

SHEAR STRENGTH OF STRUCTURAL CONCRETE MEMBERS USING A UNIFORM SHEAR ELEMENT APPROACH

by

Afshin Esfandiari

B.S., BIHE, 1997

M.A.Sc., Carleton University, 2001

A THESIS SUBMITTED IN PARTIAL FULFILLMENT OF
THE REQUIREMENTS FOR THE DEGREE OF

DOCTOR OF PHILOSOPHY

in

The Faculty of Graduate Studies

(Civil Engineering)

THE UNIVERSITY OF BRITISH COLUMBIA
(Vancouver)

April 2009

© Afshin Esfandiari, 2009

Abstract

The simplest shear problem involves a two-dimensional rectangular element with uniformly distributed reinforcement parallel to the element sides, and subjected to uniform normal stresses and shear stress. Such a uniform shear element will have uniform average stresses in reinforcement and concrete. The simplest model for elements subjected to shear force and bending moment that leads to code provisions uses one uniform shear element. Shear force is assumed to be resisted by a central portion of the cross-section acting as a uniform shear element, while bending moment is assumed to be resisted by the flexural tension reinforcement and concrete compression zone at the cross-section ends. In this thesis, the shear strength of bridge girders and squat shear walls are evaluated using a uniform shear element approach.

Current code shear design provisions for beams are necessarily simplified procedures that are generally conservative. While the extra costs are small for new design, it may lead to unnecessary load restrictions on bridges or unnecessary retrofitting when used for shear strength evaluation. A new shear strength evaluation procedure for structural concrete girders is proposed. The procedure accounts for the influence of more parameters and provides more insight into the failure mode than code design methods. To verify the procedure, predicted trends are compared with Modified Compression Field theory (MCFT) for uniform shear elements, and Response-2000 for beam elements subjected to combined shear and bending moment. Shear strength predictions are also compared with results from strength tests on reinforced and prestressed concrete beams, together with predictions from current code shear design provisions.

The current Canadian building code CSA A23.3 2004 contains new provisions for the

seismic design of squat walls that were developed using a uniform shear element approach. These new code provisions are rigorously evaluated for the first time in this study. A new method to account for the flexure-shear interaction at the base of squat shear walls is proposed as well as refinements to the 2004 CSA A23.3 shear strength provisions for squat shear walls. These are verified by comparing the predicted trends with the predictions of MCFT-based nonlinear finite element program VecTor 2.

Table of Contents

Abstract.....	ii
Table of Contents	iv
List of Tables	vii
List of Figures.....	viii
List of Symbols	xvi
Acknowledgements	xxi
Chapter 1. Introduction.....	1
1.1. Shear in Concrete Structures.....	1
1.2. Modified Compression Field Theory.....	2
1.3. Simplified Shear Analysis.....	3
1.4. Shear Strength Evaluation of Bridge Girders	5
1.5. Design of Squat Shear Walls	7
1.6. Research Objectives.....	9
1.7. Thesis Organization	10
Chapter 2. Literature Review: Beam Shear Strength	13
2.1. Review of Previous Studies	13
2.2. Recent Code Approaches.....	19
2.3. Recent Studies.....	23
2.4. Concluding Remarks.....	27
Chapter 3. Uniform Shear Elements	29
3.1. General.....	29
3.2. Uniform Shear Element	29
3.3. Modified Compression Field Theory (MCFT)	30
3.4. 2007 AASHTO LRFD Method.....	44
3.5. 2006 CHBDC Method	47
3.6. Proposed Evaluation Method for Members With at Least Minimum Transverse Reinforcement.....	51
3.7. Proposed Evaluation Method for Members Without Transverse Reinforcement.....	85
Chapter 4. Beam Elements	91
4.1. General.....	91
4.2. Exact Solution.....	91
4.3. Simplified Procedures for Design.....	100
4.4. Proposed Evaluation Method for Members With At Least Minimum Transverse Reinforcement.....	104

4.5.	Proposed Evaluation Method for Members Without Transverse Reinforcement.....	115
4.6.	Members With Less than Minimum Transverse Reinforcement.....	118
4.7.	Example Evaluations of Bridge Girder With at Least Minimum Transverse Reinforcement.....	119
4.8.	Example Evaluation for Bridge Girder With Less than Minimum Transverse Reinforcement.....	136
Chapter 5.	Comparison with Beam Test Results	140
5.1.	General.....	140
5.2.	Members With at Least Minimum Transverse Reinforcement.....	140
5.3.	Members Without Transverse Reinforcement	146
5.4.	Effect of Important Parameters.....	149
5.5.	Minimum Transverse Reinforcement and Transition Between Members With and Without Minimum Transverse Reinforcement	153
Chapter 6.	Refined 2006 CHBDC Method for Shear Design.....	157
6.1.	General.....	157
6.2.	Refined CHBDC Approach for Members With at Least Minimum Transverse Reinforcement.....	157
6.3.	Bridge Examples.....	160
6.4.	Comparison with Experimental Results.....	163
Chapter 7.	Literature Review: Squat Shear Walls	168
7.1.	Shear Strength of Squat Shear Walls.....	168
7.2.	Summary of Observed Behaviour.....	176
7.3.	Recent Code Approaches.....	179
Chapter 8.	Comparison of NLFE Predictions with Experimental Results of Squat Shear Walls.....	182
8.1.	General.....	182
8.2.	Finite Element Program	182
8.3.	Comparison with Wall Test Results	185
Chapter 9.	Analytical Study of Flexural and Shear Resistance of Squat Shear Walls.....	197
9.1.	General.....	197
9.2.	Traditional Approach for Flexural Resistance of Deep Beams	197
9.3.	2004 CSA A23.3 Approach for Flexural and Shear Resistance of Squat Shear Walls	200
9.4.	Finite Element Analysis of Squat Shear Walls Failing in Flexure	204
9.5.	Proposed Sectional Model for Flexural Capacity	220
9.6.	Comparison of Finite Element Results with the Predictions of Proposed Method for Flexural Capacity of Squat Shear Walls	222
9.7.	Finite Element Analyses of Squat Shear Walls Failing in Shear.....	229

Chapter 10. Summary and Conclusions	248
10.1. General	248
10.2. Shear Strength Evaluation of Bridge Girders	248
10.3. Strength of Squat Shear Walls	255
10.4. Recommendations for Future Work.....	258
References.....	261
Appendices.....	276
Appendix A: Excel Spreadsheets for the Proposed Evaluation Methods and the Refined CHBDC Method.....	276
Appendix B: Detailed Steps in Proposed Evaluation Procedures.....	277
Appendix C: Detailed Examples of Proposed Evaluation Procedure for Members With Stirrups.....	285
Appendix D: Rating Trucks Used for Example Evaluations of Bridge Girder.....	294
Appendix E: Tested Beams Used for Comparison with Experimental Results.....	297
Appendix F: Comparison of Predictions with Beam Test Results.....	314

List of Tables

Table 4-1 Summary of predictions for example bridge girders with at least minimum transverse reinforcement.	135
Table 4-2 Comparison of nominal shear strength predictions (kN) for bridge girder example ignoring shear resisted by inclined flexural compression.	138
Table 9-1 Summary of walls analyzed to investigate flexural capacity of squat shear walls.	206
Table 9-2 Summary of walls analyzed to investigate shear strength of squat shear walls.	231

List of Figures

Fig. 1-1 Reinforced concrete simply supported beam subjected to shear and moment.....	1
Fig. 1-2 Uniform shear elements.	2
Fig. 1-3 Predicting beam shear behaviour with one uniform shear element.	4
Fig. 1-4 Predicting squat shear wall behaviour with one uniform shear element.....	5
Fig. 1-5 An example of an existing concrete bridge (BC Ministry of Transportation).	7
Fig. 3-1 Element of reinforced concrete subjected to uniform shear and normal stresses.	30
Fig. 3-2 Concrete average stress-strain relationship in compression (Vecchio and Collins, 1986).	32
Fig. 3-3 Concrete average stress-strain relationship in tension (Vecchio and Collins, 1986).....	33
Fig. 3-4 Mohr circle of stress for cracked reinforced concrete (adopted from Vecchio and Collins, 1986).....	35
Fig. 3-5 Free body diagram of a uniform shear element in the crack direction for average stresses and local stresses at the cracks (Collins et. al 1996).....	36
Fig. 3-6 Mohr circle of strains for reinforced concrete (adopted from Vecchio and Collins, 1986).....	37
Fig. 3-7 Comparison of predicted and observed shear stress – shear strain response of six uniform shear elements (Bentz et al. 2006).	39
Fig. 3-8 MCFT predictions of shear response of uniform shear elements for: (a) members with transverse reinforcement, (b) members without transverse reinforcement.....	43
Fig. 3-9 Developing procedure of CHBDC 2006/CSA A23.3-04 equation for angle of inclination of principal compression (Bentz et al., 2006).	48
Fig. 3-10 Shear strength relation with transverse reinforcement ratio (Bentz et al., 2006).	49
Fig. 3-11 Comparison of θ and β values given by CHBDC 2006/ CSA A23.3-04 with values determined from MCFT for elements without transverse reinforcement (Bentz and Collins, 2006).....	50

Fig. 3-12 Comparison of θ and β values given by CHBDC 2006/ CSA A23.3-04 with values determined from MCFT for elements with at least minimum transverse reinforcement (Bentz and Collins, 2006).....	52
Fig. 3-13 Influence of longitudinal strain ε_x and transverse strain ε_z on: (a) shear stress, (b) angle of inclination of diagonal compression, (c) longitudinal compression stress in concrete for an element with $\rho_z = 0.005$, $f_c' = 40$ MPa, $f_y = 400$ MPa.	55
Fig. 3-14 Comparison of predicted angle θ with MCFT result at: (a) yielding of transverse reinforcement, (b) crushing of concrete for $f_c' = 40$ MPa, $f_y = 400$ MPa.	57
Fig. 3-15 Comparison of predicted angle θ with MCFT result at: (a) yielding of transverse reinforcement, (b) crushing of concrete for $f_c' = 30$ MPa, $f_y = 400$ MPa.	60
Fig. 3-16 Comparison of predicted angle θ with MCFT result at: (a) yielding of transverse reinforcement, (b) crushing of concrete for $f_c' = 60$ MPa, $f_y = 400$ MPa.	61
Fig. 3-17 Comparison of predicted angle θ with MCFT result at: (a) yielding of transverse reinforcement, (b) crushing of concrete for $f_c' = 40$ MPa, $f_y = 250$ MPa.	62
Fig. 3-18 Comparison of predicted angle θ with MCFT result at: (a) yielding of transverse reinforcement, (b) crushing of concrete for $f_c' = 40$ MPa, $f_y = 600$ MPa.	63
Fig. 3-19 Comparison of predicted β with MCFT result at: (a) yielding of transverse reinforcement, (b) crushing of concrete for $f_c' = 40$ MPa, $f_y = 400$ MPa.....	66
Fig. 3-20 Comparison of predicted β with MCFT result at: (a) yielding of transverse reinforcement, (b) crushing of concrete for $f_c' = 30$ MPa, $f_y = 400$ MPa.....	68
Fig. 3-21 Comparison of predicted β with MCFT result at: (a) yielding of transverse reinforcement, (b) crushing of concrete for $f_c' = 60$ MPa, $f_y = 400$ MPa.....	69
Fig. 3-22 Comparison of predicted β with MCFT result at: (a) yielding of transverse reinforcement, (b) crushing of concrete for $f_c' = 40$ MPa, $f_y = 250$ MPa.....	70
Fig. 3-23 Comparison of predicted β with MCFT result at: (a) yielding of transverse reinforcement, (b) crushing of concrete for $f_c' = 40$ MPa, $f_y = 600$ MPa.....	71
Fig. 3-24 Comparison of predicted shear stress with MCFT result at: (a) yielding of transverse reinforcement, (b) crushing of concrete for $f_c' = 40$ MPa, $f_y = 400$ MPa.	73

Fig. 3-25 Comparison of predicted shear stress with MCFT result at: (a) yielding of transverse reinforcement, (b) crushing of concrete for $f_c' = 30$ MPa, $f_y = 400$ MPa.	74
Fig. 3-26 Comparison of predicted shear stress with MCFT result at: (a) yielding of transverse reinforcement, (b) crushing of concrete for $f_c' = 60$ MPa, $f_y = 400$ MPa.	75
Fig. 3-27 Comparison of predicted shear stress with MCFT result at: (a) yielding of transverse reinforcement, (b) crushing of concrete for $f_c' = 40$ MPa, $f_y = 250$ MPa.	76
Fig. 3-28 Comparison of predicted shear stress with MCFT result at: (a) yielding of transverse reinforcement, (b) crushing of concrete for $f_c' = 40$ MPa, $f_y = 600$ MPa.	77
Fig. 3-29 Bilinear approximation of: (a) $\cot^2 \theta$, (b) $\cot^2 \theta$ used to approximate Eq. [3-39].	79
Fig. 3-30 Comparison of predicted longitudinal concrete compression stress with MCFT result at: (a) yielding of transverse reinforcement, (b) crushing of concrete for $f_c' = 40$ MPa, $f_y = 400$ MPa.	81
Fig. 3-31 Variation of: (a) angle, (b) shear stress with concrete contribution from variable angle truss model.	84
Fig. 3-32 Comparison of predicted axial compression stress ratio $n_v / \sqrt{f_c'}$ (in MPa units) with MCFT for members without transverse reinforcement.	87
Fig. 3-33 Comparison of predicted concrete contribution β (in MPa units) with MCFT for members without transverse reinforcement.	88
Fig. 3-34 Comparison of predicted angle θ with MCFT for members without transverse reinforcement.	90
Fig. 4-1 Application of MCFT to beam elements using multi-layer analysis (Vecchio and Collins, 1986).	92
Fig. 4-2 Equilibrium of the dual sections in MCFT exact solution for beam elements (Vecchio and Collins, 1986).	93
Fig. 4-3 Algorithm of MCFT exact solution procedure for beam elements (Vecchio and Collins, 1986).	95
Fig. 4-4 Some output plots from computer program Response 2000.	97
Fig. 4-5 Some output plots from computer program Response 2000.	98

Fig. 4-6 2007 AASHTO LRFD and 2006 CHBDC approximate sectional model for beams subjected to shear and moment.....	101
Fig. 4-7 Variation of shear response over depth of prestressed I-girder with composite deck slab: (a) cross-section, (b) longitudinal strain, (c) angle θ , (d) shear flow, (e) normal stress multiplied by width.	105
Fig. 4-8 Approximate beam strain profile and forces in the proposed method.	107
Fig. 4-9 Typical shear stress-strain relationships for beams.....	113
Fig. 4-10 Response 2000 predictions for variation of shear response over the depth of a beam, $M/V = 2.0$ m, $f_y = 550$ MPa, $f_c' = 20$ MPa.	116
Fig. 4-11 Cross-sections of girders in example bridges.....	121
Fig. 4-12 Moment and shear envelopes of evaluated bridges with minimum stirrups..	123
Fig. 4-13 Comparison of predicted shear strengths along span of I-girder bridge: (a) Response 2000 and proposed method, (b) Response 2000 and code design methods. ..	125
Fig. 4-14 Comparison of Response 2000 predicted mid-depth strain along span of I-girder bridge with proposed and code design methods.	127
Fig. 4-15 Comparison of predicted shear strengths along span of box-girder bridge: (a) Response 2000 and proposed method, (b) Response 2000 and code design methods. ..	129
Fig. 4-16 Comparison of Response 2000 predicted (a) mid-depth strain, (b) flexural tension reinforcement strain along span of box-girder bridge with proposed and code design methods.....	130
Fig. 4-17 Comparison of predicted shear strengths along span of channel-girder bridge: (a) Response2000 and proposed method, (b) Response 2000 and code design methods.	132
Fig. 4-18 Comparison of Response 2000 predicted mid-depth strain of I-girder bridge with proposed and code design methods.	134
Fig. 4-19 Cross-section of the evaluated bridge girder example at 4.67 m from mid-support ($M_u = -2628$ kNm, $V_u = 662.4$ kN).	137
Fig. 5-1 Cumulative frequency of test-to-predicted ratios of proposed and code methods: (a) RC beams, (b) PC beams.....	143
Fig. 5-2 Cumulative frequency of test-to-predicted ratios of proposed and code methods: (a) 132 reinforced concrete (RC) beams, (b) 131 prestressed concrete (PC) beams.	148

Fig. 5-3 Test-to-predicted ratios of proposed and code methods versus shear stress ratio v/f_c' for 88 prestressed concrete beams with transverse reinforcement.....	150
Fig. 5-4 Test-to-predicted ratios of proposed and code methods versus effective depth for 132 reinforced concrete beams without transverse reinforcement.	152
Fig. 5-5 Test-to-predicted shear strength ratios for 76 lightly reinforced tested beams: (a) assuming no stirrups, (b) using linear interpolation approach, for members with less than minimum stirrups.	155
Fig. 6-1 Comparison of code predicted axial compression stresses n_v with MCFT for different concrete contributions to shear stress.....	159
Fig. 6-2 Linear approximation of $\cot\theta$	159
Fig. 6-3 Comparison of I-girder predicted mid-depth strain along the bridge span.	161
Fig. 6-4 Comparison of box-girder predicted (a) mid-depth strain (b) flexural tension reinforcement strain along the bridge span.	162
Fig. 6-5 Comparison of channel-girder predicted mid-depth strain along the bridge span.	163
Fig. 6-6 Cumulative frequency of test-to-predicted ratios of refined CHBDC 2006 and CHBDC 2006 methods: (a) 80 RC beams, (b) 88 PC beams, with stirrups.	164
Fig. 6-7 Cumulative frequency of test-to-predicted ratios of refined CHBDC 2006 and CHBDC 2006 methods for 132 RC beams without stirrups.....	166
Fig. 7-1 Squat walls shear failure modes.	178
Fig. 8-1 Load-deformation responses of wall DP1: (a) observed, (b) calculated (Palermo and Vecchio, 2004).	184
Fig. 8-2 Details of the three previously tested walls in the literature examined to compare experimental results with finite element predictions.	186
Fig. 8-3 Comparison of experimental load-top displacement curve with finite element prediction for wall tested by Wiradinata and Saatcioglu (1986).	187
Fig. 8-4 Comparison of finite element predictions of shear stress profiles along (a) top section, (b) mid-height section, (c) base section of the wall tested by Wiradinata and Saatcioglu (1986) and the same wall without the top beam and distributed force applied at top.	189

Fig. 8-5 Comparison of finite element predictions of vertical reinforcement stresses at the base of the wall tested by Wiradinata and Saatcioglu (1986) and the same wall without the top beam and distributed force applied at top.	190
Fig. 8-6 Comparison of experimental load-top displacement curve with finite element prediction for wall tested by Kuang and Ho (2008).	191
Fig. 8-7 Comparison of finite element predictions of shear stress profiles along (a) top section, (b) mid-height section, (c) base section of the wall tested by Kuang and Ho (2008) and the same wall without the top beam and distributed force applied at top. ...	192
Fig. 8-8 Comparison of finite element predictions of vertical reinforcement stress at the base of the wall tested by Kuang and Ho (2008) and the same wall without the top beam and distributed force applied at top.	193
Fig. 8-9 Comparison of experimental load- top displacement curve with finite element prediction for wall tested by Lefas et al. (1990).	194
Fig. 8-10 Comparison of finite element predictions of shear stress profiles along (a) top section, (b) mid-height section, (c) base section of the wall tested by Lefas et al. (1990) and the same wall without the top beam and distributed force applied at top.	195
Fig. 9-1 Comparison of a deep beam and a squat shear wall.	199
Fig. 9-2 Uniformly distributed force flow in squat shear walls.	200
Fig. 9-3 Horizontal reinforcement yielding shear failure of squat shear walls as in 2004 CSA A23.3.	202
Fig. 9-4 Typical detail of walls analyzed to investigate flexural capacity of squat shear walls.	205
Fig. 9-5 Concrete stress contour diagrams based on finite element analysis of a squat shear wall with 0.5% distributed reinforcement in both directions and height-to-length ratio of 0.5 immediately prior to flexural failure.	208
Fig. 9-6 Steel stress contour diagrams based on finite element analysis of a squat shear wall with 0.5% distributed reinforcement in both directions and height-to-length ratio of 0.5 immediately prior to flexural failure.	210
Fig. 9-7 Finite element predictions for shear stress distributions at base of four squad shear walls immediately prior to flexural failure.	211

Fig. 9-8 Finite element predictions for total normal stress distributions at base of four squat shear walls immediately prior to flexural failure.....	212
Fig. 9-9 Predicted moment capacities of 16 squat shear walls.	214
Fig. 9-10 Ratios of finite element predicted moment capacity to the plane section analysis predicted moment capacity for the 42 squat walls failing in flexure.....	215
Fig. 9-11 Truss model for a squat wall with height-to-length ratio of 0.5.....	217
Fig. 9-12 Truss model for a squat wall with height-to-length ratio of 0.3.....	219
Fig. 9-13 Proposed sectional model for flexural capacity of squat shear walls.....	221
Fig. 9-14 Comparison of finite element predictions for shear force at flexural capacity of squat shear walls with $h_w/l_w=2.0$, with 2004 CSA A23.3 and proposed method predictions.....	223
Fig. 9-15 Comparison of finite element predictions of shear force at flexural capacity of squat shear walls with $h_w/l_w=1.0$, with 2004 CSA A23.3 and proposed method predictions.....	223
Fig. 9-16 Comparison of finite element predictions for shear force at flexural capacity of squat shear walls with $h_w/l_w=0.5$, with 2004 CSA A23.3 and proposed method predictions.....	224
Fig. 9-17 Comparison of finite element predictions for shear force at flexural capacity of squat shear walls with $h_w/l_w=0.3$, with 2004 CSA A23.3 and proposed method predictions.....	224
Fig. 9-18 Proposed simple model for flexural capacity of squat shear walls.	226
Fig. 9-19 Variation of the portion of distributed vertical reinforcement α that contributes to the flexural capacity of walls.	228
Fig. 9-20 Typical details of walls analyzed to investigate shear strength of squat shear walls.	230
Fig. 9-21 Comparison of finite element predictions for shear strength with code predictions for squat walls with: (a) $\rho_v=\rho_h$, (b) $\rho_v=3\rho_h$	233
Fig. 9-22 Finite element predictions for shear stress distribution in squat walls with $\rho_v=\rho_h=0.005$ immediately prior to shear failure: (a) at base of wall, (b) at mid-height.	235

Fig. 9-23 Concrete shear stress contour diagrams based on finite element analysis of a squat shear wall with 0.5% distributed reinforcement in both directions and height-to-length ratio of 0.5 prior to diagonal tension shear failure.....	237
Fig. 9-24 Diagonal tension failure of low rise shear walls accounting for compression zone contribution.	238
Fig. 9-25 Localized sliding effect on load-displacement curve of squat shear walls with $\rho_z = \rho_v = 0.005$ and height-to-length ratio of: (a) 0.3, (b) 0.5, (c) 1.0.....	242
Fig. 9-26 Localized sliding effect on base shear stress distribution of squat shear walls with $\rho_z = \rho_v = 0.005$ and height-to-length ratio of: (a) 0.3, (b) 0.5, (c) 1.0.....	244
Fig. 9-27 Localized sliding effect on mid-height shear stress distribution of squat shear walls with $\rho_z = \rho_v = 0.005$ and height-to-length ratio of: (a) 0.3, (b) 0.5, (c) 1.0.	245
Fig. 9-28 Ratios of finite element analysis-to-2004 CSA A23.3 refined method predicted shear strength for the 44 walls failing in shear.	247

List of Symbols

- A_g, A_{cv} = Gross cross-section area of squat shear wall,
- A_s = Total reinforcement area of compression column in squat shear wall,
- A_p, A_s = Area of prestressed, nonprestressed flexural tension reinforcement;
- A_{sw}, A_{pw} = Area of prestressed, nonprestressed longitudinal reinforcement centered in web;
- A_{pwi} = Area of i^{th} layer of prestressed longitudinal reinforcement in the web,
- A_{sc} = Area of nonprestressed longitudinal reinforcement in the compression chord,
- A_{swj} = Area of j^{th} layer of nonprestressed longitudinal reinforcement in the web,
- A_{cf} = Area of concrete surrounding flexural tension reinforcement,
- A_v = Area of transverse reinforcement (stirrups) spaced at s ,
- a = Shear span,
- a_g = Maximum concrete grain size,
- b_f = Width of beam compression face width,
- b_w = Width of shear area (web),
- C = Compression column strength in squat shear wall,
- C_c = Force in the flexural compression chord,
- d = Depth from compression face to centroid of flexural tension reinforcement,
- d_{nv} = Depth of uniform compression stress n_v over diagonally cracked web,
- d_{pw} = Depth from compression face to centroid of prestressing tendons in web,
- d_w = Depth from compression face to centroid of longitudinal reinforcement in web,
- d_v = Depth of uniform shear stress,
- E_c = Modulus of Elasticity of concrete,
- E_p, E_s = Modulus of Elasticity of prestressed, nonprestressed reinforcement;
- F_l = Required tension force in longitudinal reinforcement on flexural or compression side of member,

- F_p = Prestressing tendons force,
 F_{px} = Prestressing tendons force component in the x -direction,
 F_t = Force taken by concrete tension stiffening in the cracked tension chord.
 f_c' = Specified compressive strength of concrete,
 f_{c1}, f_{c2} = Concrete tensile, compressive strain in the principal direction;
 f_{cx}, f_{cz} = Concrete normal stress in x -dir., z -dir.;
 f_p = Effective stress in prestressing tendons,
 f_{pr} = Stress in prestressing tendons at maximum resistance,
 f_{sx}, f_{sz} = Stress in x -dir., z -dir. reinforcement;
 f_{sxc}, f_{szc} = Stress in x -dir., z -dir. reinforcement at the location of diagonal cracks;
 f_x, f_z = Applied normal stress in x -direction, z -direction;
 f_y = Yield strength of reinforcement,
 h = Thickness of squat shear wall, height of beam,
 H, h_w = Height of squat shear wall,
 jd = Internal flexural lever-arm,
 l = Span of beam,
 L, l_w = Length of squat shear wall,
 M = Bending moment at the section of interest,
 N^* = Axial force in squat shear wall,
 n_v = Axial compression stress in concrete required to resist applied shear,
 n_{vo} = Predicted value of n_v at $\varepsilon_x = 0$,
 n_v^* = Axial compression stress at location of diagonal cracks required to resist applied shear,
 n_{vc} = Maximum n_v as limited by reserve capacity of longitudinal reinforcement,
 N_v, N_{vc} = Resultant of n_v, n_{vc} stress assumed uniform over effective depth d_{nv} ;
 P = Wall panel strength in squat shear wall,
 P_s = Axial load in squat shear wall,

- s = Spacing of transverse reinforcement,
 s_{\max} = Maximum spacing of transverse reinforcement,
 s_x, s_z = Crack spacing parameter in x -direction, z -direction;
 S_{xe} = Crack spacing parameter dependent on crack control characteristics of longitudinal reinforcement and aggregate size,
 s_{θ} = Crack spacing,
 T = Force in the flexural tension chord,
 T_d = Resultant force in the distributed vertical reinforcement in web of squat shear wall,
 t = Thickness of squat shear wall,
 v = Total shear stress,
 v_c, v_s = Shear stress attributed to concrete, stirrups;
 v_{ci} = Concrete stress transferred along the cracks by aggregate interlock,
 v_{ci2} = Shear stress on cracks required to achieve biaxial yielding of reinforcement,
 $v_{ci\max}$ = Maximum concrete stress that can be transferred by aggregate interlock,
 V = Total shear resistance,
 V_{biaxial} = Shear resistance when both longitudinal and transverse reinforcement yield,
 V_c, V_s = Shear resistance attributed to concrete, stirrups;
 V_{crush} = Shear resistance at concrete crushing,
 V_{yield} = Shear resistance at yielding of transverse reinforcement,
 V_p = Shear force resisted by inclined prestressing tendons,
 V_u = Total shear resistance at ultimate limit state,
 w = Crack width,
 z = Bending moment lever-arm in deep beam,
 α = Concrete tension strength factor, portion of the total amount of distributed vertical reinforcement that contributes to the flexural capacity in squat shear wall,
 α_c = Coefficient defining the relative contribution of concrete to shear resistance of

- concrete shear wall,
- β = Concrete shear contribution factor,
- Δn_v = Predicted rate of change of n_v per unit ε_x ,
- $\Delta \theta$ = Predicted rate of change of θ per unit ε_x ,
- δ_s = Shear stain caused by crack slip,
- ε_p = Strain of prestressing tendons,
- ε_x = Average longitudinal strain over depth of member,
- ε_y = Yield strain of transverse reinforcement,
- ε_z = Strain of transverse (z-direction) reinforcement,
- $\varepsilon_1, \varepsilon_2$ = Concrete tensile, compressive strain in the principal direction;
- ε_c' = Concrete strain corresponding to concrete peak compressive stress,
- ϕ_c = Concrete resistance factor,
- ϕ_p = Prestressed reinforcing steel resistance factor,
- ϕ_s = Nonprestressed reinforcing steel resistance factor,
- ϕ_{0w} = Overstrength factor in New Zealand Standards,
- γ, γ_{xz} = Shear strain in x-z plane,
- λ, λ_p = Ratio d_{pw} / d ,
- λ_s = Ratio d_w / d ,
- λ_{pi} = Ratio d_{pwi} / d ,
- λ_j = Ratio d_{wj} / d ,
- μ = Ductility Factor in New Zealand Standards,
- θ = Angle of inclination of principle compression stress (diagonal cracks),
- θ_o = Predicted value of θ at $\varepsilon_x = 0$,
- θ_p = Angle of prestressing tendons to horizontal axis (x-direction),
- ρ_h = Ratio of distributed horizontal reinforcement to concrete area in squat shear wall,

ρ_v = Ratio of distributed vertical reinforcement to concrete area in squat shear wall,

ρ_x = Ratio of distributed longitudinal (x-dir.) reinforcement area to concrete area,

ρ_z = Ratio of transverse (z-dir.) reinforcement area to concrete area,

$\rho_{z\min}$ = Minimum transverse reinforcement ratio,

σ_y = Yield stress of squat shear wall reinforcing steel,

Acknowledgements

I would like to express my sincere appreciation to my supervisor, Dr. Perry Adebar, for his valuable advice, constant guidance, and encouragement during every stage of this research.

First part of this research on shear strength evaluation of existing bridge girders was funded by the British Columbia Ministry of Transportation. Their support is gratefully acknowledged.

Special thanks to the faculty, staff, and my fellow students at the University of British Columbia who provided me with a pleasurable and peaceful environment during this work.

I am deeply grateful to my parents, Nasrin and Iraj, who have continuously supported me throughout my years of education.

At last but not the least, I would like to express my deepest appreciation to my wife, Noushin, for her love, understanding, patience, and never faltering support during this study. I should also appreciate the new addition to the family, my son Parsa, who motivated me in the last six months to work harder.

Chapter 1. Introduction

1.1. Shear in Concrete Structures

The shear behaviour of structural concrete is a complex phenomenon. One approach to developing a theory for shear behaviour is to use the results of beam tests such as the one shown in Figure 1-1. While such tests are appropriate for pure flexure behaviour, as the region between the point loads is subjected to uniform bending moment, they cannot be easily used to develop a general shear theory. The reason is that the sections in the shear spans between the point loads and supports are subjected to varying bending moment even though they are subjected to constant shear as shown by the free body diagram in Figure 1-1(b). As the applied force P is increased, shear force together with bending moment and bending moment gradient along the shear span all increase, which makes it hard to extract shear deformations from total deformations. The fact that transverse reinforcement strain is not uniform over the beam depth complicates the matter further.

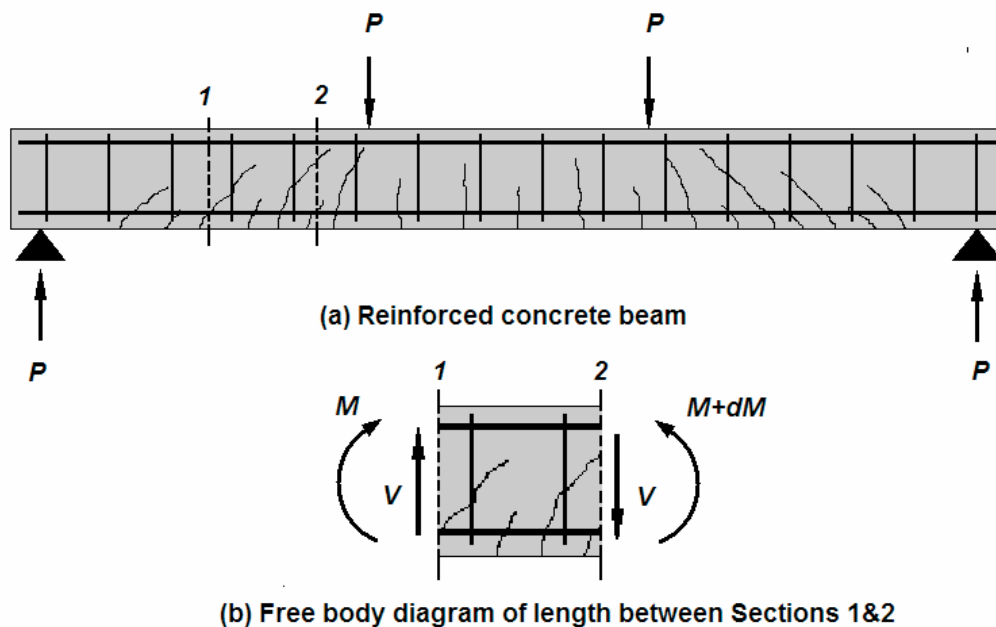


Fig. 1-1 Reinforced concrete simply supported beam subjected to shear and moment.

An alternate approach for developing a general shear theory is to use idealized elements with uniform distributed reinforcement in two directions (e.g., vertical and horizontal) subjected to uniform shear and normal stresses (uniform strains) and no bending moments (Fig. 1-2). Such elements are simpler than beams and their complete behaviour can be more easily investigated from experimental results.

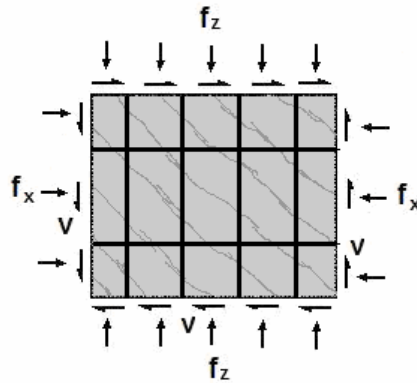


Fig. 1-2 Uniform shear elements.

1.2. Modified Compression Field Theory

The Modified Compression Field Theory (MCFT, Vecchio and Collins 1983) is a smeared crack – rotating angle model that was developed from tests performed on uniform shear elements. It predicts the behaviour of uniform shear elements throughout the whole range of loading from first cracking until failure. MCFT equations include equilibrium equations, compatibility equations, and material constitutive relationships.

MCFT has also been used for the sectional analysis of beams under combined axial load, bending moment and shear, as well as the nonlinear finite element analysis of concrete structures. For sectional analysis, the beam section is divided into layers, and

each of these layers is assumed to act as a uniform shear element. The layers are then linked by satisfying global equilibrium of the section in addition to compatibility requirements such as the well known assumption of plane sections remain plane. The procedure was implemented in computer programs such as Response 2000 (Bentz 2000) and verified against significant number of experimental results of beams. Response 2000 and equivalent programs are sophisticated research tools that provide considerable information such as stress profiles, strain profiles, and failure mechanisms.

VecTor 2 (Wong and Vecchio, 2002) is a nonlinear finite element program that employs the MCFT as constitutive relationships for uniform stress – uniform strain elements. VecTor2 can be used to analyze a variety of different concrete structures including beams and squat shear walls.

MCFT has also been used for simplified shear design procedures that utilize a single uniform shear element to approximately describe the complete sectional shear behaviour. The American Association of State Highway and Transportation Officials (AASHTO) Load and Resistance Factor Design (LRFD) bridge codes and the Canadian Highway Bridge Design Code (CHBDC) CSA S6 and the Canadian code for concrete building structures CSA A23.3 use MCFT-based methods in their shear design provisions.

1.3. Simplified Shear Analysis

Simplified shear analysis can be done by using a single uniform shear element to represent the behaviour of the shear resisting portion of a concrete structure. This approach can be applied to a beam as shown Fig. 1-3. The web of the beam is assumed to resist uniform shear stress over the shear depth of the beam (the uniform shear element), while compression and tension chords are assumed to resist the applied bending

moment. The idealized compression chord is the flexural compression zone of the beam, while the tension chord is the zone containing concentrated flexural reinforcement.

The single element shear analysis can also be applied to concrete shear walls such as the squat shear wall shown in Fig. 1-4. A certain length of the wall is assumed to resist uniform shear stress (the uniform shear element), while the ends of the wall are assumed to resist the overturning. The application of single uniform shear analysis to these two types of concrete structures are investigated in the current thesis.

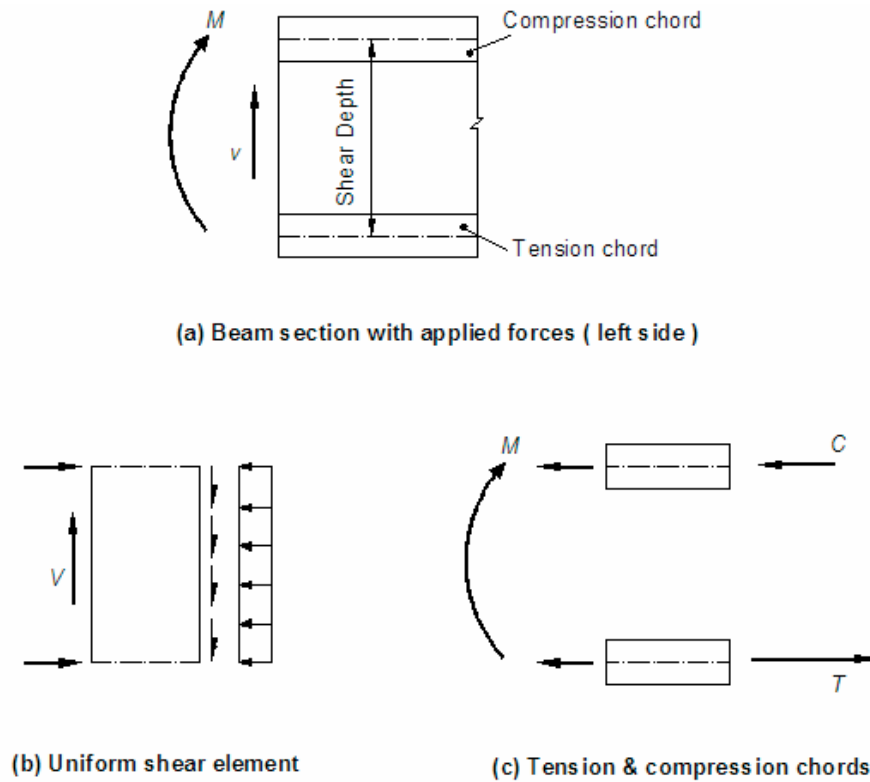


Fig. 1-3 Predicting beam shear behaviour with one uniform shear element.

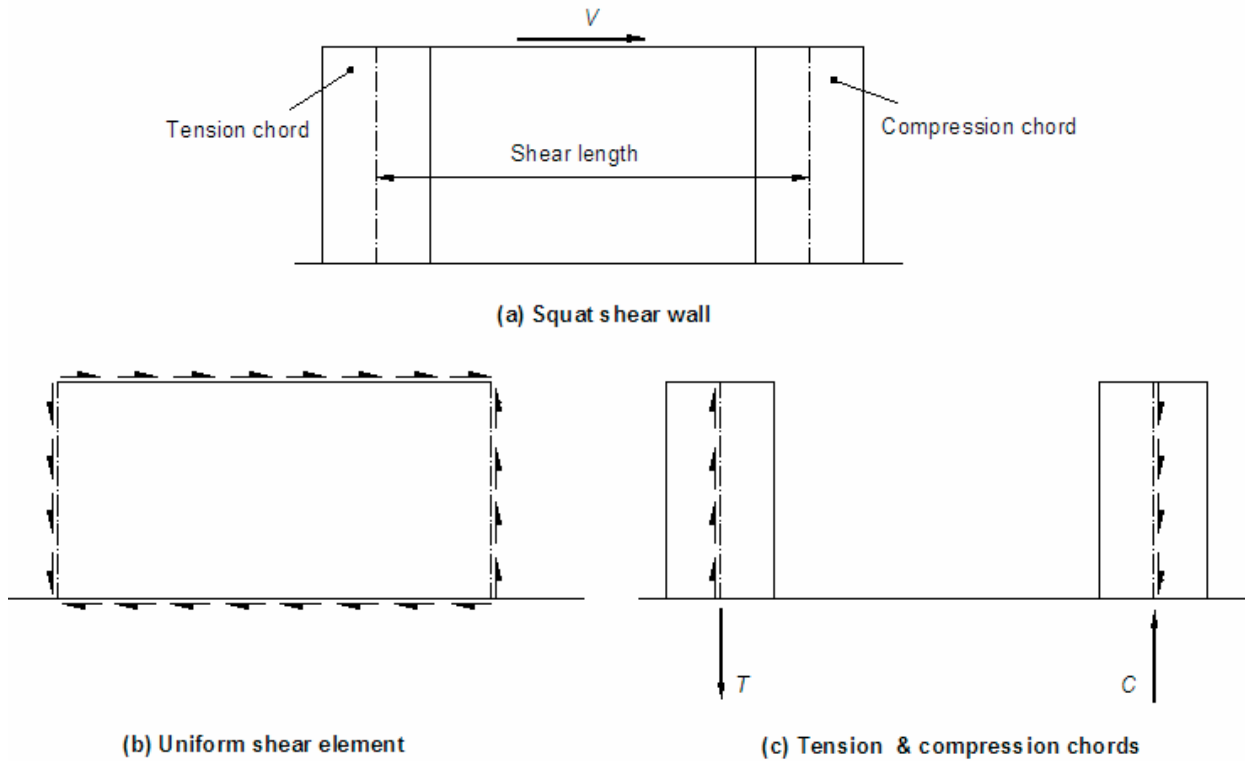


Fig. 1-4 Predicting squat shear wall behaviour with one uniform shear element.

1.4. Shear Strength Evaluation of Bridge Girders

The strength of existing concrete bridge girders (see Fig. 1-5) need to be evaluated in order to determine the load capacity rating of bridges because of increased traffic loads, or deterioration of bridges. The shear strength of concrete bridge girders often limits the load capacity ratings of bridges.

Current bridge design codes such as 2007 AASHTO LRFD and the 2006 CHBDC include simplifications that generally result in safe designs. The additional construction costs are justified by the reduced chance of a design error. On the other hand, the consequence of these same simplifications may be greater when a simplified shear design method is used to evaluate existing girders that cannot be made a little stronger. The simplifications may result in unnecessary load restrictions on bridges or unnecessary

repairs of bridge girders. Thus more complex procedures are justified for shear strength evaluation.

According to shear design procedures based on the MCFT, such as AASHTO LRFD and 2006 CHBDC, the shear strength of a girder is a function of axial strain, which depends on a number of factors including the applied shear force. Using such a design procedure to evaluate strength requires trial-and-error as the applied shear force at failure is needed to calculate shear strength.

An alternative approach for shear strength evaluation is a computer program such as Response 2000, which applies the MCFT. This would provide considerable insight such as whether the failure mode will be ductile (due to reinforcement yielding), or brittle (due to diagonal crushing of concrete). While such computer methods are very useful for special investigations, the complexity of data input and output makes it difficult to use such programs to check numerous sections along a bridge, the program options may result in different users reaching different conclusions for the same girder, and it is not possible to confirm results of such programs using hand calculations.

There is a need for a shear strength evaluation procedure that accounts for more of the complexities than a design method does and gives some insight into the shear failure mode; but yet is simple enough that a user can implement the procedure into a small computer program for checking numerous sections along a bridge, and can confirm the results of the computer program by hand calculations. Developing such a method is the objective of the current thesis.



Fig. 1-5 An example of an existing concrete bridge (BC Ministry of Transportation).

1.5. Design of Squat Shear Walls

Clause 21 of the 2004 edition of the Canadian concrete code CSA A23.3 contains new provisions for the seismic shear design of squat walls that were developed using the MCFT to describe the behaviour of a single uniform shear element. These new design provisions have not been rigorously evaluated by comparing designs resulting from the

procedure with the results of tests on squat walls or the results of nonlinear finite element analysis.

The American Concrete Institute model building code ACI 318 and New Zealand Concrete code NZS 3101 use empirical equations for the shear strength of squat shear walls that were developed from test data. Test results may not represent the true lower-bound strength that is desired in codes. For example, in almost all squat wall tests, the shear force was applied at the top of the wall to a load transfer beam that can significantly enhance the shear capacity of the wall. The diaphragm that transfers the force in a real squat wall may provide much less horizontal restraint at the top of the wall.

Squat walls are significantly restrained at the base due to the large foundation that typically supports the wall. Treating the wall as a uniform shear element may result in overly conservative designs. For example, Clause 21.7.4.7 of the 2004 CSA A23.3 states that the vertical tension force required to resist overturning at the base of squat walls shall be provided by concentrated reinforcement and vertical distributed reinforcement in addition to the amount required to resist shear. This requirement has greatly increased the required amount of vertical reinforcement in squat walls compared to traditional designs. If fan action can develop in squat walls, this requirement is too conservative.

The shear behaviour of squat walls needs to be investigated using a state-of-the-art nonlinear finite element analysis program such as VecTor 2. Of particular interest is the horizontal restraint provided at the top of the wall by loading beams used during testing, and the horizontal restraint provided at the base of the wall by real foundations. Such an analysis can be used to identify any refinements that should be made to the seismic shear design provisions in the 2004 CSA A23.3 developed from a single shear element

analysis.

1.6. Research Objectives

This thesis consists of two parts. The objective of the first, and larger of two parts, is to develop a shear strength evaluation procedure for concrete bridge girders. The evaluation procedure should give insight into the shear failure mode of concrete bridge girders and yet be simple enough that a user can implement it into a small computer program for checking numerous sections along a bridge, and can confirm the results of such a computer program by hand calculations. The procedure must be validated by comparing predictions with results from strength tests on a significant number of reinforced and prestressed concrete beams. Predictions from the procedure for actual existing bridge girders should also be compared with predictions from the more complex evaluation procedure that results from using Response 2000.

In addition to developing a standalone shear strength evaluation procedure, any refinements that can be made to the shear design procedure in the 2006 CHBDC so that the procedure is more appropriate for shear strength evaluation should also be made. An obvious possibility is to develop a refined procedure to calculate the axial strain used in the uniform shear element of bridge girders. Any such proposals must also be validated by comparing with test results and Response 2000 predictions.

The objective of the second part of the thesis is to investigate the shear behaviour of squat shear walls using nonlinear finite element analysis. The investigation should include the influence of the horizontal restraint provided at the top of the wall by loading beams used during testing, and the horizontal restraint provided at the base of the wall by real foundations. The analysis can be used to identify refinements that can be made to the

seismic shear design provisions for squat walls in the 2004 CSA A23.3 such as the requirement for vertical reinforcement for shear all along the base of the wall. Typical designs from the 2004 CSA A23.3 method need to be compared with designs using ACI 318 and NZS 3101.

1.7. Thesis Organization

This thesis contains 10 chapters and six appendices. Part 1 of the thesis, which involves the shear strength evaluation of concrete bridge girders, is presented in Chapters 2 to 6. Part 2, which involves the shear design of squat shear walls, is presented in Chapters 7 to 9. The detailed organization of the thesis is given below.

Chapter 2 presents a brief review of general literature on the shear strength of beams and bridge girders and a summary of the relevant research that has recently been done.

Chapter 3 discusses uniform shear elements and the MCFT, as well as MCFT-based design methods in the 2006 CHBDC and 2007 AASHTO LRFD shear design provisions. It presents new MCFT-based methods for shear evaluation of members with and without transverse reinforcement and compares predictions from these methods with predictions of the 2006 CHBDC and the 2007 AASHTO LRFD shear design methods.

Chapter 4 presents the application of the proposed uniform shear element method presented in Chapter 3 to beam elements. To validate the method, results from the procedure are compared with the results from Response 2000, the 2006 CHBDC and 2007 AASHTO LRFD design methods for three existing concrete bridges.

Chapter 5 compares results from large-scale tests with the proposed method predictions for both beams with and without transverse reinforcement. Chapter 6 presents the proposed refined CHBDC shear design method and its validation against test data.

Chapter 7 begins Part 2 of the thesis by presenting a summary of the previous work done on shear strength of squat shear walls. Chapter 8 briefly explains the finite element program used to predict nonlinear behaviour of squat shear walls and compares its predictions with three tests from the literature. The effect of a rigid loading beam as typically used in previous experimental work is also investigated.

Chapter 9 presents a new method to calculate flexural strength of squat walls accounting for shear – flexure interaction at base of the walls as well as the 2004 CSA A23.3 refined method for shear strength of those walls, while Chapter 10 presents summary and conclusions of the thesis.

Two Excel Spreadsheets are included with this report (Appendix A). The first is for shear strength evaluation according to the method described in Chapter 3 and 4. The second is for the refined shear design procedure described in Chapter 6.

Appendix B contains detailed instructions on how to apply the shear strength evaluation procedures described in Chapter 3. Sufficient detail is provided so that anyone can write their own spreadsheet to apply the method, or check any step in the spreadsheet provided in Appendix A.

Appendix C presents three worked examples of shear strength evaluation of actual concrete bridge girders. Appendix D provides details of rating trucks used in the bridge examples presented in Chapter 4.

Appendix E presents information on the tests used to verify the proposed methods in Chapter 5 and 6. In addition, proposed method predictions as well as other code predictions are given. Appendix F provides additional plots for comparison of test data with the proposed method and code design methods predictions. The plots illustrate the

trend of test-to-predicted shear strength ratios with important parameters in shear such as shear stress ratio, effective depth, concrete compressive strength, and longitudinal reinforcement ratio.

Chapter 2. Literature Review: Beam Shear Strength

2.1. Review of Previous Studies

Ritter (1899) and later Mörsch (1920, 1922) introduced the 45 degree truss angle to predict shear behaviour of concrete beams. The model assumes that force flow can be idealized by a truss in which concrete flexural compression chord is the horizontal compression member, longitudinal tensile reinforcement is the horizontal tensile element, compression elements formed between the cracks are the inclined elements, and stirrups are vertical elements and the angle of inclined cracks is assumed to be 45 degrees. In this method, vertical components of inclined compression forces in the diagonal struts are assumed to be balanced by stirrup forces only and no post cracking resistance is considered for concrete at the cracks.

Withey (1906, 1907) and Talbot (1909) performed experimental investigation and showed that 45 degree truss model is too conservative. This led to evaluation of 45 degree truss model by a number of researchers and the idea of contribution of concrete to shear resistance of beams and the traditional formulation of:

$$[2-1] \ V = V_c + V_s$$

$$[2-2] \ V_s = \frac{A_v f_y d_v \cot \theta}{s}$$

in which V_c is concrete contribution to shear resistance, V_s is stirrup contribution to shear resistance, A_v is the area of transverse shear reinforcement within a distance s along the member, f_y is the yield strength of the transverse reinforcement, d_v is the effective shear depth of the member traditionally assumed equal to depth from compression face to centroid of flexural tension reinforcement d , and θ is the angle of inclination (measured

from the longitudinal axis) of the concrete principal diagonal compressive stress, i.e., angle of critical diagonal crack traditionally assumed equal to 45 degrees. 45 degree truss model plus concrete contribution to shear V_c is also referred to as modified truss analogy in the literature.

Consequently, many researchers such as Morrow and Viest (1957), Bresler and Pister (1958), Hanson (1958), Guralnick (1959), Viest (1959) investigated cracked concrete contribution to shear strength of the beams and proposed different equations to quantify V_c . ACI-ASCE shear committee 326 (1962), based on available experimental investigations, suggested the following formula for shear strength of reinforced concrete beam elements.

$$[2-3] \quad V = (1.9\sqrt{f_c'} + 2500\rho_w \frac{Vd}{M})b_w d \leq 3.5\sqrt{f_c'}b_w d \quad \text{in psi units}$$

where f_c' is compressive strength of concrete, ρ_w is ratio of flexural tension reinforcement area to concrete area, b_w is web width, d is depth from compression face to centroid of flexural tension reinforcement, and M and V are factored bending moment and shear force acting at the section of interest. This formulation is still in AASHTO standards as well as ACI 318. For ordinary RC beams, Bresler and Scordelis (1963) proposed the following simple equation for V_c .

$$[2-4] \quad V_c = 2\sqrt{f_c'}b_w d \quad \text{in psi units} \quad (V_c = 0.17\sqrt{f_c'}b_w d \quad \text{in MPa units})$$

In 1962, Leohardt and Walters explained the shear failure modes of beam action and arch action through a series of tests. They showed that deep beams can transfer shear to the supports by compressive stresses in concrete whose flow is like an arch. Thus deep beams have a higher shear resistance compared to shallow beams. Later, Kani (1964)

introduced his comb theory and tooth failure mechanism to predict the shear strength of beams. In his model, inclined shear cracks along a beam would form a comb whose base is the beam top compression chord and teeth are reinforced concrete between the cracks. Shear failure then happens due to cracking of the root of one tooth as a consequence of the force caused by longitudinal reinforcement due to shear.

For prestressed concrete beams, McGregor (1960) introduced the idea of using the lesser of web shear cracking load V_{cw} and flexural shear cracking load V_{ci} for concrete contribution to shear strength by testing prestressed beams subjected to moving loads. The idea was to identify the probable cracking mode and determine concrete shear force accordingly. Two types of cracking were noticed in experimental results. Some cracks called web-shear cracking initiated in an angle at almost mid-depth of web and extended toward both compression and tension chords. Some others called flexural shear cracking initiated from flexural cracks and inclined toward the web. This was further investigated and refined by other researchers such as Hernandez et al. (1960) and Mattock and Kaar (1961), MacGregor et al. (1965 and 1966), Oleson and Sozen (1967), and MacGregor and Hanson (1969). These studies led to the following V_{ci} , V_{cw} formulas, which are semi theoretical/experimental and are still in the current AASHTO Standard Specifications and ACI 318.

$$\text{[2-5]} \quad V_{ci} = 0.6\sqrt{f'_c}b_wd + V_d + \frac{V_iM_{cr}}{M_{max}} \geq 1.7\sqrt{f'_c}b_wd \quad \text{in psi units}$$

$$\text{[2-6]} \quad V_{cw} = (3.5\sqrt{f'_c} + 0.3f_{pe})b_wd + V_p \quad \text{in psi units}$$

where V_d is dead load shear force at the section of interest, M_{max} is maximum factored moment at the section due to externally applied load, V_i is factored shear force at the

section due to externally applied load corresponding to M_{max} , M_{cr} is the external moment which causes initial flexural cracking of the section, f_{pe} is the effective stress in the prestressing steel after losses, and V_p is the vertical component of inclined prestressing force.

European researchers introduced the variable angle truss model. The model is similar to the traditional 45 degree truss model but assumes angle of inclination of diagonal compression is variable. Angle of inclination of cracked concrete could not be determined by equilibrium equations because there were three equilibrium equations versus four unknowns. Therefore, Kupfer (1964) and some others solved the problem using the principle of minimum energy while other researchers such as Leonhardt and Walter (1964), Kuyt (1972), Nielsen and Braestrup (1975), Thürlimann (1979), Thürlimann et al. (1983), and Nielsen (1984) took the plasticity approach for this purpose. It is worth mentioning that solving truss model using equilibrium approach is a lower-bound approach based on the theory of plasticity; thus, a range of possible angle of inclination may be used to determine a conservative prediction for shear strength of a concrete member.

Mitchell and Collins (1974) and Collins (1978) developed the Compression Field Theory (CFT). The theory solves equilibrium equations making use of additional equations of material constitutive relationships and compatibility equations and is capable of predicting the shear behaviour of concrete beam elements in the entire range of loading up to failure. Collins (1978) verified CFT by an experimental investigation. It should be mentioned that CFT assumes that concrete is incapable of carrying tension stresses after cracking.

Vecchio and Collins (1983) developed the Modified Compression Field Theory (MCFT) for uniform shear elements (rectangular shear elements with uniform stresses and strains in every direction). Similar to CFT, MCFT accounts for compatibility of strains, material constitutive relationships and equilibrium equations, but it also accounts for concrete contribution in tension after cracking (tension stiffening effect) as well as the effect of biaxial strains on the concrete stress-strain relationship when concrete is in compression. The theory was developed based on experimental results of the tests performed on uniform shear elements. MCFT includes two sets of equilibrium equations namely average stress equations and equations of stresses at cracks to ensure that average stresses can be transferred at cracks by aggregate interlock. It is worth mentioning that both CFT and MCFT assume that the directions of principal average stresses and principal average strains in concrete coincide; thus, crack angle changes throughout the loading after cracking. Later MCFT was used to develop more practical and simpler equations for shear design. Amongst those are the AASHTO LRFD and the 2006 CHBD (Canadian Highway Bridge Design) code approaches which were developed by Collins et al. (1996) and Bentz et al. (2006), respectively. The 2006 CHBD and 2007 AASHTO LRFD shear design methods are explained later in this chapter and Chapter 3.

Vecchio and Collins (1986) explained how uniform shear elements can be used to predict the behaviour of beam elements under shear. They used multi-layer analysis and linked the layers by the assumptions of plane sections remain plane and satisfying equilibrium at dual sections of the beam which are closely spaced. They also explained that by assuming a certain shape for shear flow profile (rectangular, parabolic, etc) the

procedure is simplified to one section rather than dual sections; however the results are approximate.

Vecchio and Collins (1988) method was later employed in computer programs Response (Felber, 1990) and Small (Ho, 1994) to predict the behaviour of concrete sections under shear force, bending moment and axial force. Bentz (2000) developed Response 2000 that also predicts the response of beam sections. Response 2000, which is the most complete program of its kind, is significantly improved in numerical techniques and is a sophisticated research tool. It provides detail information about the behavior of concrete beam sections subjected to bending moment, shear and axial force. The information, which is provided throughout the entire range of loading up to failure, include load-deformation curves, steel and concrete stress and strain profiles, shear stress on cracks, crack directions and widths, and etc. Bentz (2000) verified Response 2000 against the 534 tests reported in the literature. More details about Response 2000 are provided in Chapter 4.

Between 1987 and 1997, Hsu together with other researchers developed two methods called the Rotating Angle Softened-Truss Model (RA-STM) and the Fixed Angle Softened-Truss Model (FA-STM) to predict shear behaviour of uniform shear elements. Both methods predict the behaviour of uniform shear elements by solving equilibrium equations making use of compatibility and constitutive relations. Like MCFT, RA-STM assumes that the directions of principal stresses and strains coincide while FA-STM assumes that after cracking crack angle does not change; thus, principal compression stress does not coincide with crack direction. Both methods use different material

constitutive laws from the ones used in MCFT and account for local stress effect at cracks by reducing the average strength of reinforcement.

Other researchers such as Loov (1978, 1998), Gambarova (1987), Reineck and Hardjasaputra (1990), Reineck (1991), and Loov and Patnaik (1994) took the truss model with crack friction approach to solve shear problems of beams. In this model, two forces parallel (friction force) and perpendicular to crack surface in addition to stirrup forces are assumed to act on the shear crack plane of the beam. The summation of the vertical components of these two forces is concrete contribution to shear V_c . The equilibrium equations are solved using the constitutive laws for the transfer of forces across the cracks by friction which depend on shear load level, strain level and crack spacing. The simplified crack friction models use a constant V_c which is mostly a function of longitudinal reinforcement ratio, beam size and material properties.

2.2. Recent Code Approaches

In this section some of the recent code provisions for shear design of concrete beams are reviewed.

2.2.1. ACI 318-05 and 2002 AASHTO Standards

ACI 318-05 and 2002 AASHTO Standards assume that shear failure happens at crack angle of 45 deg and concrete contribution to shear at failure is equal to the load at which diagonal cracking is expected to occur. The method assumes shear strength is proportional to the member depth thus does not include size effect. Both codes use Eqs.[2-1] and [2-2] for shear strength of beams where $\theta=45$ deg, $d_v=d$, V_c is calculated from Eq. [2-4] for reinforced concrete members and the lesser of Eqs.[2-5] and [2-6] for

prestressed concrete members. Both codes limit the shear strength of a beam to $V_c + 8\sqrt{f'_c}b_wd$ (in psi units) to prevent concrete crushing.

2.2.2. AASHTO LRFD 2007

2007 AASHTO LRFD shear design method, which is still present in the 2008 AASHTO LRFD as an alternative method, was derived from MCFT assuming uniform shear flow along the beam effective shear depth d_v assumed to be $0.9d$. While the longitudinal strain varies over the beam depth, the method uses one longitudinal strain ϵ_x at a certain depth of the beam to determine the shear strength using a uniform shear element approach. The shear strength is given by:

$$[2-7] V = V_c + V_s + V_p = \beta\sqrt{f'_c}b_wd_v + \frac{A_vf_yd_v}{s}\cot\theta + V_p$$

where concrete contribution factor β and angle of principal compression θ are functions of longitudinal strain ϵ_x and shear stress ratio $\frac{v}{f'_c}$ for members with transverse reinforcement, while they are functions of ϵ_x and crack spacing parameter S_{xe} (a function of beam size and maximum concrete aggregate size) for members without transverse reinforcement. The values of β and θ are given in tables. The longitudinal strain ϵ_x is determined from:

$$[2-8] \epsilon_x = \frac{M/d_v + 0.5V\cot\theta - f_pA_p}{2(E_sA_s + E_pA_p)} : \text{for members with transverse reinforcement}$$

$$[2-9] \epsilon_x = \frac{M/d_v + 0.5V\cot\theta - f_pA_p}{(E_sA_s + E_pA_p)} : \text{for members without transverse reinforcement}$$

where: M = bending moment at section of interest; V = shear strength at the section of interest; f_p = effective prestressing force; A_s, A_p = area of nonprestressed and prestressed flexural tension reinforcement; and E_s, E_p = Modulus of Elasticity of nonprestressed and prestressed reinforcement, respectively.

The ε_x equations are different for members with and without transverse reinforcement by a factor of 2 as the longitudinal strain is taken at mid-depth for members with transverse reinforcement, and at the centroid of flexural tension reinforcement for members without transverse reinforcement. If the longitudinal strain is negative in the 2007 AASHTO LRFD method, the concrete compression stiffness must be added to the denominator of Eqs. [2-8] and [2-9].

2007 AASHTO LRFD method requires trial-and-error for design since ε_x , which is not known initially, is needed to determine β and θ values from the tables. In this method, it is also necessary to check if there is sufficient strength in the longitudinal reinforcement to resist the extra demand caused by shear. Also shear stress is limited to $0.25f'_c$ to avoid concrete crushing in the web prior to stirrup yielding. More details about this method is given in Chapter 3.

2.2.3. 1994 CSA A23.3 and CHBDC 2000

1994 CSA A23.3 method for shear design of beams, which is the same as 2000 Canadian Highway Bridge Design Code (CHBDC) method, is essentially the same as 2007 AASHTO LRFD method except it uses the longitudinal strain at the centroid of flexural tension reinforcement Eq. [2-9] for both members with and without transverse

reinforcement. In addition, the method does not allow negative longitudinal strains unlike 2007 AASHTO LRFD that allows negative ε_x values.

2.2.4. 2004 CSA A23.3, CHBDC 2006, and AASHTO LRFD 2008

Similar to 2007 AASHTO LRFD method, this method is based on MCFT and uses Eq. [2-7] to determine shear strength of beams, but it provides equations for β and θ rather than tabulated values. Further simplifications in this method resulted in equations for β and θ that are not functions of shear stress ratio $\frac{v}{f_c'}$ for members with transverse reinforcement. β and θ are functions of longitudinal strain ε_x only. In addition, the equations for β and θ are the same for both members with and without transverse reinforcement. The equations are:

$$\text{[2-10]} \quad \beta = \frac{4.8}{1 + 1500\varepsilon_x} \cdot \frac{1300}{1000 + s_{xe}} \quad \text{in psi units}$$

$$\text{[2-11]} \quad \theta = (29 + 7000\varepsilon_x) \left(0.88 + \frac{s_{xe}}{2500} \right) \leq 75 \text{ deg}$$

where s_{xe} is the size effect parameter taken as 300 mm for members with transverse reinforcement and varies for members without transverse reinforcement depending on depth of elements, vertical spacing of longitudinal reinforcement layers, and concrete maximum aggregate size. In 2008 AASHTO LRFD and 2004 CSA 23.3, Eq. [2-11] is conservatively simplified to $\theta = 29 + 7000\varepsilon_x$ for members without transverse reinforcement.

The method assumes that mid-depth strain is the reference strain for both members with and without transverse reinforcement. In addition, it simplifies Eq. [2-8] by

substituting $V \cos \theta$ with $2V$ in the numerator to avoid trial-and-error procedure for design purposes. ε_x is given by:

$$[2-12] \varepsilon_x = \frac{M / d_v + V - f_p A_p}{2(E_s A_s + E_p A_p)}$$

The strain ε_x used in 2008 AASHTO LRFD equations for β and θ is exactly twice the value used in 2004 CSA A23.3 and 2006 CHBDC (Eq. 2-12), and thus $1500\varepsilon_x$ in Eq. [2-10] is replaced by $750\varepsilon_x$, and $7000\varepsilon_x$ in Eq. [2-11] is replaced by $3500\varepsilon_x$. As a result, the methods final predictions for shear strength of beams remain the same. This method uses the same equations and limits as 2007 AASHTO LRFD method to check the sufficiency of longitudinal reinforcement for shear and avoid concrete crushing. More details are provided in Chapter 3.

The 2008 AASHTO LRFD also has a simple design procedure that was proposed by Hawkins et al. (2005). This method is discussed in Section 2-3.

2.3. Recent Studies

Oh and Kim (2004)

They tested two full-scale post-tensioned prestressed concrete girders that were 10600 mm long and 1200 mm deep, and had web transverse reinforcement and web width of 180 mm. The geometry of the beams were the same but one of them was high strength concrete ($f'_c = 60$ MPa) while the other one was normal strength concrete ($f'_c = 40$ MPa). 12 seven strand prestressing tendons with 12.7 mm diameter and the prestressing force of 1007.9 MPa were used in the girders. Girders were loaded by an asymmetrical point load up to failure. They calculated principal strains, shear strain and angle of

inclination based on the measured strains in the horizontal, vertical and 45 degree directions.

Based on experimental results, they concluded that the concept of compatibility of strains and rotation of crack angle throughout loading was well suited for predicting prestressed concrete beam behaviour in shear for both normal strength and high strength concrete.

Cladera and Mari´ (2004 and 2005)

They proposed simplified shear design procedures for concrete beams with and without transverse reinforcement. For beams with transverse reinforcement, they used available shear test results of 123 reinforced concrete beams in the literature and employed Artificial Neural Networks (ANNs) to develop their proposed shear design procedure.

The selected database had shear span-to-depth ratio a/d equal to or greater than 2.49, f_c' from 21 to 125 MPa (less than 80 MPa in 80% of the tests), effective depth from 198 to 925 mm (depth of less than 600 in. in 90% of the tests), transverse reinforcement $\rho_z f_y$ from 0.33 to 3.57 MPa, and longitudinal reinforcement from 0.5% to 5.8%. It was observed that AASHTO LRFD predictions were the closest to ANNs results compared to EC2 and ACI predictions. As a result, they used AASHTO LRFD tabulated values for θ to develop the following equation for members with web reinforcement, which was believed to be conservative compared to the AASHTO LRFD tabulated values:

$$[2-13] \quad \theta = 20 + 15\varepsilon_x + 45 \frac{\tau}{f_c'}$$

In the above equation, ε_x is mid-depth strain, and τ is shear stress equal to $V/b_w d_v$. They used the same formula as in the 2004 CSA A23.3 for ε_x .

For concrete contribution V_c in members with web reinforcement, they developed a formula with the same format as in EC2 but the influence of some parameters were changed based on ANNs results. Their proposed formula for V_c was:

$$[2-14] \quad V_c = [0.17\xi(1000\rho_l)^{1/2} f_c'^{0.2} \tau^{1/3} + 0.15\sigma_{cp}] b_w d_v$$

where ρ_l is ratio of flexural tension reinforcement area to concrete area, σ_{cp} is normal stress due to prestressing or axial load, and ξ is the size effect parameter equal to:

$$[2-15] \quad \xi = 1 + \sqrt{\frac{200}{s_x}} \leq 2.75$$

in which s_x is the lesser of d_v or spacing of longitudinal vertical reinforcement in the web. Finally, they verified their proposed method for members with stirrups against 162 reinforced concrete beams and 40 prestressed concrete beams reported in the literature.

Kuchma et al. (2005) (NCHRP Project 12-56)

As part of a National Cooperative Highway Research Program (NCHRP) Project 12-56, Kuchma et al. tested 6 high-strength prestressed concrete girders to investigate the applicability of available shear design procedures especially the AASHTO LRFD method for high strength prestressed concrete. They tested specimens that had 50 ft clear span, f_c' from 10 to 18 ksi, depth of 73 in., and 26 to 42 prestressing strands of 0.6 inch diameter. All girders had transverse reinforcement and were subjected to uniform load (see Kim 2004 for more details).

Some of the important conclusions from the study are:

- Draped strands (6 draped strands were used) improved the cracking shear strength 16%-23%, as well as the ultimate shear strength 15%-16%.
- Draped strands and horizontal web strands provided good crack control.

- Welded wire reinforcement (WWR) improved the ability of tested beams in redistribution of shear forces between stirrups. This is because WWR could sustain large strains.
- A sudden increase in transverse strain was noticed immediately after cracking.
- A number of the specimens failed due to web crushing at the base of the web over the support. The failure indicated that the shear stresses were not uniform over the depth; but were concentrated in a compression strut. The AASHTO LRFD approach of limiting the shear stress – assumed to be uniform over the shear depth – to $0.25 f_c'$ results in a safe prediction of these tests as well.
- AASHTO LRFD method provided accurate predictions for the shear strength of the specimens. The ratios of measured to predicted strengths for the 20 tests ranged from 0.97 to 1.29, had an average value of 1.12 and a COV of 0.09.

Hawkins et al. (NCHRP Report 549, 2005)

This project involved evaluating the most prevalent shear design procedures including the shear provisions in AASHTO LRFD, 2004 CSA A23.3, ACI 318 as well as JSCE (Ref. 44), EC2 (Ref. 28) and DIN (Ref. 27) against 1359 test results available in the literature. They found that among all the shear design procedures in building codes, AASHTO LRFD and the 2004 CSA A23.3 provide the best predictions with only 10% probability of being unconservative. Based on their evaluation results, they recommended that one use either the 2004 CSA A23.3 provisions or the following modified ACI procedure:

- For reinforced concrete beams, $\theta = 45$ deg. and

[2-16] $V_c = 1.9\sqrt{f_c'}b_wd_v$ (in psi units)

- For prestressed concrete beams, $\theta = 45$ deg. if $V_{ci} \geq V_{cw}$ or $M_u \geq M_{cr}$ otherwise:

$$[2-17] \quad \cot \theta = 1 + 3 \frac{f_{pe}}{\sqrt{f'_c}} \quad (\text{in psi units})$$

and V_c is the lesser of:

$$[2-18] \quad V_{ci} = 0.632\sqrt{f'_c}b_wd_v + V_d + \frac{V_iM_{cr}}{M_{\max}} \geq 1.9\sqrt{f'_c}b_wd_v \quad (\text{in psi units})$$

$$[2-19] \quad V_{cw} = (1.9\sqrt{f'_c} + 0.3f_{pe})b_wd_v + V_p \quad (\text{in psi units})$$

where: d_v is the effective shear depth of the member which may be taken as $0.9d$.

V_{cw} in Eq. [2-25] is significantly reduced from the traditional ACI 318 web shear cracking expression.

Hawkins et al. compared predictions from the proposed simplified method above with the results of 147 tests they selected from a database of 1359 shear tests. They selected test data of members that contained minimum transverse reinforcement ($\rho_z f_y > 50$ psi [0.35 MPa]), had an overall depth of at least 20 inches (500 mm), and were cast from concrete having a compressive strength of at least 4 ksi (28 MPa). They excluded tests in which anchorage or flexural failure occurred. The results showed that the 2006 CHBD and AASHTO LRFD shear design provisions gave the best predictions compared to the test results; however, their proposed method had considerably better predictions than those from ACI 318. Hawkins et al. also compared the predictions of Response 2000 with test results and reported that Response 2000 predictions were better than the predictions of evaluated codes.

2.4. Concluding Remarks

Recent studies (Hawkins et al. 2005, Kuchma et al. 2005, Cladera and Mari' 2004 and 2005) have shown that the 2007 AASHTO LRFD and 2006 CHBDC shear design

methods which were developed based on MCFT are two of best methods compared to other evaluated code methods when their predictions are compared with experimental results. Response 2000 which performs sophisticated MCFT-based sectional analysis for beams and explicitly accounts for moment shear interaction has also been evaluated and found to be better than MCFT-based simplified methods in 2007 AASHTO LRFD and the 2006 CHBDC (Hawkins et al. 2005). On the other hand, modified truss analogy which uses the 45 angle truss model in addition to concrete contribution to shear such as shear design methods in ACI 318 and EC2 was found not to be as consistent with experimental results (Hawkins et al. 2005, Cladera and Mari´ 2004 and 2005). As a result, MCFT as well as MCFT-based sectional analysis for beams (Response 2000) are used in this study to develop a new procedure for shear evaluation of concrete bridges. In addition, the predictions of the proposed procedure are compared to 2007 AASHTO LRFD, 2006 CHBDC, and ACI 318, which is one of the modified truss analogy methods in the literature that has been used for many years. Finally, the proposed equations are verified against numerous test results reported in the literature.

Chapter 3. Uniform Shear Elements

3.1. General

A uniform shear element has uniformly distributed reinforcement in two directions parallel to the element sides and is subjected to uniform shear and normal stresses. Such elements are simpler than beams and their complete behaviour can be more easily investigated from experimental results. This chapter presents methods that can be used to predict the behaviour of uniform shear elements. How the shear behaviour of beams can be approximated using a single uniform shear element is discussed in Chapter 4.

The Modified Compression Field Theory (MCFT, Vecchio and Collins 1983) is one of the theories used that can predict the behaviour of uniform shear elements. It is a smeared rotating crack angle model that was developed from tests. MCFT is discussed in this chapter. In addition, simplified MCFT-based methods available in codes and the literature are reviewed and discussed. A new shear evaluation procedure for uniform shear elements is proposed. The proposed evaluation procedure is compared with MCFT and the predictions from the code simplified procedures.

3.2. Uniform Shear Element

Uniform shear element is a rectangular membrane element (subjected to in-plane shear and axial stresses) with uniformly spaced longitudinal (x -direction) and transverse (z -direction) reinforcement, no inclined prestressing tendons, and subjected to uniform applied normal stresses f_x and f_z and shear stress v . Such an element will have uniform reinforcement stresses f_{sx} and f_{sz} , and uniform concrete stresses f_{cx} , f_{cz} and $v_c=v$ as shown in Fig. 3-1. Figure 3-1 also shows that this element may be used to model a portion of an I-girder subjected to in-plane shear and moment.

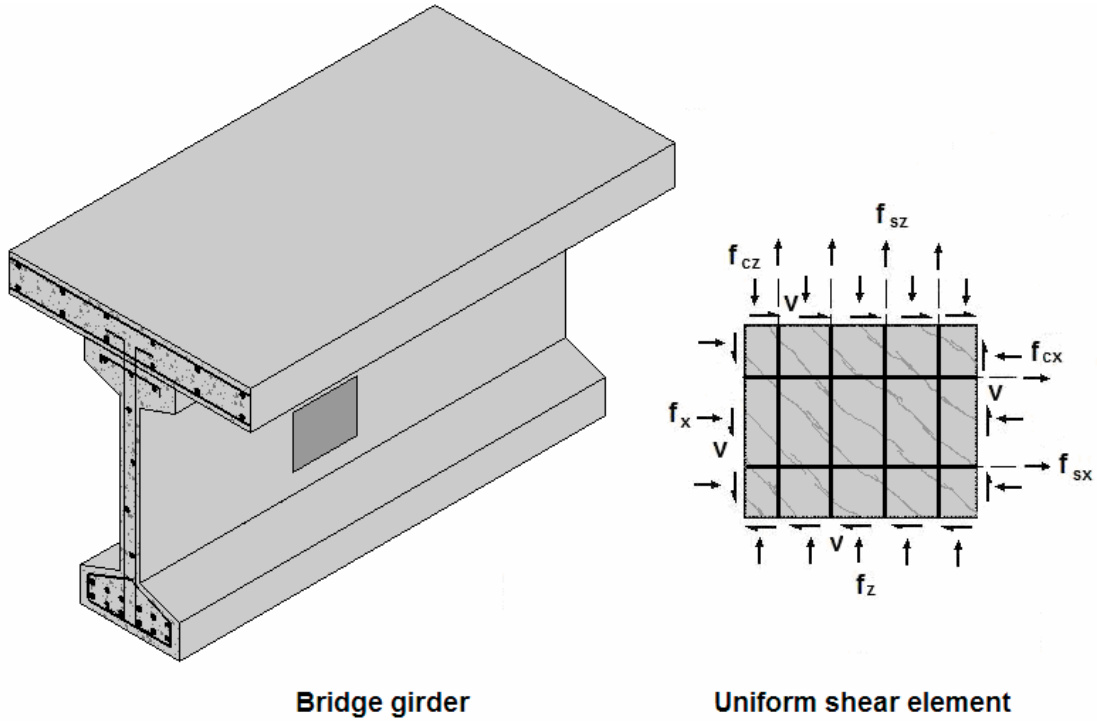


Fig. 3-1 Element of reinforced concrete subjected to uniform shear and normal stresses.

3.3. Modified Compression Field Theory (MCFT)

Modified Compression Field Theory (MCFT) was developed by Vecchio and Collins (1986) from testing reinforced concrete elements subjected to uniform shear stress. It is a smeared, rotating crack model where the inclination of diagonal cracks is determined by combining equilibrium requirements, strain compatibility assumptions and empirical average stress – average strain relationships for cracked concrete and reinforcement.

The MCFT can be used to predict the shear stress – shear strain relationships of structural concrete membrane elements with different amounts of transverse (z -direction) and longitudinal (x -direction) reinforcement. Any structure in which forces are primarily transferred through in-plane action can be idealized as a combination of uniform shear elements. In the following sections, MCFT equations for material constitutive

relationships, equilibrium equations, and compatibility are explained.

3.3.1. Material Constitutive Relationships

Parabolic stress-strain relationship as shown in Fig. 3-2 is considered for concrete in compression in the principal direction. Cracked concrete softens when subjected to biaxial strains compared to concrete uniaxial stress-strain relationship. As a result, the principal compressive strength (peak stress) may be significantly lower than the uniaxial strength when concrete is subjected to significant tension strain transverse to the principal compression. Vecchio and Collins (1986) showed that the reduction in concrete strength (peak stress) in such cases can be predicted by the following equation:

$$[3-1] \quad f_{c2\max} = \frac{f_c'}{0.8 - 0.34\varepsilon_1 / \varepsilon_c'} \leq f_c'$$

where $f_{c2\max}$ is concrete peak stress under biaxial strains, ε_1 is concrete principal tensile strain, f_c' is concrete peak stress under uniaxial compression and ε_c' is concrete strain corresponding to concrete peak compressive stress. Therefore, a parabolic stress-strain relationship of concrete in the principal compressive direction can be expressed as:

$$[3-2] \quad f_{c2} = \left[2 \frac{\varepsilon_2}{\varepsilon_c'} - \left(\frac{\varepsilon_2}{\varepsilon_c'} \right)^2 \right] f_{c2\max}$$

in which f_{c2} is concrete compressive stress in the principal direction and ε_2 is concrete compressive strain in the principal direction.

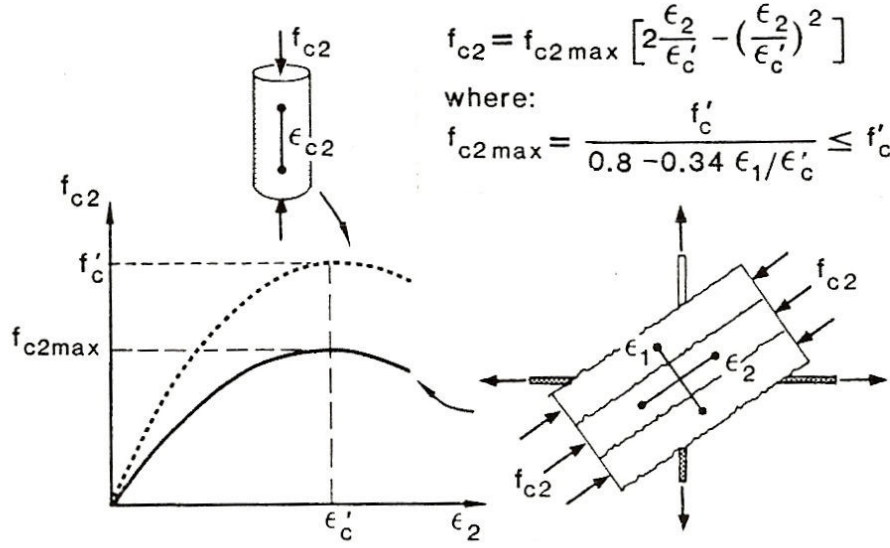


Fig. 3-2 Concrete average stress-strain relationship in compression (Vecchio and Collins, 1986).

One of the important aspects of MCFT is the model for principal concrete tension stresses. It accounts for concrete contribution to reinforcing bar stiffness after cracking, which is called tension stiffening and has significant influence on concrete contribution to shear strength of a reinforced concrete element. In MCFT concrete model, concrete tension stress increases linearly until cracking. After cracking, concrete continues to resist an average tension stress but it reduces as the principal tensile principal strain increases. The original concrete tensile stress-strain relationship in MCFT is shown in Fig. 3-3 and is given by:

$$[3-3] \quad f_{c1} = E_c \cdot \epsilon_1 \quad \epsilon_1 \leq \epsilon_{cr}$$

$$[3-4] \quad f_{c1} = \frac{f_{cr}}{1 + \sqrt{200 \epsilon_1}} \quad \epsilon_1 > \epsilon_{cr}$$

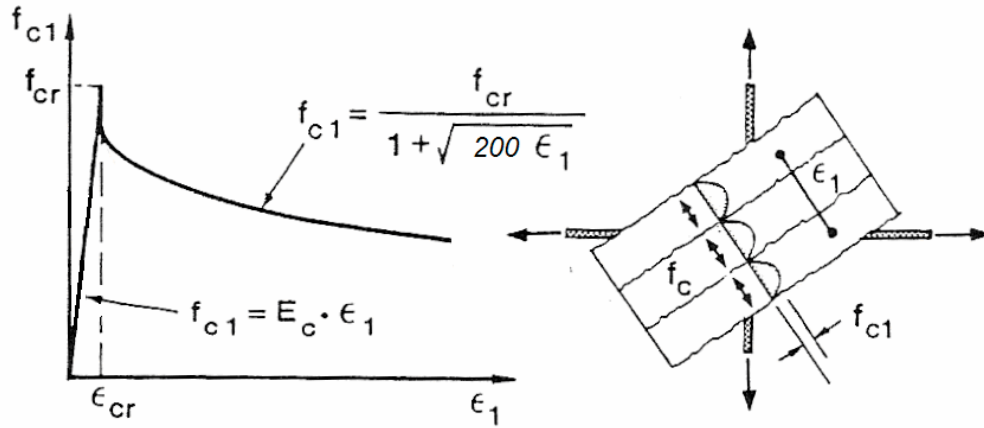


Fig. 3-3 Concrete average stress-strain relationship in tension (Vecchio and Collins, 1986).

Eq. [3-4] was later changed to a more conservative equation (Collins et. al 1996, Rahal and Collins 1999, Bentz et. al 2006, and Bentz and Collins 2006) as:

$$[3-5] f_{c1} = \frac{f_{cr}}{1 + \sqrt{500\epsilon_1}}$$

The stress-strain relationship expressed by Eqs. [3-3] to [3-5] accounts for average tensile stress in concrete in the principal direction and is valid if aggregate interlock in addition to stress increase in the reinforcing steel at the cracks are capable of equilibrating average stresses. Otherwise, tensile stress must be reduced accordingly.

The maximum shear stress that can be resisted by aggregate interlock along a crack is given by:

$$[3-6] v_{cr\max} = \frac{0.18\sqrt{f'_c}}{0.31 + 24w(a_g + 16)} \quad (\text{in MPa units})$$

where a_g is concrete maximum aggregate size, and w is crack width determined from:

$$[3-7] w = s_{\theta}\epsilon_1$$

in which s_θ is crack spacing and is assumed equal to:

$$[3-8] \quad s_\theta = \frac{1}{\left(\frac{\sin \theta}{s_x} + \frac{\cos \theta}{s_z} \right)}$$

where s_x is crack control parameter of x -direction reinforcement, and s_z is crack control parameter of z -direction reinforcement. For members with at least minimum amount of reinforcement, crack spacing may be conservatively assumed as $s_\theta = 300$ mm (Collins et. al 1996, Rahal and Collins 1999, Bentz et. al 2006, and Bentz and Collins 2006).

A bilinear stress-strain relationship is used for reinforcing steel. Prior to yielding of reinforcement, the steel stress is assumed to be $E_s \varepsilon_s$ where E_s is the Modulus of Elasticity of steel (200000 MPa) and ε_s is the average strain of reinforcement. After yielding, the steel stress remains constant and equal to f_y (steel yield stress) – no strain hardening is assumed.

3.3.2. Equilibrium Equations

Equilibrium equations of MCFT can be expressed by Mohr circles of stresses as shown in Figure 3-4. Mohr circle of cracked reinforced concrete stresses is a summation of Mohr circles of reinforcement stresses and concrete stresses. Reinforcement is considered to take axial load in the direction of the reinforcement, and thus does not resist shear stress. As a result, the shear stress in Mohr circle of concrete stresses is equal to the one in Mohr circle of reinforced concrete stresses. Mohr circles of stresses shown in Fig. 3-4 can be formulated as:

$$[3-9] \quad f_x = \rho_x f_{sx} + f_{cl} - \nu \cot \theta_c$$

$$[3-10] f_z = \rho_z f_{sz} + f_{c1} - v \tan \theta_c$$

$$[3-11] v = (f_{c1} + f_{c2}) / (\tan \theta_c + \cot \theta_c)$$

where f_x and f_z are normal stresses in x and z -directions, ρ_x and ρ_z are reinforcement ratios in x and z -directions, f_{sx} and f_{sz} are reinforcement stresses in x and z -directions, and θ_c is concrete angle of principal direction of stresses.

The equilibrium equations above are in terms of average stresses. It is also necessary to check stresses at the cracks. Fig. 3-5 compares the free body diagram of a uniform shear element on average and at the cracks. At the cracks, concrete tension stress in the principal direction f_{c1} becomes zero and aggregate interlock stress v_{ci} contributes to equilibrium instead. In addition, reinforcing steel stresses may be higher at the cracks compared to the average stresses. Equilibrium equations at the cracks are:

$$[3-12] f_x = \rho_x f_{sxcr} - v_{ci} \cot \theta_c - v \cot \theta_c$$

$$[3-13] f_z = \rho_z f_{szcr} + v_{ci} \tan \theta_c - v \tan \theta_c$$

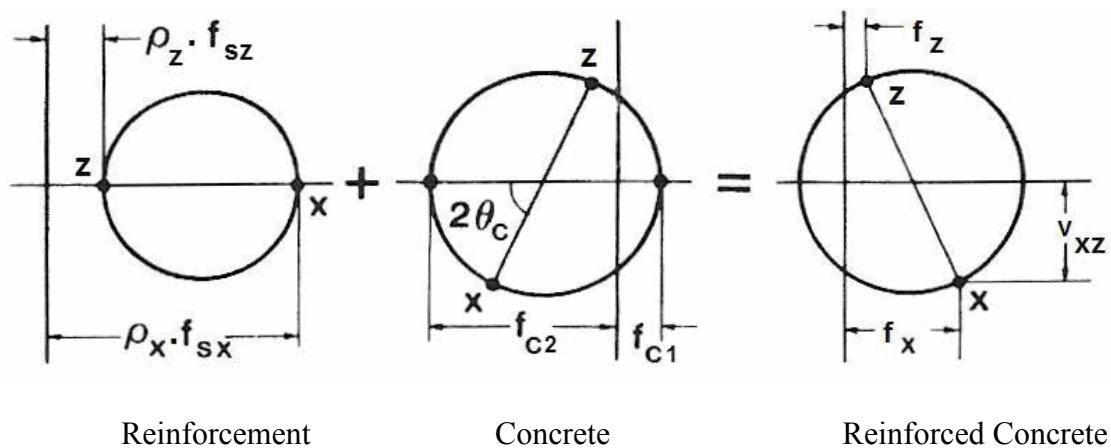


Fig. 3-4 Mohr circle of stress for cracked reinforced concrete (adopted from Vecchio and Collins, 1986).

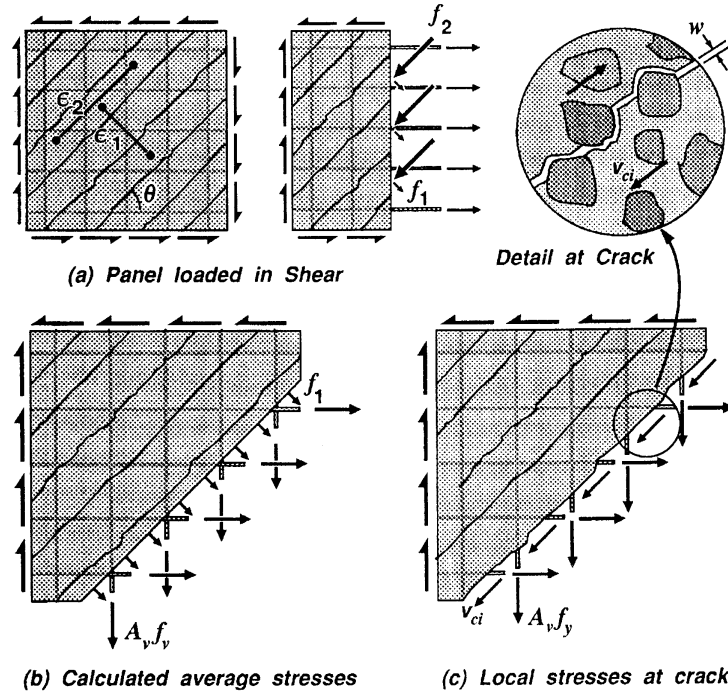


Fig. 3-5 Free body diagram of a uniform shear element in the crack direction for average stresses and local stresses at the cracks (Collins et. al 1996).

where v_{ci} is stress along the cracks due to aggregate interlock, and f_{sxcr} and f_{szcr} are reinforcement stresses at the cracks in x and z -directions, respectively. The following conditions need to be checked in order to determine whether the average tensile concrete stress can be equilibrated at the cracks or the average tensile stress in concrete needs to be reduced (Bentz 2000).

$$[3-14] \quad v_{ci2} = |\rho_x(f_{sxcr} - f_{sx}) - \rho_z(f_{szcr} - f_{sz})| \sin \theta_c \cos \theta_c$$

$$[3-15] \quad f_{c1} \leq \rho_x(f_{sxcr} - f_{sx}) \cos^2 \theta_c + \rho_z(f_{szcr} - f_{sz}) \sin^2 \theta_c$$

$$[3-16] \quad f_{c1} \leq \rho_x(f_{sxcr} - f_{sx}) + \min(v_{ci \max}, v_{ci2}) \cot \theta_c$$

$$[3-17] \quad f_{c1} \leq \rho_z(f_{szcr} - f_{sz}) + \min(v_{ci \max}, v_{ci2}) \tan \theta_c$$

In the equations above, v_{ci2} is the shear stress on cracks required to achieve biaxial yielding of reinforcement and $v_{ci\max}$ is the aggregate interlock capacity determined from Equation [3-6].

3.3.3. Compatibility Equations

Although cracks in concrete represent discontinuities, the average strains over a length containing a number of cracks are considered to satisfy requirements of continuous materials in MCFT. Consequently, like all other continuous materials, compatibility in reinforced concrete is expressed by Mohr circle of strains as shown in Figure 3-6. Some important compatibility equations are:

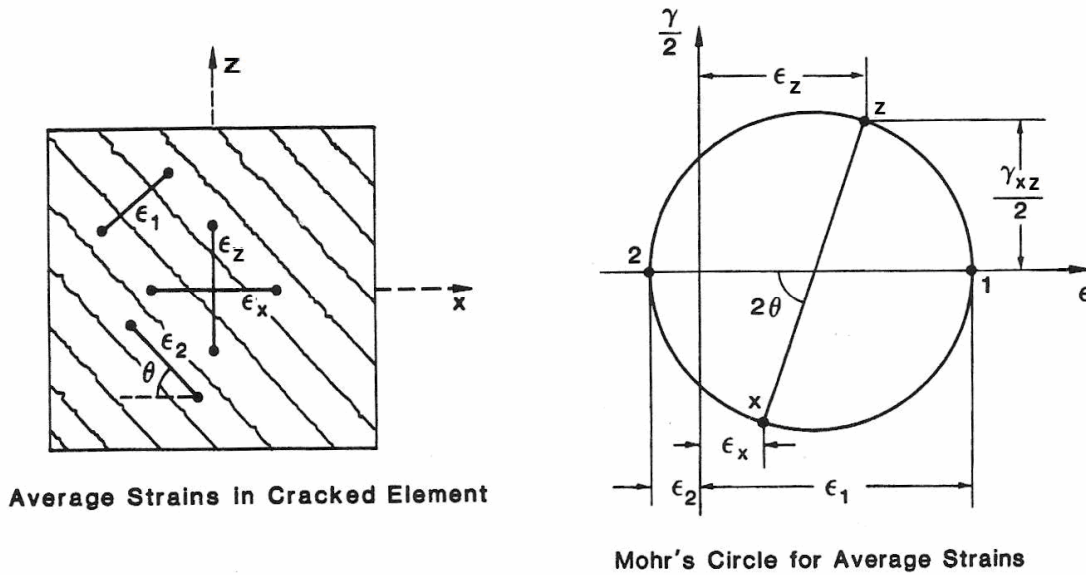


Fig. 3-6 Mohr circle of strains for reinforced concrete (adopted from Vecchio and Collins, 1986).

$$[3-18] \tan^2 \theta = \frac{\epsilon_x + \epsilon_2}{\epsilon_z + \epsilon_2}$$

$$[3-19] \epsilon_1 = \epsilon_x + \epsilon_z + \epsilon_2$$

$$[3-20] \gamma_{xz} = 2(\varepsilon_x + \varepsilon_z) \cot \theta$$

$$[3-21] \varepsilon_1 = \varepsilon_x (1 + \cot^2 \theta) + \varepsilon_z \cot^2 \theta$$

where ε_1 and ε_2 are strains in principal directions, ε_x and ε_z are strains in x and z -directions, γ_{xz} is shear strain, and θ is principal compression strain direction to x axis. It should be mentioned that MCFT assumes the direction of principal strain coincides with the direction of principal average stress. In other words, MCFT assumes $\theta_c = \theta$.

3.3.4. Solution of MCFT Equations

Determining stresses given strains using MCFT equations is an easy task; however, calculating strains from given forces is tedious and requires trial-and-error. For the latter case, two unknowns are estimated in the beginning and solving equations verifies whether the estimated values are correct or need to be changed. For example, one solution strategy is to estimate concrete stresses in the x and z -directions. Then, calculate steel stresses in the x and z -directions in addition to concrete angle of inclination θ and principal stresses from equilibrium equations. Subsequently, determine strains in the principal, x and z -directions using material constitutive laws for concrete and steel. At this stage, crack equilibrium conditions should be checked and principal tension strain should be adjusted accordingly. The calculated strains should then satisfy compatibility equations otherwise the estimated concrete stresses should be revised and the procedure should be repeated until compatibility equations are satisfied.

3.3.5. Experimental Verification

MCFT was developed (Vecchio and Collins, 1986) based on experimental tests performed on 30 uniform shear elements under the variety of uniform biaxial stresses.

Recently, Bentz et al.(2006) have compared the experimental results of 100 uniform shear element tests available in the literature with MCFT predictions and concluded that MCFT predicts the behaviour of such elements with an average test-to-predicted shear strength ratio of 1.01 and coefficient of variation of 12.2%. As shown in Fig. 3-7, Bentz et al. (2006) also compared experimental results of shear stress-shear strain relationship from six tested elements with the predictions of MCFT. The six elements consisted of two elements tested at the University of Toronto (Kirschner and Collins 1986, and Khalifa 1986) and four elements tested at the University of Houston (Pang and Hsu, 1995). University of Toronto tests are labeled by SE and University of Houston tests are labeled by A and B in Figure 3-7. The reasonable agreement of MCFT predictions with the experimental results is evident.

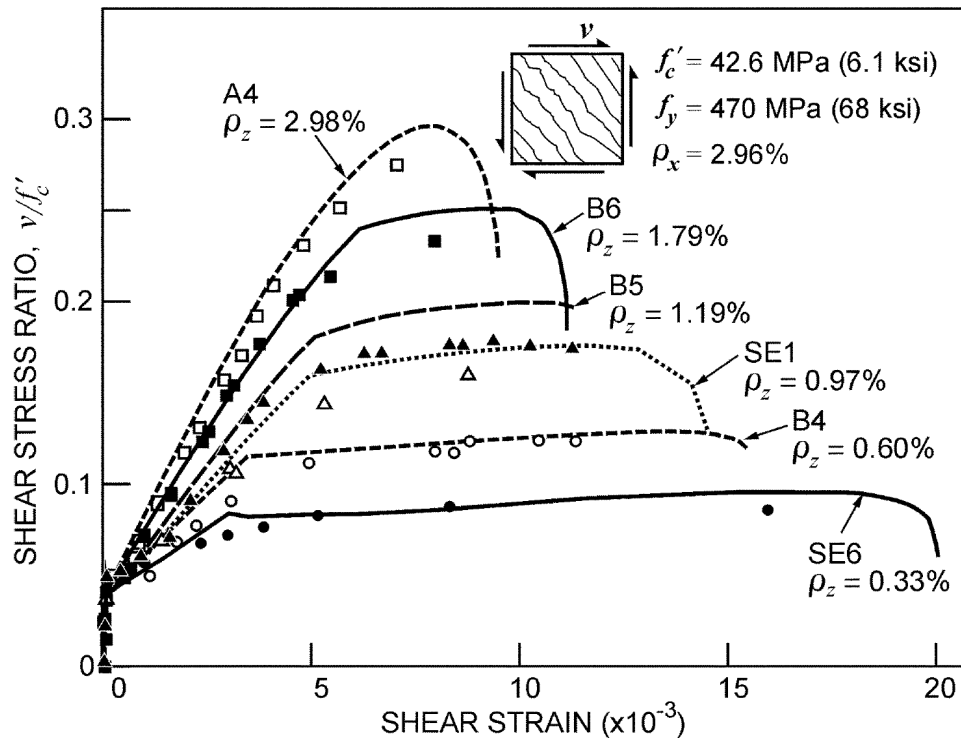


Fig. 3-7 Comparison of predicted and observed shear stress – shear strain response of six uniform shear elements (Bentz et al. 2006).

3.3.6. MCFT and Traditional Shear Design Formulation

In traditional shear design approach, the shear resistance of a structural concrete member is expressed as the sum a concrete contribution V_c , a stirrup contribution V_s and the vertical component of inclined prestressing force V_p in the general form:

$$[3-22] \quad V = V_c + V_s + V_p = \beta \sqrt{f'_c} b_w d_v + \frac{A_v f_y d_v \cot \theta}{s} + V_p$$

where β is the concrete contribution factor accounting for the shear resistance of cracked concrete, f'_c is the compressive strength of concrete, b_w is the web width, d_v is the effective shear depth of the member, A_v is the area of transverse shear reinforcement within a distance s along the member, f_y is the yield strength of the transverse reinforcement and θ is the angle of inclination (measured from the longitudinal axis) of the concrete principal diagonal compressive stress, i.e., angle of critical diagonal crack.

The concrete contribution is traditionally taken equal to the shear force at first diagonal cracking. For prestressed concrete members, β depends on the moment-to-shear ratio and level of prestress in the traditional equations. For a small member (no size-effect reduction), a conservative lower-bound value for V_c results from assuming $\beta = 2$ psi (0.17 MPa) and $d_v = d$. The transverse reinforcement contribution V_s has traditionally been calculated assuming $\theta = 45^\circ$ ($\cot \theta = 1.0$), and $d_v = d$.

For a uniform shear element, Equation [3-22] can be modified by eliminating V_p and dividing the remaining shear force components by the shear area $b_w d_v$:

$$[3-23] \quad v = v_c + v_s = \beta \sqrt{f'_c} + \rho_z f_y \cot \theta$$

where ρ_z is the transverse reinforcement ratio $A_v / b_w s$. Assuming clamping stress f_z is equal to zero and transverse reinforcement has yielded, MCFT equilibrium equation

Eq.[3-10] can also be rearranged in the same format as Eq. [3-23] where:

$$[3-24] \beta = f_{cl} \cot \theta$$

MCFT assumes $f_{cr} = 0.33\sqrt{f_c'}$; thus, from average stresses (Eq. 3-5), β can be calculated from:

$$[3-25] \beta = \frac{0.33 \cot \theta}{1 + \sqrt{500\varepsilon_1}}$$

But β is also limited depending on the maximum stresses that can be transferred at the cracks. The concrete contribution factor β and angle of inclination θ change from element to element as well as throughout the loading stages of one element after cracking up to failure.

Figure 3-8(a) depicts how MCFT predicts the shear stress – shear strain relationships of structural concrete elements with different amounts of transverse and longitudinal reinforcement in addition to the corresponding concrete contribution factors β s and crack angles θ s (from horizontal axis) of concrete for different loading stages. Notice that until concrete cracks, the inclination of diagonal compression θ in elements subjected to pure shear is 45 degrees. After cracking, θ reduces depending on the relative amount of reinforcement ρ_z / ρ_x , and the shear stress ratio v / f_c' . After transverse (z-dir.) reinforcement yields, shear strain γ increases, longitudinal strain ε_x increases, inclination of diagonal compression θ reduces, and concrete contribution factor β reduces. As v_c reduces and v_s increases, the total shear may reduce, stay constant or increase, depending on the amount of transverse reinforcement as shown in Fig. 3-8(a). The point at which diagonal compression stresses in concrete reaches the crushing strength of concrete is also shown on each curve. After this point, the shear strength of the element reduces.

For the element (with $\rho_z = 0.005$, $\rho_x = 0.02$) where all the reinforcement is already yielding, the strength reduction is sudden.

For members without transverse reinforcement, ρ_z becomes zero thus MCFT Eq.[3-23] can be presented by concrete contribution only as $v = \beta\sqrt{f_c'}$ similar to traditional method. The MCFT can predict the complete shear stress – shear strain relationships of such elements as well. It was used to predict the response of elements with no transverse (z-direction) reinforcement and 3% distributed longitudinal (x-direction) reinforcement subjected to different levels of longitudinal axial stress f_x , and the results are shown in Fig. 3-8(b). One element was subjected to constant axial compression stress f_x of 3 MPa, the second element was subjected to pure shear ($f_x=0$), and the third element was subjected to a constant axial tension stress of 1.5 MPa. The element subjected to shear and axial tension can be considered to represent the lower portion of a web subjected to shear and bending moment – the flexural stresses cause axial tension in the lower part of the web. The cracking point (indicated by a round dot in Fig. 3-8b) is very strongly influenced by the magnitude of axial stress. Axial tension reduces the shear force at cracking, while axial compression increases the shear force at cracking.

According to the MCFT, the concrete contribution V_c is not the shear force at diagonal cracking; but is the additional shear force beyond that resisted by yielding stirrups that can be transferred across diagonal cracks by interlock of rough crack surfaces. For a member without transverse reinforcement subjected to combined shear and axial tension (representing the influence of bending moment), Adebar and Collins (1996) showed that the critical point is when transfer of shear across diagonal cracks initially limits the applied stresses. In other words, the critical point is when θ and β

correspond to the solution in which β calculated from average stresses Eq. [3-25] is equal to the upper limit due to aggregate interlock capacity calculated from Equation [3-6]. This point is indicated by a square dot in Figure 3-8(b).

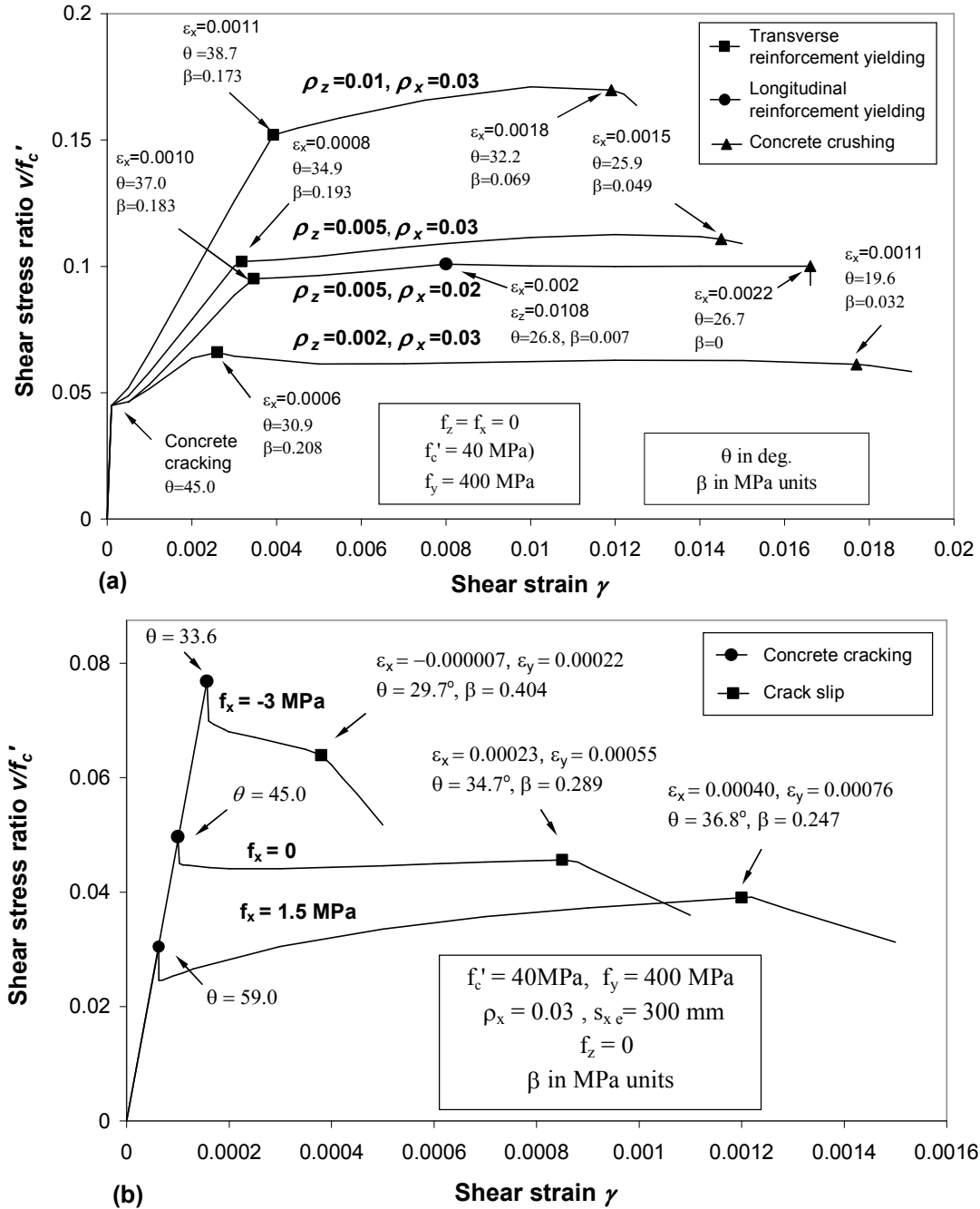


Fig. 3-8 MCFT predictions of shear response of uniform shear elements for: (a) members with transverse reinforcement, (b) members without transverse reinforcement.

It is worth mentioning that at the critical point, β and angle θ are not functions of f_c' because ε_2 is relatively small and negligible compared to ε_1 in Eq. [3-21] and therefore both β s associated with average stress condition (Eq. 3-25) and aggregate interlock capacity (Eq. 3-6) are only functions of θ at a given longitudinal strain ε_x .

3.4. 2007 AASHTO LRFD Method

The shear design method given in the 2007 and older versions of AASHTO LRFD was developed based on MCFT analysis of uniform shear elements. The derivation of this method was presented by Collins et al. (1996). The method uses the traditional shear design formula (Eq. 3-22) and includes tables with values of β and θ . MCFT analysis assumptions used in the derivation of the method are: clamping stress $f_z=0$, the crack spacing s_θ for members with transverse reinforcement is 300 mm, concrete maximum aggregate size is 19 mm, and the cracking stress of concrete is $f_{cr} = 0.33\sqrt{f_c'}$ in MPa units. Analyses were performed at a given longitudinal strains ε_x assuming that longitudinal reinforcement had sufficient capacity to provide the required axial compression force to transfer shear at the cracks. Another check as part of the method is performed to confirm this assumption.

For members with at least minimum transverse reinforcement, it was assumed that transverse reinforcement had yielded. Thus, the crack check equation for both members with at least minimum and without transverse reinforcement is Eq. [3-17] which can be rewritten as:

$$[3-26] \quad \beta \leq \frac{0.18}{0.3 + [24\varepsilon_1 s_\theta / (a_g + 16)]}$$

β is obtained from Eq. [3-25] but reduced if Eq.[3-26] is not satisfied.

For members with at least minimum transverse reinforcement, the tabulated values of β and θ depend on longitudinal strain ε_x and shear stress ratio v/f_c' according to MCFT. As for design of members with transverse reinforcement, the desired shear strength of an element can be achieved with different relative amount of transverse and longitudinal reinforcement, the values of θ and β provided in the tables for such members correspond to one particular solution. This solution uses a cost function to determine θ and corresponding β that are associated with minimum cost for the amount of longitudinal and transverse reinforcement needed for shear.

According to the AASHTO LRFD tables, for ε_x from -0.0002 to +0.001, and v/f_c' from 0.075 to 0.250, θ varies from 22 to 37 deg., and β varies from 0.13 to 0.53 in MPa units for members with transverse reinforcement. To ensure that transverse reinforcement yields prior to concrete crushing, the shear strength is limited to $\frac{v}{f_c'} = 0.25$.

For members without transverse reinforcement, as discussed earlier, critical shear strength is reached when θ and β correspond to the solution in which β calculated from average stresses Eq. [3-25] is initially limited by aggregate interlock capacity expressed by Eq [3-26]. The tabulated values of θ and β correspond to the critical point mentioned above. They are functions of longitudinal strain ε_x and effective crack spacing parameter S_{xe} that is given by:

$$[3-27] S_{xe} = \frac{35s_x}{a_g + 16}$$

It should be noted that crack spacing of members without transverse reinforcement is determined by $s_\theta = \frac{S_x}{\sin \theta}$ since crack spacing parameter in z -direction is assumed to be infinity in Eq. [3-8] for such members.

According to AASHTO LRFD tables for members without transverse reinforcement, ε_x varies from -0.0002 to +0.002, and for small members ($S_{xe} = 300$ mm), θ varies from 25 to 37 deg and β varies from 0.53 to 0.17 (in MPa units) over that range. For very large members ($S_{xe} = 2000$ mm), θ is about double, and β is about half. Specifically, θ varies from 44 to 72 deg and β varies from 0.26 to 0.05 (in MPa units) over the same range.

As discussed earlier, MCFT analyses were done at a given longitudinal strain assuming that longitudinal reinforcement had sufficient strength to transfer shear at cracks. To check the validity of this assumption, 2007 AASHTO LRFD method uses Eq. [3-28], which is derived from MCFT Eqs. [3-12] & [3-13] when $f_x = f_y = 0$.

$$\text{[3-28] } n_v^* = (2v_c + v_s) \cot \theta = 2(v - 0.5v_s) \cot \theta$$

In the equation above, n_v^* is the required axial strength (force per unit area) provided by longitudinal reinforcement to transfer shear at the crack and reinforcing steel force per unit area in the z -direction $v_s = \rho_z f_y \cot \theta$. n_v^* should be less than available longitudinal reinforcement strength per unit area for shear to ensure that the assumption explained above is valid.

3.5. 2006 CHBDC Method

The 2006 CHBDC shear design procedure, which is the same as the 2004 CSA A23.3 shear design procedure, was developed by Bentz et al. (2006) and Bentz and Collins (2006) and is again based on MCFT with the same assumptions as the ones used for 2007 AASHTO LRFD method. The method does not include tables but provides equations for θ and β instead. These equations are:

$$[3-29] \quad \beta = \frac{0.4}{1 + 1500\varepsilon_x} \cdot \frac{1300}{1000 + S_{xe}}$$

$$[3-30] \quad \theta = (29 + 7000\varepsilon_x)(0.88 + \frac{S_{xe}}{2500}) \leq 75 \text{ deg}$$

Similar to 2007 AASHTO LRFD method, θ and β equations are functions of crack spacing parameter and longitudinal strain for members without transverse reinforcement. For members with at least minimum transverse reinforcement, θ and β equations are functions of ε_x only and are independent of shear stress ratio v/f_c' unlike the 2007 AASHTO LRFD method. This is because the equation for β was developed for no transverse reinforcement (low shear stress ratio), and the solution for θ was developed for high shear stress ratio $v/f_c' = 0.25$. Combining these θ and β equations results in a simpler design procedure than using the tables in 2007 AASHTO LRFD.

First part of Eq. [3-29] $(\frac{0.4}{1 + 1500\varepsilon_x})$ was derived from Eq. [3-6] assuming

$S_{xe} = 300 \text{ mm}$ and $w = 0.2 + 1000\varepsilon_x \text{ mm}$, which is in good agreement with the MCFT predictions of crack width w when no transverse reinforcement is present. The second part of Eq. [3-29] is a correction factor when S_{xe} is different than 300 mm.

As mentioned earlier, Eq. [3-30] was developed for heavily reinforced sections where $v/f_c' = 0.25$. Figure 3-9 presents the variation of angle θ with longitudinal strain ϵ_x for such elements at yielding of transverse reinforcement and crushing of concrete based on MCFT. As shown, the 2006 CHBDC equation for angle θ falls in the region where transverse reinforcement has yielded but concrete has not crushed when $\frac{v}{f_c'} = 0.25$.

Bentz et al. (2006) explained that Eqs. [3-29] and [3-30] is a linear relationship between shear strength and transverse reinforcement ratio assuming constant longitudinal strain while in reality this relationship is concave downwards based on plastic analyses as shown in Figure 3-10. As a result, they concluded that using Eqs. [3-29] and [3-30] for members with traditional amount of transverse reinforcement is conservative and appropriate for design.

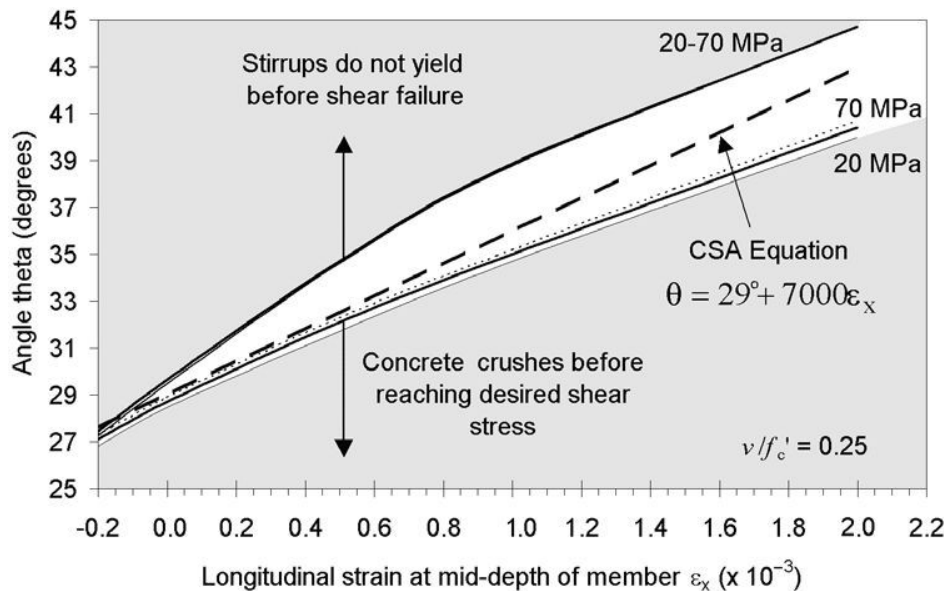


Fig. 3-9 Developing procedure of CHBDC 2006/CSA A23.3-04 equation for angle of inclination of principal compression (Bentz et al., 2006).

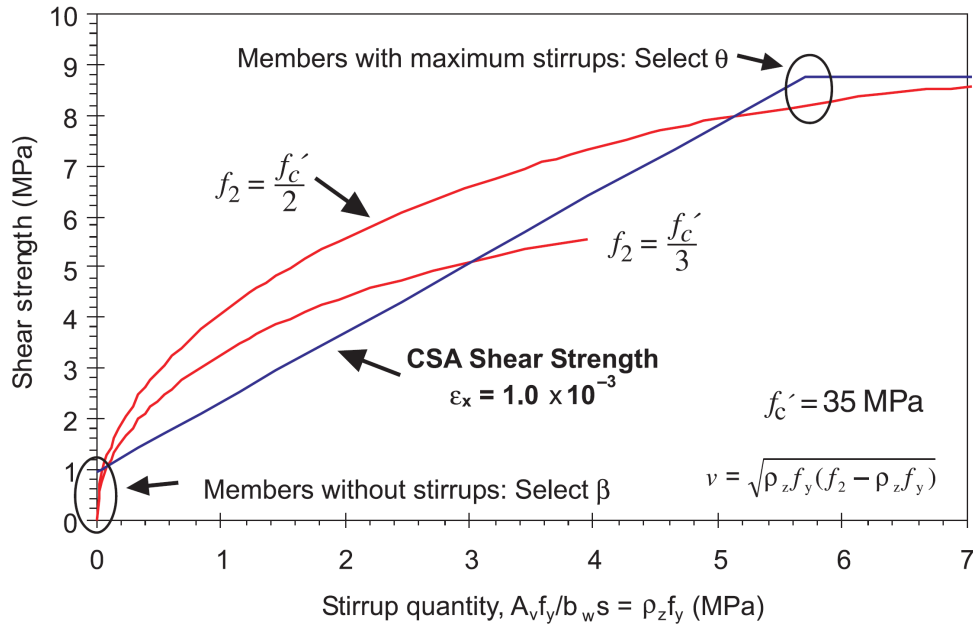


Fig. 3-10 Shear strength relation with transverse reinforcement ratio (Bentz et al., 2006).

Bentz et al. (2006) compared the 2006 CHBDC equations for θ and β with MCFT for members without transverse reinforcement and with different crack spacing parameters for longitudinal strains varying from -0.0002 to 0.0025 as shown in Figure 3-11. The MCFT results correspond to the point when v_c is maximum. The 2006 CHBDC equation for β gives a good estimate of β at large longitudinal strains but does not give a good estimate of β at low longitudinal strains. The 2006 CHBDC equation for θ is not in good agreement with MCFT predictions over a wide range of longitudinal strains. However, θ is less important than β for members without transverse reinforcement because shear capacity of these elements is a function of β not θ . The angle of principal compression θ is only used to determine the demand on longitudinal reinforcement imposed by shear. Therefore, the lower the angle, the more conservative the results.

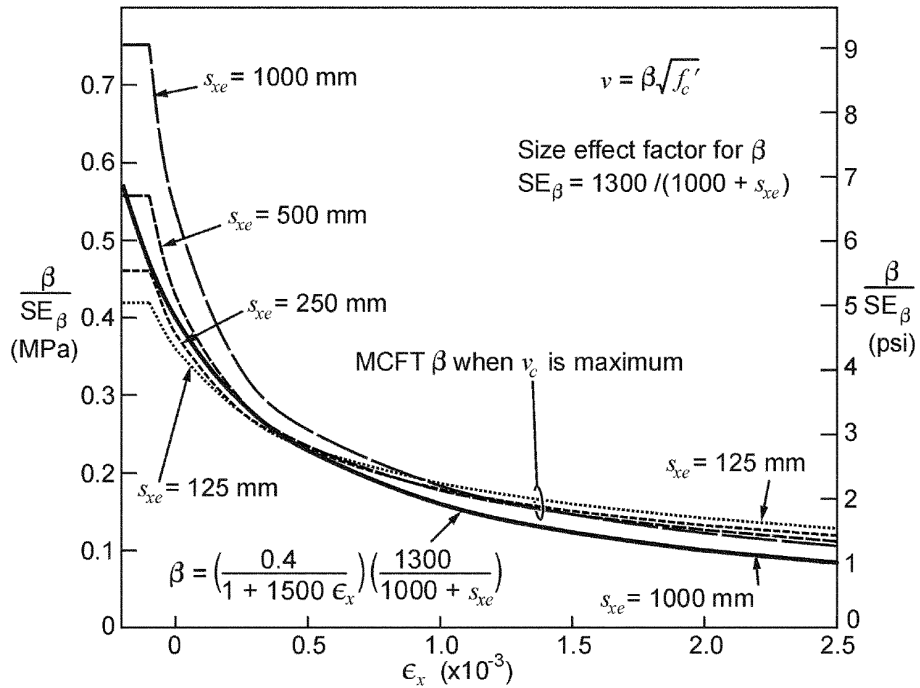
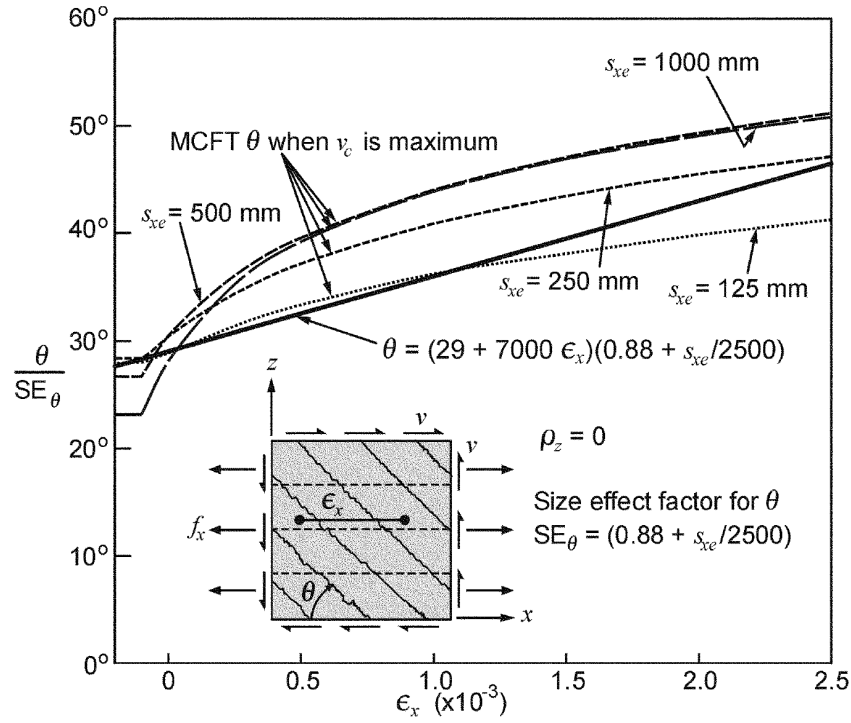


Fig. 3-11 Comparison of θ and β values given by CHBDC 2006/ CSA A23.3-04 with values determined from MCFT for elements without transverse reinforcement (Bentz and Collins, 2006).

Shown in Fig. 3-12, Bentz et al. (2006) also compared the 2006 CHBDC equation for θ and β with MCFT for members with different amount of transverse reinforcement for longitudinal strains ranged from -0.0002 to 0.0025. Once again, the MCFT predictions correspond to maximum v_c contribution to shear strength. Figure 3-12 shows that the 2006 CHBDC equation for θ is conservative compared to MCFT predictions except for a few cases. The 2006 CHBDC equation for β is also conservative except for the cases where ε_x is low. For such cases, however, Bentz et al. (2006) explained that conservative estimate of θ could compensate for the unconservative estimate of β .

In the 2006 CHBDC method, shear strength is also limited to $\frac{v}{f_c'} = 0.25$ to avoid concrete crushing prior to transverse reinforcement yielding. Moreover, the same equation as in 2007 AASHTO LRFD method (Eq. 3-28) is used to check the sufficiency of longitudinal reinforcement strength to transfer shear at cracks.

3.6. Proposed Evaluation Method for Members With at Least Minimum Transverse Reinforcement

2007 AASHTO LRFD and the 2006 CHBDC methods are intended for the design of new structures. The methods assume that the required shear capacity of a section is given and the amount of transverse reinforcement needs to be determined. As a result, the 2007 AASHTO LRFD is based on a particular MCFT solution for a given required shear capacity aimed at the cost effective combination of longitudinal and transverse reinforcement. The 2006 CHBDC uses simplified equations for angle of inclination θ and the axial stress required to transfer shear that are independent of the amount of transverse reinforcement to avoid iteration.

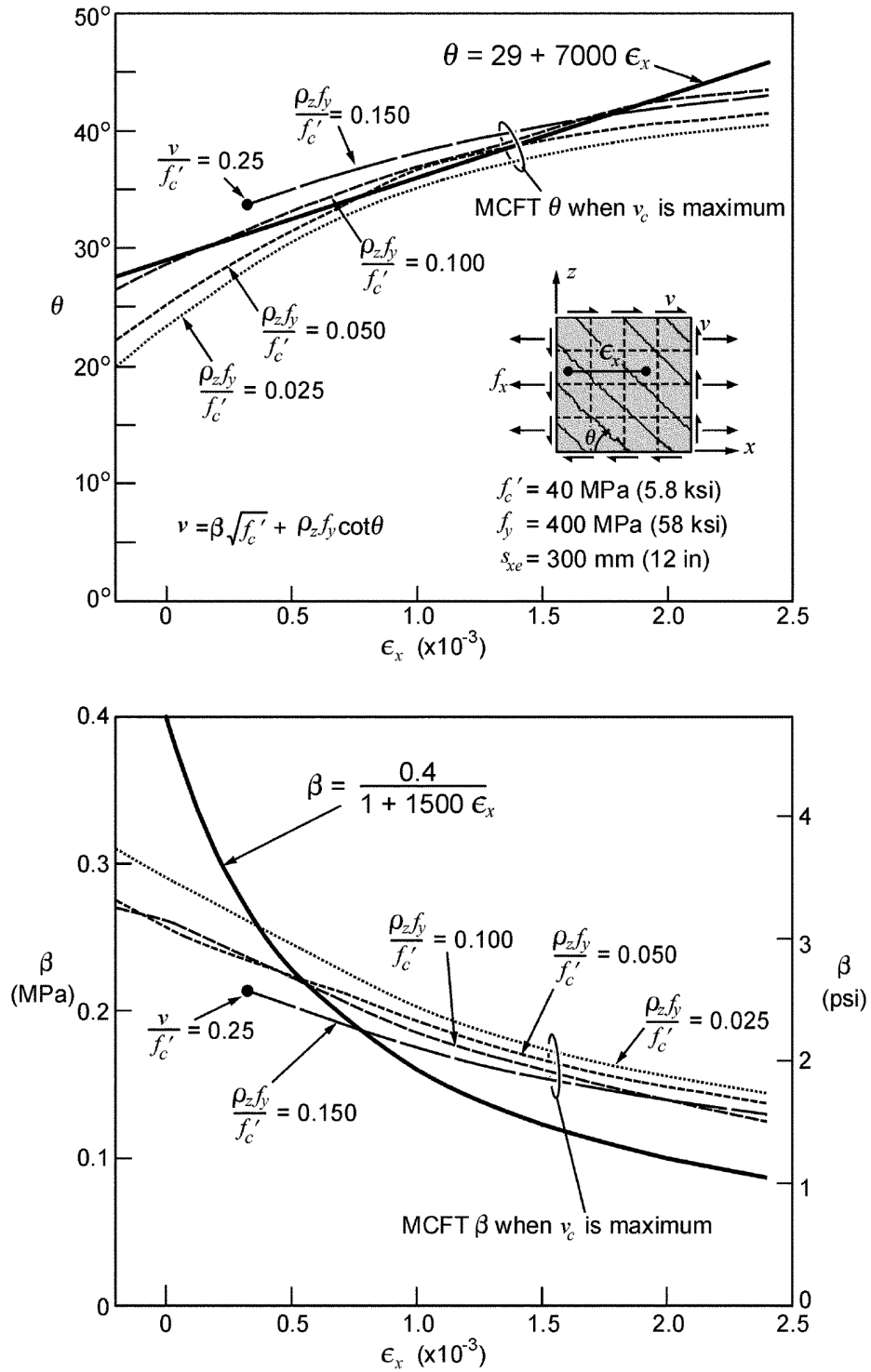


Fig. 3-12 Comparison of θ and β values given by CHBDC 2006/ CSA A23.3-04 with values determined from MCFT for elements with at least minimum transverse reinforcement (Bentz and Collins, 2006).

In contrast to design, shear evaluation deals with cases where amount of reinforcement is known and shear capacity of the section needs to be determined. As a result, applying the shear design provisions of 2007 AASHTO LRFD or 2006 CHBDC to evaluation problems require trial-and-error. Moreover, the relative amount of longitudinal and transverse reinforcement cannot be changed; therefore, the θ and β that result in a certain relative amount of reinforcement may not be the best solution. Ignoring the effect of some of parameters such as transverse reinforcement ratio on angle of principal compression and axial compression required for shear could result in conservative estimate of shear capacity which is acceptable for design but could lead to unnecessary posting of bridge load limit, retrofit or replacement of existing bridges.

In this section, a new procedure that is specifically intended for shear strength evaluation problems is presented. The method presented here is for members with at least minimum transverse reinforcement only. Section 3-7 presents a similar method for members without transverse reinforcement.

As was done to develop the shear design methods in AASHTO LRFD and 2006 CHBDC, it is assumed that in members with at least minimum transverse reinforcement, the diagonal crack spacing is 300 mm, concrete maximum aggregate size is 19 mm, and concrete cracking stress is $0.33\sqrt{f'_c}$ in MPa units. To develop equations that can be applied to beams, it is assumed that the longitudinal strain ϵ_x of the uniform shear element is constant, and the required longitudinal reinforcement is available in the beam to equilibrate the longitudinal concrete compression. A separate check is done in the evaluation procedure to ensure that this is the case.

Figure 3-13 presents a variety of results from MCFT. Specifically, it presents the influence of axial strain ε_x and transverse strain ε_z on (a) shear stress ν , (b) angle of inclination of principal average compressive stress θ and (c) axial compression stress in concrete f_{cx} all for an element with $\rho_z = 0.005$. Figure 3-8(a) demonstrates how the axial strain ε_x increases as the shear stress applied to an element with a given amount of longitudinal reinforcement ρ_x . The curves shown in Fig. 3-13 are for different constant ε_x values, and are plotted over the range of ε_z from transverse reinforcement yielding to concrete crushing.

Figure 3-13(a) illustrates how a larger ε_x results in a lower shear stress at first yielding of transverse reinforcement ($\varepsilon_z=0.002$) and lower shear stress at concrete crushing (maximum ε_z which corresponds to $\varepsilon_z = -0.002$). A larger ε_x also results in a higher shear stress increase after yielding of transverse reinforcement. For example, when $\varepsilon_x = 0$, the shear stress at $\varepsilon_z=0.002$ is the maximum shear stress, while when $\varepsilon_x = 0.001$, the shear stress at $\varepsilon_z=0.002$ is about 80 % of the maximum shear stress. Figure 3-13(b) suggests the reason for this is that the higher ε_x results in a larger compression angle θ at first yielding of the transverse reinforcement and hence less stirrup contribution. While θ varies from 24.4 to 36.7 deg at first yielding of transverse reinforcement, it varies from only 21.3 to 24.3 deg at concrete crushing.

Figure 3-13(c) gives the concrete longitudinal compression stress f_{cx} required to maintain the specified axial strain ε_x . For an element with large ε_x (e.g., 0.001), there is lower f_{cx} at transverse reinforcement yielding ($\varepsilon_z=0.002$) and a larger increase in f_{cx} as ε_z increases. For an element with small ε_x (e.g., $\varepsilon_x = 0$), there is higher f_{cx} at $\varepsilon_z=0.002$ and a

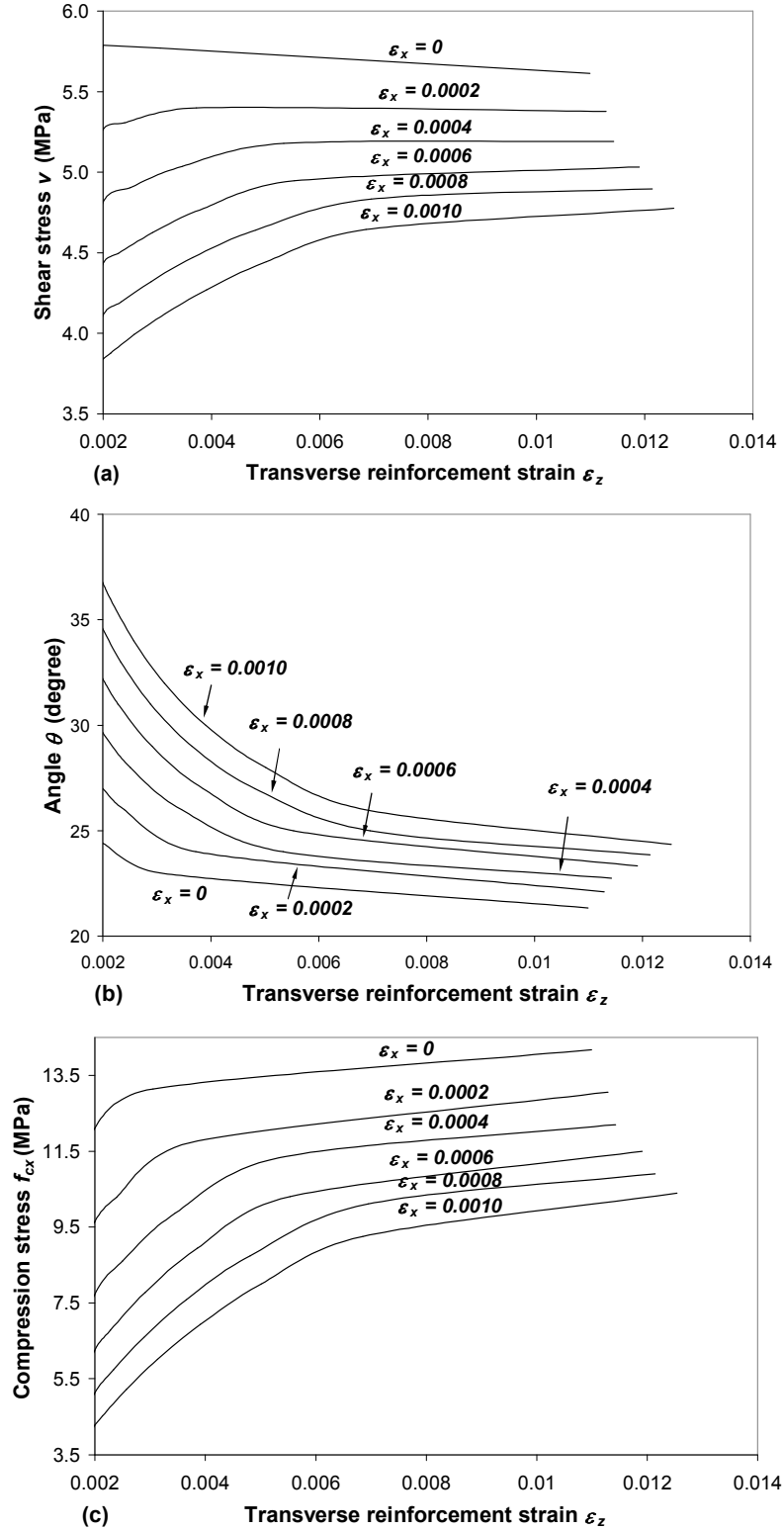


Fig. 3-13 Influence of longitudinal strain ϵ_x and transverse strain ϵ_z on: (a) shear stress, (b) angle of inclination of diagonal compression, (c) longitudinal compression stress in concrete for an element with $\rho_z = 0.005$, $f'_c = 40$ MPa, $f_y = 400$ MPa.

small increase in f_{cx} as ε_z increases.

As shown in Figure 3-13 (a), maximum shear strength of a member is generally close to the shear strength that corresponds to either yielding of transverse reinforcement or concrete crushing. However, the MCFT analyses are based on the assumption that longitudinal reinforcement does not yield as explained before. In some cases the element does not reach its maximum capacity at yielding of transverse reinforcement or crushing of concrete due to yielding of longitudinal reinforcements at cracks. For instance, the element with $\rho_z = 0.005$ and $\rho_x = 0.02$ shown in Fig. 3-8(a) reaches the maximum shear stress when the longitudinal reinforcement yields at $\varepsilon_x = 0.002$. As a result, in the proposed evaluation method, the strength is evaluated at three possible failure points. Yielding of transverse reinforcement and concrete crushing are two of the failure modes and the third failure mode involves yielding of both the transverse and longitudinal reinforcement.

3.6.1. Proposed Equations for Angle of Inclination of Principal Compression

Figure 3-14 shows the relationship between θ and the axial strain ε_x for different quantities of transverse reinforcement ρ_z , $f'_c = 40$ MPa, and $f_y = 400$ MPa at yielding of transverse reinforcement and concrete crushing stage. The solid lines show the relationships given by MCFT, which is approximately linear for a constant ρ_z . The relationships are very different at yielding of transverse reinforcement (Fig. 3-14a), and concrete crushing (Fig. 3-14b).

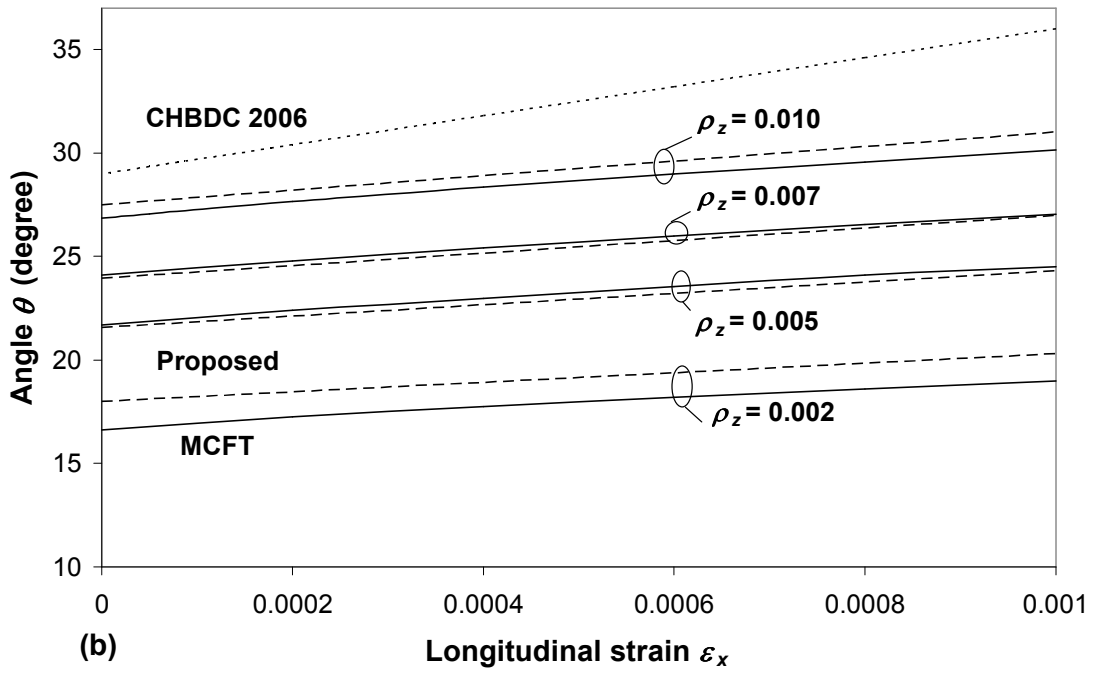
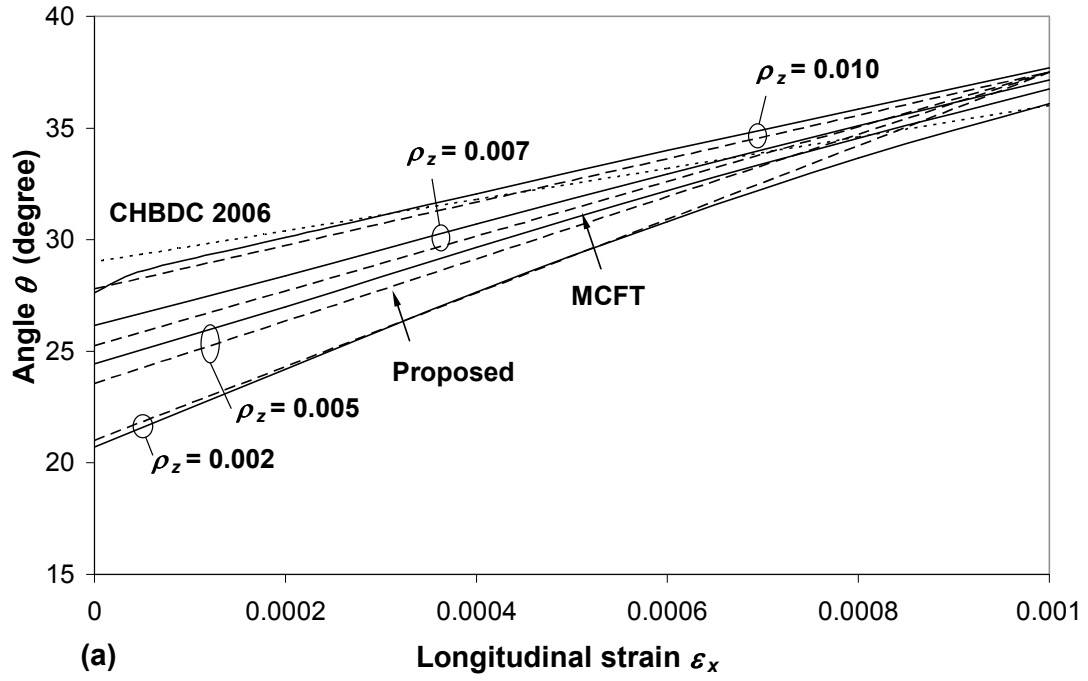


Fig. 3-14 Comparison of predicted angle θ with MCFT result at: (a) yielding of transverse reinforcement, (b) crushing of concrete for $f'_c = 40$ MPa, $f_y = 400$ MPa.

The 2006 CHBDC method has one equation for θ as a function ε_x , and this is shown in Fig. 3-14 as a dotted line. As the 2006 CHBDC approximate value for θ is generally larger than the actual value, it results in a smaller V_s than actual and is generally conservative. The 2006 CHBDC approximate value for θ is smaller than the actual value when ε_x is large at the point of transverse yielding (right-hand side of Fig. 3-14a); but as discussed with reference to Fig. 3-13(a), there will be a significant shear strength increase after yielding for large ε_x , and the 2006 CHBDC approximate angle is very conservative for all concrete crushing cases (Fig. 3-14b). The 2006 CHBDC approximate angle is also very conservative at transverse reinforcement yielding for members with low amounts of transverse reinforcement.

More accurate equations for θ were developed for the proposed method. This was done by looking at a significant number of MCFT predictions of shear strength for uniform shear elements with different amount of transverse reinforcement and material properties at transverse reinforcement yielding and concrete crushing. As indicated by the AASHTO LRFD method, the angle θ depends on the shear stress ratio v/f_c' . In design, the shear stress v is known; but not during strength evaluation. Thus the parameter $\rho_z f_y / f_c'$ was used in place of v/f_c' . It was also found that angle θ at yielding of transverse reinforcement is a function of transverse steel strain at yielding ε_y . The proposed equation for θ is:

$$[3-31] \quad \theta = \theta_o + \Delta\theta \varepsilon_x \leq 45$$

where at yielding of transverse reinforcement:

$$[3-32] \quad \theta_o = (85 \frac{\rho_z f_y}{f_c'} + 19.3)(-50\varepsilon_y + 1.1); \quad \varepsilon_y \leq 0.002$$

$$[3-33] \Delta\theta = 1000 [37.5(-200\varepsilon_y + 1.4) - \theta_o]$$

in which ε_y is the reinforcing steel yield strain and shall not be taken greater than 0.002

and at concrete crushing:

$$[3-34] \theta_o = 119 \frac{\rho_z f_y}{f_c'} + 15.6$$

$$[3-35] \Delta\theta = 15000 \frac{\rho_z f_y}{f_c'} + 2000$$

The angles predicted by these equations are also shown in Figs. 3-14(a) and (b) as dashed lines, and they are clearly in good agreement with MCFT. When the longitudinal strain equals the transverse strain, the MCFT angle is equal to 45 deg. For 400 MPa grade reinforcement, the transverse reinforcement yields at a strain of 0.002, thus the angles converge to 45 deg. in Fig. 3-14(a) at a longitudinal strain of 0.002. The largest longitudinal strain used in the shear analysis of beams is 0.001, and at this strain, the MCFT angles have almost converged. For simplicity, Eqs. [3-32] and [3-33] predicted angles converge at a longitudinal strain of 0.001, and for 400 MPa grade reinforcement, that angle is 37.5 deg.

Figures 3-15 to 3-18 are similar to Fig. 3-14 except they involve steel grades 250 MPa and 600 MPa, or concrete compression strengths 30 MPa and 60 MPa. Figures 3-14 to 3-18 illustrate that the proposed equations adequately capture the effect of concrete strength f_c' and steel grade on the angle of inclination θ at both yielding of transverse reinforcement and crushing of concrete. This validates the approach of using the parameters $\rho_z f_y / f_c'$ and ε_y in the proposed equations for angle θ .

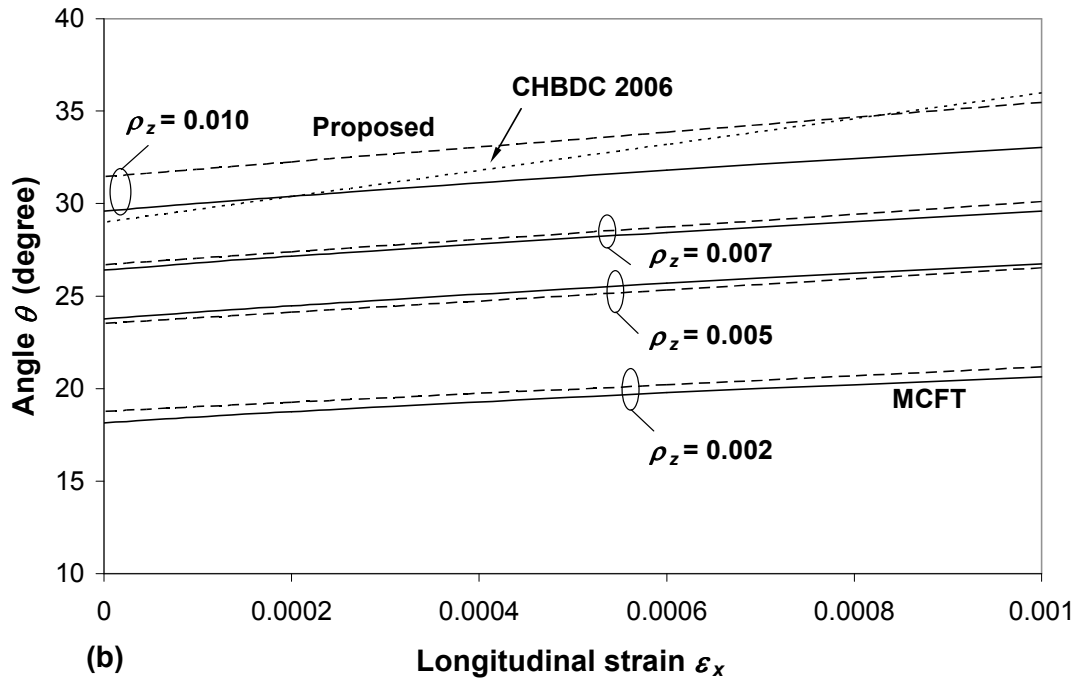
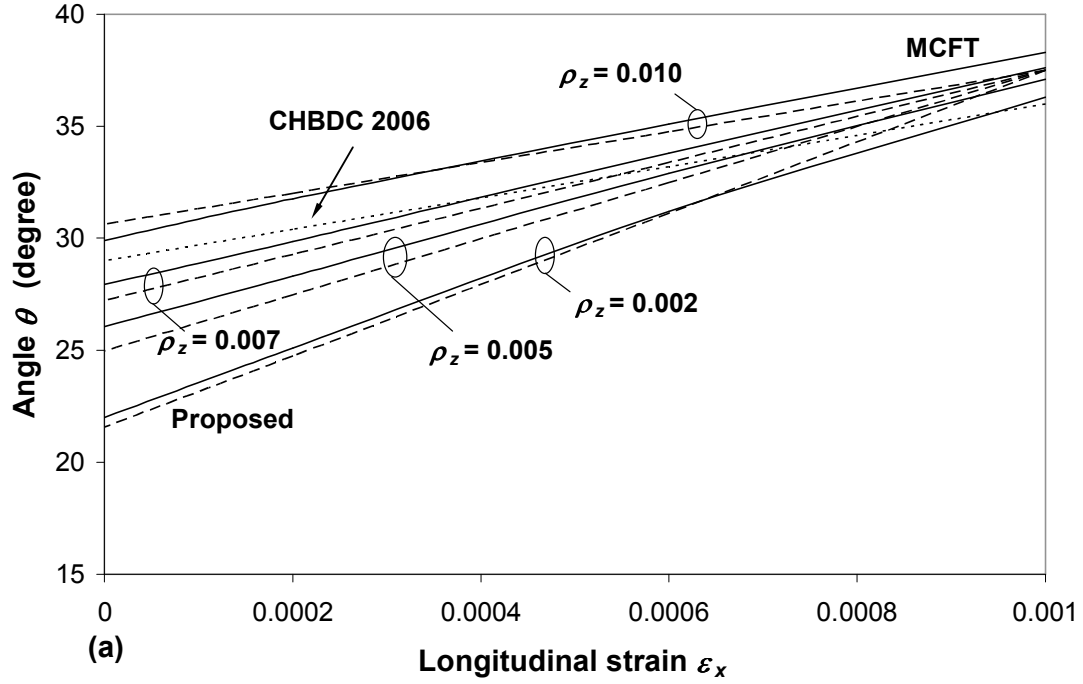


Fig. 3-15 Comparison of predicted angle θ with MCFT result at: (a) yielding of transverse reinforcement, (b) crushing of concrete for $f'_c = 30$ MPa, $f_y = 400$ MPa.

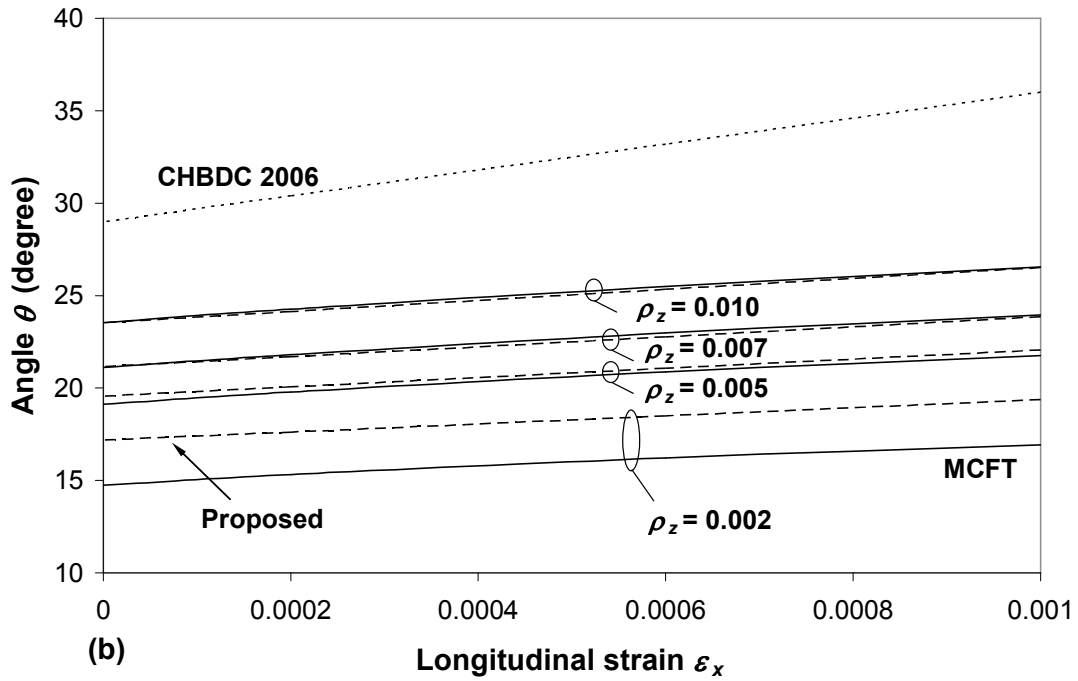
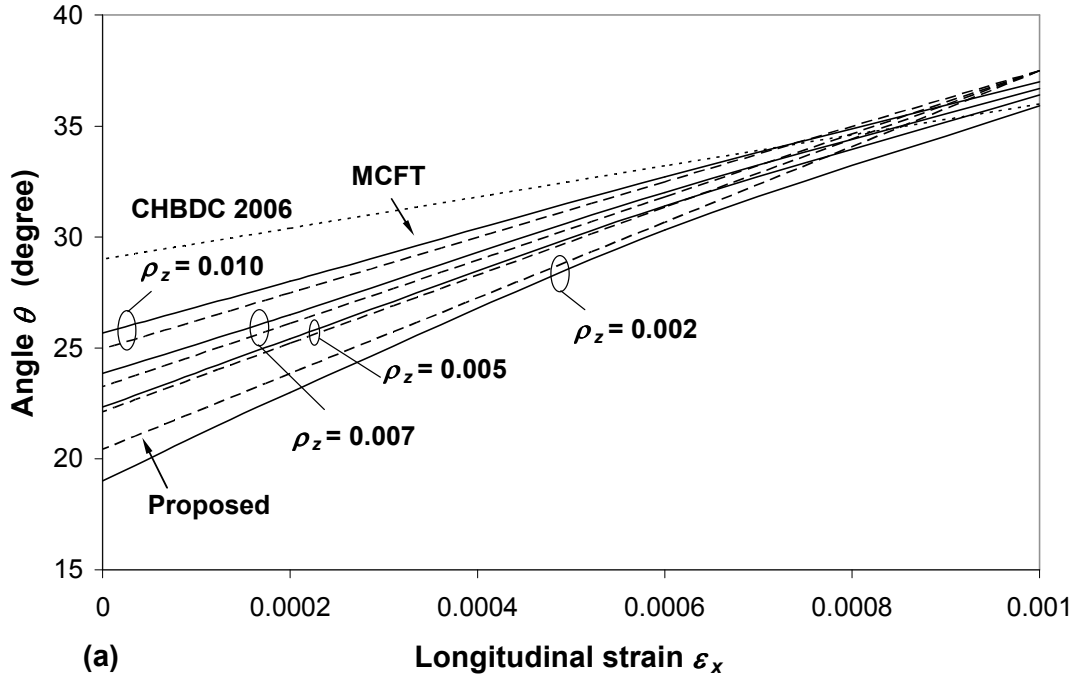


Fig. 3-16 Comparison of predicted angle θ with MCFT result at: (a) yielding of transverse reinforcement, (b) crushing of concrete for $f'_c = 60$ MPa, $f_y = 400$ MPa.

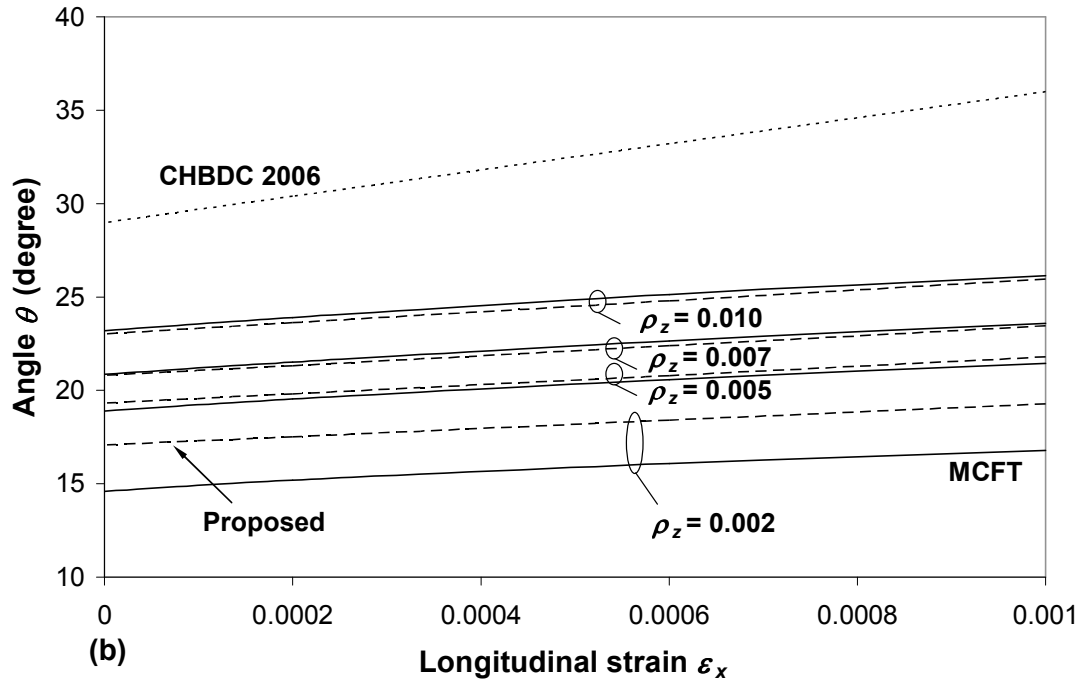
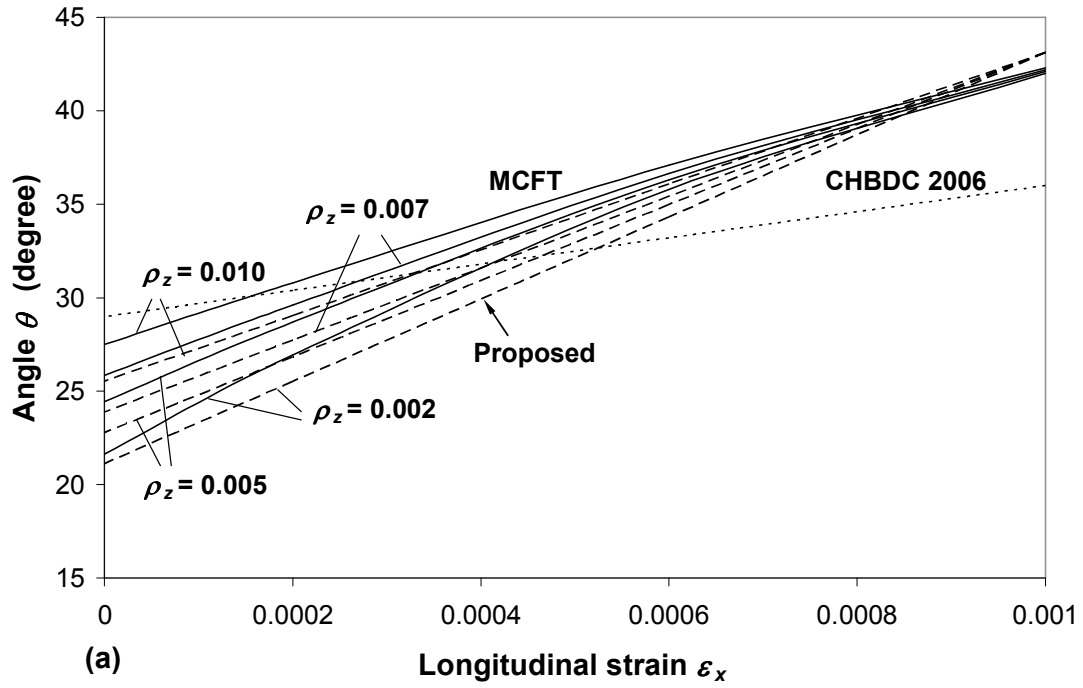


Fig. 3-17 Comparison of predicted angle θ with MCFT result at: (a) yielding of transverse reinforcement, (b) crushing of concrete for $f'_c = 40$ MPa, $f_y = 250$ MPa.

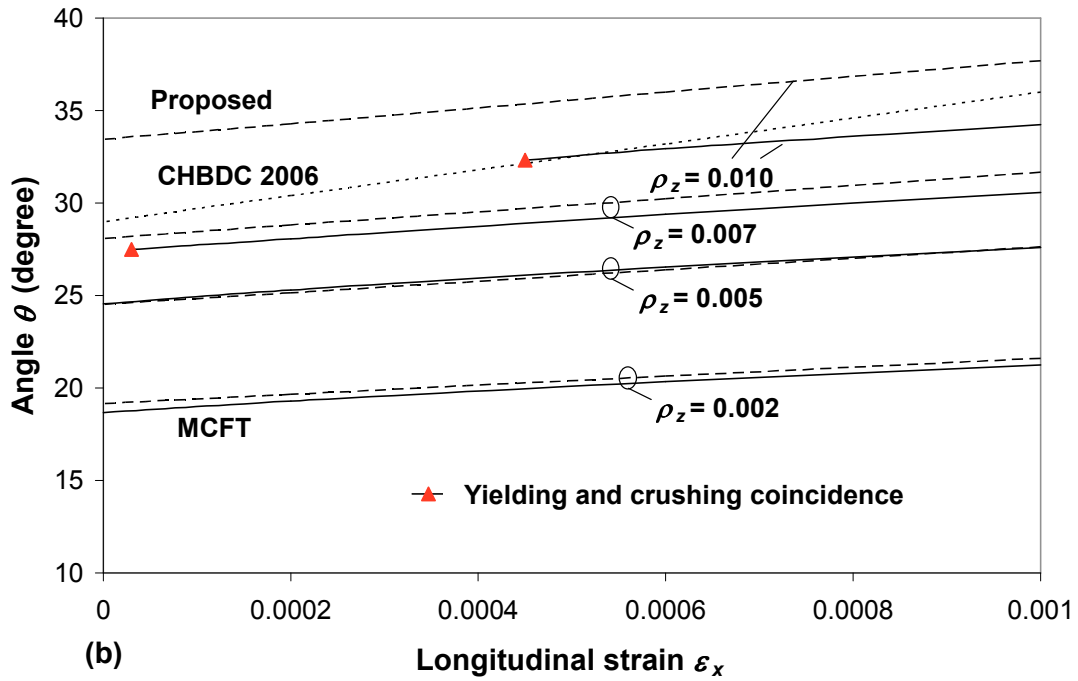
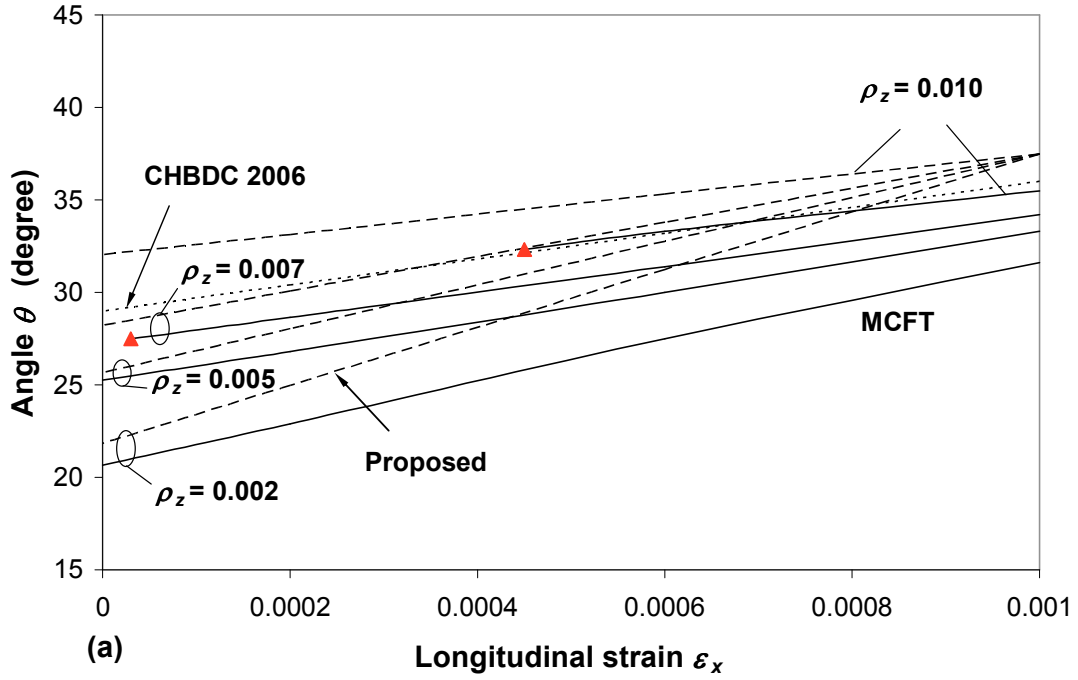


Fig. 3-18 Comparison of predicted angle θ with MCFT result at: (a) yielding of transverse reinforcement, (b) crushing of concrete for $f'_c = 40$ MPa, $f_y = 600$ MPa.

Figure 3-17(a) indicates that the predicted angles at $\varepsilon_x=0$ from the proposed equations are slightly smaller than the MCFT results for lower grade steel 250 MPa ($f_y = 250$ MPa) and thus are slightly unconservative; this compensates for the conservative estimate of proposed β equation for such steel as will be discussed later in this chapter. MCFT results showed that angle θ is not significantly sensitive to steel grade at yielding of transverse reinforcement once steel grade is higher than 400 MPa; thus ε_y shall not be taken greater than 0.002 in the proposed method equations. This is, however, ignored in the proposed method when applied to beam elements due to the fact that concrete crushing is normally the governing failure mode at larger strains.

Figure 3-18 shows that the proposed method predicted angles at yielding of transverse reinforcement are slightly conservative for steel grade 600 MPa. It will be shown later in this chapter that the unconservative prediction of concrete contribution factor β compensates for it. Notice in Fig. 3-18 that MCFT predictions had to stop for lower strains and higher transverse reinforcement ratios because concrete crushing happened prior to yielding of transverse reinforcement. Shown in Figs. 3-17(b) and 3-18(b), the proposed method equation of angle at concrete crushing is in good agreement with MCFT predictions for different steel grades.

Figure 3-15 to 3-18 show that the 2006 CHBDC predictions of angle are always smaller and thus conservative compared to the MCFT predictions at crushing of concrete while they are mostly conservative but sometimes unconservative compared to MCFT predictions at yielding of transverse reinforcement.

3.6.2. Proposed Equations for Concrete Contribution Factor

The solid lines in Figs. 3-19 show the concrete contribution factor β according to MCFT at yielding of transverse reinforcement (Fig. 3-19a) and concrete crushing (Fig. 3-19b) for 40 MPa concrete and 400 MPa reinforcing steel. The 2006 CHBDC approximate β value is shown as a dotted line. As this equation was developed for members without transverse reinforcement, it gives unconservative values of β for low ε_x values in members with at least minimum transverse reinforcement. Bentz et al. (2006) explained that the unconservative estimate of V_c in these members, compensates for the conservative estimate of V_s due to the larger than actual value of θ .

Figure 3-19(a) indicates that the concrete contribution factor β does not vary significantly at transverse reinforcement yielding. It will be shown later that the concrete contribution factor β does vary with steel grade for steel grades lower than 400 MPa. As was done to develop the equations for θ , the proposed equations for β were developed by looking at a significant number of MCFT results for uniform shear elements with varying amount of transverse reinforcement and different material properties. The proposed equation for concrete contribution factor at yielding of transverse reinforcement is:

$$[3-36] \quad \beta = 0.18(-300\varepsilon_y + 1.6) \text{ in MPa units}$$

Figure 3-19(b) indicates that β does vary somewhat more at concrete crushing. The 2007 AASHTO LRFD method assumes β is a function of both ε_x and v/f_c' . As described above in reference to the proposed expression for θ , using v/f_c' would require iteration in evaluation, thus the parameter $\rho_z f_y / f_c'$ was substituted for v/f_c' . For simplicity, β was not made a function of ε_x .

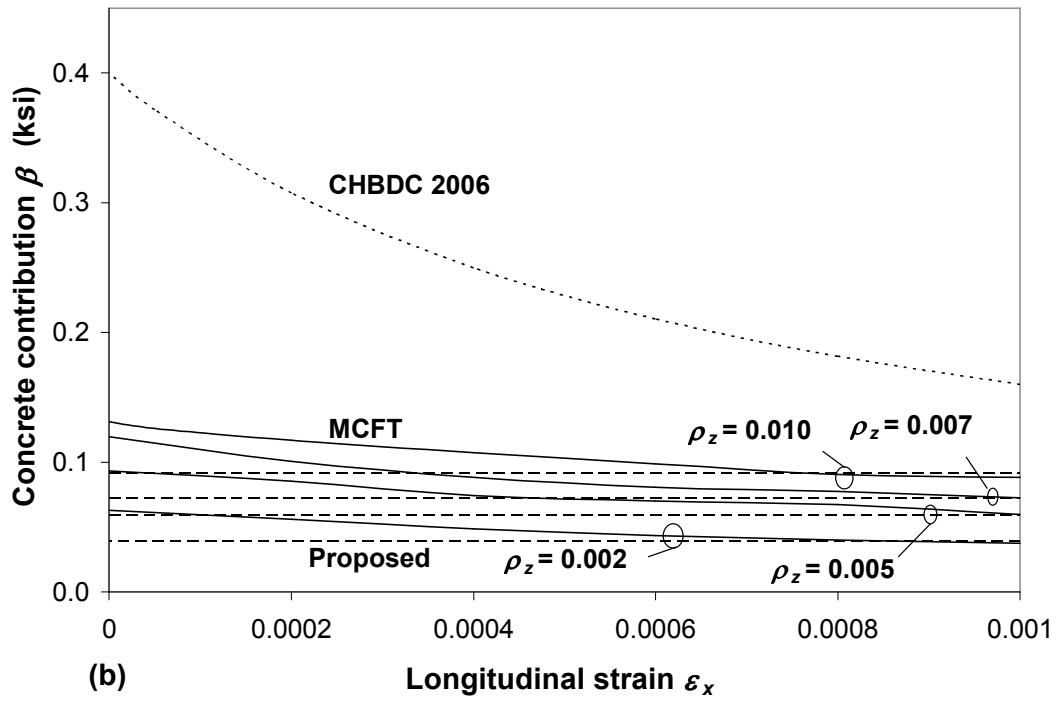
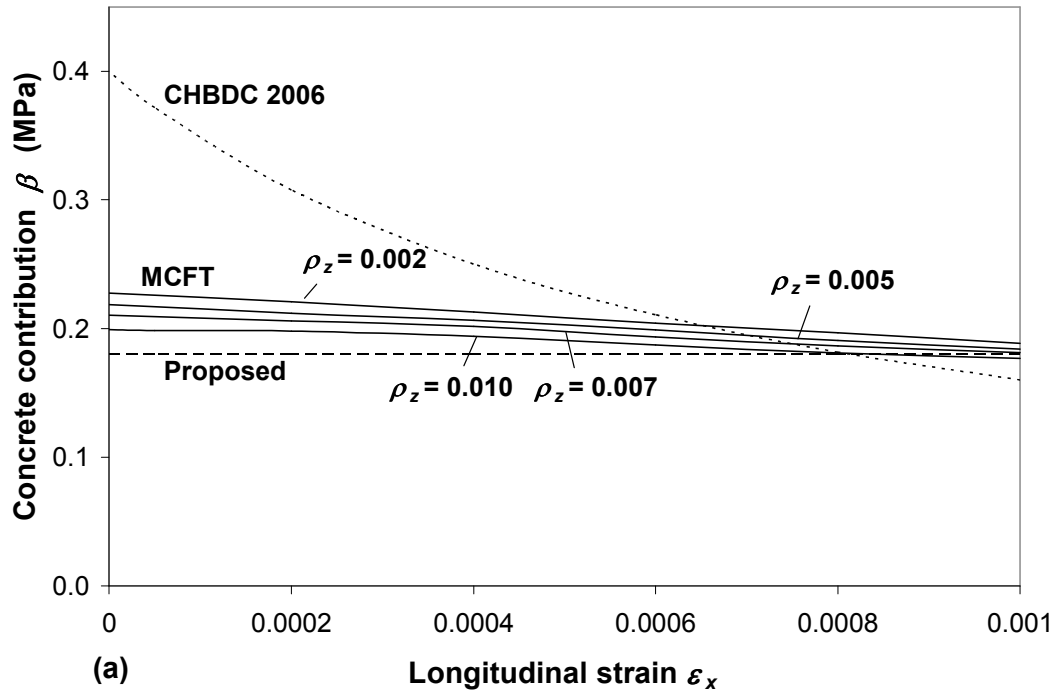


Fig. 3-19 Comparison of predicted β with MCFT result at: (a) yielding of transverse reinforcement, (b) crushing of concrete for $f'_c = 40$ MPa, $f_y = 400$ MPa.

The proposed expression for concrete contribution factor at concrete crushing is:

$$[3-37] \quad \beta = 0.65 \frac{\rho_z f_y}{f_c'} + 0.03 \text{ in MPa units}$$

Figure 3-19 shows the proposed expressions are conservative and agree well with MCFT.

Figures 3-20 to 3-23 examine the proposed equations for concrete contribution factor β and compare them with MCFT and the 2006 CHBDC method when concrete compressive strength is 30 and 60 MPa, or steel grade is 250 and 600 MPa. The same trend as in Fig. 3-19 is noticed in Figs. 3-20 and 3-21 in which the concrete compressive strength is 30 and 60 MPa, respectively. Once again, the current CHBDC predictions are unconservative for low longitudinal strains and the proposed method is conservative and consistent with MCFT results.

For steel grade 250 MPa shown in Fig. 3-22(a), the trend is somewhat different at yielding of transverse reinforcement as the variation of concrete contribution factor with longitudinal strain is more significant. As a result, the proposed method equation is conservative for low longitudinal strains. However, this is compensated for by the slightly unconservative estimate of angle as explained in the previous section. The 2006 CHBDC predictions are more consistent with MCFT at yielding of transverse reinforcement for 250 MPa reinforcing steel compared to those for 400 and 600 MPa steel grades. As shown in Figs. 3-23, the concrete contribution factors given by the proposed equation for steel grade 600 MPa are unconservative but this is compensated for by the conservative estimate of corresponding angles as mentioned before. Figs. 3-22(b) and 3-23(b) illustrate that the proposed equation for concrete contribution factor at concrete crushing is consistent with the MCFT.

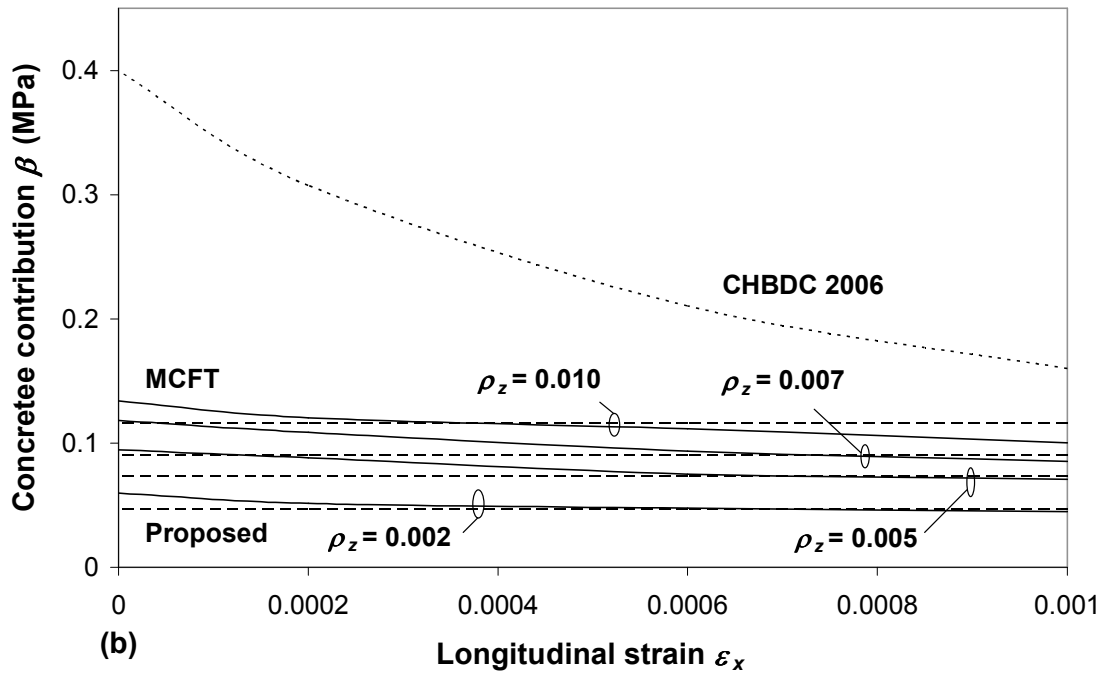
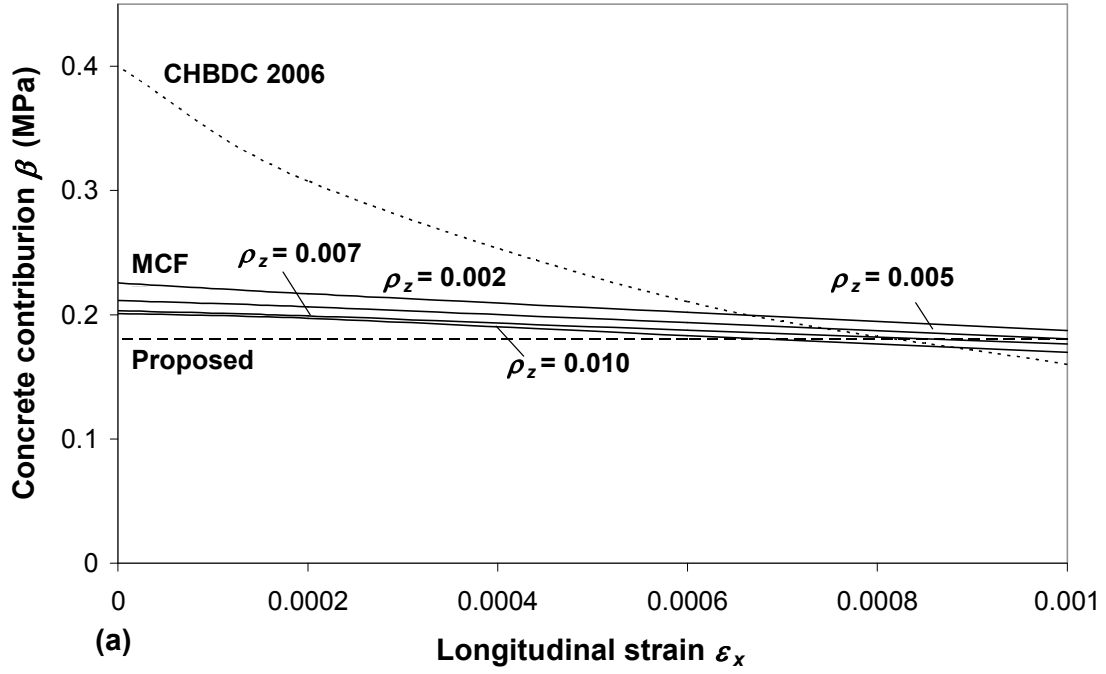


Fig. 3-20 Comparison of predicted β with MCFT result at: (a) yielding of transverse reinforcement, (b) crushing of concrete for $f'_c = 30$ MPa, $f_y = 400$ MPa.

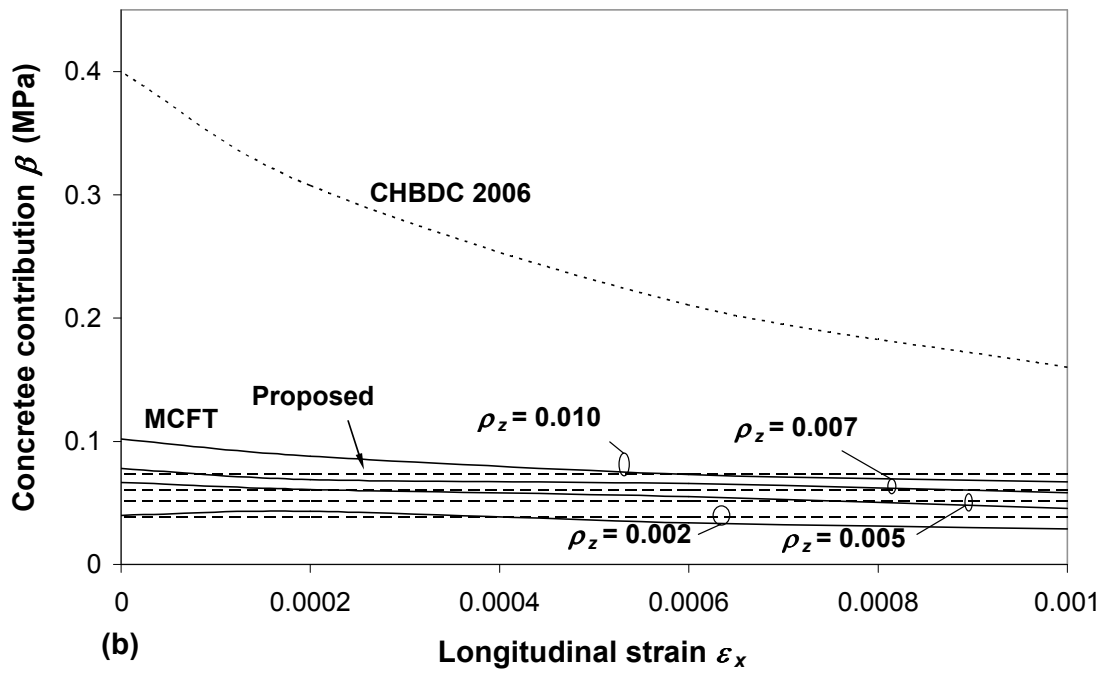
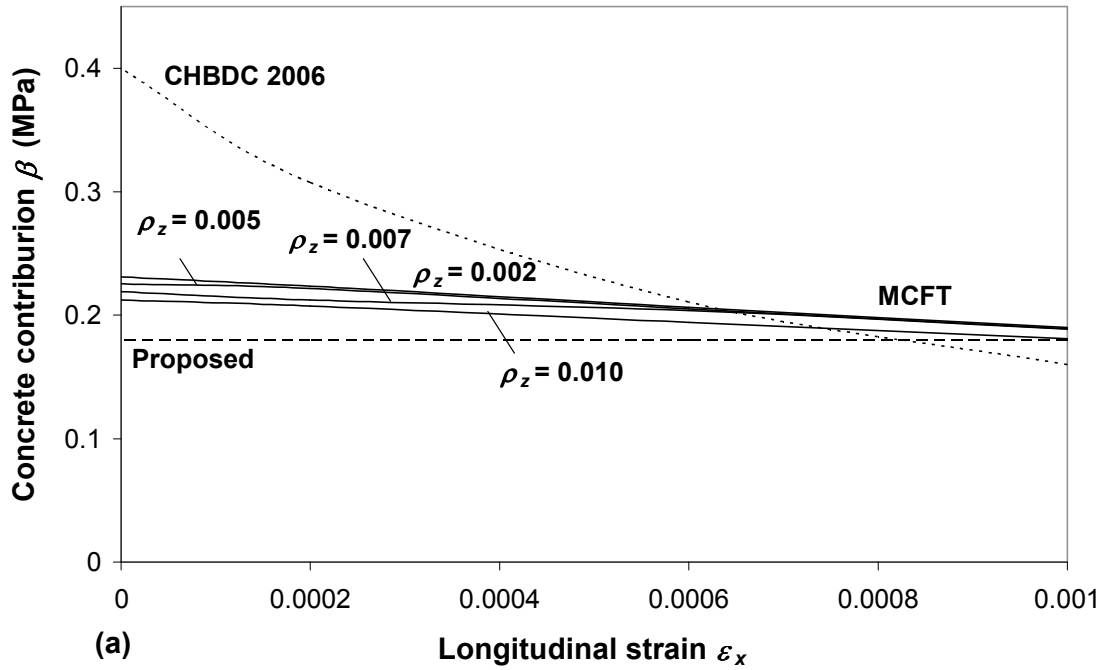


Fig. 3-21 Comparison of predicted β with MCFT result at: (a) yielding of transverse reinforcement, (b) crushing of concrete for $f'_c = 60$ MPa, $f_y = 400$ MPa.

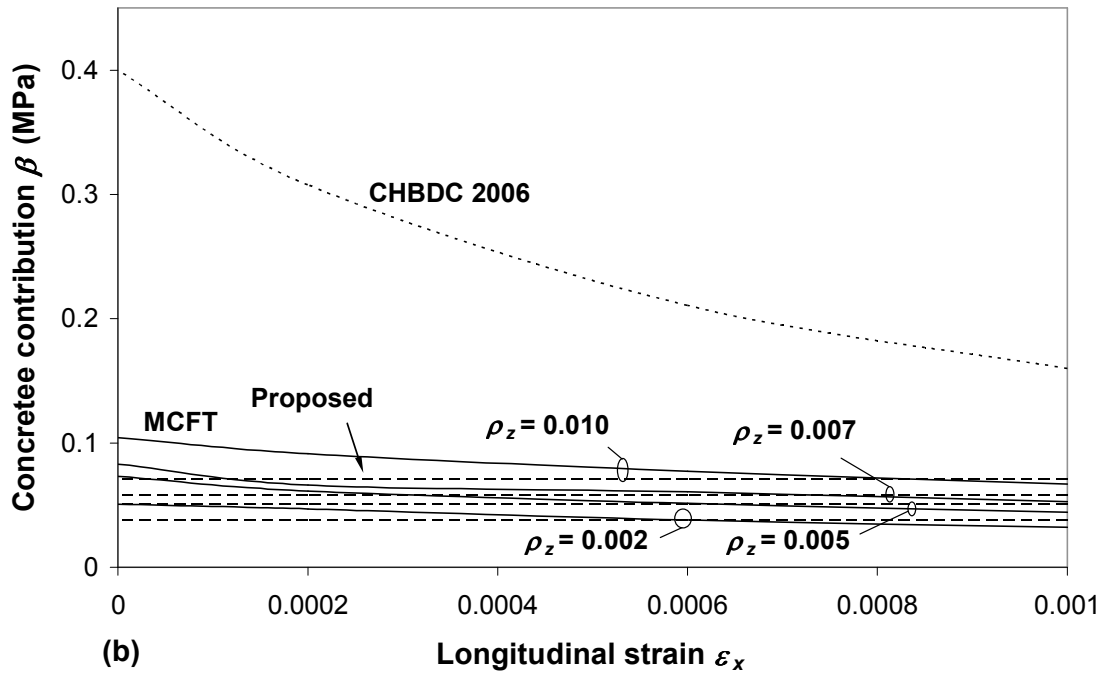
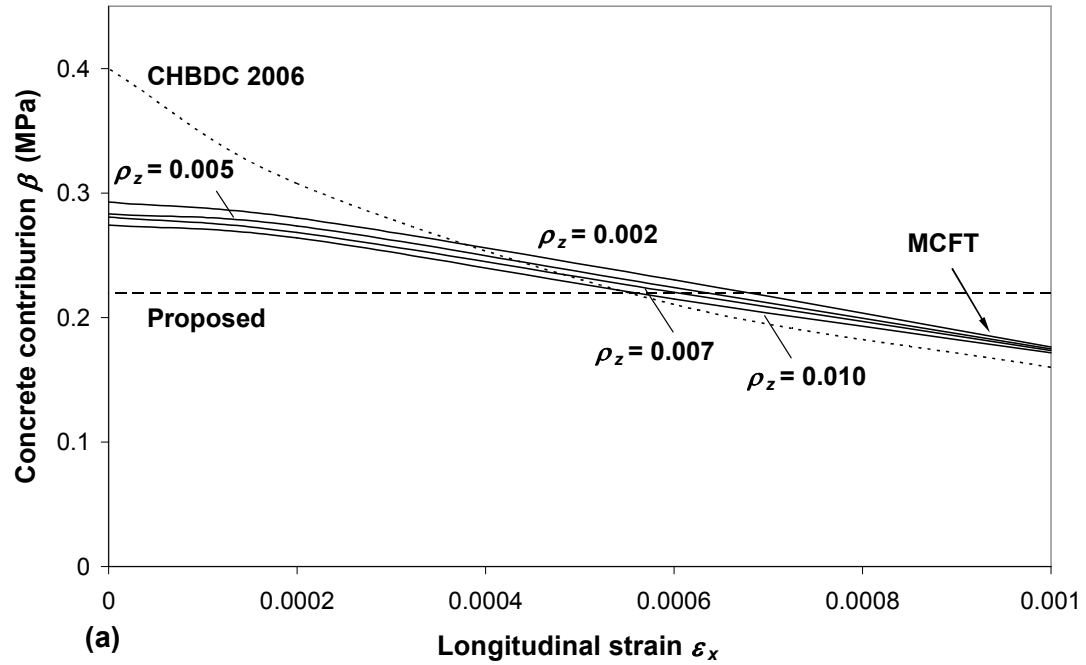


Fig. 3-22 Comparison of predicted β with MCFT result at: (a) yielding of transverse reinforcement, (b) crushing of concrete for $f'_c = 40$ MPa, $f_y = 250$ MPa.

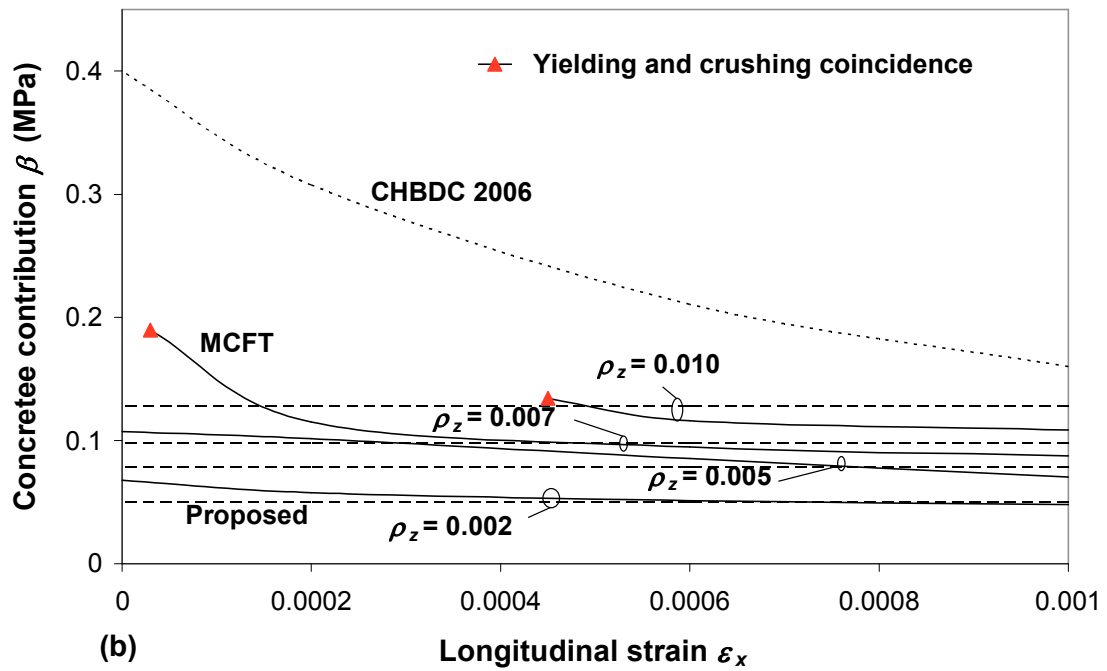
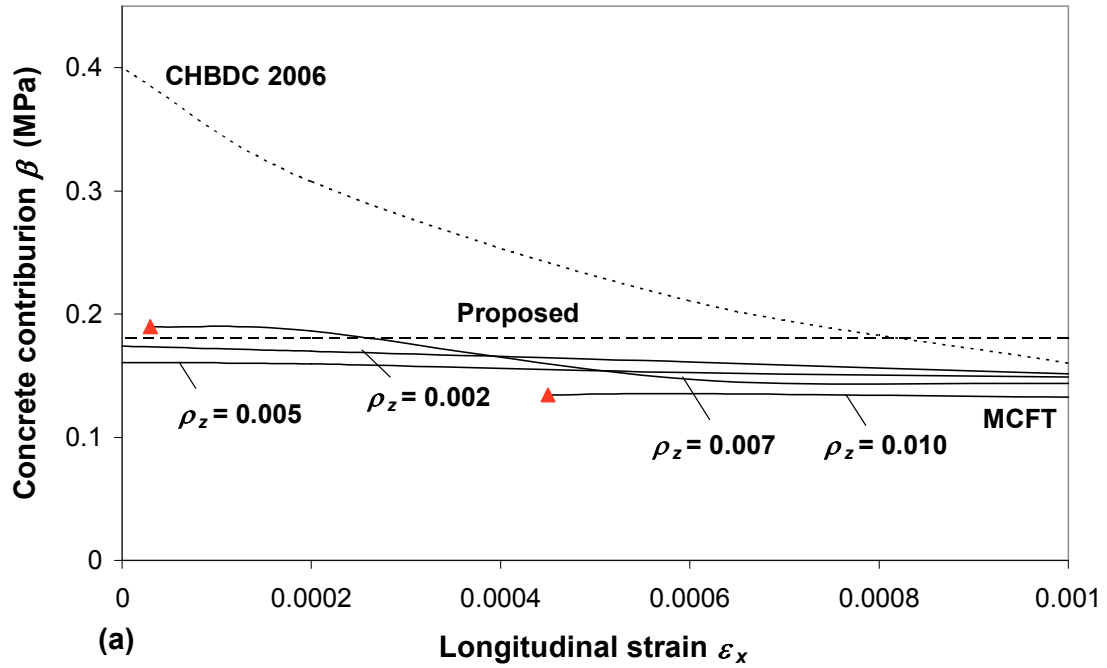


Fig. 3-23 Comparison of predicted β with MCFT result at: (a) yielding of transverse reinforcement, (b) crushing of concrete for $f'_c = 40$ MPa, $f_y = 600$ MPa.

3.6.3. Predicted Total Shear Stress

Total shear stress v is the sum of the concrete contribution v_c , which depends on β and the stirrup contribution v_s , which depends on the angle θ . As different combinations of θ and β can result in the same total shear stress, different methods can be really compared by comparing the predictions for total shear stress. Figures 3-24 to 3-28 compare MCFT predictions of total shear stress with the results from the proposed method at transverse reinforcement yielding and concrete crushing for concrete compressive strength of 30, 40, and 60 MPa and steel grade of 250, 400, and 600 MPa. In all cases, the proposed method agrees better with MCFT results than the 2006 CHBDC. Generally, the 2006 CHBDC predictions are unconservative for low longitudinal strains but it becomes less unconservative for concrete strength of 60 MPa. The 2006 CHBDC predictions are mostly conservative compared to MCFT results at concrete crushing except for low longitudinal strains.

As explained before, the 2006 CHBDC limits the maximum shear strength to $0.25f_c'$ to ensure that concrete crushing occurs after yielding of transverse reinforcement. Figures 3-28 proves that this is consistent with MCFT results, and thus this is adopted in the proposed method. Notice that for 40 MPa concrete and 600 MPa reinforcing steel, concrete crushing and steel yielding coincide at shear stress of 9.3 MPa and 10.3 MPa for transverse reinforcing steel ratios of $\rho_z = 0.007$ and 0.010, respectively. This is close to $0.25f_c' = 10$ MPa predicted by the 2006 CHBDC.

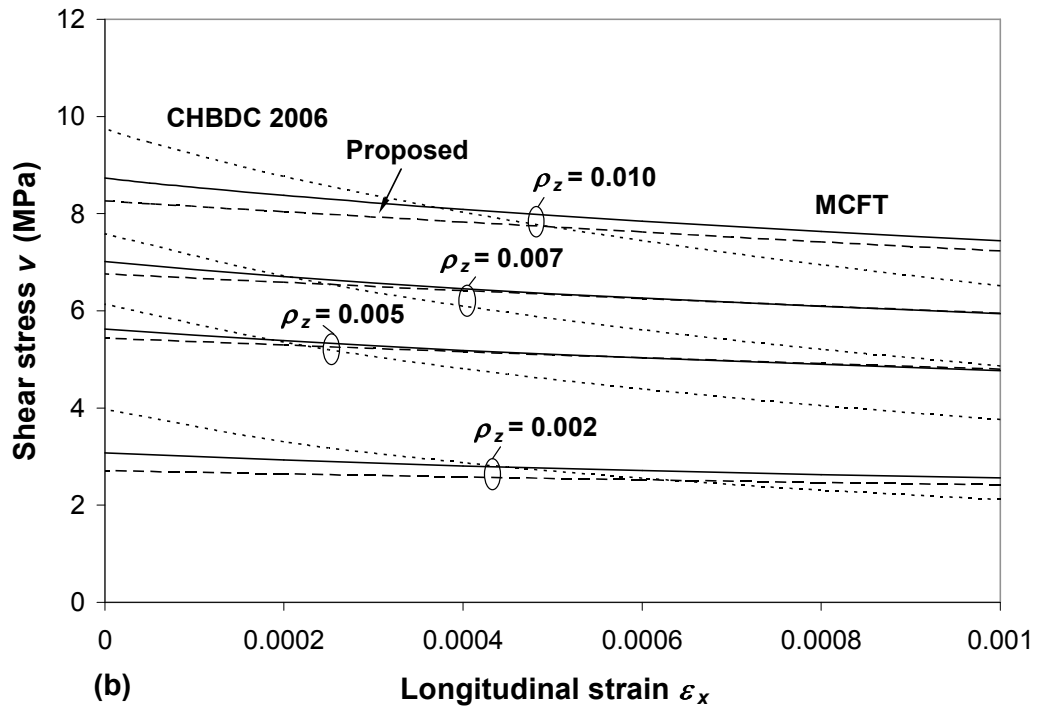
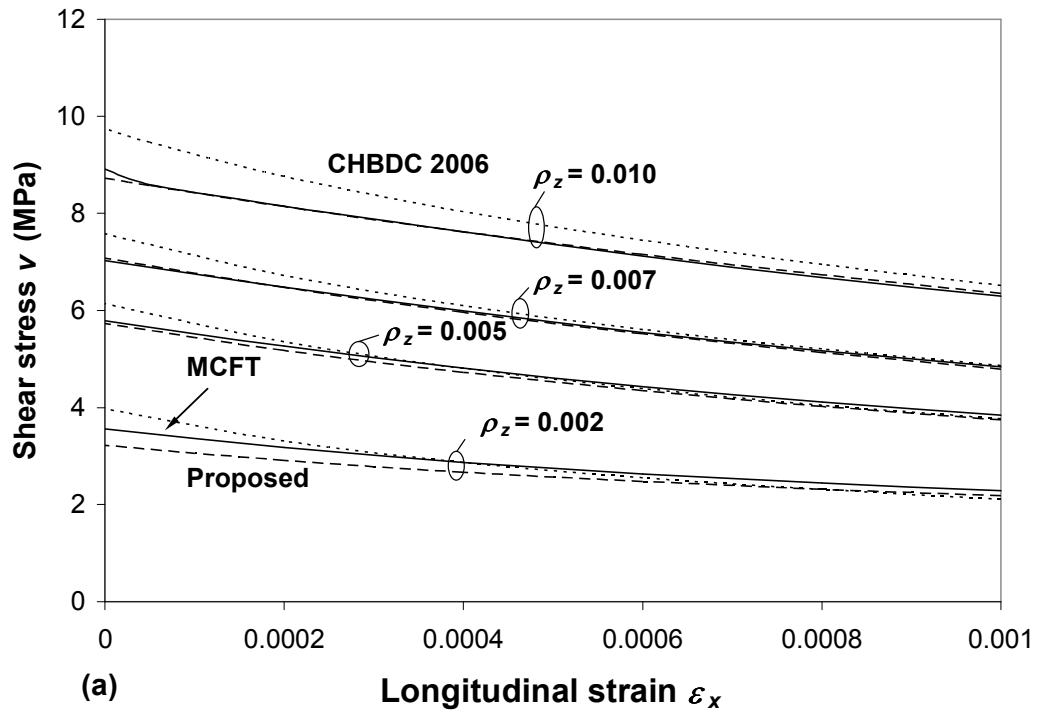


Fig. 3-24 Comparison of predicted shear stress with MCFT result at: (a) yielding of transverse reinforcement, (b) crushing of concrete for $f'_c = 40$ MPa, $f_y = 400$ MPa.

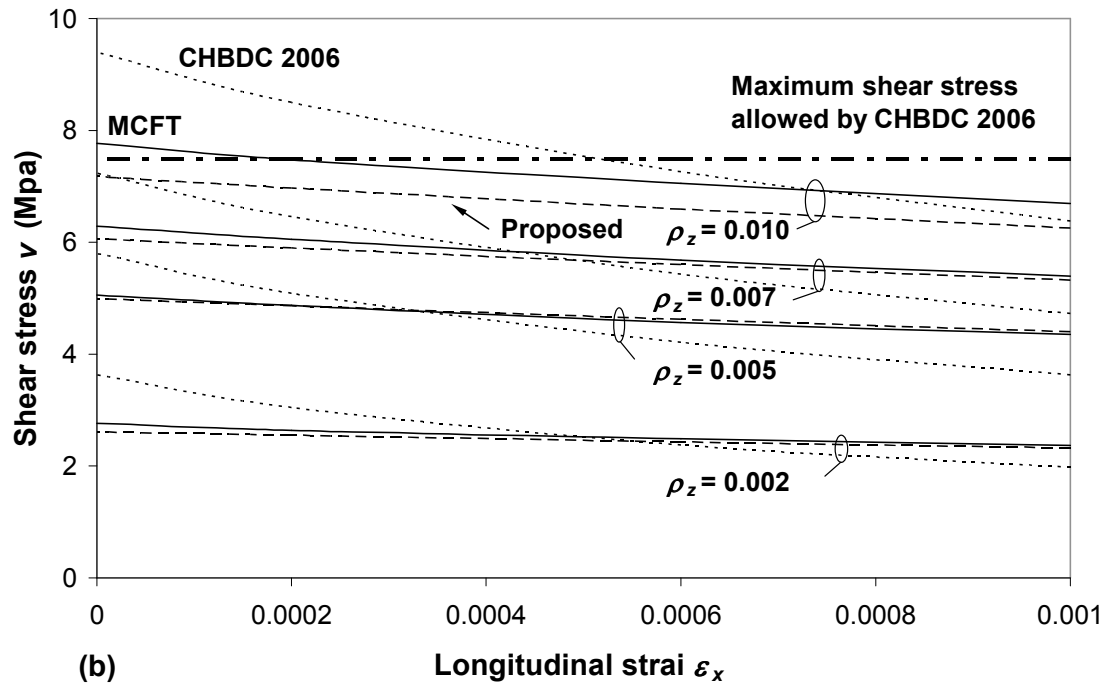
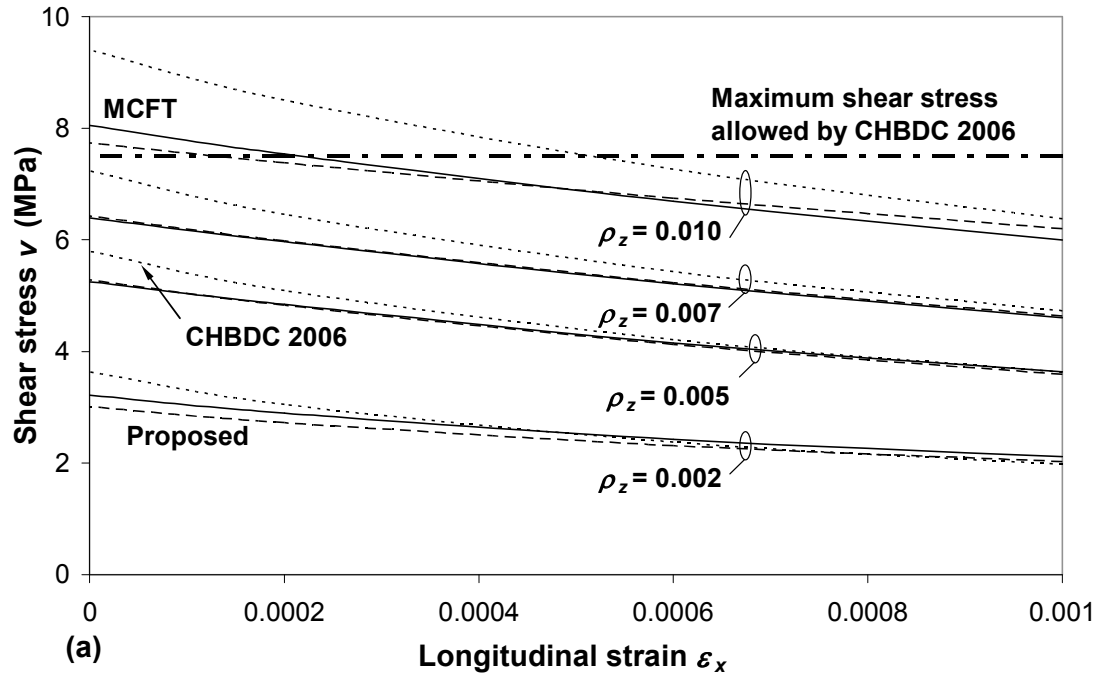


Fig. 3-25 Comparison of predicted shear stress with MCFT result at: (a) yielding of transverse reinforcement, (b) crushing of concrete for $f'_c = 30$ MPa, $f_y = 400$ MPa.

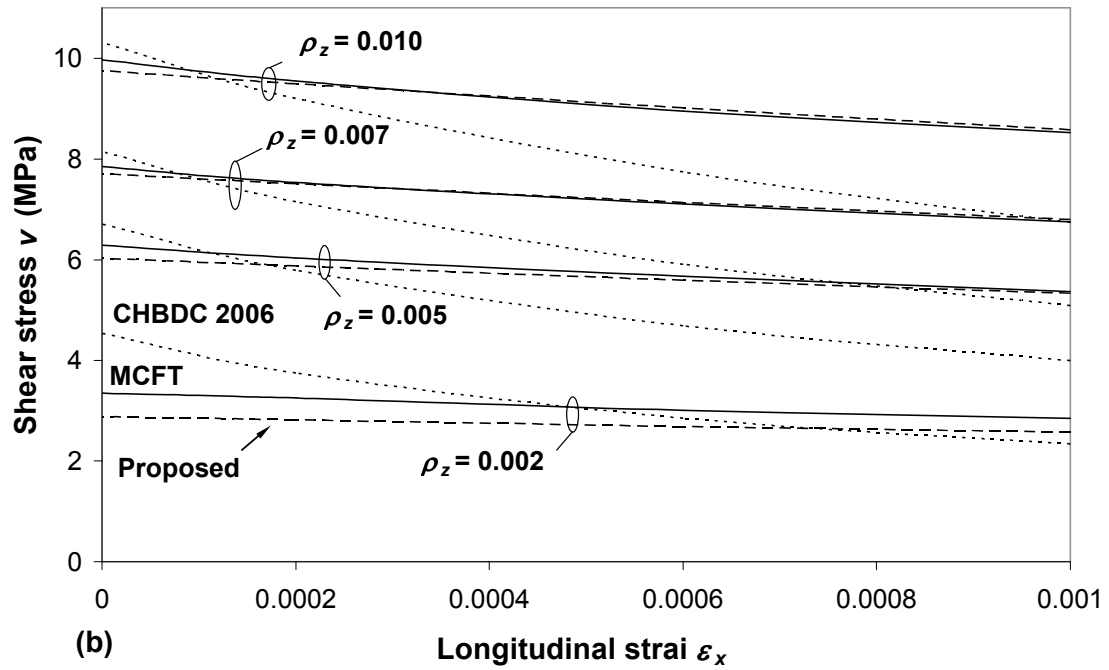
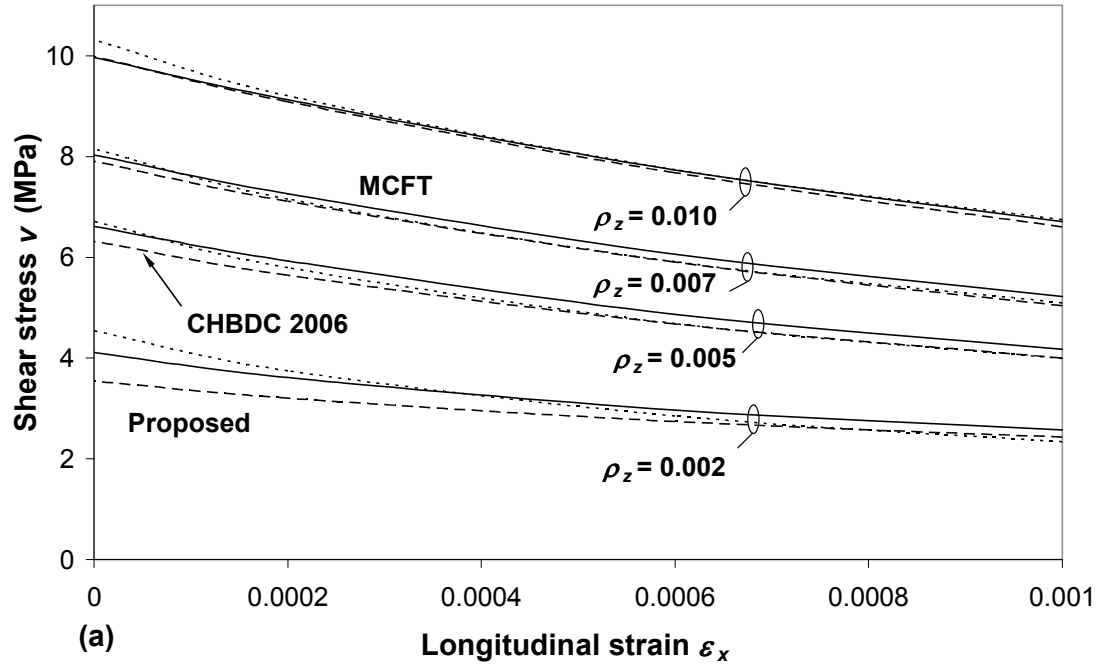


Fig. 3-26 Comparison of predicted shear stress with MCFT result at: (a) yielding of transverse reinforcement, (b) crushing of concrete for $f'_c = 60$ MPa, $f_y = 400$ MPa.

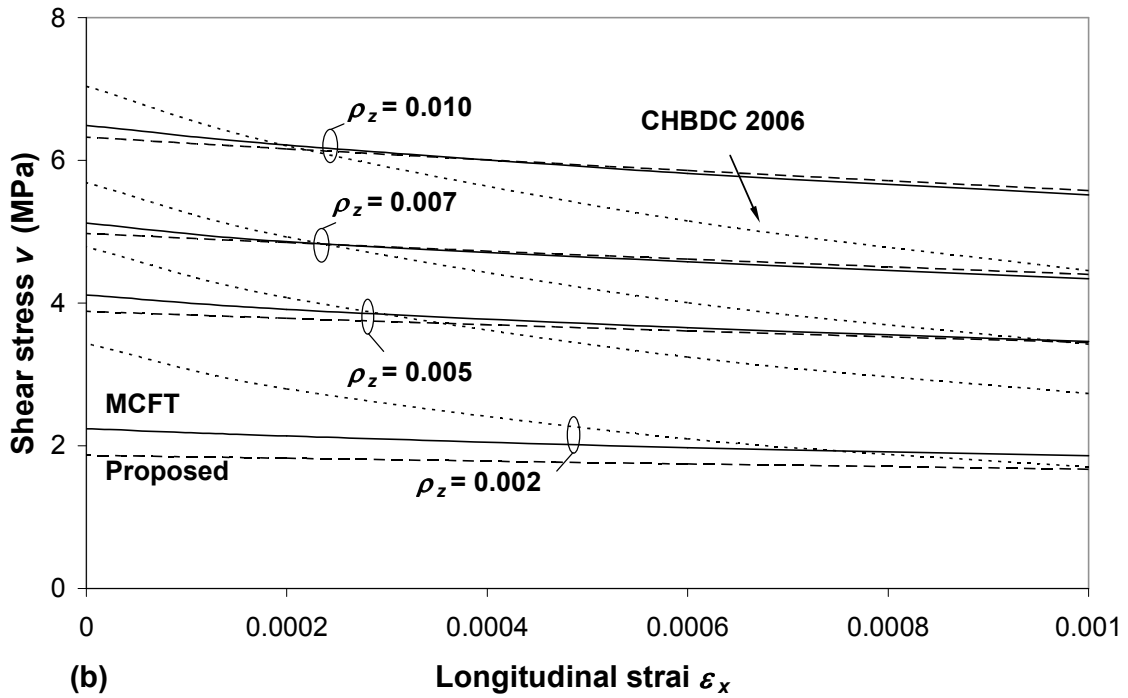
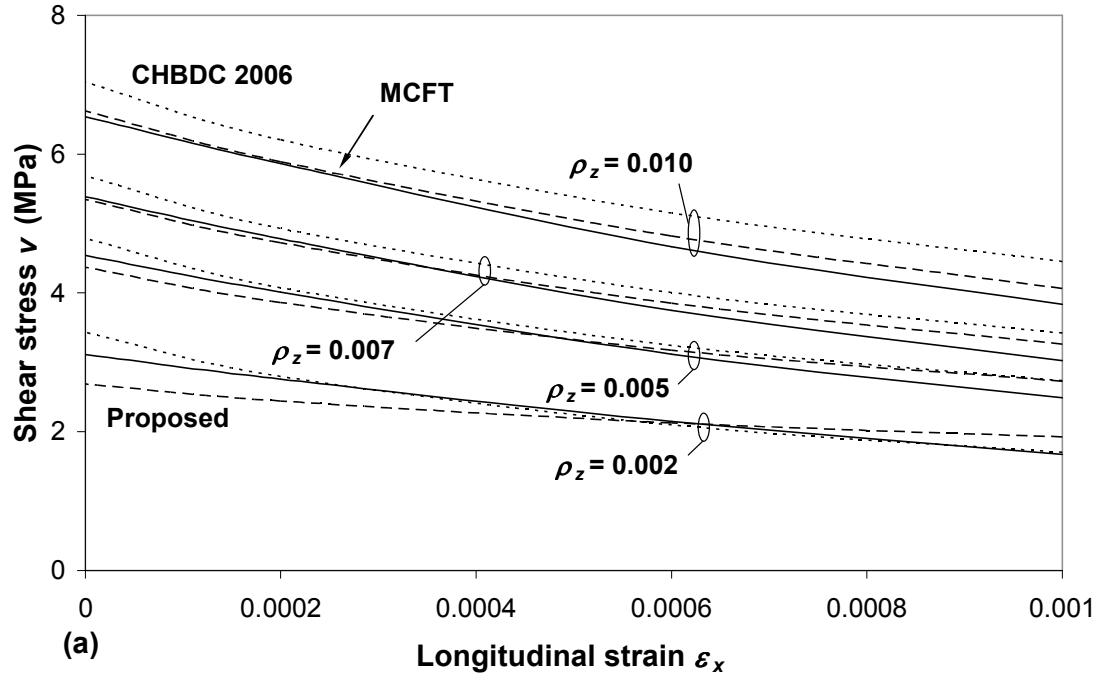


Fig. 3-27 Comparison of predicted shear stress with MCFT result at: (a) yielding of transverse reinforcement, (b) crushing of concrete for $f'_c = 40$ MPa, $f_y = 250$ MPa.

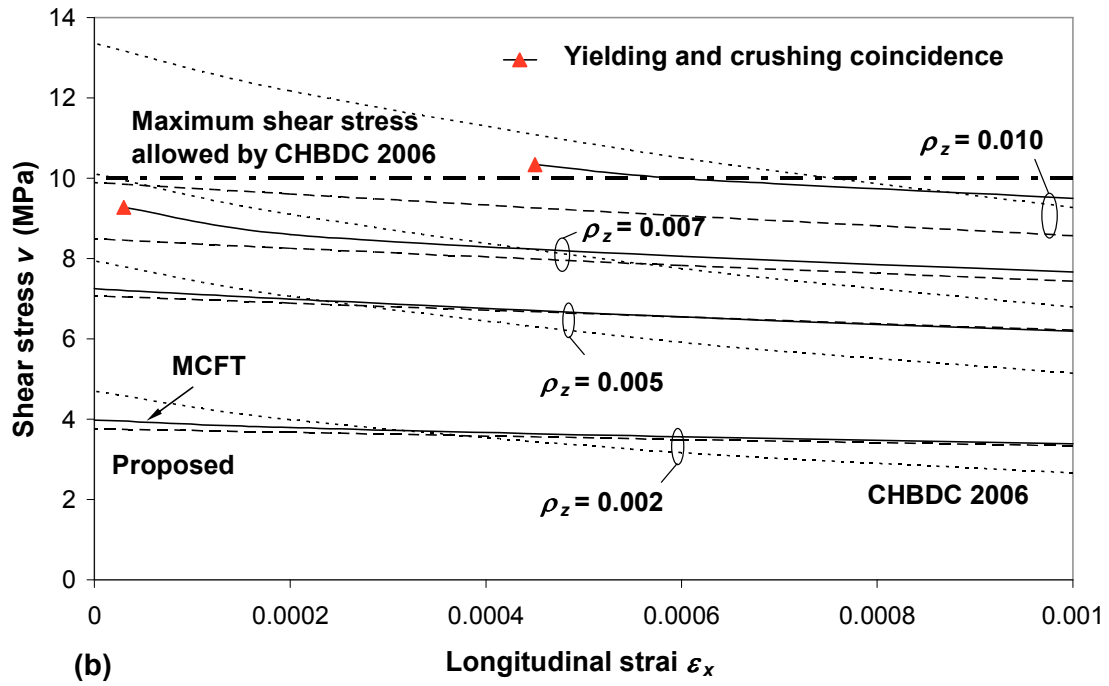
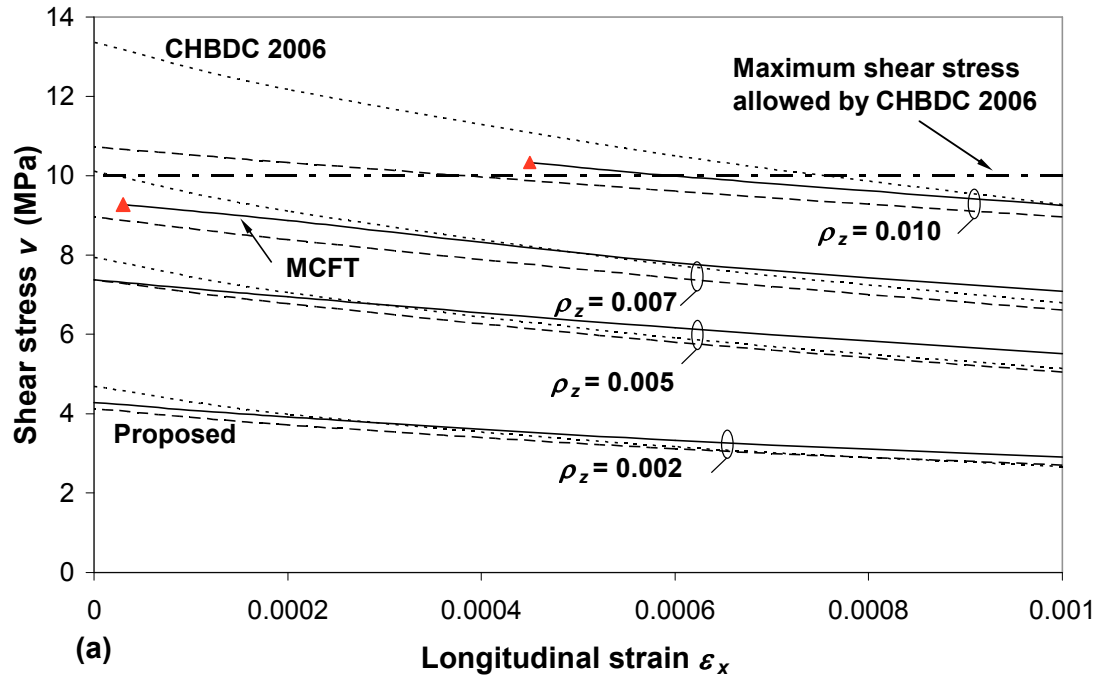


Fig. 3-28 Comparison of predicted shear stress with MCFT result at: (a) yielding of transverse reinforcement, (b) crushing of concrete for $f'_c = 40$ MPa, $f_y = 600$ MPa.

3.6.4. Proposed Equations for Longitudinal Concrete Compression Stress

The resultant of the longitudinal concrete compression stress f_{cx} is the axial compression force N_v required in a beam web to resist shear, thus this stress is also referred to as n_v . In order to estimate ε_x , which influences β and θ , an estimate of n_v is needed. As the longitudinal compression n_v in concrete must be balanced by tension in steel, n_v is equal to $\rho_x f_s$ where ρ_x is the reinforcement ratio in the x -direction and f_s is the stress in the horizontal reinforcement. As $f_s = E_s \varepsilon_x$, ε_x for a uniform shear element is given by:

$$[3-38] \quad \varepsilon_x = \frac{n_v}{\rho_x E_s}$$

In the 2007 AASHTO LRFD shear design method, it is assumed for simplicity that $n_v = v \cot \theta$, while in the 2006 CHBDC shear design method, this has been further simplified to $n_v = 2v$. According to MCFT, substituting for f_{c1} in Eq. [3-10] from Eq. [3-9] and assuming $f_x = f_z = 0$, the actual relationship is:

$$[3-39] \quad n_v = 2v_c \cot 2\theta + \rho_z f_y \cot^2 \theta$$

To simplify this equation in the proposed method, $\cot 2\theta$ and $\cot^2 \theta$ have been approximated as linear functions for $\theta > 25^\circ$ and $\theta \leq 25^\circ$ as illustrated in in Fig. 3-29. Substituting these linear functions, as well as $v_c = \beta \sqrt{f'_c}$, and Eq. [3-31] for θ as a function of ε_x gives:

$$[3-40] \quad n_v = n_{v0} + \Delta n_v \varepsilon_x$$

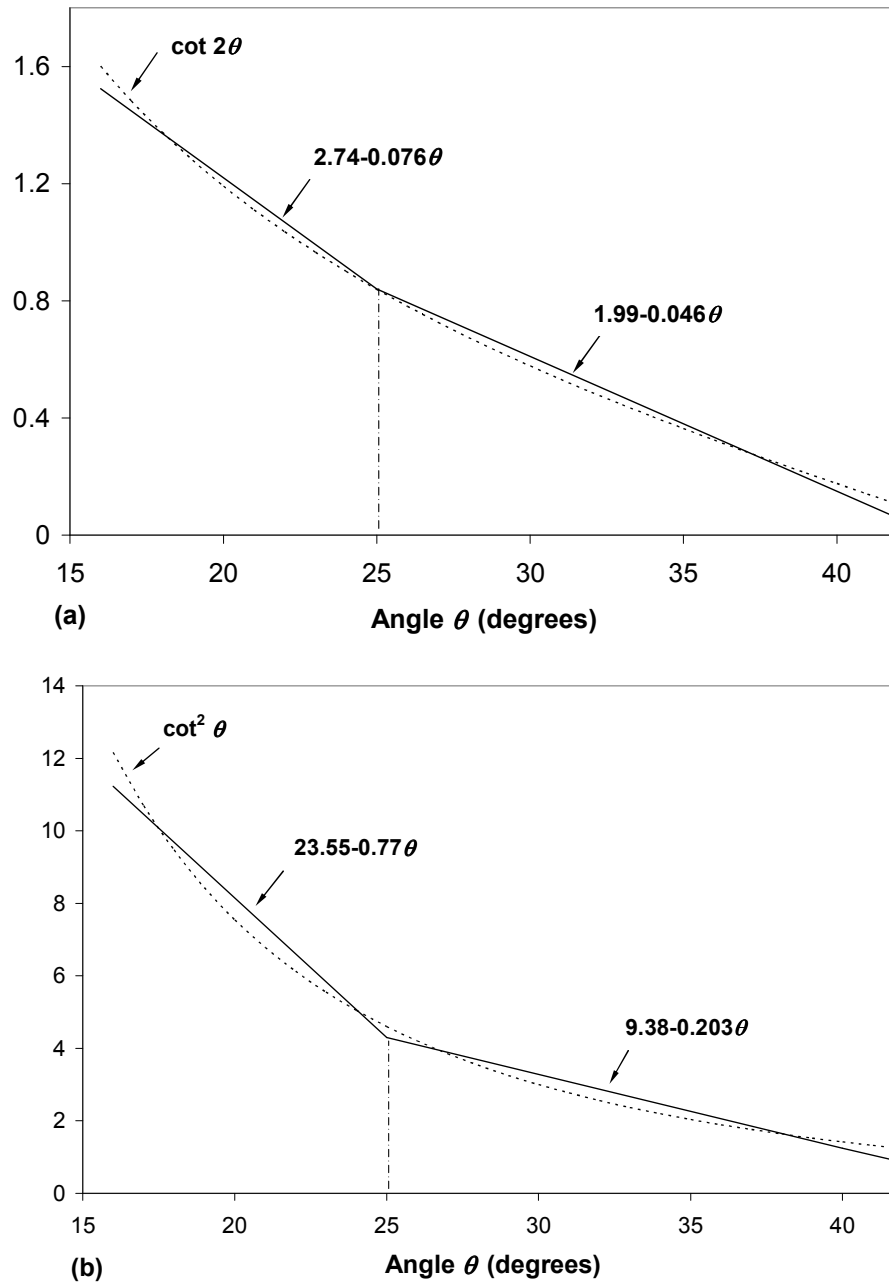


Fig. 3-29 Bilinear approximation of: (a) $\cot 2\theta$, (b) $\cot^2 \theta$ used to approximate Eq. [3-39].

where for $\theta > 25$ deg:

$$[3-41] \Delta n_v = (-0.09\beta\sqrt{f'_c} - 0.20\rho_z f_y)\Delta\theta$$

$$[3-42] n_{vo} = \frac{\Delta n_v}{\Delta\theta}\theta_o + 4.0\beta\sqrt{f'_c} + 9.4\rho_z f_y$$

and for $\theta \leq 25$ deg:

$$[3-43] \Delta n_v = (-0.15\beta\sqrt{f'_c} - 0.77\rho_z f_y)\Delta\theta$$

$$[3-44] n_{vo} = \frac{\Delta n_v}{\Delta\theta}\theta_o + 5.5\beta\sqrt{f'_c} + 23.6\rho_z f_y$$

A simplification that avoids trial-and-error is to only use Eqs. [3-41] and [3-42] for transverse reinforcement yielding, use Eqs. [3-43] and [3-44] if $\theta_o \leq 23$ deg and use Eqs. [3-41] and [3-42] if $\theta_o > 23$ deg for concrete crushing. Although this simplification results in slightly unconservative estimate of axial compression stress at reinforcement yielding for members with low amount of transverse reinforcement and low longitudinal strain (members with angle of principal compression of less than 25 deg), this unconservatism is compensated for by conservative estimate of β for such elements as shown in Figures 3-19 to 3-23. At concrete crushing, angle rate of change with longitudinal strain is not high (see Figs. 3-14 to 3-18); thus θ_o is a good representative of θ . For average strain of $\epsilon_x = 0.005$, θ_o is almost 2 deg smaller than θ (see Figs. 3-14 to 3-18). In addition, approximated linear functions of $\cot 2\theta$ and $\cot^2 \theta$ for $\theta > 25$ deg shown in Fig. 3-29 are still consistent with actual values at $\theta = 23$ degrees.

The n_v calculated from MCFT as well as estimated by Eqs. [3-40] to [3-44] together with the simplification explained above are compared at yielding of transverse reinforcement in Fig. 3-30(a) and concrete crushing in Fig. 3-30(b).

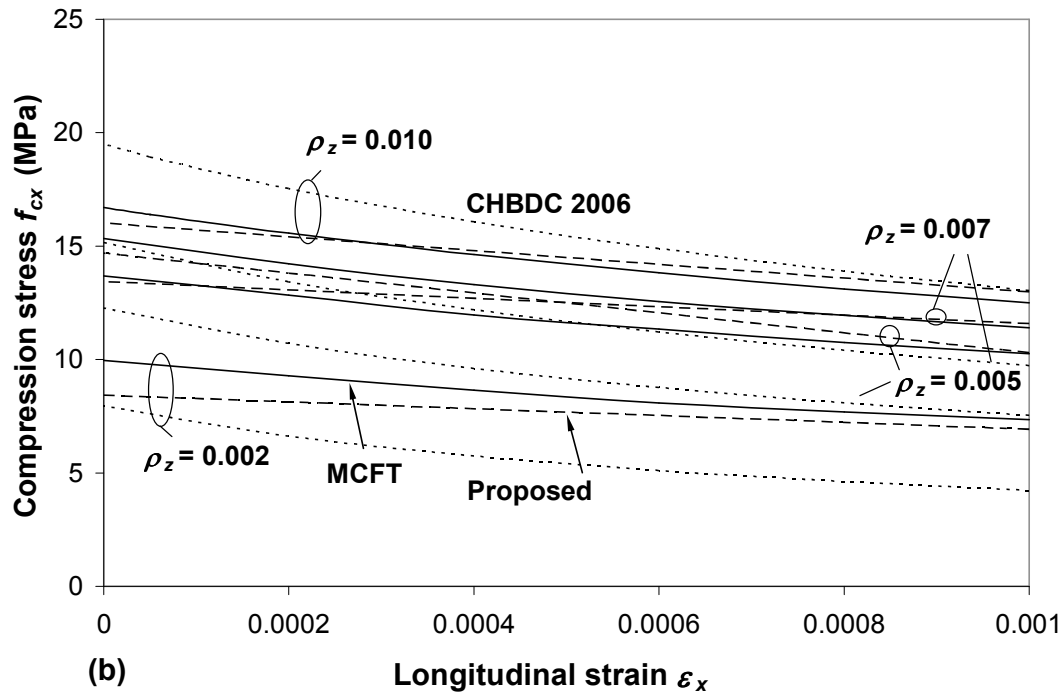
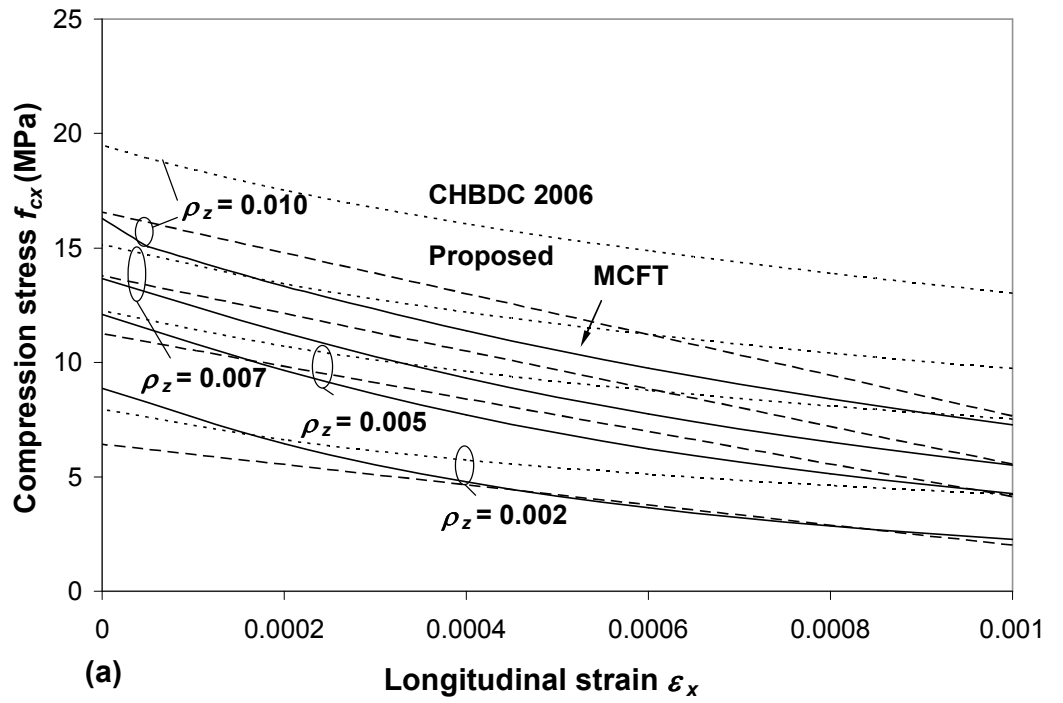


Fig. 3-30 Comparison of predicted longitudinal concrete compression stress with MCFT result at: (a) yielding of transverse reinforcement, (b) crushing of concrete for $f'_c = 40$ MPa, $f_y = 400$ MPa.

The 2006 CHBDC approximation of $n_v = 2v$ is generally conservative (larger estimate of n_v than actual) at yielding of transverse reinforcement. Thus the estimated axial tension force in the longitudinal reinforcement that balances the axial compression force N_v will be larger than actual, and the estimated axial strain ϵ_x will be larger than actual. When this trend is combined with the trend shown in Fig. 3-24, the 2006 CHBDC method generally gives conservative predictions of shear strength for a member with a given amount of longitudinal reinforcement. The predictions of the proposed equations for n_v are not compared with the MCFT predictions for other material properties since the proposed equation has been directly derived from the MCFT actual equation.

3.6.5. Longitudinal Reinforcement Yielding

There are some cases where an element cannot reach the capacity at yielding of transverse reinforcement or concrete crushing because the longitudinal reinforcement does not have the capacity – beyond that needed to resist the applied bending moment – to equilibrate the longitudinal compression stress in concrete due to shear. The average longitudinal compression stress n_v which influences the strain of the member was discussed above. This average stress is reduced by the ability of cracked concrete to resist some average tension stresses. The axial compression stress required locally at diagonal cracks to resist shear is considerably larger and is given by Eq. [3-28] as discussed before. The concrete contribution factor β and angle of principal compression θ determined at transverse reinforcement yielding and concrete crushing can be used in Eq. [3-28] to determine the longitudinal compression at diagonal cracks that must be balanced by tension in longitudinal reinforcement; but as shown in Fig. 3-8(a), yielding of longitudinal reinforcement may occur somewhere between the point of transverse

reinforcement yielding and concrete crushing.

Rather than determine a third pair of β and θ values associated with the point of longitudinal reinforcement yielding, a simpler approach is to ignore the concrete contribution when determining the shear to cause yielding of both the transverse and longitudinal reinforcement. Setting $v_c=0$ in Eqs. [3-23] and [3-28], and solving these two equations for v (eliminating θ) results in the following expression for shear strength given the maximum n_v^* controlled by the capacity of distributed longitudinal reinforcement denoted n_{vc} :

$$[3-45] \quad v = \sqrt{\rho_z f_y n_{vc}}$$

Actual concrete contribution cannot be determined by equilibrium equations only and require more complicated analysis using material constitutive relations and compatibility equations. However, concrete contribution is small in common cases at biaxial yielding of reinforcement as both transverse and longitudinal strains are large at this stage and thus the stress that can be resisted by aggregate interlock is very small.

Figure 3-31 illustrates the variation of angle θ and shear strength per unit area with shear stress resisted by concrete v_c ranging from 0% to 40% of the shear strength when the longitudinal compression stress n_v is 3 MPa and 6 MPa. θ s and β s shown in Fig. 3-31 were determined from equilibrium equations. From equilibrium, v is given by Eq. [3-23] and n_v is given by Eq. [3-28]. Substituting for v_c and n_v , the equations can be solved for angle θ and shear stress v .

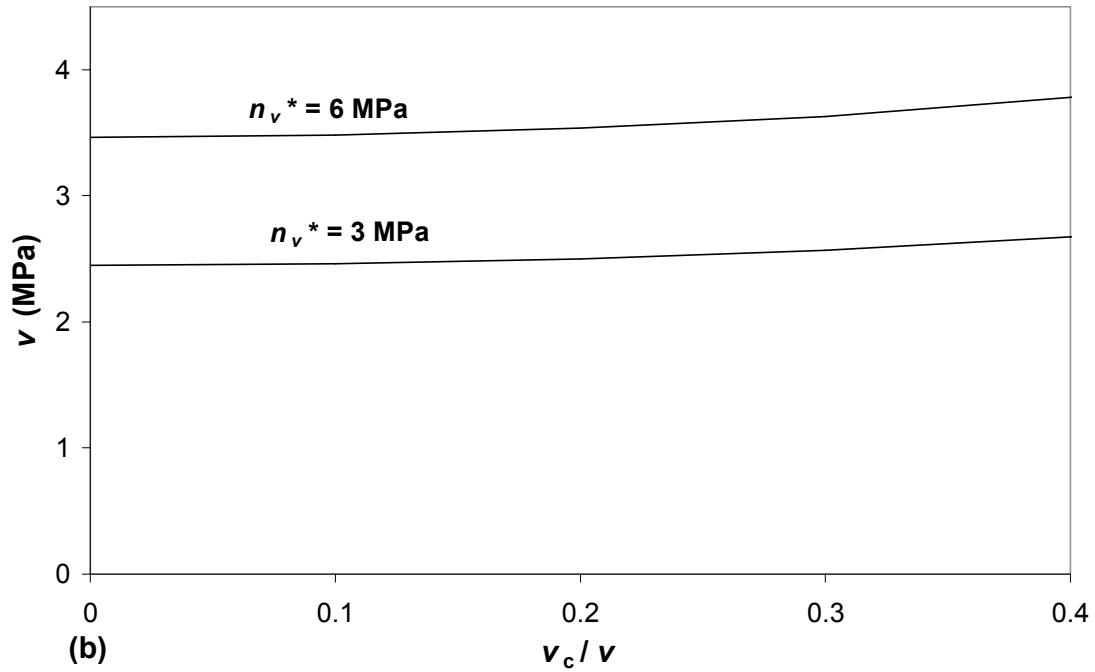
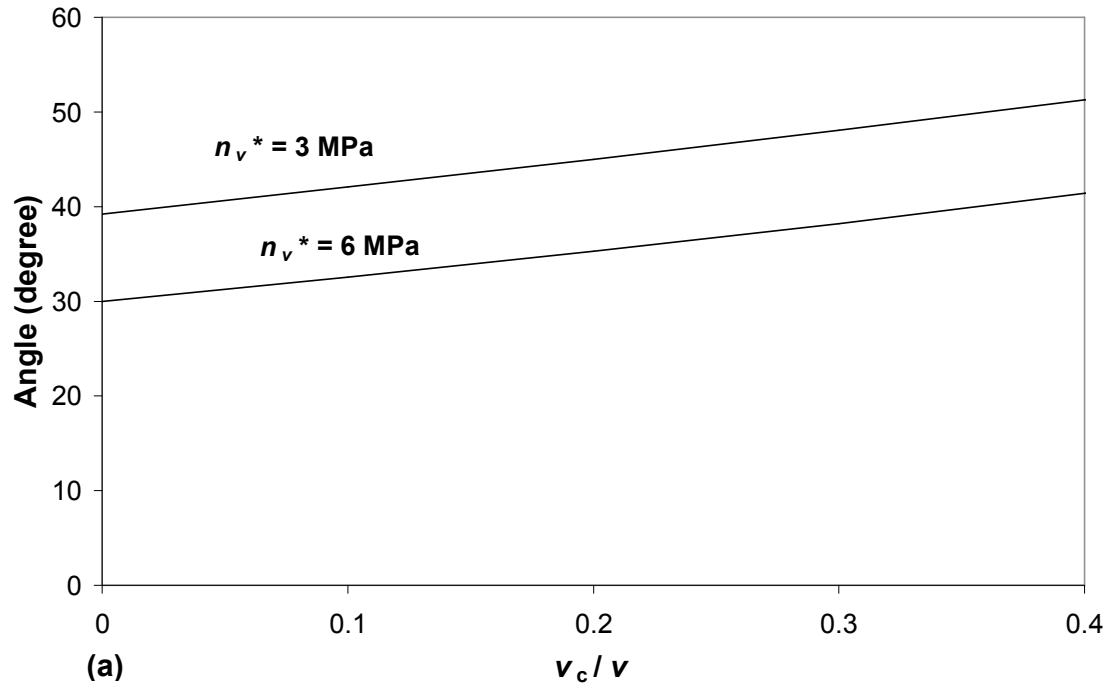


Fig. 3-31 Variation of: (a) angle, (b) shear stress with concrete contribution from variable angle truss model.

Figure 3-31 shows that angle is steeper when concrete contribution is higher; therefore shear does not change significantly with concrete contribution. Notice that there is only an increase of less than 10% in shear strength once concrete contribution changes from 0 to 40%.

3.7. Proposed Evaluation Method for Members Without Transverse Reinforcement

Members without transverse reinforcement behave differently than members with at least minimum transverse reinforcement. As a result, the proposed evaluation procedure for members without transverse reinforcement is different from the procedure for members with at least minimum transverse reinforcement.

Figures 3-8(a) and 3-8(b) show the predicted shear behaviour of both members with at least minimum and without transverse reinforcement, and these are clearly different. Figure 3-8(b) illustrates that after cracking of concrete, there is a sudden drop in shear stress; however, the shear stress normally increases as the stress resisted by aggregate interlock increases. Adebar and Collins (1996) showed that the critical point is when transfer of shear across diagonal cracks initially limits the applied stresses. The corresponding shear stress is taken as the shear strength per unit area of a uniform shear element without transverse reinforcement. The proposed evaluation procedure to determine the shear strength at this critical point is presented here.

At the critical failure points (shown as square dots in Fig. 3-8b), a diagonally cracked element with only longitudinal reinforcement – no stirrups – resists shear by a combination of diagonal compression and tension stresses that must satisfy two requirements. The first is that the resultant normal stress on any horizontal plane must be

zero as there is no transverse reinforcement to balance concrete normal stress. The second requirement is that the resultant stresses acting on a plane parallel to the assumed crack direction θ must be the required combination of shear and compression stress needed to transmit the shear across the crack. As a result of these two requirements, axial compression stress will exist on vertical planes in the element, and the resultant of the axial compression n_v must be equilibrated by tension in the longitudinal reinforcement. According to the MCFT n_v is given by Eq.[3-39]. As discussed earlier, this has been simplified to $n_v = v \cot \theta$ in the AASHTO LRFD shear design method, which is a reasonable simplification for members with significant transverse reinforcement, and in the 2006 CHBDC shear design method, this has been further simplified to $n_v = 2v$. For members without transverse reinforcement, $v_s = 0$ and $v = v_c$. As the axial strain of a member depends on the magnitude of n_v , which is a function of the applied shear stress, shear strength evaluation requires trial-and-error for the 2007AASHTO LRFD and 2006 CHBDC methods.

Fig. 3-32 compares the axial compression stress n_v from the two code approximate expressions, and the MCFT for two different sized members ($S_{xe} = 300$ and 2000 mm) without transverse reinforcement. As v_c is proportional to $\sqrt{f'_c}$, the ratio $n_v / \sqrt{f'_c}$ plotted in Fig. 3-32 is independent of f'_c . The two code approximate expressions for n_v , which are used for both members with and without transverse reinforcement, give much higher compression stress than MCFT predictions for members without transverse reinforcement. In the proposed evaluation method for members without transverse reinforcement, it is assumed that $n_v = 0$. This is a better approximation and greatly simplifies the shear strength evaluation of such members and also removes the need for

trial-and-error procedure.

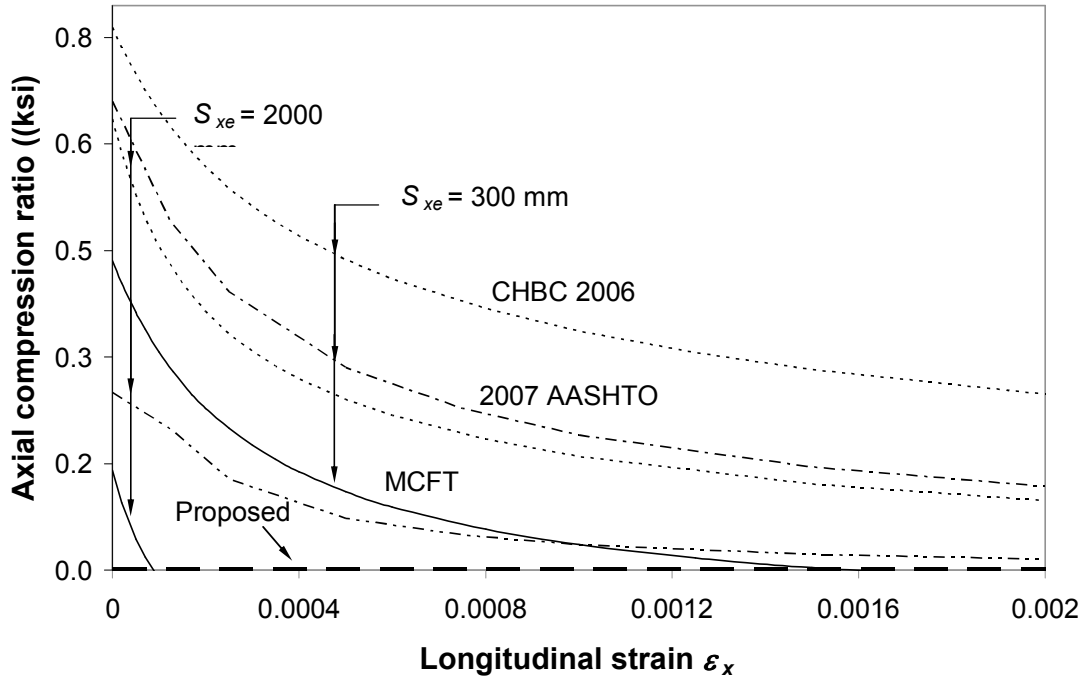


Fig. 3-32 Comparison of predicted axial compression stress ratio $n_v / \sqrt{f'_c}$ (in MPa units) with MCFT for members without transverse reinforcement.

The expression for concrete contribution factor β was selected to compensate for the assumption of zero longitudinal compression stress n_v , and was adjusted to give a good fit with test results on girders. The proposed expression is:

$$[3-46] \quad \beta = \frac{0.35}{1 + (600 + 2.1S_{xe})\epsilon_x} \leq \frac{400}{(500 + 0.5S_{xe})} \quad (\text{in MPa units})$$

The limit imposed on Eq. [3-46] is a cut-off for large members with very low longitudinal strain as shown for $S_{xe} = 2000$ in Figure 3-34. This prevents Eq. [3-46] predictions from being unconservative compared to MCFT for such members.

Fig. 3-33 compares β from Eq. [3-46] with that from the MCFT and the 2007 AASHTO LRFD table and 2006 CHBDC Eq. [3-29]. As the 2006 CHBDC method was primarily developed for $S_{xe} = 300$ mm, its predictions are in good agreement with MCFT

for that size member. The 2007 AASHTO LRFD values for β are almost exactly the same as the MCFT as the tabulated values were derived from the MCFT. 2007 AASHTO LRFD curves shown in Fig. 3-33 are based on linear interpolation between tabulated values.

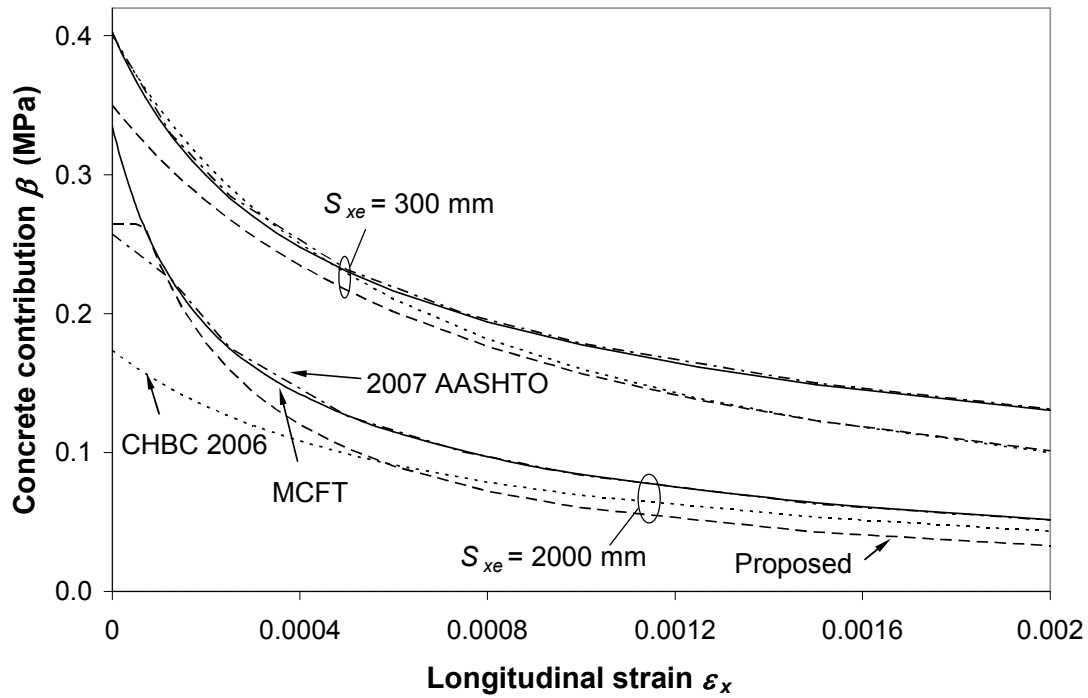


Fig. 3-33 Comparison of predicted concrete contribution β (in MPa units) with MCFT for members without transverse reinforcement.

For members without transverse reinforcement, the angle θ is only used to determine the demand imposed on longitudinal reinforcement by shear. As shown in Fig. 3-34, the 2007 AASHTO LRFD tabulated values are essentially identical to the MCFT. As the 2006 CHBDC expression for θ is a simple linear function of axial strain, it does not fit nearly as well to the MCFT values. The proposed expression for inclination of average principal compression stress in concrete, which is assumed to be parallel to the critical diagonal cracks is:

$$[3-47] \quad \theta = (35 + 7000\varepsilon_x)(0.6 + 0.02\sqrt{S_{xe}}) \quad (\text{in MPa units})$$

The predictions of Eq. [3-47] are also shown in Figure 3-34. The predictions are closer to MCFT results compared to the 2006 CHBDC predictions for longitudinal strains of greater than $\varepsilon_x = 0.0004$. Longitudinal reinforcement unlikely yield at cracks once the strain is lower.

As in members with transverse reinforcement, in some cases, yielding of longitudinal reinforcement will limit the shear capacity of an element because the longitudinal reinforcement does not have the capacity to equilibrate the longitudinal compression stress in concrete due to shear. The average longitudinal compression stress n_v that influences the strain of the member was discussed above. This average stress is reduced by average tension stresses in cracked concrete. The axial compression stress required locally at diagonal cracks to resist shear is considerably larger. For members without transverse reinforcement it is given by:

$$[3-48] \quad n_v^* = 2v_c \cot \theta$$

The v_c and θ determined for maximum post-cracking capacity of an element can be used in Eq. [3-48] to determine the longitudinal compression at diagonal cracks that must be balanced by tension in longitudinal reinforcement. How the demand on longitudinal reinforcement from shear is combined with the demand from bending moment is explained in Chapter 4.

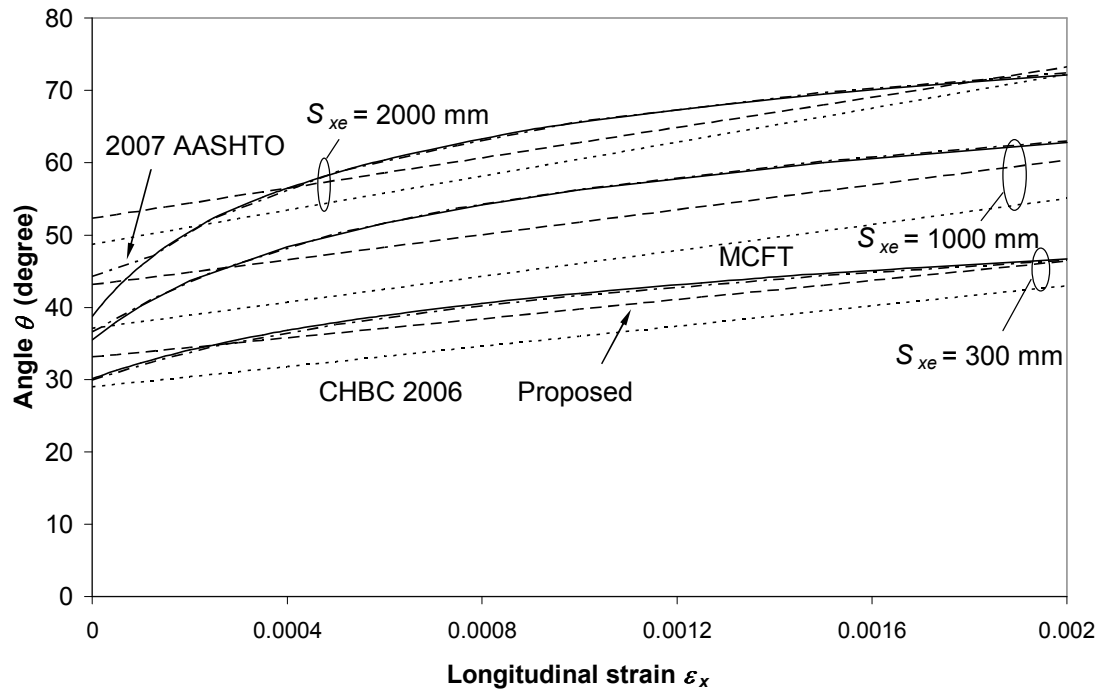


Fig. 3-34 Comparison of predicted angle θ with MCFT for members without transverse reinforcement.

Chapter 4. Beam Elements

4.1. General

A rigorous analysis of a beam subjected to axial load, bending moment and shear force can be done using a multi-layer analysis where the response of each layer is modeled as a uniform shear element. Response 2000 is a computer program that does such analyses. A simpler shear analysis can be done by using a single uniform shear element to approximate the complete shear behavior of a beam and this is consistent with shear design provisions in 2007 AASHTO LRFD and 2006 CHBDC.

In this chapter, the multi-layer analysis procedure for beams subjected to shear is briefly reviewed, and the simplified procedures used in 2007 AASHTO LRFD and 2006 CHBDC are summarized. The proposed procedure to apply the uniform shear element model from Chapter 3 is introduced and the predictions from the proposed procedure are compared with predictions using the shear design provisions in 2007 AASHTO LRFD and 2006 CHBDC, and the predictions from Response 2000.

4.2. Exact Solution

The procedure explained here was developed by Vecchio and Collins (1986). To account for moment-shear interaction at a beam section, a beam cross-section is divided to multiple layers as shown in Figure 4-1. Each layer is assumed to behave like a uniform shear element i.e. undergoes uniform stresses and strains in every direction. As a result, the MCFT formulation explained in Chapter 3 can be applied to each individual layer. Each layer may have different stresses, strains and angle of principal compression. To link the layers in this procedure, the well known assumption of plane sections remain

plane is used. In addition, global equilibrium should be satisfied meaning that stresses acting on the layers should balance bending moment, shear, and axial force acting at the cross-section. It is worth mentioning that any shear flow distribution at the section can result in a set of stresses in beam layers which satisfy both section equilibrium and compatibility assumption of plane sections remain plane. Consequently, one other check is needed to ensure that the assumed shear flow distribution would not violate equilibrium between the beam sections. This check is done by looking at the second section close to the primary one assuming that the second section has to have the same shear flow distribution as in the primary section. As shown in Figure 4-2, the normal stresses calculated at individual layers should then be consistent with the assumed shear flow distribution determined from the equilibrium of each layer between the dual sections. Shown in Fig. 4-2, Vecchio and Collins (1986) suggested that the second section should be spaced about $d/6$ from the primary one.

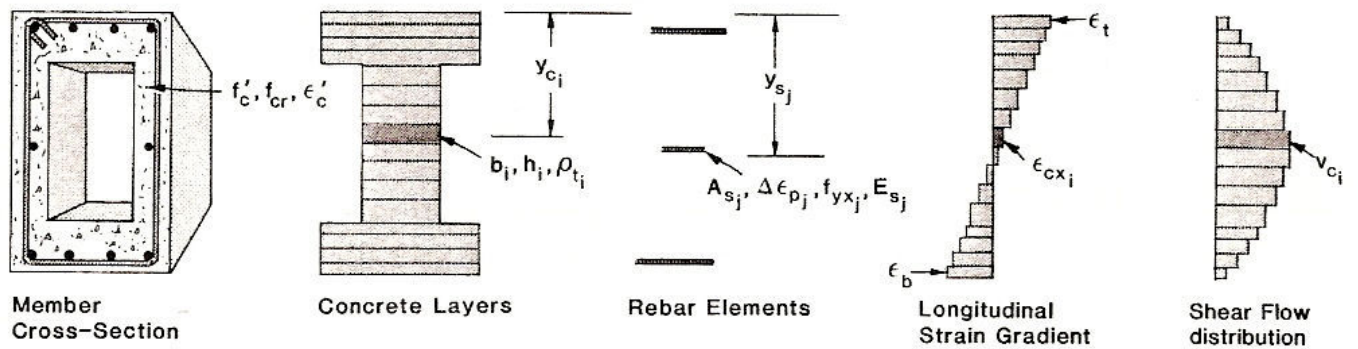


Fig. 4-1 Application of MCFT to beam elements using multi-layer analysis (Vecchio and Collins, 1986).

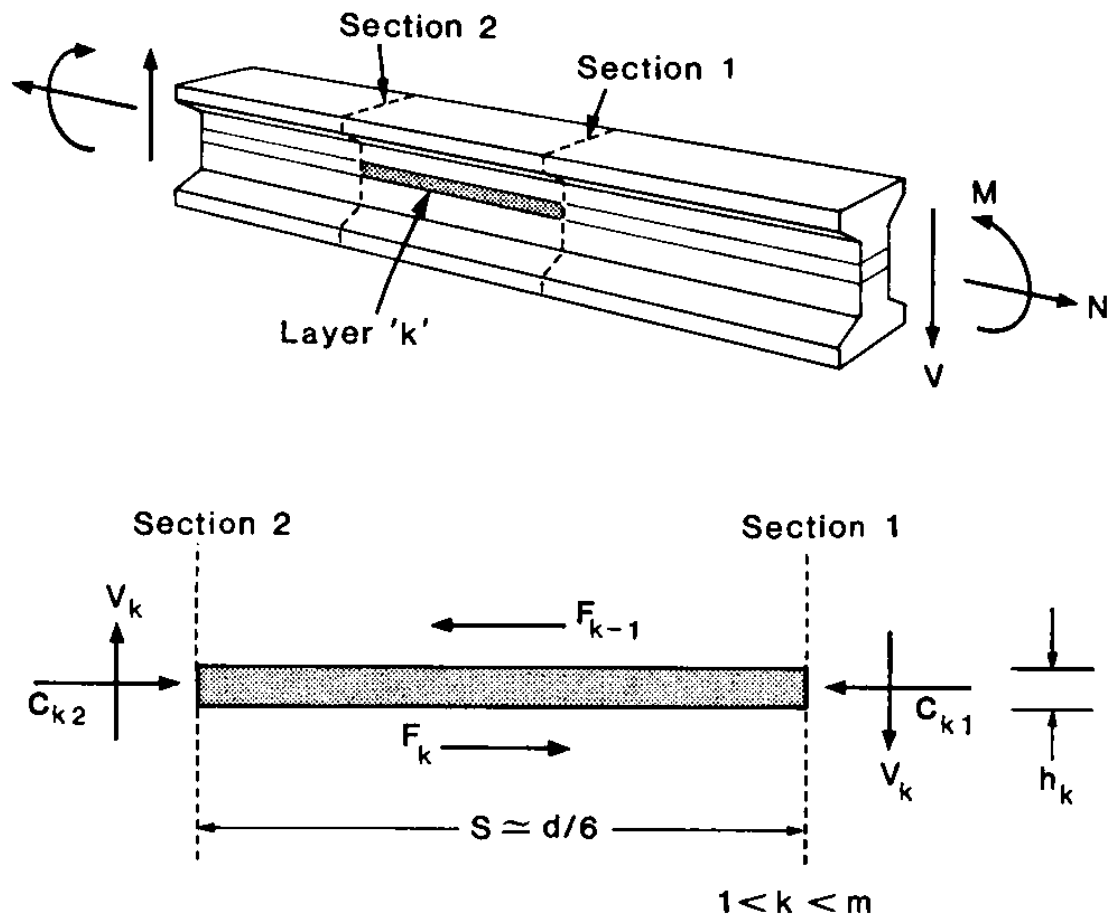


Fig. 4-2 Equilibrium of the dual sections in MCFT exact solution for beam elements (Vecchio and Collins, 1986).

Figure 4-3 presents the algorithm of the procedure as presented by Vecchio and Collins (1986). In summary, a shear flow distribution is assumed in the beginning. Then, longitudinal strain profiles (which are linear) are adjusted at the dual sections in a way that MCFT equations for individual layers, as well as global sectional equilibrium at both sections, are satisfied. Note that dual sections might have different longitudinal strain profiles but they have the same shear flow profile. In addition, shear force remains the same at both sections but moment varies to comply with equilibrium. Once longitudinal strain profiles and normal stresses are determined at all layers for both sections, shear flow distribution may then be calculated by looking at equilibrium of each layer between the sections as illustrated in Figure 4-2. The procedure should be repeated until the calculated shear flow profile is the same as the assumed one.

The procedure is complicated since it involves multi-layer MCFT analysis of two sections and trial-and-error. Vecchio and Collins (1986) explained that the procedure might be simplified by assuming an approximate shear flow profile or approximate shear strain profile. Common assumptions are constant shear flow (uniform shear flow) or parabolic shear strain profiles. This reduces the analysis procedure to one section only but the results are approximate. Vecchio and Collins (1986) compared the shear-moment interaction predictions from the exact method with predictions assuming constant shear flow and parabolic shear strain profile for three different concrete sections. In all cases, the approximate predictions using the assumption of constant shear flow gave similar results to the exact procedure. As it will be shown later in this thesis, the constant shear flow is the basic assumption of the 2007 AASHTO LRFD and the 2006 CHBDC shear provisions for beam elements.

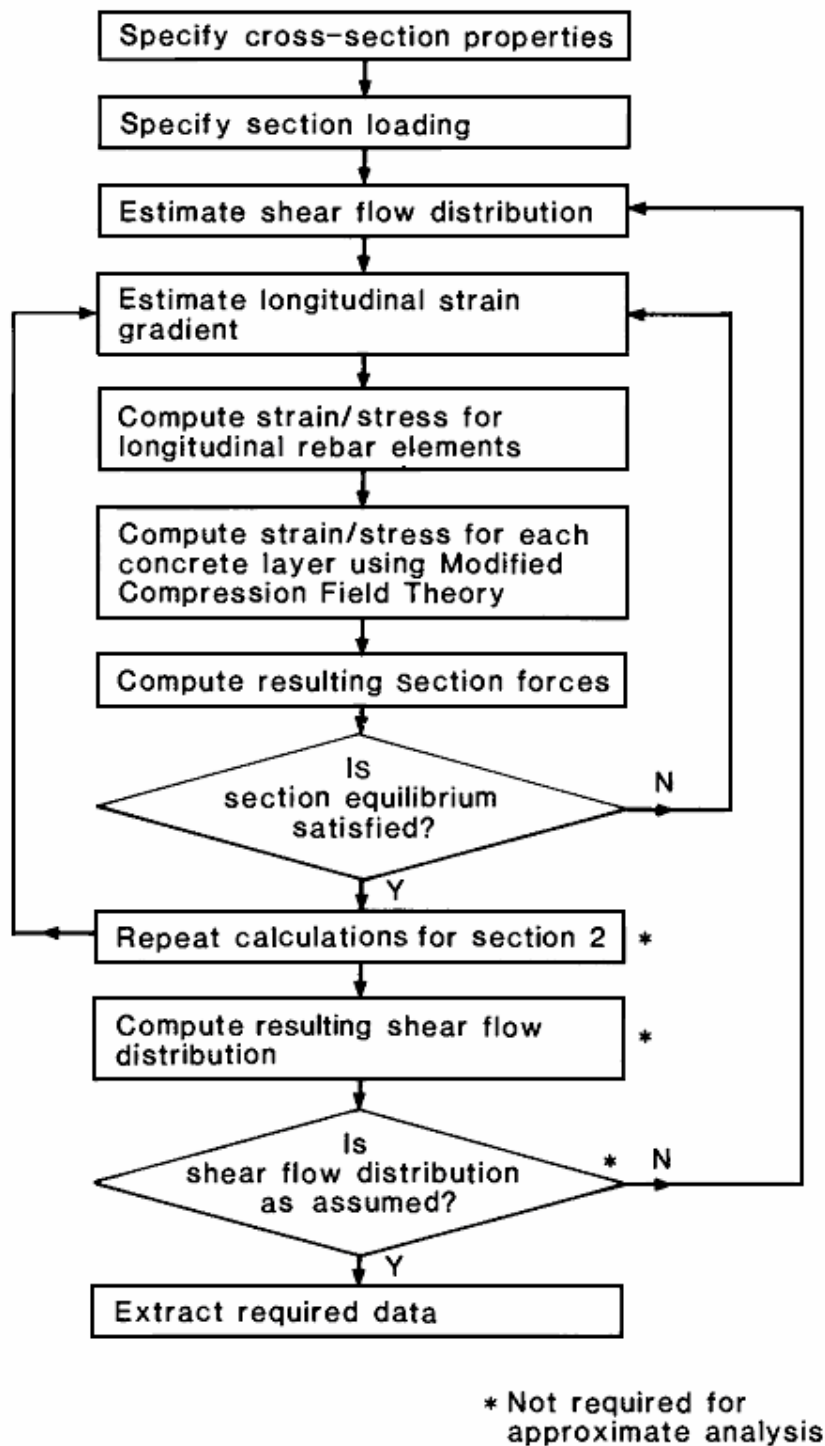


Fig. 4-3 Algorithm of MCFT exact solution procedure for beam elements (Vecchio and Collins, 1986).

4.2.1. Response 2000

Response 2000 (Bentz, 2000) is a computer program that applies the MCFT to beams using a multi-layer analysis. The unique aspect of Response 2000 is that instead of using dual sections to predict the shear flow distribution over the depth of a beam section, it uses tangent stiffness of layers meaning that it looks at two sections with infinitesimal distance apart instead. Response begins the analysis with an assumed shear flow distribution to determine the strains and stresses in the layers. Knowing strain condition of layers, stiffness of each layer can be determined using material constitutive laws of steel and concrete explained in Chapter 3. The layers tangent stiffness matrix will then be integrated over the depth to determine global stiffness matrix of the section which is then used to calculate shear strain and shear flow profiles from external forces acting at the section. The calculated shear strain profile is the assumed shear strain profile for the next iteration and the procedure is repeated until convergence is reached.

Response 2000 is a sophisticated research tool that provides detailed output of results including concrete and steel stresses and strains, shear on cracks, concrete angle of principal compression, crack spacing at all layers, and force deformation plots as well as shear-moment interaction diagrams. Figures 4-4 and 4-5 present some example output plots from Response 2000 for a typical prestressed I-girder cross-section used in bridges. The depth with darker color in the cross-section is an uncracked depth and the portion of transverse reinforcement that is yielding is also shown in darker color. Among other plots, Figure 4-4 shows the sectional profiles for principal compression stress and shear stress on cracks.

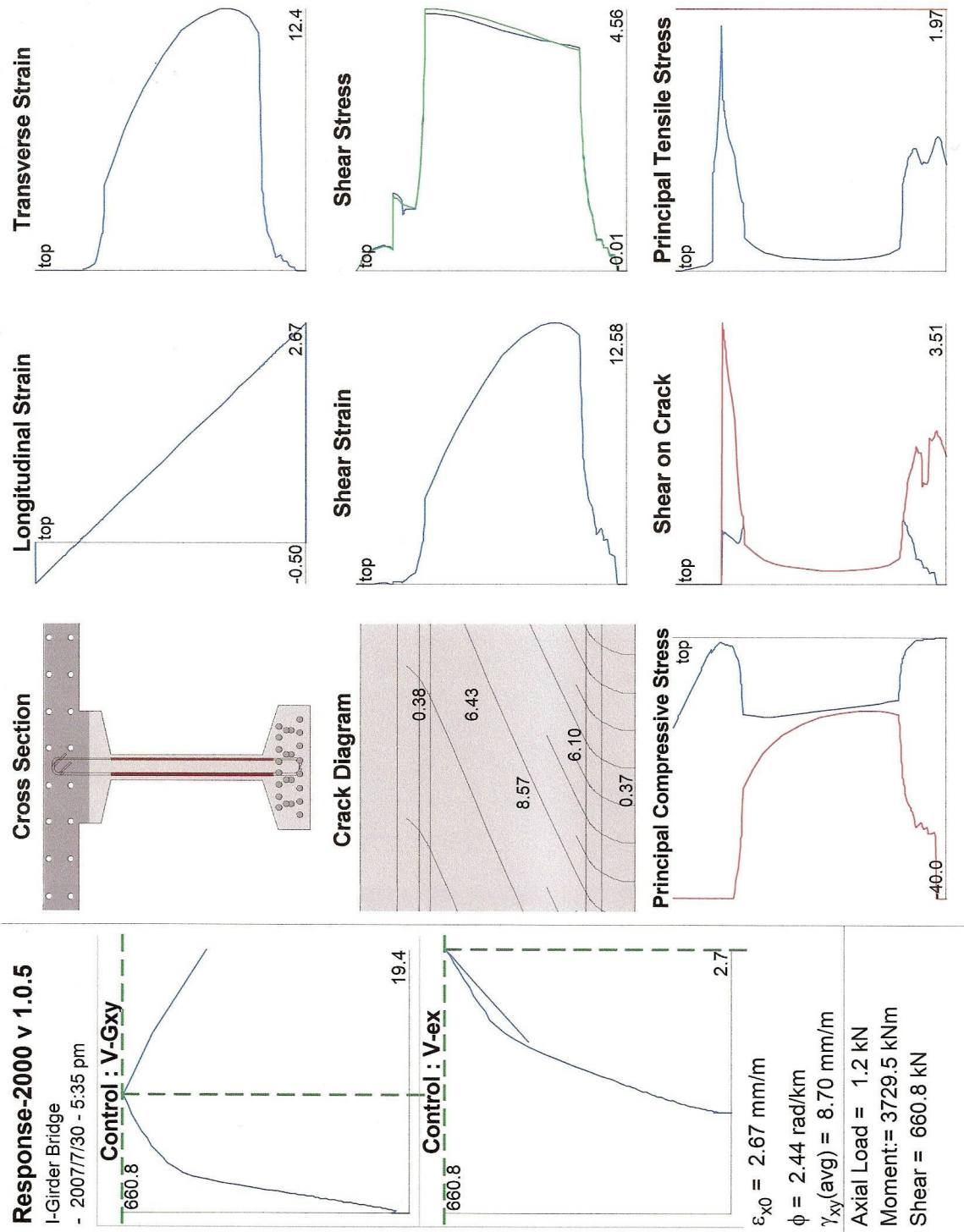


Fig. 4-4 Some output plots from computer program Response 2000.

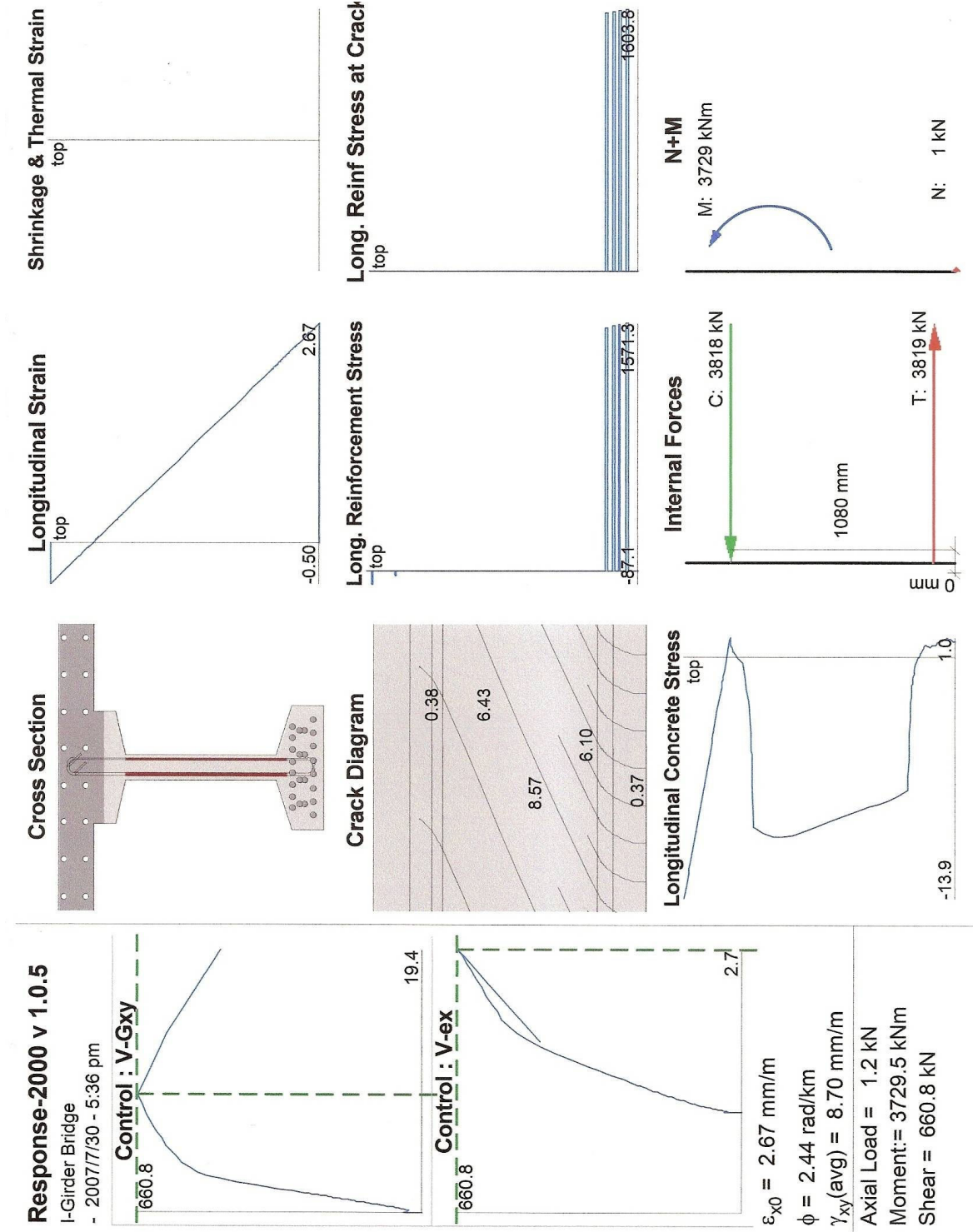


Fig. 4-5 Some output plots from computer program Response 2000.

The allowable stresses are also shown in a different color on the same plots. Two shear stress profiles in different colors are also provided. One is determined from MCFT equations for individual layers and the other one is determined from tangent stiffness method explained previously. As shown, the two profiles should be close if the analysis procedure has reached convergence.

Bentz (2000) verified Response 2000 against 534 tests reported in the literature on a variety of member types, and found a mean ratio of measured to predicted shear strength of 1.05 and a COV of 12%. In the report on the shear strength of bridge girders, Hawkins et al. (2005) compared Response 2000 predictions with the results of 149 tests they selected from a database of 1359 shear tests. They selected members that contained minimum transverse reinforcement ($\rho_z f_y > 50$ psi [0.35 MPa]), had an overall depth of at least 500 mm, and were cast from concrete having a compressive strength of at least 28 MPa. Also, tests in which anchorage or flexural failure occurred were not included. The 149 tests they selected included 85 prestressed concrete girders. They found a mean ratio of measured to predicted shear strength of 1.02 and 1.11, and a COV of 11% and 17% for reinforced and prestressed girders, respectively.

Response 2000 is not as appropriate for design and evaluation since different users may get different results by adjusting parameters such as material constitutive models and crack spacing options available in the program. Also, as the program was developed for investigating a number of sections in detail, it is not ideal for evaluating many different sections in a normal design office environment.

4.3. Simplified Procedures for Design

The shear design procedures in both the 2007 AASHTO LRFD and 2006 CHBDC are based on a single-layer shear analysis. The shear stress is assumed to be uniform over the shear depth d_v , which is estimated as $0.9d$. Similarly, the principal average compression stress (diagonal crack) angle θ and the longitudinal compression stress in concrete due to shear stress n_v are also both assumed to be constant over the shear depth d_v . For members with transverse reinforcement, the longitudinal strain ϵ_x used in the shear analysis is taken as the average value over the section, and for simplicity, this is estimated as half the strain of the flexural tension reinforcement. The longitudinal strain ϵ_x used in the shear analysis for members without transverse reinforcement is different in the two codes. It is equal to the maximum longitudinal strain in the 2007 AASHTO LRFD, while it is taken as the average longitudinal strain over the section in the 2006 CHBDC.

Both codes assume that bending moment is carried by the concrete compression chord and the tension chord reinforcement and the flexural internal lever-arm is equal to effective shear depth ($jd = d_v$). As a result of the assumption of uniform longitudinal compression stress over d_v , half of longitudinal compression force required for shear N_v is carried by the tension chord reinforcement and the other half is carried by the compression chord. These assumptions are shown in Figure 4-6.

As mentioned previously, both 2007 AASHTO LRFD and 2006 CHBDC methods assume that the effective shear depth can be idealized as one uniform shear element thus one longitudinal strain is needed to determine the maximum shear force taken by the effective shear depth. In 1994 AASHTO LRFD and the 2000 CHBDC, this strain was the maximum longitudinal strain over the shear depth, which is equal to the longitudinal

strain at the center of the flexural reinforcement, but this was later found to be too conservative for members with at least minimum transverse reinforcement. Consequently, the mid-depth strain was chosen as the longitudinal strain in the 2007 AASHTO LRFD and the 2006 CHBDC for members with at least minimum transverse reinforcement. In both codes, the mid-depth strain is approximated by half the maximum strain at the center of flexural tension reinforcement.

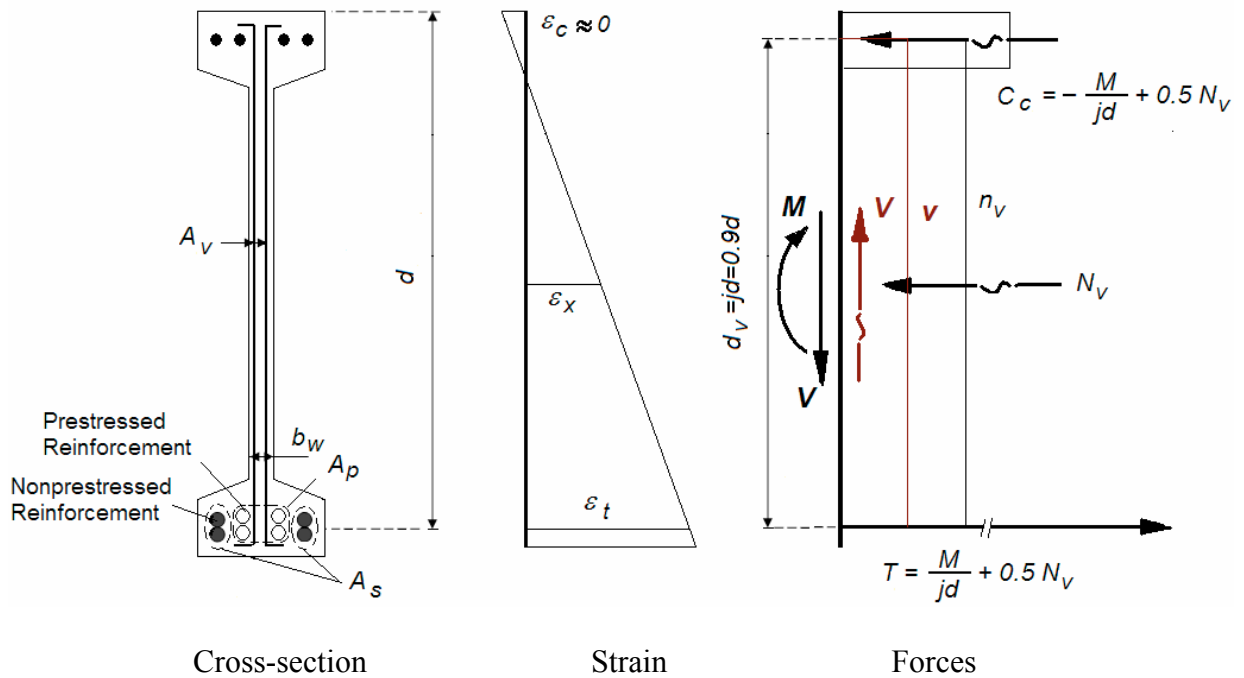


Fig. 4-6 2007 AASHTO LRFD and 2006 CHBDC approximate sectional model for beams subjected to shear and moment.

The maximum longitudinal strain is given by:

$$[4-1] \quad \epsilon_x = \frac{\frac{M}{jd} + 0.5 N_v - f_p A_p}{(E_s A_s + E_p A_p)}$$

in which $M/jd+0.5N_v$ is the force in the flexural tension reinforcement, $f_p A_p$ is prestressing force at zero longitudinal strain, and $(E_s A_s + E_p A_p)$ is the stiffness of flexural tension reinforcement. The mid-depth strain, which is taken as half the maximum longitudinal strain, is calculated from:

$$[4-2] \quad \varepsilon_x = \frac{\frac{M}{jd} + 0.5N_v - f_p A_p}{2(E_s A_s + E_p A_p)}$$

where: M = bending moment at section of interest; jd = internal flexural lever-arm (M/jd = flexural tension force); N_v = axial compression force needed to resist shear in web; A_s , A_p = area of nonprestressed and prestressed flexural tension reinforcement; and E_s , E_p = Modulus of Elasticity of nonprestressed and prestressed reinforcement, respectively.

As explained in Chapter 3, 2007 AASHTO LRFD and the 2006 CHBDC use Eqs. [4-3] and [4-4] for N_v , respectively. These equations are presented in the form of stresses in Chapter 3.

$$[4-3] \quad N_v = V \cot \theta$$

$$[4-4] \quad N_v = 2V$$

For members without transverse reinforcement, the 2006 CHBDC still uses the mid-depth strain thus uses Eq. [4-2] to calculate the longitudinal strain. In contrast, 2007 AASHTO LRFD uses the maximum longitudinal strain over the section depth given by Eq. [4-1].

To design a section by 2007 AASHTO LRFD, mid-depth strain is estimated to determine θ and β values from tables. The longitudinal strain ε_x can then be calculated from Eqs. [4-1] or [4-2]. This is repeated until the calculated ε_x is equal or less than the

estimated ε_x . Knowing θ and β , the required amount of transverse reinforcement can be calculated using Eq.[3-22]. In contrast, the 2006 CHBDC shear provisions do not require trial-and-error for design since ε_x is not a function of θ . ε_x is calculated from Eq. [4-2] where N_v is obtained from Eq. [4-4], θ and β are determined from Eqs. [3-30] and [3-29], and the required amount of transverse reinforcement is then given by Eq.[3-22]. Both methods require trial-and-error for shear strength evaluation as the longitudinal strain ε_x is a function of shear resistance (shear force at failure level) and shear resistance is not known until the evaluation is complete.

As stated earlier, θ s and β s in the 2007 AASHTO LRFD and the 2006 CHBDC are based on the assumption that there is enough capacity provided in the axial direction by longitudinal reinforcement at the cracks. To check the validity of this assumption, the codes require that:

$$[4-5] \quad F_t = \frac{M}{jd} + (V - 0.5V_s) \cot \theta$$

be equal to or greater than the top and the bottom chord longitudinal reinforcement capacity. The bending moment is negative if the equation is used for compression chord. In Eq. [4-5], M/jd is the demand on the flexural reinforcement due to the bending moment and $(V - 0.5V_s) \cot \theta$ is the demand on the flexural reinforcement due to the shear force. The demand $(V - 0.5V_s) \cot \theta$ due to the shear force is half the demand in uniform shear elements given by Eq. [3-28] as half N_v is assumed to be resisted by the flexural reinforcement in beam elements (see Fig. 4-6).

4.4. Proposed Evaluation Method for Members With At Least Minimum Transverse Reinforcement

Figure 4-7 shows the Response 2000 predictions for a typical prestressed I-girder at the point of transverse reinforcement yielding (dotted line) and concrete crushing (solid line). Information about the I-girder is provided in Section 4-7. The longitudinal strains vary linearly over the depth as shown in Fig. 4-7(b). The transverse shear flow (Fig. 4-7d) varies in a complex nonlinear way with the maximum value being in the deck slab, which is modeled composite with the girder. The inclination of the principal compression stress (Fig. 4-7c) varies from 0 on the top of the deck slab to 90 deg at the bottom face of the girder. Over the height of the web, the angle generally varies between 27 and 39 deg at transverse reinforcement yielding and between 24 and 26 deg at concrete crushing. The longitudinal concrete normal stress is multiplied by width of member (analogous to shear flow) in Fig. 4-7(e) to facilitate comparison with the proposed method prediction, which assumes a constant web width.

The proposed method uses a single shear analysis and thus assumes uniform shear stress over the shear depth d_v . The mid-depth strain is used as the longitudinal strain in the shear analysis. The actual shear stress is not uniform as shown in Fig. 4-7(d); however, the shear stress at mid-height is a reasonable estimate of the average shear stress. In the 2007 AASHTO LRFD and 2006 CHBDC simplified design procedures, the longitudinal concrete compression stress n_v required to resist shear is also assumed to be uniform over the shear depth d_v . Figure 4-7(e) indicates that n_v at mid-height is a reasonable estimate of n_v over the web region of the member; but is not a good estimate of the average n_v over the complete shear depth. The shear depth extends well into the deck slab, the maximum shear flow occurs in this region; however this portion of the

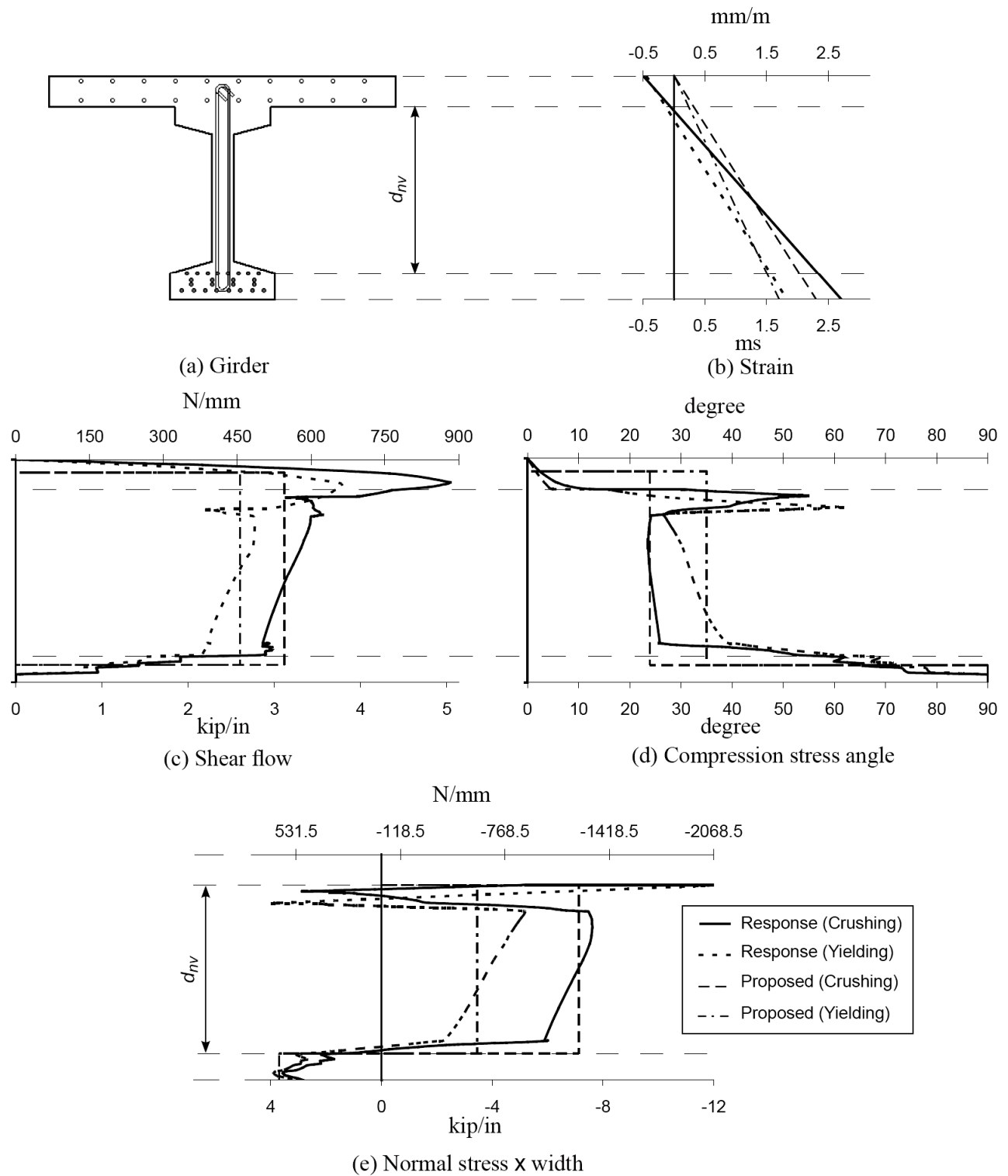


Fig. 4-7 Variation of shear response over depth of prestressed I-girder with composite deck slab: (a) cross-section, (b) longitudinal strain, (c) angle θ , (d) shear flow, (e) normal stress multiplied by width.

member does not experience any diagonal cracking and thus does not develop the additional longitudinal concrete compressive stresses n_v due to shear. There is flexural compression in the deck slab that is balanced by flexural tension and therefore should not be part of N_v . The longitudinal concrete compressive stresses due to shear n_v also do not extend down into the flexural tension flange. The concrete in this region is in tension, which helps to stiffen the reinforcement. Thus the n_v estimated at section mid-height is assumed to be uniform over a reduced depth d_{nv} from top of bottom flange to the bottom of top flange (see Fig. 4-7e). As a result, N_v is determined by longitudinal compression stress calculated from Eq. [3-40] multiplied by the effective area of $b_w d_{nv}$. The proposed equation for N_v is:

$$[4-6] \quad N_v = (n_{v0} + \Delta n_v \varepsilon_x) b_w d_{nv}$$

The tension stiffening effect of concrete in the tension flange of the girder, which has a cross-sectional area of A_{tf} , is also accounted for in the proposed method. This is done by assuming an average concrete tension force of $F_t = \alpha \sqrt{f'_c} A_{tf}$ over this area; where $\alpha = 0.165$ in MPa units (0.0125 in psi units). α is calculated from Eq. [3-5] assuming longitudinal strain of 0.002 at the center of flexural tension reinforcement. Another refinement in the proposed method is to accurately account for reinforcement in the web, which may be in any number of layers and be located at any elevations.

Figure 4-8 shows the beam approximate sectional model that is used in the proposed method. One layer of web nonprestressed reinforcement distanced d_w from the compression face and one layer of web prestressed reinforcement distanced d_{pw} from the compression face are shown. The longitudinal strain at the center of web nonprestressed

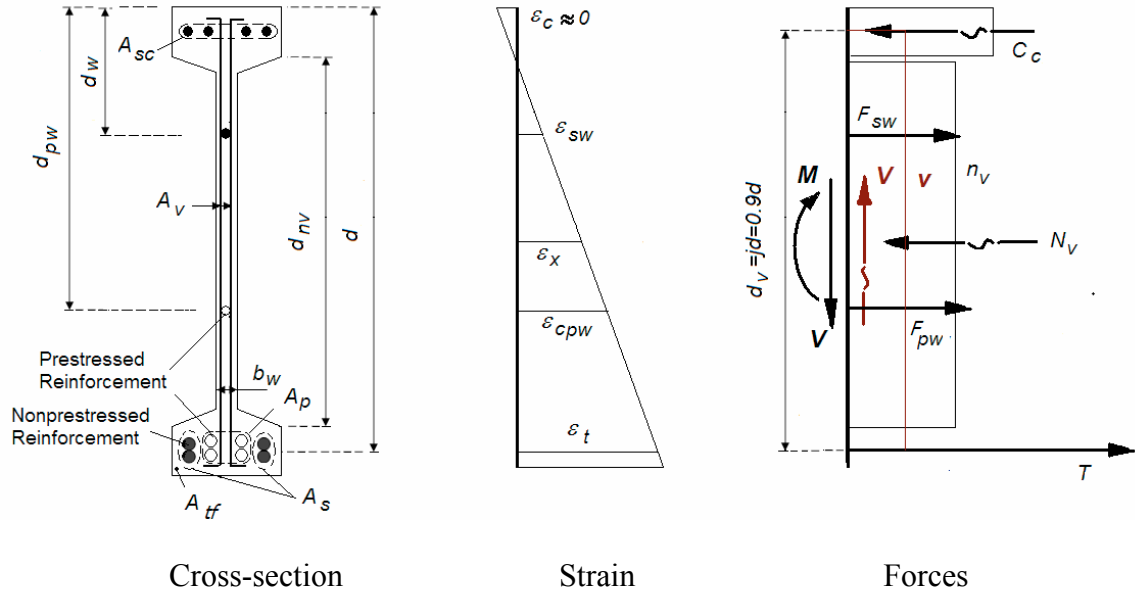


Fig. 4-8 Approximate beam strain profile and forces in the proposed method.

reinforcement is ε_{sw} and at the center of web prestressed reinforcement is ε_{cpw} . Thus the forces in the web nonprestressed and prestressed reinforcement are:

$$[4-7] F_{sw} = E_s A_{sw} \varepsilon_{sw}$$

$$[4-8] F_{pw} = E_p A_{pw} \varepsilon_{cpw} + A_{pw} f_p$$

where A_{sw} is web nonprestressed reinforcement area, A_{pw} is web prestressed reinforcement area, and f_p is prestressing force at zero strain. From strain compatibility and assuming extreme compression fiber strain is equal to zero:

$$[4-9] \varepsilon_{sw} = 2 \frac{d_w}{d} \varepsilon_x$$

$$[4-10] \varepsilon_{cpw} = 2 \frac{d_{pw}}{d} \varepsilon_x$$

A factor of 2.0 in Eqs. [4-9] and [4-10] comes from the assumption of mid-depth longitudinal strain ε_x is half the longitudinal strain at the center of the flexural tension

reinforcement. Substituting for ε_{sw} and ε_{cpw} from Eqs. [4-9] and [4-10] in Eqs. [4-7] and [4-8]:

$$[4-11] \quad F_{sw} = 2\lambda_s E_s A_{sw} \varepsilon_x$$

$$[4-12] \quad F_{pw} = 2\lambda_p E_p A_{pw} \varepsilon_x + A_{pw} f_p$$

where $\lambda_s = \frac{d_w}{d}$ and $\lambda_p = \frac{d_{pw}}{d}$. Force T in the flexural tension reinforcement shown in

Fig. 4-8 is determined from taking moments about the point of application of compression force C_c :

$$[4-13] \quad T = \frac{M}{jd} + 0.5N_v - \lambda_s F_{sw} - \lambda_p F_{pw}$$

In deriving Eq. [4-13], it is assumed that the distance from the point of application of C_c to the compression face is very small and almost equal to zero. Substituting for F_{sw} and F_{pw} from Eqs. [4-11] and [4-12] and for N_v from Equation [4-6]:

$$[4-14] \quad T = \frac{M}{jd} + 0.5(n_{v0} + \Delta n_v \varepsilon_x) b_w d_{nv} - 2\lambda_s^2 E_s A_{sw} \varepsilon_x - 2\lambda_p^2 E_p A_{pw} \varepsilon_x - \lambda_p A_{pw} f_p$$

The mid-depth longitudinal strain, which is assumed to be equal to half the longitudinal strain at the center of flexural tension reinforcement, is determined from:

$$[4-15] \quad \varepsilon_x = \frac{T - \alpha \sqrt{f_c'} A_{tf} - f_p A_p}{2(E_s A_s + E_p A_p)}$$

where, as explained previously, $\alpha \sqrt{f_c'} A_{tf}$ is the force in the tension chord resisted by concrete tension stiffening and $f_p A_p$ is the force in the prestressed reinforcement at zero longitudinal strain. Substituting for T from Eq. [4-14] and solving for ε_x , the proposed equation for mid-depth strain is:

$$[4-16] \quad \varepsilon_x = \frac{M / jd + 0.5n_{v0}b_w d_{nv} - \alpha\sqrt{f'_c}A_{tf} - f_p(A_p + \lambda_p A_{pw})}{2 [E_s(A_s + \lambda_s^2 A_{sw}) + E_p(A_p + \lambda_p^2 A_{pw})] - 0.5 \Delta n_v b_w d_{nv}}$$

The longitudinal strain at section mid-height is assumed to be half the strain of the flexural tension reinforcement. This is generally a conservative assumption as the strain on the opposite face is usually compressive (see Fig. 4-7b). If the bending moment is small and the shear force is large, the section may be subjected to tension strains over the full depth. This would be the case if total force in compression chord C_c shown in Fig. 4-8 is greater than zero. In that case, the section mid-height strain calculated by Eq. [4-16] should be multiplied by 2. From Equilibrium and strain compatibility using the same procedure used to determine T , C_c is given by:

$$[4-17] \quad C_c = -\frac{M}{jd} + 0.5(n_{v0} + \Delta n_v \varepsilon_x) b_w d_{nv} - 2(1 - \lambda_s) \lambda_s E_s A_{sw} \varepsilon_x - 2(1 - \lambda_p) \lambda_p E_p A_{pw} \varepsilon_x - (1 - \lambda_p) A_{pw} f_p$$

For typical problems, nonprestressed reinforcement may be assumed to be uniformly distributed over the full web centered at mid-depth. For such cases, Eqs. [4-16] and [4-17] can be simplified to:

$$[4-18] \quad \varepsilon_x = \frac{M / jd + 0.5n_{v0}b_w d_{nv} - \alpha\sqrt{f'_c}A_{tf} - f_p(A_p + \lambda_p A_{pw})}{2 [E_s(A_s + 0.25 A_{sw}) + E_p(A_p + \lambda_p^2 A_{pw})] - 0.5 \Delta n_v b_w d_{nv}}$$

$$[4-19]$$

$$C_c = -\frac{M}{jd} + 0.5(n_{v0} + \Delta n_v \varepsilon_x) b_w d_{nv} - 0.5 E_s A_{sw} \varepsilon_x - 2(1 - \lambda_p) \lambda_p E_p A_{pw} \varepsilon_x - (1 - \lambda_p) A_{pw} f_p$$

Note area of flexural tension reinforcement A_s in denominator of Eq. [4-18] is multiplied by a factor of 4 compared to area of longitudinal reinforcement A_{sw} centered in the web. A factor of 2 comes from the assumption that mid-height strain is half the strain of the flexural tension reinforcement and a second factor of 2 comes from the need to provide

twice as much reinforcement at section mid-depth to resist bending compared reinforcement on the flexural tension face.

Unlike the other simplified procedures, ε_x equation in the proposed method is not a function of shear resistance but is a function of section geometry, amount of reinforcement and material properties. These variables are known in evaluation problems thus ε_x can be determined without a need for trial-and-error. Once ε_x is known β and θ are known from Eq. [3-31] to [3-37]; therefore section shear strength can be calculated from Eq. [3-22] without trial-and-error. Note that ε_x and the corresponding shear strength should be evaluated at yielding of transverse reinforcement and concrete crushing failure modes using the same equations for ε_x and θ (Eqs. 4-16 and 3-31), but the parameters β , n_{v0} , Δn_v , θ_0 , $\Delta\theta$ have different values at each failure mode (see Eqs. 3-32 to 3-37 and 3-41 to 3-44). For yielding of longitudinal reinforcement, another approach explained in the next section is used.

In the case of multiple layers of nonprestressed and prestressed reinforcement in the web, Eqs. [4-16] and [4-17] can be expressed in a more general form as:

$$[4-20] \varepsilon_x = \frac{M / jd + 0.5n_{v0}b_w d_{nv} - \alpha\sqrt{f_c'}A_{tf} - f_p(A_p + \sum_{i=1}^n \lambda_{pi}A_{pwi})}{2[E_s(A_s + \sum_{j=1}^m \lambda_j^2 A_{swj}) + E_p(A_p + \sum_{i=1}^n \lambda_{pi}^2 A_{pwi})] - 0.5\Delta n_v b_w d_{nv}}$$

$$C_c = -M / jd + 0.5n_{v0}b_w d_{nv} + \varepsilon_x[0.5\Delta n_v b_w d_{nv} - 2\sum_{j=1}^m \lambda_j(1-\lambda_j)E_s A_{swj} - 2\sum_{i=1}^n \lambda_{pi}(1-\lambda_{pi})E_p A_{pwi}]$$

$$- \sum_{i=1}^n (1-\lambda_{pi})f_p A_{pwi}$$

where m and n are number of layers of nonprestressed and prestressed reinforcement in the web, A_{pwi} and A_{swj} are total area of the i^{th} and j^{th} layer of prestressed and

nonprestressed reinforcement. The parameters $\lambda_{pi} = d_{pwi} / d$ and $\lambda_j = d_{wj} / d$ are used to account for the location of prestressed and nonprestressed reinforcement in the web where d_{pwi} is the distance from the flexural compression face to centroid of i^{th} layer of web prestressed reinforcement and d_{wj} is the distance from the flexural compression face to centroid of j^{th} layer of web nonprestressed reinforcement.

4.4.1. Evaluation at Yielding of Longitudinal Reinforcement

In the proposed method, shear strength of a section is limited to the shear force causing biaxial yielding of reinforcement at the crack. The stress corresponding to this shear force is determined from Eq. [3-45]. Expressing Eq. [3-45] in terms of forces, the shear force which causes biaxial yielding of reinforcement is given by:

$$[4-21] \quad V \leq \sqrt{\rho_z f_y (b_w d_v) N_{vc}}$$

where N_{vc} is the longitudinal compression force reserved for shear. Assuming all longitudinal nonprestressed reinforcement has yielded and all longitudinal prestressed reinforcement has reached their capacity f_{pr} in Figure 4-8:

$$[4-22] \quad T = A_s f_y + A_p f_{pr}$$

$$[4-23] \quad F_{sw} = A_{sw} f_y$$

$$[4-24] \quad F_{pw} = A_{pw} f_{pr}$$

Substituting for T , F_{sw} , and F_{pw} in Eq. [4-13] and solving for N_v , the axial compression force reserved for shear in the flexural tension reinforcement is given by:

$$[4-25] \quad N_{vc} = 2 \left[f_y (A_s + \lambda_s A_{sw}) + f_{pr} (A_p + \lambda_p A_{pw}) - M / jd \right]$$

Similarly, the same procedure for the compression side results in Eq. [4-26] for the axial compression force reserved for shear in the flexural reinforcement in the compression chord.

$$[4-26] \quad N_{vc} = 2 \left[f_y (A_{sc} + (1 - \lambda_s) A_{sw}) + f_{pr} (1 - \lambda_p) A_{pw} + M / jd \right]$$

Equation [4-21] must be evaluated separately for the flexural tension and flexural compression sides of the member and the smaller value controls the shear strength.

In Eqs. [4-25] and [4-26], the internal flexural lever-arm jd has a direct influence on longitudinal reinforcement force and therefore the reserved capacity in longitudinal reinforcement to resist shear. In the 2006 CHBDC, jd is estimated as $0.9d$. Response 2000 predictions for numerous sections that failed due to biaxial yielding of reinforcement showed that a more accurate estimate is given by:

$$[4-27] \quad jd = d - \frac{f_{pr} A_p + f_y A_s}{1.2 f_c' b_f}$$

where b_f is the compression face width of the section. In Eq. [4-27], the average flexural compression stress over the concrete flexural compression zone is assumed to be $0.6 f_c'$.

4.4.2. Governing Failure Mode

Figure 4-9 depicts typical shear stress-shear strain relationships for reinforced concrete beams. Solid lines show the typical curves if yielding of longitudinal reinforcement does not limit the shear strength. Such cases involve yielding of transverse reinforcement and concrete crushing failure modes and the higher of these two is the governing failure mode that determines the shear strength. Dashed lines illustrate possible changes in the curves if longitudinal reinforcement yields prior to yielding of transverse reinforcement or after yielding of transverse reinforcement. In the upper curve shown in Fig. 4-9 the shear stress

increases after yielding of transverse reinforcement until concrete crushes. In the lower curve the shear stress reduces after yielding of transverse reinforcement. When longitudinal reinforcement yields before yielding of transverse reinforcement in both curves, the shear stress increases up until yielding of transverse reinforcement and then remains constant. In such cases, biaxial yielding of reinforcement failure mode is the highest shear stress throughout the loading and thus is the governing failure mode.

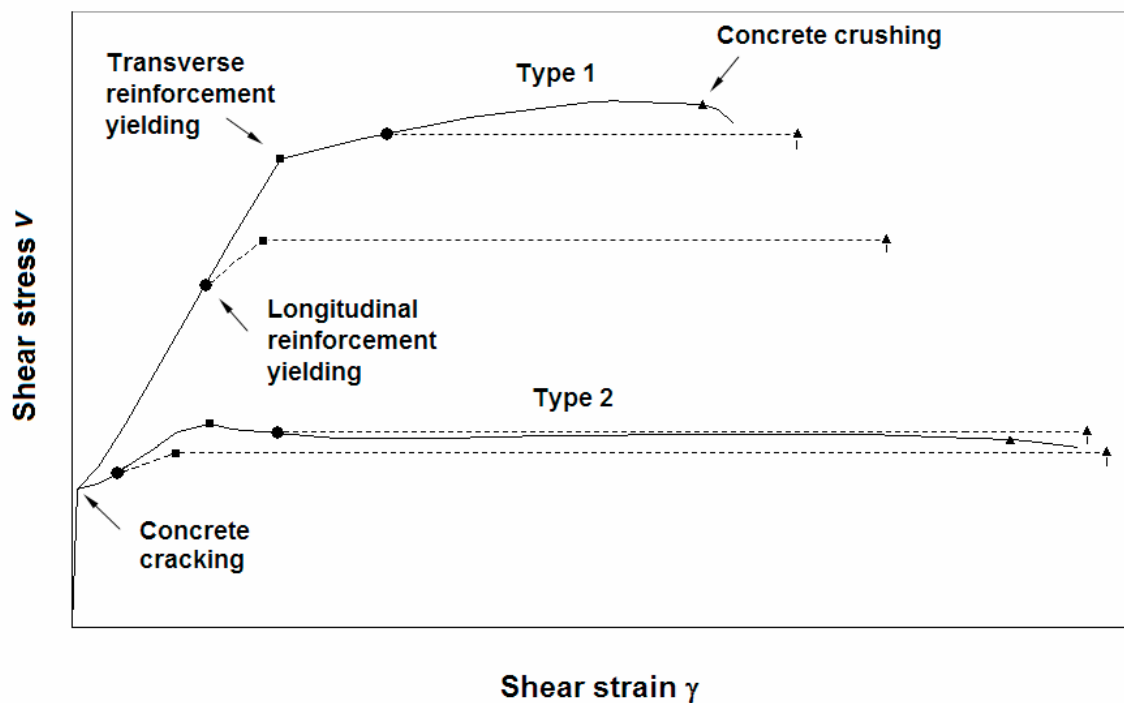


Fig. 4-9 Typical shear stress-strain relationships for beams.

Another possibility is that longitudinal reinforcement yields after transverse reinforcement yielding. If this happens, shear stress remains almost unchanged after longitudinal reinforcement yielding until concrete crushes (see Fig. 4-9). However, this shear stress is only the highest and governing shear stress throughout the load deformation curve if the concrete crushing shear stress is higher than the shear stress

corresponding to yielding of transverse reinforcement (curve type 1). For the type 2 curve, on the other hand, yielding of transverse reinforcement is the governing failure mode since it corresponds to the highest shear stress in the load deformation curve.

If the shear strength corresponding to the biaxial yielding of reinforcement is lower than yielding of transverse reinforcement shear stress for curve type2, the problem would be how to determine whether longitudinal reinforcement yielding has happened prior to or after yielding of transverse reinforcement. This can be examined by checking the condition given by Eq. [4-5] at transverse reinforcement yielding stage; longitudinal reinforcement will yield after transverse reinforcement yielding if the condition is satisfied. Since curve type 2 corresponds to sections with low amount of transverse reinforcement close to minimum in which concrete crushing shear stress is not significantly lower than transverse reinforcement yielding shear stress, the proposed method uses the biaxial reinforcement yielding shear strength as the governing shear strength if it is lower than any of the other two failure modes. In summary, the governing failure mode in the proposed method is:

- V_{yield} if greater than V_{crush} and less than $V_{biaxial}$
- V_{crush} if greater than V_{yield} and less than $V_{biaxial}$
- $V_{biaxial}$ if less than $\text{Max} (V_{yield} , V_{crush})$

where V_{yield} , V_{crush} , and $V_{biaxial}$ are the beam shear strength corresponding to yielding of transverse reinforcement, crushing of concrete, and biaxial yielding of reinforcement, respectively. As explained in Chapter 3, the governing failure mode should not be greater than $0.25f'_c b_w d_v$ to avoid concrete crushing prior to transverse reinforcement yielding.

4.5. Proposed Evaluation Method for Members Without Transverse Reinforcement

Fig. 4-10 shows the Response 2000 predictions for a reinforced concrete beam (Fig. 4-10a) without transverse reinforcement at the maximum applied shear force. The longitudinal strains are assumed to vary linearly over the depth (Fig. 4-10b), while the transverse strain (Fig. 4-10c) is highly nonlinear and the maximum value is mid-way between the flexural tension reinforcement and the section mid-depth. The shear stress distribution (Fig. 4-10d) is not uniform; but can be reasonably approximated as uniform over the shear depth d_v .

Fig. 4-10(e) examines the distribution of longitudinal normal stress over the beam depth. The flexural compression over the top third of the beam is very prominent. The tension force needed to equilibrate this compression is calculated as part of the flexural analysis. Immediately below the flexural compression zone, there is a peak tension stress, and below that, the beam is diagonally cracked. Over the diagonally cracked portion of the beam, there are small longitudinal compression stresses. In fact, the tension stresses above the diagonal cracks and the tension stiffening (average tension stresses in cracked concrete) around the longitudinal reinforcement are larger than the longitudinal compression. In Chapter 3, it is shown that the longitudinal compression stress n_v is small and can be assumed equal to zero for a uniform shear element without transverse reinforcement. The assumption of no longitudinal compression force due to shear in a diagonally cracked member without transverse reinforcement is even more valid for a beam than a uniform shear element as shown in Figure 4-10(e).

Numerous analyses of members without stirrups (similar to that shown in Fig. 4-10) indicated that the maximum transverse strain typically occurs mid-way between the level

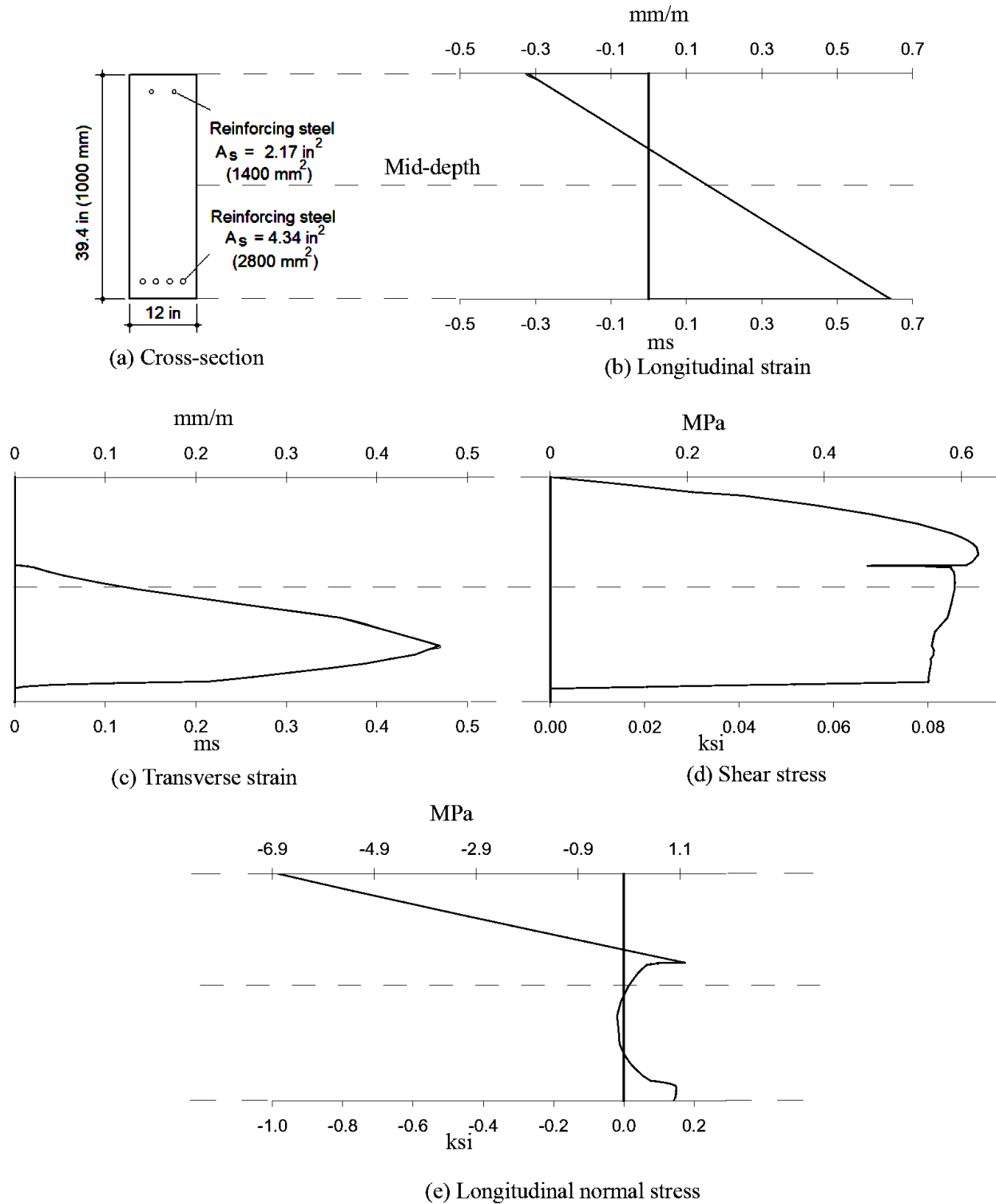


Fig. 4-10 Response 2000 predictions for variation of shear response over the depth of a beam, $M/V = 2.0 \text{ m}$, $f_y = 550 \text{ MPa}$, $f_c' = 20 \text{ MPa}$.

of the flexural tension reinforcement and the section mid-depth as shown in Fig. 4-10(c). Thus in the proposed procedure, the longitudinal strain ε_x used in the shear analysis for members without stirrups is the maximum longitudinal strain divided by 1.5. As in the 2006 CHBDC and 2007 AASHTO LRFD methods, the shear flow is uniform over the effective shear depth d_v .

Assuming the axial compression force due to shear and tension stiffening force in the tension chord are zero, accounting for the tension force resisted by distributed non-pressed reinforcement, and accounting for the prestressing tendons in the web, the same procedure used to derive Eq. [4-18] results in the following proposed longitudinal strain:

$$[4-28] \quad \varepsilon_x = \frac{M / jd - f_p (A_p + \lambda_p A_{pw})}{1.5 [E_s (A_s + 0.25 A_{sw}) + E_p (A_p + \lambda_p^2 A_{pw})]}$$

Since ε_x is not a function of shear demand or angle of principal compression, the proposed method does not require trial-and-error for evaluation.

While the influence of longitudinal compression due to shear is negligible in the proposed method when calculating the axial strain of the member, it cannot be ignored when checking whether the longitudinal reinforcement yields at a diagonal crack. The longitudinal compression stress required locally at diagonal cracks to resist shear is much larger than the average longitudinal compression stress, and is given by MCFT as:

$$[4-29] \quad N_v^* = 2V_c \cot \theta$$

Thus the longitudinal reinforcement yields if this axial compression force (N_v^*) is greater than reserved axial compression force in the tension or compression chords given by Equations [4-25] and [4-26]. For cases in which longitudinal reinforcement yields, the shear strength is taken as:

$$[4-30] \quad V = \frac{N_{vc}}{2}$$

which is determined by solving Eq. [4-29] for V_c with θ equal to 45 degrees. MCFT results shown in Fig. 3-34 indicate that angle of principal compression is mostly greater than 45 degrees thus 45 deg is generally a conservative assumption. Note that the higher the angle, the more conservative the predictions for members with no stirrups. This is because the angle for such members is only used to determine shear demand on longitudinal reinforcement.

4.6. Members With Less than Minimum Transverse Reinforcement

In the 2006 CHBDC and 2007 AASHTO LRFD shear design provisions, minimum amounts of transverse reinforcement are different. Thus one of these minimum amounts was selected to be used in the proposed method. The 2006 CHBDC requirements for minimum amount of transverse reinforcement ρ_{zmin} and maximum transverse reinforcement spacing s_{max} are:

$$[4-31] \quad \rho_{zmin} = 0.060 \frac{\sqrt{f_c'}}{f_y}$$

$$[4-32] \quad s_{max} = 0.75d_v \leq 600 \text{ mm for } v_u < 0.10f_c'$$

$$[4-33] \quad s_{max} = 0.33d_v \leq 300 \text{ mm for } v_u \geq 0.10f_c'$$

The minimum percentage of transverse reinforcement is 38% larger in 2007 AASHTO LRFD but the maximum permitted spacing of this reinforcement is slightly larger. Comparison of shear strength predictions from the proposed method with beam test results in Chapter 5 shows that the proposed evaluation procedure can reasonably predict the shear strength of beams with transverse reinforcement amount as low as the 2006

CHBDC minimum amount. Consequently, the 2006 CHBDC minimum amount of transverse reinforcement was adopted in the proposed method.

In the 2006 CHBDC and 2007 AASHTO LRFD shear design provisions, if a section has less than the minimum amount of transverse reinforcement, the shear strength is calculated assuming no transverse reinforcement. Angelakos et al. (2001) found that this approach results in a conservative estimate of shear strength for members with slightly less than the minimum transverse reinforcement. Based on the results of 21 large reinforced concrete beam tests, they proposed that the shear strength increase linearly from the shear strength of a member with no stirrups to the shear strength of the member with minimum stirrups. In the evaluation section, the 2006 CHBDC recommends the same approach; but the linear increase in shear strength starts when the member has more than one-third of the minimum transverse reinforcement. Members with less than one third of minimum transverse reinforcement are assumed to have the same shear strength as members with no transverse reinforcement. In the proposed method, the 2006 CHBDC linear approach was adopted for members with less than minimum transverse reinforcement based on comparison of the shear strength predictions from the proposed method with the experimental results that is presented in Chapter 5.

4.7. Example Evaluations of Bridge Girder With at Least Minimum Transverse Reinforcement

The trends predicted by the proposed expressions for inclination of diagonal cracks θ , concrete contribution factor β , total shear stress v , and longitudinal compression stress n_v for an element subjected to uniform shear were compared with MCFT in Chapter 3. In order to verify the complete shear strength evaluation procedure including the

assumptions used to apply the uniform shear approach to bridge girders, the results obtained for three example bridge girders are compared with the results obtained using computer program Response 2000. The predicted shear strengths determined from the 2007 AASHTO LRFD, 2006 CHBDC, and ACI 318 shear design methods are also presented. Note that the 2008 AASHTO LRFD shear design provisions are similar to the 2006 CHBDC shear design provisions.

Figure 4-11 shows the cross-sections of the three different girders in the three bridges. The following material properties were assumed in all cases: $f_c' = 40$ MPa, $f_y = 400$ MPa, $f_{pu} = 1860$ MPa, and $E_p = E_s = 200000$ MPa. In order to compare resistances from different codes, the nominal resistances (without resistance factors) were calculated.

The I-girder bridge is a 21 m single span bridge with six prestressed concrete I-girders spaced at 2 m. The cross-section of the girders near the support is shown in Fig. 4-11(a). The four prestressing tendons near the top of the web are draped toward the bottom flange at 7.75 m from the support. The bridge transverse reinforcement ratios change from $\rho_z = 0.834\%$ to 0.437% and from $\rho_z = 0.437\%$ to 0.327% at locations of 7.32 m and 8.69 m from the supports. The box-girder bridge has a single span of 29.80 m and consists of nine prestressed concrete box girders. The cross-section of the girders near the support is shown in Fig. 4-11(b). The 16 prestressing tendons distributed over the web are draped toward the bottom half of the web at 11.91 m from the support. The channel-girder (Fig. 4-11c) bridge consists of 14 precast nonprestressed channel girders interconnected by reinforcing bars grouted in place. Each of the simple spans of this multi-span bridge is 8.40 m.

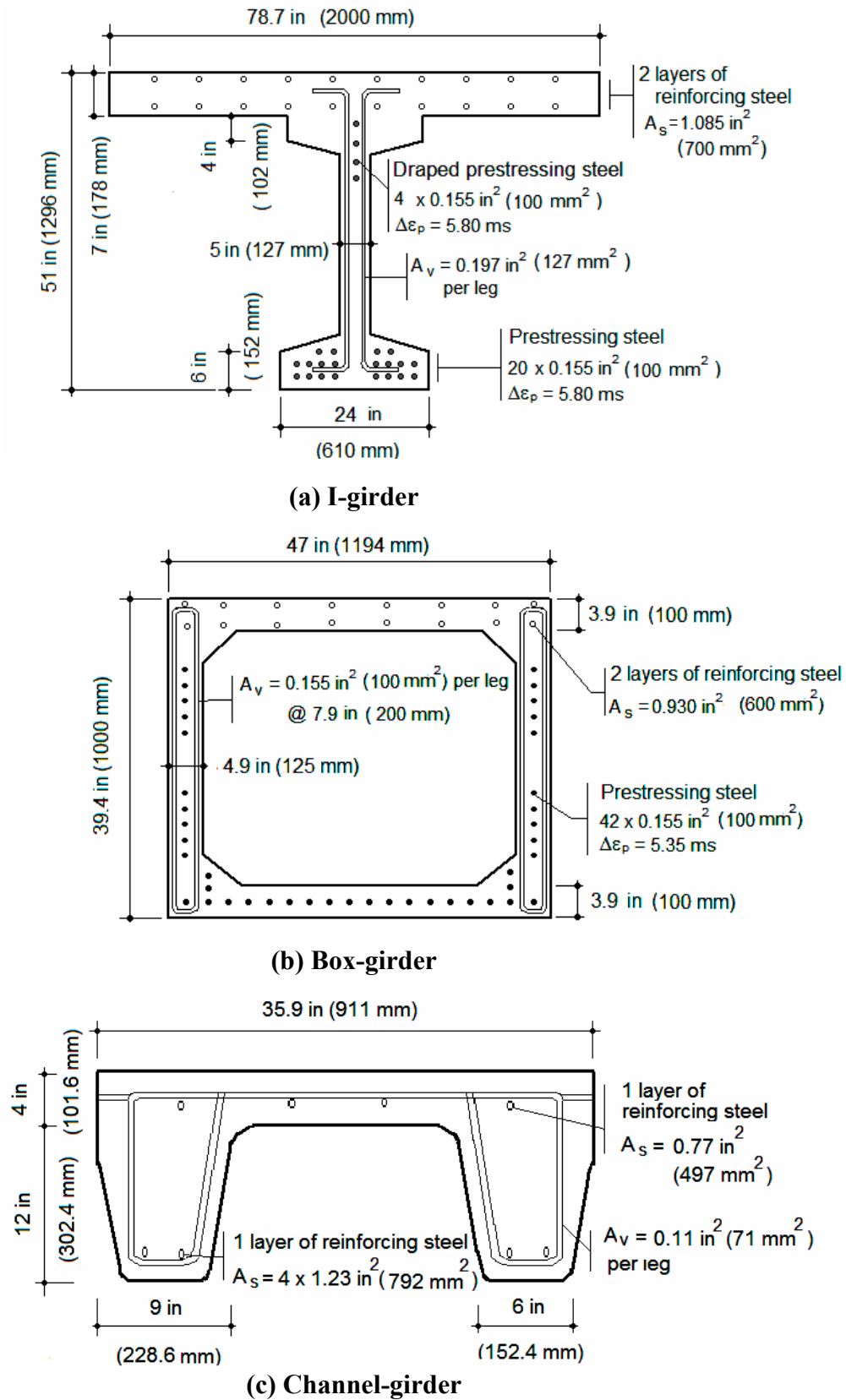


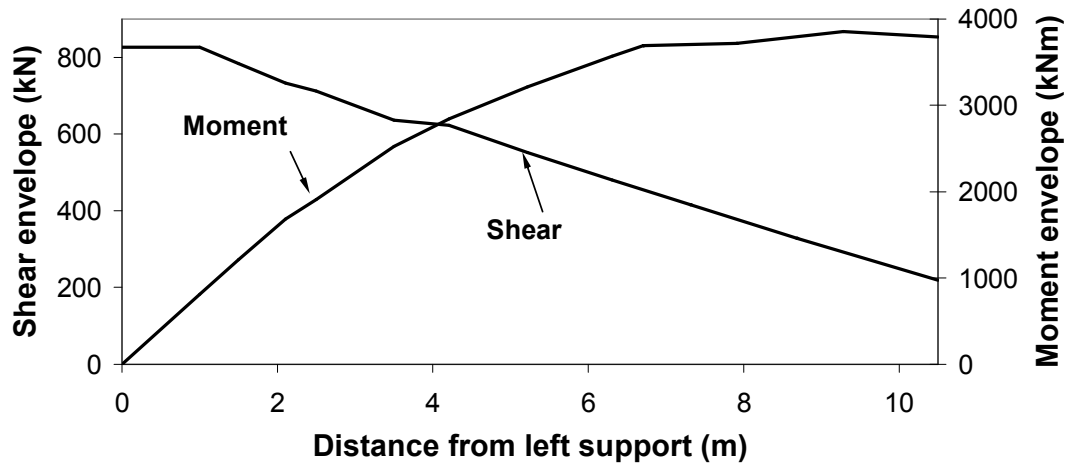
Fig. 4-11 Cross-sections of girders in example bridges.

The bridge girder amounts of transverse reinforcement change from $\rho_z = 0.588\%$ to 0.294% and from $\rho_z = 0.294\%$ to 0.098% at locations of 1.39 m and 1.75 m from the supports. All bridges had two traffic lanes.

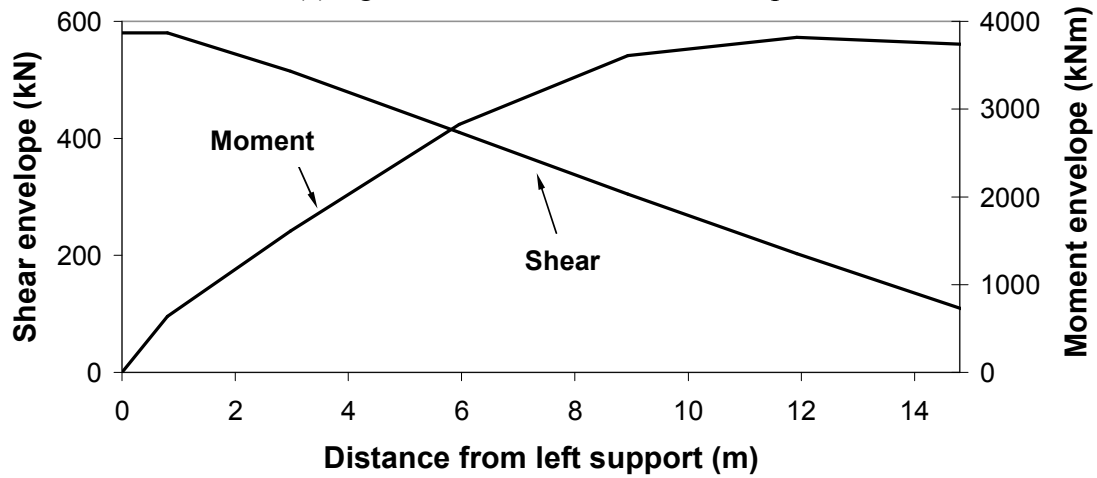
Bridge live load (truck load) for I-girder Bridge consisted of CHBDC standard truck with five axels and total weight of 625 kN in addition to one special permit truck with eight or 11 axles and total weight of 839 kN (85.5 tonnes) or 1699 kN (173.2 tonnes). For the other two bridges, however, the CHBDC standard truck or 839 kN (85.5 tonnes) permit truck were only used. Lane load and dynamic allowance factor, as well as a multi-lane reduction factor were included as per the 2006 CHBDC. The load factors were based on the 2006 CHBDC for Level 2 Inspection. Live load was transversely distributed according to the 2006 CHBDC. Factored moment and shear envelope diagrams for all three bridges are shown in Figure 4-12. Appendix D includes information of the trucks used for evaluation in this thesis.

The bridge girders were evaluated at a number of sections along the span. At locations where the spacing of transverse reinforcement changes, the shear strength was assumed to linearly vary from shear strength of the section with lower amount of transverse reinforcement to shear strength of the section with higher amount of transverse reinforcement over the length d_v centered at the location of change in the amount of transverse reinforcement. This is permitted in the 2006 CHBDC evaluation section.

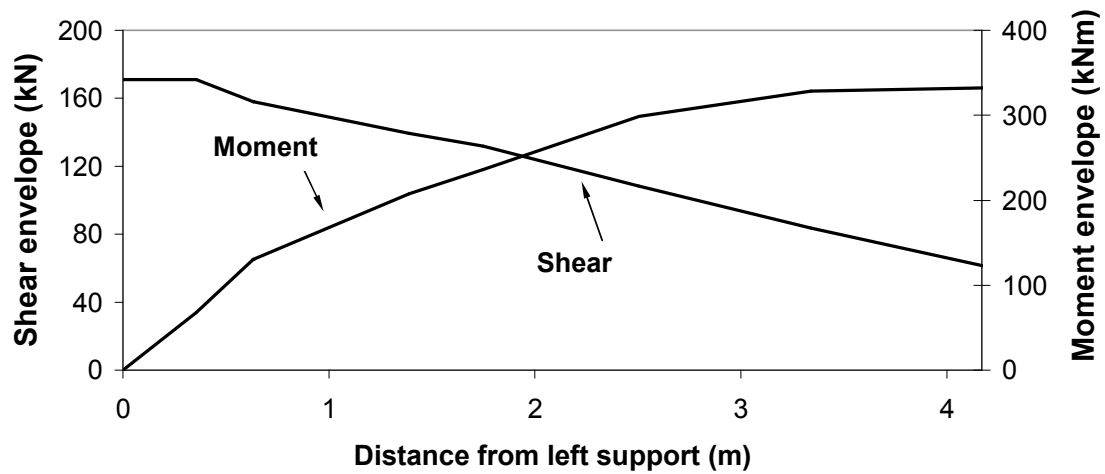
At each section, evaluation was done at a constant moment equal to the factored moment demand corresponding to maximum shear demand acting at that section. To evaluate the example bridge girders by the 2006 CHBDC method, shear capacity was estimated and ε_x was calculated accordingly.



(a) I-girder shear and moment envelopes



(b) Box-girder shear and moment envelopes



(c) Channel-girder shear and moment envelopes

Fig. 4-12 Moment and shear envelopes of evaluated bridges with minimum stirrups.

Using ε_x , θ and β were determined, and shear capacity was calculated. The same procedure was repeated until the estimated shear capacity was equal to the calculated shear capacity.

To evaluate example bridge girders by the 2007 AASHTO method, θ and β were first estimated. Shear capacity was then calculated using the estimated θ , β . Subsequently, ε_x was determined substituting the calculated shear capacity and estimated angle in the equation for longitudinal strain ε_x . Entering the tables with ε_x and shear capacity ratio (v/f_c'), θ and β were determined; linear interpolation was used for intermediate values. The same procedure was repeated until the estimated θ and β were equal to the θ and β extracted from the tables.

To evaluate prestressed bridge girders by the ACI 318 shear design method, the well known V_{ci} , V_{cw} approach was used to determine the concrete contribution. For V_{ci} calculations, it was assumed that top deck concrete weight as well as girder weight is supported by girders only while other added load (wearing and live loads) are supported by composite action of deck and girders. For the channel-girder bridge, which was nonprestressed, V_c was assumed to be $2\sqrt{f_c'}b_wd$ in psi units ($0.17\sqrt{f_c'}b_wd$ in MPa units) as specified by ACI 318.

4.7.1. Comparison of Results for I-girder Bridge

The variation of predicted strengths over about half the span of the I-girder is shown in Fig. 4-13. Both the proposed method and Response 2000 can predict the shear strength at yielding of transverse reinforcement and crushing of concrete.

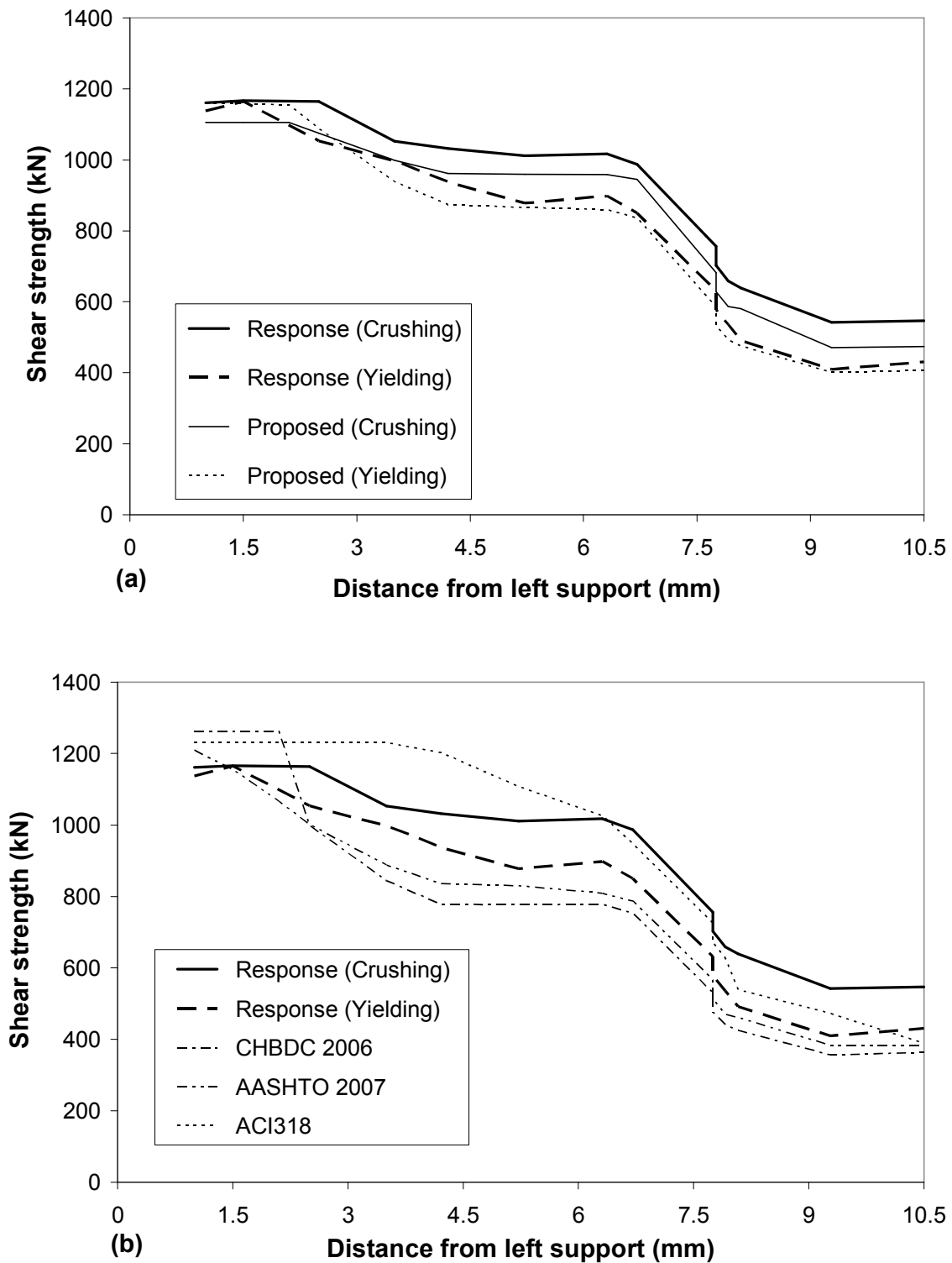


Fig. 4-13 Comparison of predicted shear strengths along span of I-girder bridge: (a) Response 2000 and proposed method, (b) Response 2000 and code design methods.

Figure 4-13(a) compares the shear strength determined from Response 2000 and the proposed method for the concrete crushing mode (solid lines) and transverse reinforcement yielding mode (dashed lines). Generally, there is very good agreement along the span. Note that the information presented in Fig. 4-7 is for the I-girder explained here at 7.92 m from the support.

Fig. 4-13(b) compares the shear strength from Response 2000 with shear strengths according to the 2007 AASHTO LRFD, 2006 CHBDC and ACI 318 shear design methods. 2007 AASHTO LRFD gives a safe prediction almost all along the span; the predictions become slightly unconservative near the support. The 2006 CHBDC shear design method gives an unsafe prediction near the support where the axial strains are very low. On the other hand, the method gives a very low prediction at 4.21 m from the support, where the predicted strength is 778 kN while the shear strength according to Response 2000 is 938 kN at transverse reinforcement yielding and 1032 kN at concrete crushing. Near mid-span, the 2006 CHBDC prediction corresponds well with transverse reinforcement yielding. The ACI 318 shear design method gives very unsafe predictions where V_{cw} controls the shear strength from the support up to 6.10 m from the support. This equation was previously recognized as being unsafe (Hawkins et al. 2005).

Figure 4-14 compares the Response 2000 predictions for mid-depth strain over about half the span with the predictions from 2007 AASHTO LRFD, 2006 CHBDC, and the proposed method. Similar to Response 2000, the proposed method can predict the mid-depth strains at yielding of transverse reinforcement and crushing of concrete. The 2006 CHBDC and 2007 AASHTO LRFD can only predict one mid-depth strain at a section. The proposed method predictions agree well with the predictions from Response 2000

both at yielding of transverse reinforcement and crushing of concrete. The 2006 CHBDC and 2007 AASHTO LRFD predictions are significantly larger than Response 2000

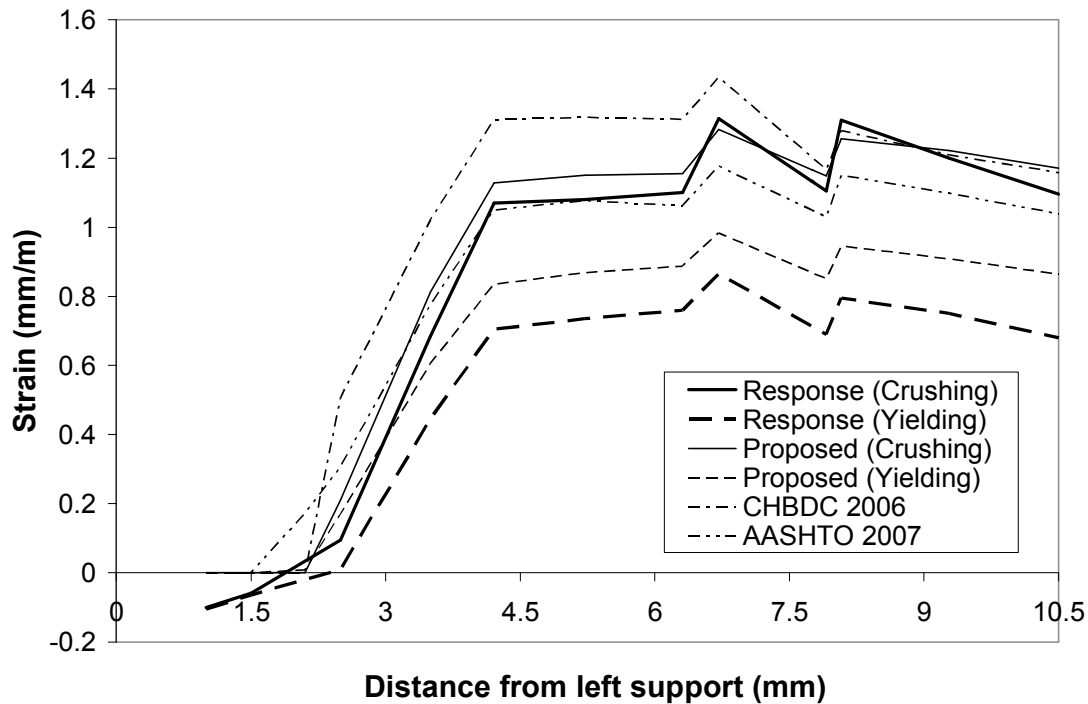


Fig. 4-14 Comparison of Response 2000 predicted mid-depth strain along span of I-girder bridge with proposed and code design methods.

predictions at yielding of transverse reinforcement; however, the predicted shear forces at failure (shear strength) from the 2006 CHBDC and 2007 AASHTO LRFD are slightly lower than the Response 2000 predictions at yielding of transverse reinforcement. This suggests that both 2007 AASHTO LRFD and 2006 CHBDC methods conservatively estimate the mid-depth longitudinal strain. The predictions from the 2007 AASHTO LRFD method are less conservative compared to the predictions from the 2006 CHBDC method. Notice that shear strength at yielding of transverse reinforcement from the proposed method (Fig. 4-13a) is greater than the shear strength at concrete crushing near

the support where the predicted longitudinal strain (Fig. 4-14) is small and almost zero. This was also noticed in MCFT predictions for uniform shear elements presented in Chapter 3 (see Fig. 3-13a).

4.7.2. Comparison of Results for Box-girder Bridge

In Fig. 4-15(a), the proposed method predictions of shear strength for the box-girder along almost half the span are compared with the Response 2000 predictions at yielding of transverse reinforcement and concrete crushing. The proposed method predictions compare well with the predictions from Response 2000. In the proposed method predictions, shear strength at transverse reinforcement yielding governs at sections that are near the support as it is greater than the shear strength corresponding to the crushing of concrete. This is consistent with Response 2000 predictions. Figure 4-15(b) compares the shear strength predictions from Response 2000 with the predictions from 2007 AASHTO LRFD, 2006 CHBDC, and ACI 318. As also noticed in the I-girder, ACI 318 method results in unconservative shear strength predictions for sections that are close to the support (up to 3.7 m from support). The ACI 318 method predictions become conservative for sections close to mid-span compared to the predictions from Response 2000. The 2006 CHBDC method predictions are unconservative close to the support; however, become conservative near mid-span compared to the Response 2000 predictions at crushing of concrete.

Figures 4-16(a) and 4-16(b) present Response 2000 predicted mid-depth strains and flexural reinforcement strains (strain at the center of flexural tension reinforcement) for the box-girder over about half the span with the predictions from the proposed method.

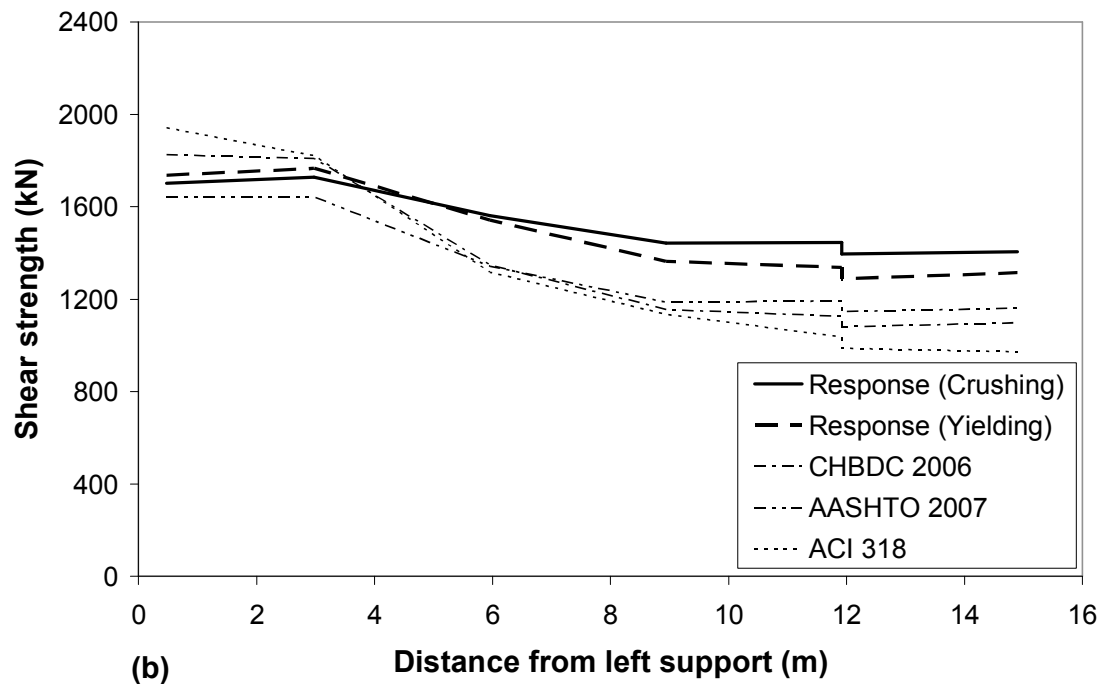
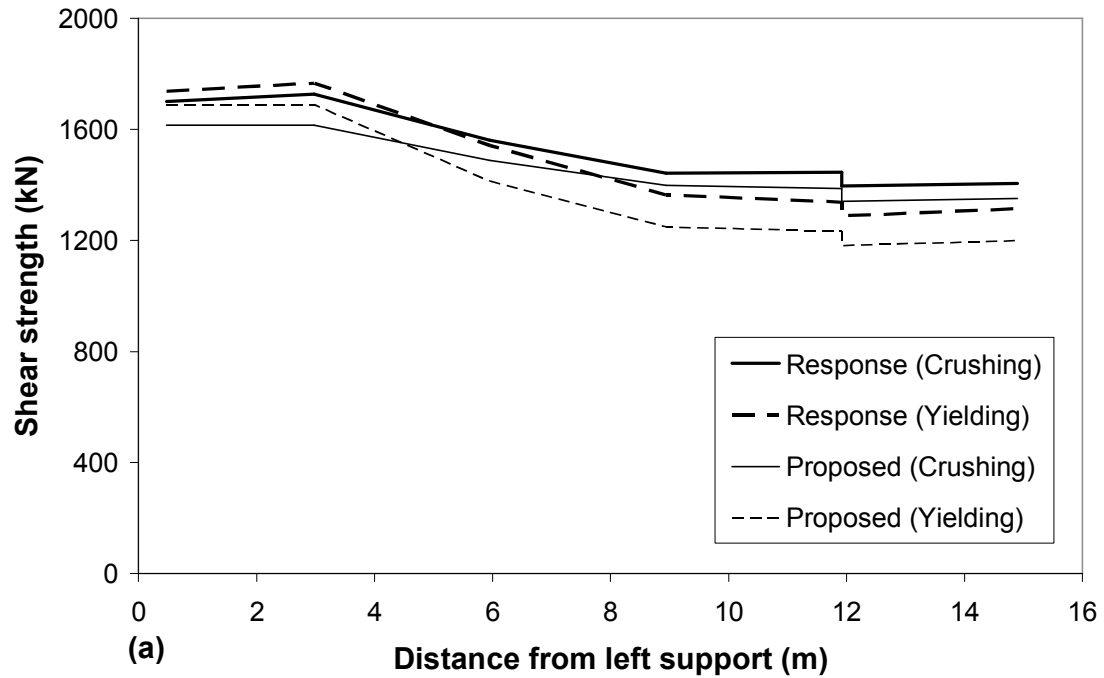


Fig. 4-15 Comparison of predicted shear strengths along span of box-girder bridge: (a) Response 2000 and proposed method, (b) Response 2000 and code design methods.

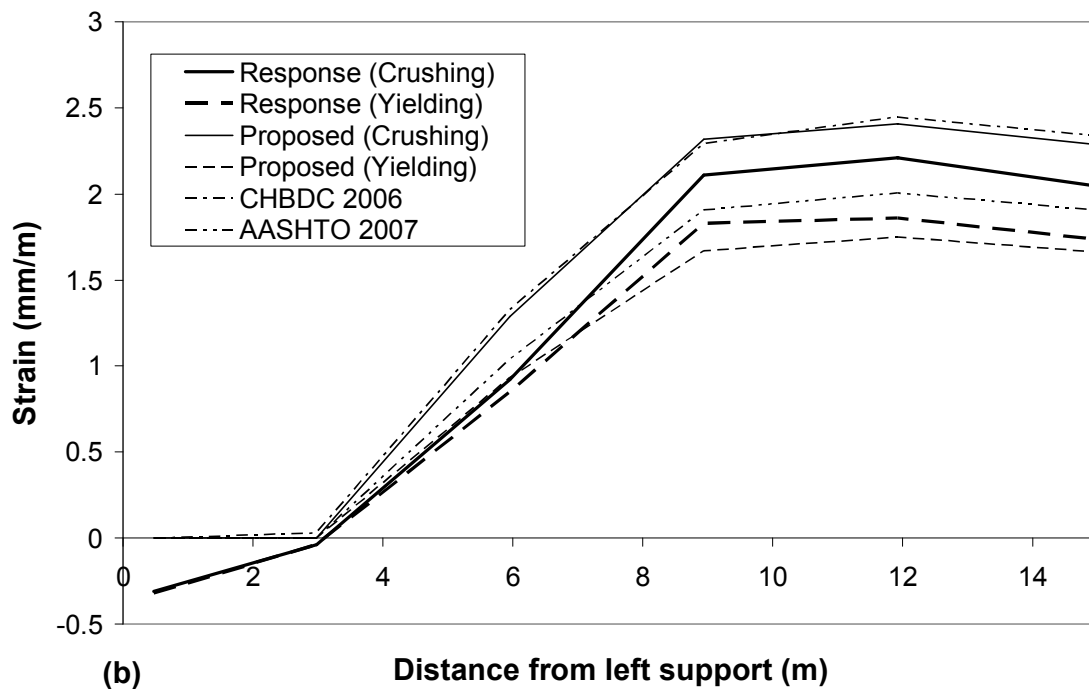
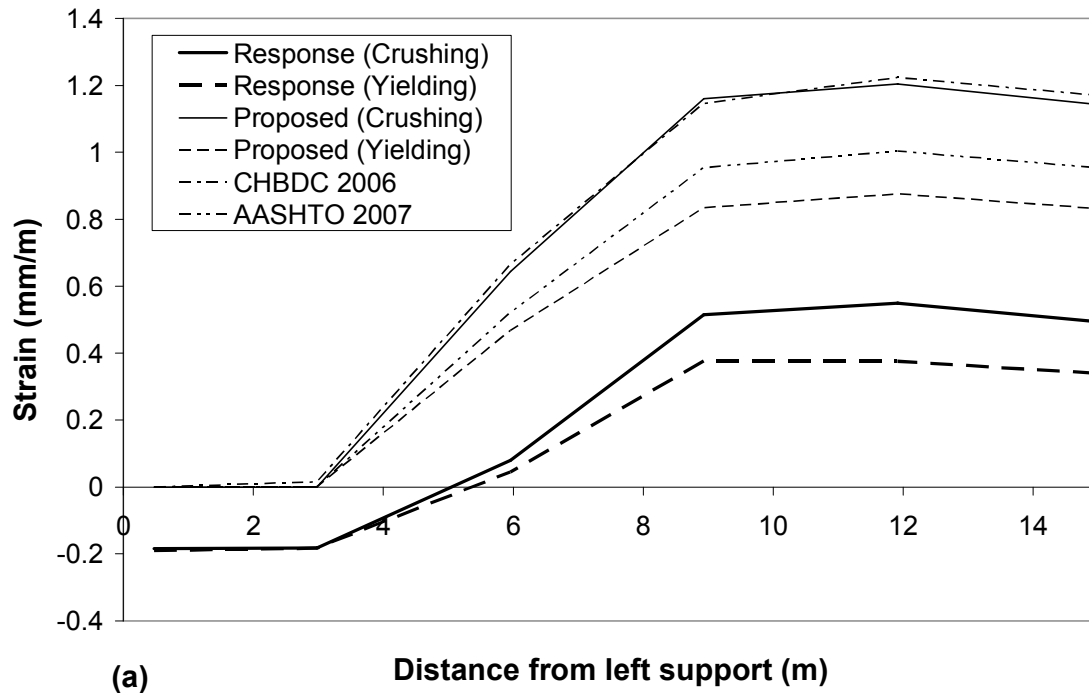


Fig. 4-16 Comparison of Response 2000 predicted (a) mid-depth strain, (b) flexural tension reinforcement strain along span of box-girder bridge with proposed and code design methods.

The predictions from 2007 AASHTO LRFD, and the 2006 CHBDC methods are also presented. The proposed method predictions of mid-depth strain (Fig. 4-16a) are the closest to those predicted by Response 2000 but the difference is still significant. The difference, however, is due to the assumption of mid-depth strain is half the strain at the center of flexural tension reinforcement. As shown in Fig. 4-16(b), the predictions of flexural tension reinforcement strain from the proposed method agree well with Response 2000 predictions.

The 2007 AASHTO LRFD predictions for flexural tension reinforcement strain compare well with the Response 2000 predictions at yielding of transverse reinforcement but are lower than Response 2000 predictions at concrete crushing. The 2006 CHBDC predictions of flexural tension reinforcement strain are conservative and even larger than Response 2000 predictions at concrete crushing along a significant portion of the span.

4.7.3. Comparison of Results for Channel-girder Bridge

Shear strength predictions of Response 2000 for almost half the span of the channel-girder bridge are shown with the predictions from the proposed method in Fig. 4-17(a), and with the predictions from 2007 AASHTO LRFD, 2006 CHBDC, and ACI 318 in Figure 4-17(b). Figure 4-17(a) illustrates that Response 2000 predictions of shear strength are compatible with those predicted by the proposed method both at yielding of transverse reinforcement and crushing of concrete. Near mid-span, the proposed method shear strength predictions at yielding of transverse reinforcement is higher than those at concrete crushing since the amount of transverse reinforcement is low (0.098%) and slightly higher than the 2006 CHBDC minimum amount (0.095%). Similar trend is also noticed but is less significant in the Response 2000 predictions.

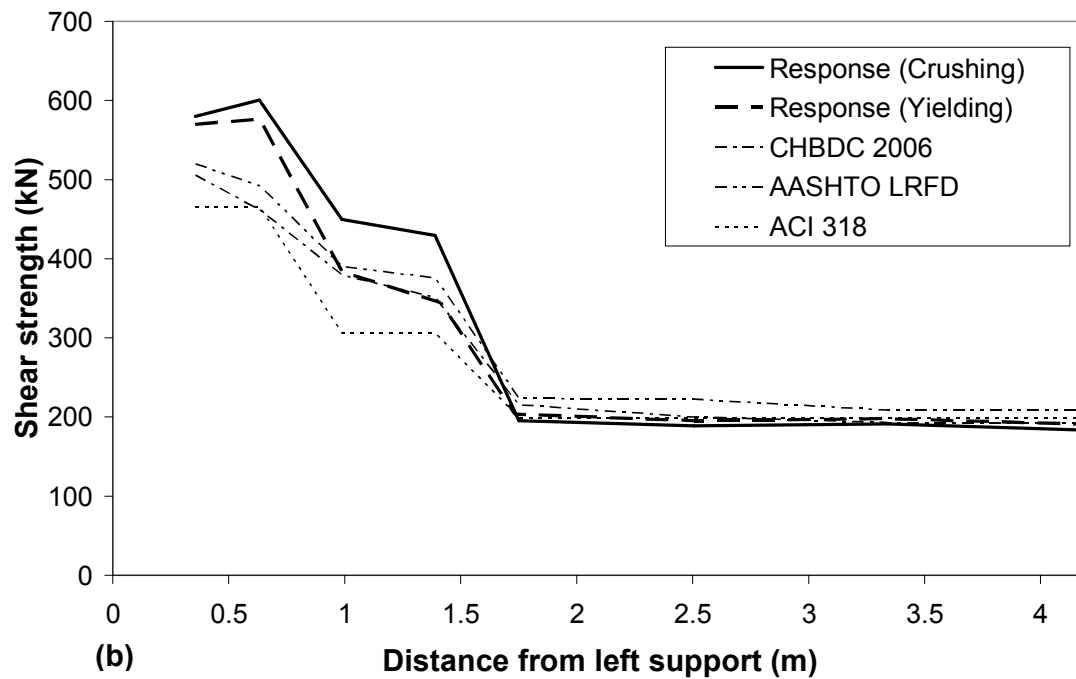
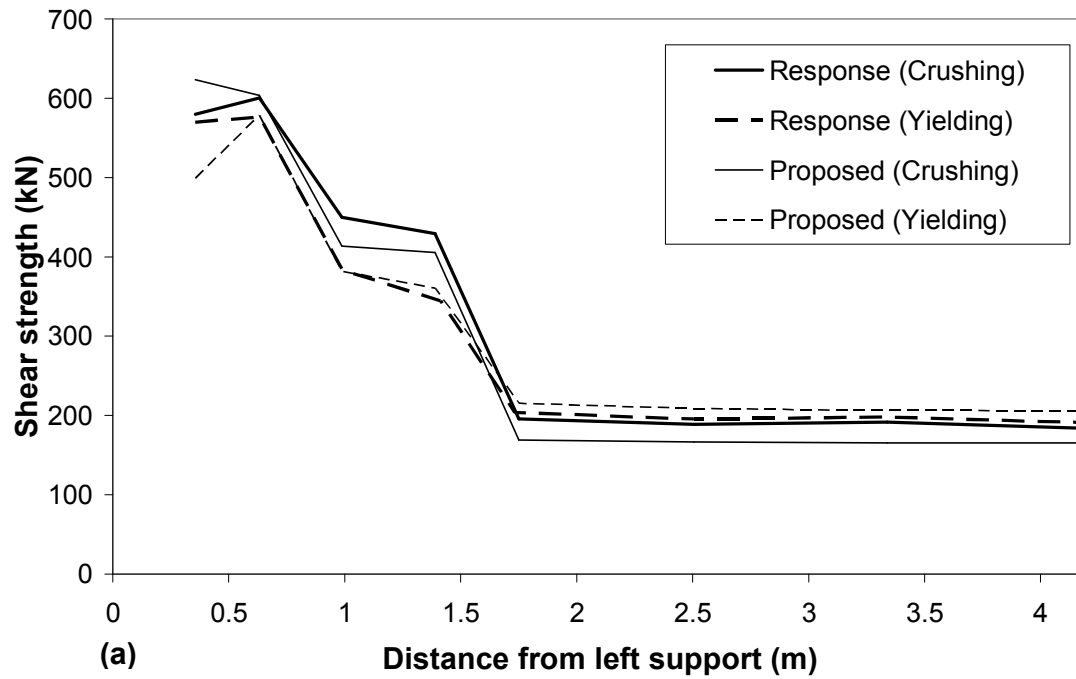


Fig. 4-17 Comparison of predicted shear strengths along span of channel-girder bridge: (a) Response2000 and proposed method, (b) Response 2000 and code design methods.

The 2006 CHBDC predictions are slightly lower than the 2007 AASHTO LRFD predictions and ACI 318 predictions are too conservative except for the portion of the span that is near mid-span. 2007 AASHTO LRFD predictions as well as predictions from the proposed method are slightly unsafe (with Response 2000-to-predicted shear strength ratio of about 0.95) near mid-span. Response 2000 results showed that yielding of transverse reinforcement does not extend over the full effective shear depth as the amount of transverse reinforcement is low. This does not cause significant reduction in shear strength for members containing minimum transverse reinforcement as shown in Fig. 4-17(b). Notice that the predictions from the proposed method are not significantly higher than Response 2000 predictions near mid-span.

In Fig. 4-18, Response 2000 predictions of channel girder mid-depth strain over about half the span with the predictions from the proposed method, and from the 2007 AASHTO LRFD and the 2006 CHBDC methods are presented. The proposed method predictions are the closest to Response 2000 predictions. The 2007 AASHTO LRFD predictions are better than the 2006 CHBDC predictions compared to Response 2000 predictions. It should be mentioned that the large mid-depth strains predicted by the codes as well as the proposed method near the support is because the axial force N_v due to shear has caused tension in the compression chord. The same trend is also noticed in Response 2000 predictions.

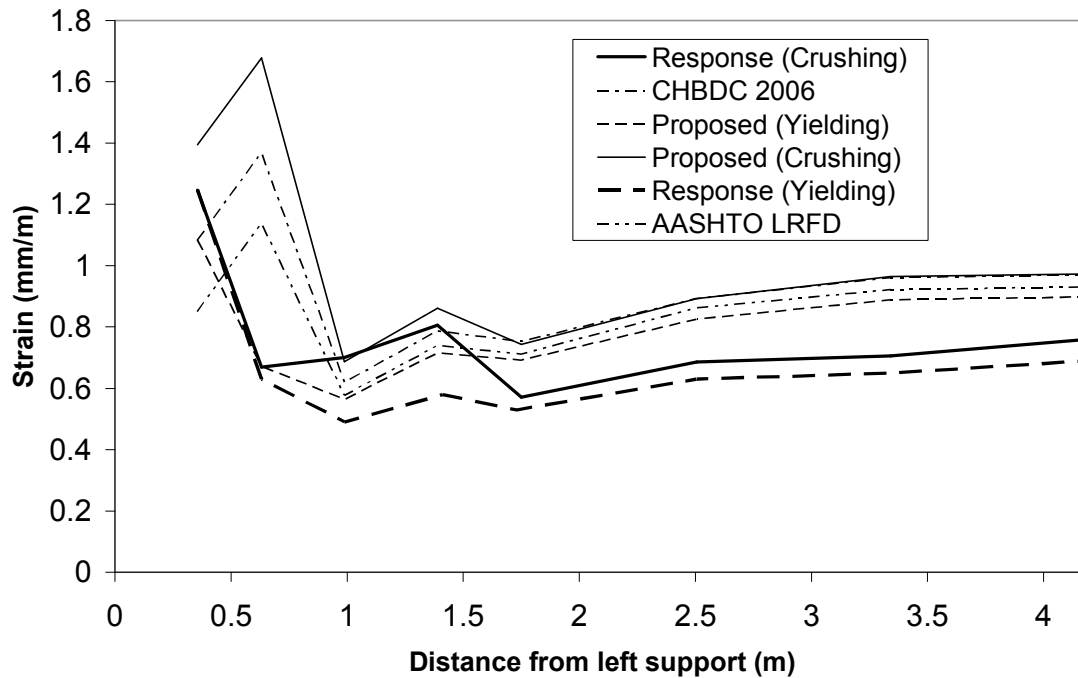


Fig. 4-18 Comparison of Response 2000 predicted mid-depth strain of I-girder bridge with proposed and code design methods.

4.7.4. Summary of Results for Example Bridge Girders

The predicted shear strengths at three sections along each of the three bridge girders are summarized in Table 4-1. For each bridge, one section is located in the low-moment region close to the support, another section is located in the high-moment region near mid-span, and the third section was located between the other two. The shear strength at transverse reinforcement yielding and concrete crushing according to Response 2000 are both shown, and the lower (critical) one is identified (*). Unlike the shear design methods, the proposed method also gives two shear strengths, and these generally agree well with Response 2000 results.

Table 4-1 Summary of predictions for example bridge girders with at least minimum transverse reinforcement.

Section information					Predicted shear strength (kN) (ratio Response 2000 shear to predicted shear)					Response 2000 shear strength (kN)	
Bridge	Dist. from supp. (m)	ρ_z (%)	V_u (kN)	M_u (kNm)	AASHTO 2007	CHBDC 2006	ACI 318	Proposed		Yielding	Crushing
								Yielding	Crushing		
I-girder	1.50	0.87	783.7	1211	1155.8 (1.01)	1261.8 (0.92)	1230.6 (0.95)	1158.6* (1.01)	1105.0	1164.8	1166.2*
	5.22	0.87	139.3	3213	830.3 (1.22)	776.6 (1.30)	1107.9 (0.91)	865.2	959.4* (1.05)	878.1	1011.0*
	7.91	0.44	83.7	3719	470.2 (1.40)	441.2 (1.49)	628.1 (1.05)	493.0	587.4* (1.12)	535.8	658.7*
Box-girder	2.98	0.80	514.6	1610	1693.0 (1.04)	1807.8 (0.98)	1820.8 (0.97)	1689.8* (1.05)	1614.6	1766.7*	1727.5
	5.96	0.80	410.1	2830	1392.6 (1.12)	1348.8 (1.16)	1316.3 (1.19)	1413.2	1487.9* (1.05)	1542.5	1561.6*
	8.94	0.80	304.3	3610	1237.8 (1.17)	1156.1 (1.25)	1133.7 (1.25)	1248.4	1398.3* (1.03)	1363.9	1442.7*
Channel-girder	0.63	0.59	157.9	130	492.2 (1.22)	462.2 (1.30)	465.8 (1.29)	581.8	603.6* (1.00)	576.5	600.6*
	1.39	0.29	139.3	208	375.6 (1.14)	351.1 (1.22)	305.9 (1.40)	360.4	405.4* (1.06)	344.6	429.2*
	3.34	0.10	83.7	328	209.1 (0.95)	193.2 (1.03)	199.3 (0.99)	206.1* (0.96)	165.4	192.3*	191.3
Mean					1.14	1.18	1.11	1.04		-	
COV (%)					11.8	15.4	15.9	4.3		-	

The ratios of Response 2000 shear strengths to predicted shear strengths are shown within brackets. For the proposed method, the ratios vary from 0.96 to 1.12, and have a mean of 1.04 and a COV of 4.3%. For the 2007 AASHTO LRFD shear design method the ratios vary from 0.92 to 1.40, with a mean of 1.14 and a COV of 11.8%. The ratios from the 2006 CHBDC shear design method vary from 0.92 to 1.49, with a mean of 1.18 and COV of 15.4%. Finally, for the ACI 318 method, the ratios vary from 0.91 to 1.40; have a mean of 1.11, and a COV of 15.9%. Note that 2007 AASHTO LRFD and the proposed method predictions are slightly unsafe only for the third section of the channel girder bridge that contains very low amount of transverse reinforcement close to the 2006

CHBDC minimum amount. The CHBDC and ACI 318 methods, however, resulted in unsafe estimate of shear strength at the first two sections of the I-girder and channel girder bridges where the moment shear ratios were low.

4.8. Example Evaluation for Bridge Girder With Less than Minimum Transverse Reinforcement

To demonstrate the proposed evaluation method, it was also applied to T-girders with less than minimum transverse reinforcement in a two-span continuous bridge with a span of 24.7 m. The 8.8 m wide bridge has two lanes of traffic, and four girders. The girders are 1067 mm deep at the ends of the bridge, and are haunched to 2286 mm deep over a 9.754 m length near the middle support. The girders were strengthened by post-tensioned 32 mm Dywidag bars located near the top flange and attached to the girders by steel diaphragms.

The results from the shear strength evaluation at the section located 4.67 m from the middle support are discussed below. The details of the section at that location are shown in Fig. 4-19. At this section, the amount of transverse reinforcement in the girders was $\rho_z = 0.042\%$, which is 62% of the 2006 CHBDC minimum transverse reinforcement $\rho_{zmin} = 0.068\%$. The 610 mm spacing of the stirrups is exactly the maximum allowed spacing. The concrete cylinder compression strength $f'_c = 21$ MPa and reinforcement yield strength $f_y = 400$ MPa. The longitudinal crack spacing parameter at the section of interest is $S_{xe} = 1469$ mm.

Bridge live load (truck load) consisted of CHBDC standard truck with total weight of 625 kN as well as 3 special permit trucks with 7, 8 and 9 axles and total weights of 750 kN (76.5 ton), 839 kN (85.5 ton) and 819 kN (83.5 ton). In addition, a 6-axle mobile

crane with 118 kN (12 ton) axle load was considered. Lane load and dynamic allowance factor, as well as a multi-lane reduction factor were included as per the 2006 CHBDC. The load factors were based on the 2006 CHBDC for Level 2 Inspection. Live load was transversely distributed according to the 2006 CHBDC. Factored moment and shear envelope values at the section of interest were $M_u = -2628$ kNm, $V_u = 662.4$ kN. Truck details are presented in Appendix D.

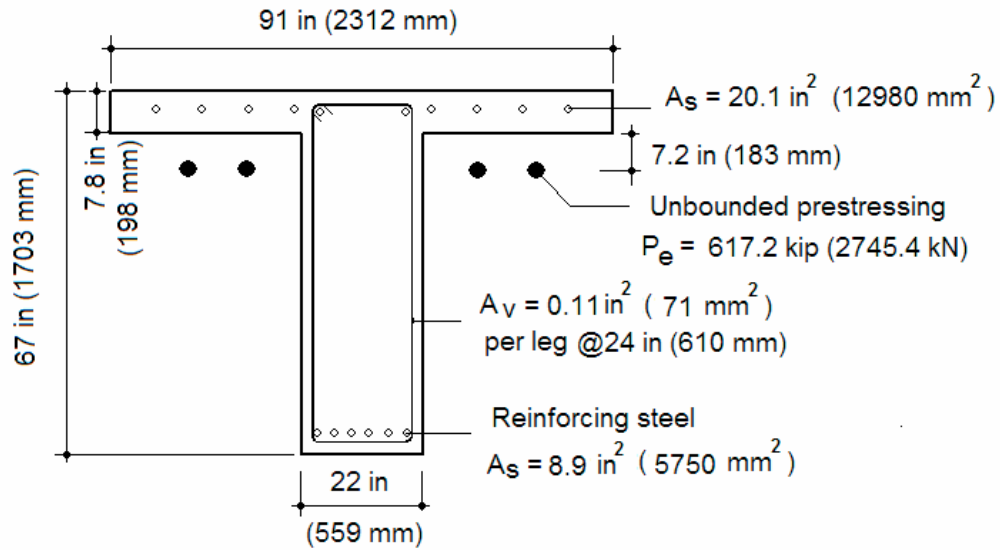


Fig. 4-19 Cross-section of the evaluated bridge girder example at 4.67 m from mid-support ($M_u = -2628$ kNm, $V_u = 662.4$ kN).

Table 4-2 compares the shear strength predictions for the critical section of the bridge girders. The first row of predictions are assuming the amount of transverse reinforcement is less than minimum, and therefore V_c is calculated assuming no transverse reinforcement and $V_s = 0$. The second row of predictions was made assuming the section had minimum stirrups $\rho_{zmin} = 0.068\%$ even though the actual stirrups were only 62% of this amount. The third row gives the predicted strength using the 2006

CHBDC linear interpolation method. As the actual amount of transverse reinforcement ($\rho_z = 0.042\%$) is a 43% increase from one-third minimum to minimum ($\rho_z = 0.068\%$), the shear strength in row three is equal to the value in row one plus 43% of the difference between rows one and two. The prediction given in the third row of the column for Response 2000 is the prediction using the actual amount of reinforcement. For the ACI 318 predictions, the external prestressing was treated as an axial compression.

Table 4-2 Comparison of nominal shear strength predictions (kN) for bridge girder example ignoring shear resisted by inclined flexural compression.

	AASHTO 2007	2006 CHBDC	ACI 318	Proposed	Response 2000
Assuming no stirrups	1028	787	825	1210	1201
Assuming min. stirrups	1319	1729	1067	1235	1220
Using 2006 CHBDC Interpolation	1152	1189	928	1221	1216 ⁽¹⁾

⁽¹⁾ Based on actual amount of stirrups not CHBDC interpolation method.

The 2006 CHBDC prediction for the section without transverse reinforcement is 787 kN, which is significantly lower than all other predictions, and the 2006 CHBDC prediction for the section with minimum transverse reinforcement is 1729 kN, which is significantly higher than all other predictions. There are two reasons for this. First, the predicted longitudinal strain ε_x that influences the shear response is very small for which the 2006 CHBDC values of β are conservative for large members without stirrups (see Fig. 3-33). Secondly, the 2006 CHBDC uses the same β equation for members with transverse reinforcement (Eq. 3-29) except S_{xe} becomes 300 mm, which results in a

significantly higher β value for a large member with transverse reinforcement compared to the same member without transverse reinforcement. The predictions from the proposed method are similar to the Response 2000 results in all cases.

It is interesting to note that the evaluated section was within the hunched portion of the girder. As a result, the inclined flexural compression force contributes to the shear strength of the bridge. Accounting for this effect results in 222 kN additional shear strength using simple hand calculations assuming $jd=0.9d$, and 547 kN additional shear strength using Program Response 2000. The Response 2000 prediction is much higher because a considerable portion of the section is in compression and therefore jd is smaller and hence the flexural compression is larger.

Chapter 5. Comparison with Beam Test Results

5.1. General

In this chapter, the proposed shear evaluation method is verified by comparing predictions of shear strength with the measured shear strengths of beams that failed in shear. The shear strengths of the beams were also predicted using the shear design provisions of 2007 AASHTO LRFD, 2006 CHBDC, and ACI 318.

The minimum amount of transverse reinforcement required in the shear design provisions of 2006 CHBDC and 2007 AASHTO LRFD are different. Results from tests on beams with a low percentage of transverse reinforcement are used in this chapter to show the 2006 CHBDC limit is appropriate for use with the proposed method. The 2006 CHBDC has an interpolation procedure that can be used to evaluate the shear strength of a member with less than the minimum percentage of transverse reinforcement. The results from tests on beams with a low percentage of transverse reinforcement are also used to show this procedure is appropriate for use with the proposed method.

5.2. Members With at Least Minimum Transverse Reinforcement

To verify the proposed method for members with at least minimum transverse reinforcement, predictions for 80 reinforced concrete beams and 88 prestressed concrete beams with at least minimum transverse reinforcement as specified by 2006 CHBDC

($\rho_z \geq 0.06 \frac{\sqrt{f'_c}}{f_y}$ in MPa units) were compared with the measured test results. The

selected tests were mostly extracted from the shear database collected for National Cooperative Highway Research Program (NCHRP) Project 12-61 (Hawkins et al. 2005)

and presented by Kim (2004). The shear database includes 160 reinforced concrete beams with transverse reinforcement, and 164 prestressed concrete beams with transverse reinforcement. A total of 156 of these beams that had a depth of at least 300 mm and transverse reinforcement ratio not greater than 0.015 were selected from the database. Among the tests selected for comparison are ten prestressed I-girders that were 73 in. (1854 mm) deep tested for NCHRP project 12-56 at the University of Illinois (Kim 2004, Kuchma et al. 2005) as well as seven prestressed I-girders that were 44 in. (1118 mm) tested by the Structural Research Center in Florida (Shahawy and Batchelor, 1996). In addition to the results from the database, seven reinforced concrete beams tested by Mphonde and Frantz (1985) and five reinforced concrete beams tested by Rahal and Al-Shaleh (2004) were included.

To predict the shear strength of the tested beams using the proposed method, 2007 AASHTO LRFD, and 2006 CHBDC, trial-and-error is needed as the applied moment-to-applied shear force ratio is known at the critical section. Evaluation of a bridge girder using the proposed method does not need trial-and-error as the accompanying bending moment is known in this case. Trial-and-error is not needed to predict the shear strength of tested beams using ACI 318 as the shear strength is a function of applied moment-to-applied shear force ratio in the method. Linear interpolation was used to determine β and θ values from the tables provided in the 2007 AASHTO LRFD shear design provisions.

The loading for most of the tests consisted of one or two concentrated loads. The critical shear section for these was assumed to be at a distance d (effective depth) from the concentrated load toward the support. For tests with uniformly distributed loading, the critical section was assumed to be at distance d from the support or from the location of

change in the amount of transverse reinforcement toward mid-span. For beams with inclined tendons, the vertical component of the effective prestressing force V_p was added to the shear strength.

Figures 5-1(a) and (b) present the cumulative frequency diagrams of test-to-predicted shear strength ratios of 80 reinforced concrete (RC) beams and 88 prestressed concrete (PC) beams, respectively. These diagrams show the number of ratios (as a portion of the total number) that are equal to or less than the corresponding test-to-predicted ratio on the horizontal axis. A “perfect model” would have a cumulative frequency of zero for a ratio of test-to-predicted less than 1.0, and a cumulative frequency of 1.0 for a ratio of test-to-predicted greater than 1.0. The closer the actual result is to this, the better is the prediction.

Figure 5-1(a) shows that the proposed method has the largest (safest) minimum test-to-predicted shear strength ratio of 0.88 compared to 0.84, 0.72, and 0.80 which are the minimum test-to-predicted shear strength ratios associated with ACI 318, 2007 AASHTO LRFD, and 2006 CHBDC predictions, respectively. Figure 5-1(a) also shows that about 20% of predictions of the proposed method, as well as the 2006 CHBDC and AASHTO LRFD methods have test-to-predicted ratios below 1.0. However, only about 10% of proposed method and 2006 CHBDC test-to-predicted ratios are below 0.95 while about 15% of test-to-predicted ratios from 2007 AASHTO LRFD are less than 95% of the actual test results.

Beyond test-to-predicted shear strength ratio of 1.0, the proposed method and the 2007 AASHTO LRFD ratios have the closest cumulative frequency diagram to the “perfect” prediction. ACI 318 predictions are the safest as only 7% of the predicted

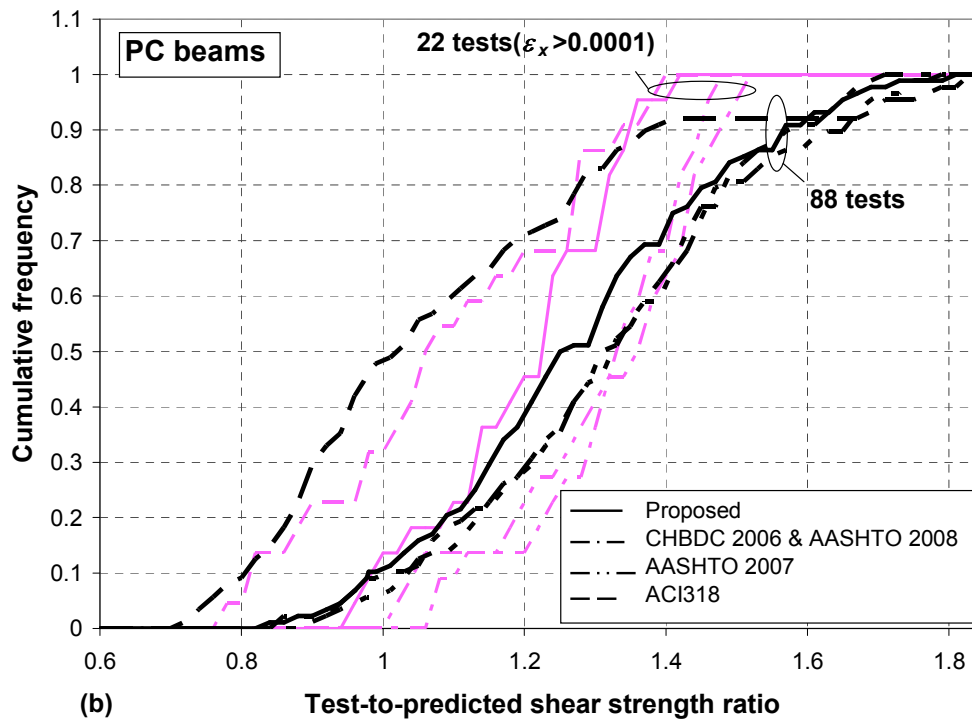
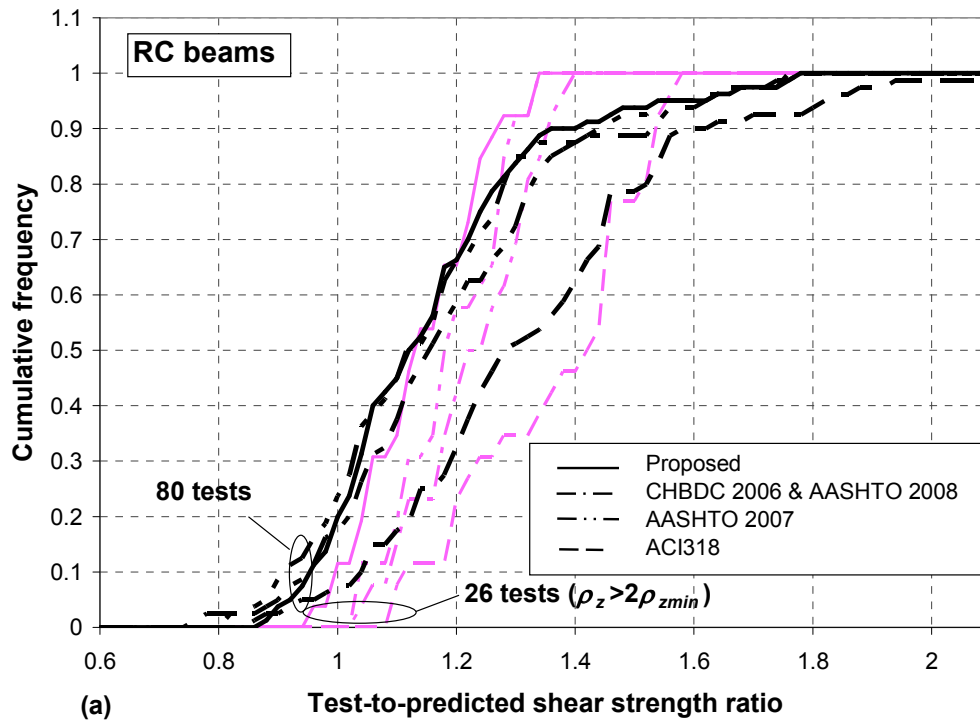


Fig. 5-1 Cumulative frequency of test-to-predicted ratios of proposed and code methods:
(a) RC beams, (b) PC beams.

values have a test-to-predict shear strength ratio less than 1.0, but the method is generally overly conservative compared to the other methods. For example, ACI 318 has a maximum test-to-predicted ratio of 2.1, while all other methods have a maximum ratio less than about 1.8. The proposed method has a mean value of test-to-predicted shear strength ratios of 1.15 and COV of 16.5%. The mean values of test-to-predicted shear strength ratios are 1.15, 1.19, and 1.32 for 2007 AASHTO LRFD, 2006 CHBDC, and ACI 318, and the corresponding COV of ratios are 18.0%, 17.6%, and 18.7%, respectively.

Figure 5-1(b) compares the cumulative frequency distribution of test-to-predicted shear strength for 88 PC beams, and once again, the proposed method gives the closest to the “perfect” prediction. For the ratios of less than 1.0, the 2006 CHBDC and the proposed method test-to-predicted ratios show almost the same cumulative frequency distribution while 2007 AASHTO LRFD predictions are safer. However, only 10% of the 2006 CHBDC and the proposed method predictions are less than actual test results, which is reasonably acceptable given the fact that their minimum actual test-to-predicted shear strength ratios are about 0.85. About 50% of the ACI 318 predictions are unsafe (have test-to-predicted ratios less than 1.0). The mean values of test-to-predicted shear strength ratios are 1.07, 1.27, 1.32, 1.31 for ACI 318, the proposed method, 2007 AASHTO LRFD, and CHBDC 2006 predictions. Also, the corresponding COV of test-to-predicted shear strength ratios are 24.8%, 16.7%, 16.0%, 15.8%.

The difference of the proposed method predictions with the 2006 CHBDC and 2007 AASHTO LRFD predictions could be more significant in real bridge girders than what is shown in Figure 5-1 as was shown in the bridge examples in Chapter 4. This is due to the

fact that a significant number of the tested reinforced concrete beams had transverse reinforcement amount of less than two times the minimum amount specified by 2006 CHBDC whereas in real practice, reinforced concrete bridge girders often contain significantly more transverse reinforcement. There were only 26 RC members among the examined tests that had at least two times the minimum amount of transverse reinforcement for which the cumulative frequency distribution of test-to-predicted shear strength ratios from the proposed method as well as from the code methods are shown in Figure 5-1(a). The proposed method predictions are the closest to a “perfect model” predictions. The mean of ratios are 1.14, 1.18, 1.23 while COV of ratios are 9.1%, 7.8%, 8.4% for the proposed method, the 2007 AASHTO LRFD and the 2006 CHBDC, respectively.

Most tested prestressed concrete beams had a very low predicted mid-depth strain (almost zero) but many real prestressed concrete bridge girders are expected to experience larger strains at mid-depth especially for sections that are close to mid-span. The reason is that in the tested beams, failure usually occurs at section close to the support whereas in bridge girders failure can also happen close to mid-span at locations where amount of transverse reinforcement changes.

There were only 22 tests which had the predicted mid-depth strain higher than 0.0001 from the proposed method. The cumulative frequency distribution of test-to-predicted ratios of those tests is also shown in Figure 5-1(b). Notice that the median of the proposed method ratios is 1.24 (cumulative frequency value corresponding to test-to-predicted ratio of 0.5) while it is 1.34 and 1.36 from the 2007 AASHTO LRFD and the 2006 CHBDC methods. The mean of test-to-predicted ratios are 1.20, 1.30, and 1.33 for

the proposed method, 2007 AASHTO LRFD, and 2006 CHBDC predictions. The corresponding COV of ratios are 11.0%, 10.5%, and 9.8%, respectively.

In summary, the proposed method predictions for the tested beams with at least minimum amount of transverse reinforcement are in better agreement with the test results compared to the predictions from the 2006 CHBDC shear design procedure, which is the same as 2008 AASHTO LRFD shear design procedure. The test-to-predicted shear strength ratios from the proposed method are on average about 4% lower than the predictions from the 2006 CHBDC method for both RC and PC beams and they are still reasonably conservative. As the amount of transverse reinforcement increases to two times the minimum amount and more, the proposed method predictions are even better and the difference with the predictions from the 2006 CHBDC method becomes more significant. In case of PC beams, as the mid-depth predicted strain gets larger, the proposed method predictions compare better with the test results. In real bridge girders, shear failure can happen close to mid-span at locations where the amount of transverse reinforcement changes. At these locations, the mid-depth longitudinal strain is large.

5.3. Members Without Transverse Reinforcement

To verify the proposed method for members without transverse reinforcement, predictions for 132 reinforced concrete beams and 131 prestressed concrete beams without transverse reinforcement were compared with the measured test results. The selected tests were extracted from the same database used for members with transverse reinforcement (Kim 2004). The reinforced concrete members that were selected had a minimum depth of 380 mm, while the prestressed members had a minimum depth of 300 mm and a minimum effective prestressing stress of 550 MPa. The reinforced concrete

members included a number of tests with a depth of about 1000 mm and up to a depth of 2000 mm. In contrast, the depth of the prestressed members ranged from 300 mm to about 460 mm. The shear span-to-depth ratios of all the members ranged from 2.5 to 8.0.

As in members with minimum transverse reinforcement, the loading for most of the tests consisted of one or two concentrated loads, and again, the critical shear section for these was assumed to be at a distance d (effective depth) from the concentrated load toward the support. For test with uniformly distributed loading, the critical section was assumed to be at distance d from the support or from the location of change in transverse reinforcement amount toward mid-span. For beams with inclined tendons, the vertical component of the effective prestressing force V_p was included in the calculated shear strength.

Fig. 5-2 presents the cumulative frequency distribution of the test-to-predicted shear strength ratios. As explained previously, a “perfect prediction” would have a cumulative frequency of zero for test-to-predicted shear strength ratios less than 1.0, and a cumulative frequency of 1.0 for test-to-predicted shear strength ratios greater than 1.0.

Fig. 5-2(a) shows that ACI 318 predictions are unsafe (test-to-predicted shear strength ratios less than 1.0) for about 45% of the tests (cumulative frequency of 0.45) on reinforced concrete beams without stirrups. This well known issue is because ACI 318 ignores size effect in members without stirrups. The proposed method and 2006 CHBDC predictions are similar – the predicted shear strengths for about 15% of the tests are somewhat unsafe. The 2007 AASHTO LRFD shear strength predictions are a little lower. The proposed method has a mean value of test-to-predicted strength of 1.17 and COV of 17.3%. The mean values of test-to-predicted shear strength are 1.05, 1.26, and 1.16 for

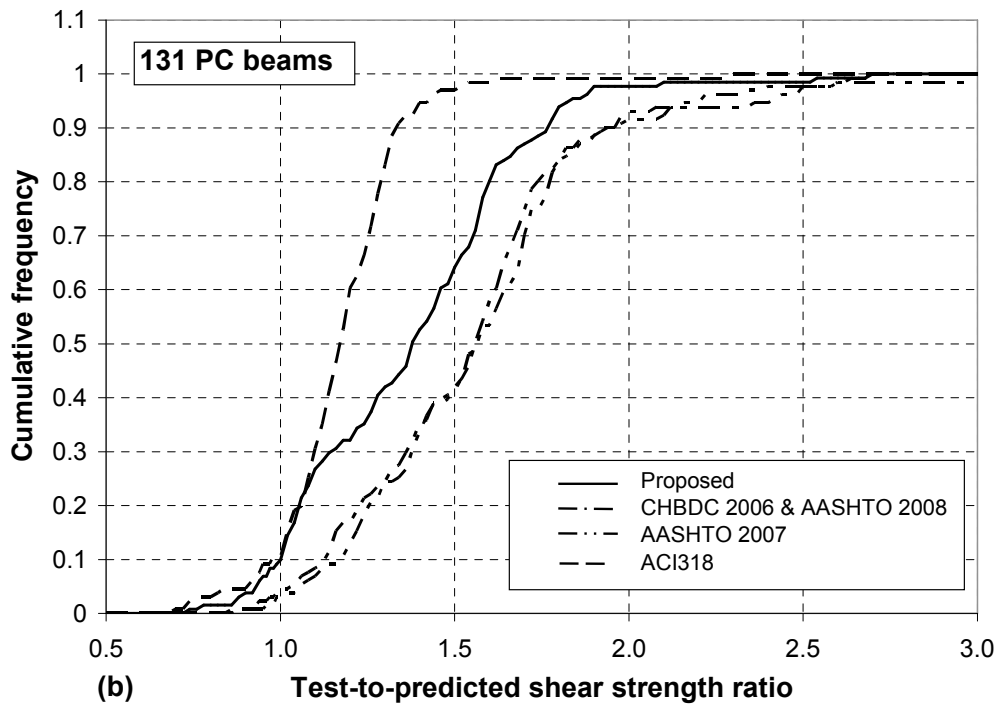
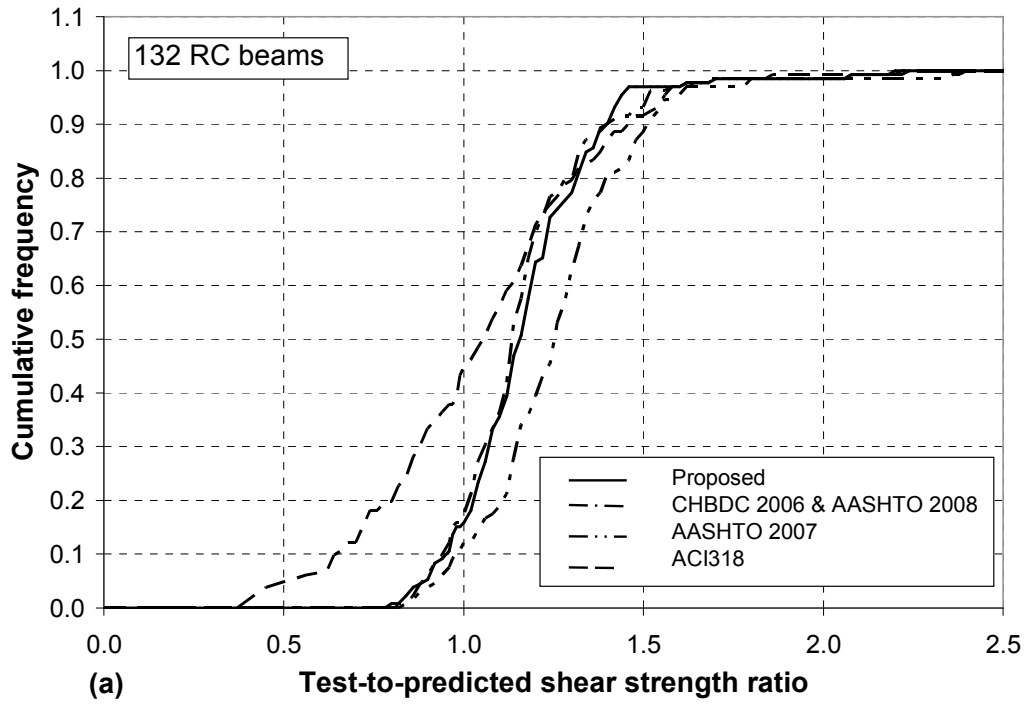


Fig. 5-2 Cumulative frequency of test-to-predicted ratios of proposed and code methods:
 (a) 132 reinforced concrete (RC) beams, (b) 131 prestressed concrete (PC) beams.

ACI 318, 2007 AASHTO LRFD, and 2006 CHBDC, and the COV are 30.3%, 18.5%, and 17.8%, respectively.

Fig. 5-2(b) indicates that the ACI 318 method gives the best predictions for the 131 prestressed concrete beams that are not very large. The proposed method does better than 2006 CHBDC and 2007 AASHTO LRFD. Mean of test-to-predicted shear strength ratios is 1.17 from ACI 318, 1.57 from 2007 AASHTO LRFD, 1.37 from the proposed method, 1.55 from the 2006 CHBDC. The COV of these ratios is 16% from ACI 318, 17% from the proposed method, and about 23.1% and 23.2% from 2007 AASHTO LRFD and the 2006 CHBDC.

5.4. Effect of Important Parameters

To ensure that the proposed method accurately captures the effect of important parameters in shear, the test-to-predicted shear strength ratios presented in Sections 5-2 and 5-3 were plotted versus a number of parameters and also compared with ratios from the codes. 80 plots are presented in Appendix F and only 6 of these are presented here in Figures 5-3 and 5-4. Appendix F includes plots for RC and PC beams both with and without transverse reinforcement. Five parameters including beam depth, shear stress ratio $\frac{v}{f'_c}$, shear span-to-depth ratio, longitudinal reinforcement ratio, and effective prestressing force were looked at and the results are presented in Appendix F.

Figure 5-3 shows test-to-predicted shear strength ratios from ACI 318, 2006 CHBDC and the proposed method versus shear stress ratios ($\frac{v}{f'_c}$) for 88 prestressed concrete beams with minimum amount of transverse reinforcement.

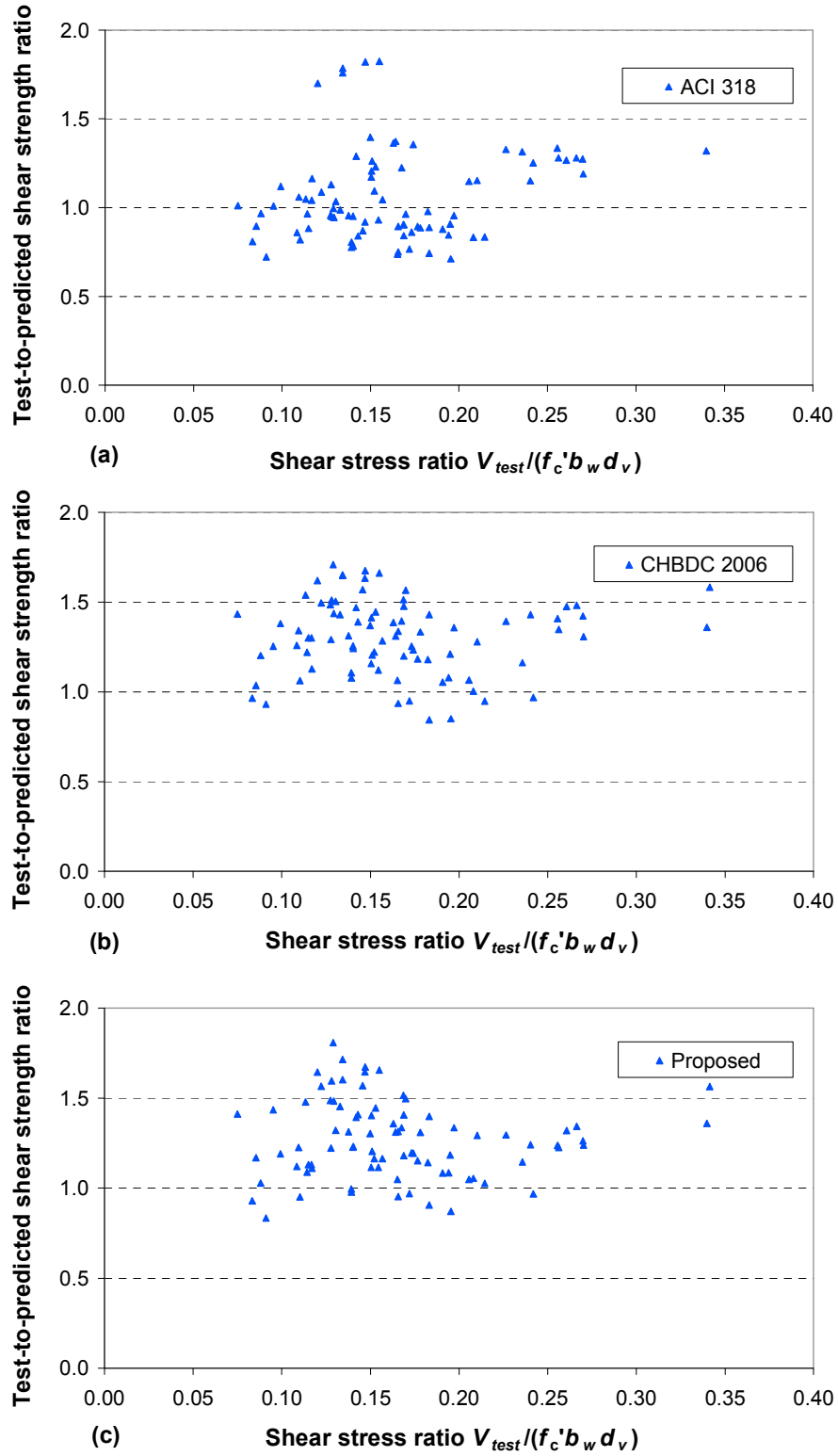


Fig. 5-3 Test-to-predicted ratios of proposed and code methods versus shear stress ratio v/f_c' for 88 prestressed concrete beams with transverse reinforcement.

To calculate actual shear stress ratios, shear strength from the actual test results was divided by the beam effective shear area ($b_w d_v$) and concrete compressive strength f'_c . As shown in Fig. 5-3(a), ACI 318 is unconservative over the whole range of practical shear stress ratio ($\frac{v}{f'_c} \leq 0.25$), but conservative for higher shear ratios. The reason is that ACI 318 assumes that concrete contribution to the shear strength is equal to cracking strength of concrete whereas concrete contribution decreases after cracking due to increase in strains and therefore reduction in aggregate interlock capacity.

Figures 5-3(b) and (c) illustrate that both 2006 CHBDC and the proposed method reasonably predict shear strength of the tested beams over the entire range of shear stress ratios. Notice that as shear stress ratio increases (transverse reinforcement ratio increases), the proposed method predictions are closer to actual test results compared to the predictions from the 2006 CHBDC.

Figure 5-4 presents the variation of test-to-predicted shear strength ratios of the 131 reinforced concrete beams with beam depth for ACI 318, 2006 CHBDC, and the proposed method. As shown in Fig. 5-4(a) and explained before, ACI 318 predictions becomes highly unconservative as beam depth increases since it fails to account for beam size effect in shear. Both 2006 CHBDC and the proposed method reasonably capture the effect of beam size on shear strength of the tested beams as shown in Figures 5-4(b) and (c).

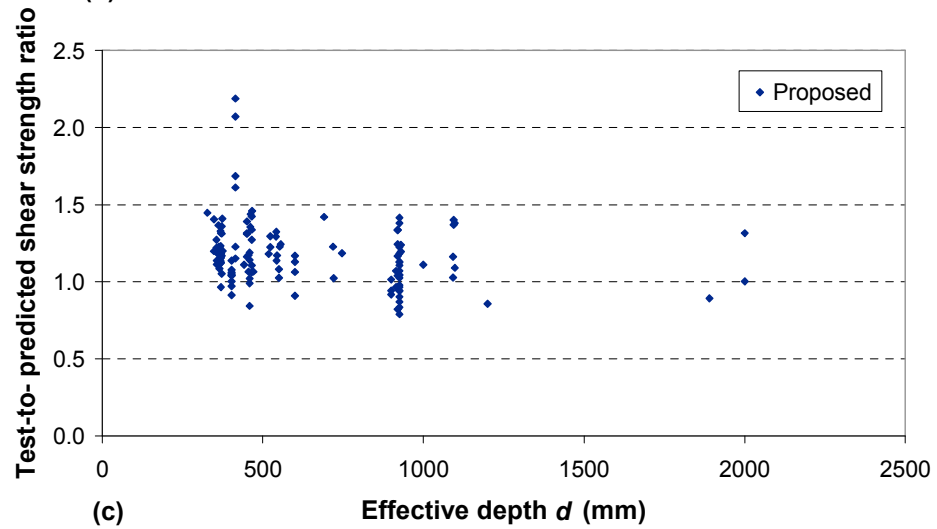
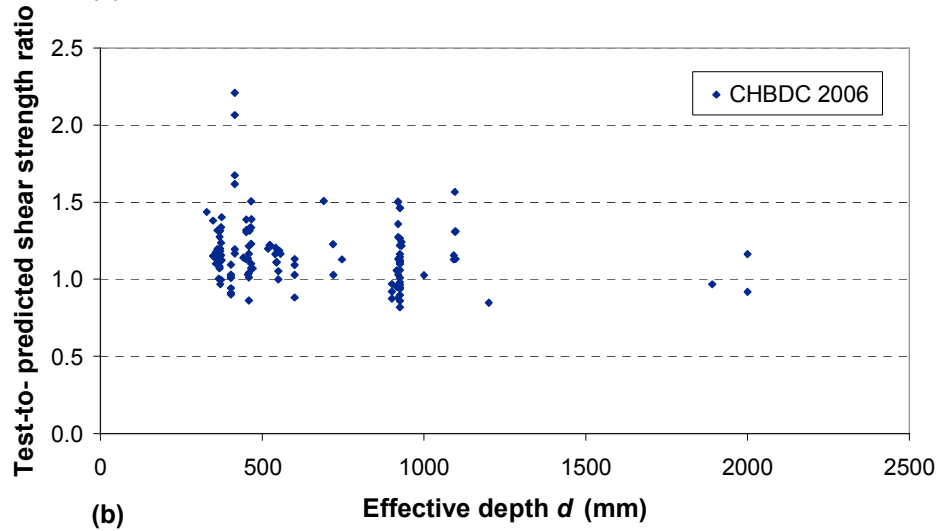
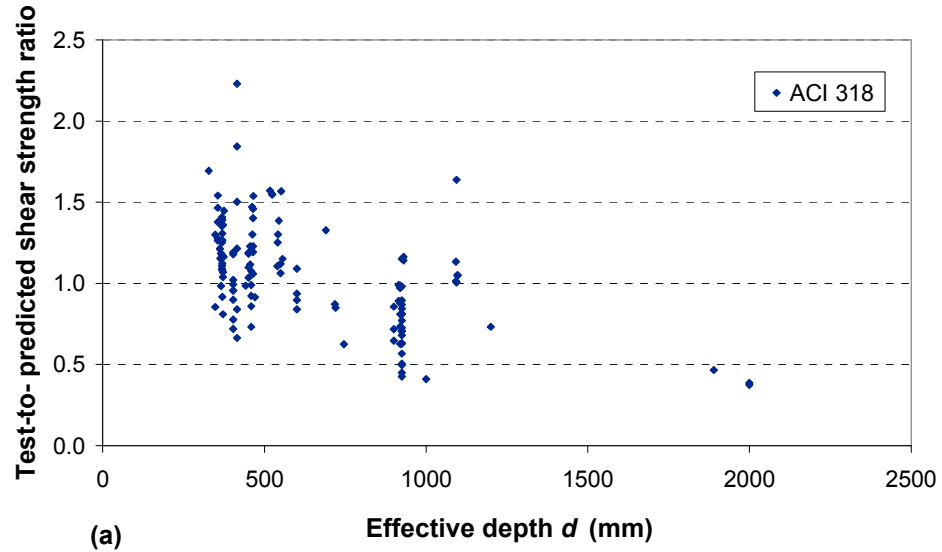


Fig. 5-4 Test-to-predicted ratios of proposed and code methods versus effective depth for 132 reinforced concrete beams without transverse reinforcement.

5.5. Minimum Transverse Reinforcement and Transition Between Members With and Without Minimum Transverse Reinforcement

As explained previously in Chapter 4, the 2006 CHBDC minimum transverse reinforcement ratio is $\rho_{zmin} = 0.06 \frac{\sqrt{f_c'}}{f_y}$. This minimum amount is 30% higher than the minimum amount specified by the 2007 AASHTO LRFD method.

Codes normally treat members with less than minimum transverse reinforcement as members with none. Based on the experimental study by Angelakos et al. (2001), the 2006 CHBDC uses a different approach in the evaluation section. According to the 2006 CHBDC evaluation section, shear strength of lightly reinforced members with less than one third of minimum amount of transverse reinforcement is the same as members with no transverse reinforcement. The shear strength increases linearly from the shear strength of the member with no stirrups to the shear strength of the member with minimum stirrups as the transverse reinforcement amount increase from one third of minimum to minimum.

To investigate if the 2006 CHBDC minimum transverse reinforcement ratio (ρ_{zmin}) may be adopted in the proposed method and if the 2006 CHBDC linear approach for members with less than minimum transverse reinforcement is appropriate for use with the proposed method, predictions of proposed method were compared with reinforced concrete beam test results containing transverse reinforcement ratio ranging from $0.49\rho_{zmin}$ to $1.8\rho_{zmin}$. 76 beams were selected from the shear database (Kim 2004) and 9 reinforced concrete beams tested by Rahal and Al-Shaleh (2004) were included. 50 of the selected beams contained more than the 2006 CHBDC minimum transverse

reinforcement and the remaining 26 tests contained less than minimum transverse reinforcement.

Figure 5-5 examines the variation of test-to-predicted shear strength ratios from the proposed method with transverse reinforcement amount as a ratio of minimum transverse reinforcement specified by the 2006 CHBDC. In Fig. 5-5(a) members with less than minimum transverse reinforcement is treated as members without transverse reinforcement, while in Fig. 5-5(b) the linear interpolation approach permitted by 2006 CHBDC is used for members with less than minimum transverse reinforcement. For members with more than minimum transverse reinforcement, the predictions in Figs. 5-5(a) and 5-5(b) are the same. For those members, 12 tests out of 50 tests have ratios of less than 1.0 for which the predictions are unsafe; however, only 5 of them (10%) have ratios of less than 0.95. This is also consistent with predictions from the proposed method for the 80 reinforced concrete beams in Fig. 5-1(a) meaning that the safety level of the predictions would not change significantly as the transverse reinforcement amount decreases to the 2006 CHBDC minimum transverse reinforcement ratio. As a result, the 2006 CHBD minimum transverse reinforcement is adopted in the proposed method.

In Figs. 5-5(a) and 5-5(b) members with less than minimum amount of transverse reinforcement have $\rho_z/\rho_{\min} < 1.0$. Figure 5-5(a) shows treating these members as members without stirrups leads to conservative estimates of shear strength for members with transverse reinforcement amount of less but close to minimum amount. In Fig. 5-5(b), in which the linear interpolation approach is used, a more uniform trend is observed. Notice that the overall consistency of the predictions with the actual test results has been improved considerably. Seven predictions out of 26 predictions (28%) are unsafe but

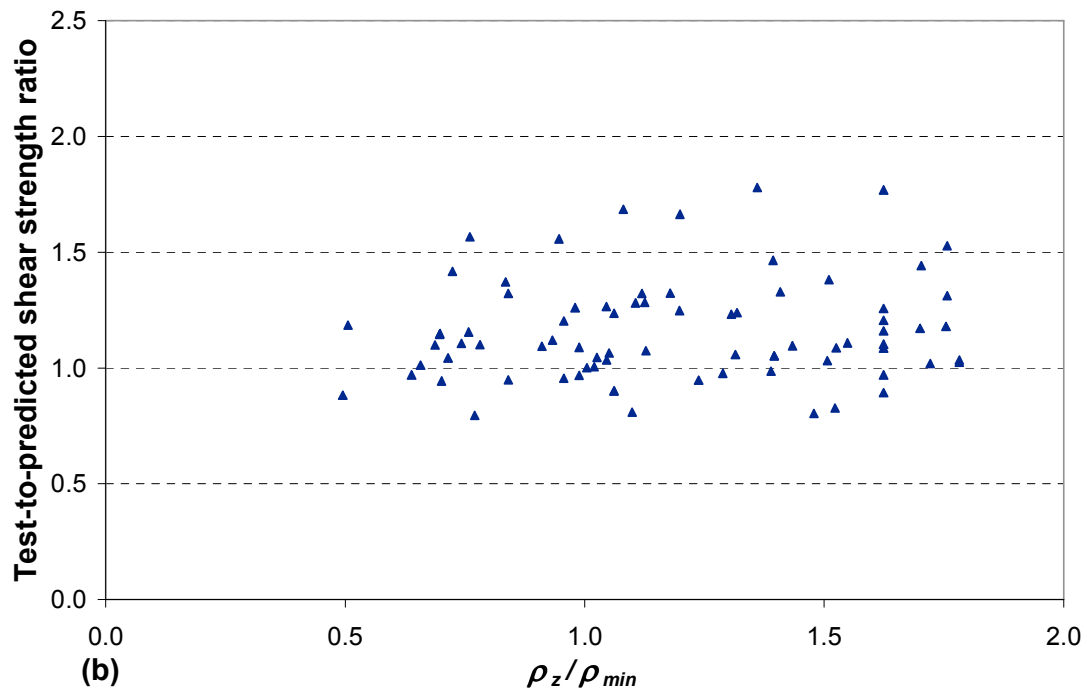
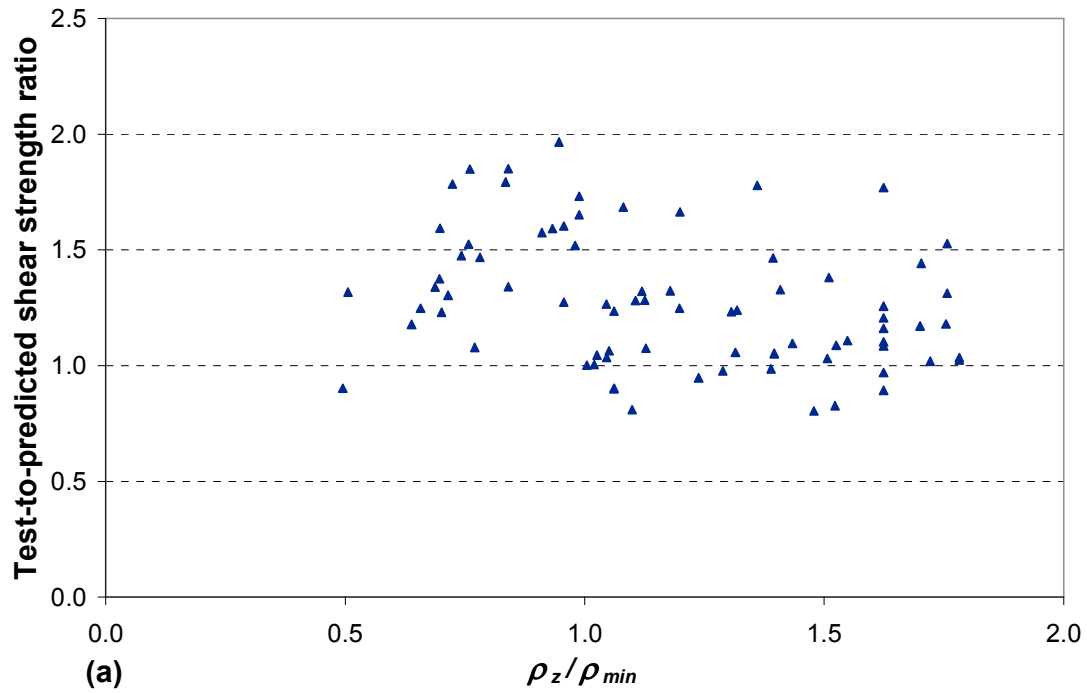


Fig. 5-5 Test-to-predicted shear strength ratios for 76 lightly reinforced tested beams: (a) assuming no stirrups, (b) using linear interpolation approach, for members with less than minimum stirrups.

only two predictions (7.7%) are less than 95% of the actual test results. This is again consistent with the safety level of the proposed method predictions for the 80 reinforced concrete tested beams with more than minimum transverse reinforcement.

Chapter 6. Refined 2006 CHBDC Method for Shear Design

6.1. General

The 2006 CHBDC shear design provisions include an equation for mid-depth longitudinal strain ε_x that is simplified and conservative; however, the code permits the use of more accurate procedures to determine mid-depth longitudinal strain. The proposed method for shear strength evaluation presented in Chapters 3 and 4 includes a more accurate equation for mid-depth longitudinal strain that is not a function of applied shear force. In this chapter a similar equation for mid-depth longitudinal strain for shear design, which is a function of applied shear force, is presented. It is investigated whether the more accurate equation is appropriate for use in shear design using the 2006 CHBDC shear design provisions. The predicted longitudinal strains in bridge girders are compared with strains determined using Response 2000. In addition, predictions of shear strength from the 2006 CHBDC with the proposed equation for mid-depth longitudinal strain ε_x are compared with available test results.

6.2. Refined CHBDC Approach for Members With at Least Minimum Transverse Reinforcement

Some of the refinements introduced in Chapter 3 for the proposed method namely the assumption of n_v acts over a depth of d_{nv} that can be different from effective shear depth d_v , accounting for tension stiffening effect in the tension chord, and how to include the effect of web nonprestressed and prestressed reinforcement can well be implemented in ε_x equation of the 2006 CHBDC without any changes. However, the proposed N_v equation used to derive ε_x equation in Chapter 4 is for evaluation problems and thus is a function

of transverse reinforcement amount. For design, ε_x equation and thus N_v equation should be a function of applied shear force to avoid iteration.

As explained in Chapter 3, the 2006 CHBDC uses the approximation of $2v$ for axial compression stress needed to transfer shear along the cracked depth n_v , which is too conservative. In contrast, 2007 AASHTO LRFD uses a more accurate approximation $v \cot \theta$. Figure 6-1 compares the 2006 CHBDC and 2007 AASHTO LRFD predictions of n_v with MCFT for varying concrete contribution and angle of inclination of 29 and 36 deg, which are the corresponding angles to $\varepsilon_x = 0$ and $\varepsilon_x = 0.001$ in the 2006 CHBDC method, respectively. As illustrated, 2007 AASHTO LRFD approximate equation for n_v is more accurate; thus is used to develop a refined equation for ε_x .

Using $v \cot \theta$ to approximate n_v in the ε_x equation requires trial-and-error in design since θ is not initially known. To overcome this problem, as shown in Figure 6-2, $\cot \theta$ may be replaced with a linear function of θ given below for the range of θ between 28 and 40 deg, which is the suggested range of θ by the 2006 CHBDC equation (Eq. 3-30).

$$\text{[6-1]} \quad \cot \theta = 3.4 - 0.056\theta$$

Substituting for $\cot \theta$ from Eq. [6-1] and θ from Eq. [3-30], $v \cot \theta$ can be approximated as:

$$\text{[6-2]} \quad n_v = v \cot \theta = 1.8v - 392v\varepsilon_x$$

Using the same procedure as used to derive Eq. [4-18] but using the n_v equation above results in the following ε_x equation for design.

$$\text{[6-3]} \quad \varepsilon_x = \frac{M / jd + 0.9Vd_{nv} / d_v - \alpha \sqrt{f'_c} A_{tf} - f_p (A_p + \lambda_p A_{pw})}{2 [E_s (A_s + 0.25A_{sw}) + E_p (A_p + \lambda_p^2 A_{pw})] + 196Vd_{nv} / d_v}$$

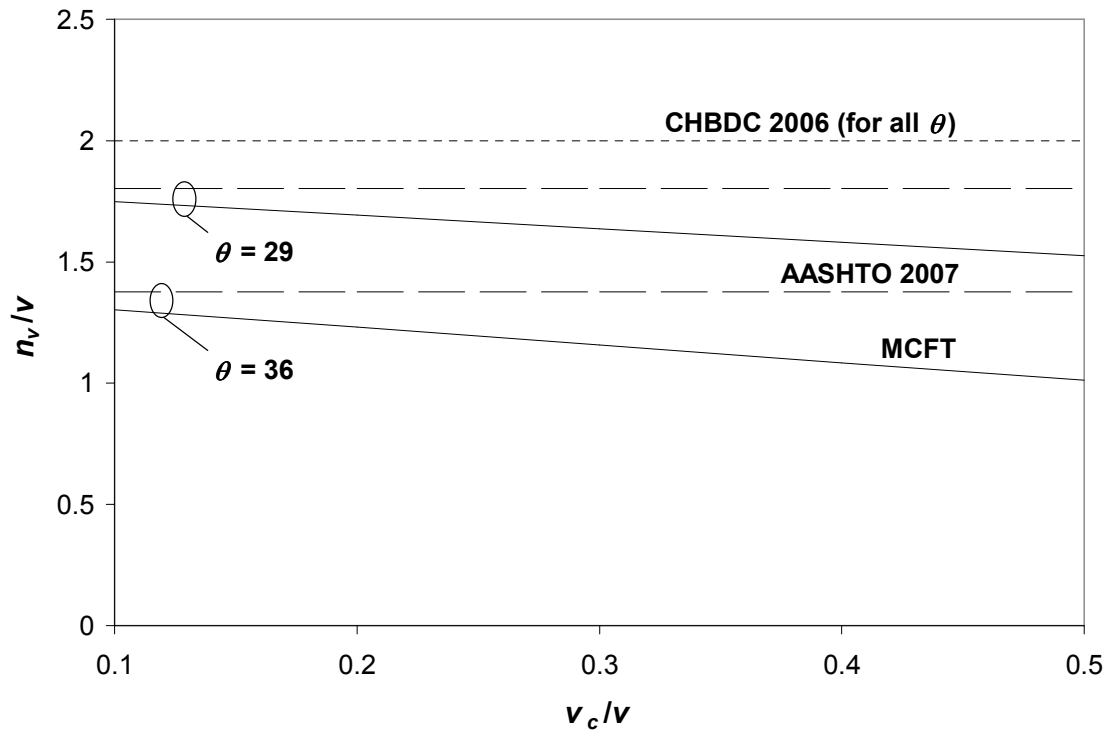


Fig. 6-1 Comparison of code predicted axial compression stresses n_v with MCFT for different concrete contributions to shear stress.

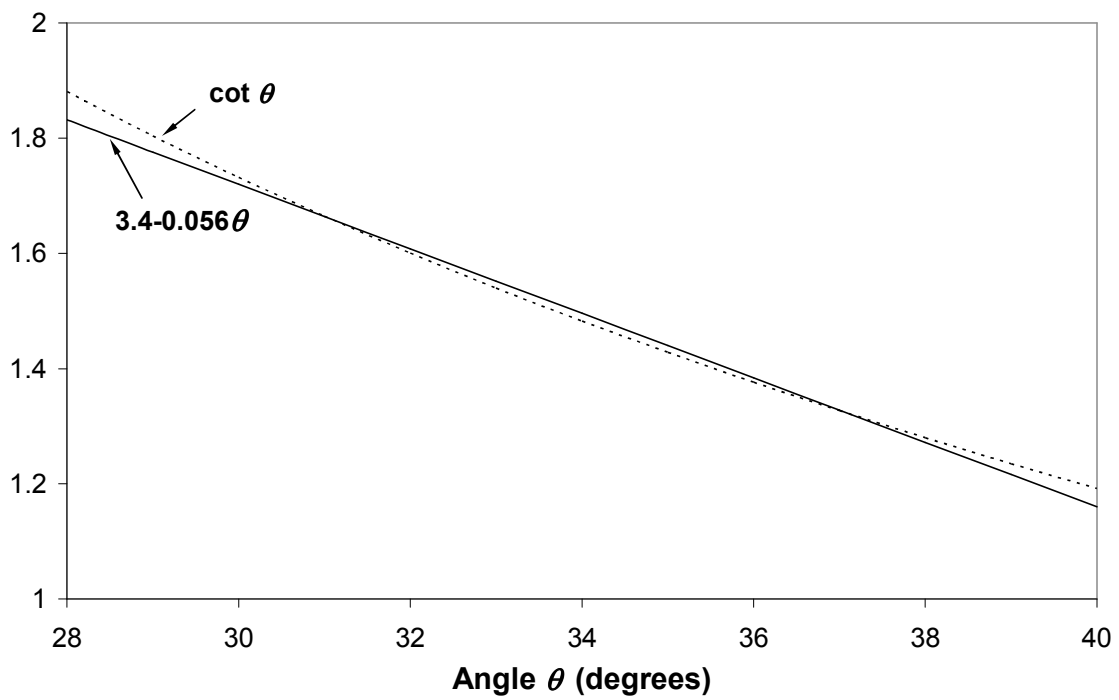


Fig. 6-2 Linear approximation of $\cot \theta$.

where V is the applied shear force. The more general form of Eq. [6-2] for m layers of web nonprestressed reinforcement and n layers of web prestressed reinforcement is:

$$\text{[6-4]} \quad \varepsilon_x = \frac{M / jd + 0.9Vd_{nv} / d_v - \alpha\sqrt{f_c'}A_{fc} - f_p(A_p + \sum_{i=1}^n \lambda_{pi}A_{pwi})}{2 [E_s(A_s + \sum_{j=1}^m \lambda_j^2 A_{swj}) + E_p(A_p + \sum_{i=1}^n \lambda_{pi}^2 A_{pwi})] + 196Vd_{nv} / d_v}$$

in which A_{swj} is total area of the j^{th} layer of web nonprestressed reinforcement, A_{pwi} is total area of the i^{th} layer of web prestressed reinforcement. λ_j and λ_{pi} are the ratios of d_{pwi} / d and d_{wj} / d in which d_{pwi} and d_{wj} are the distances from the centroids of the i^{th} layer of web prestressed reinforcement and the j^{th} layer of web nonprestressed reinforcement to the flexural compression face, respectively.

6.3. Bridge Examples

Figures 6-3 to 6-5 compare Eq. [6-2] and the 2006 CHBDC equation for ε_x with Response 2000 predictions for the same three bridge girders that were evaluated with the proposed evaluation method in Chapter 4. Comparisons are made at yielding of transverse reinforcement stage since, as shown in Chapter 4, the 2006 CHBDC predictions of shear strength is close to that stage. In other words, shear strength at yielding of transverse reinforcement given by Response 2000 is used in Eq. [6-2] and the ε_x equation of 2006 CHBDC and the results are compared with Response 2000 predictions of mid-depth strain at yielding of transverse reinforcement.

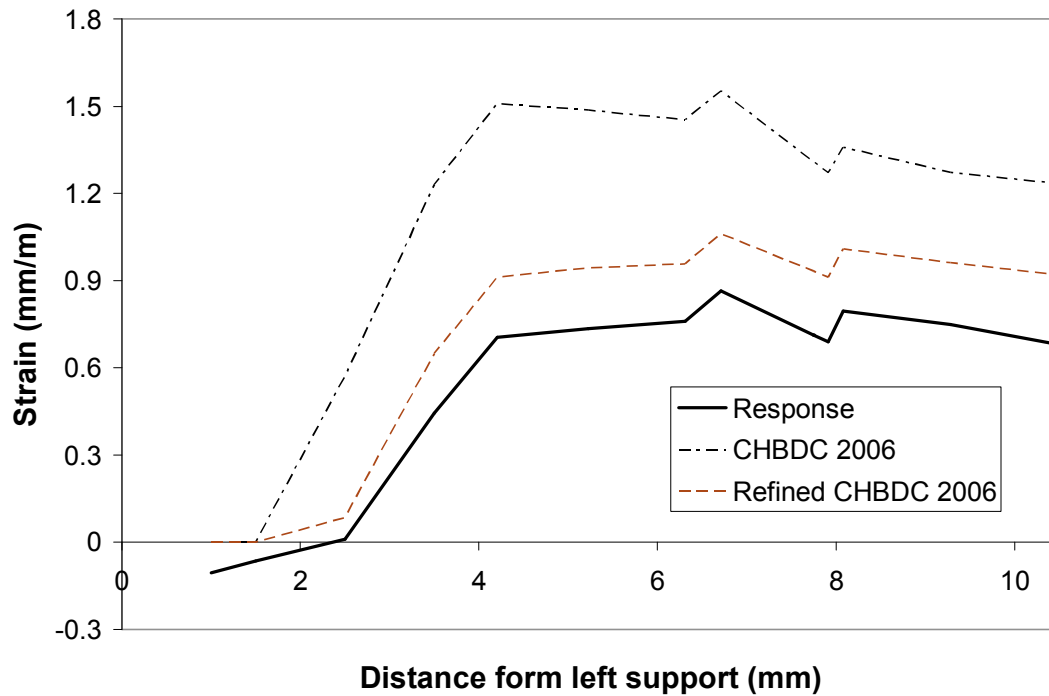


Fig. 6-3 Comparison of I-girder predicted mid-depth strain along the bridge span.

As shown in Figures 6-3 to 6-5, the refined ϵ_x equation is closer to the Response predictions in all cases. The refined equation improves the predictions of strains up to 40%, 35%, and 15% for I-girder, box-girder, and channel-girder bridges compared to the 2006 CHBDC ϵ_x equation, respectively. Figure 6-4 also includes the comparison of Response 2000 predictions of flexural tension reinforcement strain with those from the 2006 CHBDC and the refined ϵ_x equation for the box-girder. Note that the flexural tension reinforcement strain is two times the mid-depth strain in the 2006 CHBDC method. The refined ϵ_x equation for mid-depth strain is also half the refined ϵ_x equation for flexural tension reinforcement strain.

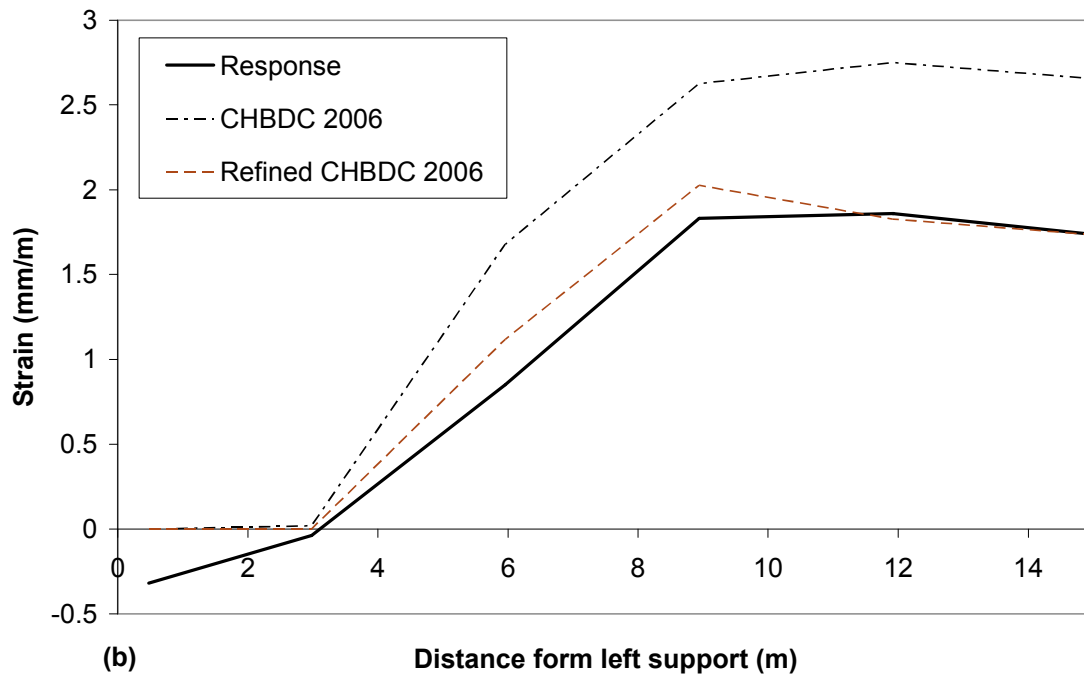
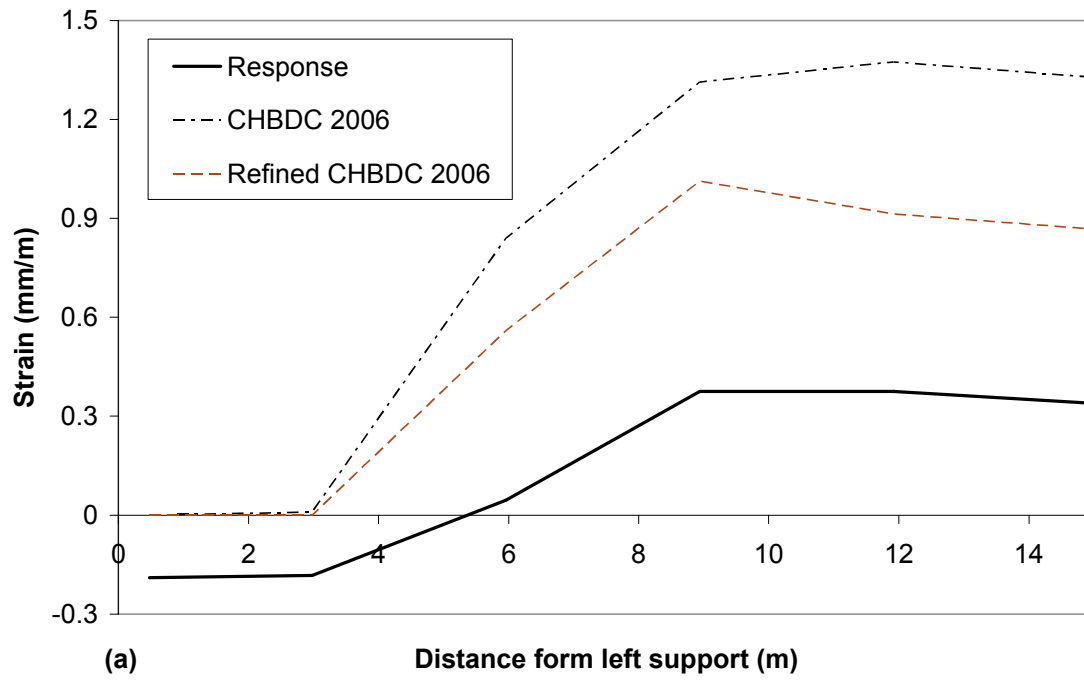


Fig. 6-4 Comparison of box-girder predicted (a) mid-depth strain (b) flexural tension reinforcement strain along the bridge span.

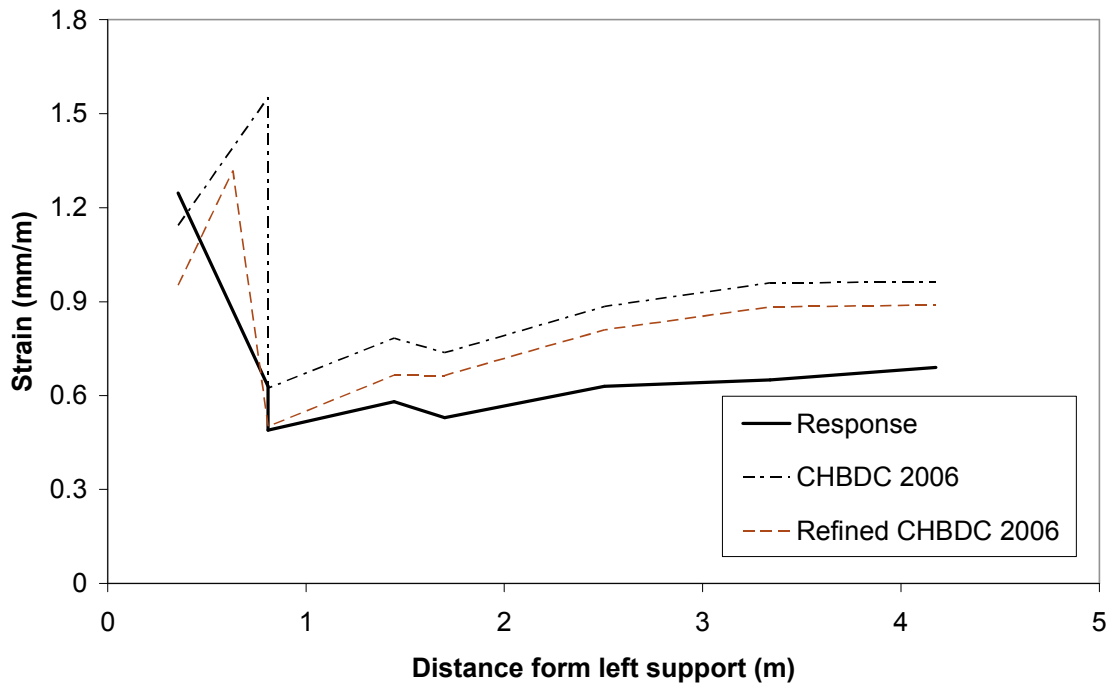


Fig. 6-5 Comparison of channel-girder predicted mid-depth strain along the bridge span.

Notice that the refined equation adequately estimates the flexural tension reinforcement strain compared to the Response 2000 results (Fig. 6-4b). The refined equation prediction of mid-depth strains shown in Fig. 6-4(a) is not as good due to the approximation of mid-depth strain is half the flexural tension reinforcement strain.

6.4. Comparison with Experimental Results

To verify if the refined ε_x equation can be used in the 2006 CHBDC shear design procedure, the shear strength predictions of the refined 2006 CHBDC method, in which the original ε_x equation is replaced with Eq. [6-2], are compared with experimental results from the 80 reinforced concrete beams and 88 prestressed concrete beams. The results are also compared with the shear strength predictions from the 2006 CHBDC method.

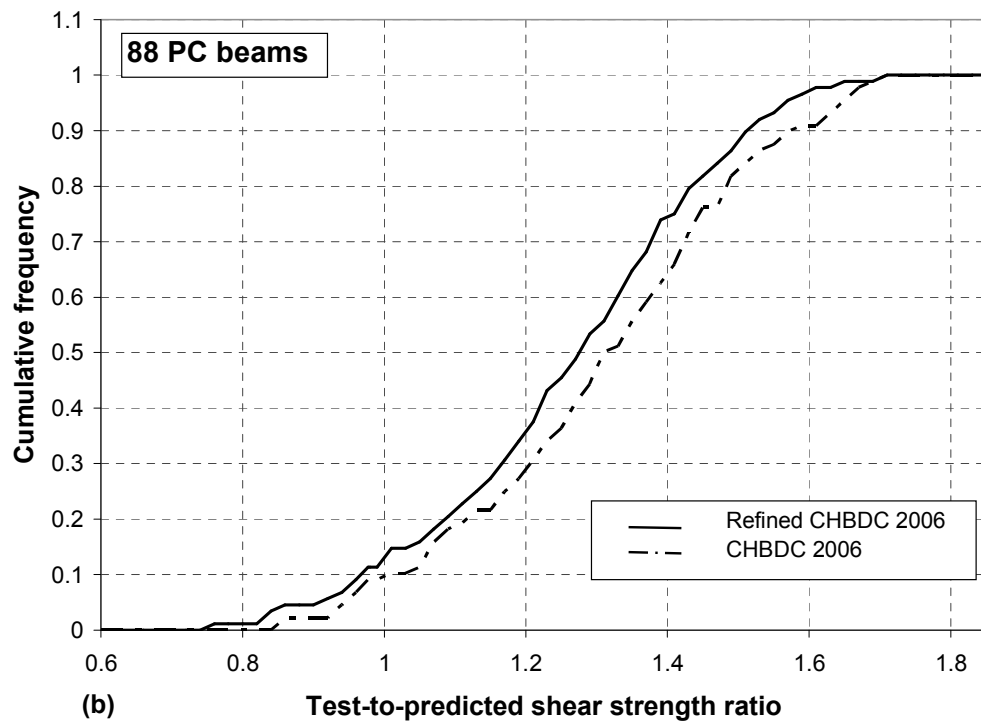
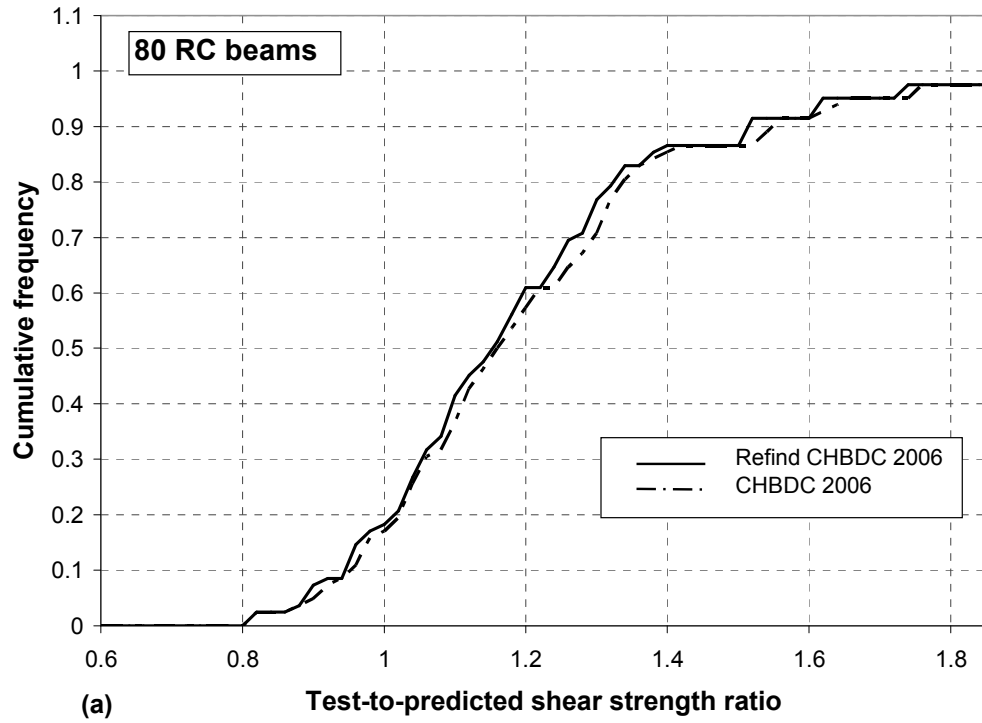


Fig. 6-6 Cumulative frequency of test-to-predicted ratios of refined CHBDC 2006 and CHBDC 2006 methods: (a) 80 RC beams, (b) 88 PC beams, with stirrups.

Note that the same experimental results were also used to verify the proposed evaluation method in Chapter 5.

Figure 6-6 compares the cumulative frequency diagram of the test-to-predicted shear strength ratios from the refined 2006 CHBDC method with the one from the 2006 CHBDC method. Fig. 6-6(a) shows that the refined ε_x equation does not have a significant effect on the predictions for reinforced concrete beams. As also explained in Chapter 5, the reason is there were not many tested beams with transverse reinforcement amount more than twice the minim amount specified by the 2006 CHBDC while bridge girders generally contain higher amount of transverse reinforcement. Note that more amount of reinforcement results in higher shear strength thus higher longitudinal strain due to shear. As a result, the higher the transverse reinforcement, the more significant the influence of the proposed refined ε_x equation on the predicted shear strength.

As shown in Fig. 6-6(b), the refined ε_x equation does improve the 2006 CHBDC predictions for prestressed members. Using the refined ε_x equation in the 2006 CHBDC shear design procedure improves the average test-to-code predicted shear strength ratio from 1.31 to 1.26 while the COV of ratios remains about the same. Although Figure 6-6(b) shows that refined ε_x equation increases the cumulative frequency values of the test-to-predicted ratios of less than 1.00, 14% of the refined method predictions are unsafe and only less than 5% of the ratios are below 0.90. This is still reasonable and even safer than the 2006 CHBDC prediction for the 80 RC members shown in Figure 6-6(a).

To more accurately predict the longitudinal strain of members with no stirrups in the 2006 CHBDC method, one can replace the simplified equation of $N_v = 2V$ with the one from MCFT $N_v = 2V \cot 2\theta$ in the 2006 CHBDC equation for ε_x . This was done to

predict shear strength of the 132 reinforced concrete tested beams with no stirrups, which were also used to verify the proposed evaluation method in Chapter 5.

The cumulative frequency diagram of the test-to-predicted shear strength ratios from the refined 2006 CHBDC method is shown together with the one from the original 2006 CHBDC in Figure 6-7.

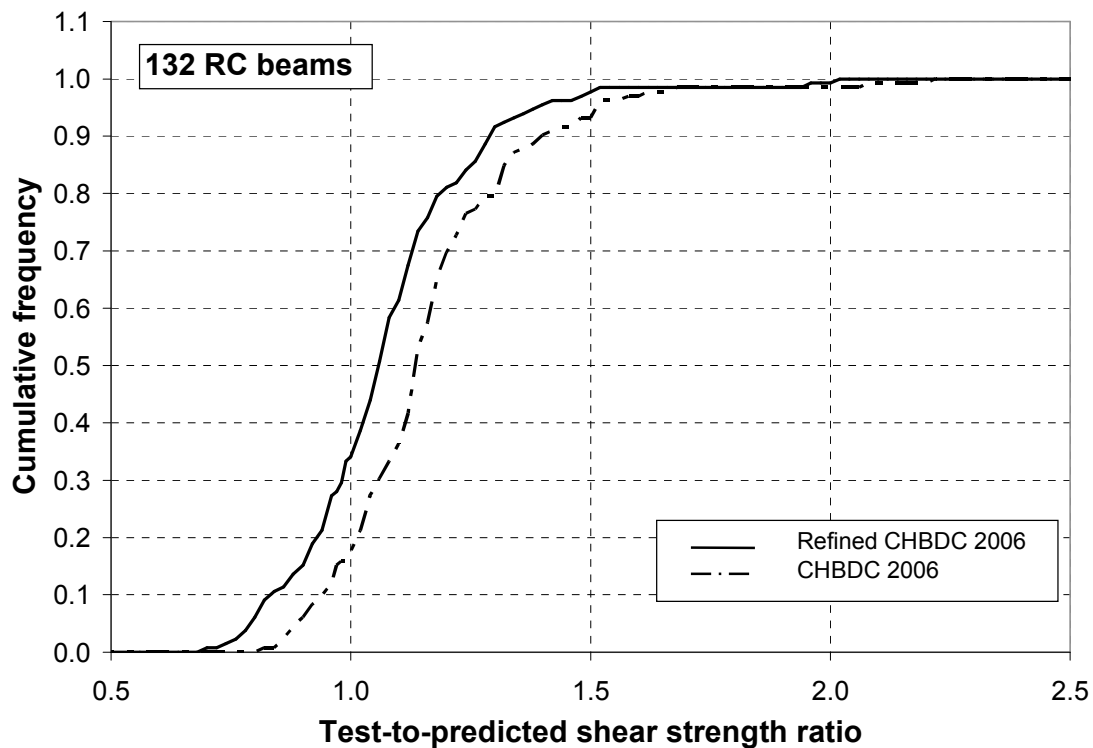


Fig. 6-7 Cumulative frequency of test-to-predicted ratios of refined CHBDC 2006 and CHBDC 2006 methods for 132 RC beams without stirrups.

As shown, the refined ε_x equation increases the number of unsafe predictions from 18% to 32% of the tested beams. It is due to the reason that the 2006 CHBDC uses the mid-depth longitudinal strain to predict the shear strength of a beam while Response 2000 shows that failure usually occurs at locations closer to flexural tension chord (see Fig. 4-10). The 2006 CHBDC uses a simplified equation for axial compression which is overly

conservative for members without stirrups and this compensates for the unconservative approach of using the mid-depth longitudinal strain in the shear analysis. Consequently, it is not recommended to use a more accurate ε_x in the 2006 CHBDC shear design provisions for members with no stirrups.

Chapter 7. Literature Review: Squat Shear Walls

7.1. Shear Strength of Squat Shear Walls

Benjamin and Williams (1953-1958) studied the behaviour of reinforced concrete squat walls at the Stanford University. In their experimental program, they tested walls surrounded by concrete frames and applied a monotonic concentrated lateral load at the tension side of the wall (top of tensile column). Some of their findings were size effect was not significant, vertical reinforcement had more influence on shear strength than horizontal reinforcement, and shear strength was considerably higher for the walls with smaller height-to-length ratios. Their last version of proposed empirical equation to estimate shear strength of squat shear walls is:

$$[7-1] V_u = \frac{0.1}{P} C + 2.2P$$

where:

$$[7-2] C = A_s f_c' \left[15 + 1.9 \left(\frac{L}{H} \right)^2 \right]$$

$$[7-3] P = \sigma_y \rho t L$$

in which L is wall length, H is wall height, ρ is distributed reinforcement ratio which is the same for both vertical and horizontal directions, t is wall thickness, A_s is compression column total reinforcement area, σ_y is wall reinforcement yield stress, P is wall panel strength, and C is compression column strength. The limitations they identified for their equations are as follows: $\rho \leq 1.5\%$, $42 \leq \sigma_y \leq 52$ ksi, $0.9 \leq L/H \leq 3$, $P/C \leq 3.26$.

Later an extension of Benjamin and William's research was conducted at the Massachusetts Institute of Technology (MIT) whose results were reported by Antebi et

al. (1960). The primary aim of the program was to predict the shear strength of low rise walls under blast loading. Once again, the walls were surrounded by concrete frames. The majority of walls were tested under blast loading while a few of them were tested under monotonic static loading.

Using results of the tests done at Stanford University and MIT, Antebi et al. (1960) proposed two sets of empirical equations to predict the shear strength of low rise walls under static and dynamic (blast) loading. Based on the proposed equations, shear strength of low rise walls was a function of height-to-length ratio, frame reinforcement area and yield stress, and amount of equal vertical and horizontal distributed reinforcement in the wall. They also identified limitations in their method; however, these were less restricting than those identified by Benjamin and Williams.

dePaiva and Seiss (1965) conducted a series of tests of simply supported deep beams with applied concentrated load at the top. They found that in deep beams, stirrups would not engage appreciably in shear force transfer since load was directly transferred to the supports by concrete compression struts (arch action). These results on deep beams led to a number of recommendations in the 1960s for shear strength of shear walls. For example, Uniform Building Code (UBC 1967) shear wall provisions considered no steel contribution in walls with height-to-length ratio equal to or less than 1.0 and limited total shear stress of walls with height-to-length ratio equal to or greater than 2.0 to $v_u \leq 10\sqrt{f_c'}$ in psi units. On the other hand, it considered concrete contribution of $v_c = 5.4\sqrt{f_c'}$ in psi units for walls with height-to-length ratio equal to or less than 1.0 and $v_c = 2\sqrt{f_c'}$ in psi units (as in shallow beams) for walls with height-to-length ratio of equal to or greater than 2.7. Linear interpolation was used for intermediate values.

Additional tests on deep beams by Crist (1966) and Leonhardt and Walther (1966) showed that arch action (a direct strut from the load to the support) depends upon how the load is applied. In deep beams, the load is usually applied on the compression face which results in significant arch action. When a deep beam is loaded indirectly using a transverse beam, the arch action is greatly reduced and the quantity of stirrups becomes very important.

In 1971, shear wall provisions first appeared in ACI 318. The background to these provisions was presented by Cardenas et al. (1973). Steel contribution in shear was developed based on truss analogy which resulted in the same formula as for steel contribution in shallow beams. Concrete contribution was developed to be the lesser of shear forces that resulted in web cracking and flexural shear cracking. Below is ACI 318-71 shear provisions for shear walls in psi units.

$$[7-4] \quad v_c \leq 3.3\sqrt{f'_c} + \frac{N_u}{4l_w h}$$

$$[7-5] \quad v_c \leq 0.6\sqrt{f'_c} + \frac{l_w(1.25\sqrt{f'_c} + 0.2N_u / l_w h)}{M_u / V_u - l_w / 2}$$

$$[7-6] \quad v_c \geq 2(1 + 0.002N_u / A_g)\sqrt{f'_c}$$

$$[7-7] \quad v_s = \rho_h f_y$$

$$[7-8] \quad v_c + v_s \leq 10\sqrt{f'_c}$$

$$[7-9] \quad V_u = (v_c + v_s)hd$$

in which V_u is ultimate shear strength, h is wall thickness, l_w is wall length, ρ_h is horizontal reinforcement ratio, d is distance from extreme compression fiber to centroid

of concentrated flexural reinforcement, and A_g is wall cross-section gross area. The above equations are still in the current ACI non-seismic shear design provisions for walls.

Equation [7-4] is the shear stress causing web cracking, which almost always governed for low rise walls, while Eq. [7-5] is shear stress causing flexural shear cracking. In ACI 318-71, the concrete contribution to shear strength in walls is not taken less than the concrete contribution in shallow beams as given by Eq. [7-6]. Total shear stress was limited to avoid diagonal crushing of concrete (Eq. 7-8). Cardenas et al. (1973) compared the predictions from ACI 318-71 with previous test data and found that ACI 318-71 predictions were safe and satisfactory.

Barda (1972) conducted tests on eight squat shear walls which had flanges and top concrete beam to transfer the load to the top edge of the wall. Six walls were tested under cyclic loading while the remaining two were subjected to monotonic loading. Barda investigated the effect of wall aspect ratio, flexural reinforcement, horizontal and vertical distributed reinforcement ratios on shear strength of squat walls and proposed the following equation:

$$[7-10] V_u = (8.4\sqrt{f'_c} + 0.95\rho_n f_y)hd \quad (\text{in psi units})$$

where h is wall thickness, and ρ_n is vertical reinforcement ratio. Later Barda et al. (1977) proposed another equation that accounted for the influence of wall aspect ratio and axial force.

$$[7-11] V_u = (8\sqrt{f'_c} - 2.5\sqrt{f'_c} \frac{h_w}{l_w} + \frac{N_u}{4l_w h} + \rho_n f_y)hd \quad (\text{in psi units})$$

where h_w is wall height, l_w is wall length and N_u is wall axial compression force.

Park and Paulay (1975) and Paulay et al. (1982), based on walls tested at the University of Canterbury, reported that ductile behaviour of squat shear walls were achievable if horizontal shear reinforcement was sufficient to avoid shear failure at flexural capacity level. They also proposed no reliance on concrete contribution to shear strength of squat shear walls should be made if ductile behaviour was desired. From their experimental program, Paulay et al. (1982) concluded that diagonal bars at the base of squat shear walls avoided sliding shear failure under load reversals thus improved the ductile behaviour of squat shear walls.

Hernandez (1980) tested 23 walls all with top slab and some with intermediate slabs under cyclic loading. He investigated the effect of wall aspect ratio, horizontal and vertical reinforcement ratios, concrete compressive strength, axial load, and boundary conditions. Based on the results, Hernandez proposed the following equations to determine shear strength of walls.

$$[7-12] V_0 = (1.6 - 0.3(\frac{h_w}{l_w})^2)\sqrt{f_c'} \geq 0.5\sqrt{f_c'}$$

$$[7-13] V_c = A \left(V_0 \sqrt{1 + \frac{\sigma}{V_0}} \right); \quad \frac{\sigma}{V_0} \leq 5$$

$$[7-14] V_s = A(\rho f_y)$$

where σ is wall compressive stress (axial force/ gross concrete area), A is area of wall cross-section, ρ is vertical reinforcement ratio if $h_w/l_w \leq 1$ or horizontal reinforcement ratio otherwise. In these equations, all forces are in kgf, stresses are in kgf/cm², and lengths are in cm.

Seven rectangular squat walls with aspect ratio of 1.0 were tested by Cardenas et al. (1980). The load was transferred to the top edge of the wall by means of a stiff beam at the top. All walls were subjected to monotonic load except one, which was subjected to cyclic loading. They concluded that ACI318-77 design provisions for squat shear walls were reasonably safe for monotonic loading as well as cyclic loading. Furthermore, both horizontal and vertical reinforcement were found to contribute to shear strength of the tested walls.

Maier and Thürlimann (1985) tested ten flanged squat shear walls with height-to-length ratio of 1.0 and concluded horizontal reinforcement influence on shear resistance of squat walls was negligible, and cyclic loading did not reduce shear capacity of tested walls considerably. The dominant mode of failure in their test was crushing of concrete at the base.

Between 1985 and 1994, Saatcioglu together with other researchers tested 8 squat shear walls under cyclic loading to investigate the effect of vertical and horizontal reinforcement, aspect ratio, and reinforcement detailing at the base. All walls had top rigid beams and did not have flanges. The results were presented in a number of publications including Wirandianta (1985), Wirandianta and Saatcioglu (1986), Pieleette (1987), Wasiewicz (1988), Mohammadi-Doostdar (1994). They concluded that shear strength of squat shear walls were mostly influenced by the wall aspect ratio and base sliding due to shear was more critical for squat walls with height-to-length ratio of 0.25. They also concluded that special detailing at the base could improve shear sliding behaviour that would result in a more ductile behaviour of walls.

Wirandianta (1985) proposed a modification to ACI 318-83 special provisions for earthquake (which is still the same in ACI 318-05) to explicitly account for aspect ratio when determining concrete contribution to shear strength of walls. His proposed equation was:

$$[7-15] \quad v_c = \alpha_c \sqrt{f'_c} \quad (\text{in psi units})$$

where

$$[7-16] \quad \alpha_c = 6 - \frac{h_w}{l_w} \geq 2$$

Wood (1990) compared ACI 318 shear strength predictions for 143 previously tested squat shear walls with test results. She concluded that ACI 318 predictions were safe for walls with horizontal reinforcement ratio of $\rho_h f_y \leq 2.1$ MPa, which could be as little as 1.5 times the minimum reinforcement, while they became unsafe for other walls. She also concluded that modified truss analogy which assumes a constant concrete contribution in addition to steel contribution corresponding to a constant angle i.e. 45 degrees was not consistent with test results. She showed that shear strength of tested walls was considerably less sensitive to the amount of horizontal reinforcement compared to the predictions from the modified truss analogy. Based on experimental data and shear friction model, Wood proposed a lower-bound semi-empirical equation for shear strength prediction of squat walls:

$$[7-17] \quad V_n = \frac{A_{vf} f_y}{4A_{cv}}; \quad \sqrt{f'_c} \leq v_n \leq 10\sqrt{f'_c} \quad (\text{in psi units})$$

where A_{vf} is shear reinforcement area crossing the shear plane at the base, and A_{cv} is wall cross-section gross area.

Lefas et al. (1990) and Lefas and Kotsovos (1990) conducted a series of tests on seventeen reinforced concrete squat walls with height-to-length ratio of 1.0 and 2.0 under cyclic and monotonic loading. Walls included different amount of concentrated flexural reinforcement as well as vertical and horizontal distributed reinforcement and load was transferred to the walls by means of a rigid beam built on each wall top edge. From their experimental program, they concluded that dominant failure mode was vertical tension splitting of the concrete compression zone near the wall compression face at the base. Vertical reinforcement did not have a significant effect.

26 squat shear walls tested under cyclic loading were tested by Hidalgo et al. (1998, 2002). They evaluated the method proposed by Wood (1990) as well as ACI 318-95 provisions by comparing the predictions with the results they obtained. Their study showed that horizontal reinforcement had insignificant influence on the wall shear resistance. ACI predictions were conservative and satisfactory, but Wood's method predictions were slightly better.

Gulec et al. (2008) compared test results of 120 rectangular squat shear walls reported in the literature with predictions from Barda (1977) method, Wood (1990) method, and ACI 318-05 shear design provisions. The walls had minimum thickness of 51 mm, no diagonal reinforcement or additional reinforcement to control sliding shear, and height-to-length ratio of less than 2.0. It was concluded that sliding of the wall base was the dominant failure mode in the tested walls. The scatter in shear strength test-to-predicted ratios was substantial for all methods and Wood (1990) predictions were the best compared to experimental results. While ACI 318 predictions were conservative, Barda (1977) method predictions consistently overestimated the shear capacity of walls. It was

also seen that most of the conservative predictions of shear strength were associated with lightly reinforced walls.

7.2. Summary of Observed Behaviour

In all available test results reviewed in the literature, load was introduced at the top edge of the wall by a rigid beam. As a result, it is not surprising that many researches such as Benjamin and Williams (1953-1958), Barda (1972), Lefas et al. (1990), Wood (1990), and Hidalgo et al. (1998, 2002) have found the effect of horizontal reinforcement to be insignificant in shear and others such as Gulec et al. (2008) identified that base sliding was the dominant failure mode. If the top beam had been removed in the tests and load was distributed at top of the wall, it could have resulted in a larger contribution of horizontal reinforcement, as well as failure at lower load levels due to diagonal tension rather than at the base at higher load levels.

Although such a rigid beam increases the wall shear strength mostly against diagonal tension failure, such rigidity is not always available in real structures especially in the case of flexible diaphragms. The effect of such beams is investigated in the next chapter.

In contrast to diagonal tension failure mode, base sliding failure mode is not sensitive to how the load is applied at top of the wall. Based on comparisons made with experimental results of tested walls which generally had a top loading beam, current ACI code provisions have been found to conservatively capture this failure mode by many researchers such as Cardenas et al. (1980), Hidalgo et al. (1998, 2002), and (Gulec et al. 2008); thus should also be appropriate for walls without a top loading beam and with distributed load at top.

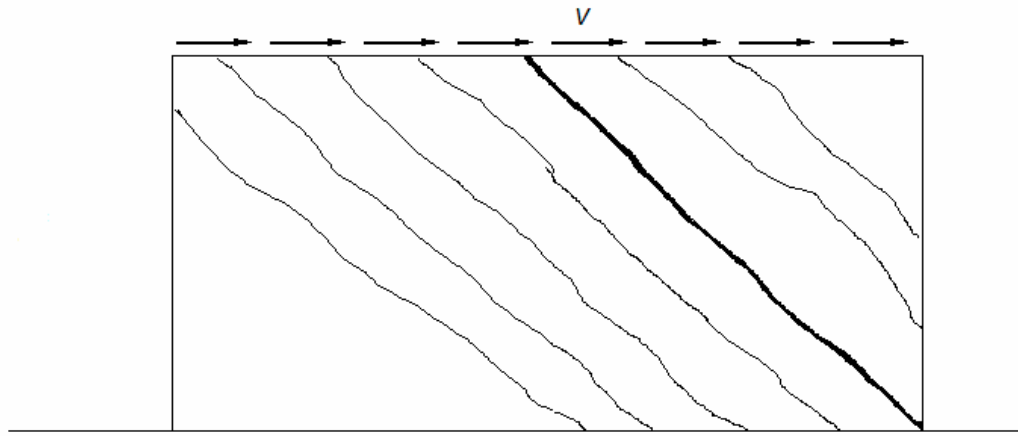
The most common shear failure modes of squat shear walls reported in the literature are diagonal tension failure mode, diagonal concrete crushing failure mode, and base sliding shear failure mode. These failure modes, which are explained in Paulay et al. (1982), are shown in Figure 7-1.

Diagonal tension failure mode (Fig. 7-1a) occurs when there is an insufficient amount of horizontal reinforcement to balance the diagonal compression force that does not go directly to the base. The diagonal tension failure plane that will develop is shown in Figure 7-1(a).

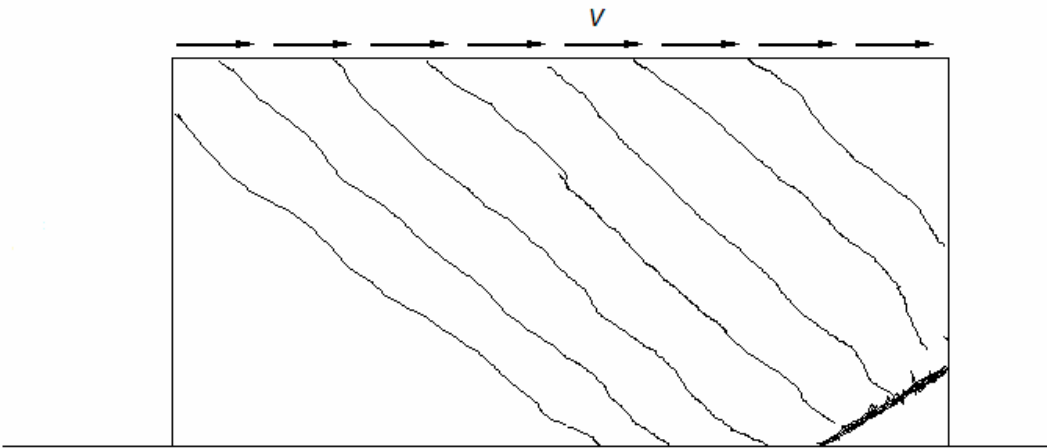
When there is sufficient distributed reinforcement to transfer shear, squat shear walls may fail in diagonal crushing of concrete which mostly happens near the compression face of wall base as shown in Figure 7-1(b). This usually happens in walls with large horizontal reinforcement ratio and large flexural capacity. Diagonal concrete crushing failure is undesirable since it is a sudden and brittle failure mode.

Third failure mode which is called base sliding failure mode is caused by cyclic loading. As a consequence of cyclic loading, compression face of the wall which had been in significant tension when the load was reversed, is cracked and thus the wall slides along the base (Fig. 7-1c) when it experiences high shear force and a significant number of load cycles.

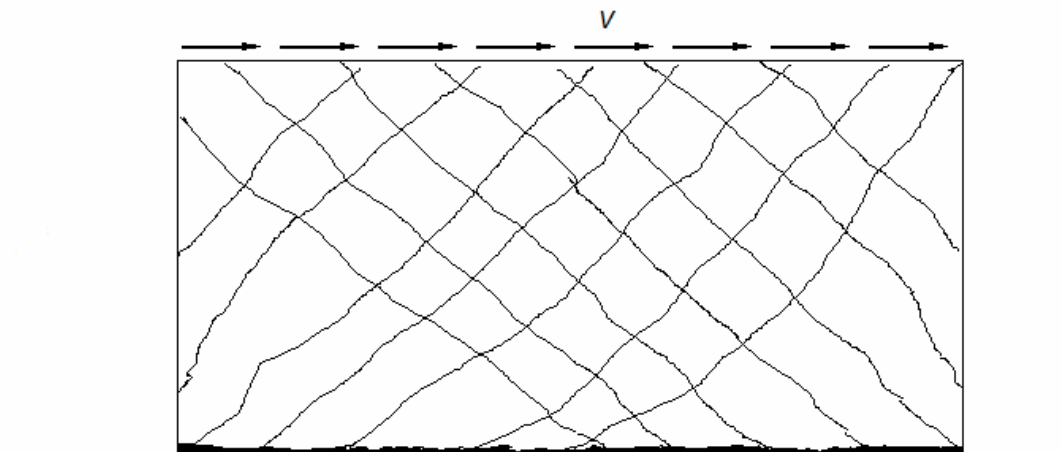
The last two failure modes are controlled in the codes by limiting the total shear stress. Some codes suggest using diagonal reinforcement at the base- foundation interface to avoid base sliding failure.



(a) Diagonal tension failure



(b) Concrete crushing failure



(c) Base sliding shear failure

Fig. 7-1 Squat walls shear failure modes.

7.3. Recent Code Approaches

7.3.1. ACI 318-05

The non-seismic provisions for the shear strength of squat walls in ACI 318 are the same approach as in ACI 318-71 given by Eqs. [7-4] to [7-9]. It also requires the same minimum amount of distributed vertical reinforcement as in the 1971 edition:

$$[7-18] \rho_n = 0.0025 + 0.5\left(2.5 - \frac{h_w}{l_w}\right)(\rho_h - 0.0025) \geq 0.0025$$

where ρ_n is distributed vertical reinforcement ratio and ρ_h is distributed horizontal reinforcement ratio. ρ_n need not to be taken greater than ρ_h .

In the additional requirements for seismic design, ACI 318 provides the following equation for shear strength of squat shear walls.

$$[7-19] V_n = A_{cv}(\alpha_c \sqrt{f'_c} + \rho_h f_y) \quad (\text{in psi units})$$

where A_{cv} is the total area of wall cross-section, $\alpha_c=3.0$ for $h_w/l_w \leq 1.5$, and $\alpha_c=2.0$ for $h_w/l_w \geq 2.0$. For intermediate values, linear interpolation is used. Based on ACI 318, vertical reinforcement ratio may not be less than horizontal reinforcement ratio.

To avoid concrete crushing, the total shear force is limited to $8A_{cv}\sqrt{f'_c}$ for all wall piers sharing a common lateral force and to $10A_{cv}\sqrt{f'_c}$ for individual wall piers. A wall pier refers to a vertical wall segment between two openings.

7.3.2. New Zealand Standards (NZS 3101-95)

According to NZS 3101, the shear strength of squat shear walls is:

$$[7-20] V = V_c + V_s = v_b d = (v_c + v_s) b_w d$$

$$[7-21] \quad v_c = (\sqrt{f_c'} + \frac{N^*}{A_g}) \quad (\text{in MPa units})$$

$$[7-22] \quad v_s = \rho_h f_y$$

where N^* is axial force, A_g is gross area of the wall cross-section, b_w is wall thickness, and effective depth d is equal to $0.8 l_w$ in which l_w is wall length. Moreover, the total shear stress v is limited to the lesser of $0.2f_c'$, $1.1\sqrt{f_c'}$, and 9 MPa.

In the seismic provisions, shear stress provided by concrete is given by

$$[7-23] \quad v_c = (\frac{5-\mu}{4})(0.27\sqrt{f_c'} + \frac{N^*}{4A_g}) \geq 0 \quad (\text{in MPa units})$$

$$[7-24] \quad v_c \geq 0.6 \sqrt{\frac{N^*}{A_g}} \quad (\text{in MPa units})$$

where μ is ductility factor and limited to 3.0 for squat shear walls. Concrete crushing is avoided by:

$$[7-25] \quad v \leq (\frac{\phi_{0w}}{\mu} + 0.15)\sqrt{f_c'} \quad (\text{in MPa units})$$

where ϕ_{0w} is overstrength factor.

7.3.3. 2004 CSA A23.3

In the 2004 CSA A23.3, the same equation as the one given for beams is used to determine shear strength of squat shear walls:

$$[7-26] \quad V = \beta \sqrt{f_c'} b_w d_v + \rho_h f_y b_w d_v \cot \theta$$

where shear length $d_v = 0.8 l_w$ in which l_w is wall length, concrete contribution factor $\beta = 0$, b_w is wall thickness, ρ_h is horizontal reinforcement ratio, and angle of principal compression θ can be freely chosen between 30 and 45 deg. The chosen angle is then

used to determine the amount of distributed vertical reinforcement from the following equation.

$$[7-27] \quad \rho_v = \rho_h \cot^2 \theta - \frac{P_s}{f_y A_g}$$

where ρ_h is the horizontal reinforcement ratio, P_s is axial load, and A_g is wall gross cross-section area. To avoid concrete crushing in the 2004 CSA A23.3, shear strength is limited to:

$$[7-28] \quad V \leq 0.15 f_c' b_w d_v$$

According to the 2004 CSA A23.3, distributed vertical reinforcement needed for shear given by Eq. [7-27] does not contribute to the wall flexural capacity. As a result, additional vertical reinforcement for flexure must be provided in addition to the distributed vertical reinforcement needed for shear.

Chapter 8. Comparison of NLFE Predictions with Experimental Results of Squat Shear Walls

8.1. General

In this chapter, experimental results of three squat shear wall tests reported in the literature are compared with nonlinear finite element predictions. The walls had different aspect ratios and different reported failure modes.

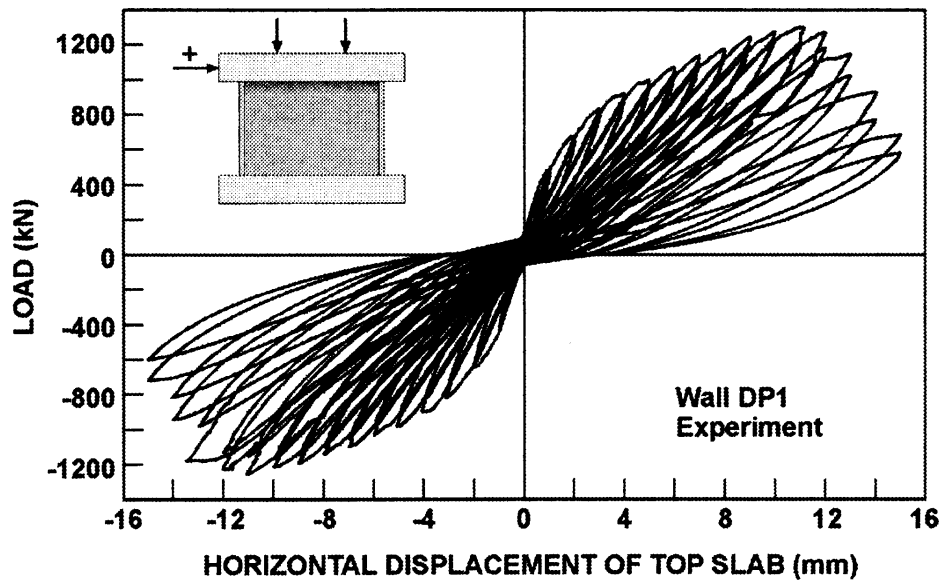
A brief introduction to the nonlinear finite element program VecTor 2 used in this study is given. The finite element program predicted behaviour for the squat shear walls is then presented. The implementation of the program is verified by comparing the finite element predictions with the wall test results. In addition, the influence of the top loading beam on the wall strength is studied. This is done by presenting the finite element results for the same three walls in which the top loading beam was removed and the load was distributed along the wall top edge.

8.2. Finite Element Program

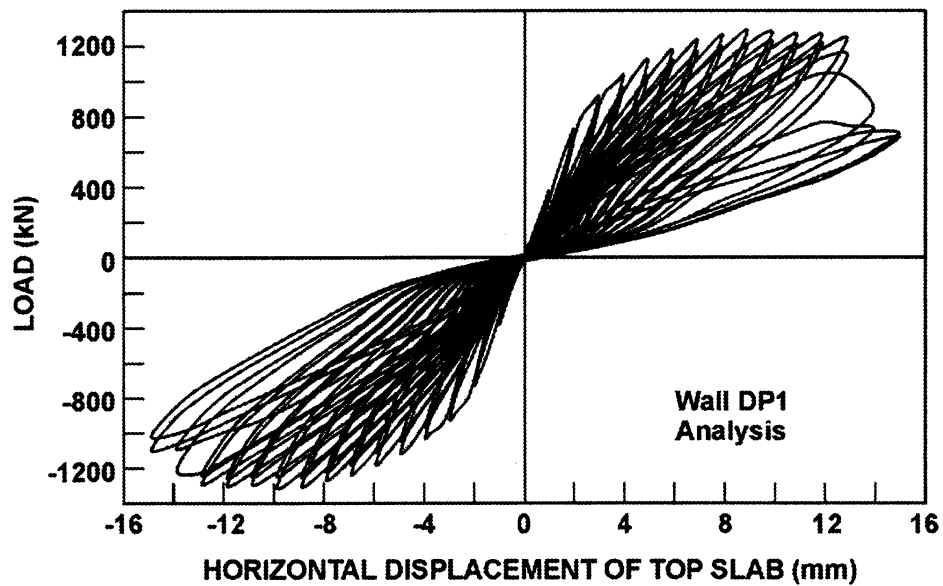
Program VecTor2 developed by Wong and Vecchio (2002) at the University of Toronto was used for nonlinear finite element analysis. The program performs nonlinear finite element analysis of concrete structures and explicitly accounts for interaction of moment and shear. Although VecTor 2 has simple elements and employs simple numerical techniques, it uses the state of the art material models to relate biaxial element strains to biaxial element stresses. In-plane elements of uniform stress and strain field are used in the program.

Two models for cracked reinforced concrete subjected to biaxial strains have been implemented in VecTor 2. One of the models is MCFT, which was explained in Chapter 3, and the other one is Disturbed Stress Field Model DSFM (Vecchio 2000). DSFM is conceptually similar to MCFT but it allows different orientations for the principal stress and strain directions. DSFM determines the difference between principal stress and principal strain orientations by calculating additional strains caused by crack slip. MCFT and DSFM predictions of shear strength are basically the same for ordinary structures. DSFM becomes more accurate for structural concrete that is heavily or very lightly reinforced in the orthogonal directions (Vecchio 2000).

Palermo and Vecchio (2004) verified VecTor 2 for shear walls. They compared the program predictions for four slender walls and two squat walls with the experimental results. All walls were subjected to cyclic loadings. The walls included two slender barbell shaped walls with height-to-length ratio of 2.4 (height = 4570 mm, width = 1910 mm) tested by Portland Cement Association (Oosterle et al. 1976), two rectangular slender walls with concealed end columns and height-to-length ratio of 2.0 (height = 1200 mm, length = 600 mm) tested by Pilakoutas and Elnashai (1995), and two flanged squat walls with height-to-length ratios of 0.70 and 0.67 (height = 2020 mm, width = 2885 mm and 3045 mm) tested at the University of Toronto (Palermo and Vecchio, 2002). The finite element predictions were in good agreement with the test results. As an example, comparison of the predicted load displacement curve with the test results for one of the squat walls (height = 2020 mm, width = 2885 mm) is shown in Figure 8-1.



(a)



(b)

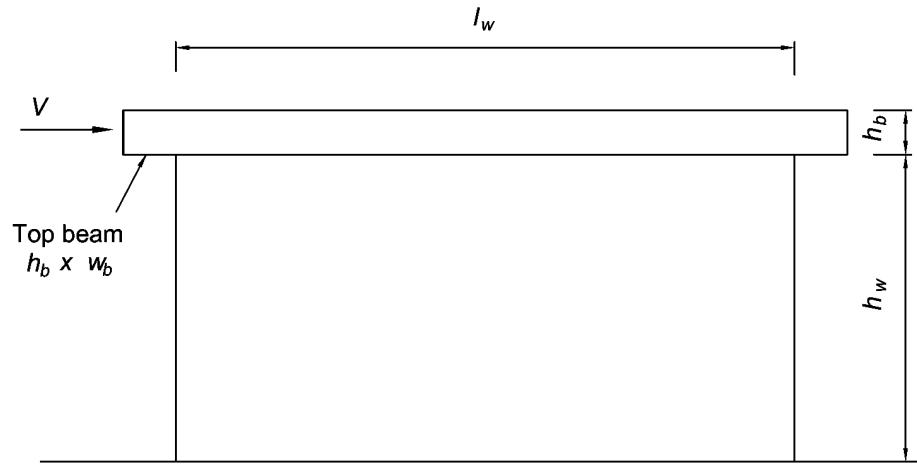
Fig. 8-1 Load-deformation responses of wall DP1: (a) observed, (b) calculated (Palermo and Vecchio, 2004).

8.3. Comparison with Wall Test Results

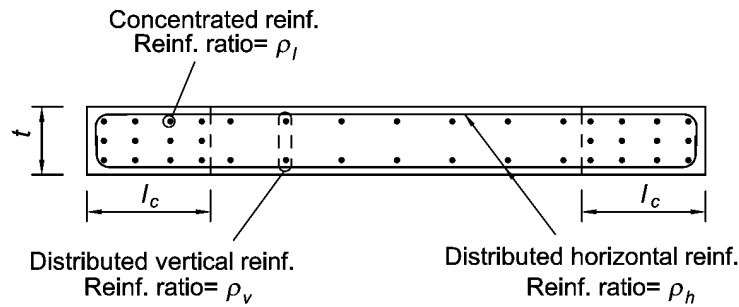
The squat shear walls that were previously tested generally had a rigid loading beam at the top. While such a rigid beam allows redistribution of shear force at top and therefore can significantly increase the shear resistance of a wall, it is not guaranteed that such a top rigidity or strength is available in real squat walls. Codes, however, should provide lower-bound predictions, which are not unconservative in any cases, thus for shear design purposes it is reasonable to ignore any top rigidity in squat walls.

The main purpose of this section is to show how the top loading beam in the tested walls may have influenced the shear capacity of walls and what type of failure is mostly affected by such a beam. Experimental results of three previously tested walls are compared with the finite element predictions for the walls with and without the top loading beam. In the walls without the top beam, the load is uniformly applied along the top of the wall.

Wall details as well as material properties are presented in Figure 8-2. The walls were tested by Wiradinata and Saatcioglu (1986), Kuang and Ho (2008), and Lefas et al. (1990) and had height-to-length ratios of 0.5, 1.0, and 2.0, respectively. The first two walls were tested under cyclic loading while the third one was tested under monotonic loading. They were selected since they had different reported failure modes i.e. diagonal tension failure (yielding of horizontal reinforcement), flexural failure (yielding of vertical reinforcement), and diagonal crushing of concrete. In the finite element analysis, all walls were monotonically loaded and shear force was applied in the left-to-right direction. The results presented hereafter are separated based on the wall reported failure modes.



Wall Elevation



Wall Cross Section

Geometry and Material Properties

Researcher Name	Specimen	h_w (mm)	l_w (mm)	l_c (mm)	t (mm)	h_b (mm)	w_b (mm)	ρ_v (%)	ρ_h (%)	ρ_l (%)	f_{vy} (MPa)	f_{hy} (MPa)	f'_c (MPa)
Wiradinata, Saatcioglu (1986)	Wall 1	1000	2000	-	100	300	500	0.80	0.25	-	435	425	25.0
Kuang, Ho (2008)	U1.0	1200	1200	-	100	300	300	0.92	1.05	-	520	520	30.4
Lefas et al. (1990)	SW26	1300	650	140	65	150	200	2.5	0.40	3.3	470	520	25.0

Fig. 8-2 Details of the three previously tested walls in the literature examined to compare experimental results with finite element predictions.

8.3.1. Diagonal Tension Failure

This wall tested by Wiradinata and Saatcioglu (1986) had a height-to-length ratio of 0.5. Figure 8-3 presents the load-displacement curves for the wall from the experimental results (dotted line) as well as finite element predictions (solid line). Finite element predictions are in reasonably good agreement with the experimental results. Sectional analysis for pure flexure assuming plane sections remain plane (plane section analysis) predicts the flexural capacity of the wall is at $V = 544$ kN. Actual wall maximum strength was reached at $V = 575$ kN and the reported failure mode was diagonal tension. In comparison, finite element prediction of wall maximum strength is $V = 527$ kN.

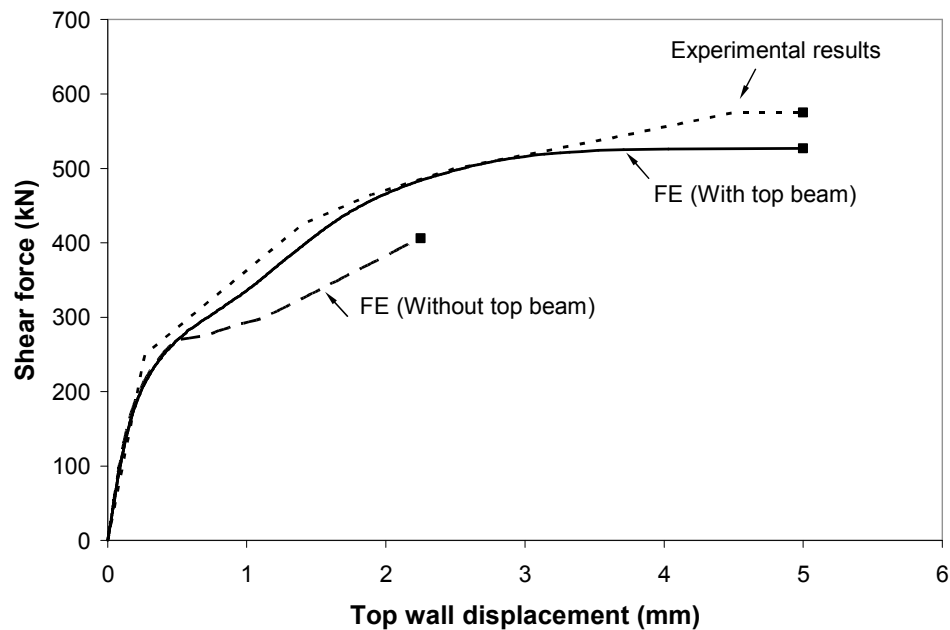


Fig. 8-3 Comparison of experimental load-top displacement curve with finite element prediction for wall tested by Wiradinata and Saatcioglu (1986).

As was mentioned above, wall strength from test results is higher than those predicted by the plane section analysis for pure flexure and finite element analysis. The reason

might be the strain hardening in the vertical reinforcement. As the steel strain hardening information was not reported, finite element analysis as well as plane section analysis were done assuming no strain hardening for steel.

Finite element prediction of load-displacement curve for the same wall in which the top beam was removed and shear force was uniformly distributed over the wall top edge is also presented (dashed line). Displacements correspond to the wall top edge mid-point as the top wall displacement varies over the wall top edge because there is not a rigid beam at top to make the top displacement uniform over the wall top edge. Notice that the wall strength is reduced to 408 kN due to diagonal tension shear failure, which is 23% reduction in strength compared to finite element predictions for the wall with the top beam.

The reason is examined in Figure 8-4, which shows sectional shear stress distributions of both walls (with and without a top beam) at top, mid-height, and base of the walls prior to failure. Shear is redistributed by the top beam toward the left side of the wall (Fig. 8-4a) in order to be transferred through diagonal struts that go directly to the base without a need for horizontal reinforcement. This is not the case in the wall without the top beam and therefore it reaches its strength earlier due to yielding of horizontal reinforcement (diagonal tension shear failure). Figures 8-4(b) and 8-4(c) show that shear stress distributions at the mid-height and the base are more uniform for the wall without the top beam.

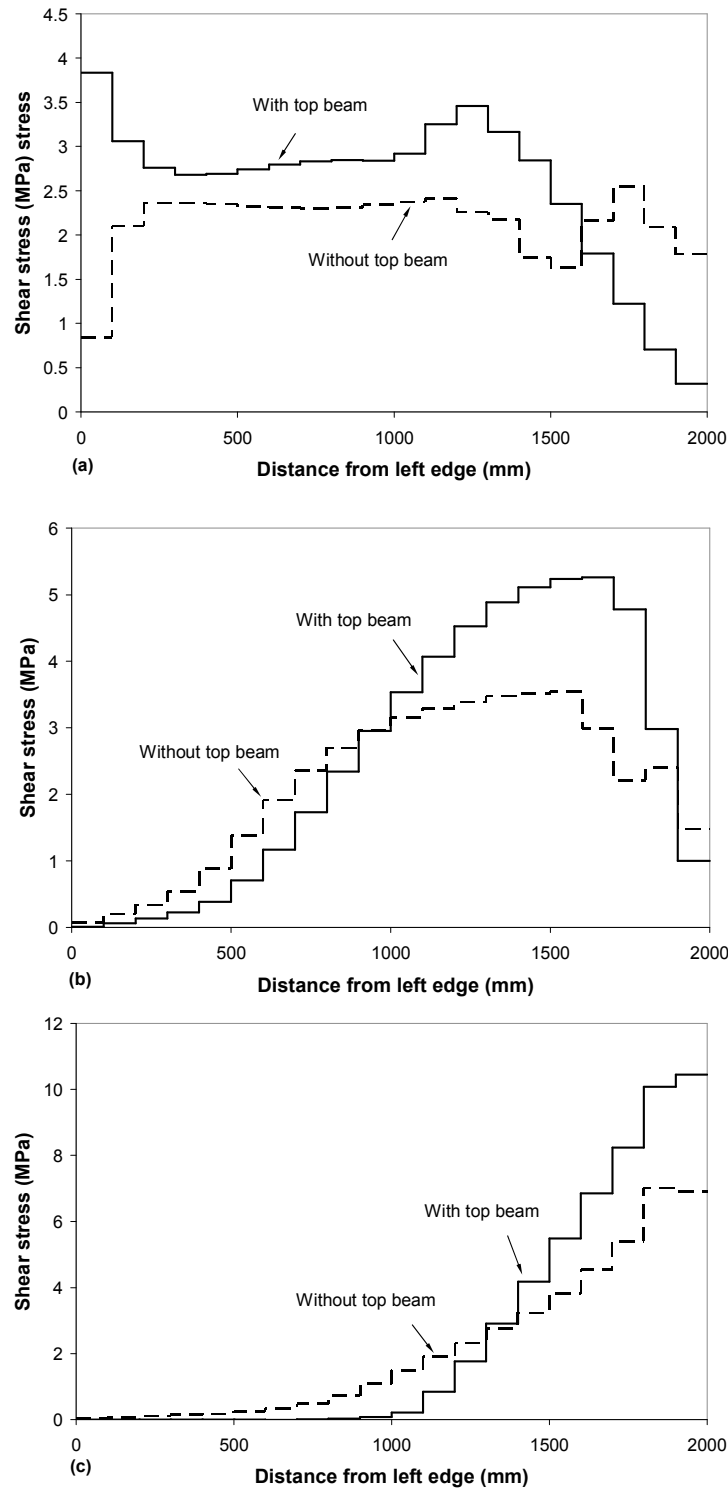


Fig. 8-4 Comparison of finite element predictions of shear stress profiles along (a) top section, (b) mid-height section, (c) base section of the wall tested by Wiradinata and Saatcioglu (1986) and the same wall without the top beam and distributed force applied at top.

In Figure 8-5 the vertical steel stress profiles at the base immediately prior to failure are compared. The wall with the top beam reaches the flexural capacity while the other wall does not. Notice that all vertical reinforcement has yielded in the flexural tension side of the wall with the top beam.

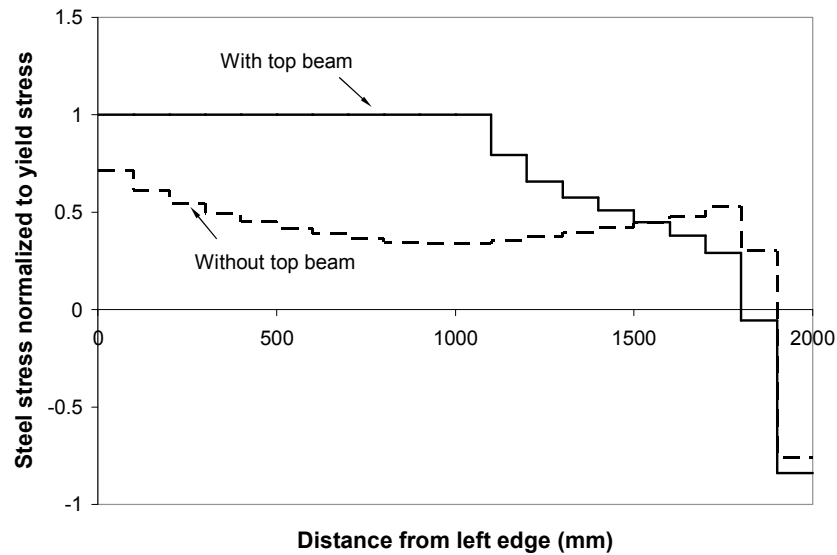


Fig. 8-5 Comparison of finite element predictions of vertical reinforcement stresses at the base of the wall tested by Wiradinata and Saatcioglu (1986) and the same wall without the top beam and distributed force applied at top.

8.3.2. Yielding of Vertical Reinforcement Failure

The wall tested by Kuang and Ho (2008) had a height-to-length ratio of 1.0. It was expected to fail in flexure since a sufficient amount of horizontal reinforcement was provided for shear. As opposed to the other two walls discussed in this chapter which did not have axial compression, this wall was subjected to an axial compression of 300 kN.

Figure 8-6 compares the actual load-deformation curve with the finite element predictions. Sectional analysis for pure flexure assuming plane sections remain plane predicts a shear force at flexural capacity equal to 321 kN. The actual wall strength and

the finite element predicted strength are also about 330 and 325 kN. Finite element predictions for the same wall with no top beam and distributed force at top are also shown in Figure 8-6 (dashed line). It is shown that the top beam does not significantly influence the flexural capacity and load deformation curve of the wall if shear reinforcement is sufficient.

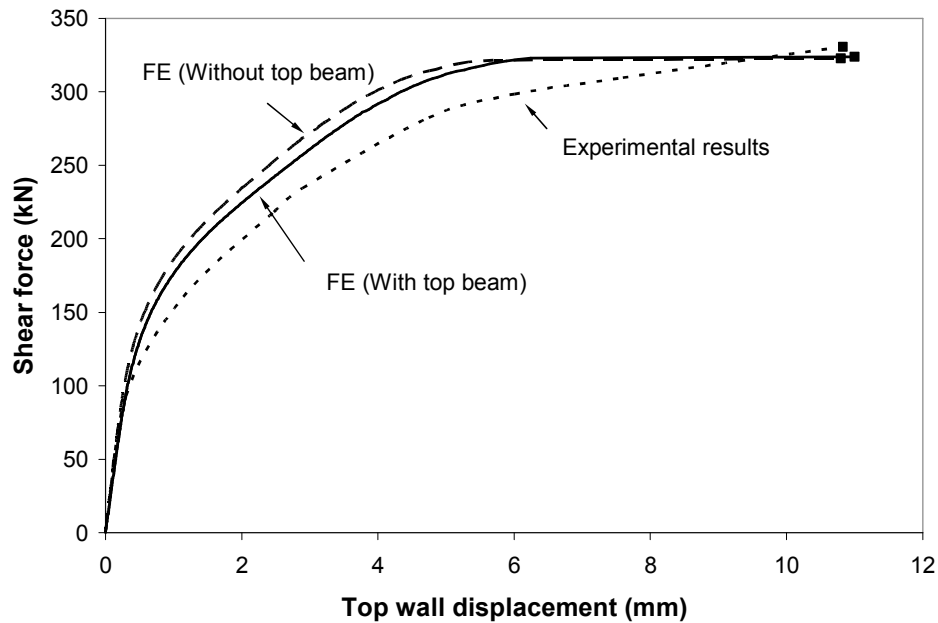


Fig. 8-6 Comparison of experimental load-top displacement curve with finite element prediction for wall tested by Kuang and Ho (2008).

Figure 8-7 shows finite element predictions of sectional shear stress distributions for walls with and without top beam at top, mid-height, and base of the walls prior to their failure. Once again, shear is redistributed toward left side of the wall at top of the wall

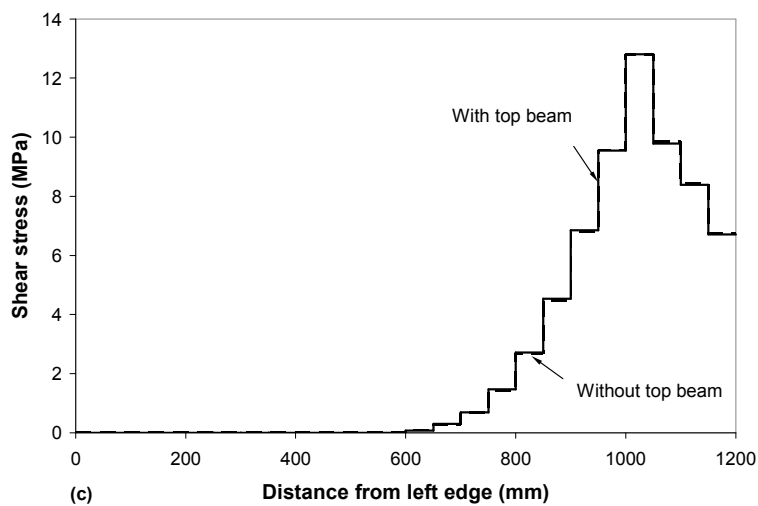
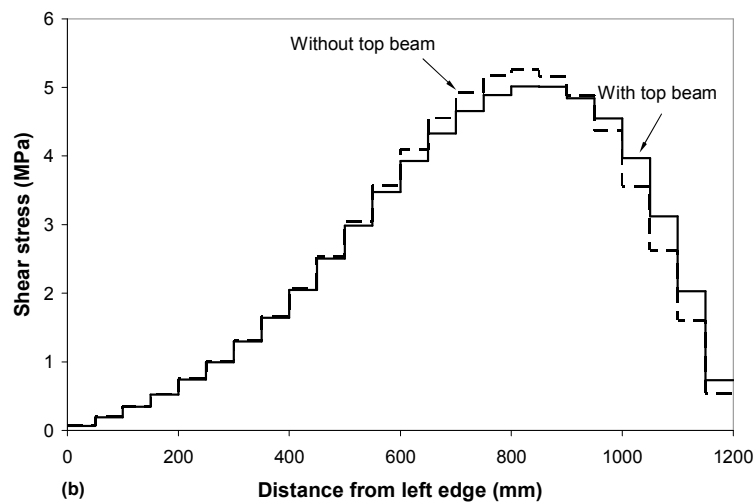
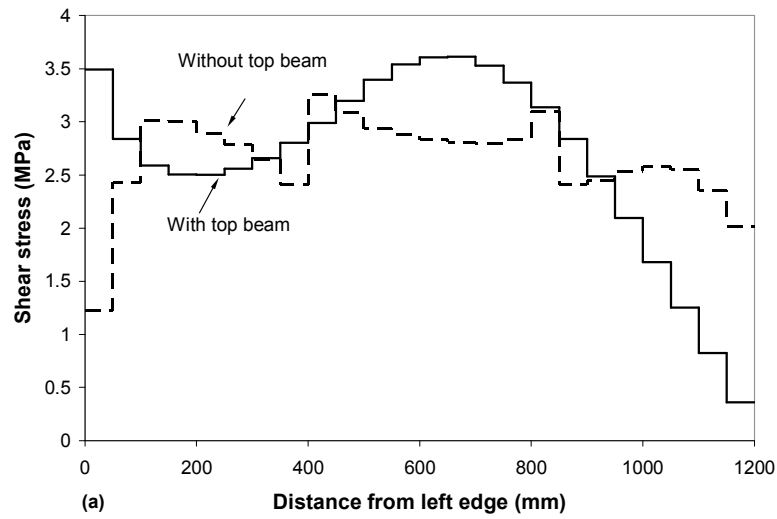


Fig. 8-7 Comparison of finite element predictions of shear stress profiles along (a) top section, (b) mid-height section, (c) base section of the wall tested by Kuang and Ho (2008) and the same wall without the top beam and distributed force applied at top.

with the top beam (Fig. 8-7a). This does not influence the shear distribution at mid-height and the base as shown in Figures 8-7(b) and 8-7(c) thus does not affect the flexural strength.

Figure 8-8 illustrates the vertical steel stress profiles at base of the walls prior to failure. As shown, both walls are predicted to fail in flexure since a significant portion of vertical reinforcement at the tension side of the wall is yielding.

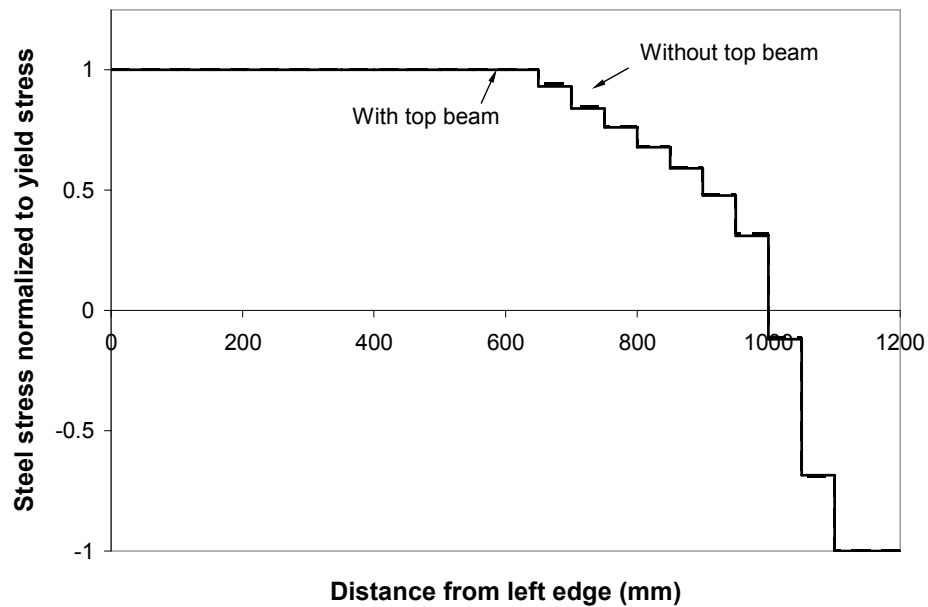


Fig. 8-8 Comparison of finite element predictions of vertical reinforcement stress at the base of the wall tested by Kuang and Ho (2008) and the same wall without the top beam and distributed force applied at top.

8.3.3. Concrete Crushing Failure

Leftas et al. (1990) reported that their wall specimen SW26 failed due to crushing of the concrete at compression side of the wall base. Finite element analysis also predicts the same failure mode for the wall. The experimental load-deformation curve and the finite element prediction are presented in Fig.8-9. Finite element predictions and experimental

results are in good agreement. Finite element prediction of shear strength is $V=110$ kN. This is less than the shear force at flexural failure predicted by the plane section analysis for pure flexure, which is equal to 124 kN. The reason is that concrete crushes in the principal direction at the compression side of the base. Finite element predictions for the same wall without the top beam and distributed force at top are also shown in Figure 8-9. Finite element predicted failure mode for the latter wall is also crushing of concrete and as shown shear strength is not highly affected by the top beam.

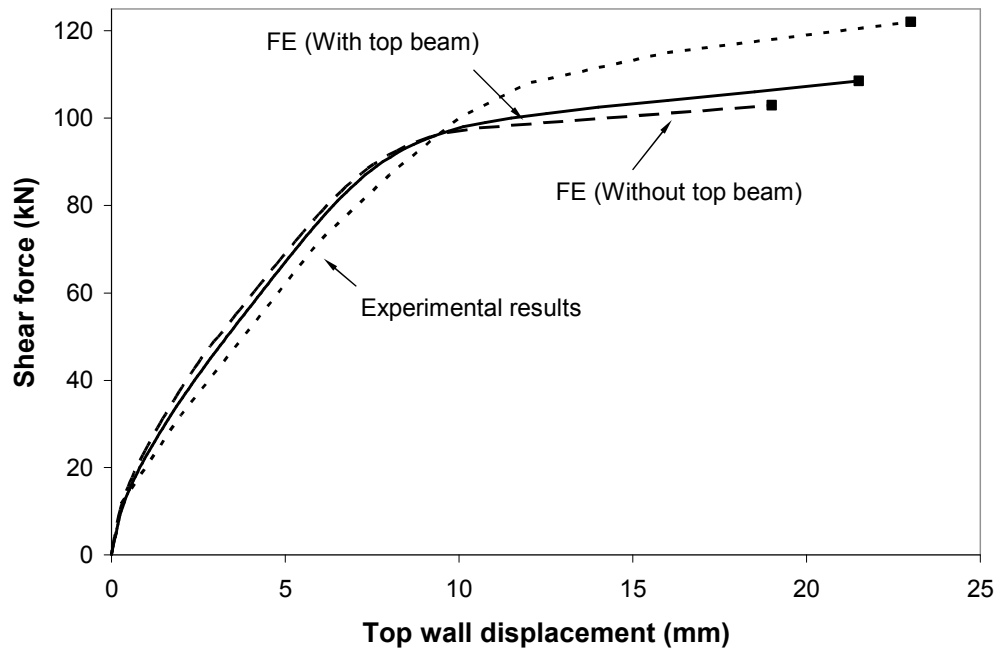


Fig. 8-9 Comparison of experimental load- top displacement curve with finite element prediction for wall tested by Lefas et al. (1990).

Figure 8-10 compares the finite element predictions of sectional shear profiles at top, mid-height, and base for the walls with and without the top beam. Notice again that the wall with the top beam carries significant portion of shear by redistributing the shear toward the left side at top and therefore making use of diagonal concrete struts that go

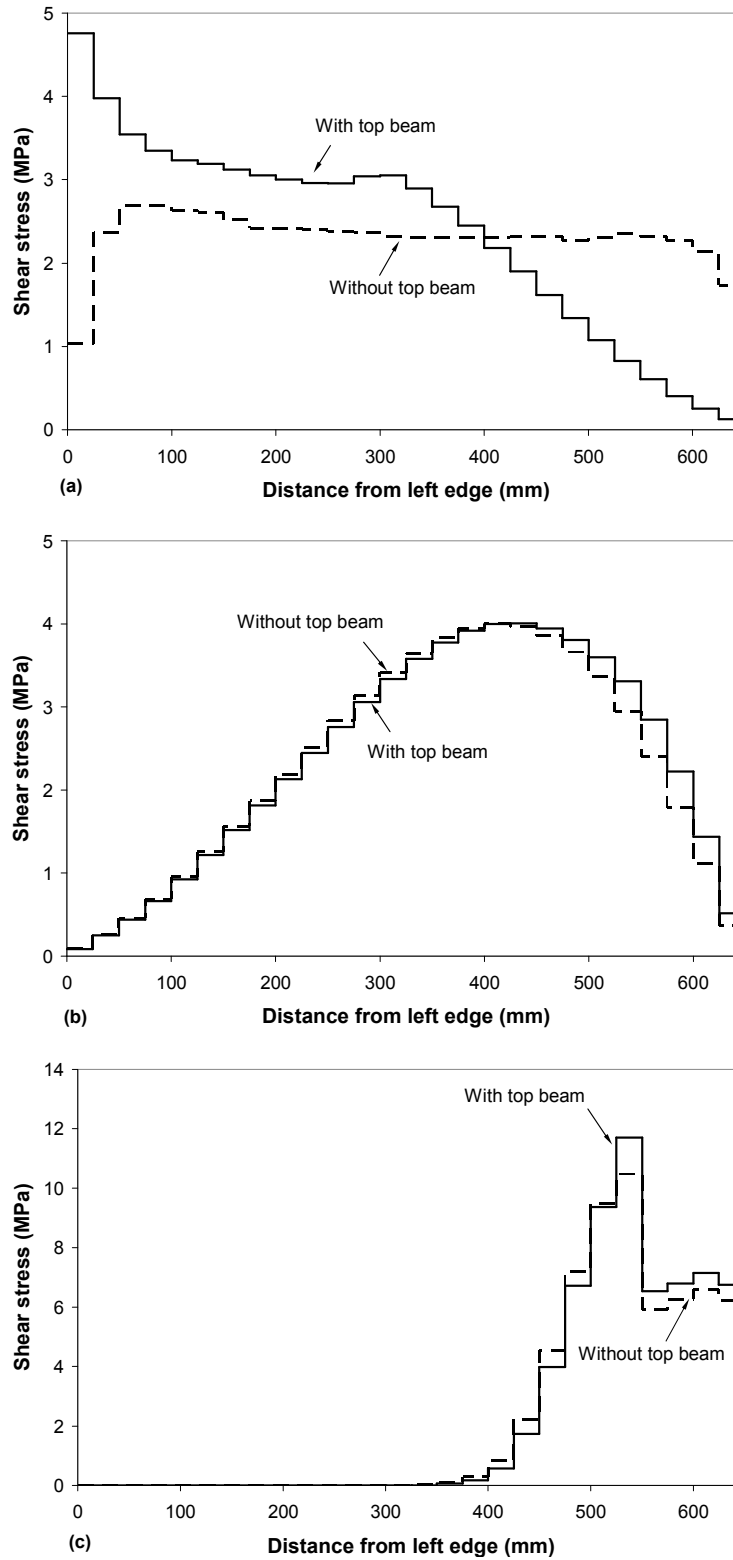


Fig. 8-10 Comparison of finite element predictions of shear stress profiles along (a) top section, (b) mid-height section, (c) base section of the wall tested by Lefas et al. (1990) and the same wall without the top beam and distributed force applied at top.

directly to the support. On the other hand, the shear distribution at top is more uniform for the wall without the top beam (see Fig. 8-10a). Top beam, however, does not significantly influence the shear stress distribution at mid-height or the base of the wall (see Fig. 8-10b and 8-10c) thus the wall shear strength is not significantly influenced by the top beam.

Sectional models for shear predict insignificant contribution of flexural compression chord in shear. This is not true at the base of a squat wall as shown in Fig. 8-10(c). Compression stress in the principal direction is maximum in the compression zone at the base of the wall due to the combination of stresses caused by flexure and shear. This results in concrete crushing in the wall compression zone at the base for highly reinforced walls.

In conclusion, comparison of finite element program (VecTor 2) predictions with the actual behaviour of three previously tested walls presented in this chapter show that the shear strength at diagonal tension shear failure (yielding of horizontal reinforcement) may be greatly increased by the top rigid loading beam commonly used in the squat shear wall tests to transfer shear to the wall top edge. In contrast, flexural failure as well as concrete crushing shear failure is not significantly influenced by the top beam. It can also be concluded that base sliding shear failure is not influenced by the top beam. In highly reinforced walls where horizontal reinforcement does not yield, shear distribution at the base is not significantly influenced by the top loading beam.

Chapter 9. Analytical Study of Flexural and Shear Resistance of Squat Shear Walls

9.1. General

This chapter involves flexural and shear resistance of squat shear walls. The brief background of some available methods to predict the shear strength of squat shear walls is presented. In addition, nonlinear finite element analysis (VecTor 2) is used to determine shear and flexural capacity of such walls and the results are compared with the code predictions. A new method to determine the flexural resistance of squat shear walls which accounts for flexure-shear interaction at the wall base is presented and the predictions are compared with the finite element results. Proposed refinements to the 2004 CSA A23.3 provisions for squat shear walls are also introduced.

As explained earlier in Chapters 7 and 8, tested squat shear walls generally had a top loading beam which increases the shear resistance of such walls if they fail due to horizontal reinforcement yielding. In the walls analyzed here, shear force is uniformly distributed over the wall top edge and no top loading beam is included since the purpose is to determine the lower-bound resistance of the walls.

9.2. Traditional Approach for Flexural Resistance of Deep Beams

Leonhardt and Walther (1966) performed linear finite element analysis of uncracked concrete to determine flexural capacity of single span deep beams. They concluded that internal flexural lever-arm for a deep beam is less than what is predicted by the plane section analysis. This phenomenon resulted in lower flexural capacity of such beams compared to the plane section analysis predictions. They proposed equations for internal flexural lever-arm of a deep beam. In the proposed equations, internal flexural lever-arm

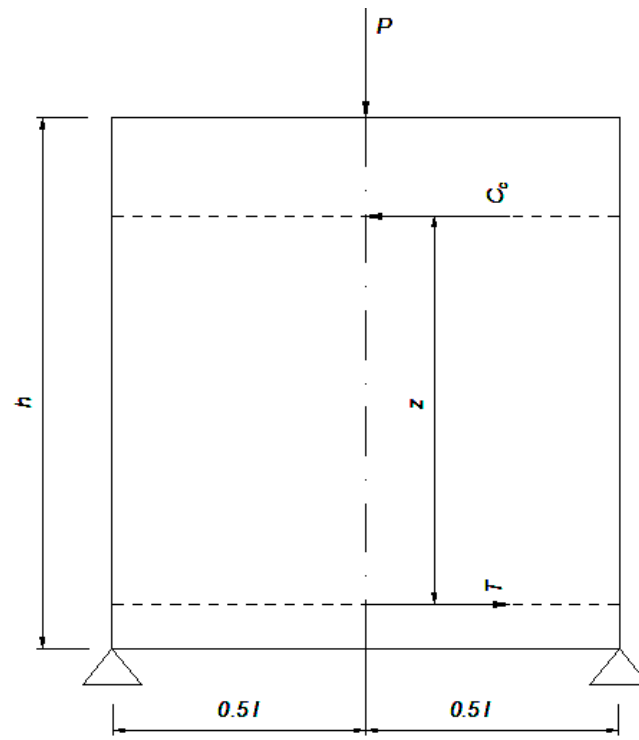
is equal to 0.6 times beam height for a deep beam with span-to-height ratio less than or equal to 1.0 and is equal to 0.8 times the beam height for a beam with span-to-height ratio of 2.0 and linearly varies from a beam with span-to-height ratio of 1.0 to a beam with span-to-height ratio of 2.0.

Half of a single span deep beam has a similar geometry and similar boundary conditions as a squat shear wall. A deep beam and a squat shear wall are shown in Figs. 9-1(a) and (b). While parameters shown in Fig. 9-1(a) are the ones used by Leonhardt and Walther (1966) equations, parameters shown in Fig. 9-1(b) are the parameters commonly used for squat shear walls. To apply the Leonhardt and Walther (1966) equations to a squat shear wall, internal flexural lever-arm z in Fig. 9-1(a) becomes jd shown in Fig. 9-1(b) ($z = jd$), beam span l in Fig. 9-1(a) becomes two times wall height h_w shown in Fig. 9-1(b) ($l = 2h_w$), and beam height h in Fig. 9-1(a) becomes wall length l_w shown in Fig. 9-1(b) ($h = l_w$). Leonhardt and Walther (1966) equations for internal flexural lever-arm applied to a squat shear wall are:

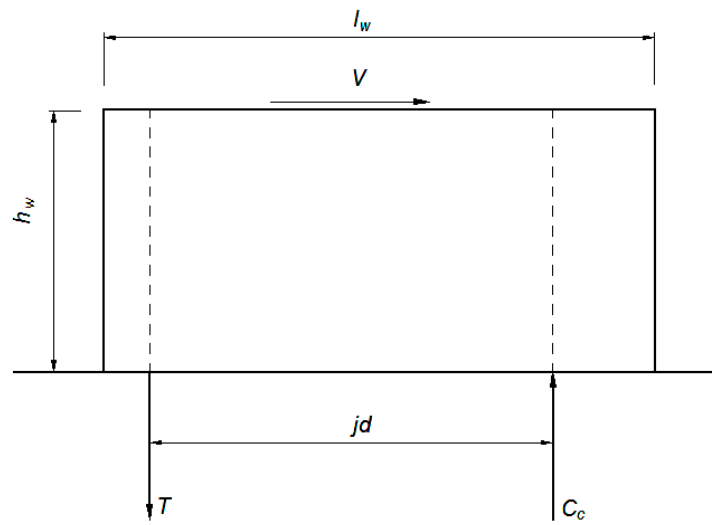
$$[9-1] \quad jd = 0.4(h_w + l_w) \quad \text{where} \quad 0.5 \leq \frac{h_w}{l_w} \leq 1.0$$

$$[9-2] \quad jd = 1.2h_w \quad \text{where} \quad \frac{h_w}{l_w} < 0.5$$

in which l_w is wall length, h_w is wall height, and jd is internal flexural lever-arm at the base of the wall. Leonhardt and Walther (1966) also proposed that the flexural tension zone of a deep beam is small; therefore, flexural tension reinforcement should be concentrated at the flexural tension face.



(a) Deep beam



(b) Squat shear wall

Fig. 9-1 Comparison of a deep beam and a squat shear wall.

9.3. 2004 CSA A23.3 Approach for Flexural and Shear Resistance of Squat Shear Walls

The 2004 CSA A23.3 requires that a squat shear wall behaves as a single uniform shear element. Figure 9-2 shows a truss model for uniform shear stress distribution in a squat shear wall when the axial force is small and therefore neglected.

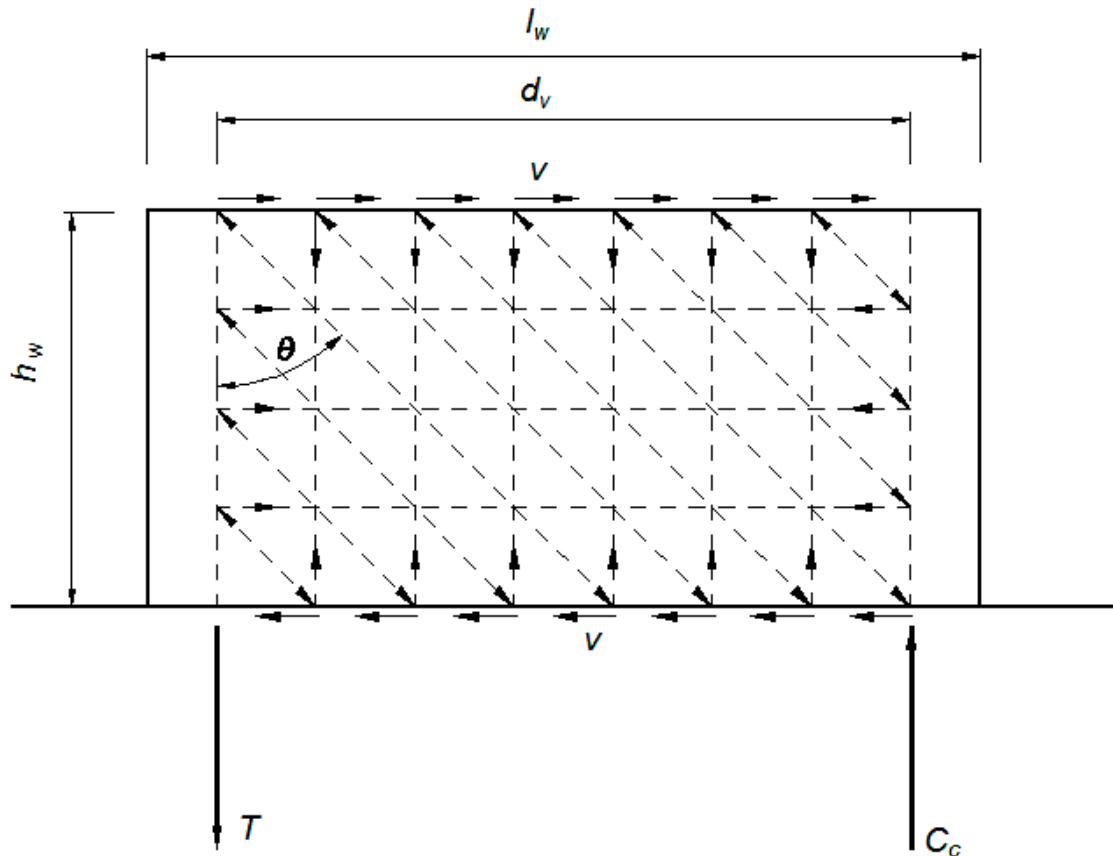


Fig. 9-2 Uniformly distributed force flow in squat shear walls.

The web is assumed to resist shear along the length d_v taken as $0.8 l_w$ in the 2004 CSA A23.3. Thus vertical reinforcement distributed over the shear length is required to balance the vertical component of diagonal compression force needed for shear as shown

in Figure 9-2. In the model shown in Fig. 9-2, the overturning moment is resisted by the concentrated vertical reinforcement force T and the compression force C_c . The 2004 CSA A23.3 requires that the distributed vertical reinforcement needed for shear not contribute to the flexural capacity of squat shear walls. The requirement for additional vertical reinforcement for shear can also be expressed as a reduced internal flexural lever-arm as was done for deep beams by Leonhardt and Walther (1966).

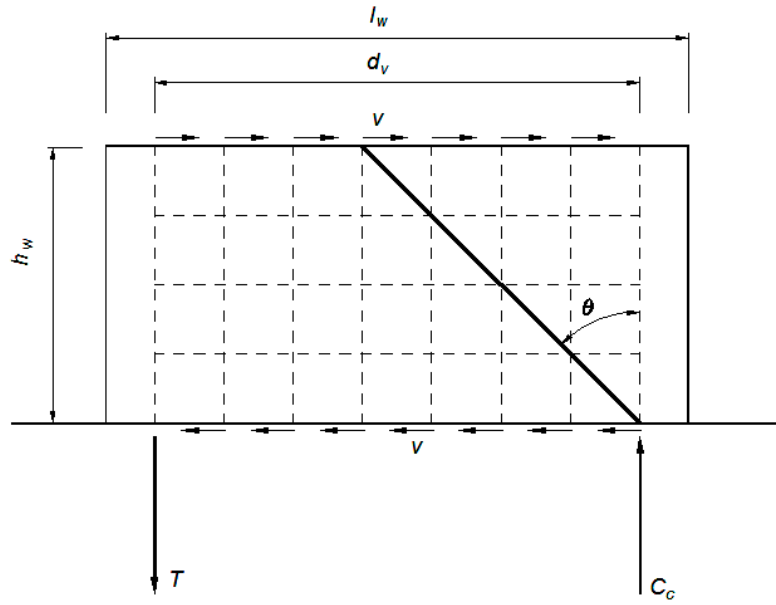
When shear stress is uniformly distributed, there is an infinite number of possible failure planes with horizontal reinforcement yielding; however, all planes correspond to the same total force applied to the wall. One such failure plane is shown in Figure 9-3(a). Fig.9-3(b) illustrates the free body diagram of the element bounded by the failure plane. The horizontal force $\rho_h f_y b_w h_w$ and vertical force $\rho_h f_y b_w h_w \tan \theta$ are the resultant forces resisted by distributed horizontal and vertical reinforcement, respectively. ρ_h and ρ_v are distributed horizontal and vertical reinforcement ratios, and b_w is wall thickness. In the free body diagram shown in Fig. 9-3(b), the force due to aggregate interlock at the crack is not included as it is ignored by the 2004 CSA A23.3.

As shear stress is uniformly distributed (Fig. 9-3a), the wall shear strength V is determined from:

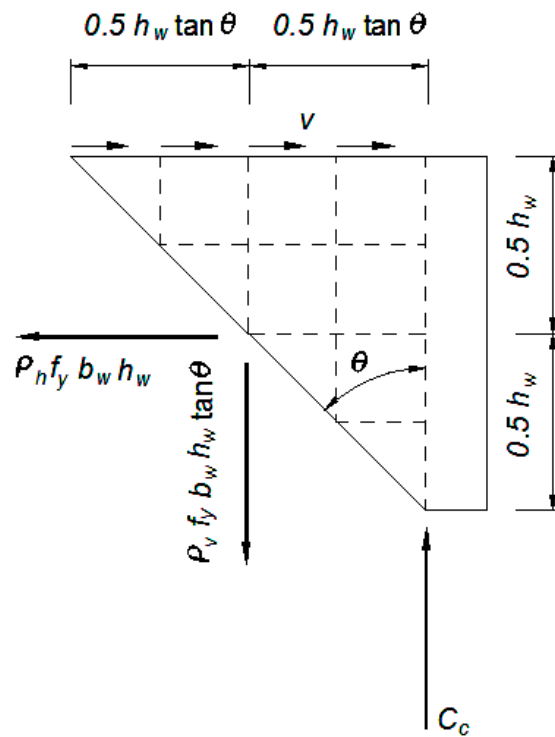
$$[9-3] V = v b_w d_v$$

where v is shear stress. From equilibrium in the horizontal direction in Fig.9-3(b):

$$[9-4] v = \rho_h f_y \cot \theta$$



(a) Failure plane



(b) Free body diagram of wall element bounded by failure plane

Fig. 9-3 Horizontal reinforcement yielding shear failure of squat shear walls as in 2004 CSA A23.3.

Substituting v from Eq. [9-4] in Eq. [9-3] results in the following shear strength equation for squat shear walls given in the 2004 CSA A23.3.

$$[9-5] \quad V = \rho_h f_y b_w d_v \cot \theta$$

The relationship between the amount of distributed horizontal and vertical reinforcement can be obtained by taking moments about the point of application of concrete compression force C_c in Figure 9-3(b).

$$[9-6] \quad \rho_v = \rho_h \cot^2 \theta$$

2004 CSA A23.3 allows any angle θ between 30 and 45 deg in Eq. [9-5] as long as distributed vertical reinforcement needed for shear, given by Eq. [9-6], is calculated using the same angle. When $\theta = 45$ deg, distributed vertical reinforcement ratio is equal to the distributed horizontal reinforcement ratio while when $\theta = 30$ deg, distributed vertical reinforcement ratio is 3 times the distributed horizontal reinforcement ratio.

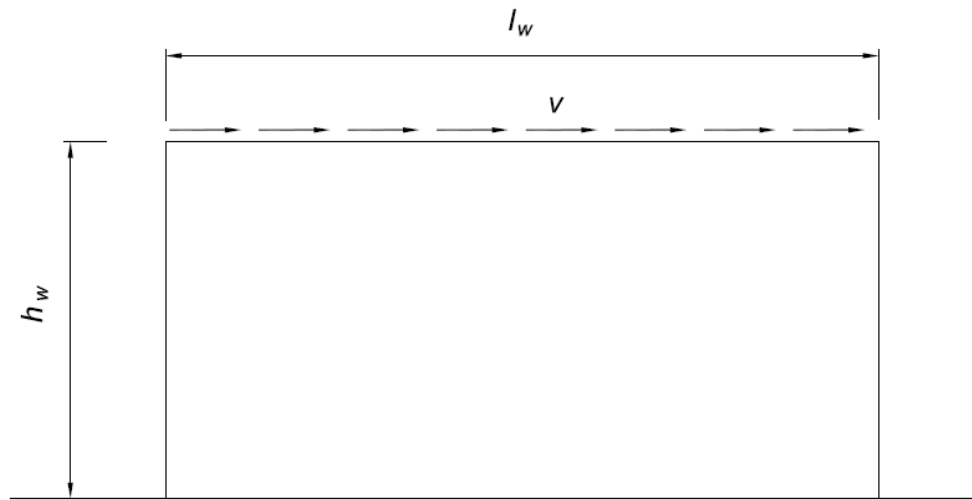
In the above derivations wall is not subjected to axial force for simplicity. For walls with gross cross-section area A_g and subjected to axial force P_s , the amount of distributed vertical reinforcement given by Eq. [9-6] is reduced by $\frac{P_s}{f_y A_g}$. The reason is part of axial force needed for shear is provided by the applied axial force and the remaining part is resisted by the distributed vertical reinforcement. As explained in Chapter 7, the 2004 CSA A23.3 limits the shear strength to $0.15 f_c' b_w d_v$ to avoid concrete crushing.

9.4. Finite Element Analysis of Squat Shear Walls Failing in Flexure

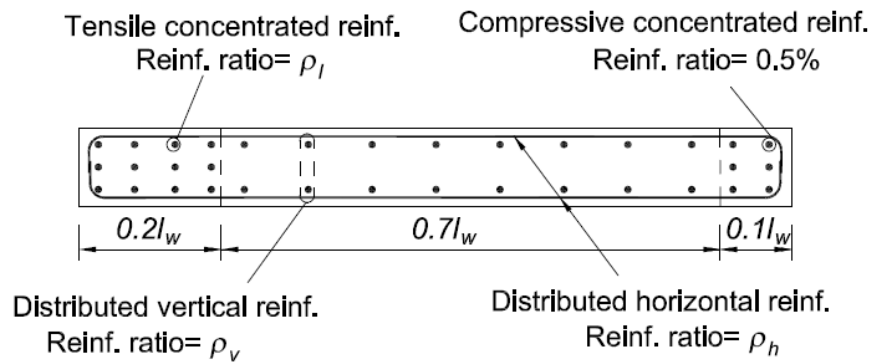
A total of 42 walls in four groups with aspect ratios of $h_w/l_w=0.3, 0.5, 1.0,$ and 2.0 were analyzed. Concrete compressive strength of $f'_c = 40$ MPa and steel yield stress of $f_y = 400$ MPa without strain hardening were assumed. The walls were designed to fail due to yielding of vertical reinforcement at the base of the wall according to the 2004 CSA A23.3 predictions. Typical details of the walls that were analyzed in this study are shown in Figure 9-4. Wall cross-sections were uniform along the wall height and no top loading beam was assumed.

All walls were monotonically loaded and the load was applied from left-to-right uniformly distributed over the wall top edge. To achieve a lower-bound solution, the contribution of the compression zone was minimized by placing the minimum amount of concentrated reinforcement permitted by the 2004 CSA A23.3 in 10% of the wall length on the compression side. In order to increase the flexural capacity of the walls, a large amount of concentrated vertical reinforcement was placed on the tension side of the wall.

Table 9-1 presents the concentrated and distributed vertical reinforcement ratios as well as the distributed horizontal reinforcement ratios of the 42 walls that were analyzed. The concentrated vertical reinforcement ratios ρ_l in the tension zone, which is the ratio of the total amount of concentrated reinforcement over the tension zone, ranged from 0.5% to the maximum of 3.0% depending on the height-to-length ratios. The ratio of the total amount of concentrated reinforcement over the compression zone ρ'_l was kept constant and equal to the minimum amount according to the 2004 CSA A23.3 ($\rho'_l = 0.5\%$).



Wall Elevation



Wall Cross Section

Fig. 9-4 Typical detail of walls analyzed to investigate flexural capacity of squat shear walls.

Horizontal reinforcement ratios were varied from 0.25% to 1.0% for every combination of aspect ratio and concentrated vertical reinforcement except for a few in which distributed horizontal reinforcement ratios of 0.25% and slightly higher caused shear failure. For walls with height-to-length ratio of 2.0, distributed vertical

Table 9-1 Summary of walls analyzed to investigate flexural capacity of squat shear walls.

h_w/l_w	$\rho_l(\%)$	$\rho_h(\%)$	$\rho_v(\%)$	$\rho'_l(\%)$
0.3	0.50	0.40	0.40	0.50
	0.50	0.50	0.50	0.50
	0.50	0.75	0.75	0.50
	0.50	1.00	1.00	0.50
0.5	0.50	0.25	0.25	0.50
	0.50	0.50	0.50	0.50
	0.50	0.75	0.75	0.50
	0.50	1.00	1.00	0.50
	1.00	0.45	0.45	0.50
	1.00	0.75	0.75	0.50
	1.00	1.00	1.00	0.50
1.0	0.50	0.25	0.25	0.50
	0.50	0.50	0.50	0.50
	0.50	0.75	0.75	0.50
	0.50	1.00	1.00	0.50
	1.00	0.25	0.25	0.50
	1.00	0.50	0.50	0.50
	1.00	0.75	0.75	0.50
	1.00	1.00	1.00	0.50
	2.00	0.45	0.45	0.50
	2.00	0.75	0.75	0.50
	2.00	1.00	1.00	0.50
2.0	0.50	0.25	0.25	0.50
	0.50	0.50	0.50	0.50
	0.50	0.75	0.75	0.50
	0.50	1.00	1.00	0.50
	1.00	0.25	0.25	0.50
	1.00	0.50	0.50	0.50
	1.00	0.75	0.75	0.50
	1.00	1.00	1.00	0.50
	2.00	0.25	0.25	0.50
	2.00	0.50	0.50	0.50
	2.00	0.75	0.75	0.50
	2.00	1.00	1.00	0.50
	3.00	0.33	0.33	0.50
	3.00	0.50	0.50	0.50
	3.00	0.75	0.75	0.50
	3.00	1.00	1.00	0.50
	3.00	0.25	0.75	0.50
	3.00	0.50	1.50	0.50
	3.00	0.75	2.25	0.50
	3.00	1.00	3.00	0.50

ρ_l = concentrated flexural reinforcement ratio, ρ'_l = concentrated reinforcement ratio in concrete compression zone, ρ_v = distributed vertical reinforcement ratio, ρ_h = distributed horizontal reinforcement ratio

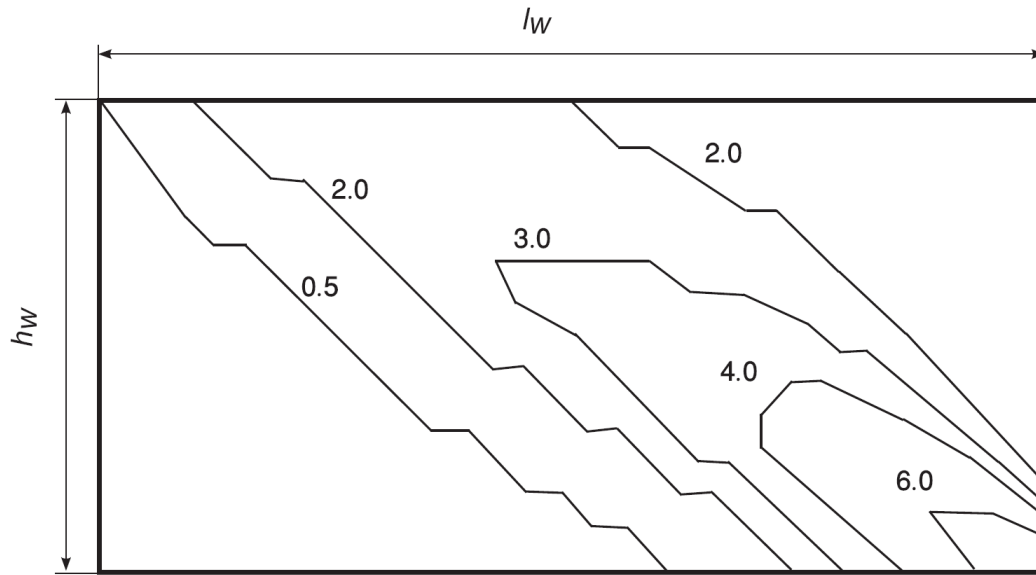
reinforcement ratios were assumed to be either equal to the distributed horizontal reinforcement ratio ($\rho_v / \rho_h = 1.0$) or 3 times the horizontal reinforcement ratio ($\rho_v / \rho_h = 3.0$). For all other walls, the amount of distributed vertical reinforcement was equal to the amount of distributed horizontal reinforcement as distributed reinforcement amounts of $\rho_v / \rho_h = 3.0$ caused shear failure.

9.4.1. Finite Element Model

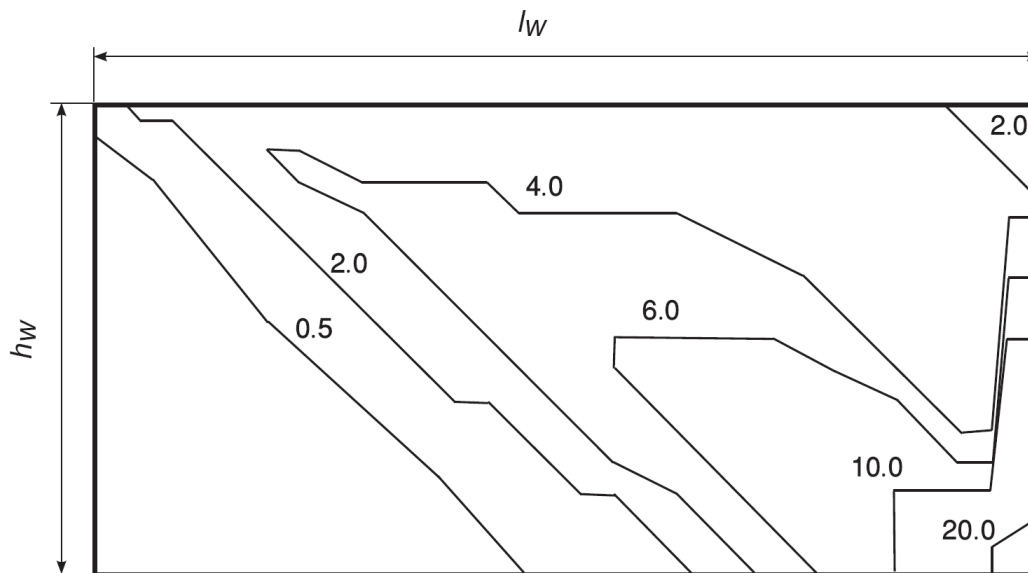
Uniform shear elements discussed in Chapter 8 were used. All walls were modeled with 30 square elements along the length while number of elements along the height was varied depending on the wall aspect ratio. 60 elements were used over the height of walls with height-to-length ratio of 2.0, while nine elements were used over the height of walls with height-to-length ratio of 0.3. All nodes along the wall base were constrained in both vertical and horizontal directions and no other constraint was provided. As was explained previously, the applied shear force at the top was uniformly distributed over the wall length and a top loading beam was not provided.

9.4.2. Finite Element Results

Figure 9-5 presents the shear stress and principal compression stress distributions immediately prior to flexural failure in the wall with 0.5% distributed horizontal and vertical reinforcement ratio and height-to-length ratio of 0.5. At that load level, the wall had experienced lots of cracking and reinforcement was yielded over a significant portion of the wall in both horizontal and vertical directions. Stress flow is shown by stress contours which connect the equal stress points in the wall.



(a) Shear stress (MPa)



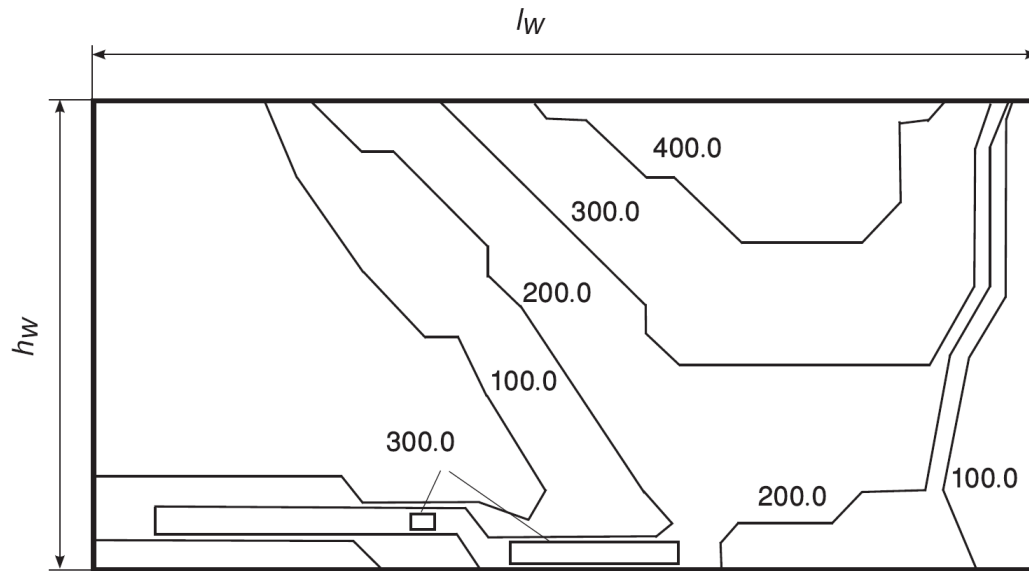
(b) Principal compression stress (MPa)

Fig. 9-5 Concrete stress contour diagrams based on finite element analysis of a squat shear wall with 0.5% distributed reinforcement in both directions and height-to-length ratio of 0.5 immediately prior to flexural failure.

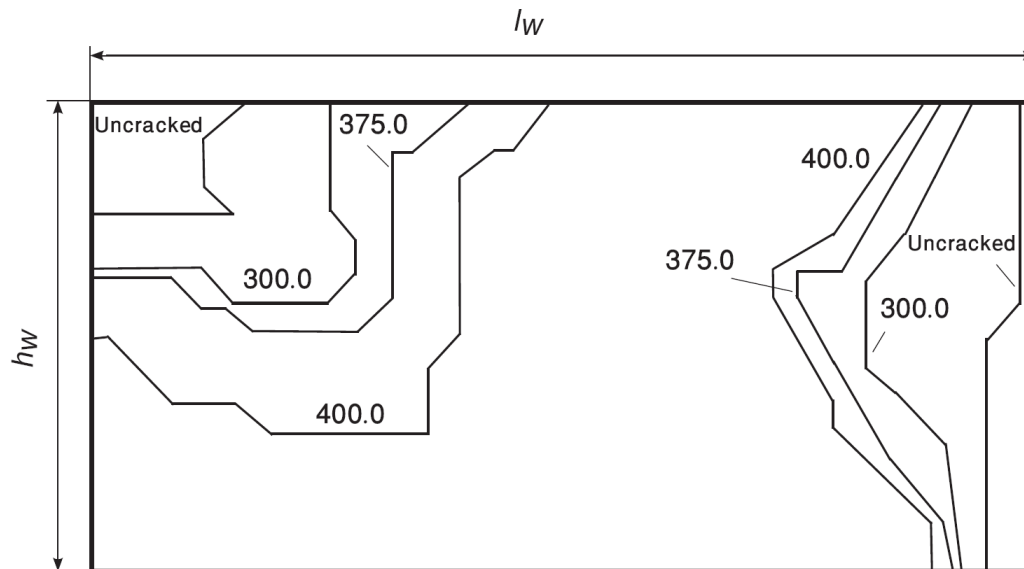
As shown, shear stress distribution is not uniform at the base even though shear is applied uniformly at the top. Shear stress at the base is almost zero along the tension side to mid-length beyond where it increases as it approaches the flexural compression zone. The same trend is also noticed in the distribution of concrete principal stress. Concrete principal stress is almost zero in the triangular area in the tension side of the wall separated by a line from left top corner to the wall base mid-length.

The reason can be examined in Fig. 9-6, which illustrates the stress in the vertical and horizontal reinforcement at cracks for the same wall. The 2004 CSA A23.3 assumes shear force carried by horizontal reinforcement is transferred to the concentrated flexural reinforcement and then directed to the base by concrete diagonal struts (see Fig. 9-1). In contrast, Fig. 9-6(a) presents a different distribution predicted by the finite element analysis. Horizontal reinforcement transfers the shear to concrete diagonal struts before it reaches the concentrated flexural reinforcement. Notice that horizontal reinforcement stress is less than 100 MPa on left side of the wall over the considerable portion of the length except close to the wall base where forces are redistributed to provide more flexural capacity.

Figure 9-6(b) examines stress distribution in the vertical reinforcement of the same wall. Vertical distributed reinforcement has mostly yielded. Flexural concentrated reinforcement has also yielded at the base and yielding has extended well over almost half of wall height. This is again due to the fact that horizontal reinforcement is anchored in the concrete diagonal struts and does not transfer the load to the concentrated vertical reinforcement.



(a) Horizontal steel stress at cracks (MPa)



(b) Vertical steel stress at cracks (MPa)

Fig. 9-6 Steel stress contour diagrams based on finite element analysis of a squat shear wall with 0.5% distributed reinforcement in both directions and height-to-length ratio of 0.5 immediately prior to flexural failure.

The shear stress distributions at the base of four walls are examined in Figure 9-7. The walls all had a same cross-section with horizontal and vertical reinforcement ratio of 0.5% and had different aspect ratios of $h_w/l_w = 0.3, 0.5, 1.0$, and 2.0 . The results shown in Fig. 9-7 correspond to the load level immediately prior to flexural failure. As the height-to-length ratio decreases, shear is carried by a larger portion of wall length at the base. For example, for the wall with $h_w/l_w=0.3$, about 60% of the wall length is subjected to significant shear. For the wall with $h_w/l_w=0.5$, shear is resisted over about 40% of the wall length. For walls with height-to-length ratios of 1.0 and 2.0, almost all shear force is resisted by the compression zone. This means that the demand on distributed vertical reinforcement due to shear is not significant, thus reduction of flexural capacity due to shear is also not significant.

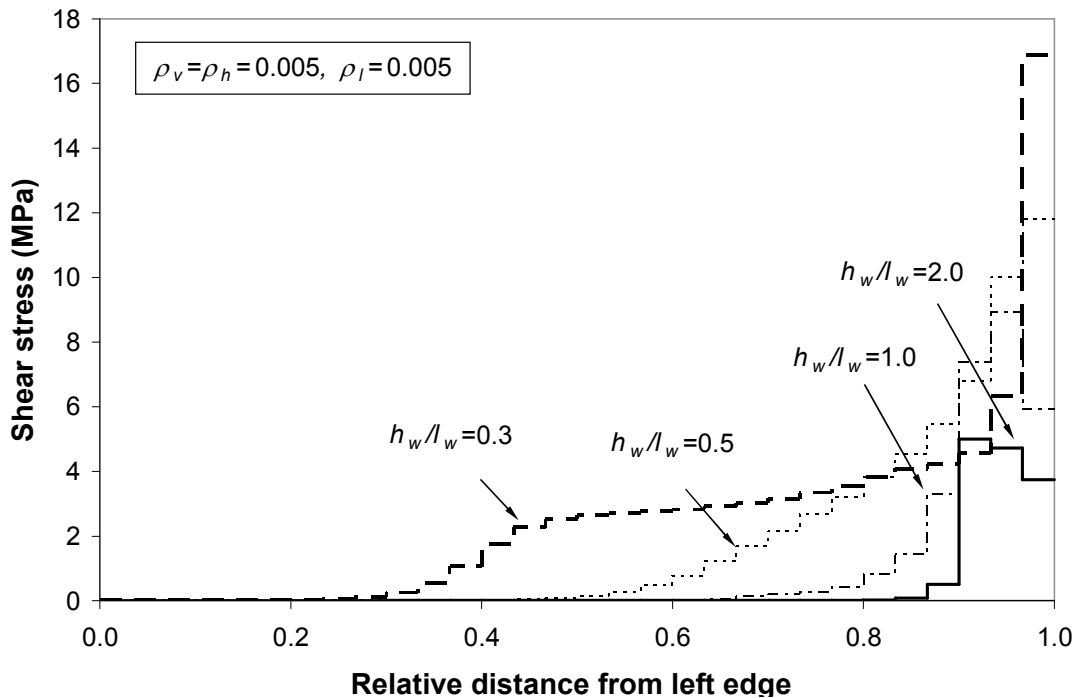


Fig. 9-7 Finite element predictions for shear stress distributions at base of four squat shear walls immediately prior to flexural failure.

Figure 9-8 shows total normal stress (vertical force per unit length divided by thickness of wall) distributions of the same walls at the base. The total normal stress is equal to the vertical compression stress in concrete n_v plus the stress $\rho_v f_s$ that is resulted from steel stress f_s . When vertical reinforcement is yielding and there is no vertical compression stress due to shear, the total normal stress is equal to $\rho_v f_y$. Vertical reinforcement ratio is 0.5%, thus total normal stress of $\rho_v f_y = 2.0$ MPa is the maximum tensile stress which corresponds to yielding of vertical reinforcement. For walls with height-to-length ratios of 1.0 and 2.0, normal stress in a significant portion of the wall from the tension face to the flexural compression zone reaches the maximum value of 2.0 MPa which again suggests an insignificant reduction in flexural capacity due to shear.

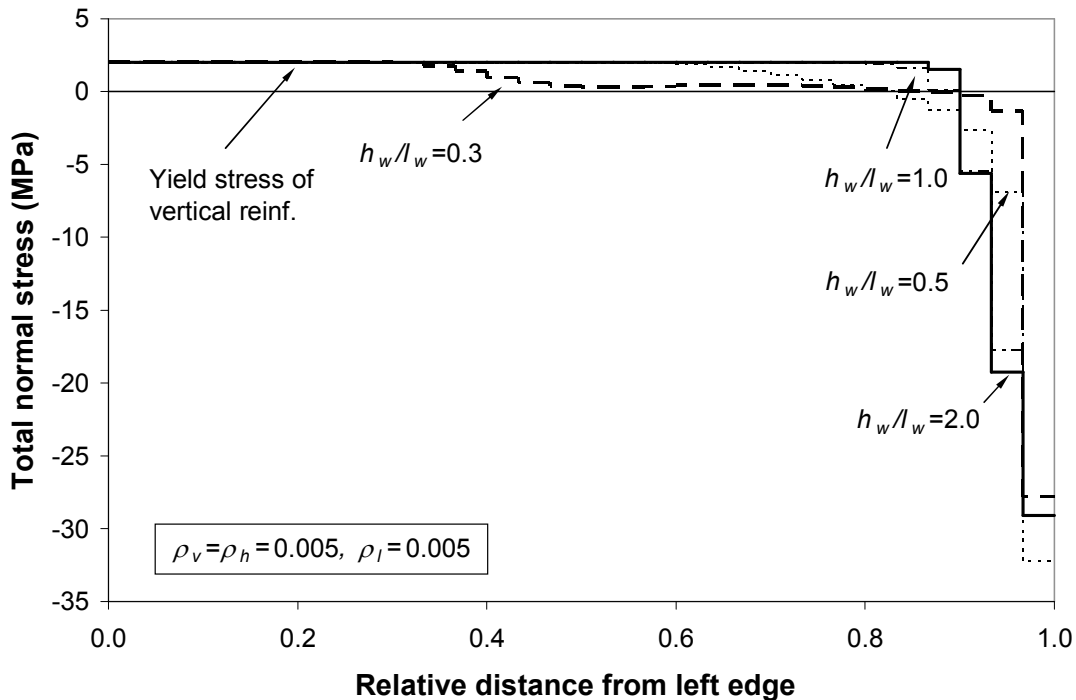


Fig. 9-8 Finite element predictions for total normal stress distributions at base of four squat shear walls immediately prior to flexural failure.

In the wall with height-to-length ratio of 0.3, the total shear stress equals $\rho_v f_y$ (2.0 MPa) at about $0.4l_w$ from the tension face. For the wall with an aspect ratio of 0.5, the total normal stress equals $\rho_v f_y$ (2.0 MPa) at about $0.6l_w$ from the tension face. This is the consequence of shear being present in the rest of wall portion at the base that results in normal compression stresses that balances diagonal compression stresses. This results in a reduction of the moment capacity of the walls with low height-to-length ratios compared to the walls with height-to-length ratios of 1.0 or higher.

Finite element predicted moment capacities of 16 walls with $\rho_l = 0.5\%$ are presented in Figure 9-9 (solid lines with markers). The predictions of plane section analysis (Response 2000) are also shown as a dotted line. The amount of distributed vertical reinforcement in these walls was equal to the amount of distributed horizontal reinforcement and ranged from 0.25% to 1.0%. The predicted flexural capacity from plane section analysis depend only on the amount of distributed vertical reinforcement, which is equal to the amount of distributed horizontal reinforcement. Walls with height-to-length ratios of 1.0 and 2.0 almost reach the capacity predicted by plane section analysis. In contrast, walls with height-to-length ratios of 0.3 and 0.5 have relatively less flexural capacity due to the influence of shear. The flexural strength reduction is more significant as the wall height-to-length ratio decreases.

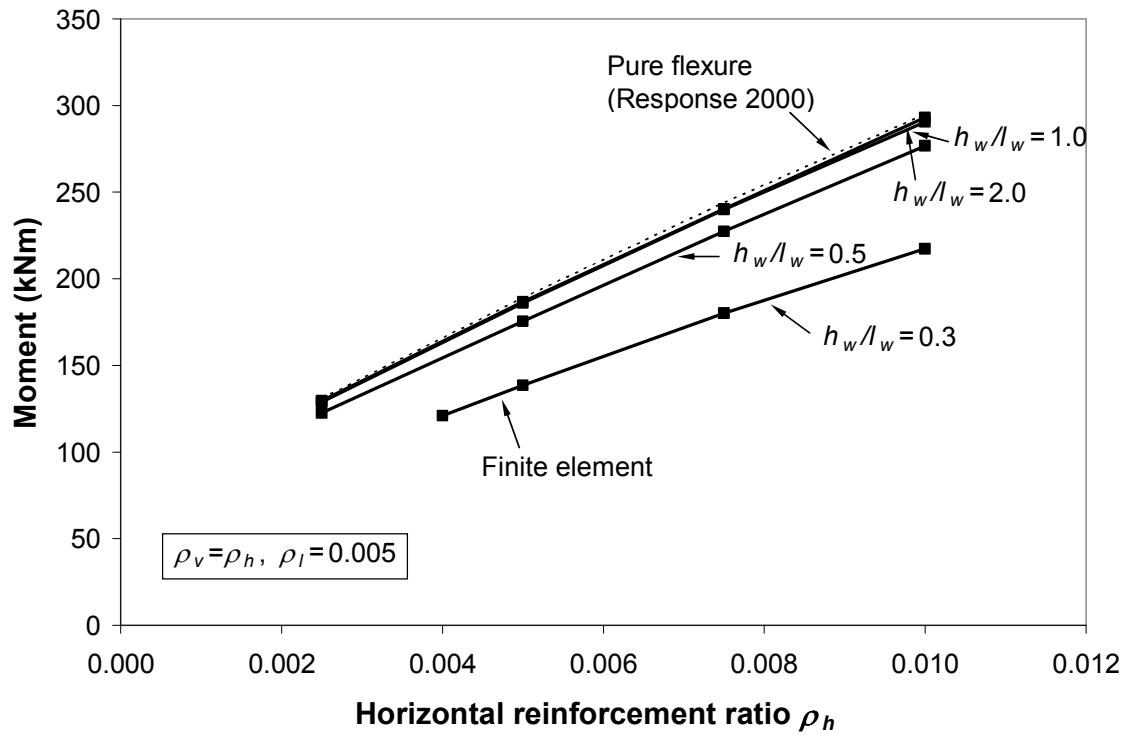


Fig. 9-9 Predicted moment capacities of 16 squat shear walls.

The ratios of finite element predictions of moment capacity to the plane section analysis predictions of moment capacity for the 42 walls are illustrated in Figure 9-10. Once again the reduction of moment due to shear is insignificant for the walls with height-to-length ratios of 1.0 and 2.0 while it becomes more significant for the walls with height-to-length ratio of 0.3. For example, the reduction in moment capacity with respect to the plane section analysis predictions is about 9% for the walls with height-to-length ratio of 0.5 and about 27% for the walls with height-to-length ratio of 0.3.

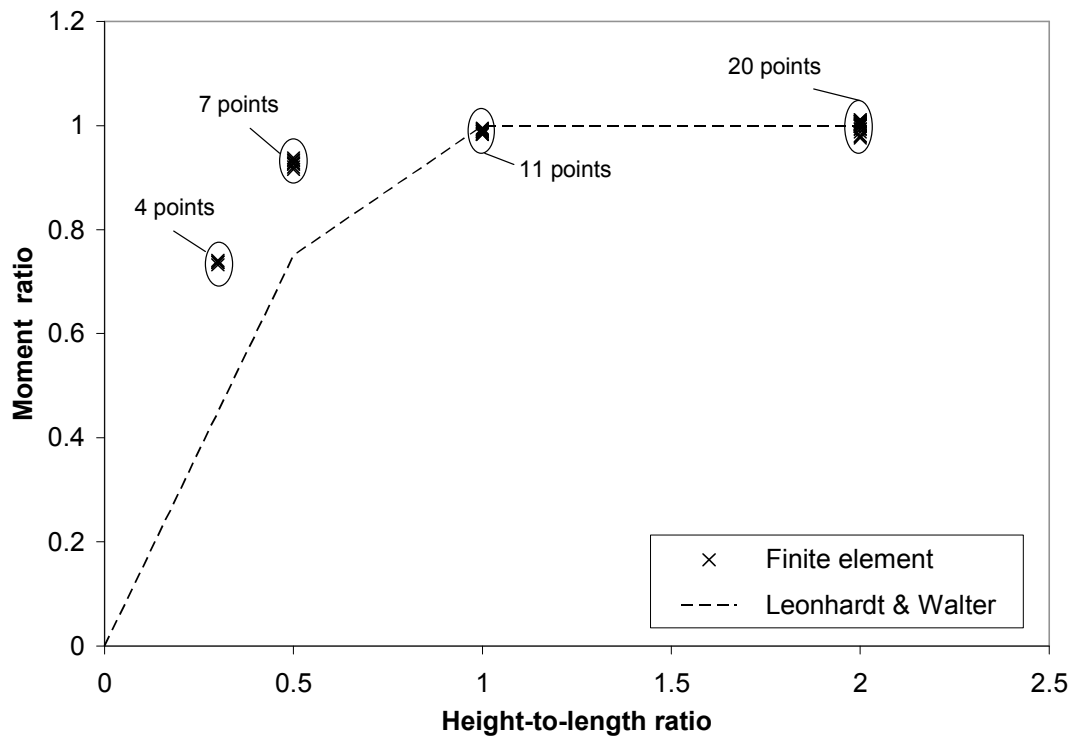


Fig. 9-10 Ratios of finite element predicted moment capacity to the plane section analysis predicted moment capacity for the 42 squat walls failing in flexure.

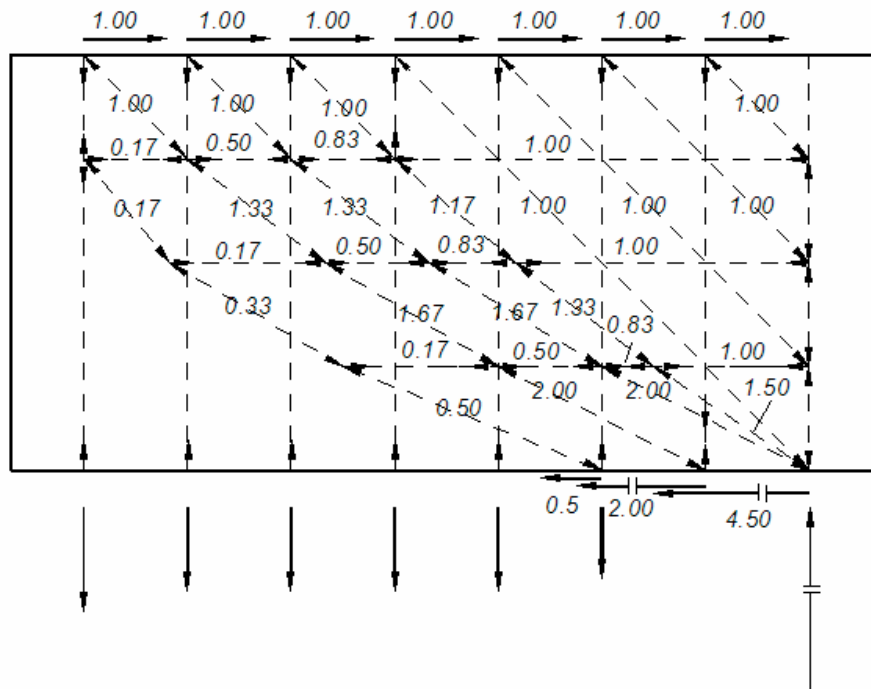
Leonhardt and Walther (1966) presented equations for the internal flexural lever-arm in deep beams that can be applied to squat shear walls. As Leonhardt and Walther solution does not include the contribution of distributed vertical reinforcement, the predictions of flexural capacity from their equations could be very different compared to the nonlinear finite element predictions. Finite element analysis, as explained previously, shows that distributed vertical reinforcement contributes to the wall flexural strength. However, if the predictions of both methods are converted to the ratio of flexural capacity with respect to the capacity predicted by the plane section analysis, there are similarities between nonlinear finite element predictions for squat walls and Leonhardt and Walther linear solution for deep beams. Assuming that internal lever-arm is about 80% of the wall

length from the plane section analysis, the reduction in moment capacity with respect to the plane section analysis can be assumed to be proportional to the reduction in the flexural lever-arm and this is presented in Figure 9-10. Both Leonhardt and Walther equations and finite element predict no reduction in flexural capacity for walls with h_w/l_w greater than or equal to 1.0.

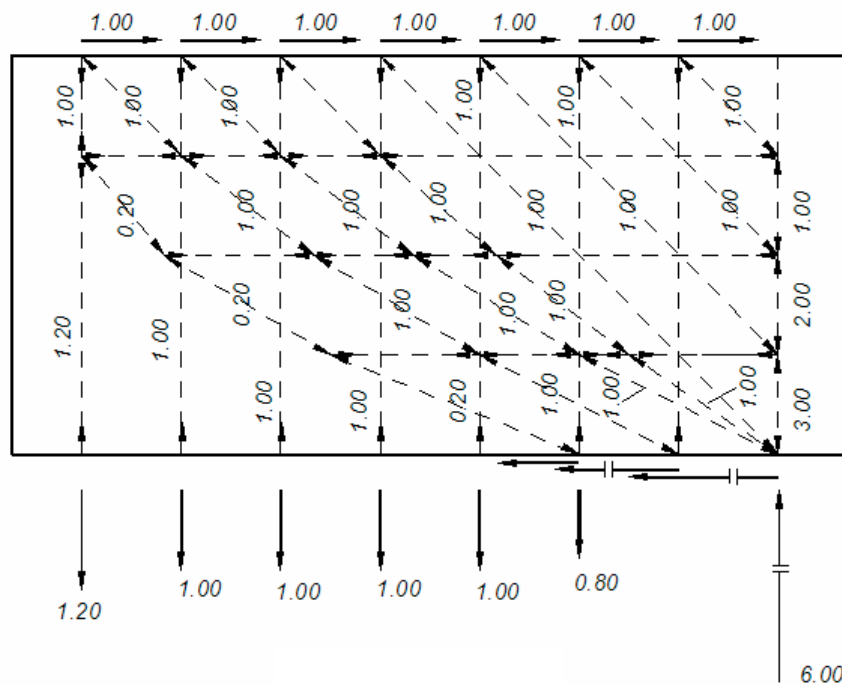
9.4.3. Presentation of NLFE with Simple Truss Model

This section explains how the force flow in squat shear walls predicted by the finite element analysis can be presented using simple truss models in which reinforcing steel is assumed to resist all tension and concrete resists diagonal compression.

The forces in a wall with height-to-length ratio of 0.5 are presented in Figure 9-11. Fig. 9-11(a) presents the forces in the horizontal reinforcement in addition to the horizontal components of the diagonal member forces, while the forces in the vertical reinforcement and vertical components of the diagonal member forces are shown in Figure 9-11(b). Horizontal elements are the distributed horizontal reinforcement, tensile vertical elements are the concentrated vertical reinforcement and distributed vertical reinforcement, and elements in compression represent concrete. Uniformly distributed shear force is applied over the effective shear length $d_v = 0.8l_w$ along the top. Unit horizontal force is applied on each node of the truss along the top. All forces in truss members relate to this unit force, which represents shear resisted by each member if the shear is uniformly distributed.



(a) Horizontal components of diagonal compression forces and tension forces in horizontal reinforcement

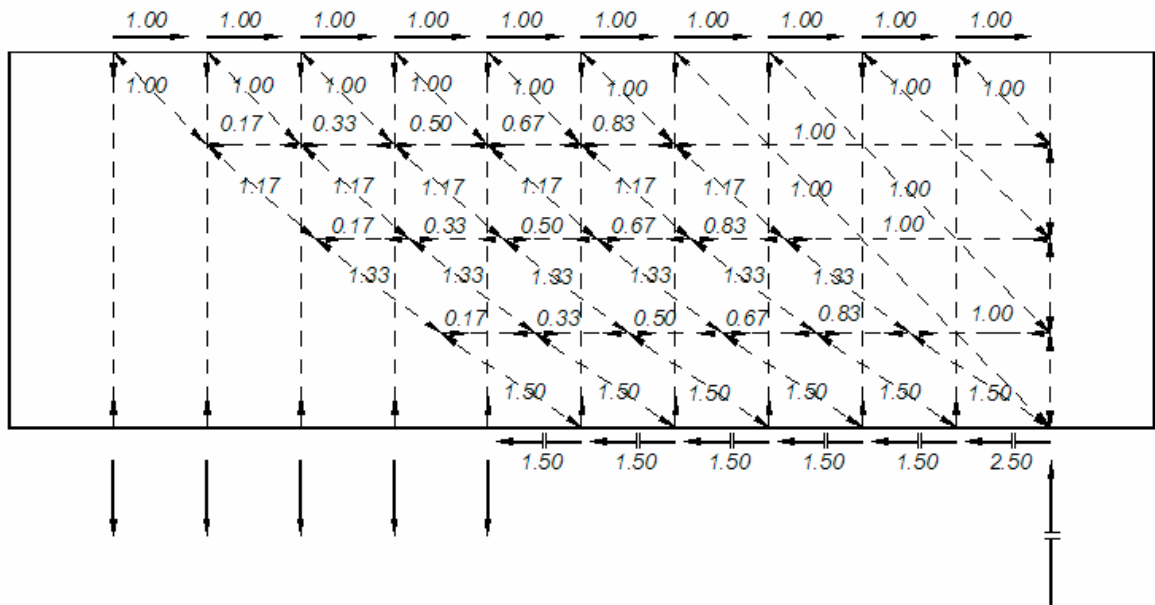


(b) Vertical components of diagonal compression forces and tension forces in vertical reinforcement

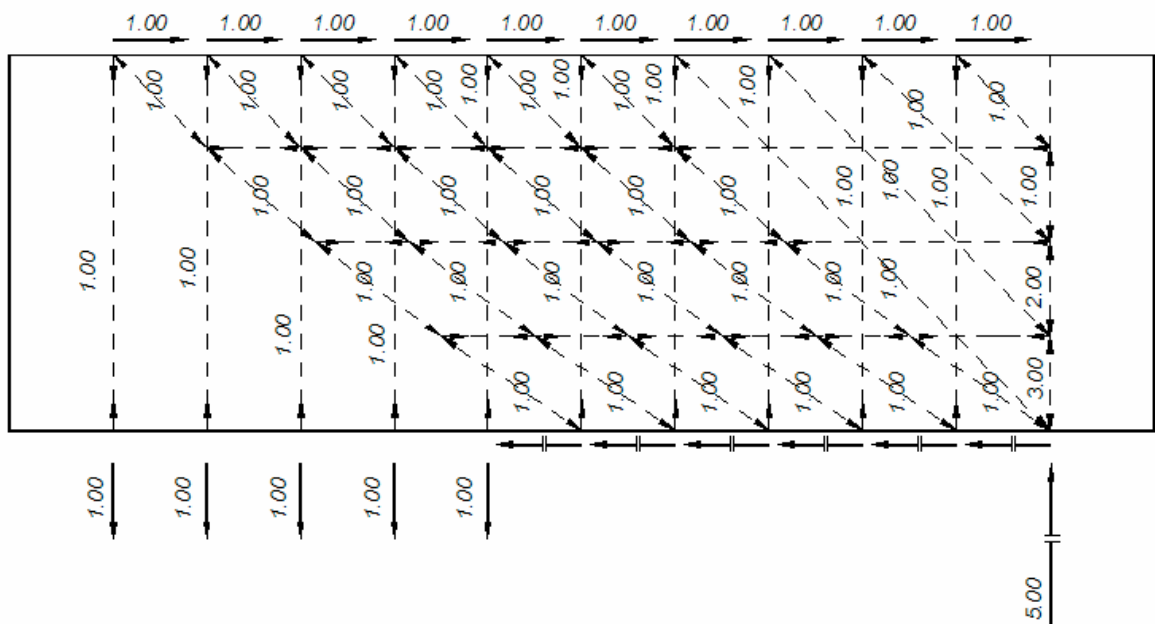
Fig. 9-11 Truss model for a squat wall with height-to-length ratio of 0.5.

As was noticed in the finite element results, the truss model shows that forces carried by horizontal reinforcement could be anchored in the diagonal struts and do not need to be transferred to the tensile concentrated vertical reinforcement. This is possible because the direction of diagonal struts change to balance the horizontal force that is carried by the horizontal reinforcement. Notice in Fig. 9-11 that the first two diagonal struts at the top of the wall on the left side as well as the one below them change direction to balance the horizontal forces as they cross the vertical elements. This results in an increase in the diagonal strut force due to the increase of its horizontal component only. Figure 9-11 also shows that from 6 vertical elements in the wall web representing distributed vertical reinforcement, 4.8 of them (80%) contribute to the flexural capacity of the wall. Furthermore, as was also seen in finite element results, shear at the base is resisted by only a portion of the wall length on the compression side.

In Fig. 9-12, another truss example for a wall with height-to-length ratio of 0.3 is provided. The same trend is noticed; however, shear is resisted by a larger portion of the wall length at the base and less contribution of the distributed vertical reinforcement to the flexural capacity is noticed compared to the wall with height-to-length ratio of 0.5 shown in Figure 9-11. About 50% of the distributed vertical reinforcement contributes to the flexural capacity of the wall based on the truss model shown in Figure 9-12. It is worth mentioning that the magnitude of vertical component of diagonal struts remains constant throughout the height of the wall even though the diagonal struts, which go directly to the base, change direction as they cross the horizontal reinforcement.



(a) Horizontal components of diagonal compression forces and tension forces in horizontal reinforcement



(b) Vertical components of diagonal compression forces and tension forces in vertical reinforcement

Fig. 9-12 Truss model for a squat wall with height-to-length ratio of 0.3.

9.5. Proposed Sectional Model for Flexural Capacity

This section presents a proposed sectional model that includes the influence of shear on the flexural capacity of squat shear walls. As was noticed in the finite element results and was later presented by simple truss models, distribution of normal compression stress at the base of a squat shear wall is over a longer length than predicted by plane section analysis. This phenomenon, which results in a reduction of wall moment capacity compared to what is predicted by the plane section analysis, is more significant when the wall height-to-length ratio is small. It becomes insignificant for walls with height-to-length ratios close to 1.0 or greater. The proposed model can capture this behaviour by including an axial force N_v in addition to the other forces that act at the wall base. N_v , which is the force needed for shear, is zero for walls with greater height-to-length ratios and becomes significant as the wall height-to-length ratio becomes smaller. For N_v equal to zero, the model becomes the same as sectional analysis under pure flexure and thus no reduction due to shear is calculated.

Figure 9-13 shows the proposed sectional model at the base to calculate flexural capacity of squat shear walls. T in Figure 9-13 is the force in the concentrated reinforcement and T_d is the resultant force in the distributed vertical reinforcement. At flexural capacity, T is equal to the area of concentrated reinforcement times steel yield stress. Assuming distributed reinforcement yields over the wall entire length, T_d can also be reasonably approximated by total area of distributed vertical reinforcement times steel yield stress.

Axial force N_v is the resultant force of the normal stress acting over a portion of wall length d_{nv} at the base. As was presented by the truss model in Fig. 9-12, rotation of

diagonal struts that go directly to the wall base does not affect the magnitude of N_v per unit length. Notice in Fig. 9-12(b) that the magnitude of the vertical components of all diagonal struts that go directly to the base is equal to 1.0 and it does not increase as they rotate. This suggests that normal stress at the base is equal to the normal stress at the top of the wall. One good approximation, as explained in previous chapters, for the normal stress needed for shear is $v \cot \theta$ and thus:

$$[9-7] \quad N_v = v \cot \theta (b_w d_{nv})$$

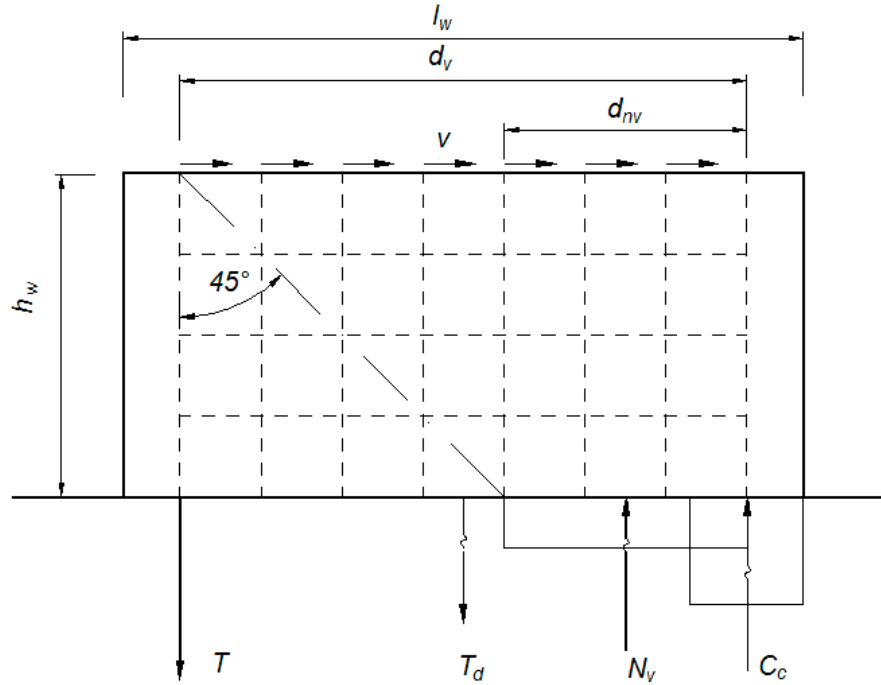


Fig. 9-13 Proposed sectional model for flexural capacity of squat shear walls.

In which angle θ is the angle of diagonal compression and $v = \frac{V}{b_w d_v}$. In the proposed model, angle of inclination is determined from the 2004 CSA A23.3 equilibrium-based equation Eq. [7-27] given the amount of distributed vertical and horizontal reinforcement and wall axial force. The model becomes similar to the 2004 CSA A23.3 when $d_{nv} = d_v$

and it becomes a typical sectional analysis under pure flexure when $d_{nv}=0$. Based on the finite element results, d_{nv} is a function of wall aspect ratio. The proposed d_{nv} shown in Fig. 9-13 is given by:

$$[9-8] \quad d_{nv} = d_v - h_w \geq 0$$

In the proposed model shown in Fig. 9-13, the magnitude and location of C_c is determined from equilibrium in the vertical direction using the equivalent stress block for concrete compression stress in the flexural compression zone. Moment capacity is then determined from moment equilibrium at the base. This is an iterative procedure for a given wall with a given amount of distributed reinforcement because the wall flexural capacity as well as shear force corresponding to the wall flexural capacity is unknown. Notice that flexural capacity is a function of shear force at flexural capacity in the proposed model. For design, however, the procedure is not iterative as the applied bending moment and shear force are known.

9.6. Comparison of Finite Element Results with the Predictions of Proposed Method for Flexural Capacity of Squat Shear Walls

Figures 9-14 to 9-17 compare the finite element predictions for the flexural capacity of the 42 squat shear walls failing in flexure with the predictions of the 2004 CSA A23.3 as well as the proposed method predictions. In these figures, the relationship between the average shear stress over the wall length $\frac{V}{b_w l_w}$ immediately prior to flexural failure with the horizontal reinforcement ratio is presented.

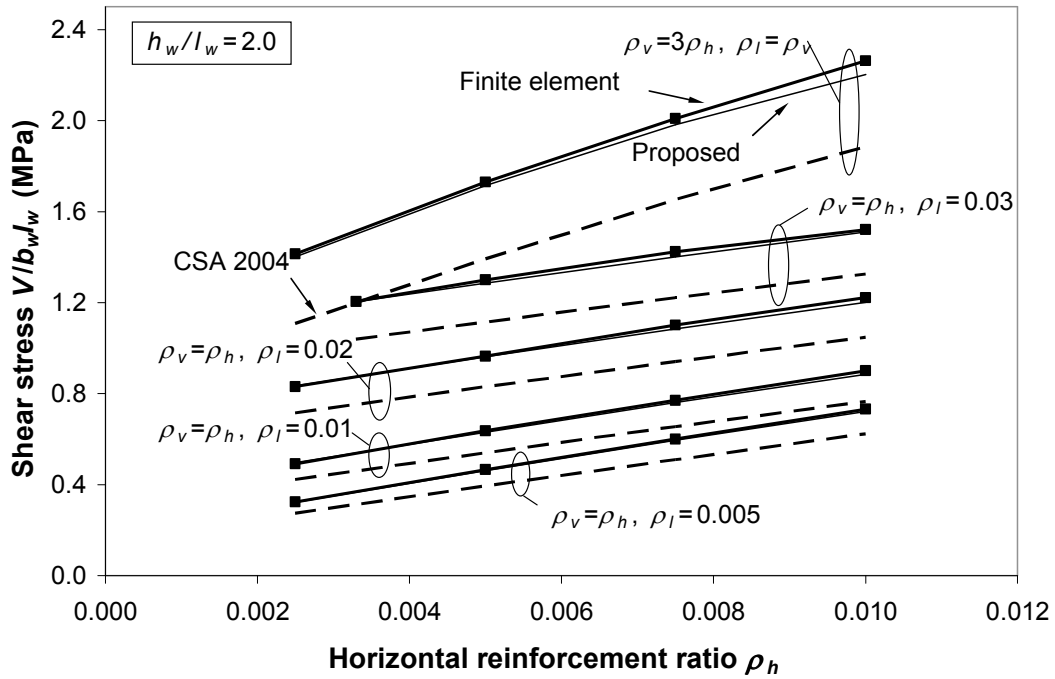


Fig. 9-14 Comparison of finite element predictions for shear force at flexural capacity of squat shear walls with $h_w/l_w=2.0$, with 2004 CSA A23.3 and proposed method predictions.

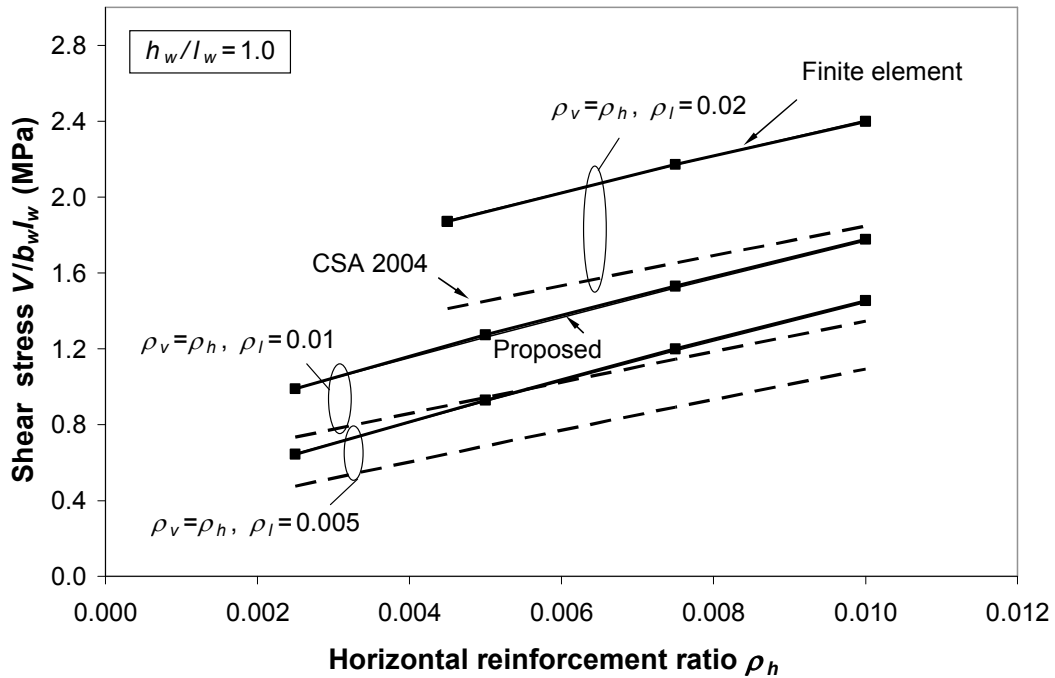


Fig. 9-15 Comparison of finite element predictions of shear force at flexural capacity of squat shear walls with $h_w/l_w=1.0$, with 2004 CSA A23.3 and proposed method predictions.

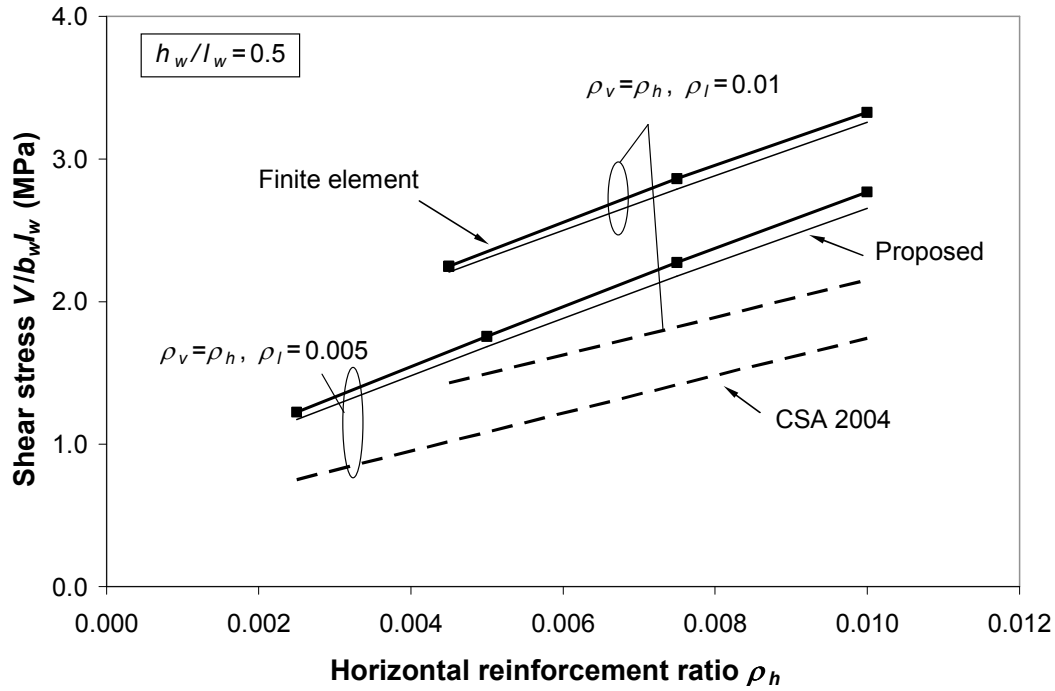


Fig. 9-16 Comparison of finite element predictions for shear force at flexural capacity of squat shear walls with $h_w/l_w=0.5$, with 2004 CSA A23.3 and proposed method predictions.

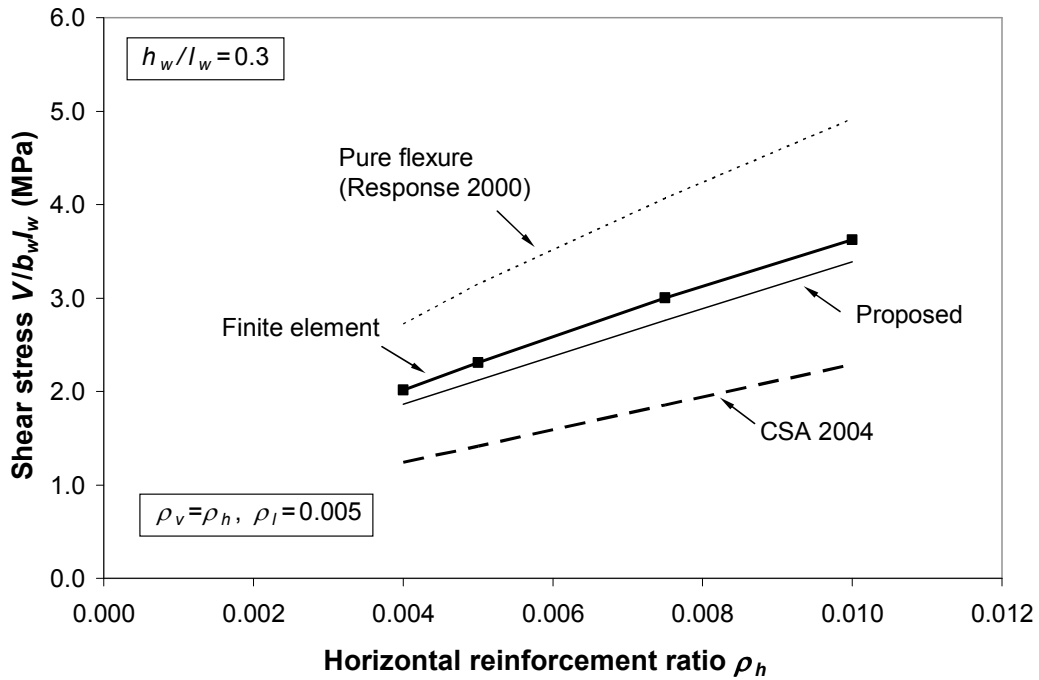


Fig. 9-17 Comparison of finite element predictions for shear force at flexural capacity of squat shear walls with $h_w/l_w=0.3$, with 2004 CSA A23.3 and proposed method predictions.

Finite element predictions are shown with thick solid lines with markers, while the proposed method predictions are presented by the thinner solid lines. The predictions of the 2004 CSA A23.3 method are shown by dashed lines. To determine the flexural capacity of the walls according to the 2004 CSA A23.3 method, only the portion of distributed vertical reinforcement that is not needed for shear was included in the sectional analysis. This was an iterative procedure because the wall flexural capacity was not known and therefore shear at flexural capacity was also unknown.

Figures 9-14 and 9-15 compare the finite element predictions with those from the 2004 CSA A23.3 and the proposed method for the walls with height-to-length ratios of 2.0 and 1.0. The proposed method predictions compare well with the finite element results. Note that the proposed method predictions are so close to the finite element predictions in some cases that the lines cannot be distinguished. The 2004 CSA A23.3 predictions are conservative as it totally excludes the contribution of distributed vertical reinforcement needed for shear.

Figures 9-16 and 9-17 present the finite element predictions with the 2004 CSA A23.3 and the proposed method predictions for the walls with height-to-length ratios of 0.5 and 0.3. The 2004 CSA A23.3 predictions are conservative. The proposed method predictions are in reasonably good agreement with the finite element predictions.

9.6.1. Simplified Proposed Method

A simpler model than the proposed model presented in Section 9.5 is to use a reduced amount of distributed vertical reinforcement when calculating the flexural capacity at the base of a squat shear wall. For example, the current CSA A23.3 does not use any of the distributed reinforcement needed for shear. The model is shown in Fig. 9-18 where T_d is

again the resultant tension force in the distributed vertical reinforcement assumed to be yielding over the wall length and α is the portion of the total amount of distributed vertical reinforcement that contributes to the flexural capacity of the wall. While $\alpha=1.0$ means that all of the distributed vertical reinforcement contributes to the flexural capacity, $\alpha = 0$ means none of the distributed vertical reinforcement contributes to the flexural capacity. In order to get the same results from the model presented here in Fig. 9-18 and the proposed model presented before in Fig. 9-13, taking moments about the point of application of compression force C_c in both models should yield equal moments. Thus:

$$[9-9] \alpha T_d (0.5d_v) = T_d (0.5d_v) - N_v (0.5d_{nv})$$

Substituting for $T_d = \rho_v f_y b_w d_v$ and solving for α :

$$[9-10] \alpha = 1 - \frac{N_v}{\rho_v f_y b_w d_v} \left(\frac{d_{nv}}{d_v} \right)$$

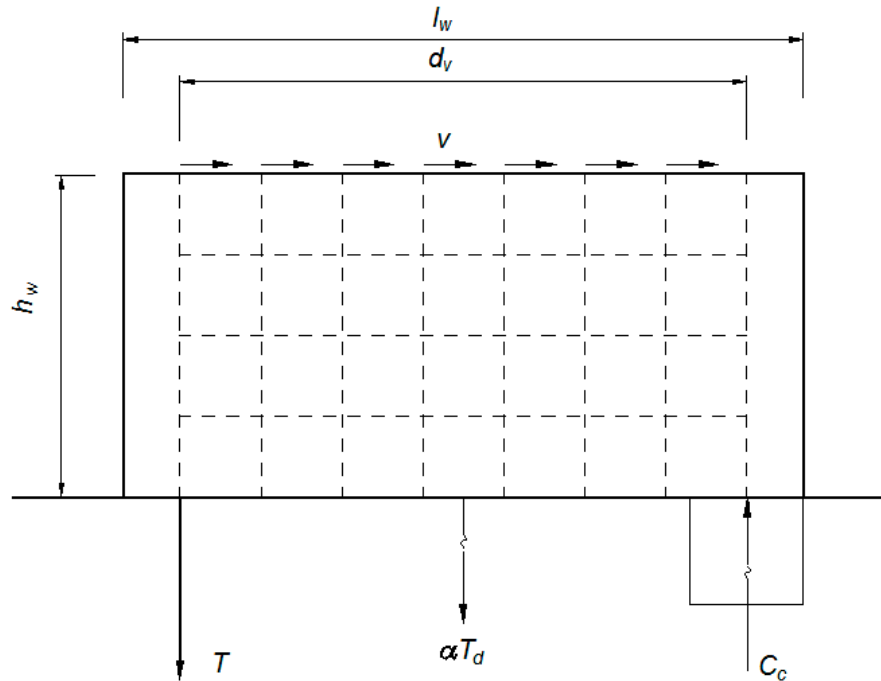


Fig. 9-18 Proposed simple model for flexural capacity of squat shear walls.

Substituting for N_v from Eq. [9-7], Eq. [9-10] can be written as:

$$[9-11] \quad \alpha = 1 - \left(\frac{v \cot \theta}{\rho_v f_y} \right) \left(\frac{d_{nv}}{d_v} \right)^2$$

Assuming flexural and shear failure occur at the same load level and $v_c = 0$ as assumed by the current CSA A23.3, from equilibrium:

$$[9-12] \quad v = \rho_v f_y \tan \theta$$

Substituting v from Eq. [9-12] in Eq. [9-11] results in the following simplified equation:

$$[9-13] \quad \alpha = 1 - \left(\frac{d_{nv}}{d_v} \right)^2$$

in which d_{nv} is determined from Eq. [9-8] and α is the portion of distributed vertical reinforcement needed for shear that contributes to the flexural capacity. d_{nv} can be expressed as a function of wall aspect ratio $\frac{h_w}{l_w}$ assuming $d_v = 0.8l_w$ as in the 2004

CSAA23.3. Substituting $d_v = 0.8l_w$ in Equation [9-8]:

$$[9-14] \quad \frac{d_{nv}}{l_w} = (0.8 - \frac{h_w}{l_w}) \geq 0$$

As $\frac{h_w}{l_w}$ increases $\frac{d_{nv}}{d_v}$ decreases thus the reduction of flexural capacity due to shear also

decreases. For walls with $\frac{h_w}{l_w} \geq 0.8$, no reduction in flexural capacity due to shear is

predicted by the proposed simplified method since d_{nv} becomes zero. Substituting d_{nv}

from Eq. [9-14] in Eq. [9-13], α is given as a function of wall aspect ratio $\frac{h_w}{l_w}$:

$$[9-15] \quad \alpha = \frac{h_w}{l_w} \left(2.5 - 1.56 \frac{h_w}{l_w} \right) \leq 1.0$$

This function is plotted in Figure 9-19 (solid line). As shown, about 80% and 40% of distributed vertical reinforcement needed for shear contribute to the flexural capacity for walls with $\frac{h_w}{l_w} = 0.5$ and 0.2, respectively. No reduction in flexural capacity due to shear for walls with $\frac{h_w}{l_w} \geq 0.8$ is predicted. Equation [9-15] can be conservatively approximated by Eq. [9-16] which is also plotted in Figure 9-19.

$$[9-16] \quad \alpha = 1.5 \frac{h_w}{l_w} \leq 1.0$$

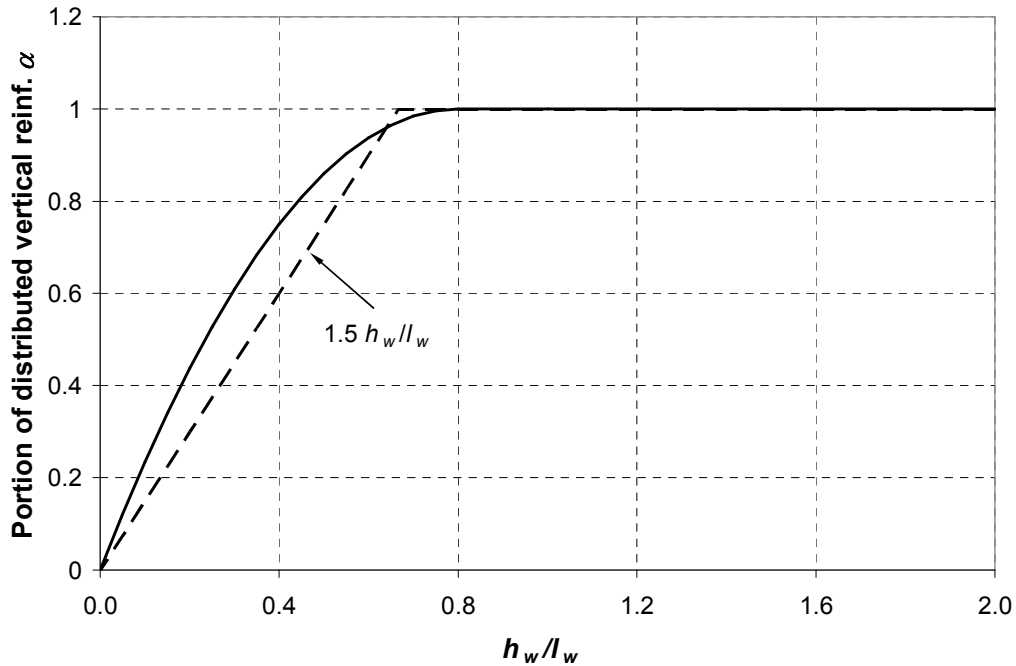


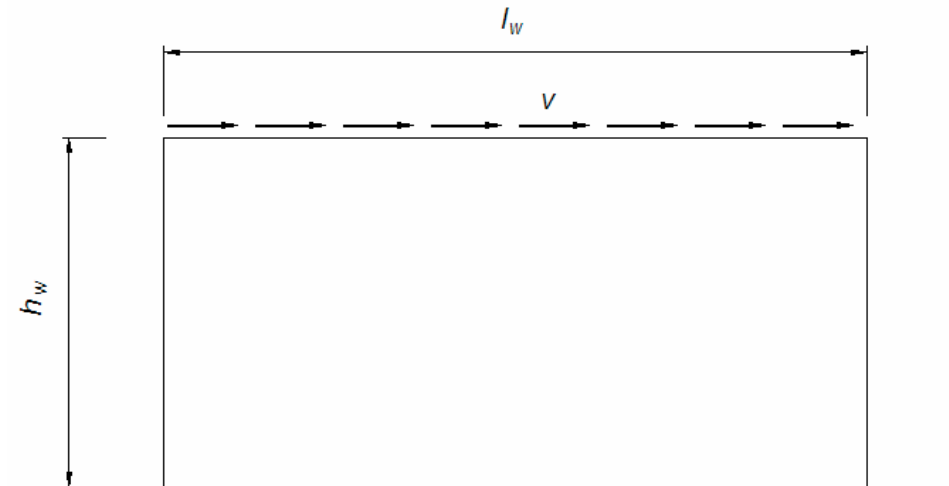
Fig. 9-19 Variation of the portion of distributed vertical reinforcement α that contributes to the flexural capacity of walls.

A simpler approach for code provisions is to use all of the distributed vertical reinforcement in walls with $\frac{h_w}{l_w} \geq 0.8$ and use none of vertical distributed reinforcement needed for shear in walls with $\frac{h_w}{l_w} < 0.8$ when calculating flexural capacity of a squat shear wall.

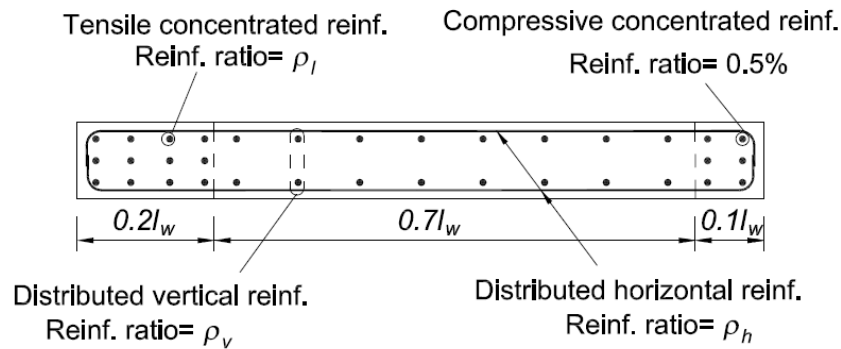
9.7. Finite Element Analyses of Squat Shear Walls Failing in Shear

44 walls were designed to fail in shear and analyzed by VecTor 2. The walls, which were monotonically loaded at the top from the left-to-right direction, had aspect ratios of $h_w/l_w=0.3, 0.5, 1.0$, and 2.0 , with concrete compressive strength of $f'_c = 40$ MPa and steel yield stress of $f_y = 400$ MPa. Typical wall details are shown in Figure 9-20. Two types of cross-sections were used. Type 1 cross-section, which was rectangular, was used for height-to-length ratios of 0.3 and 0.5 while Type 2 cross-section, which included a flange on the flexural tension side, was used for the remaining taller walls to avoid flexural failure. A wall with a flange on one side only is perhaps unrealistic but gives a lower-bound shear strength. Previous studies have shown that if a squat shear wall has a flange on the compression side, the compression zone contribution to the wall shear resistance significantly increases and thus the shear resistance of the wall increases. All walls had uniform cross-sections over the height, and no top beam was provided.

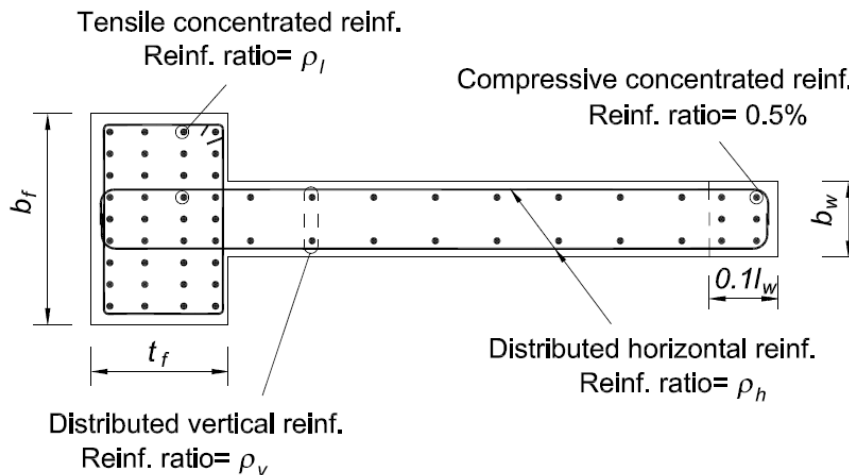
Table 9-2 presents the wall cross-section details including concentrated and distributed vertical reinforcement ratios and distributed horizontal reinforcement ratios. Once again, to minimize the contribution of the flexural compression zone to the



Wall Elevation



Type 1 Wall Cross Section



Type 2 Wall Cross Section

Fig. 9-20 Typical details of walls analyzed to investigate shear strength of squat shear walls.

Table 9-2 Summary of walls analyzed to investigate shear strength of squat shear walls.

h_w/l_w	Wall type	t_f/l_w	b_f/b_w	$\rho_l(\%)$	$\rho_h(\%)$	$\rho_v(\%)$	$\rho'_l(\%)$
0.3	1	-	-	1.00	0.25	0.25	0.50
	1	-	-	1.00	0.50	0.50	0.50
	1	-	-	1.50	0.75	0.75	0.50
	1	-	-	2.00	1.00	1.00	0.50
	1	-	-	2.50	1.25	1.25	0.50
	1	-	-	3.00	1.50	1.50	0.50
	1	-	-	1.00	0.25	0.75	0.50
	1	-	-	1.33	0.50	1.50	0.50
	1	-	-	2.00	0.75	2.25	0.50
	1	-	-	2.66	1.00	3.00	0.50
0.5	1	-	-	3.33	1.25	3.75	0.50
	1	-	-	1.00	0.25	0.25	0.50
	1	-	-	1.00	0.50	0.50	0.50
	1	-	-	1.50	0.75	0.75	0.50
	1	-	-	2.00	1.00	1.00	0.50
	1	-	-	2.50	1.25	1.25	0.50
	1	-	-	3.00	1.50	1.50	0.50
	1	-	-	1.00	0.25	0.75	0.50
	1	-	-	1.33	0.50	1.50	0.50
	1	-	-	2.00	0.75	2.25	0.50
1.0	2	0.1	4.0	2.66	1.00	3.00	0.50
	2	0.1	4.0	3.33	1.25	3.75	0.50
	2	0.1	4.0	1.25	0.25	0.25	0.50
	2	0.1	4.0	1.25	0.50	0.50	0.50
	2	0.1	4.0	1.88	0.75	0.75	0.50
	2	0.1	4.0	2.50	1.00	1.00	0.50
	2	0.1	4.0	3.13	1.25	1.25	0.50
	2	0.1	4.0	3.75	1.50	1.50	0.50
	2	0.1	4.0	1.25	0.25	0.75	0.50
	2	0.1	4.0	1.25	0.50	1.50	0.50
2.0	2	0.1	4.0	1.88	0.75	2.25	0.50
	2	0.1	4.0	2.50	1.00	3.00	0.50
	2	0.1	4.0	3.13	1.25	3.75	0.50
	2	0.2	4.0	1.25	0.25	0.25	0.50
	2	0.2	4.0	1.25	0.50	0.50	0.50
	2	0.2	4.0	1.88	0.75	0.75	0.50
	2	0.2	4.0	2.50	1.00	1.00	0.50
	2	0.2	4.0	3.13	1.25	1.25	0.50
	2	0.2	4.0	3.75	1.50	1.50	0.50
	2	0.2	4.0	1.25	0.25	0.75	0.50
2.0	2	0.2	4.0	1.25	0.50	1.50	0.50
	2	0.2	4.0	1.88	0.75	2.25	0.50
	2	0.2	4.0	2.50	1.00	3.00	0.50
	2	0.2	4.0	3.13	1.25	3.75	0.50
	2	0.2	4.0	3.13	1.25	3.75	0.50

ρ_l = concentrated flexural reinforcement ratio, ρ'_l = concentrated reinforcement ratio in concrete compression zone, ρ_v = distributed vertical reinforcement ratio, ρ_h = distributed horizontal reinforcement ratio.

shear resistance, concentrated vertical reinforcement ratio in the compression zone was taken equal to the 2004 CSA A23.3 minimum ratio of 0.5%. In addition, concentrated vertical reinforcement was placed over only 10% of the wall length on the wall compression side.

Distributed horizontal reinforcement ratios were varied from 0.25% to 1.5%. According to the 2004 CSA A23.3 provisions, diagonal compression angle θ is freely chosen from 30 to 45 degrees. If $\theta=45$ deg is chosen and there is no axial compression, the amount of distributed vertical reinforcement needed for shear is equal to the amount of distributed horizontal reinforcement (see Eq. [9-6]). If $\theta=30$ deg is chosen, the amount of distributed vertical reinforcement needed for shear is 3.0 times the amount of distributed horizontal reinforcement (see Eq. [9-6]). Thus distributed vertical reinforcement ratios were either equal to the distributed horizontal reinforcement ratios ($\rho_v / \rho_h = 1.0$) or 3.0 times the horizontal reinforcement ratios ($\rho_v / \rho_h = 3.0$). The same finite element mesh discussed for walls failing in flexure (Section 9.4.1) was used.

9.7.1. Comparison of Finite Element Results with Code Predictions

Figure 9-21 compares the finite element predictions (solid lines with markers) for shear strength of the walls failing in shear with the predictions of ACI 318 (dashed line), NZS 3101 (dashed-dotted line), and the 2004 CSA A23.3 (dotted line). While Fig. 9-21(a) presents the results for walls with equal amount of distributed reinforcement in both directions, Fig. 9-21(b) shows the results for the walls with distributed vertical reinforcement ratios of 3 times horizontal distributed reinforcement ratios. NZS 3101 predictions were determined assuming ductility factor of 2.0 and overstrength factor of

1.0. NZS 3101 method is explained in Section 7.3.2. Note that the 2005 National Building Code of Canada specifies a ductility factor of 2.0 for squat shear walls.

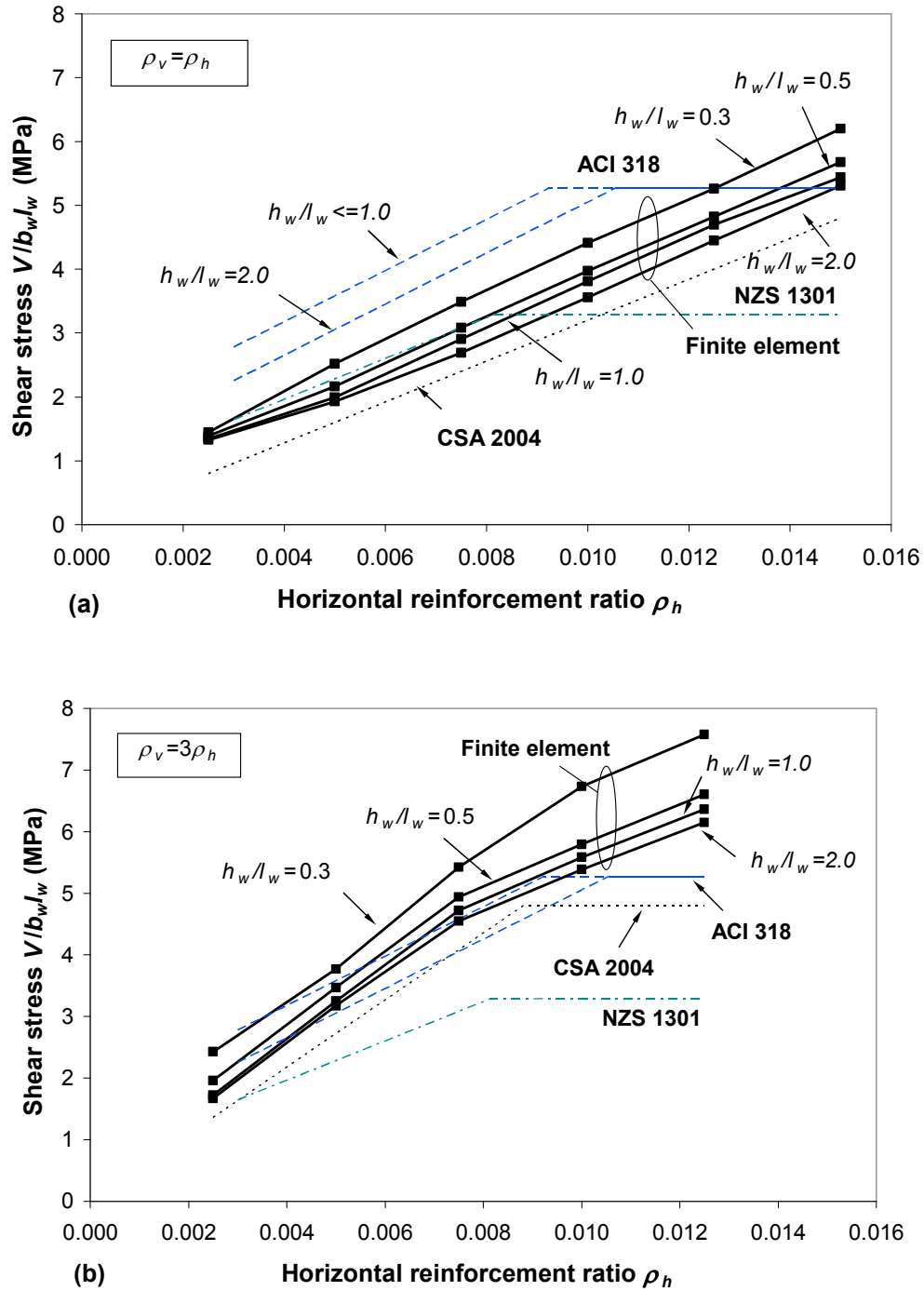


Fig. 9-21 Comparison of finite element predictions for shear strength with code predictions for squat walls with: (a) $\rho_v = \rho_h$, (b) $\rho_v = 3\rho_h$.

The end horizontal lines in the code prediction curves in Figs. 9-21(a) and (b) correspond to the code total shear force limits to avoid concrete crushing and base sliding due to shear. These limits are explained in Chapter 7. The change in the slopes of finite element curves beyond horizontal reinforcement ratio of about 0.008 in Fig. 9-21(b) is also due to the change of failure mode from diagonal tension shear failure to concrete crushing failure.

ACI 318 and NZS 3101 predictions are the same in Figs. 9-21(a) and 9-21(b) as they are not influenced by ρ_v / ρ_h ratios. In contrast, the 2004 CSA A23.3 predictions are higher in Fig. 9-21(b) compared to Fig. 9-21(a) that is consistent with the finite element results. ACI 318 predictions are consistently unconservative for $\rho_v / \rho_h = 1.0$ until they reach concrete crushing limit. NZS 3101 predictions are less unconservative for $\rho_v / \rho_h = 1.0$; they are slightly unconservative for the taller walls with horizontal reinforcement ratios of less than 0.008.

For walls with $\rho_v / \rho_h = 3.0$ (Fig. 9-21b), ACI 318 predictions are in better agreement with the finite element results compared to those for the walls with $\rho_v / \rho_h = 1.0$ (Fig. 9-21a), but they are still unconservative in some cases. NZS 3101 predictions are highly conservative for walls with $\rho_v / \rho_h = 3.0$. The 2004 CSA A23.3 trend of predictions is similar to that from the finite element results, but they are conservative in all cases. While the 2004 CSA A23.3 predictions are closer to the finite element results for walls with height-to-length ratios of 1.0 and 2.0, they become more conservative for walls with height-to-length ratio of 0.3.

Shear stress distributions at the wall base and mid-height are shown in Figs. 9-22 (a) and (b) for the four walls with $\rho_v = \rho_z = 0.005$. Shear stress at base (Fig. 9-22a) is not

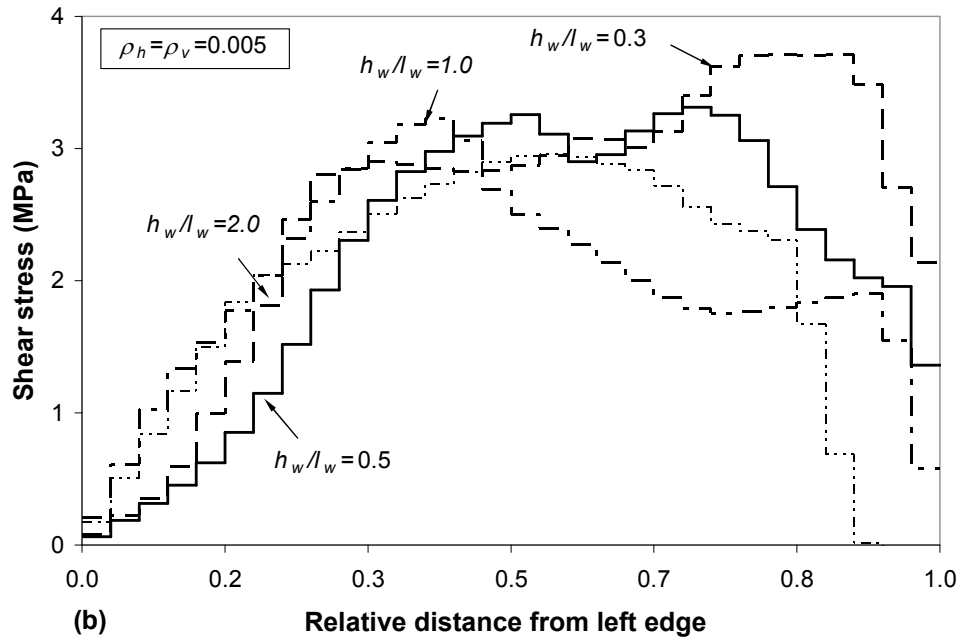
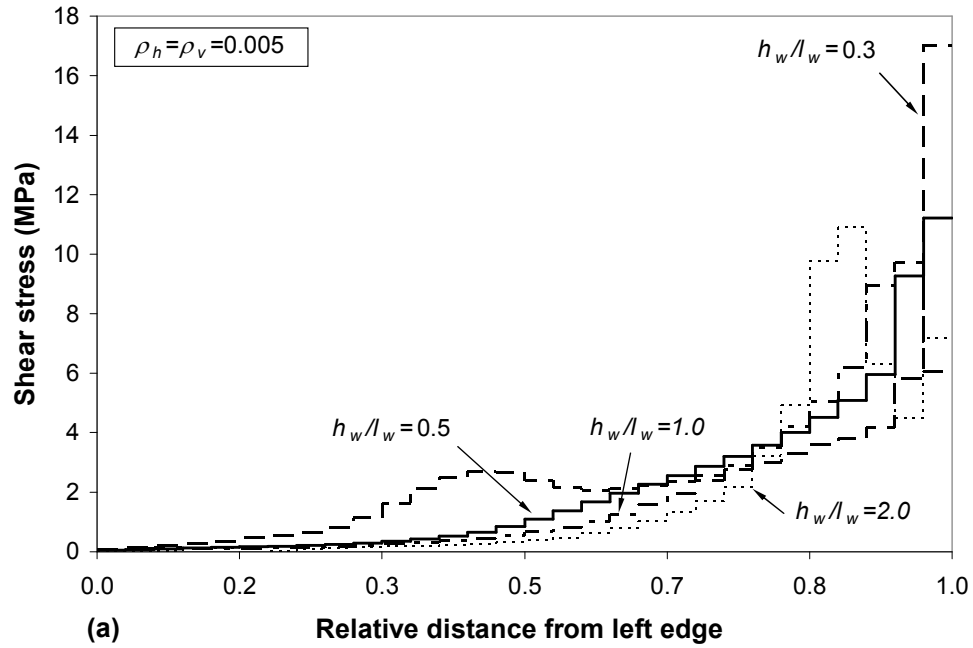


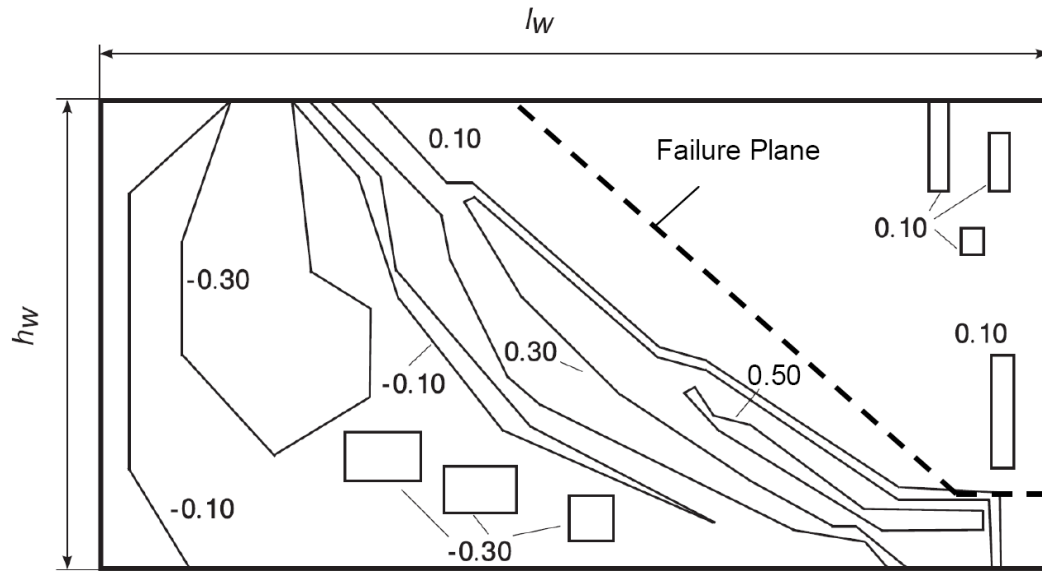
Fig. 9-22 Finite element predictions for shear stress distribution in squat walls with $\rho_v = \rho_h = 0.005$ immediately prior to shear failure: (a) at base of wall, (b) at mid-height.

uniform; shear is mostly carried by compression side of the wall especially in the taller walls. Maximum shear stress in the compression side of the walls is as high as 17 MPa in the wall with height-to-length ratio of 0.3.

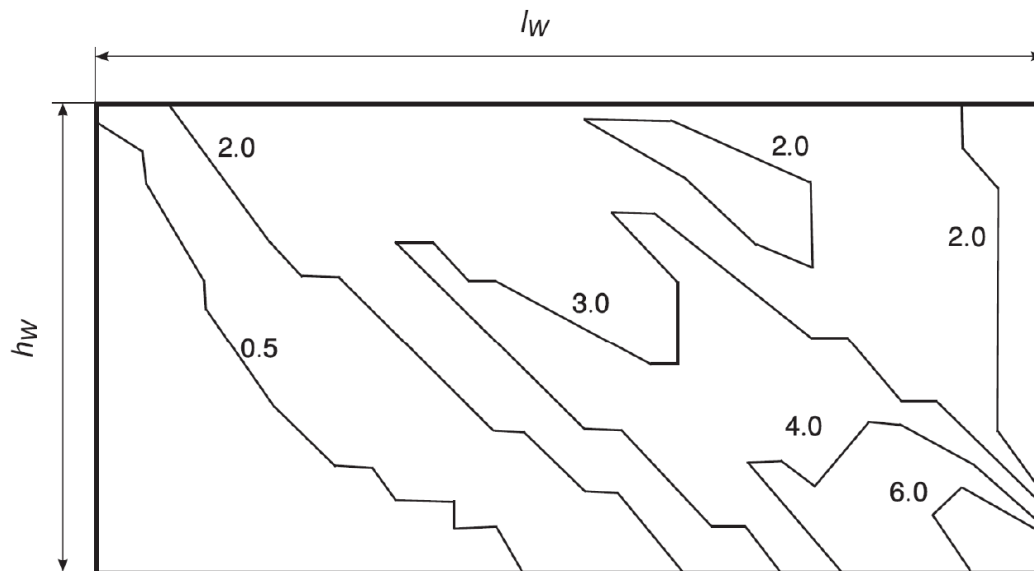
Mid-height shear stress distributions (Fig. 9-22b) are closer to uniform distribution. As the wall height-to-length ratios decrease, contribution of the compression side of the walls to shear resistance is more significant. The 2004 CSA A23.3 assumes that shear is resisted by 80% of the wall length ($d_v=0.8l_w$) which is conservative since the compression zone significantly contributes to the wall shear strength especially for walls with a height-to-length ratio of 0.3.

Aggregate interlock contribution to shear resistance was found to be negligible in the finite element results. This is shown in Fig. 9-23(a), which illustrates the stress contour diagram of shear stress on cracks together with approximate failure plane based on the finite element results. Notice that shear stress on cracks is less than 0.1 MPa in the region that failed in shear. This confirms that the assumption of $V_c=0$ in the 2004 CSA A23.3 is reasonable.

Figure 9-23(b), which illustrates the stress contour diagram of total shear stress, shows that the shear flow pattern is the same as the one for the wall failing in flexure shown in Figure 9-5(a). Fig. 9-23(b) also illustrates that shear stress in the compression zone is significant, thus it significantly contributes to the shear strength of squat walls. The 2004 CSA A23.3 ignores the compression zone contribution to shear strength as it assumes that shear force is resisted by 80% of the wall length. It was found that the significant increase in the finite element predicted shear strength of squat



(a) Shear stress on cracks v_c (MPa)

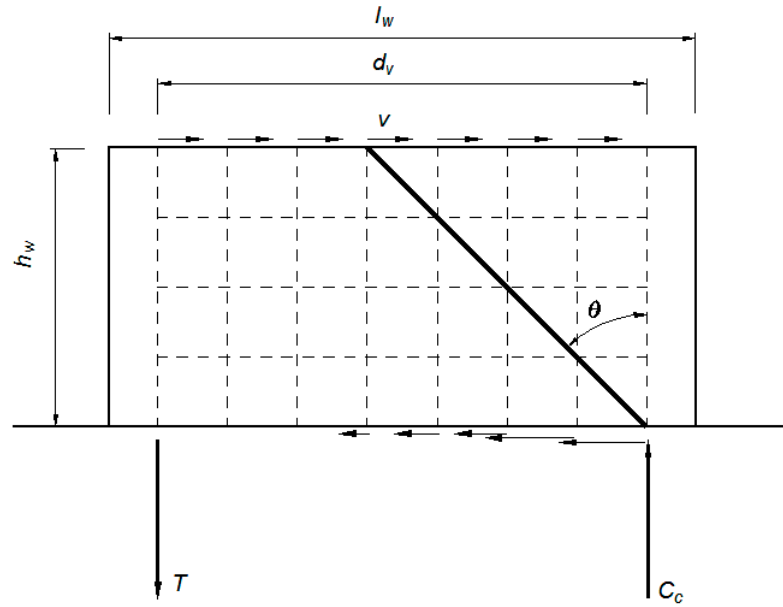


(b) Shear stress (MPa)

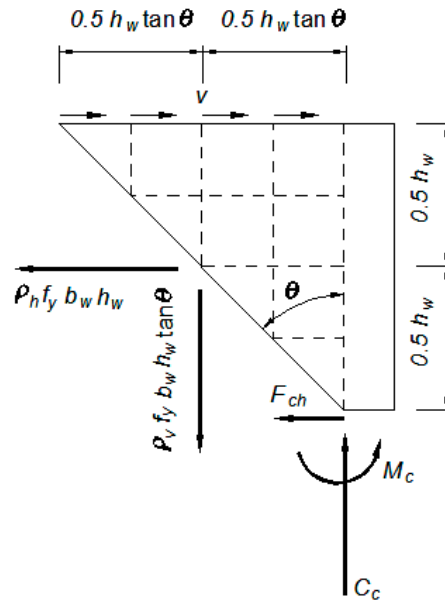
Fig. 9-23 Concrete shear stress contour diagrams based on finite element analysis of a squat shear wall with 0.5% distributed reinforcement in both directions and height-to-length ratio of 0.5 prior to diagonal tension shear failure.

walls with height-to-length ratio of 0.3 compared the shear strength of the taller walls was due to the compression zone contribution to shear resistance.

To include the effect of compression zone in shear resistance, the free body diagram shown in Fig. 9-3(b) can be revised as shown in Fig. 9-24(b).



(a) Failure plane



(b) Free body diagram of wall element bounded by failure plane

Fig. 9-24 Diagonal tension failure of low rise shear walls accounting for compression zone contribution.

According to equilibrium equation in the horizontal direction:

$$[9-17] \quad v b_w h_w \tan \theta = V_{sh} + F_{ch} = \rho_h f_y b_w h_w + F_{ch}$$

F_{ch} is a function of compression zone length which in turn is a function of wall length and concrete cracking stress. Concrete cracking stress is a function of $\sqrt{f'_c}$, thus F_{ch} can be estimated as:

$$[9-18] \quad F_{ch} = \kappa \sqrt{f'_c} b_w l_w$$

where κ is a coefficient. Substituting F_{ch} from Eq. [9-18] in Eq. [9-17] and solving for v :

$$[9-19] \quad V = v b_w d_v = [\rho_h f_y \cot \theta + \alpha_c \sqrt{f'_c} \left(\frac{l_w}{h_w} \right)] b_w d_v$$

in which α_c is another coefficient equal to $\kappa \cot \theta$. Eq. [9-17] is similar to the ACI 318 shear strength equation for squat shear walls and other proposed methods in the literature such as the method proposed by Wirandianta (1985). It includes a steel contribution V_s that is equal to $\rho_h f_y \cot \theta b_w d_v$ and is independent of wall aspect ratio, and concrete contribution $V_c = \alpha_c \sqrt{f'_c} \left(\frac{l_w}{h_w} \right) b_w d_v$ which is a function of wall aspect ratio. $\alpha_c = 0.1$ in

Eq. [9-19] results in predictions that are in good agreement with the finite element results for the 44 walls failing in shear when θ is determined from the 2004 CSA A23.3 equation Eq. [7-27]. As it will be shown later, compression zone contribution to shear is significantly reduced if localized sliding along previously existing cracks at the base is

modeled in the finite element analysis, and thus the model explained above is not advocated in this thesis.

9.7.2. Sliding along Previously Existing Cracks

As described earlier, it was assumed in the finite element analysis that the wall base was fully constrained in the horizontal direction. As a result of this assumption, finite element predictions of shear stress carried at the base in the compression zone region was as high as 17 MPa in some cases. Such a high shear stress is appropriate for reinforced concrete that is monotonically loaded; however, under load reversals, the compression zone will have horizontal cracks as it was the tension zone in the reverse direction of loading thus may not be able to resist such a high shear stress.

Equation [3-6], which was developed from experimental results, gives the maximum shear stress that can be transferred across cracks. This equation limits the shear stress of cracked concrete to $0.58\sqrt{f'_c}$ (3.7 MPa for 40 MPa concrete) when the crack width is zero. NZS 3101, on the other hand, limits the shear stress on walls to $0.65\sqrt{f'_c}$ (4.1 MPa for 40 MPa concrete) for a wall with overstrength factor of 1.0 and ductility factor of 2.0 (see Eq. 7-25), while the 2004 CSA A23.3 limits the shear stress to $0.15 f'_c$ (6 MPa for 40 MPa concrete). A similar limit in ACI 318 is $0.83\sqrt{f'_c}$ for individual wall piers, which is 5.25 MPa for 40 MPa concrete. Based on these numbers, it was decided to limit the shear stress of walls to the conservative value of 4 MPa for 40 MPa concrete to account for sliding along previously existing cracks. Only three walls with horizontal and vertical distributed reinforcement ratios of 0.005 were analyzed in this way.

VecTor 2 is not capable of limiting the horizontal shear stress in an element to a specified value. Thus the analysis was done using VecTor 2 together with an event-to-event procedure that was manually carried out. The analysis started for the case where all nodes along the wall base were constrained both in vertical and horizontal directions. The analysis was then stopped when reaction at any node at the base reached the magnitude that corresponds to 4 MPa shear stress in the horizontal direction. The node constraint in the horizontal direction was then removed and the force corresponding to 4MPa shear stress was applied at the node. The analysis continued until the reaction at the next node reached the magnitude corresponding to 4MPa shear stress. The procedure was repeated until all reactions at the nodes had the magnitude of less than or equal to the magnitude corresponding to 4 MPa shear stress.

Figure 9-25 shows the finite element predictions of load-displacement relationships for the walls with height-to-length ratios of 0.3 (Fig 9-25a), 0.5 (Fig. 9-25b), and 1.0 (Fig. 9-25c) when horizontal shear stress is limited to 4MPa. The finite element predictions when shear stress is not limited are also presented. The results show that the shear strength of the wall with height-to-length ratio of 0.3 is significantly affected by limiting the shear stress in the compression zone, while the shear strength of the wall with height-to-length ratio of 1.0 is not affected significantly. When the shear stress in the compression zone is limited, the finite element predicted shear strength for the wall with height-to-length ratio of 0.3, shown in Fig. 9-25(a), is only 10% greater than the finite element predicted shear strength of the wall with height-to-length ratio of 1.0 shown in Figure 9-25(c). This indicates that wall aspect ratio does not significantly influence the

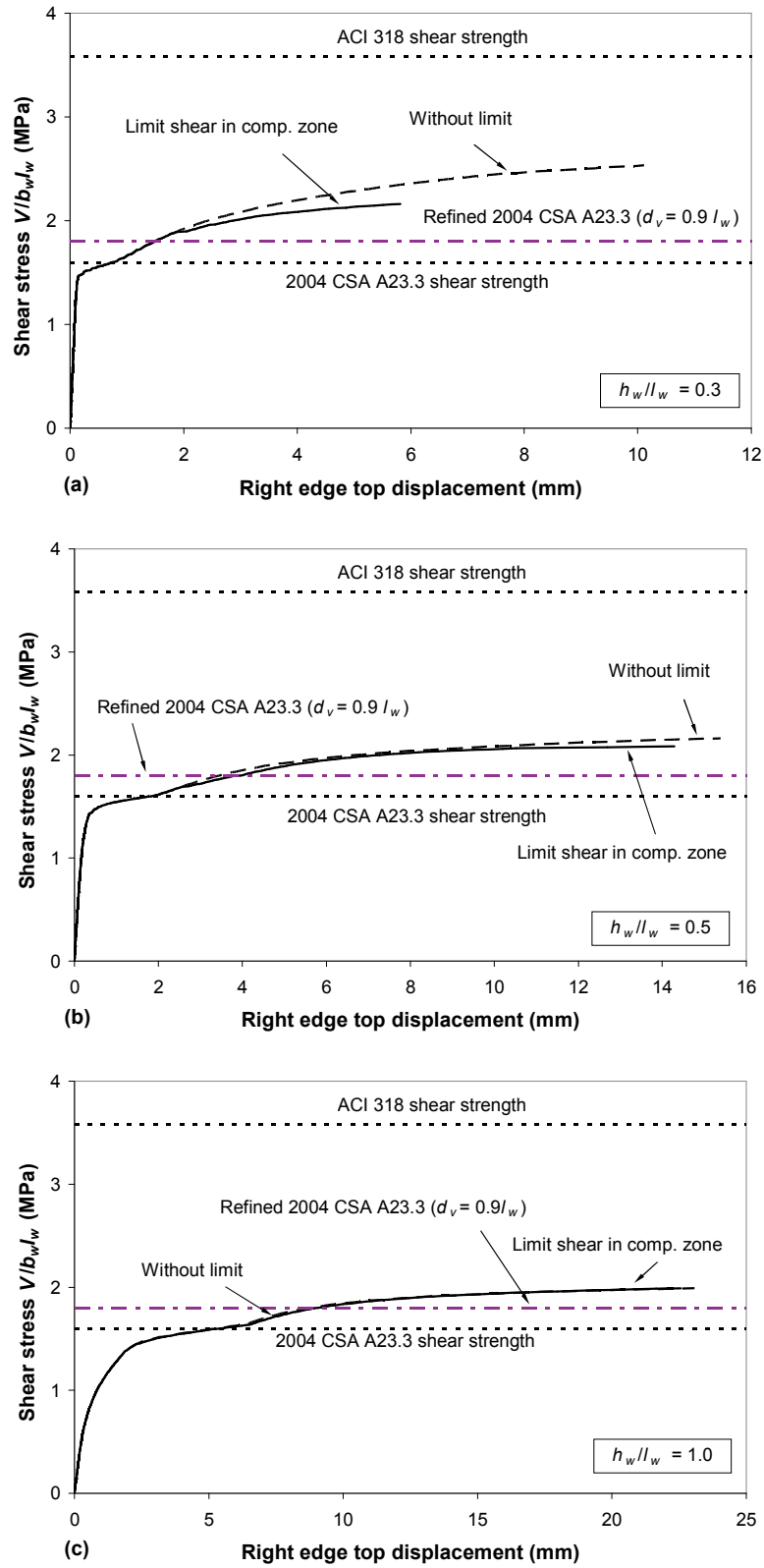


Fig. 9-25 Localized sliding effect on load-displacement curve of squat shear walls with $\rho_z = \rho_v = 0.005$ and height-to-length ratio of: (a) 0.3, (b) 0.5, (c) 1.0.

shear strength of squat shear walls when the shear stress in the compression zone is limited. This is consistent with the 2004 CSA A23.3 provisions.

Figure 9-26 illustrates base shear stress distributions of the walls when shear stress is limited together with the distributions for the walls when shear stress is not limited. As expected, shear stress is more uniform for walls in which shear stress is limited. The mid-height shear stress distributions of the walls are examined in Figure 9-27. It is evident that the compression zone contribution to shear resistance is highly reduced due to limiting the shear stress in the compression zone for the wall with height-to-length ratio of 0.3 while it does not have an influence for the wall with height-to-length ratio of 1.0.

As shown in Fig. 9-27, shear stress is still considerable in the compression zone for all walls, but this shear stress is not accounted for in the 2004 CSA A23.3; it assumes only 80% of the wall lengths contribute to shear resistance. To account for the influence of compression zone on the shear resistance, it is proposed to take $d_v=0.9l_w$ rather than $d_v=0.8l_w$ as in the 2004 CSA A23.3. The resulted predictions of shear strength are compared with finite element predictions in Figure 9-25. The good agreement between the finite element predictions of shear strength when shear stress in the compression zone is limited and the predictions from the 2004 CSA A23.3 method with the proposed refinement is evident.

9.7.3. Comparison of Finite Element Results with the 2004 CSA A23.3

Refined Method

As explained in the previous section, the proposed refinement to the CSA A23.3 provisions for shear strength of squat shear walls is to use an effective shear length $d_v=0.9l_w$. In the current provisions, $d_v=0.8l_w$. In this section, the finite element predictions

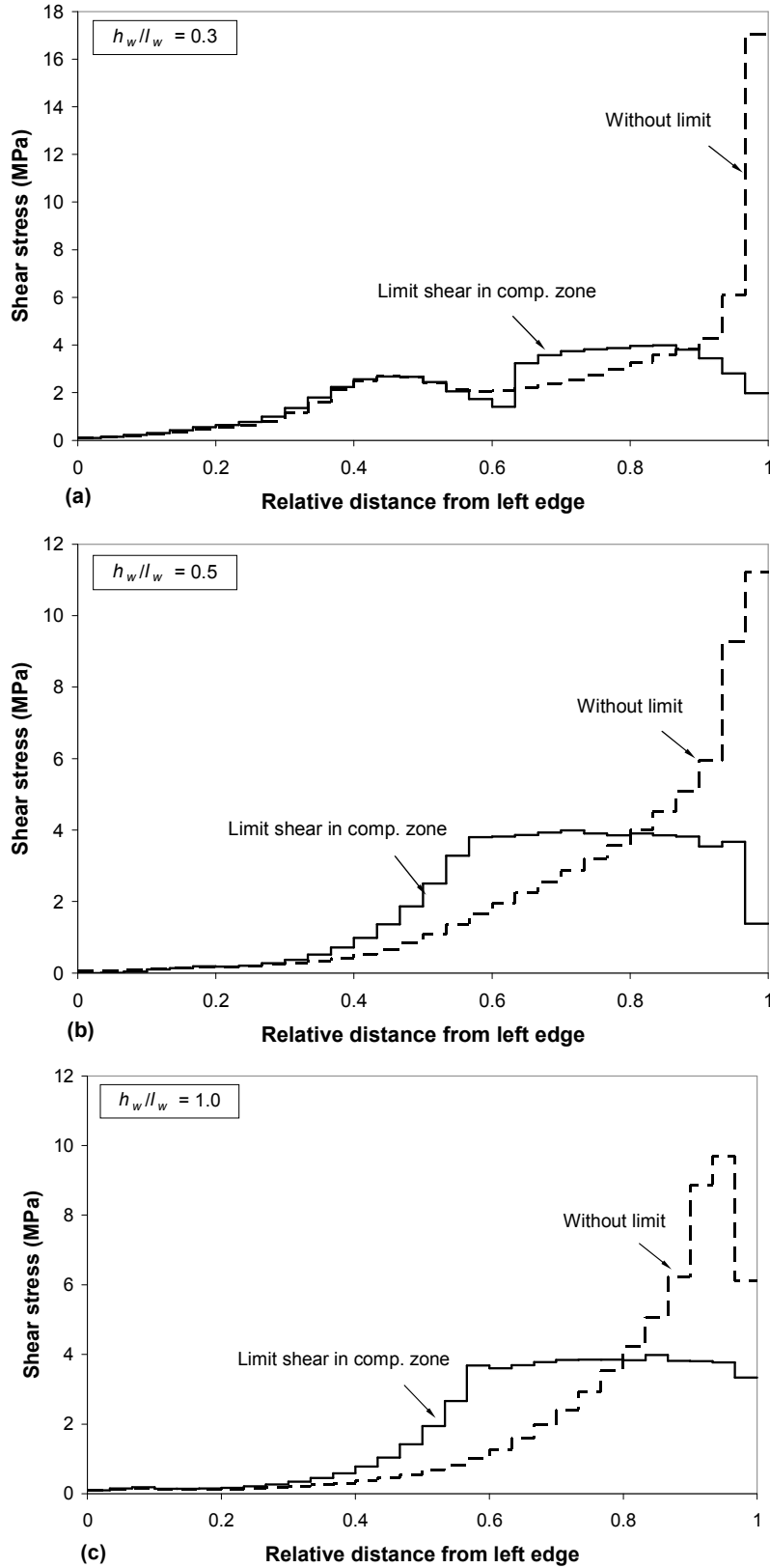


Fig. 9-26 Localized sliding effect on base shear stress distribution of squat shear walls with $\rho_z = \rho_v = 0.005$ and height-to-length ratio of: (a) 0.3, (b) 0.5, (c) 1.0.

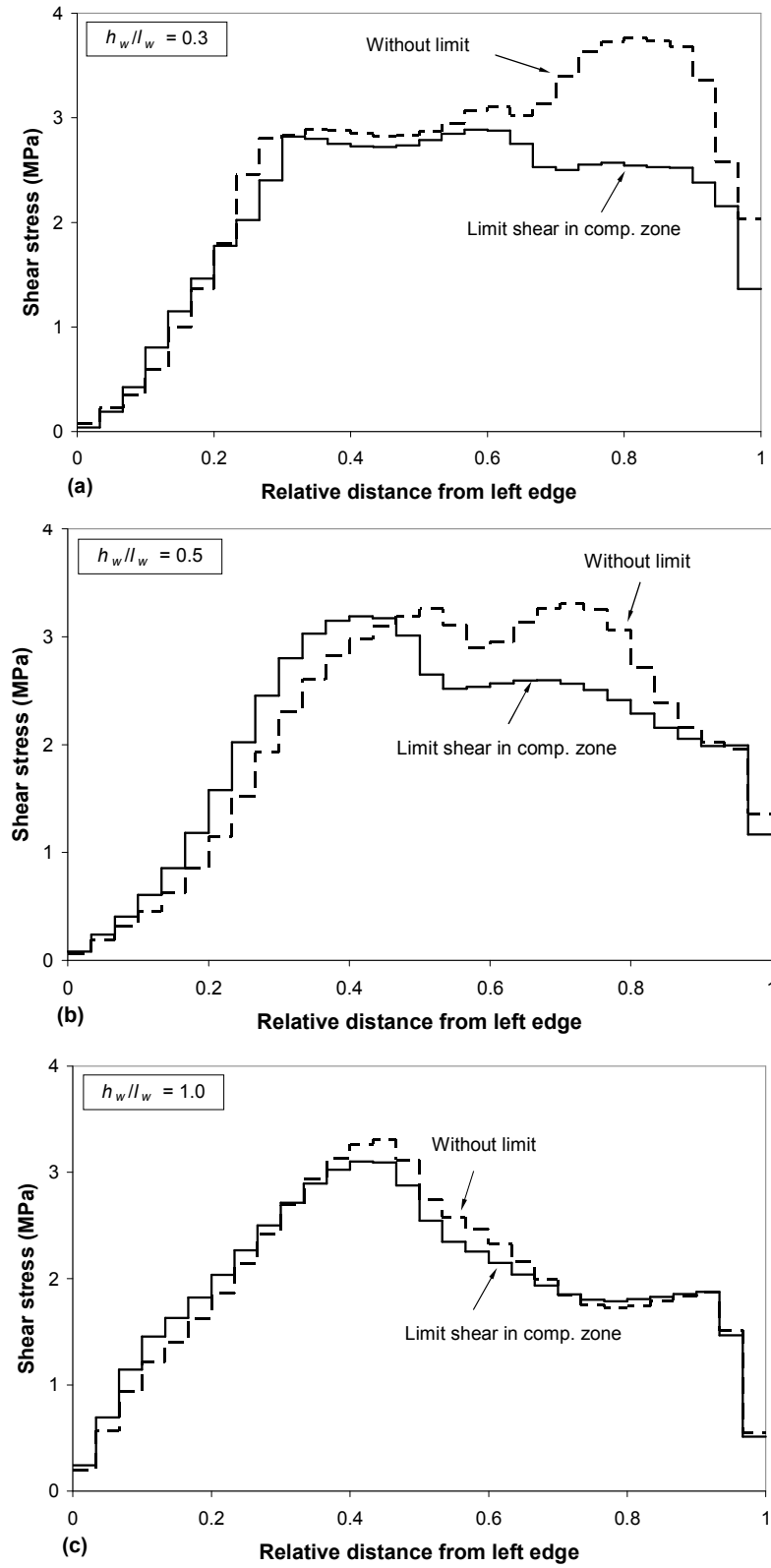


Fig. 9-27 Localized sliding effect on mid-height shear stress distribution of squat shear walls with $\rho_z = \rho_v = 0.005$ and height-to-length ratio of: (a) 0.3, (b) 0.5, (c) 1.0.

of shear strength for the 44 walls failing in shear are compared with the predictions from the 2004 CSA A23.3 with the proposed refinement.

Figure 9-28 compares the finite element predictions of shear strength with the 2004 CSA A23.3 predictions using $d_v=0.9l_w$ for the 44 walls failing in shear in which shear stress is not limited. The horizontal axis is the wall height-to-length ratio while the vertical axis is the ratio of finite element predicted shear strength to the 2004 CSA A23.3 predicted shear strength using $d_v=0.9l_w$. Clearly using $d_v=0.9l_w$ in the 2004 CSA A23.3 is conservative as the ratios vary from about 1.0 to about 1.60.

The finite element predictions compare well with the revised 2004 CSA A23.3 method for walls with height-to-length ratios of 1.0 and 2.0. The shear strength ratios are below 1.25 in most cases. Note that in walls with height-to-length ratios of 1.0 and 2.0 limiting the shear stress in the compression zone has insignificant influence on shear strength as shown in the previous section. Only one wall with a height-to-length ratio of 1.0 and one wall with a height-to-length ratio of 2.0 has a high shear strength ratio close to 1.50. Those two walls had a low amount of distributed reinforcement – 0.25% in both horizontal and vertical directions. The strength of the two walls are significantly higher than the 2004 CSA A23.3 refined method predictions because their shear strength at concrete diagonal cracking was higher than shear strength at yielding of horizontal reinforcement.

The 2004 CSA A23.3 revised method becomes more conservative for walls with smaller height-to-length ratios especially for those with height-to-length ratio of 0.3. For those walls, limiting the shear stress in the compression zone decreases the shear strength about 15% as shown in the previous section. Thus, it could be concluded that the 2004

CSA A23.3 method with the proposed refinement can reasonably predict the shear strength of squat shear walls. Limiting the shear stress in the compression zone is very time consuming and therefore it was not possible to repeat the predictions for all walls accounting for this.

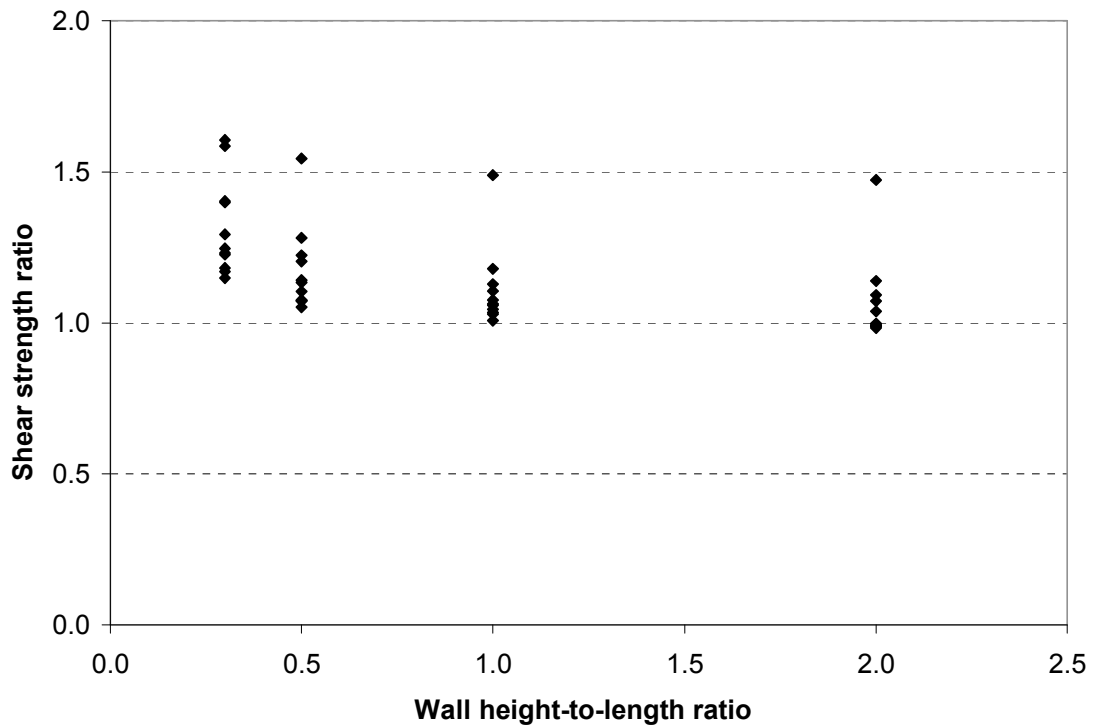


Fig. 9-28 Ratios of finite element analysis-to-2004 CSA A23.3 refined method predicted shear strength for the 44 walls failing in shear.

Chapter 10. Summary and Conclusions

10.1. General

This thesis involves two related topics which are shear strength of concrete bridge girders and strength of squat shear walls. The summary and conclusions for the two topics are reported separately below.

10.2. Shear Strength Evaluation of Bridge Girders

Beam shear design provisions of AASHTO LRFD and the 2006 CHBDC are based on simplified versions of Modified Compression Field Theory (MCFT, Vecchio and Collins 1983) which is one of the theories developed to predict the behaviour of uniform shear elements. As a result of simplifications for design, these methods are conservative which is preferred for design; but may cause unnecessary bridge load restrictions or retrofit when these methods are used for evaluation.

Response 2000 (Bentz 2000), which performs beam sectional analysis employing a smeared layered approach, provides a more accurate prediction for beam shear strength and is able to predict the behaviour of beams throughout the entire range of loading. While such a computer program is a powerful research tool, it is not convenient for engineering practice since it requires advanced knowledge of shear and high level of judgment. It requires a significant number of input parameters and includes different material models and the results cannot be easily checked by hand calculations. Use of Response 2000 for evaluation of numerous sections of a bridge is also time consuming since it requires detailed information of each cross-section and provides significant amount of information from which user should extract the needed information.

10.2.1. Proposed Evaluation Method

A new method for shear evaluation of beams was developed and is presented in this thesis. The new method accounts for the effect of more parameters in shear, provides more insight than other simplified approaches, and still is simple enough to be easily implemented in an Excel spreadsheet. Also, the results can be easily checked by hand calculations. The proposed evaluation procedure, which is different for members with and without stirrups, was developed so that trial-and-error is not required; but also includes a number of refinements such as accounting for: (i) influence of V_c (concrete tension stresses) on average longitudinal compression force N_v required to resist shear in a diagonally cracked web (V_c reduces average tension strain of member), (ii) difference between total shear depth d_v and depth of diagonally cracked web d_{nv} , (iii) tension force resisted by distributed longitudinal reinforcement in web, (iv) location of prestressed tendons in web, and (v) tension-stiffening provided by cracked concrete in tension chord.

The procedure was verified by comparing predictions of shear strength for members with and without stirrups with the MCFT predictions for a single uniform shear element. The proposed method predictions were in better agreement with MCFT predictions compared to the 2006 CHBDC method for both members with and without transverse reinforcement.

To further validate the method, shear strength predictions for four existing bridge girders were compared with the results from Response 2000. The girders in three of these bridges had more than minimum transverse reinforcement while the girders in the fourth had less than minimum transverse reinforcement. Three of the bridges had prestressed concrete girders. Predictions of the 2007 AASHTO LRFD, 2006 CHBDC,

and ACI 318-05 were also compared with the results from the proposed method. The proposed method predictions were found to be closer to Response 2000 predictions compared to the code predictions. For example, Response 2000 predictions for the nine evaluated sections of the three girders with more than minimum transverse reinforcement were on average only 4% higher than the results from proposed method. The COV of the ratios of Response 2000 predicted shear strength to the predicted shear strength from the proposed method was only 4%. Among the evaluated code methods, the 2007 AASHTO LRFD procedure was the most consistent with Response 2000. The predictions were on average 13% higher than the Response 2000 predictions and COV of predicted shear strength ratios was 11%. ACI 318-05 had the largest deviation from Response 2000 with COV of predicted shear strength ratios equal to 16%. Further verification of the method by comparing with experimental results is summarized in Section 10.2.3

10.2.2. Proposed Refinement for the 2006 CHBDC Shear Design Method

In the 2006 CHBDC and 2004 CSA A23.3 codes, the shear resistance of a beam with or without transverse reinforcement is a function of mid-depth longitudinal strain ε_x . These codes provide a simple equation to estimate ε_x , and allow the use of a more sophisticated procedure to determine ε_x ; but do not describe how this procedure is to be done. One approach that could be used to estimate the mid-depth longitudinal strain is a sectional analysis using Response 2000.

A more complex version of the code equation for ε_x was developed as part of this thesis. This equation includes a better estimate of the axial compression force needed in the web of a girder to resist shear. It also rigorously accounts for the influence of

distributed longitudinal reinforcement in the web and tension stiffening of the flexural tension reinforcement. A comparison with the mid-depth longitudinal strain determined with Response 2000 indicates the proposed equation for ε_x is more accurate than the code simplified equation. The mid-depth longitudinal strains predicted by the simple equation in the codes were up to 40% larger than predicted by the proposed equation and Response 2000. It is recommended that when the 2006 CHBDC method is used to evaluate the shear strength of an existing bridge girder with transverse reinforcement, the proposed equation for ε_x be used to obtain a higher shear strength estimate.

While 2006 CHBDC and 2004 CSA A23.3 codes permit the use of a more sophisticated procedure to determine ε_x in members without transverse shear reinforcement, a comparison with test results has shown that this may be unsafe. This is explained in Section 10.2.3.

10.2.3. Comparison of Predictions with Experimental Results

Members with at least minimum transverse reinforcement

The proposed shear evaluation method for members with transverse reinforcement was verified against actual shear strengths determined from tests of 80 reinforced concrete beams and 88 prestressed concrete beams reported in the literature. Comparisons with 80 reinforced concrete beam tests showed that the predictions from the proposed evaluation method are the closest to the test results compared to the 2006 CHBDC, 2007 AASHTO LRFD, and ACI 318 design methods.

Only 26 of the 80 reinforced concrete beams that have been previously tested had transverse reinforcement ratios more than twice the minimum, while most existing bridge girders have more than twice the minimum transverse reinforcement. For the 26 beams

with more than twice the minimum transverse reinforcement, predictions from the proposed method compare even better with the test results than the code methods.

The proposed evaluation method predictions were also in better agreement with experimental results than the code design methods for the 88 prestressed concrete beam tests with stirrups. As was also determined in previous studies (Hawkins et. al, 2005), ACI 318 method is unsafe with about 50% of the shear strength predictions being greater than the actual test results.

Of the 88 prestressed concrete beams, only 22 beams had a predicted mid-depth longitudinal strain higher than 0.0001. While the proposed method shear strength predictions for those members were in good agreement with actual test results, the 2006 CHBDC gave on average 13% more conservative results for those beams compared to the proposed method predictions.

The 2006 CHBDC shear strength predictions with the proposed refined ε_x equation was validated against the same 80 reinforced concrete and 88 prestressed concrete tested beams. Using the proposed ε_x equation in the 2006 CHBDC shear design provision improved the average test-to-code predicted shear strength ratio from 1.31 to 1.26 in prestressed concrete members while the COV of shear strength ratios remained about the same.

Members without transverse reinforcement

The proposed procedure for members without transverse reinforcement was validated by comparing shear strength predictions with test results for 132 reinforced concrete and 131

prestressed concrete beams. The proposed evaluation method gave the best overall agreement with test results.

For the reinforced concrete beams, the proposed method had an average value of test-to-predicted shear strength ratio of 1.17 and COV of 17.3%. The average values of test-to-predicted shear strength ratios were 1.26 and 1.16 for the 2007 AASHTO LRFD and 2006 CHBDC methods, respectively. The COV of these ratios were 18.5% and 17.8%, respectively. The ACI 318 predictions for the shear strength of beams without transverse reinforcement were very unsafe due to the well known size effect phenomenon.

For the prestressed concrete beams, the average test-to-predicted shear strength ratios were 1.37 for the proposed method, 1.55 for 2006 CHBDC, 1.57 for 2007 AAHTO LRFD, and 1.17 for ACI 318. The corresponding COV of these ratios were 17%, 23.2%, 23.1%, and 16%, respectively.

Using a more refined equation for ε_x to predict the shear strength of 132 reinforced concrete beams without stirrups increased the number of unsafe predictions from the 2006 CHBDC from 18% to 32% of the tests. The reason is that the 2006 CHBDC method uses the mid-depth longitudinal strain to predict shear strength, but Response 2000 results show that shear failure initiates closer to flexural tension reinforcement where the longitudinal strain is larger. The conservative simple equation given for the mid-depth longitudinal strain in the 2006 CHBDC compensates for the unconservative assumption of using mid-depth strain to determine shear strength. Therefore, the use of more accurate ε_x in the 2006 CHBDC shear design provision may result in unconservative shear strength predictions for members without transverse reinforcement. It is recommended

that the 2006 CHBDC and the 2004 CSA A23.3 code shear design provisions be modified so as not to permit the use of a refined procedure to calculate ε_x for members without transverse reinforcement.

Members with less than minimum transverse reinforcement

Although the 2006 CHBDC and 2008 AASHTO LRFD shear design provisions are similar procedures that are both based on MCFT, the 2006 CHBDC minimum transverse reinforcement is 30% lower than the 2008 AASHTO LRFD minimum transverse reinforcement. An investigation was made to determine which minimum transverse reinforcement should be used in the proposed evaluation method. This was done by comparing predictions from the proposed method with the test results for 76 tested beams which were lightly reinforced for shear. The predictions of the propose method were still consistent with test results for beams with transverse reinforcement as low as the 2006 CHBDC minimum. Thus, the 2006 CHBDC lower minimum amount of transverse reinforcement was adopted in the proposed evaluation method.

In the code shear design procedures, beams with less than minimum stirrups are often assumed to have the same shear strength as members with no stirrups. In the section on evaluation, the 2006 CHBDC assumes that members with less than one third of minimum transverse reinforcement shall have the same shear strength as members with no stirrups. For higher amount of transverse reinforcement, it assumes that shear strength of a section increases linearly from the strength with no transverse reinforcement to the strength with minimum transverse reinforcement as transverse reinforcement amount varies from one third of minimum reinforcement to the minimum amount. This procedure was examined

and found to be consistent with experimental results from the 76 beams with light amount of stirrups.

10.3. Strength of Squat Shear Walls

ACI 318 building code and New Zealand concrete code (NZS 3101) shear design provisions for squat shear walls are empirical procedures determined from squat shear wall tests. Such tests might not represent the lower-bound shear strength of actual squat shear walls in buildings because the test specimens typically had very large load transfer beams at the top of the walls.

In this study, it was examined how the top load transfer beams may have influenced the shear strength of such walls. This was done by comparing the behaviour of three previously tested walls with the nonlinear finite element predictions. In one case, the walls were analyzed with the top load transfer beam as in the test, while in the other case, the top beam was removed and the shear force was uniformly distributed over the wall length at the top of the wall. Finite element results showed that the top load transfer beams could considerably enhance the shear capacity of such walls where diagonal tension failure mode is the governing failure mode. In contrast, it does not have a significant effect on the wall flexural capacity, and the wall shear capacity when diagonal concrete crushing is the governing shear failure mode.

The 2004 CSA A23.3 uses a single uniform shear element to predict the shear behaviour of squat shear walls. As a result, the vertical distributed reinforcement needed for shear should be provided in addition to the distributed vertical reinforcement considered to resist flexure in the 2004 CSA A23.3 provisions. In other words, the 2004 CSA A23.3 provisions do not allow using vertical distributed reinforcement needed for

shear to resist flexure at the wall base. This was investigated using nonlinear finite element method and was found to be conservative especially for walls with height-to-length ratios equal to and greater than 1.0. Finite element analyses were performed on 42 different walls that were shear dominated but the capacity of the wall was limited by yielding of the vertical reinforcement at the base. These walls did not have a top loading beam. The results showed all or part of vertical distributed reinforcement is available to resist flexure depending on the wall aspect ratio. A truss model to explain why all or part of distributed vertical reinforcement is not needed for shear was presented.

A method to determine flexural strength of squat shear walls accounting for flexure shear interaction at the wall base was proposed. The method accounts for the effect of wall height-to-length ratio and allows full contribution of vertical distributed shear reinforcement in flexure for walls with height-to-length ratios of equal to or greater than 0.8. The proposed method was verified against finite element predictions for the 42 shear dominated walls where the capacity was limited by yielding of vertical reinforcement. The walls had height-to-length ratios of 2.0, 1.0, 0.5 and 0.3 and had varying amounts of distributed horizontal reinforcement, distributed vertical reinforcement, and concentrated vertical reinforcement.

The shear design provisions for squat shear walls of ACI 318, NZS 3101, 2004 CSA A23.3 were evaluated by comparing predictions with the finite element predictions of 44 walls failing in shear, which were monotonically loaded and subjected to uniformly distributed horizontal load at top. The walls had height-to-length ratios of 2.0, 1.0, 0.5 and 0.3, did not contain a top load transfer beam, and had varying amounts of distributed

horizontal reinforcement, distributed vertical reinforcement, and concentrated vertical reinforcement.

The results showed that ACI 318-05 shear strength predictions were unconservative especially for walls with the same percentage of distributed horizontal and vertical reinforcement. NZS 3101 predictions were also unconservative but closer to the finite element results compared to ACI318-05. The 2004 CSA A23.3 predictions were always conservative and were increasingly conservative for walls with lower height-to-length ratios. The 2004 CSA A23.3 predictions were in reasonably good agreement for walls with height-to-length ratios equal to and greater than 1.0. Finite element results indicated that the increase in the shear strength of walls compared to the single uniform shear prediction, which is the basis for the 2004 CSA A23.3 equations for shear strength of squat shear walls, is due to the contribution of the flexural compression zone in shear.

The flexural compression zone in one direction of loading will be the flexural tension zone in the reverse direction of loading. Thus the flexural compression zone will likely have previously existing horizontal cracks that are closed by the vertical compression. Under high shear stress, these cracks may slip locally and thus the shear resisted by the compression zone will be reduced. This is a complex phenomenon that is not modeled by the nonlinear finite element program that was used. In order to investigate the influence of local slip along previously existing cracks in the compression zone a simple model was used. The shear stress at any point was limited to 10% of the concrete compressive strength. As CSA A23.3 limits the average shear stress across the shear length of a squat wall to 15% of the concrete compressive strength, the lower limit on local shear stress is clearly conservative. Three walls were analyzed and the results were compared with the

finite element results for the same walls in which shear stress at base was not limited as well as the predictions from the 2004 CSA A23.3. Localized sliding resulted in a significant reduction in shear strength of the walls with low height-to-length ratios, while it did not influence the shear strength of the wall with height-to-length ratio of 1.0. When localized sliding was accounted for, the 2004 CSA A23.3 predictions were in better agreement with the finite element predictions but they were still conservative as the contribution from the compression zone was still significant. A refinement to the 2004 CSA A23.3 shear strength method for squat shear walls was proposed. The proposed refinement accounts for the contribution of flexural compression zone in shear by assuming shear is resisted by 90% of the wall length while the current CSA A23.3 assumes shear is resisted by only 80% of the wall length.

10.4. Recommendations for Future Work

10.4.1. Bridge Girders

As part of this study, many test results were reviewed and it was observed that the available results are from beams that are generally very similar. Thus, there is a need for additional tests to verify new shear design methods and shear strength evaluation procedures for bridge girders.

Many tested reinforced concrete beams with stirrups had an amount of transverse reinforcement close to the minimum. Available test results for shear strength of reinforced concrete beams that contain more than two times the minimum transverse reinforcement are very limited. In real bridges, on the other hand, transverse reinforcement is often more than twice the minimum amount. Of 720 tests available for

reinforced concrete beams in the literature only 26 had a depth equal to or greater than 300mm and had more than twice the minimum amount of stirrups.

Available test results for prestressed concrete beams are from beams in which the predicted mid-depth longitudinal strain is very small. Of 88 prestressed concrete beams only 23 beams had a predicted mid-depth longitudinal strain greater than 0.0001. The reason for this was that the critical section for shear was generally close to the support where the moment-to-shear ratio was small and thus the longitudinal strain was small. In real bridge girders, failure could happen close to mid-span at locations where the amount of transverse reinforcement changes. At these locations, the moment-to-shear ratio may be much larger and thus the mid-depth longitudinal strain will be much larger.

10.4.2. Squat Shear Walls

Squat shear walls that were tested generally had a large loading beam that introduced the load on the wall top. As shown in this study, such a load transfer beam will strengthen the wall top and thus significantly increase the shear strength of the walls. In real buildings, load is transferred to the shear walls by means of diaphragms. Diaphragms may not have the same strength and stiffness as the loading beams used in the tests. The current study looked at the lower-bound strength when the load is assumed to be uniformly distributed over the wall top edge. A study is needed to investigate the influence of different types of diaphragms on the load distribution over the wall top edge as well as the wall shear strength. This could be done making use of nonlinear finite element analysis and squat shear wall tests.

Concrete slabs, which are assumed to be rigid diaphragms, are very stiff and strong when they remain uncracked. However, they might be cracked and thus their stiffness

could be greatly reduced because they are lightly reinforced. Cracking of slabs need not always be due to the externally applied loads and could also be due to other effects such as shrinkage. As a result of cracking, concrete slabs might not have the same stiffness and strength as the large top loading beams used in the tests.

Flexible diaphragms such as steel deck diaphragms do not have sufficient strength to transfer the loads to the top of shear wall. The load is normally transferred to the wall by a steel angle that is connected to the wall. Depending on the stiffness of this angle and the spacing of the connections, the load distribution could be very different from the distribution in the top loading beam commonly used in the wall tests.

References

- 1- AASHTO LRFD Bridge Design Specifications (2007) including interim revision for 2008, American Association of State and Highway Transportation Officials, Washington D.C.
- 2- ACI 318 (2005), Building Code Requirements for Structural Concrete, American Concrete Institute, Farmington Hills, MI.
- 3- ACI-ASCE Committee 326 (1962) “Shear and Diagonal Tension”, Proceeding of ACI Journal, Vol. 59, January, February and March, pp. 1-30, 277-344, 352-396.
- 4- Angelakos, D., Bentz, E. C., and Collins, M. P. (2001). “Effect of Concrete Strength and Minimum stirrups on Shear Strength of Large Members”, ACI Structural Journal, Vol. 98, No.3, May, pp. 290-300.
- 5- Antebi, J., Utku, S., and Hansen, R. J. (1960). “ The Response of Shear Walls to Dynamic Loads”, Department of Civil Engineering, Massachusetts Institute of Technology, Cambridge, MA.
- 6- Barda, F. (1972). “ Shear Strength of Low-Rise Walls with Boundary Elements”, PhD thesis, Lehigh University, Bethlehem, 278pp.
- 7- Barda, F., Hanson, J. M., and Corley, W. G. (1977). “Shear Strength of Low-Rise Walls with Boundary Elements”, Reinforced Concrete Structures in Seismic Zones, SP-53, American Concrete Institute, Farmington Hills, MI, pp. 149-202.
- 8- Benjamin, J. R., and Williams, H. (1954). “Investigation of Shear Walls, Part 6 – Continued Experimental and Mathematical Studies of Reinforced Concrete Walled Bents Under Static Shear Loading”, Department of Civil Engineering, Stanford University, 59pp.

- 9- Benjamin, J. R., and Williams, H. (1957). "Behaviour of One-Storey Reinforced Concrete Shear Walls", Journal of Structural Division, ASCE, Vol. 83, ST3, pp 1-49.
- 10- Benjamin, J. R., and Williams, H. (1958). "Behaviour of One-Storey Reinforced Concrete Shear Walls Containing Openings", ACI Journal, Vol. 55, No. 11, pp. 605-618.
- 11- Bentz, E. C. (2000). "Sectional Analysis of Reinforced Concrete Members", PhD thesis, Department of Civil Engineering, University of Toronto.
- 12- Bentz, E. C., and Collins, M. P. (2006). "Development of the 2004 Canadian Standards Association (CSA) A23.3 Shear Provisions for Reinforced Concrete", Canadian Journal of Civil Engineering, Vol. 33, pp. 521-534.
- 13- Bentz, E. C., Vecchio, F. J., and Collins, M. P. (2006). "Simplified Modified Compression Field Theory for Calculating Shear Strength of Reinforced Concrete Elements", ACI Structural Journal, July, Vol. 103, No. 4, pp. 614-624.
- 14- Bresler, B., and Pister, K.S.(1958). "Strength of Concrete under Combined Stresses", Proceedings, ACI Journal, September, Vol. 55, No. 9, pp. 321-46.
- 15- Bresler, B., and Scordelis, A. C. (1963). " Shear Strength of Reinforced Concrete Beams", Proceedings of ACI, Detroit, Michigan, January, Vol. 60, pp. 51-74.
- 16- Cardenas, A. E., Hanson J. M., Corley, W. G., and Hognestad, E. (1973). "Design Provisions for Shear Walls", ACI Journal, Vol. 71, No. 3, pp. 221-230.
- 17- Cardenas, A. E.; Russell, H. G.; and Corley, W. G. (1980). "Strength of Low Rise Structural Walls", Reinforced Concrete Structures Subjected to Wind and Earthquake Forces, SP-63, American Concrete Institute, Farmington Hills, MI, pp. 221-241.

- 18- CHBDC (2000&2006), Canadian Highway Bridge Design Code, CAN/CSA-S6-06, CSA international, Toronto.
- 19- Cladera, A., and Mari', A. R. (2004). "Shear Design Procedure for Reinforced Normal and High-Strength Concrete Beams Using Artificial Neural Networks. Part II: Beams with Stirrups", Engineering Structures, Vol. 26, pp. 927-936.
- 20- Cladera, A., and Mari', A. R. (2005). "Shear Design Procedure for Reinforced and Prestressed High and Normal-Strength Concrete Beams", Special Publications of ACI, Vol. 228, 651-668.
- 21- Collins, M. P. (1978). "Towards the rational theory for RC members in shear", Journal of the Structural Division, April, Vol. 104, ST4, pp. 649-666.
- 22- Collins, M. P., Mitchell, D., Adebar, P., and Vecchio, F. J. (1996). "A General Shear Design Method", ACI Structural Journal, February, Vol. 93, No.1, pp. 36-45.
- 23- Collins, M. P., and Rahal, K. N. (1999). "Background to the General Method of Shear Design in the 1994 CSA-A23.3 Standard", Canadian Journal of Civil Engineering, Vol. 26, pp. 827-839.
- 24- Crist, R. (1966). " Shear Behaviour of Deep Reinforced Concrete Beams – V. 2: Static Tests", Proceedings, RILEM International Symposium on Effect of Repeated Loading on Materials and Structures, Instituto de Ingenieria, Mexico City, Vol. 4, Theme 4, 31pp.
- 25- CSA A23.3 (1994&2004), Design of Concrete Structures, Canadian Standard Association, Mississauga, Ontario.
- 26- dePaiva, R. H. A., and Siess, C. P. (1965). "Strength and Behaviour of Deep Beams in Shear", Journal of Structural Division, ASCE, Vol. 91, ST5, pp. 19-41.

- 27- DIN 1045-1 (2001), Concrete, Reinforced and Prestressed Concrete Structures - Part 1: Design and Construction Standard, Deutsches Institut für Normung e. V. (the German Institute for Standardization), Berlin.
- 28- EC2 (2002), Design of Concrete Structures, European Committee for Standardization, Brussels, Belgium.
- 29- Felber, A. J. (1990). “Response, a Program to Determine the Load Deformation Response of Reinforced concrete section”, M.A.Sc thesis, Department of Civil Engineering, University of Toronto.
- 30- Gambarova, P. G.(1987) “ Aggregate Interlock Role in RC Thin-Webbed Beams in Shear” Journal of Structural Division”, ASCE, Vol. 113, ST1, pp. 1-19.
- 31- Gulec, C. K., Whittaker, A. S., and Stojadinovic, B. (2008). “Shear Strength of Squat Rectangular Reinforced Concrete Walls”, ACI Structural Journal, Vol. 105, No. 4, pp. 488-497.
- 32- Guralnick, S. A. (1959). “Shear Strength of Reinforced Concrete Beams”, Proceedings, ASCE, January, Vol. 85, ST1, pp. 1-42.
- 33- Hanson, J.A. (1958) “Shear Strength of Lightweight Reinforced Concrete Beams”, ACI Journal, Vol. 55, pp. 387–404.
- 34- Hawkins, N. M., Kuchma, D. A., Mast, R. F., Marsh, M. L., and Reineck, K. H. (2005). “Simplified Shear Design of Structural Concrete Members”, National Cooperative Highway Research Program Report 549, American Association of State Highway and Transportation Officials, Washington D.C.
- 35- Hernandez, G., Sozen, M. A., and Siess, C. P. (1960). “Shear Tests on Beams with Web Reinforcing”, ACSE Regional Convention, New Orleans, LA, March.

- 36- Hernandez, B. O. (1980). "Diseno de Muros de Concreto con Falla por Cortante", Instituto de Ingenieria, Universidad Nacional Autonoma de Mexico, Mexico, 165 pp.
- 37- Hidalgo, P. A., Jordan, R., and Ledezma, C. A. (1998). "Experimental Study of Reinforced Concrete Walls under Shear Failure", Proceedings, Sixth U.S. National Conference on Earthquake Engineering, Seattle, WA.
- 38- Hidalgo, P. A., Ledezma, C. A., and Jordan, R. M. (2002). "Seismic Behaviour of Squat Reinforced Concrete Shear Walls", Earthquake Spectra, Paper No. 297, EERI, Vol. 18, No. 2, pp. 287-308.
- 39- Ho, G. (1994). "Nonlinear Analysis of Reinforced Concrete Beams Subjected to Shear, Moment and Axial Load", M.A.Sc thesis, Department of Civil Engineering, University of Toronto.
- 40- Hsu, T. T. C. (1988). "Softened Truss Model Theory for Shear and Torsion", ACI Structural Journal, November-December, Vol. 85, No.6, pp. 624-633.
- 41- Hsu, T. T. C. (1993). "Unified Theory of Reinforced Concrete", CRC Press, Boca Raton, Fla.
- 42- Hsu, T. T. C. (1996). "Toward a Unified Nomenclature for Reinforced Concrete Theory", Journal of Structural Engineering, ASCE, March, Vol. 22, No. 3, pp. 275-283.
- 43- Hsu, T. T. C., and Zang L. X. (1997). "Nonlinear Analysis of Membrane Elements by Fixed Angle-Softened Truss Model", ACI Structural Journal, September, Vol. 94, No. 5, pp. 483-492.
- 44- JSCE (1986), Specification for Design and Construction of Concrete Structures, JSCE Standard, Japan Society of Civil Engineers, Tokyo.

- 45- Kani G. N. J. (1964). "The Riddle of Shear Failure and its Solution", Proceedings, ACI Journal, Vol. 64, No. 3, pp. 441-467.
- 46- Khalifa, J. (1986) "Limit Analysis of Reinforced Concrete Shell Elements", PhD thesis, Department of Civil Engineering, University of Toronto, Toronto, Ontario, Canada, 312 pp.
- 47- Kim, K. S. (2004). "Shear Behaviour of Reinforced Concrete Beams and Prestressed Concrete Beams", PhD thesis, University of Illinois, July.
- 48- Kirschner, U., and Collins, M. P. (1986). "Investigating the Behaviour of Reinforced Concrete Shell Elements", Publication No. 86-09, Department of Civil Engineering, University of Toronto, Toronto, Ontario, Canada, 209 pp.
- 49- Kuang, J. S., Ho, Y. B. (2008). "Seismic Behaviour and Ductility of Squat Reinforced Concrete Shear Walls with Nonseismic Detailing", ACI Structural Journal, Vol. 105, No. 2, pp. 225-231.
- 50- Kuchma, D. A., Kim, K. S., Hawkins, N. M. (2005). "Application of Load and Resistance Factor Design Specifications to High-Strength Structural Concrete: Shear Provisions", Proc. of 6th International Bridge Engineering Conference: Reliability, Security, and Sustainability in Bridge Engineering, Boston, July, pp. 87-97.
- 51- Kupfer, H. (1964). "Erweiterung der Mörsch'schen Fachwerkanalogie mit Hilfe des Prinzips vom Minimum der Formänderungsarbeit", CEB Bulletin d'Information No. 40, Comite European du Beton, Paris Franse, pp. 44-57.
- 52- Kuyt, B. (1972). "Oer de Dwarskrachtsterkte van Slanke Balken met Verticale Beugels. (I) en (II)", Cement, Amsterdam, The Netherlands, Vol. 24, No. 6, 1972, pp. 243-251 and Vol. 24, No.9, pp. 346-353.

- 53- Lefas, I. E., and Kotsovos, K. D., and Ambraseys, N. N. (1990). “ Behaviour of Reinforced Concrete Structural Walls: Strength, Deformation Characteristics, and Failure Mechanism”, ACI structural Journal, Vol. 87, No. 1, pp. 23-30.
- 54- Lefas, I. E., and Kotsovos, K. D. (1990). “ Strength and Deformation Characteristics of Reinforced Concrete Walls Under Load Reversals”, ACI structural Journal, Vol. 87, No. 6, pp. 716-726.
- 55- Leonhardt, F., and Walter, R. (1966). “ Wandartiger Träger”, Deutscher Ausschuss für Stahlbeton, Bulletin No. 178, Wilhelm Ernst & Sohn, Berlin, 159 pp.
- 56- Loov, R. E. (1998). “Review of A23.3-94 Simplified Method of Shear Design and Comparison with Results Using Shear Friction”, Canadian Journal of Civil Engineering, June, Vol. 25, No. 3, pp. 437-450.
- 57- Leonhardt, F., and Walther, R. (1962). “The Stuttgart Shear Tests, 1961” , 1961- Contribution to the Treatment of the Problem of Shear in Reinforced Concrete Construction, Translation No. 111, Cement and Concrete Association, London, 133p.
- 58- Leonhardt, F., and Walther, R. (1964). “Schubversuche an Durchlaufträgern”, Deutscher Ausschus für Stahlbeton, Heft 163, Ernst, Berlin, W. Germany.
- 59- Loov, R. E. (1978). “Design of Precast Connections” Paper presented at a seminar organized by Compa International Pte, Ltd., Singapore, pp. 1-8.
- 60- Loov, R. E., and Patnaik, A. K. (1994). “Horizontal Shear Strength of Composite Concrete Beams with Rough Interface”, PCI Journal, January -February, Vol. 39, No. 1, pp. 48-108.

- 61- Ma, Z., Tadros, M. K., and Baishya, M. (2000). "Shear Behaviour of Pretensioned High-Strength Concrete Bridge I-Girders", ACI Structural Journal, Vol. 97, No. 1, pp. 185-192.
- 62- MacGregor, J. G. (1960). "Strength and Behaviour of Prestressed Concrete Beams with Web Reinforcement", PhD thesis, University of Illinois.
- 63- MacGregor, J. G., and Hanson, J. M. (1969). "Proposed Changes in Shear Provisions for Reinforced and Prestressed Concrete Beams", Proceedings, ACI Journal, April, Vol. 66. No. 4, pp. 276-288.
- 64- MacGregor J. G., Sozen, M. A., and Siess, C. P. (1965)." Strength of Prestressed Concrete Beams with Web Reinforcement", Proceedings, ACI Journal, December, Vol. 62, No. 12, pp. 1503-1522.
- 65- MacGregor J. G., Sozen, M. A., and Siess, C. P. (1966)." Behaviour of Prestressed Concrete Beams under Simulated Moving Loads", Proceedings, ACI Journal, August, Vol. 63, No. 8, pp. 835-842.
- 66- Maier, J., and Thürlimann, B. (1985). "Bruchversuche an Stahlbetonscheiben", Institut für Baustatik und Konstruktion ETH Zürich, Bericht Nr. 8003-1.
- 67- Mattock, A. H. (1957). Discussion of "Shear Strength of Reinforced Concrete Members without Web Reinforcement" by J. Morrow and I. M. Viest, Proceedings, ACI Journal, December, Vol. 53, pp. 1352-1354.
- 68- Mattock, A. H., and Kaar, P. (1961), "Precast- Prestressed Concrete Bridges, 4 Shear Tests of Continuous Girders", Journal of Portland Cement Association Research and Development Labs, January, Vol. 3, No. 1, pp. 19-46.

- 69- Metwally, A. S. (2004). "Shear Strength of Reinforced and Prestressed Concrete Beams Using Shear Friction", PhD thesis, Department of Civil Engineering, University of Calgary, April 2004.
- 70- Mitchell, D., and Collins, M. P. (1974). "Diagonal Compression Field Theory- a Rational Model for Structural Concrete in Pure Torsion", ACI journal, August, Vol. 71, pp. 396-408.
- 71- Mohammadi-Doostdar, H. (1994). "Behaviour and Design of Earthquake Resistant Low-Rise Shear Walls", PhD thesis, Department of Civil Engineering, University of Ottawa, Ottawa, ON, 250 pp.
- 72- Mörsch, E.(1920). "Der Eisenbetonbau-Seine Theorie und Anwendung", 5th edition, Wittwer, Stuttgart, Vol. 1, Part 1.
- 73- Mörsch, E. (1922). "Der Eisenbetonbau-Seine Theorie und Anwendung", 5th edition, Wittwer, Stuttgart, Vol. 1, Part 2.
- 74- Morrow, J. and Viest, I. M. (1959). "Shear Strength of Reinforced Concrete Members without Web Reinforcement", Proceedings, ACI Journal, March, Vol. 53, No. 3, pp. 833-869.
- 75- Mphonde, A. G., and Frantz, G. C. (1985). "Shear Tests of High- and Low-Strength Concrete Beams with Stirrups", American Concrete Institute, High-Strength Concrete, SP-87, pp. 179-196.
- 76- NBCC (2005), National Building Code of Canada, National Research Council of Canada, Ottawa.
- 77- NZS 3101: Part 1 (2006), Concrete Structures Standards, Standards New Zealand.

- 78- Nielsen, M. P., and Braestrup, M. W. (1975). "Plastic Shear Strength of Reinforced Concrete Beams", Bygningsstatistiske Meddelelser, Copenhagen, Denmark, Vol. 46, No. 3, pp. 61-99.
- 79- Nielsen, M. P. (1984). "Limit Analysis and Concrete Plasticity", Prentice-Hall Inc., Englewood Cliffs, NJ, 420 pp.
- 80- Oesterle, R. G., Fiorato, A.E., Johal, L.S., Carpenter, J.E., Russell, H.G., and Corley, W.G. (1976). "Earthquake-Resistant Structural Walls-Test of Isolated Walls", Report to National Science Foundation, Construction Technology Laboratories, Portland Cement Association, 315pp.
- 81- Oh, H. B., and Kim, K. S. (2004). "Shear Behaviour of Full-Scale Post-Tensioned Prestressed Concrete Bridge Girders", ACI Structural Journal, March-April, Vol. 101, No. 2, pp. 176-182.
- 82- Oleson, S.O., Sozen, C.P., (1967). "Investigation of Prestressed Reinforced Concrete for Highway Bridges. Part IV: Strength in Shear of Beams with Web Reinforcement", UIUC Bulletin 493, University of Illinois.
- 83- Oleson, S.O., and Sozen, C.P. (1967). "Investigation of Prestressed Reinforced Concrete for Highway Bridges. Part IV: Strength in Shear of Beams with Web Reinforcement", UIUC Bulletin 493, University of Illinois.
- 84- Palermo, D., and Vecchio, F.J. (2002). "Behaviour of 3-D Reinforced Concrete Shear Walls", ACI Structural Journal, Vol. 99, No. 1, pp. 81-89.
- 85- Palermo, D., and Vecchio, F.J. (2004). "Compression Field Modeling of Reinforced Concrete Subjected to Reversed Loading: Verification", ACI Structural Journal, Vol. 101, No. 2, pp. 155-164.

- 86- Pang, X., and Hsu, T. T. C. (1995). "Behavior of Reinforced Concrete Membranes in Shear", *ACI Structural Journal*, Vol. 92, No. 6, Nov.-Dec., pp. 665-679.
- 87- Pang, X. B., and Hsu, T. T. C. (1996). "Fixed-Angle Softened-Truss Model for Reinforced Concrete", *ACI Structural Journal*, Vol. 93, No. 2, pp. 197-207.
- 88- Park, R., Paulay, T. (1975). "Reinforced Concrete Structures", John Wiley and Sons, New York, 769pp.
- 89- Paulay, T., Priestley, M. J. N., and Syngge, A. J. (1982). "Ductility in Earthquake Resisting Squat Shearwalls", *ACI Journal*, Vol.79, No. 4, pp. 257-269.
- 90- Pilakoutas, K., and Elnashai, A. (1995). "Cyclic Behavior of Reinforced Concrete Cantilever Walls, Part I: Experimental Results", *ACI Structural Journal*, Vol. 92, No. 3, pp. 271-281.
- 91- Pilette, F. C. (1987). "Behavior of Earthquake Resistant Squat Shear Walls", MS thesis, Department of Civil Engineering, University of Ottawa, Ottawa, ON, 177 pp.
- 92- Rahal, K. N., and Al-Shaleh, K. S.(2004) "Minimum Transverse Reinforcement in 65 MPa Concrete Beams", *ACI Structural Journal*, Vol. 101, No. 6, pp. 872-878.
- 93- Reineck, K. H. (1991). "Ultimate Shear Force of Structural Concrete Members without Transverse Reinforcement Derived from a Mechanical Model", *ACI Structural Journal*, September-October, Vol. 88, No. 5, pp. 592-602.
- 94- Reineck, K. H., and Hardjasaputra, H. (1990). "Zum Dehungszustand bei der Querkraftbemessung profilierter Stahlbeton- und Spannbetontraeger", *Bauingenieur*, February, Vol. 65, No. 2, pp. 73-82.

- 95- Ritter, W. (1899). “Die Bauweise Hennebique”, Schweizerische Bauzeitung, Vol. 33, No. 7, pp. 59–61.
- 96- Standard Specifications for Highway Bridges (2002), 17th edition, American Association of State highway and Transportation Officials, Washington D.C.
- 97- Shahawy, M. A., and Batchelor, B. (1996), “Shear Behavior of Full-Scale Prestressed Concrete Girders: Comparison between AASHTO Specifications and LRFD Code”, PCI Journal, Vol. 41, No. 3, May-June, pp. 48-62.
- 98- Sozen, M.A., and Hawkins, N.M. (1962). “Discussion of Report of ACI- ASCE Committee 326, Shear and Diagonal Tension.”, ACI Structural Journal, September, Vol. 59, No.9, pp. 1341–1347.
- 99- Talbot, A. N. (1909). “Tests of Reinforced Concrete Beams: Resistance to Web Stresses Series of 1907 and 1908”, Engineering Experiment Station, Bulletin 29, University of Illinois.
- 100- Thürlimann, B. (1979). “Plastic Analysis of Reinforced Concrete Beams”, IABSE Colloq. Plasticity in Reinforced Concrete, Copenhagen, pp. 71-90.
- 101- Thürlimann, B., Marti, P., Pralong, J., Ritz, P., and Zimmerli, B. (1983). “Anwendung der Plastizitätstheorie Stahlbeton”, Institut für Baustatik und Konstruktion, Eidgenössische Technische Hochschule, Zurich, April, 252 pp.
- 102- Uniform Building Code (1967), International Conference of Building Officials, Pasadena.
- 103- Vecchio, F. J., and Collins, M. P. (1986). “The Modified Compression-Field Theory for Reinforced Concrete Elements Subjected to Shear”, Proceedings, ACI Journal, May-June, Vol. 83, No. 2, pp. 219-231.

- 104- Vecchio, F. J., and Collins, M. P. (1988). "Predicting the Response of Reinforced Concrete Beams Subjected to Shear Using Modified Compression Field Theory", ACI Structural Journal, May-June, Vol. 85, No.3, pp. 258-268.
- 105- Vecchio, F. J. (1989). "Nonlinear Finite Element Analysis of Reinforced Concrete Members", ACI Structural journal, Vol. 86, No. 1, pp. 26-35.
- 106- Vecchio, F. J. (2000). "Disturbed Stress Field Model for Reinforced Concrete: Formulation", Journal of Structural Engineering, Vol. 126, No. 9, pp. 1070-1077.
- 107- Vecchio, F. J. (2001). "Disturbed Stress Field Model for Reinforced Concrete: Implementation", Journal of Structural Engineering, Vol. 127, No. 1, pp. 12-20.
- 108- Vecchio, F. J. (2001). "Disturbed Stress Field Model for Reinforced Concrete: Validation" Journal of Structural Engineering, Vol. 127, No. 4, pp. 350-358.
- 109- Viest, I. M. (1959). Discussion of "Shear Strength of Lightweight Reinforced Concrete Beams" by J. A. Hanson, Proceedings, ACI Journal, March 1959, Vol. 30.
- 110- Wanger, H. (1929). "Ebene Slechwandtrager mit sehr dunnem Stegblech", Zeitschrift für Flugtechnik und Motorluftschiffahrt, Berlin, Germany, Vol. 20, Nos. 8-12.
- 111- Wasiewicz, Z. F. (1988). "Sliding Shear in Low-Rise Shear Walls Under Lateral Load Reversals", MS thesis, Department of Civil Engineering, University of Ottawa, Ottawa, ON, 127pp.
- 112- Williams, H., and Benjamin, J. R. (1953). "Investigation of Shear Walls, Part 3 – Experimental and Mathematical of the Behaviour of Plain and Reinforced Concrete Walled Bents Under Static Shear Loading", Department of Civil Engineering, Stanford University, 142pp.

- 113- Wiradinata, S. (1985). "Behavior of Squat Walls Subjected to Load Reversals", MS thesis, Department of Civil Engineering, University of Toronto, Toronto, ON, 171 pp.
- 114- Wirandianta, S., and Saatcioglu, M. (1986). "Tests of Squat Shear Wall Under Lateral Load Reversal", Proceedings, The 3rd US Conference on Earthquake Engineering, Charleston, South Carolina.
- 115- Withey, M. O. (1907). "Tests of Plain and Reinforced Concrete Series of 1906", Bulletin, University of Wisconsin, Engineering Series, Vol. 4, No. 1, pp. 1-66.
- 116- Withey, M. O. (1908). "Tests of Plain and Reinforced Concrete Series of 1907", Bulletin, University of Wisconsin, Engineering Series, Vol. 4, No. 2, pp. 1-66.
- 117- Wong, P. S., and Vecchio, F.J. (2002). "VECTOR2 & FORMWORKS User's Manual", Department of Civil Engineering, University of Toronto.
- 118- Wood, S. L. (1990). "Shear Strength of Low-Rise Reinforced Concrete Walls", ACI Structural Journal, Vol. 87, No. 1, pp. 99-107.
- 119- Yun, Y. M. (2000). "Nonlinear Strut-Tie Model Approach for Structural Concrete", ACI Structural Journal, Vol. 97, No.4, pp. 581-590.
- 120- Yun, Y. M., and Cho, C. G. (2005). "Prediction of Behaviour and Shear Strength of Reinforced Concrete Beams Using Nonlinear Strut and Tie Mode Approach", Journal of Advanced Concrete Technology, June, Vol. 3, No. 2, pp. 309-319.
- 121- Zararis, P. D. (2003). "Shear Strength and Minimum Shear Reinforcement of Reinforced Concrete Slender Beams", ACI Structural Journal, Vol. 100, No.2, March-April, pp. 203-214.

- 122- Zararis, P. I., Karaveziroglou, M. K., and Zararis, P. D. (2006). "Shear Strength of Reinforced Concrete T-Beams", *ACI Journal of Structural Engineering*, September-October, Vol. 103, No.5, pp. 693-700.
- 123- Zwoyer, E. M., and Siess, C. P. (1954). "Ultimate Strength in Shear of Simply-Supported Prestressed Concrete Beams without Web Reinforcement", *Proceedings, ACI Journal*, October, Vol. 51, no. 10, pp. 181-200.

**Appendix A: Excel Spreadsheets for the Proposed Evaluation Methods and the Refined
CHBDC Method**

Appendix B: Detailed Steps in Proposed Evaluation Procedures

Required Information

1- Loading information:

M_f = Factored bending moment at the section of interest,

N_f = Factored axial force at the section of interest.

2- Material properties:

f'_c = Specified compressive strength of concrete,

f_y = Yield stress of reinforcing steel,

f_{pu} = Ultimate strength of prestressing tendons,

f_{pr} = Stress in prestressing tendons at maximum flexural resistance.

ϕ_c = Concrete resistance factor

ϕ_s = Nonprestressed reinforcing steel resistance factor

ϕ_p = Prestressed reinforcing steel resistance factor

3- Concrete section geometry:

H = Height of beam

d_v = Depth of uniform shear stress = jd (may be taken as $0.9d$),

d_{nv} = Depth of uniform compression stress n_v over diagonally cracked web
= (section height) – (tension flange depth) – (uncracked compression chord depth). It is recommended to take d_{nv} as distance from top of tension flange to bottom of top deck for I-girders having composite action with top deck and distance from top of tension flange to bottom of compression flange for box-girders. For rectangular sections d_{nv} should be taken equal to d_v .

b_w = Width of web

A_{tf} = Area of concrete surrounding flexural tension reinforcement (tension flange area), equals to zero for rectangular sections.

d_{pw} = Depth from compression face to centroid of web prestressing tendon.

4- Reinforcement:

A_s = Area of longitudinal reinforcement in flexural tension chord,

A_{sc} = Area of longitudinal reinforcement in flexural compression chord,

A_{sw} = Total area of distributed longitudinal reinforcement centered in web,

A_v = Area of transverse reinforcement (spaced at s),

s = Spacing of transverse reinforcement,

Appendix B: Detailed Steps in Proposed Evaluation Procedures (cont.)

S_{xe} = Effective crack spacing parameter as in 2006 CHBDC and AASHTO LRFD.

5- Prestressing tendons:

A_p = Area of prestressed reinforcement in flexural tension chord,

A_{pw} = Area of prestressed reinforcement in web,

θ_p = Angle of inclination of draped prestressed reinforcement,

f_p = Effective stress of prestressing.

Evaluation Procedure for Members With at Least Minimum Stirrups

1- Calculate additional parameters.

- Calculate $jd = d_v$ from

$$jd = d_v = \min(0.9d = 0.72H)$$

- Calculate ρ_z from

$$\rho_z = \frac{A_v f_y}{b_w s}$$

- Calculate V_p from

$$V_p = \phi_p f_p A_{pw} \sin \theta_p$$

- Calculate λ from

$$\lambda = \frac{d_{pw}}{d}$$

- Set $\alpha = 0.165$ in MPa units (2.0 in psi units)

2- Calculate shear strength at yielding of transverse reinforcement V_{yield} .

- Calculate β from

$$\beta = 0.18(-300\varepsilon_y + 1.6) \geq 0.18 \text{ in MPa units}$$

Appendix B: Detailed Steps in Proposed Evaluation Procedures (cont.)

- Calculate θ_0 and $\Delta\theta$ from

$$\theta_0 = (85 \frac{\rho_z f_y}{f_c'} + 19.3)(-50\varepsilon_y + 1.1)$$

$$\Delta\theta = 1000[37.5(-200\varepsilon_y + 1.4) - \theta_0]$$

- Calculate Δn_v and n_{v0} from

$$\Delta n_v = (-0.09\phi_c \beta \sqrt{f_c'} - 0.20\phi_s \rho_z f_y) \Delta\theta$$

$$n_{v0} = \frac{\Delta n_v}{\Delta\theta} \theta_0 + 4.0\phi_s \beta \sqrt{f_c'} + 9.4\phi_s \rho_z f_y$$

- Calculate ε_x from

$$\varepsilon_x = \frac{M / jd + 0.5n_{v0} b_w d_{nv} - \phi_c \alpha \sqrt{f_c'} A_{gf} - f_p (A_p + \lambda A_{pw}) + 0.5N_f}{2 [E_s (A_s + 0.25A_{sw}) + E_p (A_p + \lambda^2 A_{pw})] - 0.5 \Delta n_v b_w d_{nv}}$$

- Calculate force in the compression chord C_c from

$$C_c = -M / jd + 0.5n_{v0} b_w d_{nv} + \varepsilon_x [0.5 \Delta n_v b_w d_{nv} - 0.5 E_s A_{sw} - 2\lambda(1-\lambda) E_p A_{pw}]$$

$$- (1-\lambda) f_p A_{pw} + 0.5 N_f$$

- Multiply ε_x by 2 if there is tension in comp. chord (if C_c is positive).
- Calculate angle θ from

$$\theta = \theta_0 + \Delta\theta \varepsilon_x$$

- Calculate transverse reinforcement yielding shear strength from

$$V_{yield} = V_c + V_s + V_p = \phi_c \beta \sqrt{f_c'} b_w d_v + \phi_s \frac{A_v f_y d_v \cot \theta}{s} + V_p$$

3- Calculate shear strength at crushing of concrete V_{crush} .

- Calculate β from

$$\beta = 0.65 \frac{\rho_z f_y}{f_c'} + 0.03 \text{ in MPa units}$$

Appendix B: Detailed Steps in Proposed Evaluation Procedures (cont.)

- Calculate θ_0 and $\Delta\theta$ from

$$\theta_o = 119 \frac{\rho_z f_y}{f_c'} + 15.6$$

$$\Delta\theta = 15000 \frac{\rho_z f_y}{f_c'} + 2000$$

- Calculate Δn_v and n_{v0} from

For $\theta_0 > 23$:

$$\Delta n_v = (-0.09\phi_c\beta\sqrt{f_c'} - 0.20\phi_s\rho_z f_y)\Delta\theta$$

$$n_{vo} = \frac{\Delta n_v}{\Delta\theta} \theta_o + 4.0\phi_s\beta\sqrt{f_c'} + 9.4\phi_s\rho_z f_y$$

For $\theta_0 \leq 23$:

$$\Delta n_v = (-0.15\phi_c\beta\sqrt{f_c'} - 0.77\phi_s\rho_z f_y)\Delta\theta$$

$$n_{vo} = \frac{\Delta n_v}{\Delta\theta} \theta_o + 5.5\phi_c\beta\sqrt{f_c'} + 23.6\phi_s\rho_z f_y$$

- Calculate ε_x from

$$\varepsilon_x = \frac{M / jd + 0.5n_{vo}b_w d_{nv} - \alpha\phi_c\sqrt{f_c'}A_{gf} - f_p(A_p + \lambda A_{pw}) + 0.5N_f}{2 [E_s(A_s + 0.25A_{sw}) + E_p(A_p + \lambda^2 A_{pw})] - 0.5\Delta n_v b_w d_{nv}}$$

- Calculate force in the compression chord C_c from

$$C_c = -M / jd + 0.5n_{vo}b_w d_{nv} + \varepsilon_x[0.5\Delta n_v b_w d_{nv} - 0.5E_s A_{sw} - 2\lambda(1-\lambda)E_p A_{pw}] - (1-\lambda)f_p A_{pw} + 0.5N_f$$

- Multiply ε_x by 2 if there is tension in comp. chord (if C_c is positive).
- Calculate angle θ from

$$\theta = \theta_o + \Delta\theta \varepsilon_x$$

- Calculate shear strength from

$$V = V_c + V_s + V_p = \phi_c\beta\sqrt{f_c'}b_w d_v + \phi_s \frac{A_v f_y d_v \cot \theta}{s} + V_p$$

Appendix B: Detailed Steps in Proposed Evaluation Procedure (cont.)

4- Calculate shear strength at biaxial yielding of reinforcement $V_{biaxial}$.

- Calculate jd form

$$jd = d - \frac{\phi_p f_{pr} A_p + \phi_s f_y A_s - N_f}{1.2 \phi_c f_c' b_f}$$

- Calculate longitudinal reinforcement capacity reserved in the comp. chord N_{vcc} from

$$N_{vcc} = 2 [\phi_s f_y (A_{sc} + 0.5 A_{sw}) + f_{pr} (1 - \lambda) A_{pw}) + M / jd - 0.5 N_f]$$

- Calculate longitudinal reinforcement capacity reserved in the tension chord N_{vct} from

$$N_{vct} = 2 [\phi_s f_y (A_s + 0.5 A_{sw}) + f_{pr} (A_p + \lambda A_{pw}) - M / jd - 0.5 N_f]$$

- Determine axial force reserved capacity N_{vc} from

$$N_{vc} = \min(N_{vcc}, N_{vct})$$

- Calculate shear strength from

$$V = \sqrt{\phi_s \rho_z f_y (b_w d_v) N_{vc}} + V_p$$

5- Determine governing shear strength.

- V_{yield} is governing failure mode if greater than V_{crush} , and less than $V_{biaxial}$.
- V_{crush} is governing failure mode if greater than V_{yield} and less than $V_{biaxial}$.
- $V_{biaxial}$ is governing failure mode if less than Max (V_{yield} , V_{crush}).
- $V_{max} = 0.25 \phi_c f_c' b_w d_v + V_p$

Appendix B: Detailed Steps in Proposed Evaluation Procedures (cont.)

Evaluation Procedure for Members Without Stirrups

1- Calculate additional parameters.

- Calculate $jd = d_v$ from

$$jd = d_v = \min(0.9d = 0.72H)$$

- Calculate V_p from

$$V_p = \phi_p f_p A_{pw} \sin \theta_p$$

- Calculate λ from

$$\lambda = \frac{d_{pw}}{d}$$

2- Calculate shear strength at maximum concrete contribution V_c .

- Calculate ε_x from

$$\varepsilon_x = \frac{M / jd - f_p (A_p + \lambda A_{pw})}{1.5 [E_s (A_s + 0.25 A_{sw}) + E_p (A_p + \lambda^2 A_{pw})]}$$

- Calculate β from

$$\beta = \frac{0.35}{1 + (600 + 2.1 S_{xe}) \varepsilon_x} \leq \frac{400}{(500 + 0.5 S_{xe})} \quad \text{in MPa units}$$

- Calculate shear strength from

$$V = V_c + V_p = \phi_c \beta \sqrt{f_c} b_w d_v + V_p$$

3- Check for yielding of long. reinforcement and determine shear strength.

- Calculate θ from

$$\theta = (35 + 7000 \varepsilon_x)(0.6 + 0.02 \sqrt{S_{xe}}) \quad \text{in MPa units}$$

- Calculate demand on the longitudinal reinforcement due to shear

Appendix B: Detailed Steps in Proposed Evaluation Procedures (cont.)

$$N_v^* = 2V_c \cot \theta$$

- Calculate longitudinal reinforcement capacity reserved in the comp. chord N_{vcc} from

$$N_{vcc} = 2 [\phi_s f_y (A_{sc} + 0.5 A_{sw}) + f_{pr} (1 - \lambda) A_{pw}) + M / jd - 0.5 N_f]$$

- Calculate longitudinal reinforcement capacity reserved in the tension chord N_{vct} from

$$N_{vct} = 2 [\phi_s f_y (A_s + 0.5 A_{sw}) + f_{pr} (A_p + \lambda A_{pw}) - M / jd - 0.5 N_f]$$

- Determine axial force reserved capacity N_{vc} from

$$N_{vc} = \min(N_{vcc}, N_{vct})$$

- If $N_{vc} \geq N_v^*$, shear strength is equal to V_c , otherwise determine shear strength from

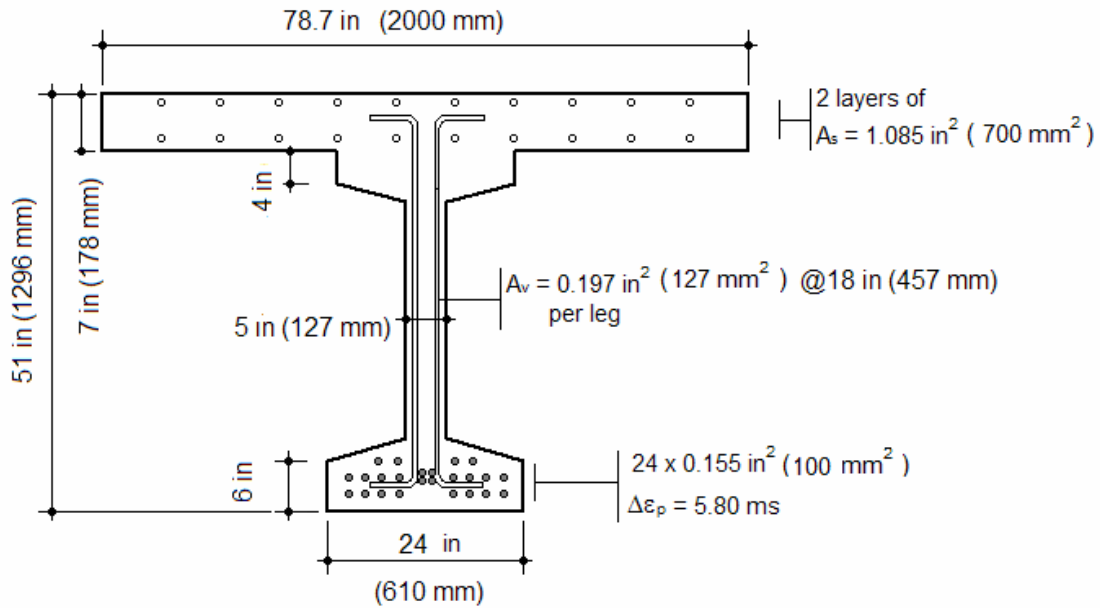
$$V = \frac{N_{vc}}{2}$$

Appendix B: Detailed Steps in Proposed Evaluation Procedures
(Summary Sheet for Proposed Method for Members With at Least Min Stirrups)

YIELDING OF TRANSVERSE REINFORCEMENT AND CONCRETE CRUSHING	
<p>Yielding of stirrups:</p> $\beta = 0.18(-300\varepsilon_y + 1.6) \geq 0.18 \text{ (MPa units)}$ $\theta_o = (85 \frac{\rho_z f_y}{f_c'} + 19.3)(1.1 - 50\varepsilon_y)$ $\Delta\theta = 1000[37.5(1.4 - 200\varepsilon_y) - \theta_o]$	<p>Concrete crushing after stirrup yielding:</p> $\beta = 0.65 \frac{\rho_z f_y}{f_c'} + 0.03 \text{ (MPa units)}$ $\theta_o = 119 \frac{\rho_z f_y}{f_c'} + 15.6$ $\Delta\theta = 15000 \frac{\rho_z f_y}{f_c'} + 2000$
<p>Yielding of stirrups, and concrete crushing if $\theta_o > 23 \text{ deg}$:</p> $\Delta n_v = (-0.09\beta\sqrt{f_c'} - 0.20\rho_z f_y)\Delta\theta$ $n_{vo} = \frac{\Delta n_v}{\Delta\theta} \theta_o + 4.0\beta\sqrt{f_c'} + 9.4\rho_z f_y$	<p>Concrete crushing if $\theta_o \leq 23 \text{ deg}$:</p> $\Delta n_v = (-0.15\beta\sqrt{f_c'} - 0.77\rho_z f_y)\Delta\theta$ $n_{vo} = \frac{\Delta n_v}{\Delta\theta} \theta_o + 5.5\beta\sqrt{f_c'} + 23.6\rho_z f_y$
$\varepsilon_x = \frac{M/d_v + 0.5n_{vo}b_w d_{nv} - 2\sqrt{f_c'}A_{tf} - f_p(A_p + \lambda A_{pw})}{2[E_s(A_s + 0.25A_{sw}) + E_p(A_p + \lambda^2 A_{pw})] - 0.5\Delta n_v b_w d_{nv}}$ <p>Multiply ε_x by 2.0 if $C_c > 0$ where</p> $C_c = -M/d_v + 0.5n_{vo}b_w d_{nv} + \varepsilon_x[0.5\Delta n_v b_w d_{nv} - 0.5E_s A_{sw} - 2\lambda(1-\lambda)E_p A_{pw}] - (1-\lambda)f_p A_{pw}$ $\theta = \theta_o + \Delta\theta \varepsilon_x$ $V_n = V_c + V_s + V_p = \beta\sqrt{f_c'}b_w d_v + (A_v f_y d_v / s) \cot \theta + V_p$ <p>Governing V_n is the greater of stirrups yielding and concrete crushing shear strength</p>	
<p align="center">CHECKS</p> <p>Longitudinal reinforcement yielding</p> $V_n \leq \sqrt{\rho_z f_y (b_w d_v) N_{vc}} + V_p$ <p>where $N_{vc} = \min(N_{vcc}, N_{vct})$</p> $N_{vcc} = 2[f_y(A_{sc} + 0.5A_{sw}) + f_{pr}(1-\lambda)A_{pw}] + M/jd$ $N_{vct} = 2[f_y(A_s + 0.5A_{sw}) + f_{pr}(A_p + \lambda A_{pw}) - M/jd]$ <p>where $jd = d - \frac{f_{pr}A_p + f_y A_s}{1.2f_c' b_f}$</p> <p>Concrete crushing before stirrups yield</p> $V_n \leq 0.25f_c' b_w d_v$	<p align="center">PARAMETERS (TOP CHORD IN COMP.)</p> <p> $d_v = \max(0.9d, 0.72H)$ $\lambda = d_{pw}/d$ $\rho_z = A_v/(b_w s)$ </p>

Appendix C: Detailed Examples of Proposed Evaluation Procedure for Members With Stirrups

Example 1: Prestressed Concrete I-girder Bridge at 7.91 m from the support.



$$M_f = 3720 \text{ kNm}$$

$$V_f = 415 \text{ kN}$$

$$N_f = 0$$

$$f_y = 400 \text{ MPa}$$

$$f_c' = 40 \text{ MPa}$$

$$f_{pu} = 1860 \text{ MPa}$$

$$\theta_p = 0$$

Appendix C: Detailed Examples of Proposed Evaluation Procedure (cont.)

Solution of Example 1:

Factored loads			Material reduction factor		
$M_f =$	3719	Factored moment (positive) , kN.m	$\phi_c =$	0.75	Concrete
$V_f =$	415.2	Factored shear (positive), kN	$\phi_s =$	0.90	Steel
$N_f =$	0	Factored axial force (positive for tension) , kN	$\phi_p =$	0.95	Prestressing
Material Properties					
$f_c' =$	40	MPa	Compressive strength of concrete		
$\alpha =$	0.165		Concrete tension stiffening factor		
$f_y =$	400	MPa	Yield strength of reinforcement		
$E_s =$	200000	MPa	Modulus of Elasticity of nonprestressed reinforcement		
$\varepsilon_y =$	0.002		Steel yield strain		
$f_p =$	1160	MPa	Effective stress in prestressing tendons		
$f_{pr} =$	1660	MPa	Stress in prestressing tendons at maximum resistance		
$E_p =$	200000	MPa	Modulus of Elasticity of prestressed reinforcement		
Section Geometry					
$A_{tf} =$	115900.0	mm ²	Area of concrete surrounding flexural tension reinforcement		
$b_f =$	2000.0	mm	Width of compression face		
$d =$	1197.0	mm	Depth from compression face to centroid of flexural tension reinf.		
$H =$	1296.0	mm	Height of section		
$d_{pw} =$	0.0	mm	Depth from compression face to centroid of prestressing reinf. in web		
$d_v =$	1077.3	mm	Depth of uniform shear stress= jd		
$\lambda =$	0.00	mm	Ratio of d_{pw} / d		
$d_{nv} =$	900.0	mm	Depth of uniform comp. stress n_v over diagonally cracked web, $\leq d_v$		
$b_w =$	127.0	mm	Width of shear area (web)		
$A_s =$	0.0	mm ²	Area of nonprestressed flexural tension reinforcement;		
$A_{sw} =$	0.0	mm ²	Area of nonprestressed longitudinal reinforcement centered in web		
$A_{sc} =$	1400.0	mm ²	Area of nonprestressed reinforcement in compression chord		
$A_v =$	254.0	mm ²	Area of transverse reinforcement (stirrups) spaced at s		
$s =$	457.0	mm	Spacing of transverse reinforcement		
$\rho_z =$	0.0044		Ratio of transverse reinforcement area to concrete area		
$A_p =$	2400.0	mm ²	Area of prestressed flexural tension reinforcement		
$A_{pw} =$	0.0	mm ²	Area of prestressed longitudinal reinforcement centered in web		
$\theta_p =$	0.0	degree	Angle of inclination of draped prestressed reinforcement		

Appendix C: Detailed Examples of Proposed Evaluation Procedure (cont.)

Solution of Example 1 (cont.):

Shear strength at yielding of transverse reinforcement

$\beta =$	0.18		Concrete shear contribution factor
$\theta_0 =$	23.0	degree	Predicted value of θ at $\varepsilon_x = 0$
$\Delta\theta =$	14480.1	degree	Predicted rate of change of n_v per unit ε_x
$\Delta n_v =$	-5675.4	MPa	Predicted rate of change of n_v per unit ε_x
$n_{v0} =$	9.2	MPa	Predicted value of n_v at $\varepsilon_x = 0$
$\varepsilon_x =$	0.000859		Average longitudinal strain over depth of member
$C_c =$	-3204.9	kN	Force in compression chord (negative for compression)
$\varepsilon_x =$	0.000859		$\varepsilon_x = 2\varepsilon_x$ if there is tension in compression chord
$\theta =$	35.5	degree	Angle of inclination of principal compression
$V_c =$	116.8	kN	Shear resistance attributed to concrete
$V_s =$	302.6	kN	Shear resistance attributed to stirrups
$V_p =$	0.0	kN	Shear force resisted by inclined prestressing tendons
$V =$	419.5	kN	Total shear resistance

Shear strength at crushing of concrete

$\beta =$	0.06		Concrete shear contribution factor
$\theta_0 =$	20.8	degree	Predicted value of θ at $\varepsilon_x = 0$
$\Delta\theta =$	2656.5	degree	Predicted rate of change of n_v per unit ε_x
$\Delta n_v =$	-3333.1	MPa	Predicted rate of change of n_v per unit ε_x
$n_{v0} =$	12.6	MPa	Predicted value of n_v at $\varepsilon_x = 0$
$\varepsilon_x =$	0.001128		Average longitudinal strain over depth of member
$C_c =$	-2947.0	kN	Force in compression chord (negative for compression)
$\varepsilon_x =$	0.001128		$\varepsilon_x = 2\varepsilon_x$ if there is tension in compression chord
$\theta =$	23.8	degree	Angle of inclination of principal compression
$V_c =$	37.9	kN	Shear resistance attributed to concrete
$V_s =$	488.6	kN	Shear resistance attributed to stirrups
$V_p =$	0.0	kN	Shear force resisted by inclined prestressing tendons
$V =$	526.6	kN	Total shear resistance

Shear strength at biaxial yielding of reinforcement

$jd =$	1144.4	mm	Internal flexural lever-arm
$N_{vcc} =$	7507.3	kN	Max. N_v as limited by reserve capacity of comp. chord long. reinf.
$N_{vct} =$	1468.7	kN	Max. N_v as limited by reserve capacity of tension chord long. reinf.
$N_{vc} =$	1468.7	kN	Max. N_v (lesser of N_{vct} and N_{vcc})
$V =$	562.7	kN	Total shear strength

Shear strength of the section

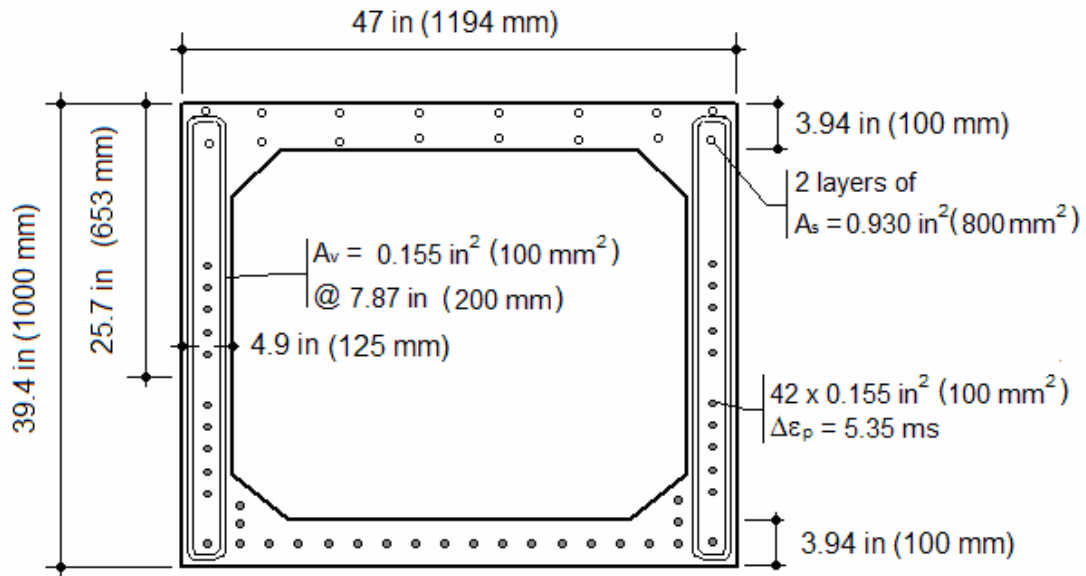
$V_{max} =$	1026.1	kN	Maximum allowable shear strength ($0.25 f_c' b_w d_v + V_p$)
$V =$	526.6	kN	Governing shear strength

Section has sufficient strength

Note: Yielding of transverse reinforcement only governs if it is greater than concrete crushing and lower than biaxial yielding

Appendix C: Detailed Examples of Proposed Evaluation Procedure (cont.)

Example 2: Prestressed Concrete Box-girder Bridge at 8.94 m from the support.



$$M_f = 3607.6 \text{ kNm}$$

$$V_f = 304.3 \text{ kN}$$

$$N_f = 0$$

$$f_y = 400 \text{ MPa}$$

$$f_c' = 40 \text{ MPa}$$

$$f_{pu} = 1860 \text{ MPa}$$

$$\theta_p = 1.3 \text{ deg. (20 web tendons are draped)}$$

Appendix C: Detailed Examples of Proposed Evaluation Procedure (cont.)

Solution of Example 2:

Factored loads			Material reduction factor		
$M_f =$	3607.6	Factored moment (positive) , kN.m	$\phi_c =$	0.75	Concrete
$V_f =$	304.3	Factored shear (positive), kN	$\phi_s =$	0.90	Steel
$N_f =$	0	Factored axial force (positive for tension) , kN	$\phi_p =$	0.95	Prestressing
Material Properties					
$f_c' =$	40	MPa	Compressive strength of concrete		
$\alpha =$	0.165		Concrete tension stiffening factor		
$f_y =$	400	MPa	Yield strength of reinforcement		
$E_s =$	200000	MPa	Modulus of Elasticity of nonprestressed reinforcement		
$\varepsilon_y =$	0.002		Steel yield strain		
$f_p =$	1070	MPa	Effective stress in prestressing tendons		
$f_{pr} =$	1800	MPa	Stress in prestressing tendons at maximum resistance		
$E_p =$	200000	MPa	Modulus of Elasticity of prestressed reinforcement		
Section Geometry					
$A_{tf} =$	119400.0	mm ²	Area of concrete surrounding flexural tension reinforcement		
$b_f =$	11940.0	mm	Width of compression face		
$d =$	950.0	mm	Depth from compression face to centroid of flexural tension reinf.		
$H =$	1000.0	mm	Height of section		
$d_{pw} =$	653.0	mm	Depth from compression face to centroid of prestressing reinf. in web		
$d_v =$	855.0	mm	Depth of uniform shear stress= jd		
$\lambda =$	0.69	mm	Ratio of d_{pw} / d		
$d_{nv} =$	800.0	mm	Depth of uniform comp. stress n_v over diagonally cracked web, $\leq d_v$		
$b_w =$	250.0	mm	Width of shear area (web)		
$A_s =$	0.0	mm ²	Area of nonprestressed flexural tension reinforcement;		
$A_{sw} =$	0.0	mm ²	Area of nonprestressed longitudinal reinforcement centered in web		
$A_{sc} =$	1600.0	mm ²	Area of nonprestressed reinforcement in compression chord		
$A_v =$	400.0	mm ²	Area of transverse reinforcement (stirrups) spaced at s		
$s =$	200.0	mm	Spacing of transverse reinforcement		
$\rho_z =$	0.0080		Ratio of transverse reinforcement area to concrete area		
$A_p =$	2200.0	mm ²	Area of prestressed flexural tension reinforcement		
$A_{pw} =$	2000.0	mm ²	Area of prestressed longitudinal reinforcement centered in web		
$\theta_p =$	1.3	degree	Angle of inclination of draped prestressed reinforcement		

Appendix C: Detailed Examples of Proposed Evaluation Procedure (cont.)

Solution of Example 2 (cont.):

Shear strength at yielding of transverse reinforcement

$\beta =$	0.18		Concrete shear contribution factor
$\theta_0 =$	26.1	degree	Predicted value of θ at $\varepsilon_x = 0$
$\Delta\theta =$	11400.0	degree	Predicted rate of change of n_v per unit ε_x
$\Delta n_v =$	-7442.4	MPa	Predicted rate of change of n_v per unit ε_x
$n_{v0} =$	13.4	MPa	Predicted value of n_v at $\varepsilon_x = 0$
$\varepsilon_x =$	0.000822		Average longitudinal strain over depth of member
$C_c =$	-4296.7	kN	Force in compression chord (negative for compression)
$\varepsilon_x =$	0.000822		$\varepsilon_x = 2\varepsilon_x$ if there is tension in compression chord
$\theta =$	35.5	degree	Angle of inclination of principal compression
$V_c =$	182.5	kN	Shear resistance attributed to concrete
$V_s =$	864.0	kN	Shear resistance attributed to stirrups
$V_p =$	47.5	kN	Shear force resisted by inclined prestressing tendons
$V =$	1094.0	kN	Total shear resistance

Shear strength at crushing of concrete

$\beta =$	0.08		Concrete shear contribution factor
$\theta_0 =$	25.1	degree	Predicted value of θ at $\varepsilon_x = 0$
$\Delta\theta =$	3200.0	degree	Predicted rate of change of n_v per unit ε_x
$\Delta n_v =$	-1955.2	MPa	Predicted rate of change of n_v per unit ε_x
$n_{v0} =$	13.3	MPa	Predicted value of n_v at $\varepsilon_x = 0$
$\varepsilon_x =$	0.001121		Average longitudinal strain over depth of member
$C_c =$	-3972.3	kN	Force in compression chord (negative for compression)
$\varepsilon_x =$	0.001121		$\varepsilon_x = 2\varepsilon_x$ if there is tension in compression chord
$\theta =$	28.7	degree	Angle of inclination of principal compression
$V_c =$	83.1	kN	Shear resistance attributed to concrete
$V_s =$	1124.1	kN	Shear resistance attributed to stirrups
$V_p =$	47.5	kN	Shear force resisted by inclined prestressing tendons
$V =$	1254.8	kN	Total shear resistance

Shear strength at biaxial yielding of reinforcement

$jd =$	941.2	mm	Internal flexural lever-arm
$N_{vcc} =$	11068.5	kN	Max. N_v as limited by reserve capacity of comp. chord long. reinf.
$N_{vct} =$	5203.5	kN	Max. N_v as limited by reserve capacity of tension chord long. reinf.
$N_{vc} =$	5203.5	kN	Max. N_v (lesser of N_{vct} and N_{vcc})
$V =$	1837.3	kN	Total shear strength

Shear strength of the section

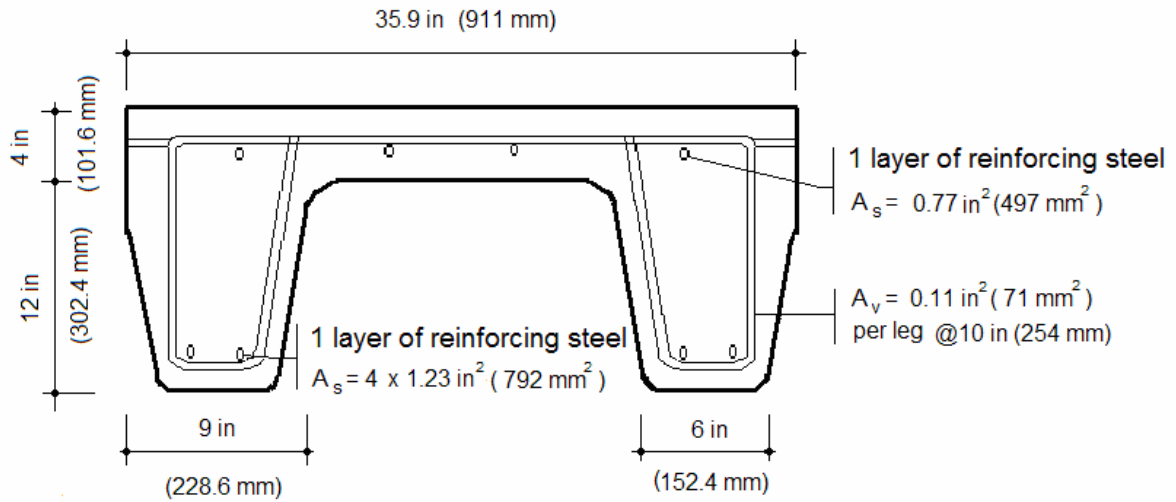
$V_{max} =$	1650.7	kN	Maximum allowable shear strength ($0.25 f_c' b_w d_v + V_p$)
$V =$	1254.8	kN	Governing shear strength

Section has sufficient strength

Note: Yielding of transverse reinforcement only governs if it is greater than concrete crushing and lower than biaxial yielding

Appendix C: Detailed Examples of Proposed Evaluation Procedure (cont.)

Example 3: Reinforced Concrete channel-girder Bridge at 1.39 m from the support.



$$M_f = 207.6 \text{ kNm}$$

$$V_f = 139.3 \text{ kN}$$

$$N_f = 0$$

$$f_y = 400 \text{ MPa}$$

$$f'_c = 40 \text{ MPa}$$

Average assumed $b_w = 381 \text{ mm}$

Appendix C: Detailed Examples of Proposed Evaluation Procedure (cont.)

Solution of Example 3:

Factored loads			Material reduction factor		
$M_f =$	207.6	Factored moment (positive) , kN.m	$\phi_c =$	0.75	Concrete
$V_f =$	139.3	Factored shear (positive), kN	$\phi_s =$	0.90	Steel
$N_f =$	0	Factored axial force (positive for tension) , kN	$\phi_p =$	0.95	Prestressing
Material Properties					
$f_c' =$	40	MPa	Compressive strength of concrete		
$\alpha =$	0.165		Concrete tension stiffening factor		
$f_y =$	400	MPa	Yield strength of reinforcement		
$E_s =$	200000	MPa	Modulus of Elasticity of nonprestressed reinforcement		
$\varepsilon_y =$	0.002		Steel yield strain		
$f_p =$	0	MPa	Effective stress in prestressing tendons		
$f_{pr} =$	0	MPa	Stress in prestressing tendons at maximum resistance		
$E_p =$	200000	MPa	Modulus of Elasticity of prestressed reinforcement		
Section Geometry					
$A_{tf} =$	15250.0	mm ²	Area of concrete surrounding flexural tension reinforcement		
$b_f =$	911.0	mm	Width of compression face		
$d =$	356.0	mm	Depth from compression face to centroid of flexural tension reinf.		
$H =$	404.0	mm	Height of section		
$d_{pw} =$	0.0	mm	Depth from compression face to centroid of prestressing reinf. in web		
$d_v =$	320.4	mm	Depth of uniform shear stress= jd		
$\lambda =$	0.00	mm	Ratio of d_{pw} / d		
$d_{nv} =$	255.0	mm	Depth of uniform comp. stress n_v over diagonally cracked web, $\leq d_v$		
$b_w =$	381.0	mm	Width of shear area (web)		
$A_s =$	3166.8	mm ²	Area of nonprestressed flexural tension reinforcement;		
$A_{sw} =$	0.0	mm ²	Area of nonprestressed longitudinal reinforcement centered in web		
$A_{sc} =$	0.0	mm ²	Area of nonprestressed reinforcement in compression chord		
$A_v =$	284.0	mm ²	Area of transverse reinforcement (stirrups) spaced at s		
$s =$	254.0	mm	Spacing of transverse reinforcement		
$\rho_z =$	0.0029		Ratio of transverse reinforcement area to concrete area		
$A_p =$	0.0	mm ²	Area of prestressed flexural tension reinforcement		
$A_{pw} =$	0.0	mm ²	Area of prestressed longitudinal reinforcement centered in web		
$\theta_p =$	0.0	degree	Angle of inclination of draped prestressed reinforcement		

Appendix C: Detailed Examples of Proposed Evaluation Procedure (cont.)

Solution of Example 3 (cont.):

Shear strength at yielding of transverse reinforcement

$\beta =$	0.18		Concrete shear contribution factor
$\theta_0 =$	21.8	degree	Predicted value of θ at $\varepsilon_x = 0$
$\Delta\theta =$	15705.5	degree	Predicted rate of change of n_v per unit ε_x
$\Delta n_v =$	-4525.4	MPa	Predicted rate of change of n_v per unit ε_x
$n_{v0} =$	7.1	MPa	Predicted value of n_v at $\varepsilon_x = 0$
$\varepsilon_x =$	0.000659		Average longitudinal strain over depth of member
$C_c =$	-449.5	kN	Force in compression chord (negative for compression)
$\varepsilon_x =$	0.000659		$\varepsilon_x = 2\varepsilon_x$ if there is tension in compression chord
$\theta =$	32.1	degree	Angle of inclination of principal compression
$V_c =$	104.2	kN	Shear resistance attributed to concrete
$V_s =$	205.3	kN	Shear resistance attributed to stirrups
$V_p =$	0.0	kN	Shear force resisted by inclined prestressing tendons
$V =$	309.5	kN	Total shear resistance

Shear strength at crushing of concrete

$\beta =$	0.05		Concrete shear contribution factor
$\theta_0 =$	19.1	degree	Predicted value of θ at $\varepsilon_x = 0$
$\Delta\theta =$	2440.2	degree	Predicted rate of change of n_v per unit ε_x
$\Delta n_v =$	-2070.3	MPa	Predicted rate of change of n_v per unit ε_x
$n_{v0} =$	10.0	MPa	Predicted value of n_v at $\varepsilon_x = 0$
$\varepsilon_x =$	0.000821		Average longitudinal strain over depth of member
$C_c =$	-244.0	kN	Force in compression chord (negative for compression)
$\varepsilon_x =$	0.000821		$\varepsilon_x = 2\varepsilon_x$ if there is tension in compression chord
$\theta =$	21.1	degree	Angle of inclination of principal compression
$V_c =$	28.4	kN	Shear resistance attributed to concrete
$V_s =$	334.3	kN	Shear resistance attributed to stirrups
$V_p =$	0.0	kN	Shear force resisted by inclined prestressing tendons
$V =$	362.7	kN	Total shear resistance

Shear strength at biaxial yielding of reinforcement

$jd =$	321.2	mm	Internal flexural lever-arm
$N_{vcc} =$	1292.5	kN	Max. N_v as limited by reserve capacity of comp. chord long. reinf.
$N_{vct} =$	987.6	kN	Max. N_v as limited by reserve capacity of tension chord long. reinf.
$N_{vc} =$	987.6	kN	Max. N_v (lesser of N_{vct} and N_{vcc})
$V =$	356.9	kN	Total shear strength

Shear strength of the section

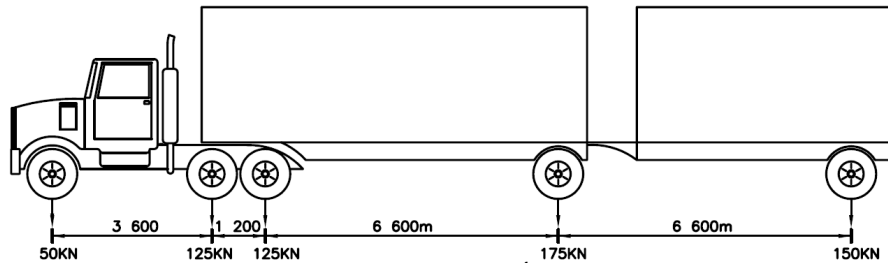
$V_{max} =$	915.5	kN	Maximum allowable shear strength ($0.25 f_c' b_w d_v + V_p$)
$V =$	356.9	kN	Governing shear strength

Section has sufficient strength

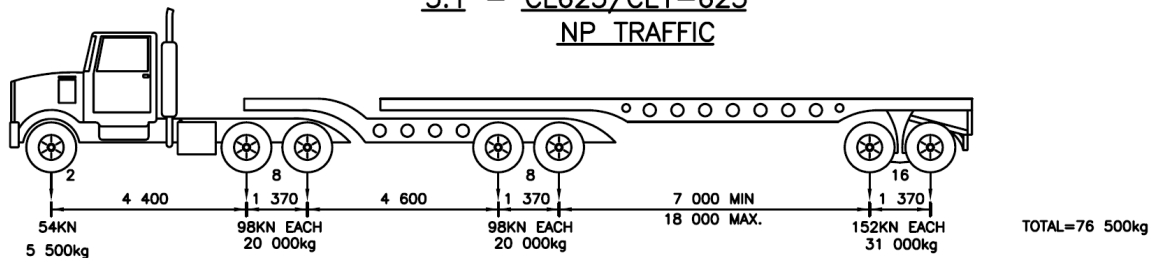
Note: Yielding of transverse reinforcement only governs if it is greater than concrete crushing and lower than biaxial yielding

**Appendix D: Rating Trucks Used for Example Evaluations of Bridge Girder
(BC Ministry of Transportation).**

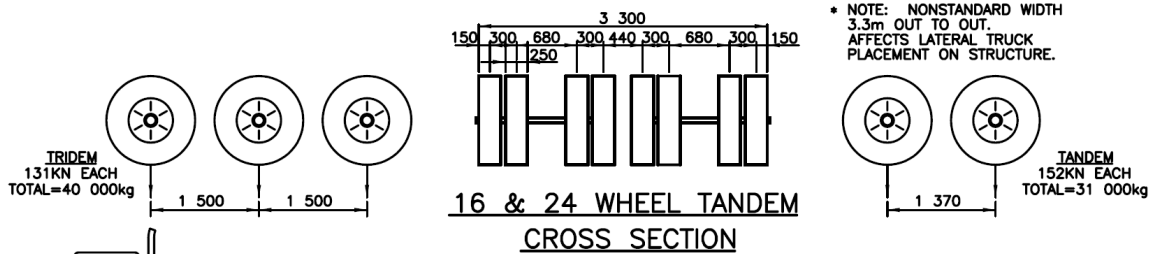
85 TONNE CEILING G.V.W. RATING TRUCKS



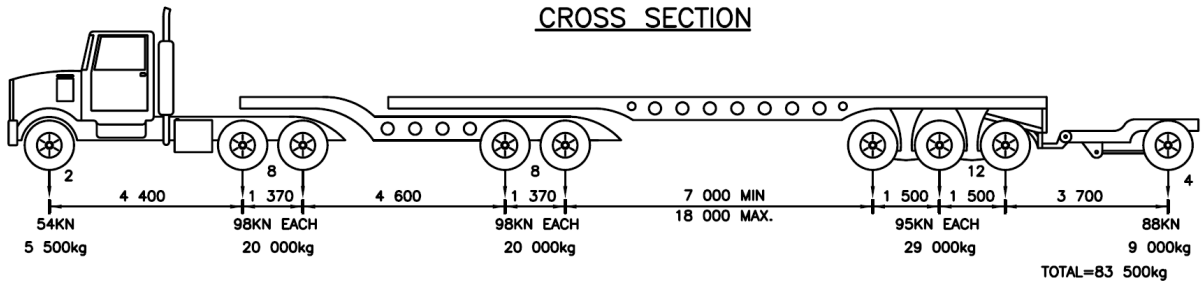
**3.1 - CL625/CL1-625
NP TRAFFIC**



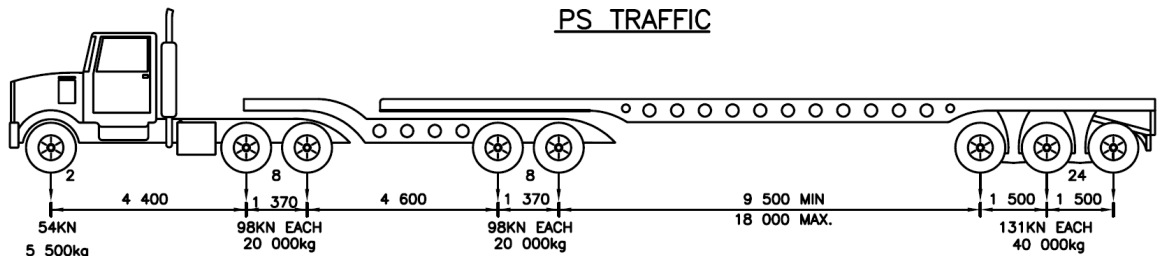
**3.2 - 7 AXLE 16 WHEEL TANDEM TRAILER
PS TRAFFIC**



**16 & 24 WHEEL TANDEM
CROSS SECTION**



**3.3 - 9 AXLE FULL PERMIT VEHICLE
PS TRAFFIC**

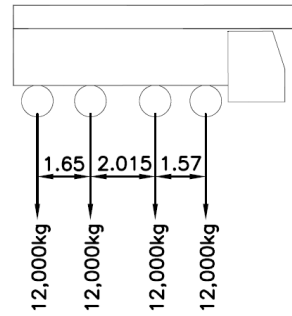


**3.4 - 8 AXLE 24 WHEEL TRIDEM TRAILER
PS TRAFFIC**

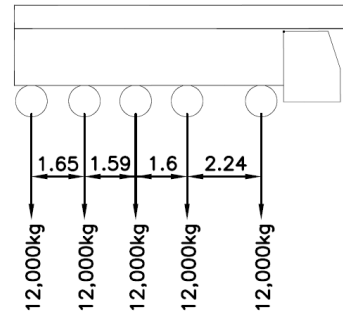
BRIDGE ENGINEERING SECTION
REVISED NOV/04

**Appendix D: Rating Trucks Used for Example Evaluations of Bridge Girder
(BC Ministry of Transportation).**

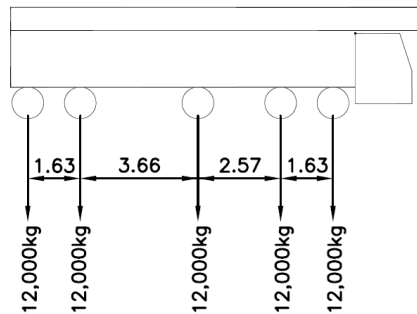
ANNUAL PERMIT CRANES



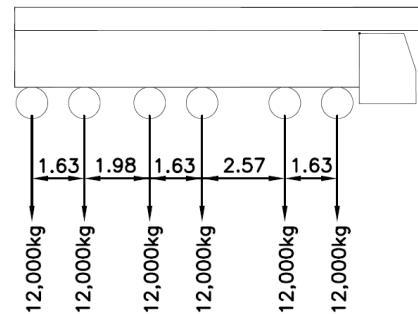
Crane-4ax



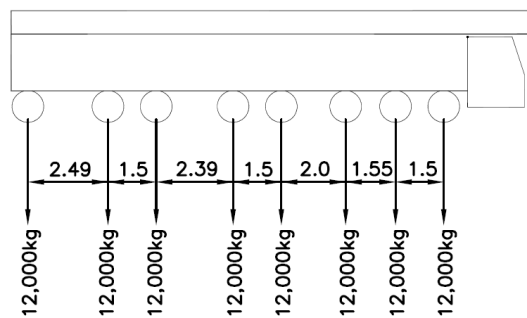
Crane-5ax



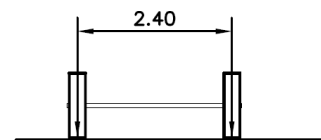
Crane-Long 5ax



Crane-6ax

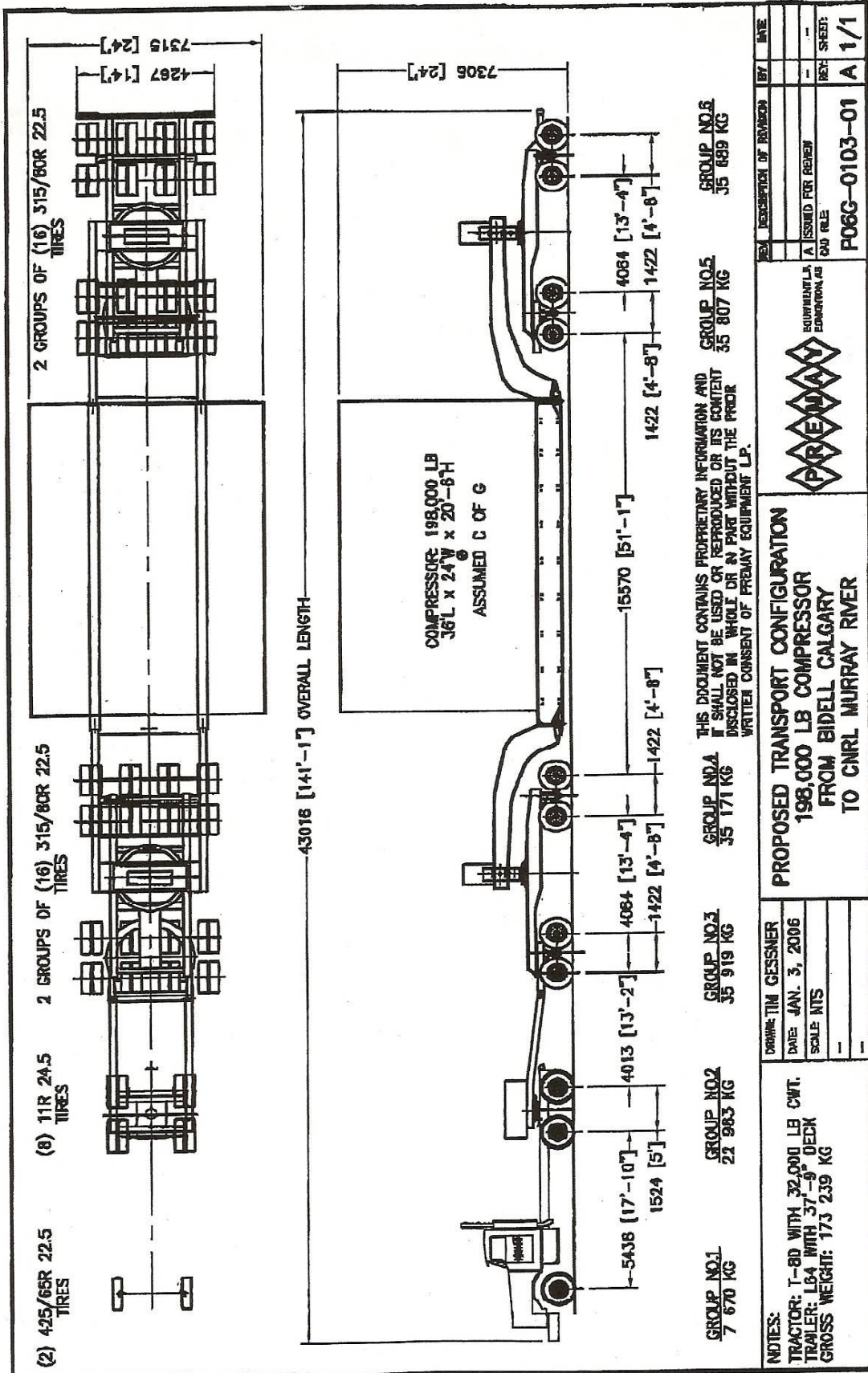


Crane-8ax



Transverse Dimension
Between \odot 's of Wheels
(Typical All Cranes) = 2.4m

**Appendix D: Rating Trucks Used for Example Evaluations of Bridge Girder
(BC Ministry of Transportation, Premay Equipment LP).**



Appendix E: Tested Beams Used for Comparison with Experimental Results (132 RC Beams Without Stirrups)

Authors (year)	Specimen	Geometry and loading information				Concrete f _c ' (MPa)	Longitudinal steel		V _{test} (kN)	Test-to-predicted shear strength ratio			
		h (mm)	b _w (mm)	L (mm)	a/d		A _s (mm ²)	f _y (MPa)		ρ (%)	ACI 318	AASHTO 2007	CHBDC 2006
Angelakos, Bentz, Collins (2001)	DB120	1000	300.0	5410	2.9	21.0	2800.0	550.2	179.0	0.84	1.14	1.10	1.04
	DB130	1000	300.0	5410	2.9	32.0	2800.0	550.2	185.0	0.71	1.03	0.98	0.94
	DB140	1000	300.0	5410	2.9	38.0	2800.0	550.2	180.0	0.63	0.94	0.90	0.87
	DB165	1000	300.0	5410	2.9	65.0	2800.0	550.2	185.0	0.50	0.95	0.95	0.90
	DB180	1000	300.0	5410	2.9	80.0	2800.0	550.2	172.0	0.45	0.82	0.82	0.79
	DB230	1000	300.0	5410	2.9	32.0	5600.0	550.2	257.0	0.98	1.14	1.12	1.03
	DBO530	1000	300.0	5410	3.0	32.0	1400.0	550.2	165.0	0.63	1.17	1.11	1.13
	B2	650	240.0	3607	3.0	29.6	1806.4	433.7	117.2	0.90	0.97	0.88	0.91
Bhal (1968)	B3	950	240.0	5410	3.0	27.5	2709.7	433.7	161.9	0.86	1.00	0.92	0.94
	B4	1250	240.0	7214	3.0	25.2	3612.9	433.7	176.6	0.73	0.90	0.85	0.86
	B5	650	240.0	3607	3.0	26.6	903.2	433.7	104.0	0.84	1.11	1.03	1.06
	B6	650	240.0	3607	3.0	24.7	903.2	433.7	111.8	0.94	1.21	1.13	1.17
	B7	950	240.0	5410	3.0	27.2	1354.8	433.7	134.9	0.72	1.03	0.97	1.02
	B8	950	240.0	5410	3.0	27.7	1354.8	433.7	122.6	0.65	0.93	0.88	0.92
	OA-1	556	309.9	3531	3.8	22.6	2580.6	555.0	166.8	1.47	1.52	1.32	1.36
	OA-2	561	305.1	4445	4.7	23.7	3225.8	555.0	177.9	1.54	1.61	1.39	1.46
Bresler, Scordelis (1963)	OA-3	556	307.1	6274	6.8	37.6	3871.0	551.6	189.0	1.30	1.54	1.34	1.44
	37623	406	202.9	2159	3.0	38.9	1258.1	477.8	96.0	1.28	1.26	1.10	1.11
	37654	406	202.9	2159	3.0	32.8	1258.1	477.8	87.4	1.26	1.29	1.14	1.14
Chana (1981)	37682	406	202.9	2159	3.0	35.7	1258.1	477.8	99.4	1.38	1.34	1.18	1.19
	B100	1000	300.0	5410	2.9	36.0	2800.0	650.2	225.0	0.81	1.20	1.14	1.11
	B100-R	1000	300.0	5410	2.9	36.0	2800.0	650.2	249.0	0.90	1.33	1.27	1.22
Collins, Kuchma (1999)	B100D	1000	300.0	5410	2.9	36.0	4000.0	650.2	320.0	1.15	1.51	1.46	1.38
	B100H	1000	300.0	5410	2.9	98.0	2800.0	475.0	193.0	0.50	0.87	0.86	0.84
	B100HE	1000	300.0	5410	2.9	98.0	2800.0	475.0	217.0	0.57	0.98	0.97	0.94
	B100L	1000	300.0	5410	2.9	39.0	2800.0	482.6	223.0	0.77	1.16	1.10	1.07
	B100L-R	1000	300.0	5410	2.9	39.0	2800.0	482.6	235.0	0.81	1.22	1.16	1.13
	B100B	1000	300.0	5410	2.9	39.0	2800.0	650.2	204.0	0.70	1.06	1.01	0.98
	BM100	1000	300.0	5410	2.9	37.2	2103.2	650.2	192.0	0.68	1.12	1.06	1.04
	BN50	500	300.0	2692	3.0	37.2	1503.2	486.1	162.7	1.18	1.46	1.32	1.31
	BND100	1000	300.0	5410	2.9	98.8	2903.2	650.2	278.0	0.73	1.23	1.22	1.18
	BHD100R	1000	300.0	5410	2.9	98.8	2903.2	650.2	333.2	0.87	1.47	1.46	1.42
	BHD50	500	300.0	2692	3.0	98.8	1503.2	486.1	192.7	1.03	1.40	1.31	1.31
	BHD50R	500	300.0	2692	3.0	98.8	1503.2	486.1	204.7	1.10	1.48	1.39	1.39
	BRL100	1000	300.0	5410	2.9	94.0	1400.0	550.2	163.0	0.43	0.97	0.94	0.96
	SE100A-45	1000	294.9	4597	2.5	50.0	2800.0	482.6	200.8	0.63	0.91	0.88	0.82
	SE100A-45-R	1000	294.9	4597	2.5	50.0	2800.0	482.6	235.4	0.73	1.07	1.03	0.96
	SE100B-45	1000	294.9	4597	2.5	50.0	3703.2	475.0	281.0	0.88	1.15	1.13	1.04
	SE100B-45-R	1000	294.9	4597	2.5	50.0	3703.2	475.0	315.8	0.99	1.29	1.27	1.17

Appendix E: Tested Beams Used for Comparison with Experimental Results (132 RC Beams Without Stirrups)

Authors (year)	Specimen	Geometry and loading information			Concrete f _c ' (MPa)	Longitudinal steel		V _{test} (kN)	Test-to-predicted shear strength ratio					
		h (mm)	b _w (mm)	L (mm)		a/d	A _s (mm ²)		f _y (MPa)	ρ (%)	ACI 318	AASHTO 2007	CHBDC 2006	Proposed
Collins, Kuchma (1999)	SE50A-45	500	168.9	2489	2.7	52.5	800.0	482.6	1.0	68.6	0.73	0.94	0.86	0.84
	SE50B-45	500	168.9	2489	2.7	52.5	800.0	482.6	1.0	80.5	0.86	1.10	1.01	0.99
	SE50B-45-R	500	168.9	2489	2.7	52.5	903.2	521.9	1.2	86.5	0.92	1.15	1.04	1.02
	SE100A-83	1000	294.9	4597	2.5	86.0	2800.0	482.6	1.0	303.2	0.81	1.33	1.36	1.24
	SE100B-83	1000	294.9	4597	2.5	86.0	3703.2	482.6	1.4	364.8	0.97	1.44	1.50	1.34
	SE100B-83-R	1000	294.9	4597	2.5	86.0	3703.2	482.6	1.4	364.1	0.97	1.44	1.50	1.34
	SE50A-83	500	168.9	2489	2.7	52.5	800.0	482.6	1.0	92.9	0.99	1.28	1.17	1.14
	SE50B-83	500	168.9	2489	2.7	52.5	903.2	482.6	1.2	100.8	1.07	1.34	1.21	1.19
Grimm (1997)	S2.2	400	300.0	2484	3.5	91.3	1961.3	468.8	1.9	187.1	1.30	1.54	1.38	1.40
	S2.3	400	300.0	2484	3.5	93.7	980.6	468.8	0.9	123.1	0.85	1.26	1.15	1.20
	S2.4	400	300.0	2484	3.8	94.1	3703.2	486.8	3.8	229.8	1.69	1.60	1.44	1.45
	S3.2	800	300.0	5283	3.7	93.7	3703.2	486.8	1.7	259.1	0.87	1.29	1.23	1.23
	S3.3	800	300.0	5283	3.5	94.4	1851.6	486.8	0.8	192.8	0.62	1.19	1.13	1.18
	S3.4	800	300.0	5283	3.8	94.1	7387.1	486.8	3.6	379.0	1.33	1.52	1.51	1.42
Hamadi, Regan (1980)	G1	400	100.1	2565	3.5	30.3	625.8	399.9	1.7	44.5	1.31	1.32	1.16	1.18
	G2	400	100.1	2565	3.4	23.5	400.0	459.9	1.1	41.0	1.36	1.50	1.34	1.36
	G3	400	100.1	2565	3.4	23.2	225.8	464.7	0.6	35.0	1.16	1.53	1.40	1.41
	G4	400	100.1	4445	6.0	22.0	400.0	799.8	1.1	30.3	1.04	1.38	1.24	1.31
Kani (1967)	63	610	154.4	5359	4.0	26.2	2322.6	351.6	2.8	93.2	1.30	1.26	1.11	1.14
	64	610	156.2	9703	8.0	25.7	2322.6	351.6	2.8	79.0	1.10	1.34	1.16	1.29
	65	610	149.6	3734	2.5	27.0	2329.0	373.7	2.8	112.3	1.57	1.29	1.18	1.23
	66	610	156.2	7518	6.0	26.4	2322.6	351.6	2.7	90.7	1.25	1.40	1.20	1.32
	71	610	154.9	4267	3.0	27.4	2245.2	373.0	2.7	102.1	1.39	1.26	1.11	1.17
	74	610	152.4	4267	3.1	27.2	2264.5	365.4	2.8	107.6	1.55	1.39	1.22	1.29
	75	610	152.4	4267	3.1	27.3	2264.5	366.8	2.8	107.9	1.55	1.39	1.22	1.22
	76	610	152.4	3734	2.6	30.8	2264.5	372.3	2.9	114.8	1.57	1.34	1.20	1.18
	79	610	153.2	9220	6.8	26.1	2316.1	381.3	2.7	83.6	1.15	1.35	1.16	1.24
	3042	1219	153.9	7518	2.5	26.4	4554.8	375.1	2.7	236.9	1.64	1.54	1.57	1.37
	3043	1219	153.7	8585	3.0	27.0	4554.8	375.8	2.7	165.0	1.13	1.15	1.13	1.03
	3044	1219	152.4	10770	4.0	29.5	4554.8	375.8	2.7	159.0	1.05	1.20	1.13	1.09
	3045	1219	154.9	5461	5.0	28.3	4554.8	380.6	2.7	152.4	1.01	1.26	1.16	1.16
	3046	1219	154.9	17399	7.0	26.7	4593.5	359.9	2.7	154.1	1.05	1.46	1.31	1.38
	3047	1219	154.9	19558	8.0	26.7	4554.8	375.8	2.7	147.0	1.00	1.46	1.31	1.40
	Kim, Park (1994)	D915-1	1000	300.0	6401	3.0	53.7	5141.9	477.1	1.9	299.2	0.89	1.04	0.95
D915-2		1000	300.0	6401	3.0	53.7	5141.9	477.1	1.9	332.1	0.99	1.16	1.06	1.07
D550-1		620	300.0	3861	3.0	53.7	3096.8	477.1	1.9	226.1	1.12	1.19	1.05	1.08
D550-2		620	300.0	3861	3.0	53.7	3096.8	477.1	1.9	214.5	1.06	1.13	1.00	1.03
Krefeld, Thurston (1966)	Ss2-Oca	508	254.0	3658	4.0	38.3	2580.6	386.1	2.2	146.8	1.23	1.30	1.13	1.17
	Ss2-Ocb	508	254.0	3658	4.0	38.3	2580.6	386.1	2.2	133.4	1.12	1.18	1.03	1.07

Appendix E: Tested Beams Used for Comparison with Experimental Results (132 RC Beams Without Stirrups)

Authors (year)	Specimen	Geometry and loading information				Concrete f_c' (MPa)	Longitudinal steel			V_{test} (kN)	Test-to-predicted shear strength ratio					
		h (mm)	b_w (mm)	L (mm)	a/d		A_s (mm ²)	f_y (MPa)	ρ (%)		ACI 318	AASHTO 2007	CHBDC 2006	Proposed		
Lambotte, Taerwe (1990)	NS-0.48	450	199.9	5004	3.0	36.3	400.0	544.7	0.5	70.0	124	0.84	1.24	1.17	1.15	
	NS-1.07	450	199.9	5004	3.0	37.2	806.5	544.7	1.0	127.0	179	1.50	1.79	1.62	1.61	
	NS-1.45	450	199.9	5004	3.0	34.0	1206.4	544.7	1.5	180.0	234	2.23	2.34	2.07	2.07	
	HS-0.48	450	199.9	5004	3.0	81.0	400.0	544.7	0.5	76.0	126	0.86	1.26	1.19	1.23	
	HS-1.07	450	199.9	5004	3.0	81.1	806.5	544.7	1.0	139.0	180	1.21	1.80	1.67	1.68	
Lambotte, Taerwe (1990)	HS-1.45	450	199.9	5004	3.0	81.6	1206.4	544.7	1.5	211.0	239	1.84	2.39	2.21	2.19	
	C3	500	199.9	2718	3.0	38.3	1206.4	424.7	1.3	110.4	125	1.19	1.25	1.13	1.16	
	C4	670	225.0	3607	3.0	38.3	1812.9	424.7	1.3	152.0	121	1.09	1.21	1.09	1.13	
	Mathey, Watstein (1963)	IIla-17	457	203.2	3658	3.8	29.2	2083.9	505.4	2.5	88.1	109	1.19	1.09	0.94	1.00
		IIla-18	457	203.2	3658	3.8	25.2	2083.9	505.4	2.5	80.7	106	1.18	1.06	0.91	0.97
Va-19		457	203.2	3658	3.8	23.5	761.3	691.5	0.9	63.3	112	0.95	1.12	1.01	1.06	
Va-20		457	203.2	3658	3.8	25.6	761.3	691.5	0.9	66.0	114	0.95	1.14	1.03	1.08	
Va-21		457	203.2	3658	2.8	26.1	690.3	704.6	0.8	71.4	114	1.02	1.14	1.03	1.04	
Va-22		457	203.2	3658	2.8	25.8	690.3	704.6	0.8	62.4	100	0.90	1.00	0.90	0.91	
Va-23		457	203.2	3658	2.8	30.5	690.3	704.6	0.8	75.1	113	0.99	1.13	1.03	1.04	
Va-24		457	203.2	3658	3.8	26.3	380.6	695.7	0.5	54.5	111	0.78	1.11	1.09	1.14	
Va-25		457	203.2	3658	3.8	25.8	380.6	695.7	0.5	50.0	103	0.72	1.03	1.01	1.05	
B40B4		406	304.8	2388	2.8	34.7	2077.4	377.8	1.9	155.7	129	1.41	1.29	1.12	1.16	
Morrow, Viest (1957)	B56B2	406	304.8	3200	3.9	14.7	2077.4	470.9	1.9	100.1	126	1.39	1.26	1.09	1.16	
	B56E2	406	304.8	3200	3.9	14.7	651.6	461.9	0.6	79.6	140	1.11	1.40	1.27	1.33	
	B56A4	406	304.8	3200	3.8	25.0	2754.8	329.6	2.4	137.9	130	1.45	1.30	1.13	1.20	
	B56B4	406	304.8	3200	3.9	27.2	2077.4	440.6	1.9	122.3	123	1.25	1.23	1.07	1.13	
	B56E4	406	304.8	3200	3.9	28.4	1387.1	428.9	1.2	109.0	121	1.09	1.21	1.07	1.13	
	B56A6	406	308.1	3200	4.0	39.9	4148.4	438.5	3.8	177.9	132	1.54	1.32	1.13	1.22	
	B56B6	406	304.8	3200	3.8	45.7	2077.4	466.1	1.8	136.8	114	1.07	1.14	1.00	1.05	
	B70B2	406	304.8	3912	4.9	16.3	2077.4	461.9	1.9	89.0	116	1.18	1.16	1.00	1.09	
	B70A4	406	304.8	3912	4.8	27.2	2754.8	435.7	2.5	132.3	131	1.35	1.31	1.14	1.23	
	B70A6	406	304.8	3912	5.0	45.0	4148.4	435.1	3.8	177.9	136	1.47	1.36	1.17	1.27	
	B84B4	406	304.8	4623	5.9	27.2	2077.4	464.7	1.9	111.2	128	1.15	1.28	1.13	1.23	
	B113B4	406	304.8	6096	7.9	32.6	2077.4	468.8	1.9	104.3	124	0.98	1.24	1.11	1.22	
	Niwa, Yamada, Yokozaawa, Okamura (1987)	1	2100	599.9	12014	3.0	27.1	3322.6	999.1	0.3	402.0	097	0.39	0.97	0.92	1.00
2		2100	599.9	12014	3.0	26.2	1664.5	999.1	0.1	382.0	113	0.37	1.13	1.16	1.32	
3		1100	300.0	6020	3.0	24.6	412.9	999.1	0.1	102.0	085	0.41	0.85	1.03	1.11	
Schoiz (1994)	A-1	400	199.9	2261	3.0	80.6	600.0	499.9	0.8	83.0	125	0.81	1.25	1.16	1.17	
	D-2	400	199.9	2184	3.0	96.8	1406.4	499.9	1.9	121.0	131	1.21	1.31	1.20	1.18	
	D-3	400	199.9	2921	4.0	96.8	1406.4	499.9	1.9	121.0	148	1.21	1.48	1.32	1.37	
Taylor (1968)	1A	406	203.2	2642	3.0	28.8	774.2	350.3	1.0	61.8	108	0.92	1.08	0.97	0.97	
	2A	406	203.2	2642	3.0	33.2	1161.3	350.3	1.5	91.6	136	1.27	1.36	1.20	1.20	
	1B	406	203.2	2642	3.0	28.8	774.2	350.3	1.0	75.6	132	1.12	1.32	1.18	1.18	

Appendix E: Tested Beams Used for Comparison with Experimental Results (132 RC Beams Without Stirrups)

Authors (year)	Specimen	Geometry and loading information				Concrete f_c' (MPa)	Longitudinal steel			V_{test} (kN)	Test-to-predicted shear strength ratio			
		h (mm)	b_w (mm)	L (mm)	a/d		A_s (mm ²)	f_y (MPa)	ρ (%)		ACI 318	AASHTO 2007	CHBDC 2006	Proposed
Taylor (1968)	2B	406	203.2	2642	3.0	33.2	1161.3	350.3	1.5	100.5	1.39	1.49	1.32	1.31
	3B	406	203.2	2642	3.0	31.6	774.2	350.3	1.0	76.1	1.08	1.29	1.15	1.15
	5A	406	203.2	2235	2.5	29.9	774.2	350.3	1.0	80.5	1.17	1.29	1.16	1.12
	5B	406	203.2	2235	2.5	29.9	774.2	350.3	1.0	80.5	1.17	1.29	1.16	1.12
Taylor (1972)	A1	1000	400.1	6477	3.0	24.6	5019.3	419.9	1.3	358.4	1.16	1.27	1.22	1.24
	A2	1000	400.1	6477	3.0	21.5	5019.3	419.9	1.3	328.4	1.14	1.33	1.24	1.20
	B1	500	199.9	3251	3.0	22.9	1258.1	419.9	1.4	104.3	1.40	1.34	1.23	1.27
	B2	500	199.9	3251	3.0	20.9	1258.1	419.9	1.4	87.2	1.23	1.26	1.10	1.11
	B3	500	199.9	3251	3.0	27.0	1258.1	419.9	1.4	85.3	1.06	1.20	1.07	1.06
Thorenfeldt (1990)	B61	500	300.0	4597	3.0	77.8	2412.9	499.9	1.8	180.3	0.99	1.23	1.14	1.11
	B63	500	300.0	4597	4.0	77.8	4012.9	499.9	2.9	229.4	1.19	1.46	1.34	1.34
	B64	500	300.0	4597	3.0	77.8	4012.9	499.9	2.9	280.7	1.46	1.59	1.51	1.42
	A2	450	199.9	2540	3.0	24.1	619.4	439.9	0.7	70.6	1.03	1.24	1.13	1.12
Walraven (1978)	A3	750	199.9	4343	3.0	24.4	1141.9	439.9	0.8	100.8	0.85	1.13	1.03	1.02
Yoshida (2000)	YB2000/0	2000	300.0	10820	2.9	33.6	4200.0	455.1	0.7	255.0	0.46	0.88	0.97	0.89
										Mean	1.05	1.26	1.16	1.17
										COV	0.302	0.185	0.178	0.173

Appendix E: Tested Beams Used for Comparison with Experimental Results (131 PC Beams Without Stirrups)

Authors (year)	Specimen	Geometry and loading information				Concrete f_{pc} (MPa)	Prestressed reinforcement				Test-to-predicted shear strength ratio			
		h (mm)	b_w (mm)	L (mm)	a/d		A_p (mm ²)	f_{pu} (MPa)	f_{pe} (MPa)	ρ (%)	ACI 318	AASHTO 2007	CHBDC 2006	Proposed
Autur (1965)	B1	305	50.8	2591	3.4	55.2	193.5	1627.2	824.6	1.40	0.82	1.24	1.23	1.14
	B2	305	50.8	2591	3.4	51.0	193.5	1627.2	799.8	1.40	0.91	1.38	1.37	1.26
	B3	305	50.8	2591	2.5	56.5	193.5	1627.2	785.3	1.40	1.21	1.78	1.72	1.50
	B5	305	50.8	2591	2.5	62.1	193.5	1627.2	877.7	1.40	1.12	1.69	1.62	1.42
	B8	305	50.8	2591	2.5	62.1	193.5	1627.2	799.8	1.40	1.13	1.64	1.59	1.40
	B9	305	50.8	2591	3.4	51.0	193.5	1627.2	785.3	1.40	0.72	1.09	1.08	1.00
	B11	305	50.8	2591	3.4	61.4	193.5	1627.2	817.0	1.40	1.04	1.53	1.54	1.44
	D1	305	50.8	2591	3.4	49.6	193.5	1627.2	829.4	1.40	1.10	1.70	1.68	1.53
	D2	305	50.8	2591	3.9	56.5	193.5	1627.2	804.6	1.40	0.97	1.36	1.38	1.34
	E1	305	50.8	2591	2.8	54.5	193.5	1627.2	780.5	1.40	1.07	1.58	1.54	1.38
	E2	305	50.8	2591	2.8	62.1	193.5	1627.2	799.8	1.40	1.18	1.72	1.69	1.53
	CW1	457	50.8	3810	2.9	76.5	561.3	1861.6	1083.2	3.05	1.27	2.58	2.69	2.08
	CW3	457	50.8	3810	5.0	76.5	561.3	1861.6	1065.2	3.05	1.09	2.20	2.41	1.77
	CW2	457	50.8	3810	3.8	76.5	561.3	1861.6	1077.0	3.05	1.15	2.33	2.48	1.88
Elzanaty, Nilson, Slate (1986)	CW4	457	50.8	3810	3.8	78.6	561.3	1861.6	1086.3	3.10	1.17	2.39	2.49	1.90
	CW5	457	50.8	3810	3.8	77.9	561.3	1861.6	1081.8	2.89	1.08	2.22	2.43	1.81
	CW7	457	50.8	3810	3.8	77.6	561.3	1861.6	1124.5	3.03	0.94	1.96	2.08	1.59
	CW6	457	50.8	3810	3.8	77.9	561.3	1861.6	812.9	3.05	1.20	2.08	2.34	1.68
	CW9	457	50.8	3810	3.8	61.0	561.3	1861.6	798.4	3.05	1.15	2.00	1.91	1.56
	CW8	457	50.8	3810	3.8	41.4	561.3	1861.6	806.0	3.05	1.12	2.16	1.99	1.68
	C11	356	76.2	3810	7.8	76.5	561.3	1861.6	1080.4	2.90	0.95	1.24	1.32	1.06
	C13	356	76.2	3810	4.0	76.5	561.3	1861.6	1066.6	2.90	1.12	1.93	1.89	1.42
	C12	356	76.2	3810	5.8	76.5	561.3	1861.6	1075.6	2.90	1.02	1.77	1.81	1.30
	C14	356	76.2	3810	5.8	78.6	561.3	1861.6	1090.1	2.98	1.01	1.71	1.73	1.25
	C15	356	76.2	3810	5.8	77.9	561.3	1861.6	1079.7	2.88	1.04	1.89	1.96	1.50
	C17	356	76.2	3810	5.8	77.6	561.3	1861.6	1121.8	2.87	0.72	1.29	1.31	0.95
	C16	356	76.2	3810	5.8	77.9	561.3	1861.6	812.9	2.90	1.00	1.44	1.55	1.24
	C19	356	76.2	3810	5.8	61.0	561.3	1861.6	797.7	2.90	1.02	1.50	1.42	1.38
	C18	356	76.2	3810	5.8	41.4	561.3	1861.6	807.4	2.90	1.07	1.78	1.63	1.51
Evans, Schumacher (1963)	S44	310	30.5	2134	2.7	32.5	77.4	1516.8	645.3	0.96	1.62	1.88	1.96	1.87
Kar (1969)	I-11	305	76.2	1524	3.3	38.6	193.5	1558.2	652.2	1.11	1.42	1.85	1.81	1.79
	I-14	305	76.2	1524	3.3	34.5	193.5	1558.2	752.2	1.11	1.35	1.75	1.64	1.76
	I-19	305	76.2	1524	3.3	33.8	193.5	1558.2	755.7	1.11	1.25	1.63	1.53	1.64
	I-20	305	76.2	1219	2.8	35.2	193.5	1558.2	551.6	1.18	1.42	1.57	1.55	1.60
	I-21	305	76.2	1727	3.8	35.2	193.5	1558.2	659.8	1.11	1.12	1.43	1.38	1.32
	D2	305	50.8	1524	3.5	35.0	129.0	1558.2	924.6	1.18	1.30	1.61	1.48	1.58
	D3	305	50.8	1092	2.5	30.8	193.5	1627.2	638.5	1.76	2.30	2.98	2.64	2.69
	D4	305	50.8	1727	4.0	34.8	193.5	1627.2	638.5	1.76	1.40	1.76	1.64	1.77

Appendix E: Tested Beams Used for Comparison with Experimental Results (131 PC Beams Without Stirrups)

Authors (year)	Specimen	Geometry and loading information				Concrete f _{pc} (MPa)	Prestressed reinforcement				Test-to-predicted shear strength ratio			
		h (mm)	b _w (mm)	L (mm)	a/d		f _{pu} (MPa)	f _{pe} (MPa)	ρ (%)	ACI 318	AASHTO 2007	CHBDC 2006	Proposed	
Kar (1969)	D5	305	50.8	1524	3.5	30.8	193.5	1627.2	755.7	1.76	1.26	1.77	1.58	1.61
	D7	305	50.8	1727	4.0	34.5	193.5	1627.2	752.2	1.76	1.31	1.79	1.63	1.71
	D8	305	50.8	2159	4.7	34.8	193.5	1627.2	737.7	1.67	1.23	1.57	1.47	1.60
MacGregor (1958)	M15	309	78.7	2743	3.5	21.3	116.1	1551.3	792.9	0.56	1.08	1.47	1.50	1.27
	M16	305	76.2	2743	3.6	20.7	154.8	1551.3	786.0	0.80	1.01	1.36	1.38	1.36
	B.14.34	305	78.7	2743	3.5	18.2	116.1	1758.2	792.9	0.56	1.13	1.51	1.56	1.37
	B.14.41	305	76.2	2743	3.6	19.9	154.8	1758.2	786.0	0.80	1.04	1.41	1.43	1.40
Moayer, Regan (1974)	P10	320	149.9	1981	3.7	41.6	296.8	1882.3	1109.4	0.74	1.33	1.68	1.84	1.57
	P11	320	149.9	1981	3.5	39.0	148.4	1882.3	1139.0	0.35	1.39	1.79	1.70	1.57
	P12	320	149.9	2997	5.3	42.3	148.4	1882.3	1139.0	0.35	1.30	1.40	1.29	1.27
	P15	320	149.9	1981	3.6	44.1	296.8	1882.3	1109.4	0.73	1.30	1.79	1.78	1.57
	P16	320	149.9	2997	5.5	42.7	296.8	1882.3	1109.4	0.73	1.46	1.71	1.64	1.57
	P17	320	149.9	2997	5.6	39.6	296.8	1882.3	1109.4	0.74	1.52	1.83	1.78	1.66
	P47	320	149.9	1981	3.6	42.5	296.8	1882.3	1109.4	0.72	1.29	1.76	1.75	1.62
	P48	320	149.9	1981	3.7	41.2	296.8	1882.3	1049.4	0.74	1.23	1.68	1.69	1.45
	B1434	305	78.7	1829	3.5	21.3	129.0	1758.2	792.9	0.63	1.03	1.38	1.42	1.26
	B1441	305	76.2	1829	3.6	20.7	129.0	1758.2	786.0	0.67	1.17	1.56	1.64	1.46
Olesen (1967)	BD1418	305	72.6	1829	3.6	44.1	129.0	1778.8	848.1	0.69	1.22	1.69	1.73	1.39
	BD1419	305	73.7	1829	3.5	46.3	129.0	1758.2	772.2	0.68	1.16	1.63	1.66	1.26
	BD1423	305	76.2	1829	3.6	29.0	129.0	1765.1	682.6	0.66	0.70	0.96	0.97	0.77
	BD1426	305	76.2	1829	3.6	21.8	129.0	1765.1	799.8	0.66	0.75	1.01	1.03	0.94
	BD1427	305	76.2	1829	3.6	26.5	129.0	1765.1	765.3	0.66	1.13	1.52	1.56	1.32
	BD1434	305	76.2	1829	3.5	18.8	129.0	1765.1	758.4	0.65	1.08	1.45	1.49	1.36
	BD1435	305	74.9	1829	3.6	18.0	129.0	1765.1	744.6	0.67	0.83	1.11	1.14	1.06
	BD1442	305	73.7	1829	3.6	20.5	129.0	1765.1	737.7	0.68	1.24	1.67	1.72	1.55
	BD2432	305	76.2	1829	3.6	21.3	129.0	1765.1	558.5	0.66	1.33	1.81	1.81	1.44
	A1	350	50.0	2007	3.2	55.1	193.5	1985.7	1079.0	1.25	1.11	1.62	1.54	1.49
Radogna (1962)	A2	350	50.0	2007	3.2	58.0	193.5	1985.7	1079.0	1.25	1.15	1.67	1.60	1.55
	A3	335	50.0	2007	3.2	57.1	193.5	1985.7	1079.0	1.25	1.07	1.56	1.49	1.45
	A.11.51	305	152.4	2743	6.4	20.0	161.3	1709.9	786.0	0.49	1.24	1.11	1.05	0.99
Sozen (1957)	A.11.53	305	152.4	2743	6.7	30.1	238.7	1709.9	858.4	0.77	1.30	1.06	0.98	0.92
	A.11.96	305	152.4	2743	6.4	20.0	303.2	1709.9	799.8	0.93	1.19	0.99	0.93	0.88
	A.12.23	305	154.9	2743	3.9	39.0	161.3	1709.9	786.7	0.44	1.25	1.41	1.37	1.20
	A.12.31	305	152.4	2743	4.2	40.0	200.0	1709.9	786.0	0.60	1.23	1.28	1.24	1.08
	A.12.34	305	152.4	2743	4.4	55.1	283.9	1654.7	758.4	0.89	1.30	1.21	1.14	1.01
	A.12.36	305	154.9	2743	3.9	23.7	148.4	1696.1	785.3	0.41	1.20	1.33	1.26	1.11
	A.12.42	305	152.4	2743	4.3	43.2	283.9	1654.7	712.9	0.88	1.31	1.23	1.15	1.04
	A.12.46	305	152.4	2743	4.4	32.1	225.8	1654.7	906.0	0.71	1.26	1.16	1.11	0.97

Appendix E: Tested Beams Used for Comparison with Experimental Results (131 PC Beams Without Stirrups)

Authors (year)	Specimen	Geometry and loading information					Concrete		Prestressed reinforcement				Test-to-predicted shear strength ratio			
		h (mm)	b _w (mm)	L (mm)	a/d	f _{pc} (MPa)	A _p (mm ²)	f _{pu} (MPa)	f _{pe} (MPa)	ρ (%)	ACI 318	AASHTO 2007	CHBDC 2006	Proposed		
Sozen (1957)	A.12.53	305	152.4	2743	4.2	23.4	200.0	1709.9	746.7	0.60	1.30	1.30	1.27	1.09		
	A.12.56	305	152.4	2743	4.2	26.1	232.3	1758.2	830.8	0.70	1.19	1.16	1.15	0.97		
	A.12.69	305	154.9	2743	4.3	20.3	219.4	1709.9	799.8	0.69	1.31	1.19	1.13	0.99		
	A.12.73	305	152.4	2743	4.3	24.5	283.9	1654.7	719.1	0.87	1.27	1.20	1.13	1.01		
	A.12.81	305	152.4	2743	4.2	17.9	232.3	1758.2	826.7	0.69	1.09	1.06	1.06	0.88		
	A.14.39	305	152.4	2134	2.9	23.1	141.9	1709.9	806.7	0.44	1.20	1.39	1.34	1.05		
	A.14.44	305	152.4	2134	2.8	23.1	161.3	1709.9	813.6	0.49	1.18	1.40	1.35	1.04		
	A.14.55	305	152.4	2134	2.8	22.9	200.0	1709.9	806.7	0.61	1.16	1.36	1.31	1.18		
	A.14.68	305	152.4	2134	2.9	16.8	180.6	1709.9	806.7	0.55	1.10	1.26	1.22	1.13		
	B.11.20	305	74.9	2743	5.3	31.2	116.1	1827.1	851.5	0.60	1.17	1.44	1.42	1.23		
	B.11.29	305	74.9	2743	5.4	28.9	154.8	1730.6	854.9	0.81	1.28	1.51	1.50	1.29		
	B.11.40	305	74.9	2743	5.4	31.0	232.3	1730.6	806.7	1.22	1.20	1.37	1.39	1.29		
	B.12.10	305	77.7	2743	3.2	38.6	77.4	1758.2	848.1	0.35	0.93	1.39	1.44	1.07		
	B.12.12	305	76.2	2743	3.2	31.5	77.4	1758.2	861.8	0.36	1.04	1.54	1.58	1.17		
	B.12.14	305	76.2	2743	3.2	26.5	77.4	1758.2	848.1	0.36	1.08	1.57	1.63	1.20		
	B.12.19	305	75.7	2743	3.3	40.6	77.4	1758.2	842.5	0.36	1.02	1.53	1.58	1.20		
	B.12.26	305	77.0	2743	3.6	30.8	148.4	1723.7	758.4	0.75	1.20	1.62	1.65	1.43		
	B.12.29	305	76.2	2743	3.7	28.8	154.8	1827.1	839.1	0.82	1.25	1.63	1.67	1.57		
	B.12.34	305	78.2	2743	3.5	33.3	225.8	1723.7	740.5	1.12	1.08	1.53	1.54	1.48		
	B.12.35	305	78.2	2743	3.6	22.1	154.8	1827.1	834.3	0.78	1.12	1.51	1.53	1.50		
	B.12.50	305	75.2	2743	3.5	20.3	193.5	1730.6	799.8	0.99	0.97	1.62	1.57	1.43		
	B.12.61	305	76.2	2743	3.6	20.5	232.3	1730.6	789.4	1.21	0.94	1.70	1.60	1.45		
	B.13.07	305	75.2	2743	2.5	59.0	77.4	1758.2	875.6	0.37	0.91	1.58	1.68	1.09		
	B.13.16	305	76.2	2743	2.7	38.2	116.1	1730.6	861.8	0.58	1.09	1.53	1.60	1.37		
	B.13.26	305	74.7	2743	2.8	31.7	154.8	1730.6	854.9	0.81	1.19	1.67	1.66	1.56		
	B.13.41	305	73.7	2743	2.8	29.8	232.3	1730.6	817.0	1.24	1.13	1.91	1.78	1.62		
	C.12.09	305	44.5	2743	3.3	44.5	77.4	1758.2	868.7	0.62	1.12	1.68	1.74	1.37		
	C.12.18	305	44.5	2743	3.7	36.6	122.6	1709.9	783.9	1.12	1.33	1.69	1.71	1.74		
	C.12.19	305	45.5	2743	3.6	41.6	148.4	1723.7	766.0	1.27	1.39	1.84	1.85	1.84		
	C.12.32	305	47.2	2743	3.7	25.0	148.4	1654.7	710.2	1.25	1.22	1.71	1.68	1.65		
	C.12.33	305	47.8	2743	3.6	37.7	238.7	1709.9	795.7	1.95	1.25	2.11	1.96	1.78		
	C.12.40	305	44.5	2743	3.7	16.5	122.6	1709.9	796.3	1.12	1.12	1.69	1.61	1.54		
	C.12.44	305	44.5	2743	3.8	19.9	161.3	1709.9	697.1	1.50	1.09	1.66	1.56	1.49		
	C.12.50	305	45.7	2743	3.6	20.8	193.5	1730.6	804.6	1.67	1.18	2.12	1.92	1.79		
	C.12.57	305	46.5	2743	3.6	21.4	232.3	1730.6	806.7	1.99	1.52	2.98	2.59	2.53		
	C.22.40	305	44.5	2743	3.7	31.9	238.7	1709.9	612.3	2.15	1.15	1.78	1.69	1.59		
Zwoyer (1953)	S-4	305	152.4	2743	4.5	21.3	283.9	1654.7	799.8	0.92	1.01	0.87	0.84	0.73		
	S-5	305	152.4	2743	4.3	43.2	283.9	1654.7	712.9	0.88	1.31	1.23	1.17	1.03		

Appendix E: Tested Beams Used for Comparison with Experimental Results (131 PC Beams Without Stirrups)

Authors (year)	Specimen	Geometry and loading information				Concrete	Prestressed reinforcement				Test-to-predicted shear strength ratio				
		h (mm)	b _w (mm)	L (mm)	a/d	f _{pc} (MPa)	A _p (mm ²)	f _{pu} (MPa)	f _{pe} (MPa)	ρ (%)	ACI 318	AASHTO 2007	CHBDC 2006	Proposed	
Zwoyer (1953)	S-6	305	152.4	2743	4.4	55.1	283.9	1654.7	758.4	0.89	1.30	1.21	1.15	1.01	
	S-7	305	152.4	2743	4.3	24.5	283.9	1654.7	719.1	0.87	1.27	1.19	1.14	1.00	
	S-15	305	152.4	2743	4.3	19.9	116.1	1654.7	606.7	0.36	1.27	1.26	1.20	1.09	
	S-16	305	152.4	2743	4.5	24.3	116.1	1654.7	616.4	0.37	1.27	1.22	1.18	1.06	
	S-23	305	152.4	2743	6.7	30.1	238.7	1709.9	858.4	0.77	1.30	1.06	0.99	0.93	
	S-24	305	152.4	2743	6.4	20.0	303.2	1709.9	799.8	0.93	1.19	0.99	0.94	0.88	
	S-25	305	152.4	2743	6.4	20.0	161.3	1709.9	786.0	0.49	1.24	1.13	1.07	1.01	
	S-29	305	152.4	2743	2.8	22.9	200.0	1709.9	806.7	0.61	1.16	1.35	1.33	1.15	
	S-30	305	152.4	2743	2.8	23.1	161.3	1709.9	813.6	0.49	1.18	1.39	1.36	1.04	
	S-31	305	152.4	2743	2.9	16.8	180.6	1709.9	812.9	0.55	1.10	1.25	1.23	1.11	
	S-32	305	152.4	2743	2.9	23.1	141.9	1709.9	806.7	0.44	1.20	1.39	1.36	1.05	
	S-33	305	152.4	2743	4.2	23.4	200.0	1709.9	746.7	0.60	1.30	1.29	1.23	1.08	
	S-34	305	152.4	2743	4.2	40.0	200.0	1709.9	786.0	0.60	1.23	1.26	1.21	1.06	
	S-35	305	44.5	2743	3.8	19.9	161.3	1709.9	697.1	1.50	1.11	1.66	1.57	1.51	
	S-36	305	44.5	2743	3.7	31.9	238.7	1709.9	612.3	2.15	1.17	1.78	1.69	1.61	
	S-37	305	44.5	2743	3.7	16.5	122.6	1709.9	796.3	1.12	1.15	1.69	1.62	1.56	
	S-38	305	44.5	2743	3.7	36.6	122.6	1709.9	783.9	1.12	1.35	1.69	1.71	1.75	
											Mean	1.17	1.57	1.55	1.37
										COV	0.158	0.228	0.232	0.184	

Appendix E: Tested Beams Used for Comparison with Experimental Results (80 RC Beams With at Least Minimum Stirrups)

Authors (year)	Specimen	Geometry and loading information				Concrete f'_c (MPa)	Stirrups		V_{test} (kN)	Test-to-predicted shear strength ratio				Proposed method failure mode
		h (mm)	b_w (mm)	L (mm)	a/d		f_{wy}	ρ_{sv} (%)		ACI 318	AASHTO 2007	CHBTC 2006	Proposed	
Adebar, Collins (1996)	ST5	310	290.1	1600	2.9	49.3	459.9	0.18	169.0	1.05	0.91	0.97	0.90	Conc. crushing
	ST6	310	290.1	1600	2.9	49.3	459.9	0.28	230.1	1.16	1.04	1.11	0.98	Long. reinf. yielding
	ST7	310	290.1	1600	2.9	49.3	459.9	0.28	275.1	1.39	1.24	1.32	1.17	Long. reinf. yielding
	ST18	310	290.1	1600	2.9	49.8	459.9	0.2	246.3	1.46	1.28	1.36	1.21	Conc. crushing
	ST19	310	290.1	1600	2.9	50.8	459.9	0.2	201.4	1.18	1.03	1.10	0.99	Conc. crushing
Clark (1951)	D2-6	381	152.4	3048	2.4	29.5	330.9	0.61	188.4	1.20	0.95	0.96	0.99	Long. reinf. yielding
	D2-7	381	152.4	3048	2.4	28.4	330.9	0.61	157.3	1.13	0.89	0.90	0.93	Long. reinf. yielding
	D2-8	381	152.4	3048	2.4	26.1	330.9	0.61	188.4	1.22	0.97	0.97	1.01	Long. reinf. yielding
	D4-1	381	152.4	3048	2.4	27.4	330.9	0.49	188.4	1.41	1.09	1.10	1.00	Conc. crushing
	D4-2	381	152.4	3048	2.4	25.6	330.9	0.49	157.3	1.33	1.03	1.03	0.95	Conc. crushing
	D4-3	381	152.4	3048	2.4	22.1	330.9	0.49	165.1	1.43	1.12	1.10	1.03	Conc. crushing
	D5-1	381	152.4	3048	2.4	27.7	330.9	0.37	146.2	1.45	1.09	1.10	1.02	Conc. crushing
	D5-2	381	152.4	3048	2.4	29.0	330.9	0.37	157.3	1.55	1.16	1.18	1.09	Conc. crushing
	D5-3	381	152.4	3048	2.4	27.1	330.9	0.37	157.3	1.57	1.18	1.19	1.11	Conc. crushing
	1	610	304.8	4267	3.1	36.4	479.2	0.14	338.1	1.23	0.96	1.03	1.04	Stirrup yielding
	S1-1	350	249.9	1956	2.5	63.6	568.8	0.16	228.3	1.39	1.17	1.16	1.17	Conc. crushing
	S1-2	350	249.9	1956	2.5	63.6	568.8	0.16	208.3	1.27	1.07	1.06	1.06	Conc. crushing
	S1-3	350	249.9	1956	2.5	63.6	568.8	0.16	206.1	1.26	1.05	1.05	1.05	Conc. crushing
Kong, Rangan (1998)	S1-4	350	249.9	1956	2.5	63.6	568.8	0.16	277.9	1.70	1.42	1.41	1.42	Conc. crushing
	S1-5	350	249.9	1956	2.5	63.6	568.8	0.16	253.3	1.55	1.29	1.29	1.29	Conc. crushing
	S1-6	350	249.9	1956	2.5	63.6	568.8	0.16	224.1	1.37	1.15	1.14	1.14	Conc. crushing
	S2-3	350	249.9	1956	2.5	72.5	568.8	0.16	208.3	1.22	1.03	1.03	1.03	Stirrup yielding
	S2-4	350	249.9	1956	2.5	72.5	568.8	0.16	206.1	1.21	1.02	1.02	1.02	Stirrup yielding
	S2-5	350	249.9	1956	2.5	72.5	568.8	0.21	277.9	1.45	1.19	1.25	1.14	Conc. crushing
	S4-1	600	249.9	3099	2.4	87.3	568.8	0.16	354.0	1.06	0.89	0.88	0.89	Stirrup yielding
	S4-2	500	249.9	2642	2.4	87.3	568.8	0.16	572.8	2.09	1.77	1.75	1.77	Stirrup yielding
	S4-3	400	249.9	2159	2.4	87.3	568.8	0.16	243.4	1.14	0.96	0.96	0.98	Stirrup yielding
	S4-4	350	249.9	1956	2.5	87.3	568.8	0.16	253.3	1.40	1.16	1.20	1.21	Stirrup yielding
	S5-1	350	249.9	2261	3.0	87.3	568.8	0.16	224.1	1.24	1.07	1.12	1.10	Stirrup yielding
	S5-2	350	249.9	2108	2.7	87.3	568.8	0.16	259.9	1.44	1.21	1.27	1.26	Stirrup yielding
	S5-3	350	249.9	1956	2.5	87.3	568.8	0.16	243.8	1.35	1.11	1.16	1.16	Stirrup yielding
	S7-3	350	249.9	1930	3.3	74.8	568.8	0.16	246.5	1.43	1.12	1.15	1.18	Stirrup yielding
	S7-4	350	249.9	1930	3.3	74.8	568.8	0.2	273.6	1.44	1.14	1.18	1.13	Conc. crushing
	S7-5	350	249.9	1930	3.3	74.8	568.8	0.22	304.4	1.54	1.22	1.27	1.17	Conc. crushing
	S7-6	350	249.9	1930	3.3	74.8	568.8	0.26	310.6	1.45	1.16	1.21	1.05	Conc. crushing
	S8-3	350	249.9	1956	2.5	74.6	568.8	0.16	309.6	1.80	1.46	1.52	1.53	Stirrup yielding
	S8-4	350	249.9	1956	2.5	74.6	568.8	0.16	265.8	1.55	1.25	1.31	1.31	Stirrup yielding
	S8-5	350	249.9	1956	2.5	74.6	568.8	0.2	289.2	1.54	1.26	1.31	1.22	Conc. crushing

Appendix E: Tested Beams Used for Comparison with Experimental Results (80 RC Beams With at Least Minimum Stirrups)

Authors (year)	Specimen	Geometry and loading information				Concrete f'_c (MPa)	Stirrups		V_{test} (kN)	Test-to-predicted shear strength ratio				Proposed method failure mode
		h (mm)	b_w (mm)	L (mm)	a/d		f_{wy}	ρ_v (%)		ACI 318	AASHTO 2007	CHBDC 2006	Proposed	
Kong, Rangan (1998)	S8-6	350	249.9	1956	2.5	74.6	588.8	0.22	283.9	1.44	1.19	1.24	1.12	Conc. crushing
	Ss2-29a-1	508	254.0	3658	4.0	38.8	423.0	0.11	159.7	0.92	0.85	0.89	0.94	Long. reinf. yielding
	Ss2-29b-1	508	254.0	3658	4.0	37.6	424.0	0.11	160.1	0.93	0.87	0.90	0.94	Long. reinf. yielding
	Ss2-29a-2	508	254.0	3658	4.0	37.2	425.0	0.11	216.6	1.26	1.14	1.19	1.25	Long. reinf. yielding
	Ss2-29b-2	508	254.0	3658	4.0	41.4	426.0	0.11	202.4	1.13	1.04	1.09	1.16	Long. reinf. yielding
Krefeld, Thurston (1996)	Ss2-29c-2	508	254.0	3658	4.0	24.1	372.3	0.11	161.5	1.13	0.95	0.98	0.99	Stirrup yielding
	Ss2-29d-2	508	254.0	3658	4.0	30.4	427.0	0.11	165.0	1.03	0.92	0.96	0.95	Conc. crushing
	Ss2-29g-2	508	254.0	3658	4.0	15.7	372.3	0.11	149.9	1.21	0.99	1.00	1.02	Stirrup yielding
	Ss2-313.5-3	508	254.0	3658	4.0	42.7	430.0	0.16	213.5	1.04	1.06	1.12	1.28	Long. reinf. yielding
	Ss2-318-1	508	254.0	3658	4.0	40.5	517.1	0.12	220.2	1.13	1.00	1.06	1.14	Long. reinf. yielding
	Ss2-318-2	508	254.0	3658	4.0	38.9	428.0	0.12	177.0	0.98	0.91	0.96	1.02	Long. reinf. yielding
	Ss2-321-1	508	254.0	3658	4.0	38.7	517.1	0.11	163.7	0.88	0.77	0.82	0.87	Long. reinf. yielding
	Ss2-321-2	508	254.0	3658	4.0	38.0	429.0	0.11	166.8	0.96	0.89	0.93	1.04	Long. reinf. yielding
	5A-0	600	119.9	5004	2.8	25.7	673.6	0.53	435.0	1.52	1.29	1.30	1.26	Conc. crushing
	5B-0	600	119.9	5004	2.8	26.6	673.6	0.53	435.0	1.52	1.28	1.30	1.24	Conc. crushing
Moayer, Regan (1974)	P5	320	149.9	1981	3.5	43.0	255.1	0.42	145.0	1.56	1.53	1.66	1.36	Long. reinf. yielding
	P20	320	149.9	1981	3.6	40.7	310.3	0.21	120.1	1.63	1.46	1.56	1.44	Stirrup yielding
	P22	320	149.9	2997	5.4	43.3	255.1	0.28	109.0	1.40	1.40	1.55	1.30	Conc. Crushing
Mphonde, Frantz (1985)	B100-3-3	337	152.0	2134	3.6	27.9	400.0	0.26	95.4	1.10	1.04	1.06	1.06	Stirrup yielding
	B100-7-3	337	152.0	2134	3.6	47.1	400.0	0.26	120.5	1.22	1.17	1.20	1.17	Stirrup yielding
	B100-11-3	337	152.0	2134	3.6	68.6	400.0	0.26	151.2	1.38	1.34	1.39	1.33	Stirrup yielding
	B150-3-3	337	152.0	2134	3.6	28.7	400.0	0.38	138.0	1.26	1.27	1.30	1.17	Conc. crushing
	B150-7-3	337	152.0	2134	3.6	46.6	400.0	0.38	133.4	1.11	1.12	1.16	1.05	Conc. crushing
	B150-11-3	337	152.0	2134	3.6	69.6	400.0	0.38	161.6	1.22	1.25	1.31	1.21	Conc. crushing
	B150-15-3	337	152.0	2134	3.6	82.8	400.0	0.38	150.0	1.09	1.12	1.18	1.11	Conc. crushing
Ozcebe, Ersoy, Tankut (1999)	TS39	360	150.1	2261	3.0	73.0	255.1	0.28	179.2	1.80	1.53	1.53	1.46	Stirrup yielding
	TS56	360	150.1	3505	5.0	61.0	433.0	0.24	129.2	1.19	1.28	1.35	1.23	Stirrup yielding
	TS36	360	150.1	2261	3.0	75.0	435.0	0.24	155.9	1.35	1.34	1.37	1.32	Stirrup yielding
	TH39	360	150.1	2261	3.0	73.0	436.0	0.21	142.9	1.31	1.29	1.31	1.27	Stirrup yielding
Rahal, Al-Shaleh (2004)	A65-140	370	200.0	2200	2.8	62.1	437.0	0.20	150.0	1.05	1.09	1.12	1.05	Stirrup yielding
	A65-110	370	200.0	2200	2.8	60.9	438.0	0.26	188.0	1.19	1.28	1.34	1.24	Stirrup yielding
	B65-140	370	200.0	2200	3.0	65.1	439.0	0.17	235.0	1.86	1.64	1.62	1.67	Stirrup yielding
	B65-125	370	200.0	2200	3.0	66.4	440.0	0.19	242.0	1.83	1.61	1.62	1.64	Stirrup yielding
	B65-110	370	200.0	2200	3.0	66.4	441.0	0.22	270.0	1.94	1.74	1.75	1.74	Stirrup yielding
Roller, Russell (1990)	No. 2	679	355.6	2794	2.5	120.1	448.2	0.44	1,097.4	1.45	1.18	1.33	1.23	Long. reinf. yielding
	No. 3	718	355.6	2794	2.5	120.1	457.8	0.89	1,655.0	1.41	1.22	1.25	1.15	Long. reinf. yielding
	No. 4	718	355.6	2794	2.5	120.1	457.8	1.27	1,940.0	1.28	0.98	1.10	1.02	Long. reinf. yielding
	No. 7	870	457.2	4572	3.0	72.4	445.4	0.16	787.9	1.06	1.00	1.04	0.99	Stirrup yielding

Appendix E: Tested Beams Used for Comparison with Experimental Results (80 RC Beams With at Least Minimum Stirrups)

Authors (year)	Specimen	Geometry and loading information				Concrete f'_c (MPa)	Stirrups		V_{test} (kN)	Test-to-predicted shear strength ratio				Proposed method failure mode
		h (mm)	b_w (mm)	L (mm)	a/d		f_{vy}	ρ_v (%)		ACI 318	AASHTO 2007	CHBDC 2006	Proposed	
Roller, Russell (1990)	No. 9	870	457.2	4572	3.0	125.3	431.0	0.16	749.4	0.84	0.76	0.82	0.90	Long. reinf. yielding
	No. 10	870	457.2	4572	3.0	125.3	445.4	0.23	1,172.2	1.16	0.99	1.09	1.06	Stirrup yielding
Yoon, Cook, Mitchell (1996)	N2-N	750	374.9	4293	3.2	36.0	430.2	0.12	483.0	1.30	1.03	1.05	1.10	Stirrup yielding
	M2-S	750	374.9	4293	3.2	67.0	432.0	0.12	552.0	1.19	1.01	1.04	1.07	Stirrup yielding
										Mean	1.15	1.19	1.15	
										COV	0.187	0.176	0.165	

Appendix E: Tested Beams Used for Comparison with Experimental Results (88 PC Beams With at Least Minimum Stirrups)

Authors (year)	Specimen	Geometry and loading information			Concrete f_{pc} (MPa)	Stirrups		V_{test} (kN)	Test-to-predicted shear strength ratio				Proposed method failure mode
		h (mm)	b_w (mm)	L (mm)		f_{vy}	ρ_v (%)		ACI 318	AASHTO 2007	CHBDC 2006	Proposed	
Bennett, Debaiky (1974)	CL-6-240	330	51.1	3607	56.5	279.9	0.25	100.0	1.00	1.78	1.71	1.81	Stirrup yielding
	CM-6-240	330	51.1	3607	56.9	417.8	0.24	100.0	0.95	1.55	1.51	1.60	Stirrup yielding
	CH-6-240	330	51.1	3607	57.8	544.7	0.22	102.5	0.94	1.46	1.44	1.48	Stirrup yielding
	CL-6-160	330	51.1	3607	58.6	279.9	0.39	102.5	0.96	1.51	1.49	1.49	Stirrup yielding
	CM-6-160	330	51.1	3607	61.2	417.8	0.34	111.5	0.99	1.44	1.43	1.45	Stirrup yielding
	CH-6-160	330	51.1	3607	59.3	544.7	0.32	112.0	0.95	1.31	1.31	1.31	Stirrup yielding
	CL-6-80	330	51.1	3607	60.3	279.9	0.72	116.0	0.95	1.26	1.25	1.23	Stirrup yielding
	CM-6-80	330	51.1	3607	59.5	417.8	0.7	126.0	0.93	1.11	1.12	1.12	Stirrup yielding
	CH-6-80	330	51.1	3607	55.9	544.7	0.64	140.0	0.98	1.14	1.18	1.14	Stirrup yielding
	NL-6-240	330	51.1	3607	41.2	279.9	0.25	82.4	0.87	1.69	1.57	1.57	Stirrup yielding
	NM-6-240	330	51.1	3607	38.5	417.8	0.24	89.0	0.90	1.61	1.51	1.51	Stirrup yielding
	NH-6-240	330	51.1	3607	35.4	544.7	0.22	89.0	0.89	1.54	1.43	1.40	Stirrup yielding
	NL-6-160	330	51.1	3607	39.1	279.9	0.39	90.5	0.90	1.59	1.48	1.41	Stirrup yielding
	NM-6-160	330	51.1	3607	38.2	417.8	0.35	93.5	0.89	1.40	1.33	1.31	Stirrup yielding
	NH-6-160	330	51.1	3607	38.8	544.7	0.32	105.0	0.95	1.44	1.36	1.34	Stirrup yielding
	NL-6-80	330	51.1	3607	39.8	279.9	0.77	106.4	0.91	1.28	1.21	1.18	Stirrup yielding
	NM-6-80	330	51.1	3607	37.1	416.4	0.7	106.0	0.83	1.10	1.00	1.05	Stirrup yielding
	NH-6-80	330	51.1	3607	38.7	544.7	0.64	114.0	0.83	1.04	0.95	1.03	Stirrup yielding
	NM-8-240	330	51.1	3607	35.3	419.9	0.41	80.0	0.74	1.15	1.06	1.05	Stirrup yielding
	NM-8-160	330	51.1	3607	41.0	419.9	0.62	93.0	0.75	1.00	0.93	0.95	Stirrup yielding
	NL-10-240	330	51.1	3607	39.3	279.9	0.58	93.5	0.86	1.33	1.25	1.19	Stirrup yielding
	NM-10-240	330	51.1	3607	40.6	410.2	0.65	95.8	0.77	1.02	0.95	0.97	Stirrup yielding
	NL-10-160	330	51.1	3607	38.5	279.9	0.88	102.5	0.85	1.16	1.08	1.08	Stirrup yielding
	NM-10-160	330	51.1	3607	38.2	410.2	0.97	102.5	0.71	0.89	0.85	0.87	Stirrup yielding
	PL-6-240	330	51.1	3607	44.2	279.9	0.26	89.0	0.92	1.74	1.63	1.65	Stirrup yielding
	PM-6-240	330	51.1	3607	43.1	417.8	0.24	84.5	0.84	1.47	1.39	1.41	Stirrup yielding
	PH-6-240	330	51.1	3607	42.1	544.7	0.22	81.0	0.78	1.31	1.24	1.23	Stirrup yielding
	PL-6-160	330	51.1	3607	42.1	279.9	0.39	98.0	0.96	1.65	1.57	1.50	Stirrup yielding
	PM-6-160	330	51.1	3607	42.2	417.8	0.35	96.0	0.89	1.42	1.34	1.31	Stirrup yielding
	PH-6-160	330	51.1	3607	40.4	544.7	0.32	93.5	0.84	1.26	1.20	1.18	Stirrup yielding
	PL-6-80	330	51.1	3607	43.8	279.9	0.77	106.0	0.89	1.23	1.18	1.15	Stirrup yielding
	PM-6-80	330	51.1	3607	43.8	417.8	0.7	114.5	0.88	1.12	1.05	1.08	Stirrup yielding
	PH-6-80	330	51.1	3607	40.8	544.7	0.64	102.5	0.74	0.93	0.85	0.91	Stirrup yielding
Durrani, Robertson (1987)	3	508	76.2	3353	46.1	503.3	0.14	154.4	1.70	1.67	1.62	1.64	Stirrup yielding
	4	508	76.2	3353	44.1	503.3	0.14	165.3	1.79	1.70	1.65	1.71	Stirrup yielding

Appendix E: Tested Beams Used for Comparison with Experimental Results (88 PC Beams With at Least Minimum Stirrups)

Authors (year)	Specimen	Geometry and loading information			Concrete f_{pc} (MPa)	Stirrups		V_{test} (kN)	Test-to-predicted shear strength ratio				Proposed method failure mode
		h (mm)	b_w (mm)	L (mm)		f_{vy}	ρ_v (%)		ACI 318	AASHTO 2007	CHBDC 2006	Proposed	
Durrani, Robertson (1987)	5	508	76.2	3353	44.6	444.0	0.18	167.0	1.76	1.55	1.65	1.60	Stirrup yielding
	8	508	76.2	3353	39.4	388.9	0.22	170.4	1.82	1.65	1.66	1.66	Stirrup yielding
	9	508	76.2	3353	41.8	518.5	0.22	172.4	1.70	1.62	1.62	1.56	Stirrup yielding
	10	508	76.2	3353	42.0	388.9	0.22	172.4	1.82	1.74	1.67	1.67	Stirrup yielding
Elzanaty, Nilson, Slate (1986)	CW 16	457	50.8	3810	73.1	434.4	0.55	186.8	1.23	1.42	1.45	1.44	Stirrup yielding
	CW 17	457	50.8	3810	69.6	434.4	0.3	142.3	1.09	1.45	1.50	1.57	Stirrup yielding
	CI 10	356	76.2	3810	73.1	434.4	0.46	141.5	1.12	1.36	1.38	1.19	Conc. crushing
	CI 11	356	76.2	3810	55.8	434.4	0.46	127.2	1.04	1.27	1.30	1.13	Conc. crushing
	CI 12	356	76.2	3810	40.0	434.4	0.46	122.3	1.04	1.28	1.28	1.16	Conc. crushing
	CI 13	356	76.2	3810	72.4	434.4	0.46	154.8	1.06	1.31	1.34	1.23	Stirrup yielding
	CI 14	356	76.2	3810	73.8	434.4	0.73	164.6	0.97	1.19	1.22	1.09	Conc. crushing
	CI 15	356	76.2	3810	70.3	434.4	0.46	121.0	0.97	1.17	1.20	1.03	Conc. crushing
	CI 16	356	76.2	3810	73.1	434.4	0.46	118.8	0.81	0.96	0.96	0.93	Stirrup yielding
	CI 17	356	76.2	3810	69.6	434.4	0.25	129.4	1.01	1.27	1.25	1.43	Stirrup yielding
	CW 10	457	50.8	3810	73.1	434.4	0.55	173.5	1.29	1.46	1.47	1.39	Stirrup yielding
	CW 11	457	50.8	3810	55.8	434.4	0.55	156.6	1.22	1.39	1.39	1.34	Stirrup yielding
	CW 12	457	50.8	3810	40.0	434.4	0.55	140.6	1.15	1.32	1.28	1.29	Stirrup yielding
	CW 13	457	50.8	3810	72.4	434.4	0.55	182.4	1.21	1.40	1.41	1.40	Stirrup yielding
	CW 14	457	50.8	3810	73.8	434.4	0.79	187.7	1.09	1.21	1.22	1.16	Conc. crushing
	CW 15	457	50.8	3810	70.3	434.4	0.55	150.3	1.13	1.28	1.29	1.22	Stirrup yielding
Gregor, Collins (1995)	CM5_A	900	150.1	2261	57.8	615.7	0.46	926.0	1.40	1.32	1.37	1.30	Conc. crushing
	CM6_A	900	150.1	2261	56.9	615.7	0.46	998.0	1.36	1.35	1.39	1.36	Conc. crushing
Kaufman, et al. (1988)	II-1	914	152.4	6096	62.7	338.5	0.33	622.8	0.89	1.09	1.03	1.17	Stirrup yielding
	1E	1854	152.4	15240	70.9	482.6	0.56	2544.4	1.17	1.13	1.16	1.12	Stirrup yielding
	1W	1854	152.4	15240	70.9	482.6	0.56	2944.6	1.36	1.21	1.23	1.19	Stirrup yielding
	2E	1854	152.4	15240	68.5	546.8	0.94	3304.8	1.15	1.07	1.07	1.05	Stirrup yielding
	2W	1854	152.4	15240	68.5	546.8	0.94	3789.2	1.31	1.16	1.16	1.14	Stirrup yielding
	3E	1854	152.4	15240	98.1	467.5	0.83	3491.7	1.26	1.16	1.20	1.20	Stirrup yielding
	3W	1854	152.4	15240	98.1	467.5	0.83	3799.0	1.37	1.27	1.31	1.31	Stirrup yielding
	5E	1854	152.4	15240	122.7	635.7	0.18	2318.3	1.26	1.33	1.29	1.45	Stirrup yielding
	5W	1854	152.4	15240	122.7	527.4	0.18	1947.4	1.09	1.22	1.15	1.32	Stirrup yielding
	6E	1854	152.4	15240	122.7	446.1	0.86	3384.0	1.16	1.13	1.13	1.11	Stirrup yielding
Lyngberg (1976)	6W	1854	152.4	15240	122.7	446.1	0.86	2723.5	1.07	1.37	1.45	1.31	Long. reinf. yielding
	2A-3	600	119.9	5004	32.6	615.7	0.53	506.0	1.28	1.46	1.48	1.34	Conc. crushing
	2B-3	600	119.9	5004	33.9	642.6	0.53	515.0	1.27	1.46	1.48	1.32	Conc. crushing

Appendix E: Tested Beams Used for Comparison with Experimental Results (88 PC Beams With at Least Minimum Stirrups)

Authors (year)	Specimen	Geometry and loading information			Concrete f_{pc} (MPa)	Stirrups		V_{test} (kN)	Test-to-predicted shear strength ratio				Proposed method failure mode
		h (mm)	b_w (mm)	L (mm)		f_{vy}	ρ_v (%)		ACI 318	AASHTO 2007	CHBDC 2006	Proposed	
Lyngberg (1976)	3A-2	600	119.9	5004	31.1	662.6	0.53	489.0	1.28	1.41	1.42	1.26	Conc. crushing
	3B-2	600	119.9	5004	27.5	624.7	0.53	433.0	1.19	1.30	1.31	1.24	Conc. crushing
	4A-1	600	119.9	5004	31.5	639.1	0.53	469.0	1.34	1.40	1.41	1.24	Conc. crushing
	4B-1	600	119.9	5004	30.4	657.8	0.53	454.0	1.28	1.34	1.35	1.23	Conc. crushing
MacGregor (1960)	FW14.06	356	44.5	2743	27.0	253.7	0.95	81.0	1.15	1.42	1.43	1.24	Conc. crushing
Malone, Ramierz (2000)	PC6S	813	151.9	4877	44.8	502.6	0.18	520.0	1.05	1.52	1.54	1.48	Stirrup yielding
Malone, Ramierz (2000)	PC10S	813	151.9	4877	69.6	502.6	0.18	534.0	1.01	1.43	1.43	1.41	Stirrup yielding
Shahawy, Batchelor (1991)	A1-00-M_N	1118	152.4	12192	50.3	482.6	0.37	627.2	0.72	0.92	0.93	0.83	Stirrup yielding
	A1-00-M_S	1118	152.4	9601	50.3	482.6	0.37	747.3	0.86	1.21	1.26	1.12	Conc. crushing
	A1-00-R/2_N	1118	152.4	12192	49.0	482.6	0.42	738.4	0.82	1.04	1.06	0.95	Stirrup yielding
	A1-00-R/2_S	1118	152.4	9601	49.0	482.6	0.38	769.5	0.88	1.24	1.30	1.13	Long. reinf. yielding
	A1-00-R_N	1118	152.4	12192	49.0	482.6	0.83	934.1	0.78	1.02	1.08	0.98	Long. reinf. yielding
	B0-00-R_N	1118	152.4	12192	51.4	482.6	0.83	978.6	0.80	1.05	1.11	1.00	Long. reinf. yielding
	B0-00-R_S	1118	152.4	9601	51.4	482.6	0.38	916.3	1.03	1.45	1.50	1.32	Long. reinf. yielding
	AR05908X	1290	149.9	18593	54.9	413.7	1.17	2800.0	1.32	1.36	1.36	1.36	Stirrup yielding
Zhongguo, Maher, Baishya (2002)	AVW14408X	1290	149.9	18593	54.9	413.7	1.19	3082.7	1.68	1.69	1.58	1.56	Stirrup yielding
	BVW20408X	1290	149.9	18593	66.5	551.6	1.7	2623.6	1.25	0.97	0.97	0.97	Stirrup yielding
	AVW14608Y	1290	149.9	18593	54.9	413.7	0.8	2045.7	1.33	1.43	1.39	1.30	Stirrup yielding
								Mean	1.08	1.32	1.31	1.27	
								COV	0.248	0.160	0.158	0.167	

Appendix E: Tested Beams Used for Comparison with Experimental Results (76 RC Beams With Less than Minimum Stirrups)

Authors (year)	Specimen	Geometry and loading information				Concrete f'_c (MPa)	Stirrups		V_{test} (kN)	Test-to-predicted shear strength ratio for proposed method	
		h (mm)	b_w (mm)	L (mm)	a/d		f_{vy}	ρ_v (%)		without linear interpolation	with linear interpolation
Angelakos, Bentz, Collins (2001)	DB120M	1000	300.0	5410	2.9	21.0	508.1	0.08	282.0	0.80	0.80
	DB140M	1000	300.0	5410	2.9	38.0	508.1	0.08	277.0	0.81	0.81
	DB165M	1000	300.0	5410	2.9	65.0	508.1	0.08	452.0	1.85	1.32
	DB180M	1000	300.0	5410	2.9	80.0	508.1	0.08	395.0	1.53	1.15
	DBO530M	1000	300.0	5410	2.9	32.0	508.1	0.08	263.0	1.25	1.25
Collins, Kuchma (1999)	BM100	1000	300.0	5410	2.9	47.0	508.1	0.08	342.0	1.73	1.09
	BM100D	1000	300.0	5410	2.9	47.0	508.1	0.08	461.0	1.65	0.97
	SE100A-M-69	1000	294.9	4597	2.5	71.0	521.9	0.15	516.3	1.11	1.11
	SE100B-M-69	1000	294.9	4597	2.5	75.0	521.9	0.15	583.2	1.03	1.03
	S2-3	350	249.9	1956	2.5	72.5	568.8	0.16	208.3	1.03	1.03
Kong, Rangan (1998)	S2-4	350	249.9	1956	2.5	72.5	568.8	0.16	206.1	1.02	1.02
	S4-1	600	249.9	3099	2.4	87.3	568.8	0.16	354.0	0.89	0.89
	S4-2	500	249.9	2642	2.4	87.3	568.8	0.16	572.8	1.77	1.77
	S4-3	400	249.9	2159	2.4	87.3	568.8	0.16	243.4	0.97	0.97
	S4-4	350	249.9	1956	2.5	87.3	568.8	0.16	253.3	1.21	1.21
	S5-1	350	249.9	2261	3.0	87.3	568.8	0.16	224.1	1.10	1.10
	S5-2	350	249.9	2108	2.7	87.3	568.8	0.16	259.9	1.26	1.26
	S5-3	350	249.9	1956	2.5	87.3	568.8	0.16	243.8	1.16	1.16
	S7-3	350	249.9	1930	3.3	74.8	568.8	0.16	246.5	1.18	1.18
	S8-3	350	249.9	1956	2.5	74.6	568.8	0.16	309.6	1.53	1.53
	S8-4	350	249.9	1956	2.5	74.6	568.8	0.16	265.8	1.31	1.31
	Ss2-213.5-1	508	254.0	3658	4.0	38.9	341.3	0.07	148.1	1.18	0.97
	Ss2-218a-2	508	254.0	3658	4.0	37.6	372.3	0.05	164.1	1.32	1.18
	Ss2-231.5a-2	508	254.0	3658	4.0	37.0	372.3	0.07	161.5	1.30	1.04
	Ss2-29-3	508	254.0	3658	4.0	34.3	237.2	0.11	177.9	1.48	1.11
Krefeld, Thurston (1996)	Ss2-29a-1	508	254.0	3658	4.0	38.8	341.3	0.11	159.7	0.95	0.95
	Ss2-29a-2	508	254.0	3658	4.0	37.2	372.3	0.11	216.6	1.25	1.25
	Ss2-29-b1	508	254.0	3658	4.0	37.6	341.3	0.11	160.1	0.95	0.95
	Ss2-29b-2	508	254.0	3658	4.0	41.4	372.3	0.11	202.4	1.16	1.16
	Ss2-29c-2	508	254.0	3658	4.0	24.1	372.3	0.11	161.5	1.00	1.00
	Ss2-29d-2	508	254.0	3658	4.0	30.4	372.3	0.11	165.0	0.95	0.95
	Ss2-29e-2	508	254.0	3658	4.0	48.5	372.3	0.11	206.4	1.52	1.26
	Ss2-29g-2	508	254.0	3658	4.0	15.7	372.3	0.11	149.9	1.02	1.02
	Ss2-313.5-3	508	254.0	3658	4.0	42.7	275.8	0.16	213.5	1.28	1.28
	Ss2-318-1	508	254.0	3658	4.0	40.5	517.1	0.12	220.2	1.14	1.14
	Ss2-318-2	508	254.0	3658	4.0	38.9	351.6	0.12	177.0	1.02	1.02
	Ss2-213.5-1	508	254.0	3658	4.0	38.9	341.3	0.07	148.1	1.18	0.97

Appendix E: Tested Beams Used for Comparison with Experimental Results (76 RC Beams With Less than Minimum Stirrups)

Authors (year)	Specimen	Geometry and loading information				Concrete f'_c (MPa)	Stirrups		V_{test} (kN)	Test-to-predicted shear strength ratio for proposed method	
		h (mm)	b_w (mm)	L (mm)	a/d		f_{vy}	ρ_v (%)		without linear interpolation	with linear interpolation
Krefeld, Thurston (1996)	Ss2-318-3	508	254.0	3658	4.0	43.0	275.8	0.12	174.8	1.34	0.95
	Ss2-321-1	508	254.0	3658	4.0	38.7	517.1	0.11	163.7	0.87	0.87
	Ss2-321-2	508	254.0	3658	4.0	38.0	351.6	0.11	166.8	1.04	1.04
	Ss2-321-3	508	254.0	3658	4.0	43.0	275.8	0.11	140.6	1.08	0.79
Moayer, Regan (1974)	P20	320	149.9	1981	3.6	40.7	310.3	0.21	120.1	1.44	1.44
	P21	320	149.9	2997	5.4	42.8	310.3	0.14	89.9	1.28	1.28
Mphonde, Frantz (1985)	B100-11-3	337	152.0	2134	3.6	68.6	269.2	0.26	151.2	1.33	1.33
	B100-15-3	337	152.0	2134	3.6	82.0	269.2	0.26	115.8	0.98	0.98
	B100-7-3	337	152.0	2134	3.6	47.1	269.2	0.26	120.5	1.17	1.17
	ACI36	360	150.1	2261	3.0	75.0	255.1	0.14	105.3	1.34	1.10
Ozcebe, Ersoy, Tankut (19999)	ACI39	360	150.1	2261	3.0	73.0	255.1	0.14	111.8	1.38	1.14
	ACI56	360	150.1	3505	5.0	58.0	255.1	0.14	93.6	1.47	1.10
	ACI59	360	150.1	3505	5.0	82.0	255.1	0.14	96.5	1.25	1.01
	TH36	360	150.1	2261	3.0	75.0	255.1	0.17	141.0	1.79	1.37
	TH39	360	150.1	2261	3.0	73.0	255.1	0.21	142.9	1.27	1.27
	TH56	360	150.1	3505	5.0	63.0	255.1	0.17	103.5	1.57	1.09
	TH59	360	150.1	3505	5.0	75.0	255.1	0.19	119.3	1.59	1.12
	TS36	360	150.1	2261	3.0	75.0	255.1	0.24	155.9	1.32	1.32
	TS39	360	150.1	2261	3.0	73.0	255.1	0.28	179.2	1.46	1.46
	TS56	360	150.1	3505	5.0	61.0	255.1	0.24	129.2	1.23	1.23
	TS59	360	150.1	3505	5.0	82.0	255.1	0.28	125.4	1.06	1.06
	A65-110	370	200.0	2200	2.8	60.9	240.0	0.257083	188.0	1.24	1.24
	A65-140	370	200.0	2200	2.8	62.1	240.0	0.202083	150.0	1.05	1.05
	A65-200	370	200.0	2200	2.8	60.9	240.0	0.14125	175.0	1.78	1.42
Rahal, Al-Shaleh (2004)	A65-95	370	200.0	2200	2.8	62.1	240.0	0.2975	220.0	1.38	1.38
	B65-110	370	200.0	2200	3.0	66.4	305.0	0.218033	270.0	1.74	1.74
	B65-125	370	200.0	2200	3.0	66.4	305.0	0.192131	242.0	1.64	1.64
	B65-140	370	200.0	2200	3.0	65.1	305.0	0.171475	235.0	1.67	1.67
	B65-160	370	200.0	2200	3.0	65.1	305.0	0.150164	208.0	1.97	1.56
	B65-200	370	200.0	2200	3.0	64.3	305.0	0.12	195.0	1.85	1.57
	No. 1	635	355.6	2794	2.5	120.1	406.8	0.08	297.3	0.90	0.88
	No. 6	870	457.2	4572	3.0	72.4	445.4	0.08	665.4	1.59	1.15
Roller, Russel (1990)	No. 7	870	457.2	4572	3.0	72.4	445.4	0.16	787.9	1.00	1.00
	No. 9	870	457.2	4572	3.0	125.3	445.4	0.16	749.4	0.90	0.90
	No. 10	870	457.2	4572	3.0	125.3	445.4	0.23	1172.2	1.09	1.06
Yoon, Cook, Mitchel (1996)	M1-N	750	374.9	4293	3.2	67.0	430.2	0.08	405.0	1.23	0.95

Appendix E: Tested Beams Used for Comparison with Experimental Results (76 RC Beams With Less than Minimum Stirrups)

Authors (year)	Specimen	Geometry and loading information				Concrete f'_c (MPa)	Stirrups		V_{test} (kN)	Test-to-predicted shear strength ratio for proposed method	
		h (mm)	b_w (mm)	L (mm)	a/d		f_{vy}	ρ_v (%)		without linear interpolation	with linear interpolation
Yoon, Cook, Mitchel (1996)	M2-S	750	374.9	4293	3.2	67.0	430.2	0.12	552.0	1.07	1.07
	N1-N	750	374.9	4293	3.2	36.0	430.2	0.08	457.0	1.60	1.20
	N2-N	750	374.9	4293	3.2	36.0	430.2	0.12	483.0	1.10	1.10
	N2-S	750	374.9	4293	3.2	36.0	430.2	0.08	363.0	1.27	0.96
									Mean	1.28	1.16
									COV	0.221	0.188

Appendix F: Comparison of Predictions with Beam Test Results (Beams Without Stirrups)

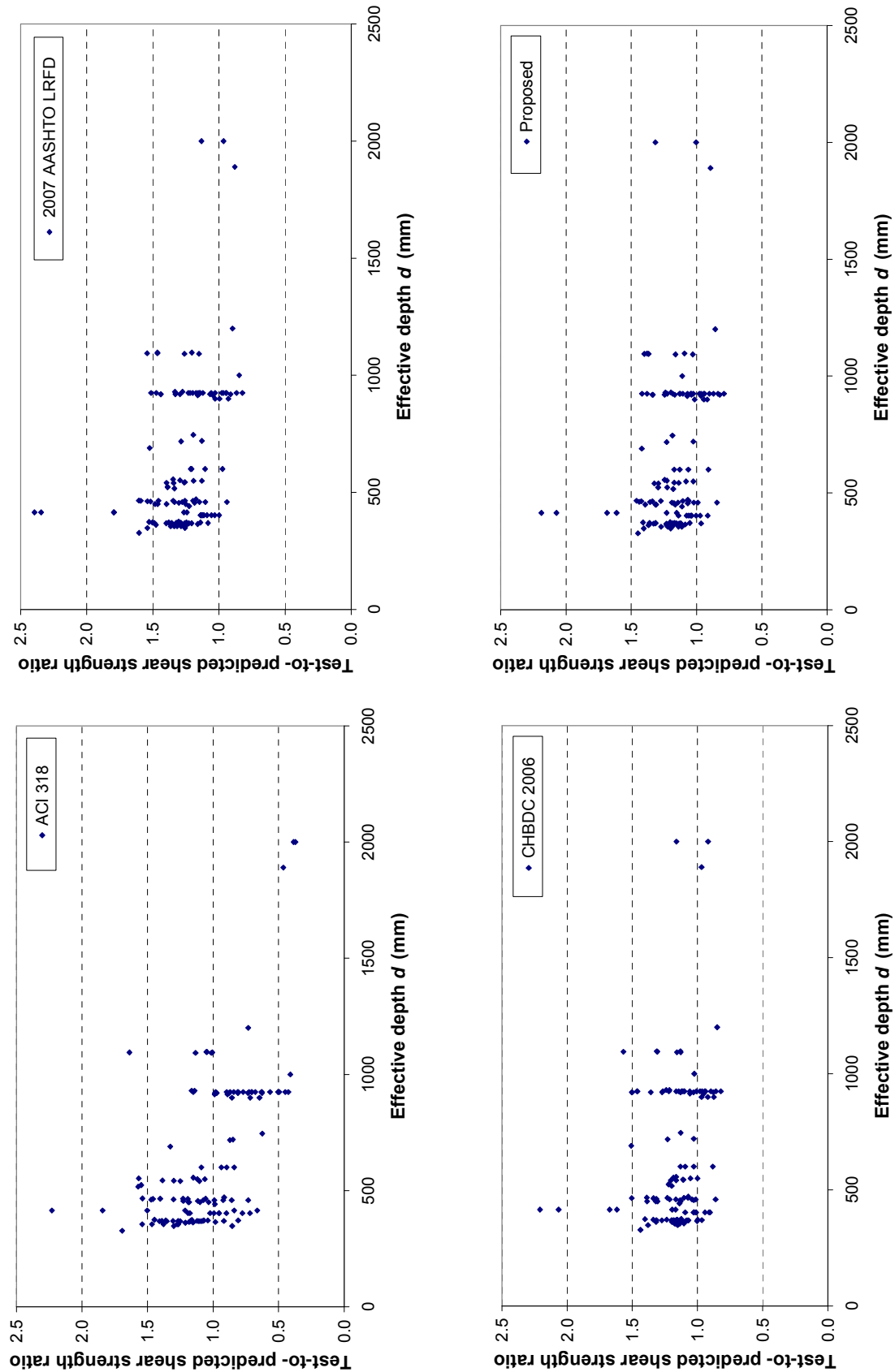


Fig. F-1 Variation of test-to-predicted shear strength ratios of 132 RC beams with effective depth.

Appendix F: Comparison of Predictions with Beam Test Results (Beams Without Stirrups)

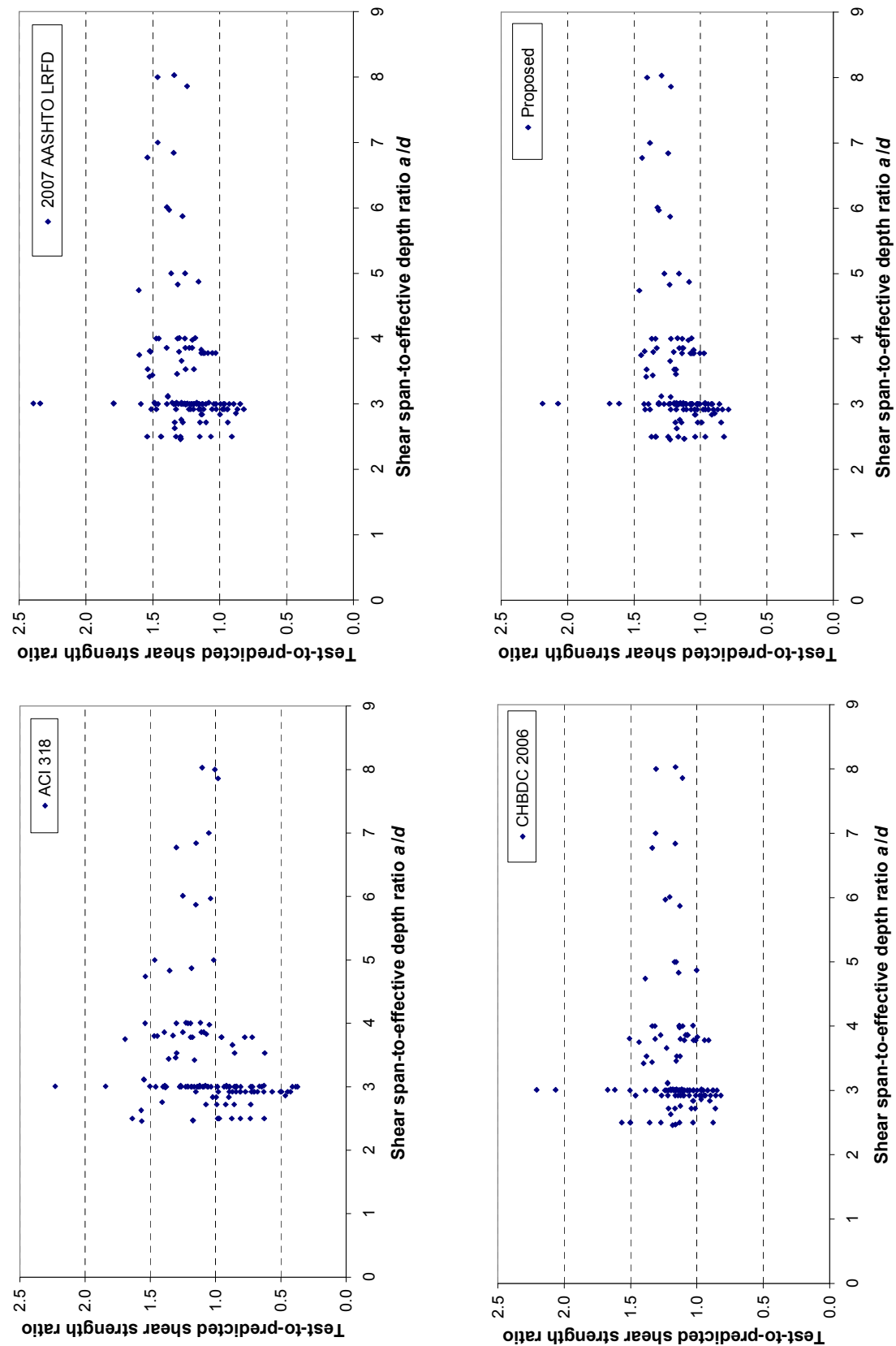


Fig. F-2 Variation of test-to-predicted shear strength ratios of 132 RC beams with shear span to effective depth ratio.

Appendix F: Comparison of Predictions with Beam Test Results (Beams Without Stirrups)

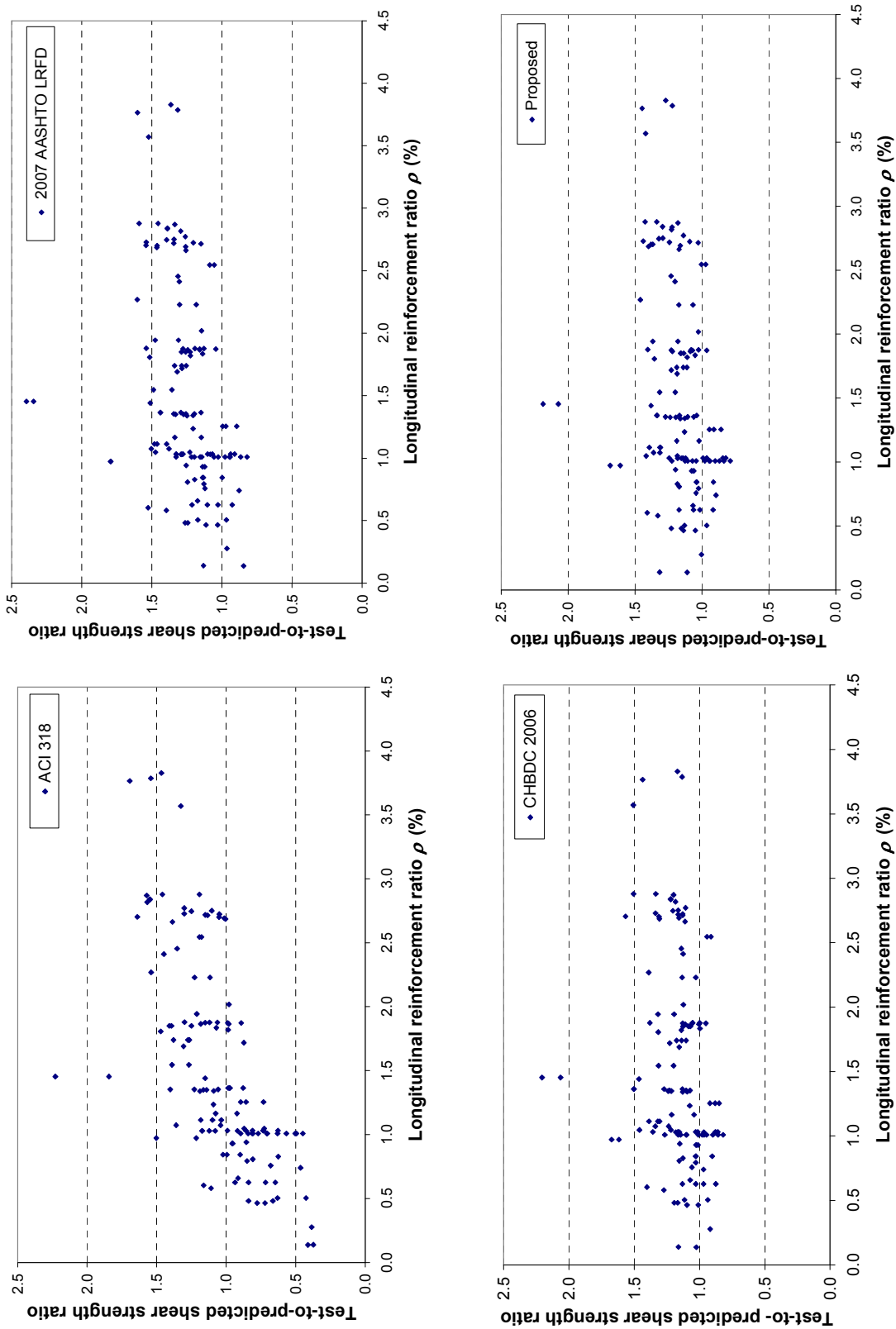


Fig. F-3 Variation of test-to-predicted shear strength ratios of 132 RC beams with longitudinal reinforcement ratio.

Appendix F: Comparison of Predictions with Beam Test Results (Beams Without Stirrups)

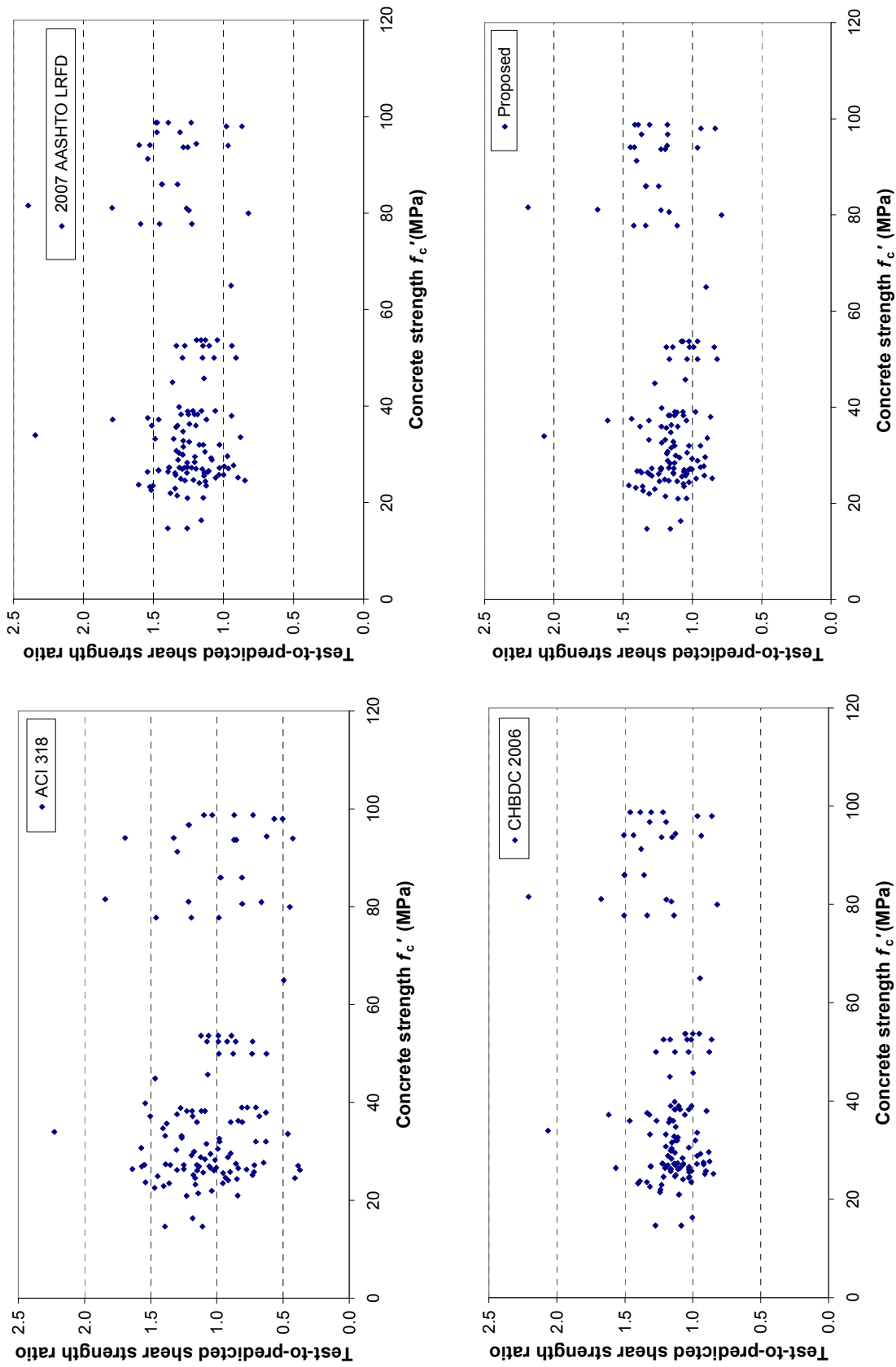


Fig. F-4 Variation of test-to-predicted shear strength ratios of 132 RC beams with concrete compressive strength.

Appendix F: Comparison of Predictions with Beam Test Results (Beams Without Stirrups)

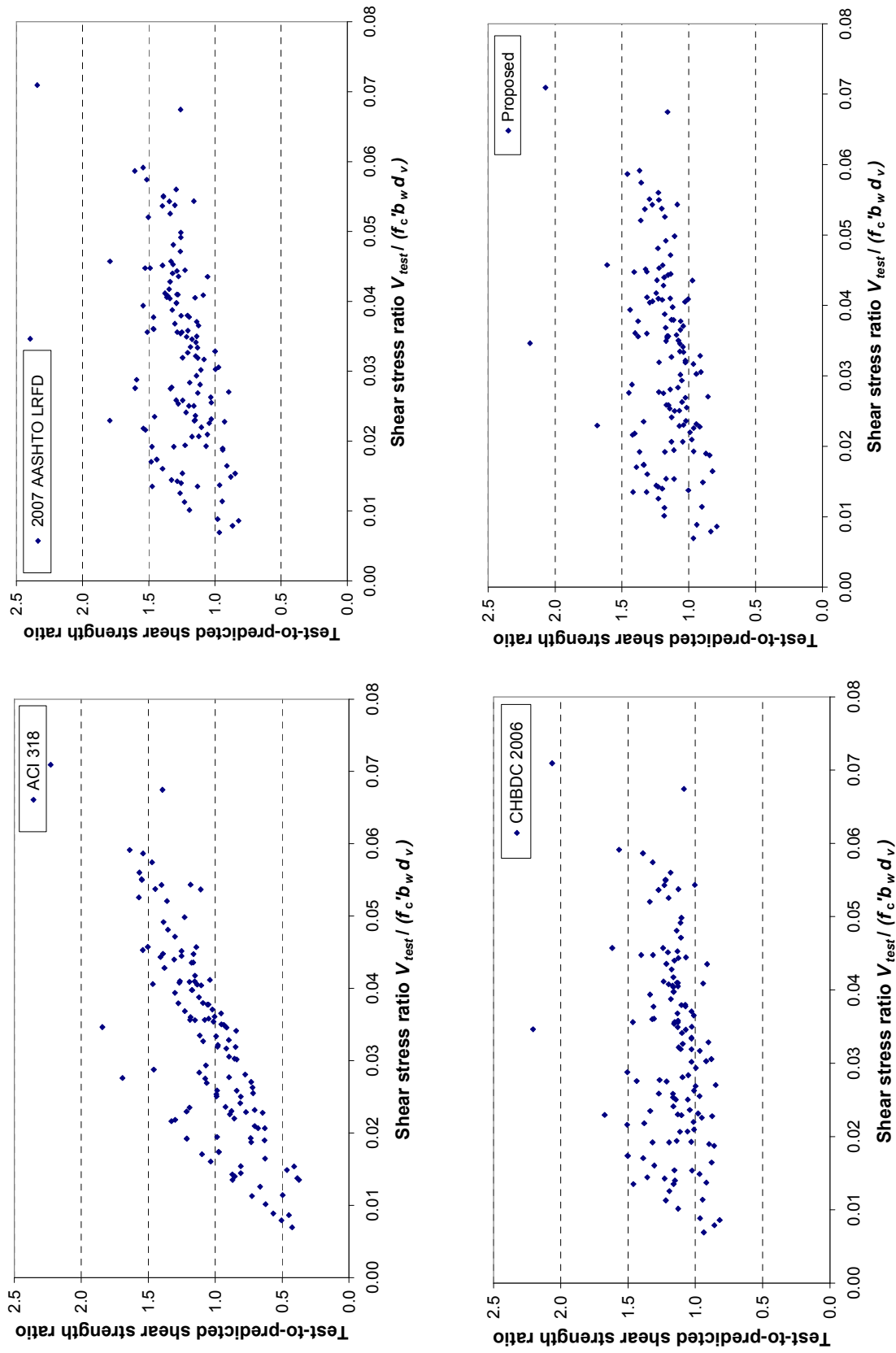


Fig. F-5 Variation of test-to-predicted shear strength ratios of 132 RC beams with shear stress ratio.

Appendix F: Comparison of Predictions with Beam Test Results (Beams Without Stirrups)

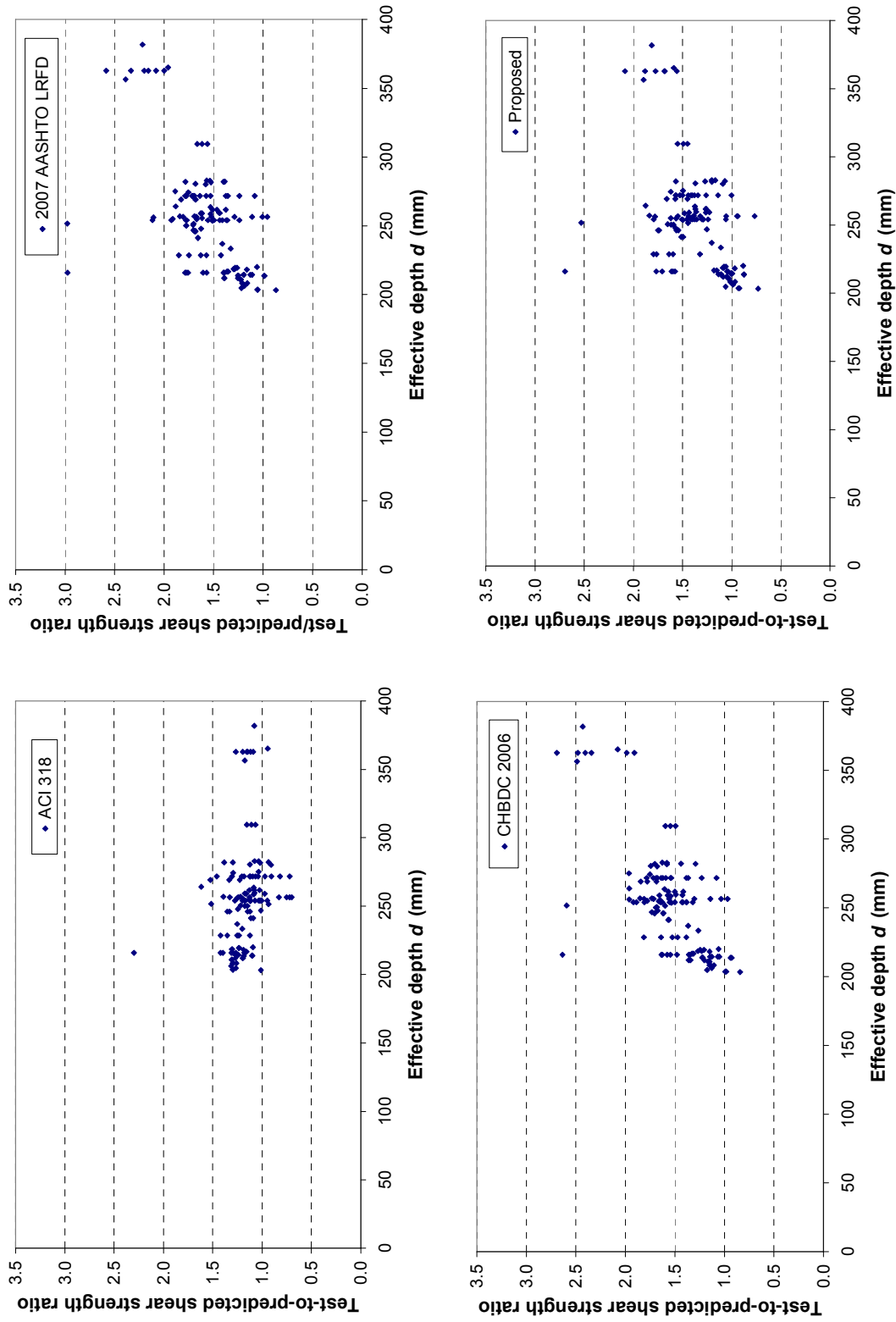


Fig. F-6 Variation of test-to-predicted shear strength ratios of 131 PC beams with effective depth.

Appendix F: Comparison of Predictions with Beam Test Results (Beams Without Stirrups)

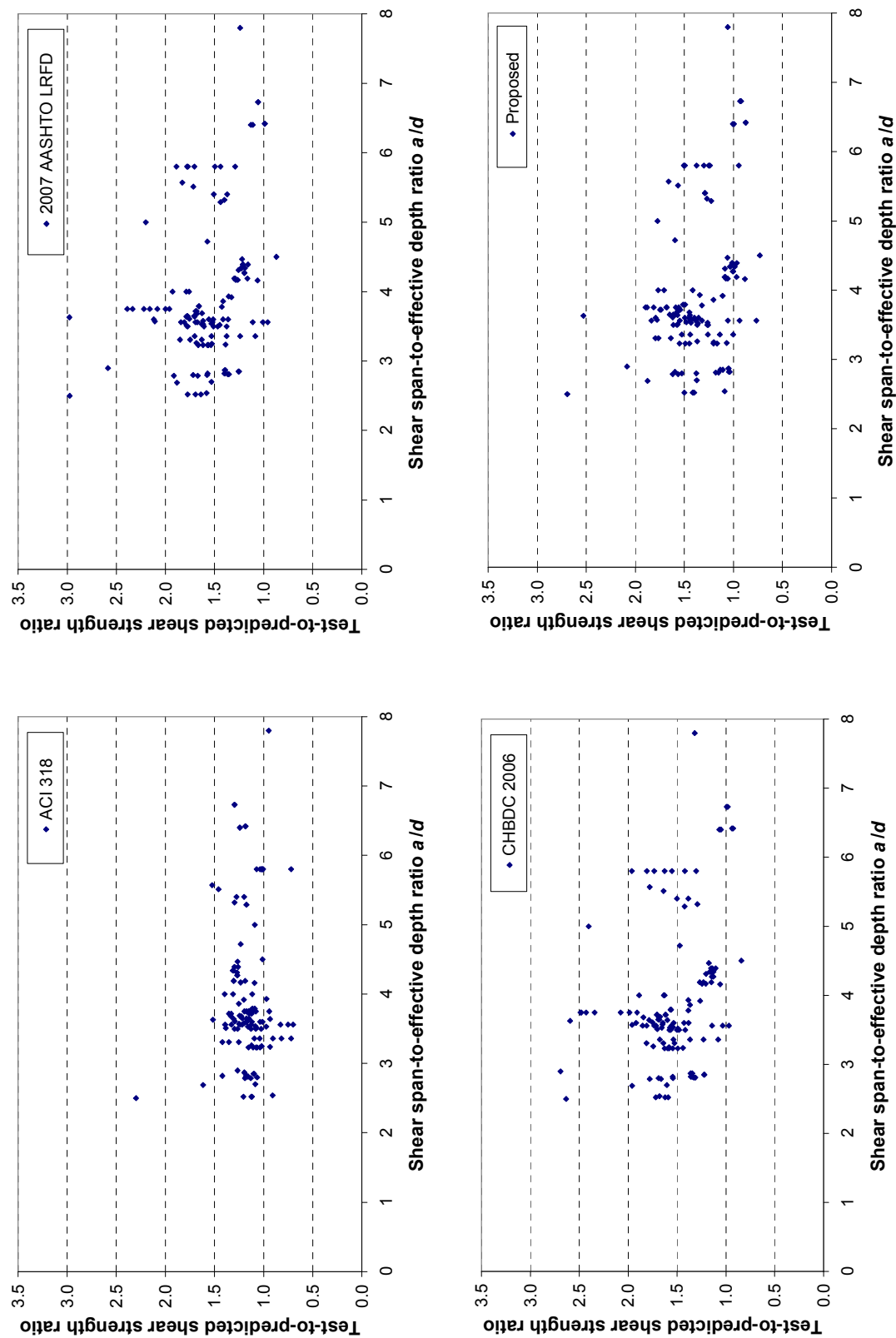


Fig. F-7 Variation of test-to-predicted shear strength ratios of 131 PC beams with shear span-to-effective depth ratio.

Appendix F: Comparison of Predictions with Beam Test Results (Beams Without Stirrups)

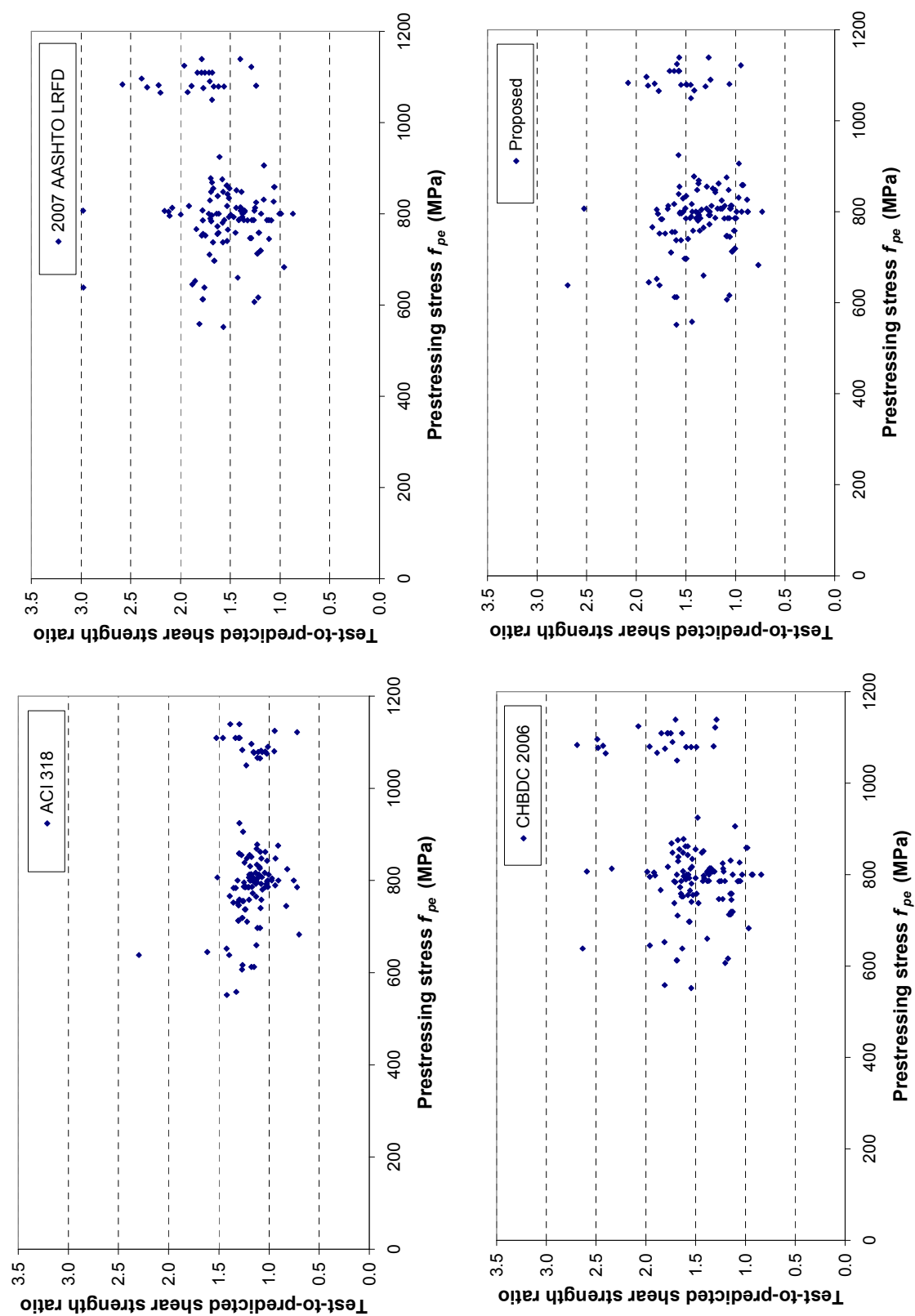


Fig. F-8 Variation of test-to-predicted shear strength ratios of 131 PC beams with effective prestressing stress.

Appendix F: Comparison of Predictions with Beam Test Results (Beams Without Stirrups)

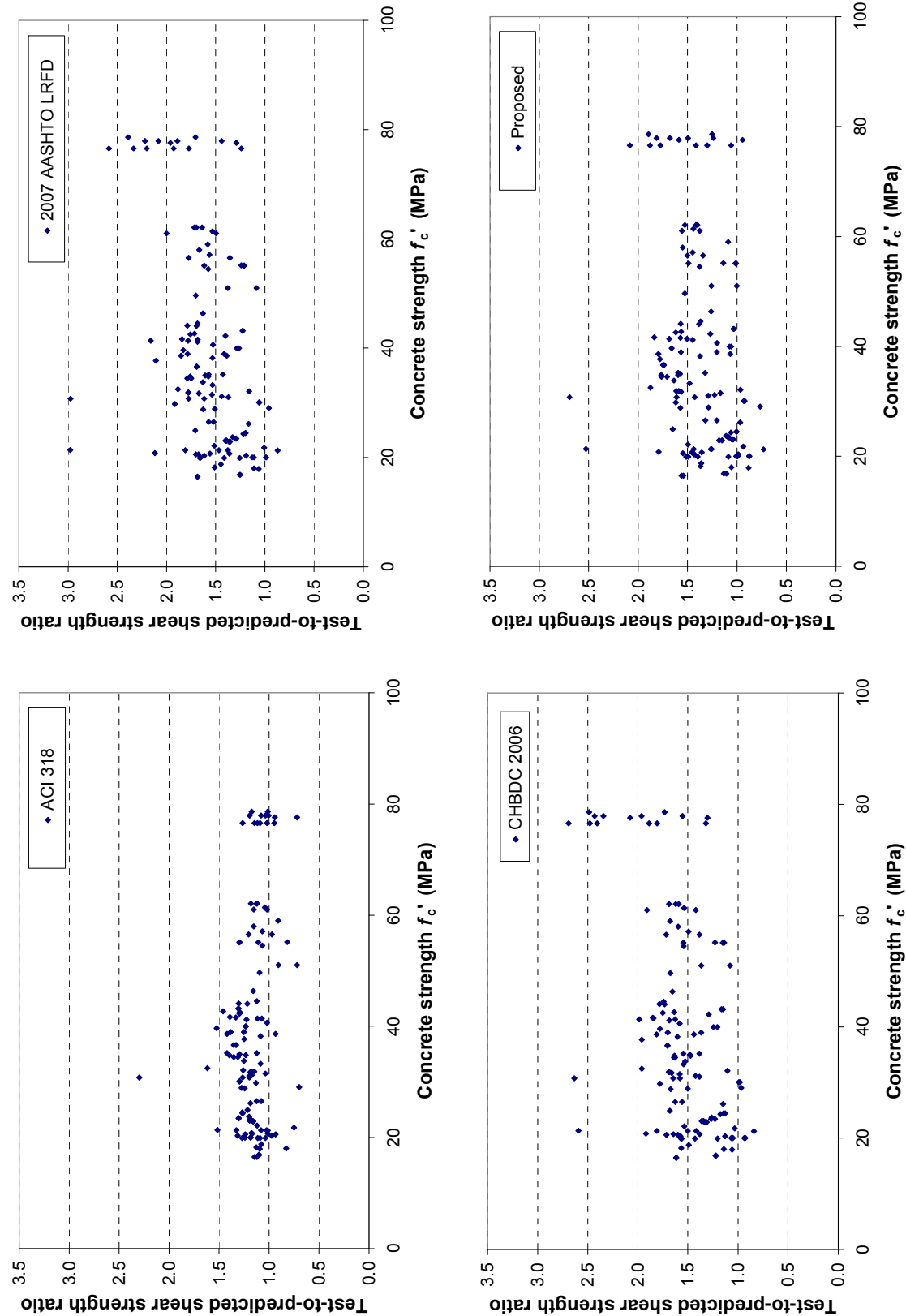


Fig. F-9 Variation of test-to-predicted shear strength ratios of 131 PC beams with concrete compressive strength.

Appendix F: Comparison of Predictions with Beam Test Results (Beams Without Stirrups)

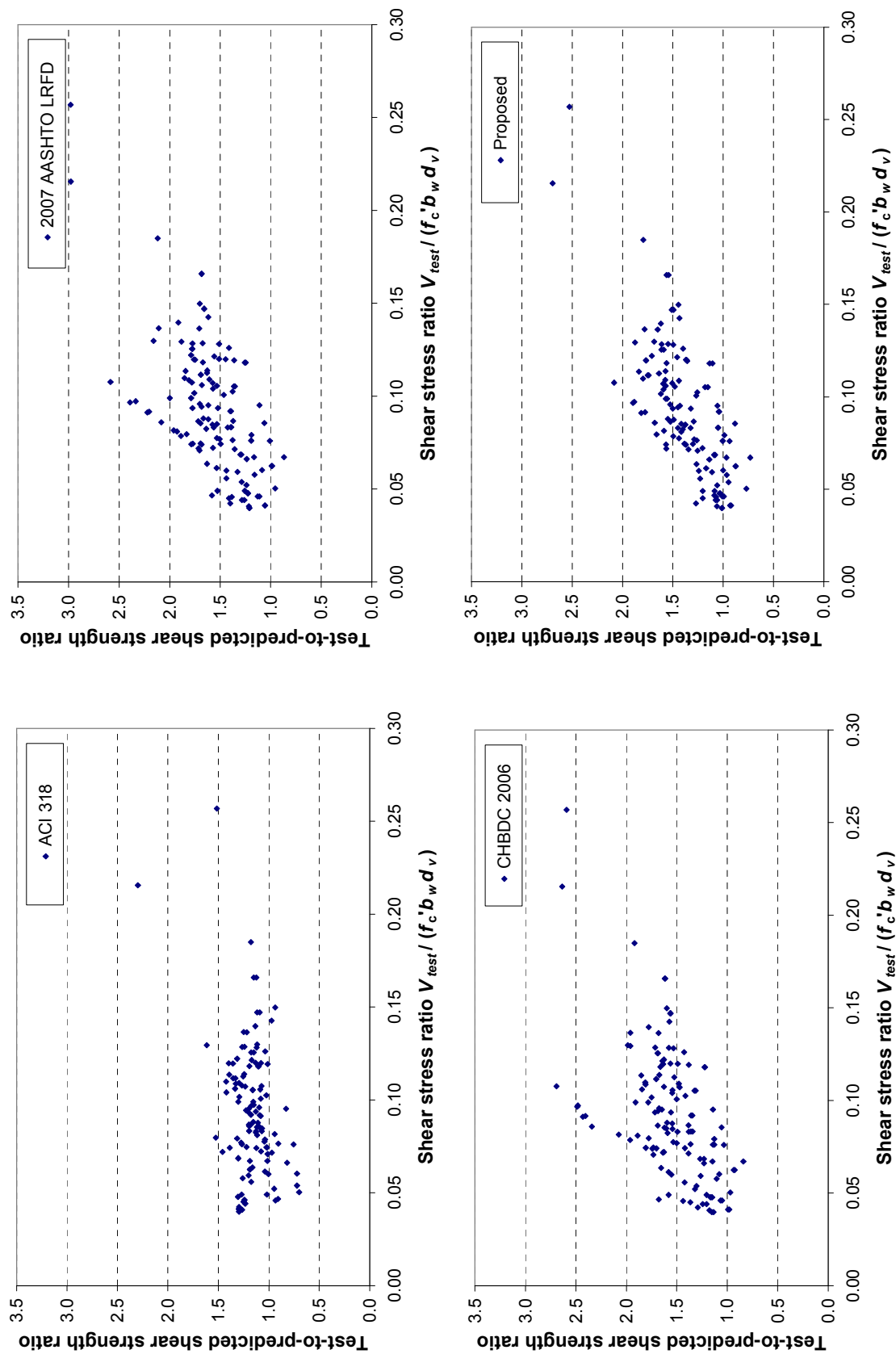


Fig. F-10 Variation of test-to-predicted shear strength ratios of 131 PC beams with shear stress ratio.

Appendix F: Comparison of Predictions with Beam Test Results (Beams With Stirrups)

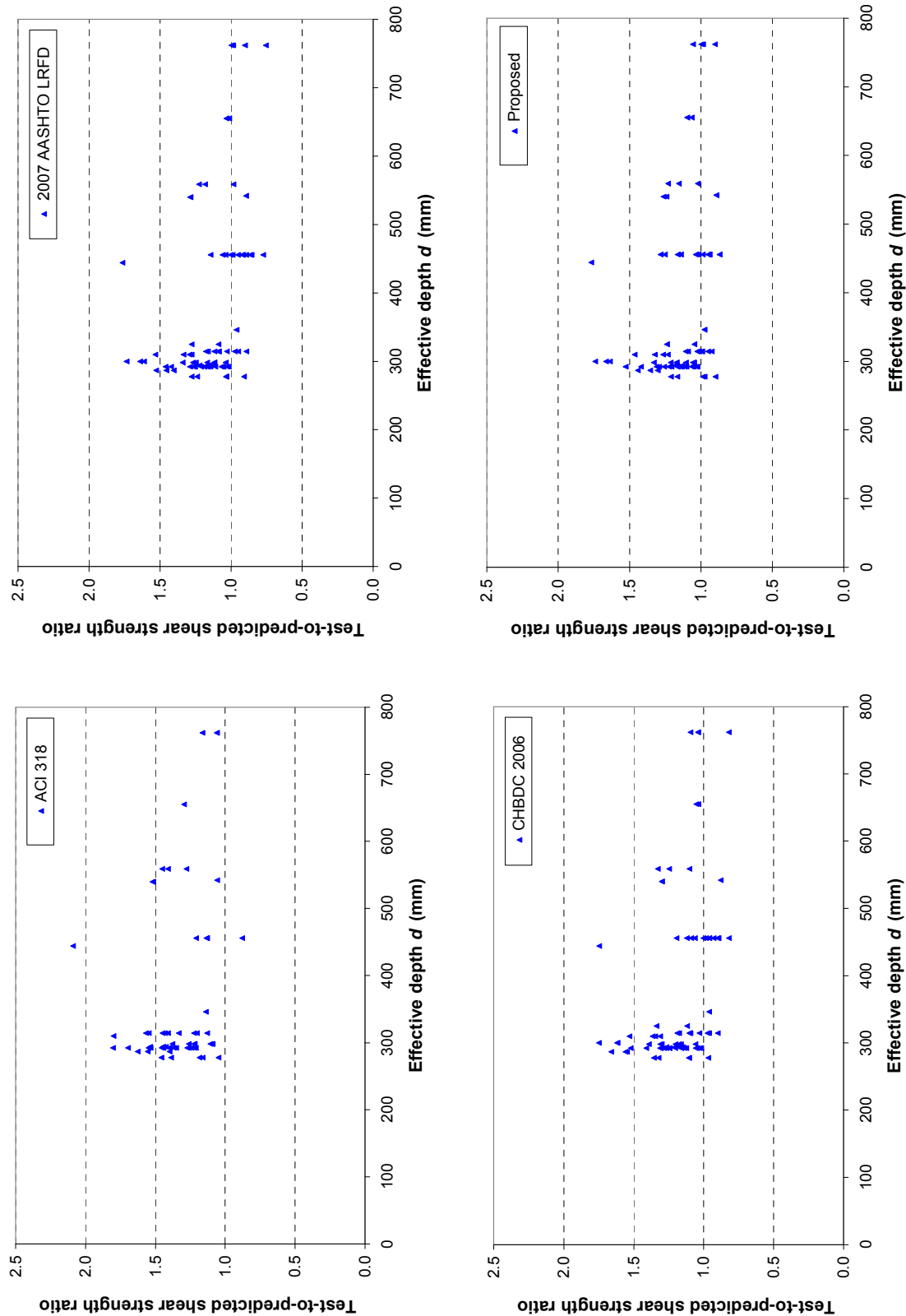


Fig. F-11 Variation of test-to-predicted shear strength ratios of 80 RC beams with effective depth.

Appendix F: Comparison of Predictions with Beam Test Results (Beams With Stirrups)

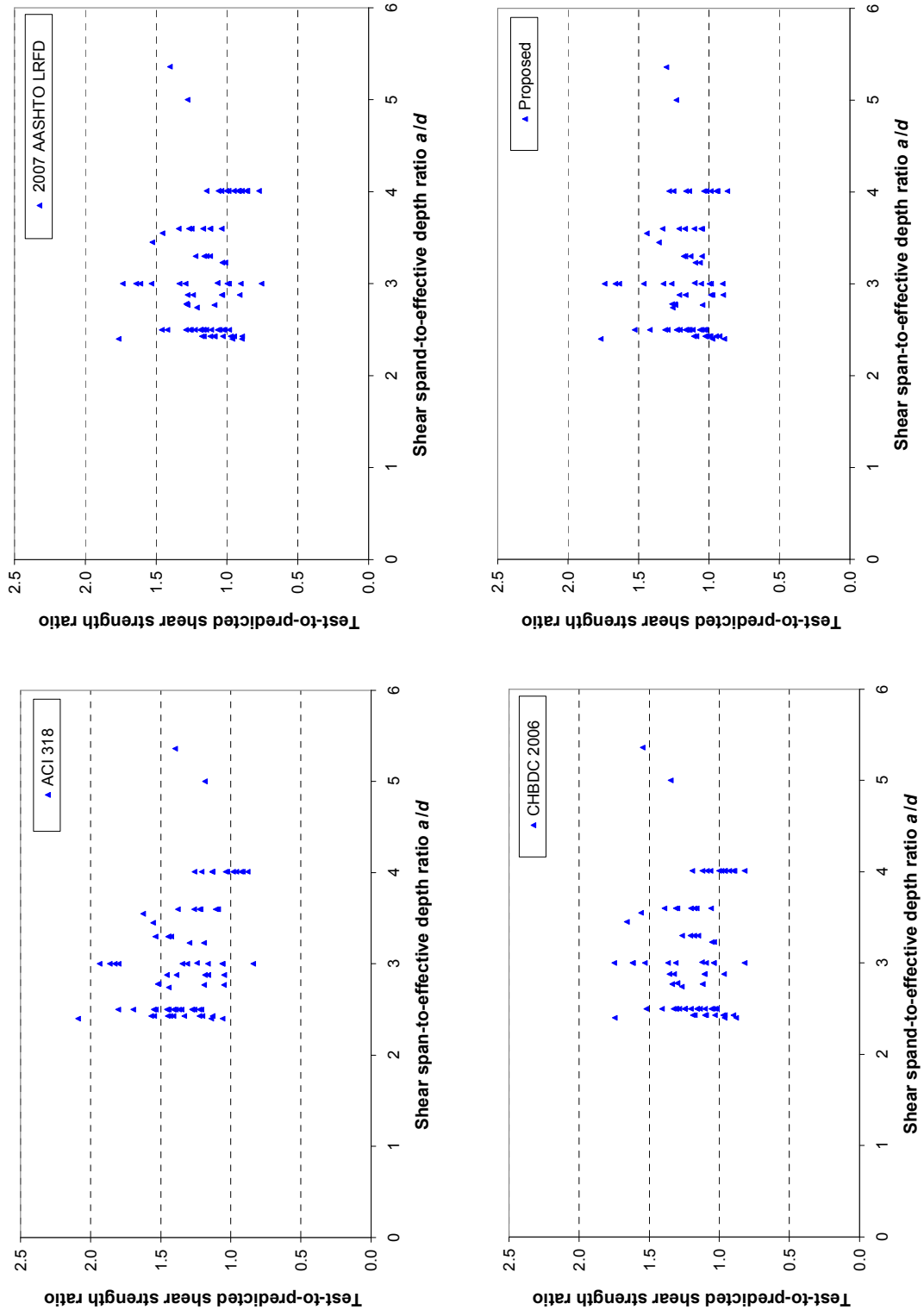


Fig. F-12 Variation of test-to-predicted shear strength ratios of 80 RC beams with shear span to effective depth ratio.

Appendix F: Comparison of Predictions with Beam Test Results (Beams With Stirrups)

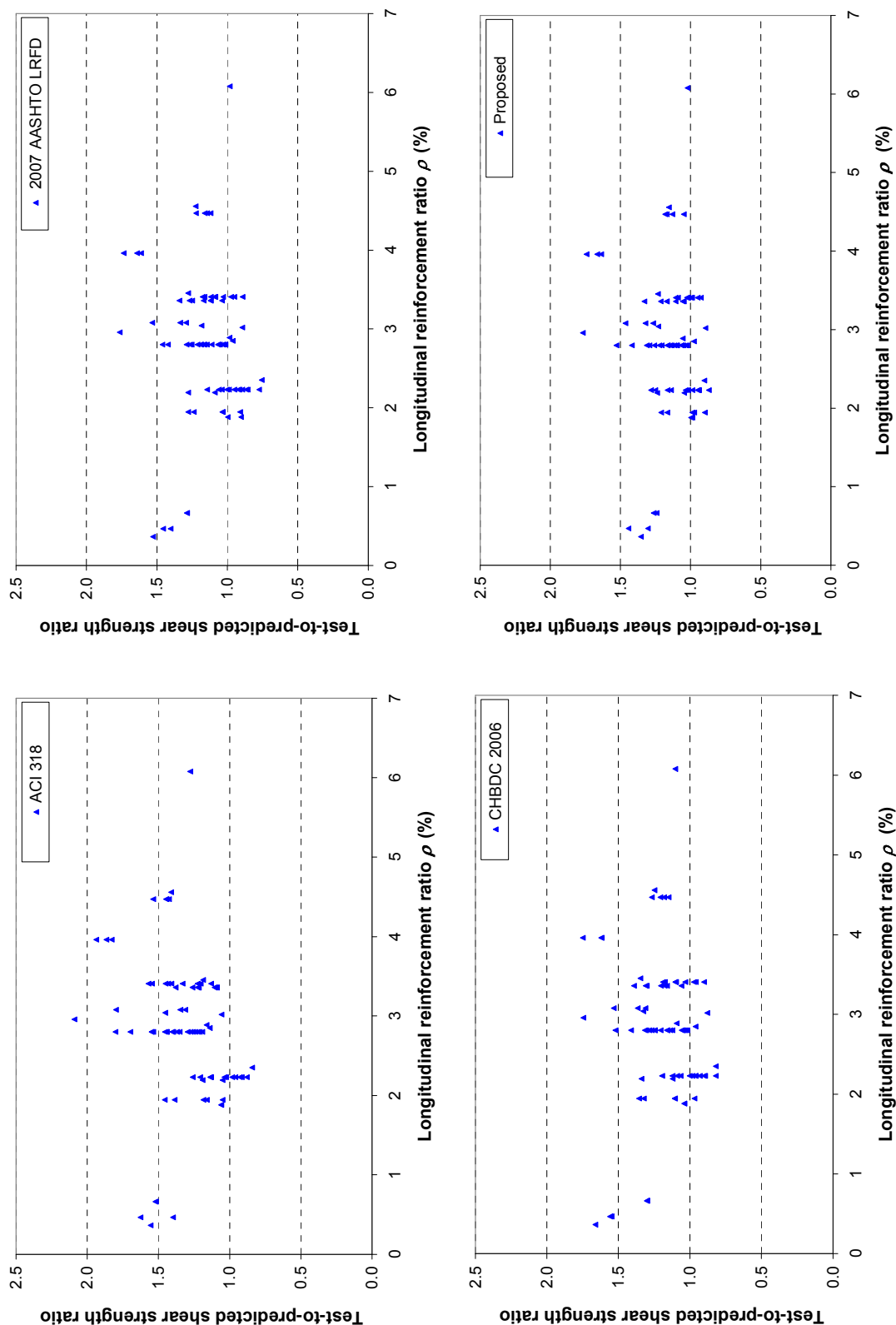


Fig. F-13 Variation of test-to-predicted shear strength ratios of 80 RC beams with longitudinal reinforcement ratio.

Appendix F: Comparison of Predictions with Beam Test Results (Beams With Stirrups)

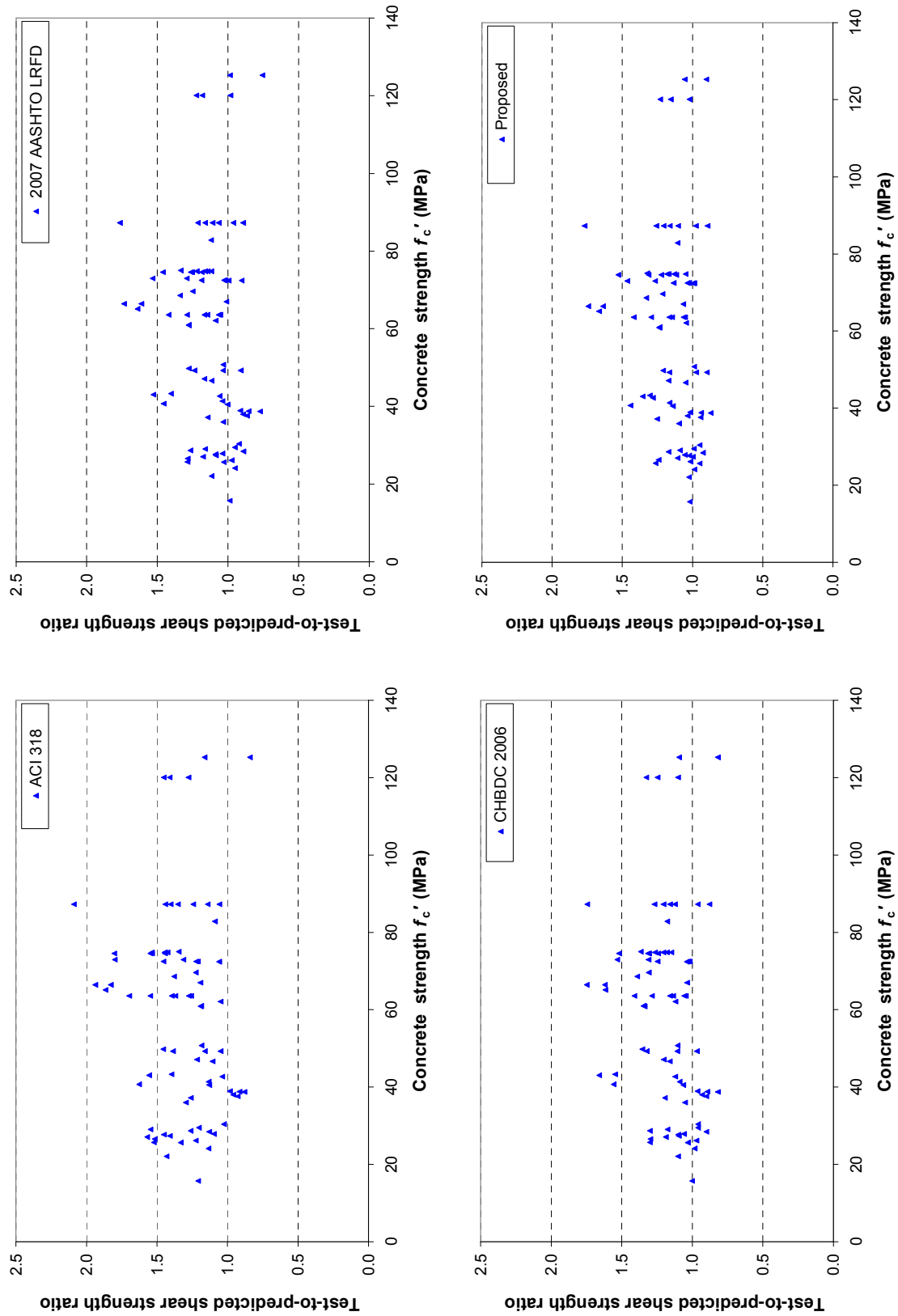


Fig. F-14 Variation of test-to-predicted shear strength ratios of 80 RC beams with concrete compressive strength.

Appendix F: Comparison of Predictions with Beam Test Results (Beams With Stirrups)

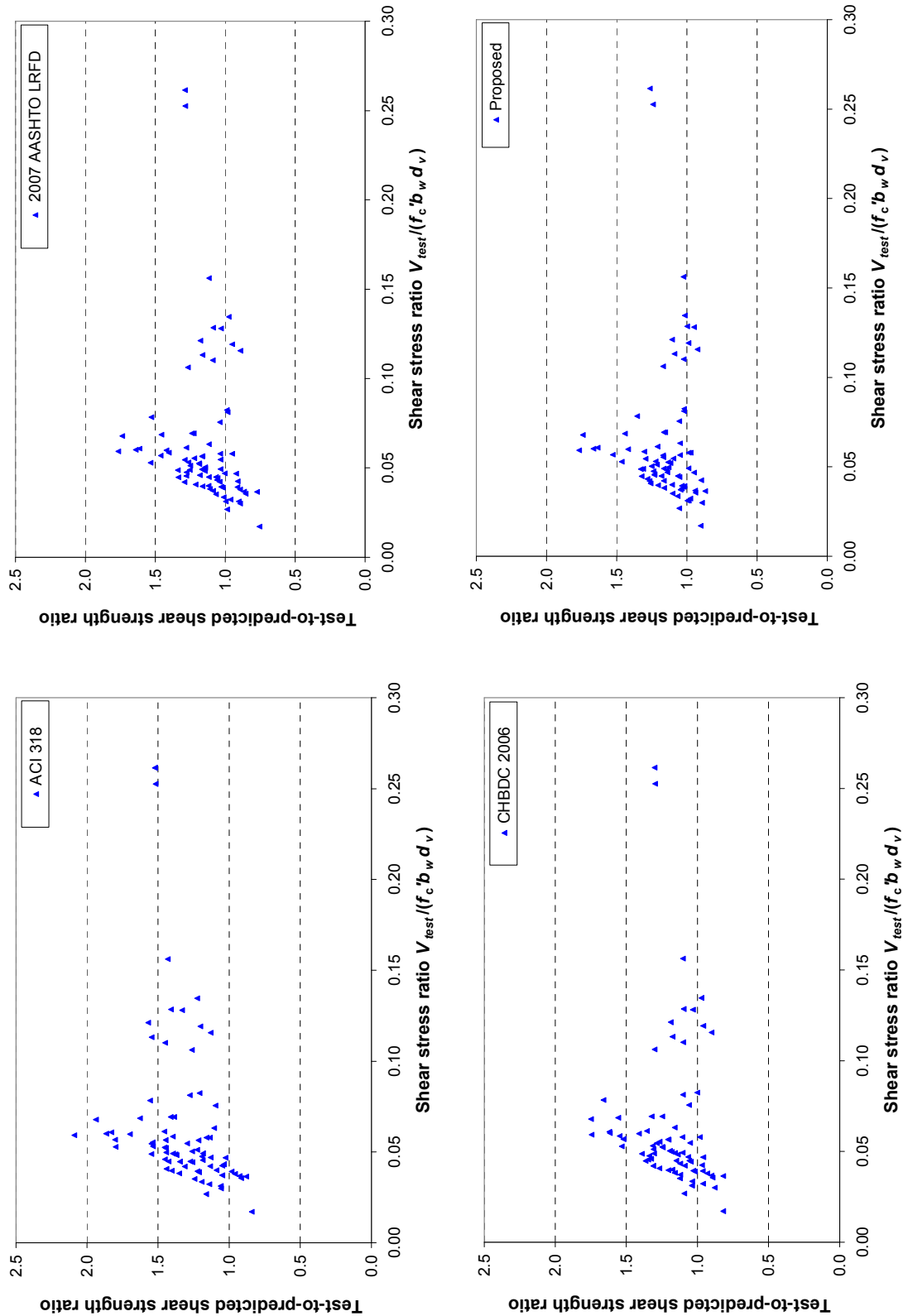


Fig. F-15 Variation of test-to-predicted shear strength ratios of 80 RC beams with shear stress ratio.

Appendix F: Comparison of Predictions with Beam Test Results (Beams With Stirrups)

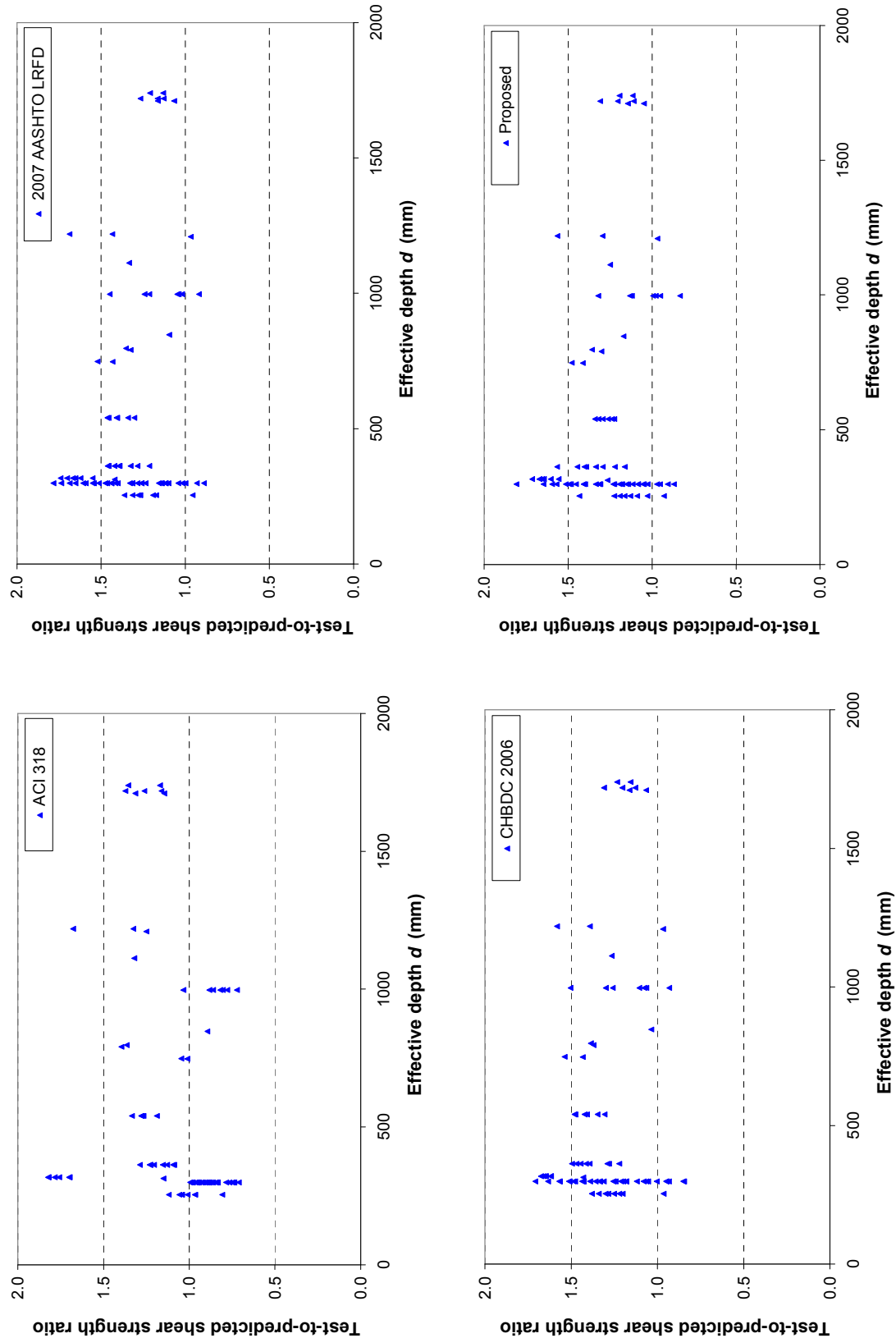


Fig. F-16 Variation of test-to-predicted shear strength ratios of 88 PC beams with effective depth.

Appendix F: Comparison of Predictions with Beam Test Results (Beams With Stirrups)

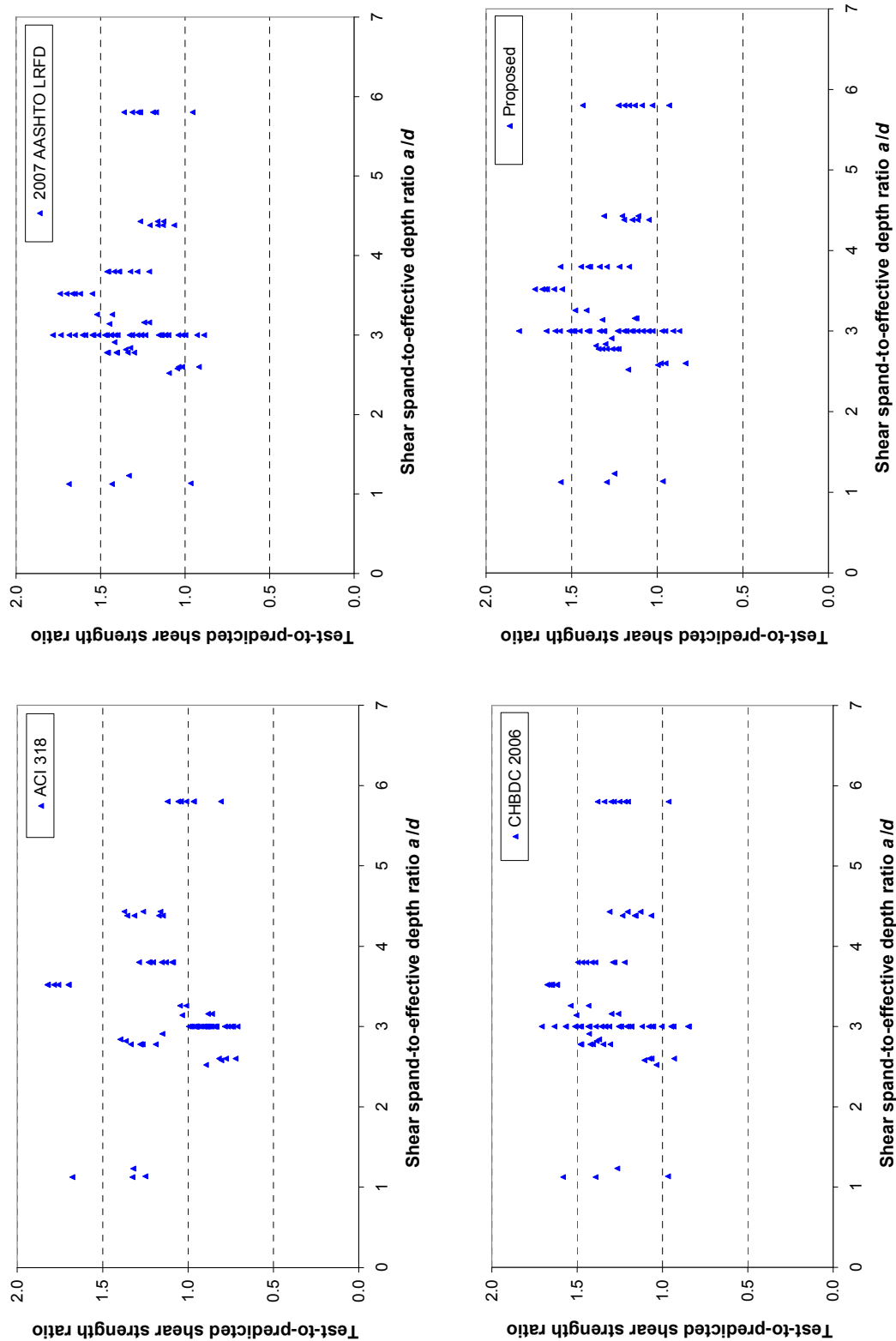


Fig. F-17 Variation of test-to-predicted shear strength ratios of 88 PC beams with shear span to effective depth ratio.

Appendix F: Comparison of Predictions with Beam Test Results (Beams With Stirrups)

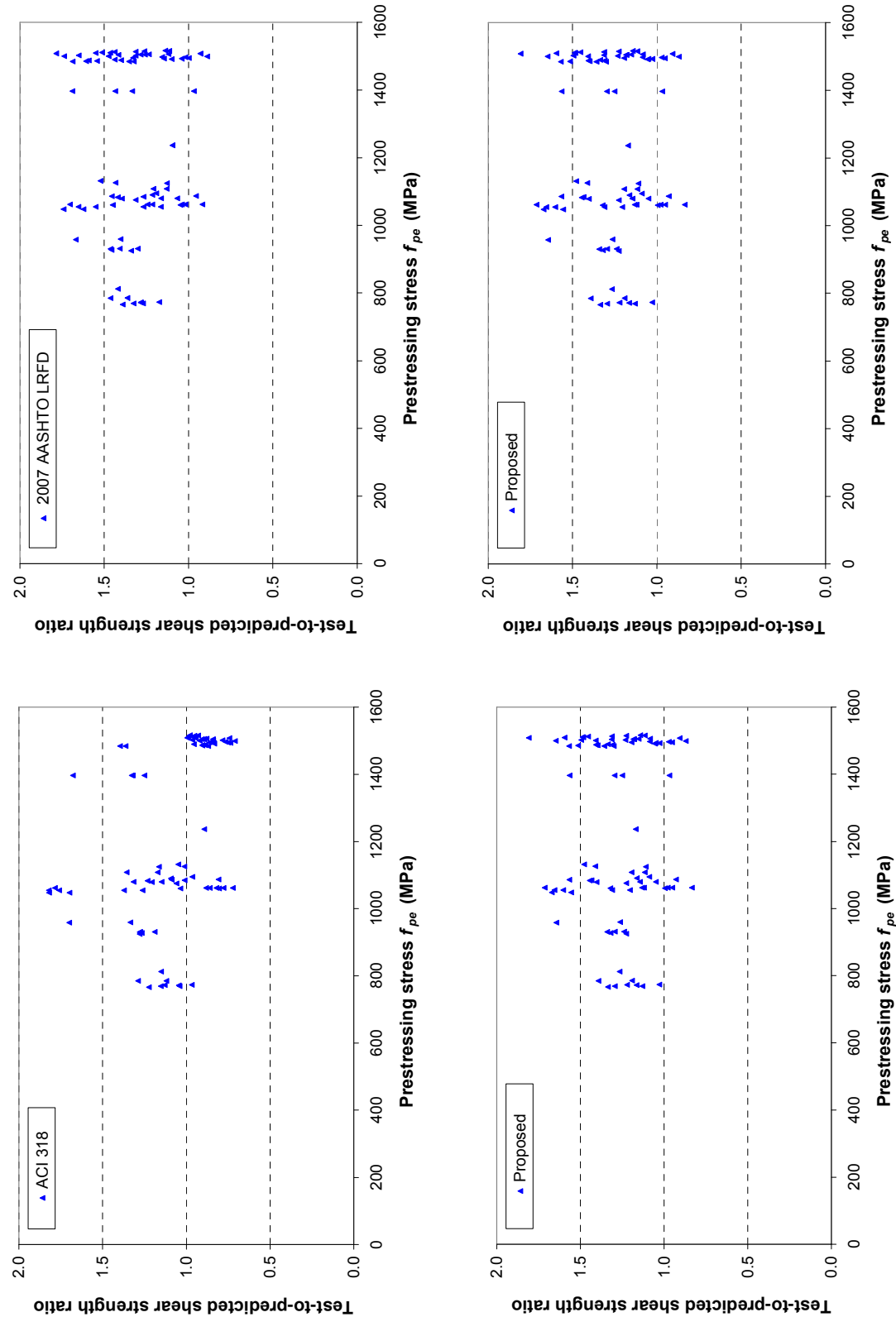


Fig. F-18 Variation of test-to-predicted shear strength ratios of 88 PC beams with effective prestressing stress.

Appendix F: Comparison of Predictions with Beam Test Results (Beams With Stirrups)

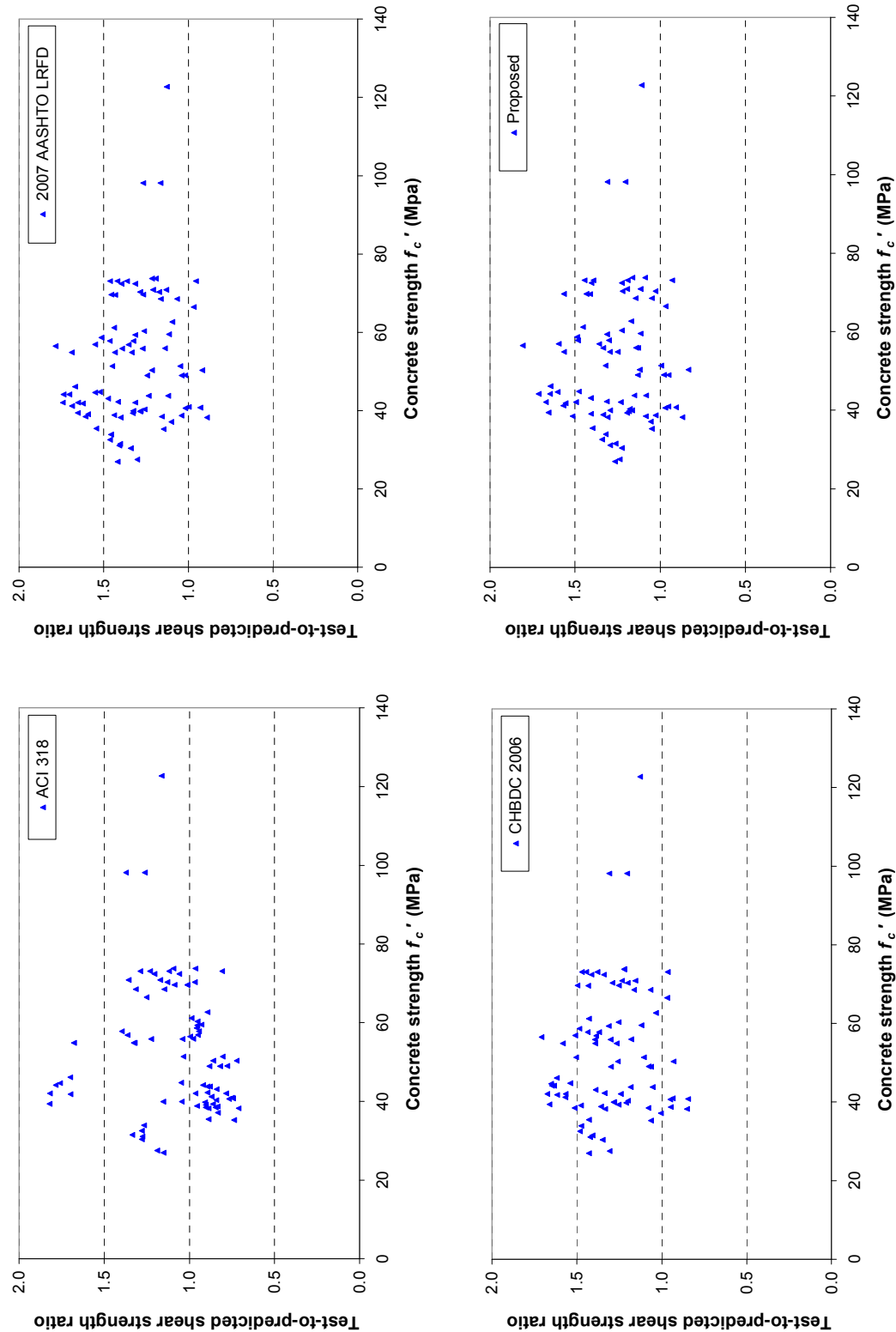


Fig. F-19 Variation of test-to-predicted shear strength ratios of 88 PC beams with concrete compressive strength.

Appendix F: Comparison of Predictions with Beam Test Results (Beams With Stirrups)

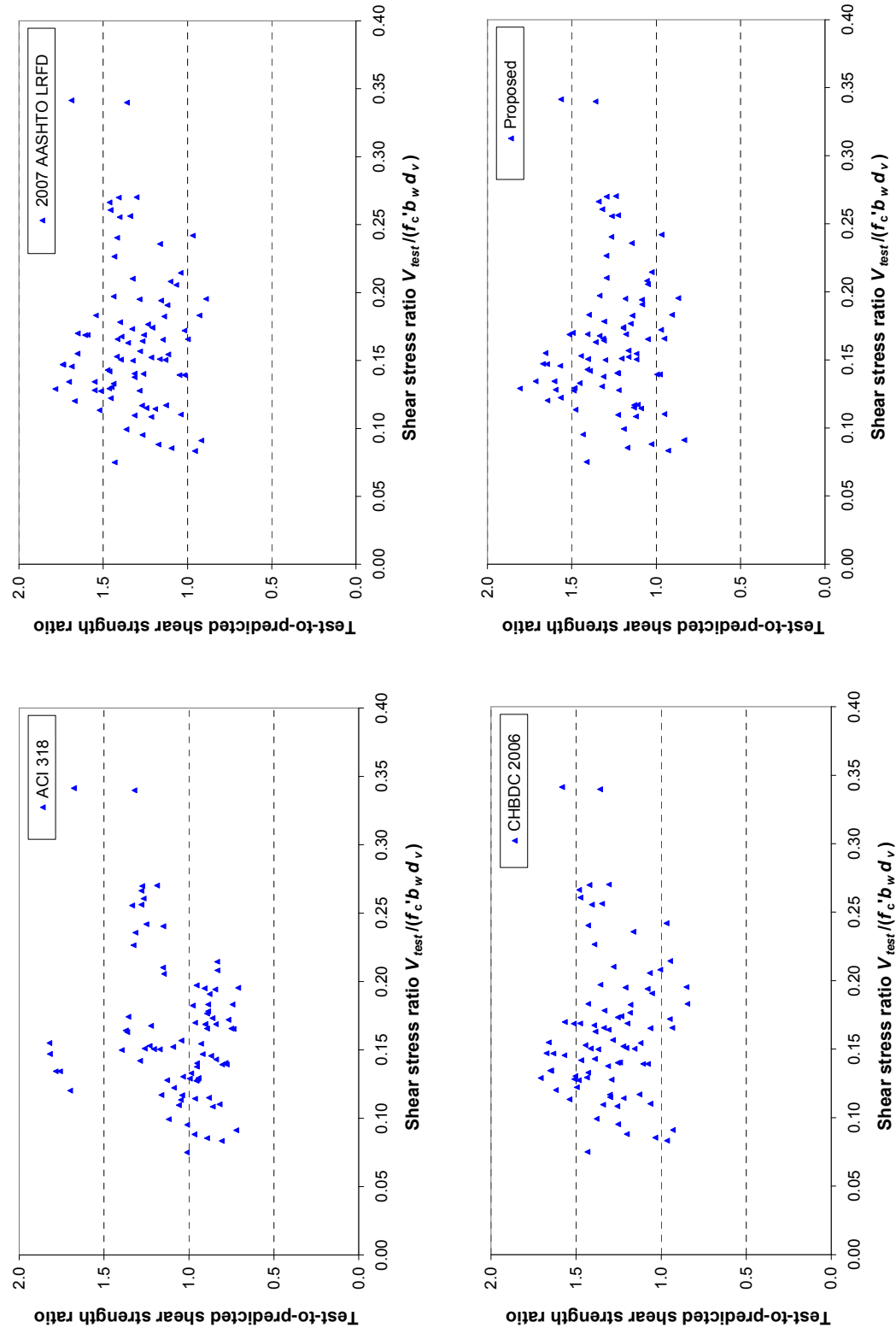


Fig. F-20 Variation of test-to-predicted shear strength ratios of 88 PC beams with shear stress ratio.